HOKKAIDO UNIVERSITY

Title	Beachrock formation mechanism and its application to developing beach sand cementation method based on microbial induced carbonate precipitation (MICP) : Case study of Krakal-Sadranan, Yogyakarta, Indonesia
Author(s)	Lutfian, Rusdi Daryono
Degree Grantor	北海道大学
Degree Name	博士(工学)
Dissertation Number	甲第14250号
Issue Date	2020-09-25
DOI	https://doi.org/10.14943/doctoral.k14250
Doc URL	https://hdl.handle.net/2115/82723
Type	doctoral thesis
File Information	Lutfian_Rusdi_Daryono.pdf

Hokkaido University Collection of Scholarly and Academic Papers : HUSCAP

Beachrock formation mechanism and its application to developing beach sand cementation method based on microbial induced carbonate precipitation (MICP): Case study of Krakal-Sadranan, Yogyakarta, Indonesia

Laboratory of Biotechnology for Resources Engineering,

Division of Sustainable Resources Engineering,

Graduate School of Engineering,

Hokkaido University,

Japan

HOKKAIDO
UNIVERSITY

Lutfian R. Daryono

Declaration

I declare that, except where specific reference is made in the text to the work conducted by other authors, this thesis is my own account of my research and contains as its main content work that has not previously been submitted for a degree at any university.

Name: Lutfian Rusdi Daryono Signature: 

Date: 17/ 08/ 2020

Acknowledgement

Foremost, I would like to express my deepest gratitude to my supervisors: Prof. Satoru KAWASAKI and associate Prof. Kazunori NAKASHIMA for their generous cooperation. Special thanks to Muhammad Hidayat, M. Zharfan Bimantoro, Reny Rafiqah, Dobrak Tirani, Jum Satriani, Fathia Lutfiananda, and Enggar Suwandi as field geology and geophysics exploration of UGM Indonesia for their constant assistance with the experiments; Dr. rer. nat. Doni Eka Prakasa, Dr. Anastasia Dewi Titisari, Ph.D., and Dr. Didit Hadi Barianto, Ph.D., who permitted access to the Get-In CICERO Laboratory that was supported by BMBF, Dept. of Geological Engineering, UGM; Drs. Imam Suyanto, M.Si., and Professor Koichi Suzuki as author's supervisor in geophysical measurement, Arief Rahmadi as author's partner in field acquisition and grateful to Embassy of the Republic of Indonesia in Tokyo regarding the permit letter-number B-00446/TOKYO/181227 for Access Benefit Sharing Knowledge Nagoya Protocol April 2018 within Hokkaido University, Japan and UGM, Indonesia. I'm extremely grateful to Mr. Ir. Arifin Tasrif (current Minister for Energy & Mineral Resources), Mr. Tri Purnajaya (Deputy Chief Representative) and also Mr. Erry Soedewo, Mrs. Dr. Sri Nurwiyanti as Agricultural Attaché and Mr. Alinda FM Zain as Education Attaché for permit correspondence in the study. Also, special thanks to my laboratory partners at Hokkaido University who made it a convivial place to work. I'd like to acknowledge the assistance to Mrs. Hitomi Tada for her support during the years I have been working on this thesis. This dissertation is dedicated to my wife Saputri Sapta Oktavianty of someone who always believe in me, my beloved son Bramadanu Kaede Daryono, and also deeply indebted to the Daryono's big family.

学 位　論　文　内　容　の　要　旨

DISSERTATION ABSTRACT

博士の専攻分野の名称 博士（工学）　　氏名　Lutfian Rusdi Daryono

学 位　論　文　題　名

Title of dissertation submitted for the degree

Beachrock formation mechanism and its application to developing beach sand cementation method based on microbial induced carbonate precipitation: Case study of Krakal-Sadranan, Yogyakarta, Indonesia

ビーチロック形成機構と微生物による炭酸塩析出に基づく海浜砂セメンテーション法の開発への応用：クラカルーサドラナン（ジョグジャカルタ，インドネシア）における事例研究

The aim of this dissertation is to assess the feasibility of exploiting ureolytic microbial adjustment activity in carbonate precipitation as a unique and novel grout, developing a countermeasure for coastal erosion using biochemical methods to improve the ground. Conducting research on the impact of direct morphology and erosional processes on in pristine or reference beachrock toward could provide essential information on the natural mechanism of the sediment and the function of microbial control in the carbonate. Microbial induced carbonate precipitation (MICP) is an effective and eco-friendly technology that can be applied to solve various environmental problems. Biominerals including calcium carbonate or calcium phosphate are involved in production of complex multifunctional composites with organic macromolecules. It is highly important to explore the multiple functionality of MICP and upscale its implementation in different areas to fully realize its potential as a versatile technique for soil improvement applications. This research framework was used to study the biological, geophysical, and engineering aspects that could deepen the understanding of MICP technology and push it closer towards field implementation.

Chapter 1 describes the research background, objectives, and originality of this thesis. A comprehensive literature review is conducted relate to various aspects of natural beachrock processes and the stability of the MICP process.

Chapter 2 presents a geophysical investigation of buried beachrock at Krakal-Sadranan beach, Yogyakarta, Indonesia. The objective of the investigation was to evaluate the feasibility

of constructing artificial beachrock using natural materials (e.g., microbes, sand, shell, pieces of coral, and seaweed) within a short time, and to propose a method to use this for coastal protection. A field survey on natural beachrock suggests that both resistivity and shear wave velocity were higher in deep deposits than in the underlying unconsolidated sand layer within a depth of approximately 1.5 m, and that this covered an area of 210.5 m^3 for the α-section and 76.9 m^3 for the β-section of the beachrock deposit.

Chapter 3 presents a detailed laboratory analysis of the investigation of the characteristics of beachrock sediment. Beachrock was also examined to determine the depositional conditions and distribution of rare earth elements therein. An increased concentration of both heavy rare earth elements (terbium, dysprosium, yttrium, holmium, erbium, thulium, ytterbium, and lutetium) and light rare earth elements (lanthanum, cerium, praseodymium, neodymium, samarium, europium, and gadolinium) suggests that the beachrock deposition process occurred under oxidative environmental conditions. This study proposes a novel use of ureolytic bacteria in a depositional environment to control the carbonate in a sedimentary process to develop artificial rock with which to mitigate coastal erosion. The resulting bacterial strains are highly homologous to the 16S rRNA nucleotide sequence of the species *Oceanobacillus profundus*, *Vibrio maritimus*, and *Pseudoalteromonas tetradonis*.

Chapter 4 describes the culturing of ureolytic bacteria from the Indonesian tropical shoreline, that was compared with that from the characteristic beachrock in Okinawa, Japan. Okinawa beachrock was classified as a biotically induced precipitate because an organism set the precipitation process in motion, although the latter then has a marginal or absent organic influence. However, Indonesian beachrock is classified as a biotically controlled precipitate, meaning that it is commonly precipitated by microorganisms, mostly bacteria and cyanobacteria.

Chapter 5 described a beach sand treatment based on the MICP process; it produced a result that mimicked the natural beachrock based on chemical compound and strength. The results revealed that the bacteria could effectively mineralize calcium carbonate between 30 °C and 40 °C, showing a more robust performance under tropical conditions. The effects of various chemical compositions were also critically investigated to deepen the understanding of the biochemical processes involved. The results of the sand solidification test in the laboratory showed that treated sand achieved an unconfined compressive strength of up to

approximately 6 MPa after a treatment period of 14 days under optimum conditions. By adding biopolymer polysaccharides, the reaction leads to crystal formation of vaterite instead of calcite. The calcium carbonate crystals studied in this research were found to be orthorhombic, rhombohedral, hexagonal, and spherical geometries.

Chapter 6 discusses the testing of durability of this material based on MICP for in the development of a countermeasure for coastal disasters. An experiment was performed to investigate the effects of environmental parameters on its long-term performance. As the tropical regions experience frequent rainfall, wetting-drying tests were performed as a potential indicator of durability. The results showed that there was significant wetting-drying damage and that this would have the foremost effect on the long-term performance of the MICP beach slope.

Chapter 7 suggests cost reduction purposes using cheap chemical reagents from cultured media and cement solution for MICP treatment. The aim of that study was to determine the feasibility of cultivating a strain of *P. tetradonis* in an economical food-grade yeast extract (beer yeast and tempeh fungi) medium and investigate its effect on bacterial production, urease activity, and biocalcification.

Chapter 8 outlines the proposal for a coastal prevention method in Indonesia based on ureolytic bacteria. The results obtained from this study are used to summarize the application guidelines for the optimal chemical compositions, suitable environmental conditions, and ways to monitor the process.

Chapter 9 summarizes and provides a conclusion that may guide future work. In summary, I have used biomechanics as a countermeasure against coastal erosion and other problems considering the potential use of a biocementation MICP treatment to develop a shoreline or beach slope. This will provide new knowledge about biotechnology and will greatly contribute to the development of environmental resource engineering.

TABLE OF CONTENTS

Declaration i
Acknowledgement ii
Dissertation abstract iii
Table of contents vi

Chapter 1. Introduction
1.1 Research background 1
1.2 Literature review 3
1.2.1 Beachrock sedimentary mechanism 3
1.2.1.1 Direct cement precipitation 5
1.2.1.2 Mixing of marine and the meteoric waters 5
1.2.1.3 Degassing of CO_2 5
1.2.1.4 Formation by biological activity 6
1.2.2 Beachrock modes of carbonate precipitation 8
1.2.2.1 Tropical factory 11
1.2.2.2 Cool-water carbonate factory 12
1.2.2.3 Mud-mound factory 12
1.2.3 Artificial beachrock development based on microbial induced carbonate precipitation (MICP) 13
1.2.3.1 Ureolytic bacteria as carbonate precipitation 15
1.2.3.2 Different polymorphs and their effects in various calcium sources 17
1.2.3.3 Isolation of ureolytic bacteria from various sources 19
1.2.3.4 Recent status of MICP applications 20
1.3 Coastal erosion 22
1.4 Current hardened structure erosion mitigation methods 24
1.4.1 Seawalls, bulkheads, and other wall structures 24
1.4.2 Breakwaters an alternative to wall-type structures are breakwaters. 24
1.4.3 Groins and jetties 25
1.4.4 Riprap and shore armoring 25
1.4.5 Beach nourishment and dune benefits 26
1.5 Objectives 26

1.6 Scope and organization 27
1.7 Originality and usefulness of the study 27
1.8 Originality of the thesis 29
References 32

Chapter 2. Geophysical investigation of buried beachrock at Krakal-Sadranan beach, Yogyakarta, Indonesia
2.1 Introduction 51
2.2 Regional geology 53
2.2.1 Physiography 53
2.2.2 Stratigraphy 54
2.2.3 Geological structure 54
2.2.4 Geology of the research area 54
2.2.5 Site study 56
2.3 Objectives 57
2.4 Material and methods 57
2.4.1 Field Investigation 57
2.4.1.1 Drone photogrammetric data processing 58
2.4.1.2 Geological identification 58
2.4.1.3 DC resistivity survey 59
2.4.1.4 MASW (Multi Analysis of Seismic Surface) 61
2.4.1.5 Seismic refraction 62
2.4.2 Laboratory tests 64
2.5 Results 64
2.5.1 Lithostratigraphy of Krakal-Sadranan beachrock 65
2.5.1.1 Trench AB 65
2.5.1.2 Trench CD 68
2.5.1.3 Trench EF 71
2.5.2 Geophysics measurements 73
2.5.2.1 α-section 73
2.5.2.2 β-section 73
2.5.2.3 γ-section 74
2.5.3 Three dimensional of subsurface model 74

2.6 Discussions 77
2.6.1 Beachrock characteristics 77
2.6.2 Geophysical beachrock imagine 82
2.6.3 Rock characteristic of natural beachrock 83
2.7 Conclusions 84
References 85

Chapter 3. Sediment Characteristics of beachrock at Krakal-Sadranan beach, Yogyakarta, Indonesia

3.1 Introduction 90
3.2 Objectives 91
3.3 Materials and methods 92
3.3.1 Sampling method 92
3.3.2 Laboratory analysis 92
3.3.2.1 Petrographic studies 92
3.3.2.2 Inductively coupled plasma-atomic emission spectroscopy and mass spectrometry (ICP-AES and MS) 93
3.3.2.3 X-Ray diffraction (XRD) and total organic carbon (TOC) 93
3.3.2.4 Algae taxonomy 95
3.3.2.5 Isolation and identification of a suitable urease active bacterium 95
3.3.2.6 Cultivation of bacteria and assessing the potential for microbial induced carbonate precipitation (MICP) 97
3.4 Results 97
3.4.1 Stratigraphy of Krakal-Sadranan beachrock 97
3.4.2 ICP-AES and MS analysis 97
3.4.3 X-Ray diffraction (XRD) and total organic carbon (TOC) 101
3.4.4 Biodiversity observations 102
3.4.4.1 Algae taxonomy 102
3.4.4.2 Isolation of indigenous ureolytic bacteria 103
3.4.4.3 Microbial population count and urease activity test 105
3.5 Discussions 106
3.5.1 Sediment characteristics 106
3.5.2 Post depositional diagenesis 107
3.5.3 Temperature and evaporation conditions 108

3.5.4 Redox condition 108
3.5.5 Terrigenous contaminant materials 109
3.5.6 Biotically controlled precipitation 112
3.5.6.1 Light 112
3.5.6 Temperature 113
3.5.6 Latitudinal zonation of skeletal production 114
3.5.6 Nutrients 114
3.5.6 Salinity 114
3.5.7 Ureolytic bacteria-controlled precipitation beachrock carbonate 115
3.6 Conclusions 116
References 117

Chapter 4. Comparative characteristics of natural beachrock from Okinawa, Japan and Yogyakarta, Indonesias

4.1 Introduction 124
4.2 Objectives 125
4.3 Methodology 126
4.3.1 Field work 126
4.3.2 Petrographic analysis 126
4.3.3 Geochemical XRD and XRF 127
4.3.4 Biodiversity microbial analysis 127
4.3.4.1 Isolation of ureolytic bacteria 127
4.3.4.2 Microbial population count and urease activity test. 127
4.4 Results 128
4.4.1 Sumuide beachrock sample, Okinawa, Japan. 128
4.4.1.1 Geology of Okinawa, East China Sea 128
4.4.1.2 Petrographic analysis result. 130
4.4.1.3 Indigenous ureolytic bacteria from Okinawa, Japan. 132
4.4.1.4 Geophysical mapping of beachrock in Okinawa, Japan 134
4.4.2 Krakal-Sadranan beachrock sample, Yogyakarta, Indonesia. 136
4.4.2.1 Geology of Gunungkidul regency, Yogyakarta. 136
4.4.2.2 Petrographic analysis result. 137
4.4.2.3 Indigenous ureolytic bacteria from Yogyakarta, Indonesia. 139

4.5 Discussion 141
4.5.1 Natural beachrock sedimentary 142
4.5.1.1 Cement characteristics 142
4.5.1.2 Geophysical properties of natural beachrock 143
4.5.2 Indigenous ureolytic bacteria from natural beachrock 144
4.5.2.1 Gram positive bacteria 142
4.5.2.1 Gram negative bacteria 147
4.5.2.3 Gram positive versus gram negative bacteria 149
4.5.3 Sediment characteristics differences of Okinawa, Japan and Yogyakarta, Indonesia natural beachrock. 149
4.6 Conclusions 150
References 151

Chapter 5. Beach sand solidification test using MICP method
5.1 Introduction 158
5.2 Objectives 159
5.3 Materials and methods 159
5.3.1 Sands 159
5.3.2 Bacteria 159
5.3.2.1 Method for urease activity test 161
5.3.2.2 Genetic analysis of microorganisms 162
5.3.3 Ureolytic bacteria characteristics of Indonesian species in various culture conditions 163
5.3.4 Cementation media 164
5.4. Experimental method 165
5.4.1 Syringe solidification test 165
5.4.2 Shoreline slope solidification model test 166
5.4.3 Needle penetration test 167
5.4.4 Experimental conditions 168
5.5 Results 170
5.5.1 Growth characteristics 170
5.5.2 Optimum pH and temperature condition 171
5.5.3 Effect of bacterial species on solidification test 172

5.5.4 Effect of bacterial population based on OD_{600} on solidification test 174
5.5.5 Effect of particle size and different sand samples on solidification test 176
5.5.6 Effect of cementation ion solutions on strength 176
5.5.7 Effect of carrageenan biopolymer on strength of MICP 182
5.5.8 Beach slope model solidification test 186
5.5.9 MICP of artificial rock properties 188
5.6 Discussions 190
5.6.1 Uniformity of cementation 190
5.6.2 Field implication and associated limitations 193
5.6.3 Permeability of cemented specimens 194
5.7 Conclusions 195
References 196

Chapter 6. Durability test of MICP beach sand treatment
6.1 Introduction 204
6.2 Objectives 205
6.3 Research methodology 205
6.3.1 Beachrock and bacteria 205
6.3.2 MICP treatment and reagents 208
6.3.3 Statistical analysis wetting-drying (WD) test 209
6.3.4 XRD test methods 209
6.3.5 Rock properties evaluation of specimens 209
6.4 Results and discussions 210
6.4.1 Aggregate stability 210
6.4.2 Mechanical characteristics 210
6.4.3 Strength deterioration ratio (SDR) 213
6.5 Conclusions 217
References 218

Chapter 7. MICP beach sand treatment using cheap chemical reagents
7.1 Introduction 221
7.2 Objectives 223
7.3 Materials and methods 223

7.3.1 Ureolytic bacteria and cultivation 223
7.3.2 Culture media 223
7.3.2.1 ZoBell2216 medium 224
7.3.2.2 Beer yeast extract 210
7.3.2.3 Tempeh starter 211
7.3.3 Nutrient cementation solution 211
7.3.3.1 Standard solution 211
7.3.3.2 Chalk powder extract 212
7.3.3.3 Snow melting reagent extract 212
7.3.4 Growth and pH profilest 213
7.3.5 Urease activity 214
7.3.6 Microbial $CaCO_3$ precipitation test 214
7.3.7 Solidifications test 215
7.3.8 Needle penetration test 216
7.3.9 Durability wet-drying test 216
7.4 Results and discussion 217
7.4.1 Culture media 217
7.4.2 Nutrient cementation solution on precipitation test 218
7.4.2.1 Standard solution 218
7.4.2.2 Chalk powder extract 219
7.4.2.3 Snow melting 219
7.4.3 Solidification test 220
7.4.4 MICP treated rock properties 220
7.4.5 Durability wetting-drying test 222
7.4.6 Cost feasibility of low-grade chemicals in MICP 224
7.5 Conclusions 226
References 226

Chapter 8. Tentative proposal of coastal preservation method
8.1 Introduction 248
8.2 Objectives 249
8.3 Material and methods 249
8.3.1 Ureolytic bacteria 249

8.3.2 Culture media 251
8.3.3 Cement solution 253
8.3.4 Soil/ sand 254
8.3.4.1 Density 254
8.3.4.2 Particle size 255
8.3.5 Treatment sand condition 256
8.3.5.1 pH and temperature 256
8.3.5.2 Marine environment 257
8.3.5.3 Injection mode and rates 258
8.4 Sustainability to the environment 258
8.4.1 Biosafety risk of indigenous ureolytic microorganisms 259
8.4.2 Biosafety risk of pure bacterial cultures 260
8.4.3 Undesired byproducts 262
8.4.4 Nonuniform injection of microbes and cementation reagents 262
8.4.5 Limitations of microbes 263
8.5 Conclusions 264
References 265

Chapter 9. General conclusions and future research
9.1 Summary of work presented and main conclusions 273
9.2 Suggestions for future works in MICP method 277
9.2.1 Froude similarity of upscale MICP 277
9.2.2 The durability of the inexpensive chemical reagents 277
9.2.3 Mechanism of MICP in clayey mineral 277

APPENDIXES
Appendix A Coastal drone mapping of Yogyakarta shoreline 279
Appendix B Measurement stratigraphy and petrographic analysis of Krakal-Sadranan beachrock, Yogyakarta, Indonesia 302
Appendix C ICP-MS and -AES results of rare earth element (REE) in the beachrock 333
Appendix D Petrography analysis of Okinawa beachrock, Japan 334
Appendix E XRD results before and after durability wetting-drying test 358
Appendix F XRD results of the MICP beach sand treatment using cheap chemical reagents 363

LIST OF TABLES

Table 1.1 Research originality. 28

Table 2.1 Coordinates of survey line. 58

Table 2.2 Comparison of the beachrock properties between Japan and Indonesia..... 82

Table 3.1 Composition of artificial seawater (Aquamarine, Japan). 96

Table 3.2 Algae species taxonomy surrounded beachrock. 102

Table 3.3 Ratio of carbonate sands and beachrock in Krakal-Sadranan, Yogyakarta, Indonesia. 109

Table 3.4 Summary of deposition process affecting the limestone sand and beachrock at Krakal-Sadranan, Yogyakarta, Indonesia.. 111

Table 4.1 Percentage composition of beachrock. 139

Table 4.2 Sedimentary characteristics differences of Okinawa natural beachrock, Japan and Yogyakarta, Indonesia natural beachrock 150

Table 5.1 The composition of the cresol red solution (per 100 mL, solvent: distilled water). 160

Table 5.2 The composition of the urease activity measurement solution (per 100 mL, solvent: distilled water). 160

Table 5.3 Genetic analysis of microorganisms.. 162

Table 5.4 Standard chemical compositions for cementation media..... 164

Table 5.5 Experimental conditions for precipitation carbonate. 165

Table 5.6 Purpose of conduction testing cases.. 170

Table 5.7 Characteristics of biopolymers considered for soil improvement. 184

Table 5.8 Rock properties of artificial beachrock using MICP method. 191

Table 6.1 The S-wave velocity values before and after subjected to WD test.. 213

Table 7.1 Composition make culture medium. 224

Table 7.2 Nutrient cementation solution of chalk powder extract with acetic acid..... 227

Table 7.3 Nutrient cementation solution of snow melting reagents (solvent in distilled water).. 228

Table 7.4 Test condition for syringe solidification test. 230

Table 7.5 Rock properties of artificial beachrock using MICP method. 237

Table 7.6 Cost comparison between pure chemicals and low-grade solutions in the MICP treatment of $1m^3$ natural sand.. 240

Table 8.1 Formula for MICP treatment of beach sand solidification test.. 264

Appendixes Table A.1 Wave height in Indian Ocean (Levitus, et al., 1994)... 283

Appendixes Table A.2 Specification of unmanned aerial vehicle (UAV) drone... 285

Appendixes Table A.3 Interval class of straightness density... 292

Appendixes Table C. Standart normalization rare earth element (REE) results concentration for sediment. The major element of beachrock (ppm), trace element result (in ppm), and REE of beachrock (in ppm)... 318

LIST OF FIGURES

Figure 1.1 Model of beachrock and cayrock formation (Gischler and Lomando, 1997).. 7

Figure 1.2 The typical material of the T factory is biotically controlled precipitate from tropical autotrophic organisms (or heterotrophic organisms with autotrophic symbionts); the C factory is dominated by heterotrophic organisms and the M factory by biotically induced precipitates, mostly micrite (Schlager, 2005)..13

Figure 1.3 Seafloor diagenesis of carbonate sedimentation in the tropical factory (Schlager, 2007; James and Jones, 2015)..... .12

Figure 1.4 Simplified Geological Map of Yogyakarta, Indonesia (modify from Surono, et al, 1992).. 23

Figure 1.5 Scope of the research.. 30

Figure 2.1 Beachrock deposits in Krakal-Sadranan, Yogyakarta, Indonesia.. 52

Figure 2.2 Geological map and stratigraphy of Yogyakarta, Indonesia..... 55

Figure 2.3 Location research area in Krakal-Sadranan, Yogyakarta, Indonesia.. 60

Figure 2.4 Schematic of acquisition plan.. 63

Figure 2.5 Stratigraphic of the Trench AB: (A) Petrographic on cross polarized nicol (XPL, A1) and plane polarized nicol (PPL, A2) with sf (skeletal fragment), mc (micrite), sp (sparite), ca (calcite) and ar (aragonite); (B) Degree of cementation based on composition of beachrock 66

Figure 2.6 Stratigraphic of the Trench CD: (A) Petrographic on cross polarized nicol (XPL, A1) and plane polarized nicol (PPL, A2) with sf (skeletal fragment), mc (micrite), sp (sparite), ca (calcite) and ar (aragonite); (B) Degree of cementation based on composition of beachrock.. 69

Figure 2.7 Stratigraphic of the Trench EF: (A) Petrographic on cross polarized nicol (XPL, A1) and plane polarized nicol (PPL, A2) with sf (skeletal fragment), mc (micrite), sp (sparite), ca (calcite) and ar (aragonite); (B) Degree of cementation based on composition of beachrock.. 72

Figure 2.8 Electrical and multi analysis surface wave results of α-section. (A1) the resistivity of line 1, (B1) the MASW of line 1, (A2) the resistivity of line 3, (B2) the MASW of line 3, (A3) the resistivity of line 2, (B3) the MASW of line 2.. 75-76

Figure 2.9 Electrical and multi analysis surface wave results of α-section. (A1) the resistivity of line 4, (B1) the MASW of line 4, (A2) the resistivity of line 5, and (B2) the MASW of line 5.....78-79

Figure 2.10 Electrical and multi analysis surface wave results of γ-section. (A) the resistivity of line 6, (B) the MASW of line 6, and (c) depth function for γ -section..... 80

Figure 2.11 Three dimensional of beachrock model calculation based on geophysical statistical anomaly data from electrical resistivity and multi analysis surface wave of α-section. 81

Figure 2.12 Three dimensional of beachrock model calculation based on geophysical statistical anomaly data from electrical resistivity and multi analysis surface wave of β-section. 81

Figure 2.13 Comparison of the geophysical properties of the sedimentary rocks and beachrocks based on P wave velocity and S wave velocity..... 84

Figure 3.1 Beachrock: (a) Baracoa, Cuba; (b) Salvador, Brazil, (c) Barcelona, Spain; (d) Athitos, N. Greece; (e) Mykonos, Greece; (f) Morrocoy, Venezuela; (g) Sifnos, Greece; (h) Attica, Greece (Vousdoukas, 2007).. 91

Figure 3.2 Petrography of beachrock samples from Krakal-Sadranan, Yogyakarta, Indonesia (a) the meniscus calcite cementation (Folk, 1962) and (b), (c) morphology of meniscus cement beachrock. 98

Figure 3.3 Spider diagrams of beachrock elements analysis (a) PAAS (Post-Archean Australian Shale) normalized major oxide diagram for limestone samples of beachrock, (b) Trace element normalizing based on Average Phaenerozoic Limestone, (c) Rare elements analysis diagram of beachrock based on shale normalization 100

Figure 3.4 Graphic XRD (a) and total organic carbon (b) from Beachrock, Krakal-Sadranan, Yogyakarta. Within abbreviation Mg-C: Magnesium Calcite, C: Calcite; A: Aragonite; SiO_2: Silica; Fe: Iron; and Al: Alumina. 101

Figure 3.5 Phylogenetic tree based on 16S rDNA nucleotide sequence of Vibrio maritimus, Psedoalteromonas tetradonis, and Oceanobacillus profundus (red-frame).. 104

Figure 3.6 Microbial induced carbonate precipitation capacity of isolated strains. 105

Figure 4.1 (A) Location map of Okinawa in Japan, (B) Research area in Sumuide, Okinawa island, (C) Location map of Indonesia, and (D) Locations Sadranan area. . 125

Figure 4.2 Sumuide beachrock sampling area, Okinawa, Japan. 129

Figure 4.3 Sumuide beachrock cement vision using 100x (yellow pattern represented grain matrix and orange pattern represented cement). 131

Figure 4.4 Cell growth and urase activity of *Pararodhobacter* sp. (a) and *Oceanisphaera* sp. (b). 133

Figure 4.5 Effect of reaction temperature on urease activity of the whole cell at pH 7 (a) and the effect of reaction pH on urease activity of the whole cell at 30°C (b). Experiment were conducted in triplicate: data represented the average of three experiments with error bars indicating the standard deviation. 134

Figure 4.6 Results of the resistivity survey (A-, B-line) (Kubo, et al., 2014). 135

Figure 4.7 Results of velocity and resistivity survey (C-, D-line) (Kubo, et al., 2014). 136

Figure 4.8 Sadranan beachrock sampling area, Yogyakarta, Indonesia. 137

Figure 4.9 Sadranan beachrock cement vision using 100x (yellow pattern represented grain matrix and orange pattern represented cement). 138

Figure 4.10 Cell growth and urase activity of *Pseudoalteromonas tetradonis* (a), *Oceanobacillus profundus* (b), and *Vibrio maritimus* (c) 140

Figure 4.11 Illustration schemes of natural beachrock occurrences (after Danjo, 2014). 142

Figure 4.12 Illustration of gram-positive bacteria (after Bailey, 2020). 147

Figure 4.13 Illustration of gram-negative bacteria (after Bailey, 2020) 148

Figure 5.1 Particle size distribution of local beach sand from Yogyakarta south coast, Indonesia. 160

Figure 5.2 Appearance of discoloration of the urease activity measurement solution (yellow is neutral, purple is alkaline). 161

Figure 5.3 Syringe solidification test. 166

Figure 5.4 Schematic diagram of the experimental arrangement of beach slope model 167

Figure 5.5 General view of the Maruto (left, from Erguler and Ulusay (2008)) and modified Eijkelkamp (right) penetrometers and their parts. (1) presser, (2) chuck, (3) penetration,(4)load scale,(5)load indication ring,(6)UCS–NPR correlation chart given by the manufacturer, (7) removable cap, (8) penetration needle produced according to the Japan Civil Engineering Society's guideline, (9) indicator ring, (10) penetrometer tube, (11) spring, (12) end cap, (13) scale, (14) extension rod, and (15) needle block 169

Figure 5.6 Effect of reaction temperature on urease activity of the whole cell at pH 7 (1 mM EDTA-disodium salt solution). Experiment were conducted in triplicate: data represented the average of three experiments with error bars indicating the standard deviation. 171

Figure 5.7 Effect of reaction pH on urease activity of the whole cell at 37 °C 1 mM EDTA-disodium salt solution). Experiment were conducted in triplicate: data represented the average of three experiments with error bars indicating the standard deviation. 172

Figure 5.8 Microbial induced carbonate precipitation test using local strain ureolytic bacteria after 14 days treatment. Black sample (left) is silica sand from Parangtritis beach sand and white sample (right) is coral sand from Krakal-Sadranan beach sand.. 173

Figure 5.9 Results of MICP-treated sample catalyzed by P.tetradonis sp. under different bacteria concentrations: (a) Estimated UCS value with the depth of the sample, (b) pH with time and (c) Ca^{2+} concentration with time. 174

Figure 5.10 (a) Solidified sample with silica Parangtritis sand, (b) solidified sample with coral Krakal-Sadranan sand, and (c) solidified sample with glass beads 175

Figure 5.11 Estimated UCS value of MICP-treated sample catalyzed by *P.tetradonis* under different particle size of sand samples. 177

Figure 5.12 Ions dependencies of MICP precipitation test 178

Figure 5.13 Estimated UCS value of MICP-treated sample catalyzed by *P.tetradonis* under different concentration of cement solution sand samples. 179

Figure 5.14 Precipitation test by *P.tetradonis* under different concentration of cement solution sand samples. 180

Figure 5.15 Graphic XRD analysis pattern using artificial beachrock. C: calcite; A: aragonite, Q; Quartz (SiO_2), V; Vaterite; Mg-Calcite 181

Figure 5.16 SEM image of $CaCO_3$ solidification test on coral sand by *P. tetradonis* at (a) λ-carrageenan and (b) κ-carrageenan at concentration 0.5% carrageenan..... 185

Figure 5.17 Estimated UCS values of solidification sand specimens at concentration 0.5% carrageenan.. 186

Figure 5.18 Profile of the cemented beach slope model (a) 15° and (b) 30° 187

Figure 5.19 Estimated UCS 3D profile along the beach slope models (t-z axis) of the treated sands (measured by needle penetrometer), (a) 15° and (b) 30°.. 187

Figure 5.20 Comparison of the UCS axial load between (a) natural beachrocks and (b) artificial rock based on MICP method with x-ray chromatography scan images of porosity.. 190

Figure 5.21 Relationship between estimated UCS versus calcium carbonate content of MICP comparing with previous study. 193

Figure 6.1 Grain size distribution curve of sands and local beach sands from Krakal-Sadranan site, Yogyakarta, Indonesia. 206

Figure 6.2 XRD pattern of (a) Krakal-Sadranan coral sands consist of $CaCO_3$ and Mg-Calcite; (b) Parangtritis sand with Ab (albite), Qtz (quartz), Mgh (maghemite), and Mgn (magnetite); (c) Mizunami sand consist of quartz; and (d) Glass beads with quartz consisted..... 207

Figure 6.3 Conceptual illustration of MICP treatment by laboratory scale (columns specimens)..... 208

Figure 6.4 Average mass loss of the specimens subjected to WD cyclic treatments based on (a) saltwater and (b) distilled fresh water. With Co = coral sand; Si = silica sand; Mizu = Mizunami.. 211

Figure 6.5 The variation of estimated UCS before and after the exposure of cyclic WD tests. With Co = coral sand; Si = silica sand; Mizu = Mizunami. 212

Figure 6.6 The variation of estimated UCS before and after the exposure of cyclic WD tests. 214

Figure 6.7 Graphic XRD analysis pattern using artificial beachrock (a) before MICP treatment, (b) after MICP treatment, (c) MICP treated after 21 WD cycle under

distilled water, and (d) MICP treated after 21 WD cycle under saltwater. With Ab (albite), Qtz (quartz), Mgh (maghemite), and Mgn (magnetite). 215
Figure 6.8 Illustration scheme of WD damages mechanism 216
Figure 6.9 Relationship between estimated UCS versus calcium carbonate content of MICP treatment period 217
Figure 7.1 Beer yeast composition (Asahi Group Research & Development, 2019) ... 225
Figure 7.2 The reaction formula of the indophenol blue method. 229
Figure 7.3 Cell growth and urase activity of *Pseudoalteromonas tetradonis* under different culture medium 232
Figure 7.4 Amino acid content of each culture medium 233
Figure 7.5 Influence of ratio of chalk powder to vinegar 234
Figure 7.6 Beach sand treatment test using microbial induced carbonate precipitation after 14 days treatment. Sample with nigrescent color (left) is Quartz silica sand from Parangtritis beach and sample with whitish color (right) is carbonate coral sand from Krakal-Sadranan beach sand.. 236
Figure 7.7 Average mass loss of the specimens subjected to WD cyclic treatments based on (a) saltwater and (b) distilled fresh water. With Co = coral sand; Si = silica sand; TM = tempeh medium; Std = standard chemical solutions 238
Figure 8.1 Schematic illustration of MICP process of urease activity. 252
Figure 8.2 Conceptual design of coastal prevention with MICP method 261

APPENDIXES

Figure A.1 Simplified geological map of Yogyakarta, Indonesia. 280
Figure A.2 Tide Pattern of South Yogyakarta coast (Sadeng tide gauge station) 284
Figure A.3 3D view of Parangtritis (Google earth) 288
Figure A.4 Shoreline change on Yogyakarta south coast since 1995-2015 (modified from Pujotomo, 2009 and Mutaqin, 2017), (A) propagation in the Parangtritis area and (B) Samas beach area.. 290
Figure A.5 3D view of digital elevation model Krakal-Sadranan beaches, Yogyakarta. 291
Figure A.6 Straightness density lineament of Krakal-Sadranan beach overlay with UAV photogrammetric. 292
Figure A.7 Beachrock zonation in Krakal-Sadranan beaches, Yogyakarta (A) α-location (B) β-location and (C) γ-location. 294
Figure A.8 Morphology of beachrock occurrences schemes (modified from Stull, 2000; Harley, et al., 2017) 296

Figure B.1 Measurement Stratigraphy and Petrographic Analysis of ABX_1 and ABX_2 samples. 302

Figure B.2 Measurement Stratigraphy and Petrographic Analysis of ABY_1 and ABY_2 samples 305

Figure B.3 Measurement Stratigraphy and Petrographic Analysis of ABZ_1 and ABZ_2 samples 308

Figure B.4 Measurement Stratigraphy and Petrographic Analysis of CDX_1, CDX_2, and CDX_3 samples. 311

Figure B.5 Measurement Stratigraphy and Petrographic Analysis of CDY_1 and CDY_2 samples 316

Figure B.6 Measurement Stratigraphy and Petrographic Analysis of CDZ_1 and CDZ_2 samples 319

Figure B.7 Measurement Stratigraphy and Petrographic Analysis of EFX_1 and EFX_2 samples. 322

Figure B.8 Measurement Stratigraphy and Petrographic Analysis of EFY_1 and EFY_2 samples 325

Figure B.9 Measurement Stratigraphy and Petrographic Analysis of EFZ_1 and EFZ_2 samples. 328

Figure D.1 Petrographic Analysis of Yomitan A samples. 334

Figure D.2 Petrographic Analysis of Yomitan B samples. 336

Figure D.3 Petrographic Analysis of Yomitan C samples. 338

Figure D.4 Petrographic Analysis of Yomitan D samples. 340

Figure D.5 Petrographic Analysis of Gima A samples. 342

Figure D.6 Petrographic Analysis of Gima B samples. 344

Figure D.7 Petrographic Analysis of Gima C samples.. 346

Figure D.8 Petrographic Analysis of Gima D (weathered) samples. 348

Figure D.9 Petrographic Analysis of Sumuide A samples. 350

Figure D.10 Petrographic Analysis of Sumuide B samples. 352

Figure D.11 Petrographic Analysis of Sumuide C samples 354

Figure D.12 Petrographic Analysis of Anthropogenic Beachrock (Synthetic). 356

Figure E.1 Graphic XRD analysis pattern of Mikawa sand (a) before MICP treatment, (b) after MICP treatment, (c) MICP treated after 21 WD cycle under distilled water, and (d) MICP treated after 21 WD cycle under saltwater.. 358-359

Figure E.2 Graphic XRD analysis pattern of Krakal-Sadranan coral sand (a) before MICP treatment, (b) after MICP treatment, (c) MICP treated after 21 WD cycle under distilled water, and (d) MICP treated after 21 WD cycle under saltwater…… 359-360

Figure E.3 Graphic XRD analysis pattern of glass beads (a) before MICP treatment, (b) after MICP treatment, (c) MICP treated after 21 WD cycle under distilled water, and (d) MICP treated after 21 WD cycle under saltwater. 361-362

Figure F.1 Graphic XRD analysis of coral sands Krakal-Sadranan 363

Figure F.2 Graphic XRD analysis pattern of MICP treatment based on standard chemical 363

Figure F.3 Graphic XRD analysis pattern of MICP treatment based on snow-melting reagent (a) sample A and (b) sample B. 364

Figure F.4 Graphic XRD analysis pattern of MICP treatment based on chalk extract (a) sample A and (b) sample B 365

CHAPTER 1
Introduction

1.1 Research background

Ureolytic bacteria which are ubiquitously abundant organisms and play important roles in most aquatic environments, are generally known to influence $CaCO_3$ precipitation by taking up organic carbon via urea hydrolysis (Vousdoukas, 2007, DeJong, et al., 2013, Dhami, et al., 2016). Although calcium carbonate formation mediated by microorganism such as cyanobacteria and ureolytic bacteria is of great importance in sedimentary deposits, the mechanisms involved are still controversial. In many cases, the precipitation of $CaCO_3$ by microbial activity has been invariably considered a noncontrolled process which raises the pH adjacent to the bacteria cells (Riding, 2006), or induced by cell-surface properties for the nucleation of $CaCO_3$ minerals (Obst et al., 2009b). In contrast, Enzyme technology is a well-established branch of biotechnology undergoing a development phase (Binod et al., 2013), and their functional significance suggests many novel applications especially for environmentally friendly industrial purposes (Binod et al., 2013). Enzymes from microorganisms are an essential source of numerous industrially relevant enzymes (Ibrahim, 2008). Microbial enzymes are relatively more stable and properties more diverse than other enzymes derived from plants and animals (Alves et al., 2014). Enzymes produced from microorganisms can be easily controlled physiologically, physio-chemically, have quantitative production and mostly extracted with low production cost extracellularly using downstream processes (Ibrahim, 2008, Pandey et al., 2011). The intracellular carbonate makes the mechanisms involved in calcification more confusing (Cam et al., 2015, 2016, 2018; Li et al., 2016). Thus, new pathways, in which some biological processes alter the carbonate system, are important to evaluate.

The coastal zone comprises a narrow strip of coastal lowlands and a vast area of coastal waters. It has become a major site for extensive and diverse economic activities. Many of the countries developing on the coasts depend heavily on the scarce coastal resources for their economic growth. Coastal resources are used and exploited for economic and social objectives: urbanization, industry, tourism and recreation, fisheries and aquaculture, energy production and transportation (Chua 1993). The dynamic and coastal constantly changing (Bird, 1980)

indicated that changes in the coast of Indonesia are consist of short term, medium term, and long term. In an era of globalization, like other coastal countries, Indonesia is the world's largest archipelagic state. By the latest official count, the archipelago consists of 18,108 islands where approximately 60% of the population lives within 50 km of the coast. Increased storm intensity, sea level rise, coastal erosion, ocean acidification, coral bleaching, and declining marine fisheries are particular sources of vulnerability (Narayan et al., 2014; Thorne et al., 2007; Zanuttigh, et al., 2013). Furthermore, the multiple drivers of change (e.g., climate change, urbanization, tourism development, and marine resource exploitation) are producing cumulative effects and conflicts that are complex, emergent, and cross-scale (Zhu, 2010; Pilkey and Cooper, 2014; Jones and Phillips, 2011; Shi, et al., 2015; Barragán and de Andrés, 2015). Considering natural hazard that drive medium term to long term changes in the coast of Indonesia, Java Island due to tectonic setting is very vulnerable to natural hazard such as high tidal and erosional beach sediment.

On other hand, Beachrock is an important feature of many tropical coastlines as it appears to have an anchoring effect for dynamic islands and provides protection from erosion. Yet, many things about its origin and properties remain unknown or debated hitherto. Beachrock outcrops may be one of the few physical records of past climate information on low-lying reef islands but research on their application as an indicator of paleo-environments in the Pacific is underdeveloped (Vousdoukas et al., 2007). In addition, through understanding the beachrock formation process, artificial rocks may be able to be formed at an accelerated speed of consolidation (Danjo, 2014). Erosion that hit by the time will have damage impact for development construction near/on the sea, such as highway, bridge concrete, and airport building. the cement materials of beachrock are mainly high-magnesium calcite and aragonite (Vousdoukas et al., 2007; Stasser, et al., 1989). In general, bedrock forms over a long period of time, but it has been reported that the formation periods of some beachrocks were only a few decades. It is assumed that if the formation periods are longer than the seismic wave velocities and the unconfined compressive strength are larger, but the porosity and the permeability are smaller. The most widely held the theory of beachrock formation involves the deposition of $CaCO_3$ between coral sand and gravel by evaporation of seawater (Neumeire, 1998; Danjo and Kawasaki, 2011; Ginsburg, 1953; Stoddart and Cann, 1965; Kubo, et al, 2014). There is much domestic and global literature on beachrock, but majority of this concern its geochemistry. In particular, its underground structure is not yet well understood. One of the few studies of this was by Psomiadis, who used electrical resistivity tomography to map the beachrock on the

island of Thassos, Greece (David, et al., 2009). On other hand, a direct current (DC) electrical survey and a seismic surface wave were conducting on Yagaji Island, Okinawa, Japan with results of the structure around the seashore to a depth of more than 10 m was obtained (Kubo, et al., 2014). Limitation data in South East Asian country related with recent beachrock sedimentary were challenged to study because of the weathering process in extremely rapid especially in the tropical equator area.

In order to address the disadvantages of current coastal countermeasures technique one could look at sustainable or "green" materials and processes using biomimetic in which lessons learned from nature form the basis for evolution of novel technological materials for the development of sustainable materials in the construction industry. When it comes to the field of geotechnical engineering, the most common "green" practices are trying to be applied for the beach's sedimentary improvement. This thesis discusses about such sustainable coast improvement techniques those are managed by science of biology, chemistry and physics together and the potential of applying this knowledge to multifunctional geotechnical engineering applications under two main topics named as sedimentary characteristic based on ureolytic bacteria isolated from natural beachrock and evaluation of their efficiency in biocementation based on microbial induced carbonate precipitation (hereafter, MICP) using local indigenous strain from natural beachrock were found in Krakal-Sadranan, Yogyakarta, Indonesia. This dissertation investigates the sustainability and effective techniques for coastal protection methods based on mimicking beachrock sedimentary process, then artificial beachrock development based on ureolytic bacteria strain were isolated from beachrock. In addition, through understanding the beachrock formation process, artificial rocks may be able to be formed at an accelerated speed of consolidation.

1.2 Literature review

1.2.1 Beachrock sedimentary mechanism

Beachrock are lithified coastal sedimentary formations consisting of various beach sediments. Lithification occurs through the precipitation of (mainly) carbonate cements (Vousdoukas et al., 2007). The beach may consist of any type of sediments, both of clastic and biogenic origin (Russell, 1962), while the cements typically consist of High-Magnesian Calcite (HMC) or Aragonite (Ar) (McKenzie, 1971). Chemical formula between HMC and Aragonite is same, $CaCO_3$, but their atoms are stacked in different configurations. Aragonite has an

orthorhombic structure and HMC a trigonal structure crystal. The first scientific mention of these cemented beach deposits has been made by Chamisso in 1815 (Gischler, 2007) who described the Radak and Ralik Island in the Pacific. Many famous 19th century scholar have later reported beachrock occurrences, including Sir Francis Beauford in 1817 (Goudie, 1969), Lyell who discovered human skeletons cemented into an "indurated beach" on the island of Guadeloupe (Lyell, 1837) and Darwin (1841).

Beachrock exposures are quite conspicuous where they can be found as pseudo-linear, elongated features in the intertidal or nearshore zone (Gischler, 2007). Given their origin on the beach and relatively recent age, these exposures are often found parallel to the present shoreline. Older beachrock exposures, in the form of isolated ridges, are thought to represent ancient shorelines and are often used in sea-level studies. Beachrock exposures commonly slow layering or sequences of bands, which may be associated with textural laminations. The bands mostly dip gently seaward following the beach slope (Russell and McIntire, 1965). However, some beachrock exposures have been found showing markedly different orientations than those of the hosting beaches (e.g. Beier, 1985 in Rutten, 2011), which might in turn be caused by diagenetic processes after cementation. Inherent to the location of origin, beachrock exposures are usually subjected to continuous destruction by fracturing and mechanical erosion caused by abrasion or erosion (e.g. McLean, 1967). During erosion-accretion cycle, older broken-off fragments of beachrock might be incorporated into younger beachrock (Stasser and Davaud, 1986). The distinction between beachrock and other coastal cemented deposits can be difficult. The term "cay sandstone" was coined for supratidal cemented deposits on reef islands (Kuenen, 1950). This cay sandstone (or cayrock) may be distinguished from beachrock based its horizontal bedding, very good sorting and the predominance of meteoric calcite cements (Ward, 1975). Similar to cayrock, cementation in this sediment is dominated by meteoric calcite. Aeolianite can be distinguished from cayrock and beachrock by sedimentary structures resulting from wind transport, such as cross-stratification (Gischler, 2007). However, very little research exists on sedimentary structure of beachrocks (Scheffers, et al., 2009 in Rutten, 2011).

Other intertidal and subtidal cementation phenomena may prove more difficult to distinguish from beachrock. Rampart and boulder rocks, consisting of cemented coral branches and fragments larger than 10 cm, sometimes show inclined bedding similar to beachrock (Scoffin and McLean, 1978). Elevated reefs and reef terraces can also be confused with beachrock (Hopley, 1986). Cemented layers of sediment formed on tidal flats, on the shallow seafloor and along lake coastlines show identical diagenetic marine-phreatic cement

characteristics to beachrock. However, they cannot, probably be regarded as beachrocks stricto sensu (Vousdoukas et al., 2007). Beachrock origin mechanism occurrences in intertidal zone still debatable many years until now, exposed beachrock and also buried or submerged beachrock. The origin of tropical beachrock has been the subject of long-standing debate, with several theories having been proposed that relate either to physiochemical or biological mechanism (Scoffin and Stoddart, 1983; Vousdoukas et al., 2007). Formation mechanisms can be classified into four main processes: direct cement precipitation, mixing of marine and the meteoric waters, degassing of CO_2, and formation by biological activity.

1.2.1.1 Direct cement precipitation

The most widely proposed mechanism for beachrock formation is by the direct precipitation of cement from marine or fresh waters (Vousdoukas et al., 2007). Cement precipitation from marine waters is considered to take place in or near the intertidal zone due to the alternating wetting and drying of the sediments (Gischler and Lomando, 1997; Kelletat, 2006), aided by increased water temperatures due to warming of the beach during the day. This theory is supported by the presence of aragonite cements, indicating a marine provenance, within most beachrokcs.

1.2.1.2 Mixing of marine and the meteoric waters

An alternative theory is that cementation is due to the mixing of marine and meteoric waters. This developed from the understanding that due to the decrease of solubility in water of $CaCO_3$ with decreasing salinity, mixing of marine and fresh water may result in carbonate saturation and lead to precipitation of the cement (Schmalz, 1971). However, Hanor (1978) showed through thermodynamically experimentation that precipitation of $CaCO_3$ cannot be induced through the mixing of marine and meteoric waters.

1.2.1.3 Degassing of CO_2

Degassing of CO_2 from groundwater can produce calcite crust similar to some cements observed in the beach sediments (Hanor, 1978). Carbon dioxide is produced in the sediment column by plants and subsequently washed seaward by the flux of groundwater. Therefore, the

concentration of CO_2 is highest in the phreatic zone and continually diffuses upwards because of the potential gradient between the phreatic zone, the vadose zone and the atmosphere. This process is self-limiting due to the relative volume of pore space, which can be obstructed by cement, as well as the maximum thickness of the cemented zone that can develop. As cement is precipitated, the porosity of the sediment decreases, which in turn decreases the ability of the system to degas (Hanor, 1978). However, this hypothesis requires waters to have sufficient residence time in the landward areas to acquire a high P_{CO_2} and dissolved calcium and carbonate, and sufficient residence time in the fore beach areas such that degassing can take place before the waters reach the oceans. Sufficient residence times may be lacking on oceanic atolls due to the small and extremely porous nature of reef islands (Stoddart and Cann, 1965).

1.2.1.4 Formation by biological activity

Many authors have considered the influence of the direct biological precipitation of beachrock cements (Davis and Kinsey, 1973; Kumbrien, 1979; Neumeier, 1999). Indirect biological precipitation may be possible in anaerobic environments where bacterial processes can control the partial pressure by CO_2 consumption (Berner, 1971). Nuemeier (1999) suggested that micro-organism have strong influence over the formation of the first micritic cement and the development of the subsequent prismatic cement probably result from abiotic precipitation during times of higher fluid circulation.

Figure 1.1 is shown about model of beachrock and cayrock formation occurrence in the surface. (1) Is idealized cross-section though a marginal barrier or atoll reef that has mangrove cays in the lagoon area. (2) Due to wave refraction at the reef crest small sand cays may build up on the reef flat. (3) Intertidal beachrock forms on the windward side of small sand and sand-shingle cays on the reef due to rapid, subaerial cementation. Supratidal cayrock forms due to vadose cementation of sand or beach ridges of larger mangrove-sand cays. (4) Due to movement of the cays, intertidal beachrock gets exposed mainly on the windward side (a), but may also be covered (b), or exposed on the leeward side (c) (Gischler and Lomando, 1997).

The formation of beachrock can be irreversibly alter the coastline, especially in highly dynamic environments such as small Pacific atolls. It has significant effects on the ecology as well as affecting beach morpho dynamics. For instance, in many cases outcrops of beachrock have been found to act as effective natural beach defenses which mitigate the erosion of the

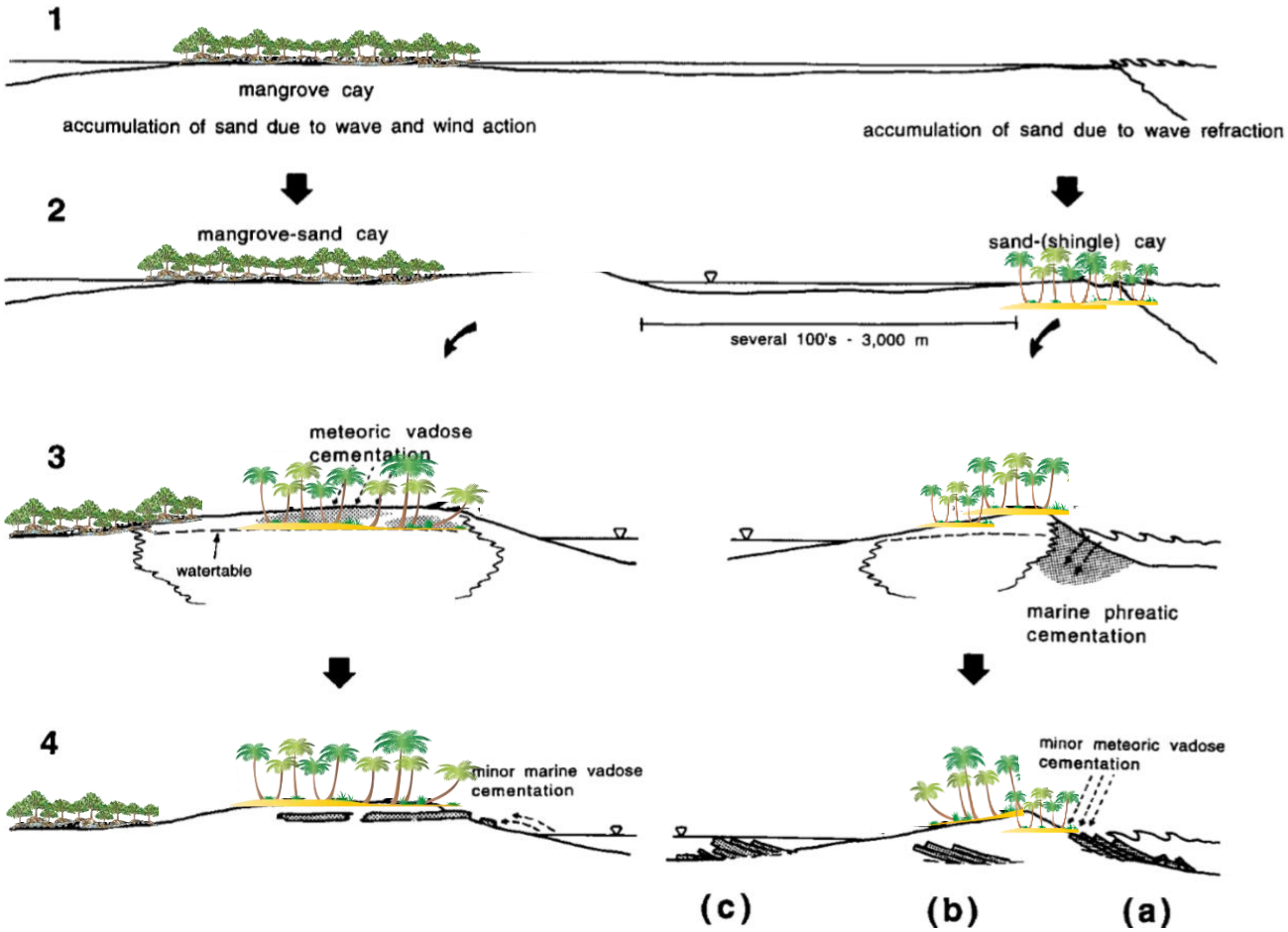


Figure 1.1. Model of beachrock and cayrock formation (Gischler and Lomando, 1997).

beach (Bird, 2000). This is particula rly true on the coasts of dynamic and fragile small islands and atolls (e.g., Dickinson, et al., 1999). Once the beachrock has formed, it sets a limit to which the beach bed can erode, in effect locking the beach profile. The expression of the beach is thus controlled by the relationship between beachrock and the nearshore hydrodynamics (Vousdoukas, et al., 2007). The nearshore hydrodynamics may also be affected by the presence of beachrock outcrops which alter seabed roughness and subsequently change the friction of the seabed (Hefegaard, et al., 1992). Additionally, outcrops of beachrock can have significant effects on the transport and supply of sediment on beaches. Vousdoukas et al., (2009) showed that submerged beachrock outcrops impede onshore transport of sediment and may act as offshore transport conduits for beach sediments. Patches of beachrock may also act as traps for sediment being transported by longshore drift (Vousdoukas et al., 2007). Beachrock may also have erosional effects on the beach. The addition of impermeable beachrock layers can modify the infiltration and extraction process of water percolation through beach sediments and

increase the volume of wetted, and thus more buoyant sediment in the swash zone that could make the sea more prone to erosion (Vousdoukas et al., 2007).

1.2.2 Beachrock modes of carbonate precipitation

Three rules capture the peculiar nature of carbonate depositional systems – carbonate sediments are largely of organic origin; they can form wave-resistant structures and they are easily altered by diagenesis because the original minerals are metastable. Precipitation of solid matter from the dissolved load of the sea occurs either abiotically, governed by inorganic thermodynamics and reaction kinetics, or biotically as a consequence of the metabolism of plants and animals. Precipitation of marine evaporites is an example of an abiotic process, precipitation of marine opal by diatoms or radiolarian an example of a biotic one (Schlager, 2005). Marine carbonate precipitation proceeds along abiotic and biotic pathways, and this makes it particularly diverse and complex. The interplay of abiotic and biotic processes of organic evolution and environmental change has led to a stunning diversity of precipitation mechanisms that are identify in this dissertation. However, even if one focuses on the practically relevant aspects of carbonate precipitation, the subdivision into abiotic and biotic precipitation is inadequate. Following Lowenstam and Weiner (1989) who recognized three degrees of biotic influence on precipitation in general and on carbonates in particular:

A. Abiotic (or quasi-abiotic) precipitates where biotic effects are negligible.
   The most conspicuous abiotic precipitate is cement formed in the pore space during the early stages of diagenesis when the deposit was still in the depositional environment. Burial cements are excluded from the abiotic carbonate factory because they are not derived from sea water but largely from remobilized sedimentary material. The case for abiotic origins particularly strong for acicular aragonite cements. Acicular magnesian calcites may be biotically influenced (Morse and Mackenzie, 1990). Associated with tropical skeletal carbonate we find abiotic precipitates in the form of ooids. Ooids form in high-energy environments by stepwise accretion on a nucleus. Field observations and laboratory experiments indicate a growth history of alternating phases of accretion and rest. The degree of organic influence on the precipitation process remains a matter of debate. However, two arguments tip the balance in favor of abiotic precipitation: (1) growth of aragonitic, Bahama-type, ooids in the laboratory where the precipitation was essentially abiotic and organic matter had only a modulating effect (Davies et al., 1978) and (2) the

similarity of ooids and cements in terms of mineralogy and chemical signature (Morse and Mackenzie, 1990). It seems that the role of organisms and organic matter in the formation of ooids is not sufficient to significantly alter the abiotic controls (Morse and Mackenzie, 1990; see Reitner et al.,1997 for contrasting view on Great-Salt-Lake ooids). The origin of carbonate in whiting's, clouds of carbonate suspended in sea water, is a much-debated issue. Morse and Mackenzie (1990) conclude that abiotic precipitation (probably on nuclei of suspended sediment) is very likely for Bahamian whiting's. However, in-situ experiments by Yates and Robbins (1999) strongly suggest that blooms of unicellular algae trigger the first precipitation, probably followed by extended abiotic growth of the original, biotically induced precipitates (Yates and Robbins, 1999). The carbonate mud from whiting's a mixture of biotically induced and abiotic precipitation.

B. Biotically induced precipitates

Where the organism sets the precipitation process in motion but organic influence on its course is marginal or absent. The reaction takes place outside the cell and the product is very similar, often indistinguishable, from abiotic precipitates. The majority of carbonate material in modern oceans is precipitated as highly structured skeletons of organisms. Precipitation is primarily controlled by the biochemistry of the respective organisms (such as algae, foraminifera or corals); the organisms, in turn, are influenced by the conditions of the sea they live in, particularly light, temperature and water chemistry (for instance the degree of carbonate saturation of the sea water). Autotrophic organisms nourish themselves by utilizing inorganic materials to synthesize their own living matter; heterotrophic organisms have to rely on organic material to do so. Autotrophic organisms among the carbonate producers are almost exclusively photo-autotrophic: they perform photosynthesis and thus depend on light for their livelihood. Some carbonate-secreting organisms are themselves heterotrophs but live in symbiosis with autotrophic algae. As a result, the system of host plus symbiont becomes autotrophic.

C. Biotically controlled precipitates

Where the organism determines location, beginning and end of the process, and commonly also composition and crystallography of the mineral. All skeletal carbonate falls in this category. A significant portion of the non-skeletal carbonate material has been precipitated under the influence of organisms and thus cannot be classified as abiotic. Commonly precipitation is induced by microorganisms, mostly bacteria and cyanobacteria. Micrite is

a major, often dominant component of these deposits. The term "(mud) mound" is commonly used as a field-geologic term (Wilson, 1975; Langevin and Bourque, 1992). It stands for autochthonous micrite as opposed to allochthonous micrite that was transported and deposited as fine-grained sediment (Wolf, 1965). Whether the micrite formed as a rigid precipitate can often be deduced from thin sections or polished slabs. The past decade brought enormous progress on the origin of mud mounds and other automicrite deposits. The combination of detailed field work, petrography and collaboration with biologists and organic chemists has led to detailed insight in a geologically very important carbonate precipitation mode that differs significantly from the more conspicuous skeletal mode (Monty et al., 1995; Reitner et al., 1995a; 1995b; Neuweiler et al., 2003, Schlager, 2005).

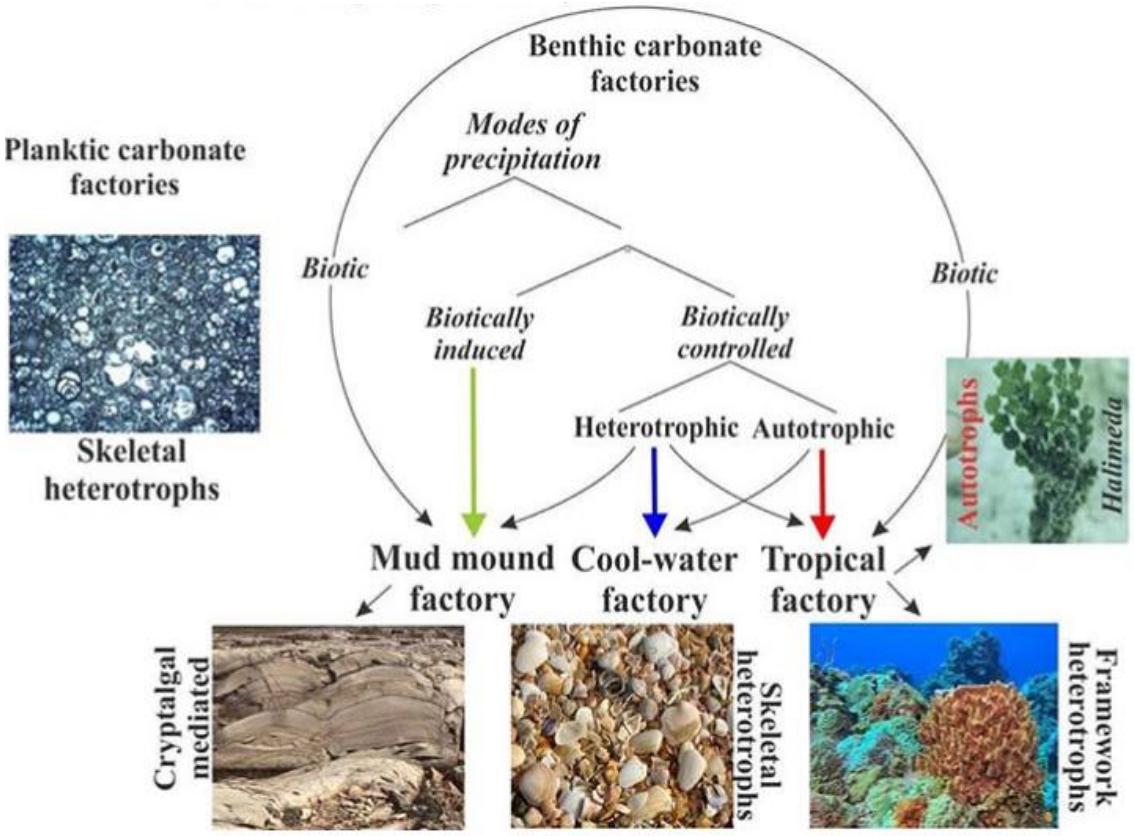


Figure 1.2. The typical material of the T factory is biotically controlled precipitate from tropical autotrophic organisms (or heterotrophic organisms with autotrophic symbionts); the C factory is dominated by heterotrophic organisms and the M factory by biotically induced precipitates, mostly micrite (Schlager, 2005).

While the categories themselves are well identifiable and useful, the designation of certain products to one of the categories remains debatable. The controversy on the origin of ooids and whiting is a case in point. In most carbonate depositional environments material is produced in

all three modes, albeit in varying proportions (Figure 1.2). If one considers carbonate precipitation not at the molecular or microscopic scale but at scales from mappable sediment bodies (±102 m) to global facies realms, different production systems or 'carbonate factories' may be distinguished. The boundaries between these systems are gradational and to some extent arbitrary. Accordingly, the number of basic types is a matter of debate with little hope of reconciling the views of lumpers and splitters. The differences from of the biotically induced and biotically controlled could be identify based on enrichment frame of microorganism in the carbonate sediment. Differences from those that are biologically induced and biologically controlled can be identified based on the framework of enrichment of microorganisms found in carbonate sediments, which are commonly found including ooids, handgrounds, cryptalgal laminates, lime mud, bioclastics, stromatolite domes, and also the meniscus cement of high magnesian calcite (HMC) or aragonite.

1.2.2.1 Tropical factory

T stands for “tropical” and “top-of-the-water-column”. Biotically controlled precipitates dominate. Most abundant among them are photo-autotrophic organisms, for instance algae and animals with photosynthetic symbiotic algae, such as hermatypic corals, certain foraminifer sand certain molluscans. The other characteristic products are abiotic precipitates in the form of marine cements and ooids. Clay-size precipitates, the “whitings”, are probably mixtures of abiotic or biotically induced precipitates (Morse and Mackenzie, 1990; Yates and Robbins, 1999; Thompson, 2001). Heterotrophs devoid of photo-symbionts are common, but non-diagnostic contributors. Construction of wave-resistant structures by organic frame building or rapid marine cementation is common, particularly at the shelf slope break. The T factory is restricted to the warm, sunlit waters of the ocean that are high in oxygen because of constant equilibration with the atmosphere and low in nutrients because of intensive competition. In modern oceans, the characteristic settings are the surface waters between 30◦ N and S of the equator. The northern and southern limit of the T factory closely follows the line where the mean temperature of the coldest month is about 20 ◦C. The T factory may also pass into the cool-water factory downward in the water column, for instance at the boundary between the warm surface layer of the ocean and the thermocline. Furthermore, transitions from T to C factory occur in shallow tropical upwelling areas where cool, nutrient-rich water comes to the surface (Lees and Buller, 1972; Pope and Read, 1997; Brandley and Krause, 1997; James, 1997; Schlager, 2005).

1.2.2.2 Cool-water carbonate factory

In the surface waters of the ocean, the cool- water factory extends poleward from the limit of the tropical factory (at about 30 ~) to polar latitudes but it also occurs in the thermocline waters of the low latitudes (Lees and Buller 1972; James 1997). Carbonate precipitation is nearly always of the biotically controlled type. Heterotrophic organisms dominate; the contribution of photoautotrophs in the form of red algae is highly variable but at times significant (Lees & Buller 1972; Henrich et aI. 1995; James 1997). The sediment typically consists of skeletal hash of sand-to- granule size. Cool-water carbonates lack herma- typic coral reefs and ooids; carbonate mud and cement are scarce. The transition to the domain of the tropical carbonate factory normally extends over more than 1000 km (Schlager 1981; Collins et al. 1997). The cool-water factory substitutes for the tropical factory in the tropics if environmental conditions are adverse. The cool-water factory extends pole ward from the limit of the tropical factory (at about 30◦) to polar latitudes. The transition to the T factory is very gradual (Betzler et al., 1997). The C factory also occurs at low latitudes in the thermocline below the warm surface waters and in upwelling areas. The oceanic environments of the C factory are photic or aphotic waters that are cool enough to exclude competition by the T factory and sufficiently winnowed to prevent burial by terrigenous fines. Nutrient levels are generally higher than in the tropical factory. These constraints set a wide depth window for the cool-water factory from upper neritic to bathyal and even abyssal depths. The most common setting is the outer neritic, current-swept part of continental shelves. The transition to the T factory normally extends over more than thousand kilometers (Schlanger, 1981; Collins et al., 1997, Schlager, 2005). Figure 1.3 is shown the seafloor diagenesis of carbonate in the tropical reagent.

1.2.2.3 Mud-mound factory

Intensive work on ancient mud-mounds and micrite precipitates in the Recent has led to two conclusions that underline the independent position of this system and the fundamental differences from the tropical and cool-water factories (Langevin and Bourque, 1992; Monty 1995; Meyer, et al., 1995; Reitner and Neuweiler 1995). First, typical mud-mounds are formed by in-situ pro- duction rather than sweeping together of fine sediment; they are fundamentally different from hydrodynamic sediment accumulations such as lagoon mudbanks or the contourite drifts of the deep sea. The micrite that constitutes the dominant component of the mounds was firm or hard during or soon after formation and does not represent lithified soft sediment. Second, the micrite is precipitated by a complex interplay of inorganic and organic

chemical reactions with microbes and decaying organic tissue playing a central role (Reitner and Neuweiler 1995; Monty 1995).

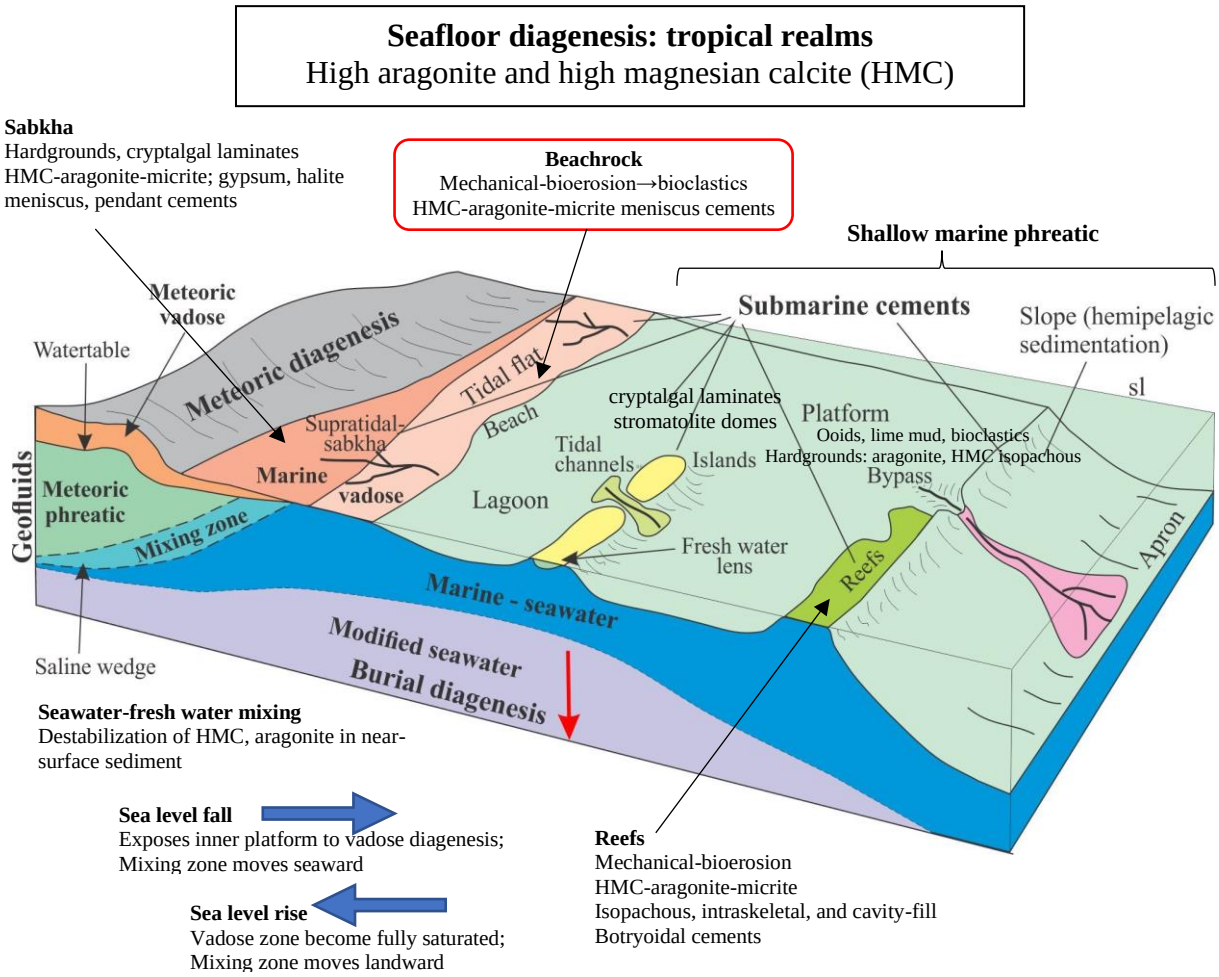


Figure 1.3. Seafloor diagenesis of carbonate sedimentation in the tropical factory (Schlager, 2007; James and Jones, 2015).

1.2.3 Artificial beachrock development based on microbial induced carbonate precipitation (MICP)

The most important environments where early marine cementation (mainly by high-magnesian calcite and aragonite) occur, are intertidal beaches and tidal flats, subtidal sandflats and reefs. Important factors controlling calcium carbonate cementation are the chemistry of the seawater (the source of the cementing material) the physical conditions, in terms of hydraulic energy, sedimentary parameters such as permeability, texture and composition of the sand, and an initially stabilizer of the loose sediment. All these factors and the way in which they relate to each other explain large variability in marine cement forms and the variability of the geotechnical properties of the cemented calcareous sediments. The factors controlling early

cementation in the shallow-marine environment are discussed in order to evaluate the boundary conditions for a laboratory model used to produce artificially cemented and by simulating natural subtidal cementation processes. The resulting cemented sands are shown to be comparable with natural sandstones and to exhibit similar behavior during strain tests (Molenaar and Venmans, 1993). Danjo and Kawasaki (2013) examined a formation mechanism of beachrock in Okinawa, Japan, because understanding this mechanism is an important step in making anthropogenic beachrock. They focused on the cement formation mechanism of beachrock, which occurs in the intertidal zone. Cement type and content have the potential to influence the strength of the material; hence, detailed knowledge of beachrock cements is valuable for producing a man-made equivalent. Beachrocks are cemented by High Magnesian Calcite (HMC) have been reported at 16 sites around the world (Danjo and Kawasaki, 2014; Erginal, A.E. et al., 2010).

MICP is considered as an environmental and economical friendly technique to stabilize soil, buildings, cracks, concrete and others. Many known ureolytic bacteria are used in different applications. *Bacillus cereus, Bacillus pasteurii, Shewanella, Sporosarcina pasteurii, Bacillus sphaericus, Bacillus pseudofirmus,* and *Bacillus cohnii* are known microorganisms used in applications for fixing cracks, remediation and self-healing of buildings (Bang et al., 2001; Ramachandran et al., 2001; Ghosh et al., 2005; Jonkers and Schlangen, 2008; De Belie et al., 2010; Achal et al., 2011a; Achal et al., 2011b). Furthermore, the ureolytic bacterial strain *Sporosarcina pasteurii* (NCIM 2477) is also used to manipulate the properties of brick by improving its quality through precipitation of calcite that deposits in the void spaces which causes reduction in the absorption of moisture (Sarda et al., 2009; Wong, 2015). Reduced permeability is another outcome of biologically modified materials such as concrete or soil. Calcium carbonate that precipitates due to biological activity deposits over the concrete resulting in reduced permeability, thereby, increasing its life span (Nolan et al., 1999). Calcium carbonate precipitation by MICP can act as an additive in decreasing the overall porosity of building materials, thereby improving the durability, strength and quality of the material. This can help to prevent the use of conventional chemicals that can be dangerous or hazardous to improve the construction materials (Annamalai et al., 2012). The effect or impact of MICP on soil properties could be at the macro-scale or micro-scale. The macro-scale behavior of soil is affected by the content of calcium carbonate precipitated, including relative density, confining stress and gradation of soil. On the other hand, micro-scale behavior of biologically treated soil will allow to study the precipitation of calcium carbonate with respect to bacterial cells as well

as the interparticle bonds formed by the precipitation of calcium carbonates between the soil grains (Lin et al., 2016).

1.2.3.1 Ureolytic bacteria as carbonate precipitation

Biologically induced mineralization is usually carried out in open environments and the process is often linked to microbial cell surface structures and metabolic activities. Microbial extracellular polymeric substances can trap and bind remarkable amounts of calcium to facilitate calcium carbonate precipitation, and most likely also play an essential role in calcium carbonate precipitation morphology and mineralogy (Arp et al., 1999; Braissant et al., 2007; Dupraz et al., 2005). The mineralization process associated with microbial metabolic activities usually leads to an increase in environmental alkalinity, thereby facilitating calcium carbonate precipitation (Douglas and Beveridge, 1998; Castanier et al., 1999). Among these metabolic activities, the most common is urea hydrolysis catalyzed by urease enzymes, which commonly occurs in large varieties of microorganisms (Mobley and Hausinger, 1989). The microbial urease enzyme hydrolyzes urea to produce carbonate and ammonia, increasing the pH and carbonate concentration, which then combines with environmental calcium to precipitate as calcium carbonate (Hammes et al., 2003; Muynck et al., 2010).

Calcite, aragonite and vaterite are three crystal polymorphs of calcium carbonate in bacterial systems, with calcite being the most common and stable bacterial carbonate polymorphs (Rodriguez-Navarro et al., 2012). Bacterial mineralization of aragonite, often representing the metastable polymorph, has also been reported (Pedone et al., 2010). The production of the polymorphs of calcite, aragonite and vaterite depend both on their growing environments and bacterial strains. It was reported that different bacteria precipitated different types of calcium carbonate and were mainly either spherical or polyhedral crystalline forms (Sanz-Rubio, et al., 2001). Bacterial-induced carbonate minerals have often been reported in a large number of bacteria, such as cyanobacteria (Jansson and Northen, 2010), sulphate-reducing bacteria (Warthmann et al., 2000), *Bacillus* (Goddette et al., 1992; Bretzel et al., 1999; Jørgensen et al., 2000), *Myxococcus* (Rodriguez-Navarro, et al., 2003; Gonzalez-Muñoz et al., 2010), *Halobacteria* (Sánchez-Román, et al., 2011) and *Pseudomonas* (Jha et al., 2009). Groth et al. (2001) tested the crystal-producing ability among cave bacteria and found that all produced calcite except for *Bacillus* sp., which precipitated vaterites. Rodriguez-Navarro et al. (2003) reported that *M. xanthus* was able to induce precipitation of calcite and vaterite. Emerging evidence suggests that bacteria do not directly influence calcium carbonate

morphology or polymorph selection (Chekroun et al., 2004; Bosak et al., 2005; Rodriguez-Navarro et al., 2012). The morphological features instead maybe influenced by the composition of the culture medium, the specific bacterial outer structures and their chemical nature, which might be crucial for the bacterial crystallization process (Gonzalez-Muñoz et al., 2010).

One of the most studied pathways of the microbial precipitation of calcite involves urea hydrolyzing bacteria. The ureolytic process is straight forward. In the first step, urea ($CO(NH_2)_2$) is hydrolyzed to ammonia (NH_3) and carbonic acid (H_2CO_3) in the series of reactions outlined below (Equations 1.1-1.4) (Burne and Chen, 2000). The ammonia and carbonic acid equilibrate in water to form bicarbonate (HCO_3^-), ammonium (NH^{4+}), and one hydroxide ion (OH^-) (Equations 1.5 and 1.6). It is at this step that the pH increase essential to calcite precipitation occurs. This rise in pH shifts the bicarbonate equilibrium to form carbonate ions (CO_3^{2-}) (Equation 1.6) which, in the presence of soluble calcium (Ca^{2+}), precipitates out of solution as calcium carbonate ($CaCO_3$) if saturation is exceeded (Burne and Chen, 2000; Castanier et al., 1999). A high carbonate concentration induces $CaCO_3$ precipitation around the cells and the presence of calcium ions in the surrounding environment is described by Equation 1.9.

$$CO(NH_2)_2 + H_2O \xrightarrow[\text{urease}]{} NH_2COOH + NH_3 \quad \text{(Eq. 1.1)}$$

$$NH_2COOH + H_2O \rightarrow NH_3 + H_2CO_3 \quad \text{(Eq. 1.2)}$$

$$CO(NH_2)_2 + 2H_2O \rightarrow 2NH_3 + H_2CO_3 \quad \text{(Eq. 1.3)}$$

$$H_2CO_3 \leftrightarrow HCO_3^- + H^+ \quad \text{(Eq. 1.4)}$$

$$2NH_3 + 2H_2O \leftrightarrow 2NH_4^+ + 2OH^- \quad \text{(Eq. 1.5)}$$

$$2HCO_3^- + 2H^+ + 2OH^- + 2NH_3 \leftrightarrow 2CO_3^{2-} + 2NH_4^+ + 2H_2O \quad \text{(Eq. 1.6)}$$

$$Ca^{2+} + cell \leftrightarrow cell : Ca^{2+} \quad \text{(Eq. 1.7)}$$

$$CO_3^{2-} + cell : Ca^{2+} \leftrightarrow cell: CaCO_3 \quad \text{(Eq. 1.8)}$$

$$CO(NH_2)_2 + 2H_2O + Ca^{2+} \leftrightarrow 2NH_4^+ + CaCO_3 \quad \text{(Eq. 1.9)}$$

Under natural conditions, the precipitation of carbonates occurs very slowly. In this sense, microorganisms would act as catalysts in the carbonate formation process. Carbonates, especially calcite ($CaCO_3$) and dolomite ($CaMg(CO_3)_2$) are found as limestones on the Earth's

surface, representing an important carbon stock in the lithosphere (Ehrlich and Newman, 2009; Kumari, et al., 2016). The mechanisms through which the biological precipitation of carbonates occurs are not fully described.

However, three mechanisms have been proposed to explain this process (Dhami, et al., 2013): i) Biomineralization occurs as a bioproduct of the microbial metabolism; ii) Extracellular molecules are involved in the carbonate mineralization process; iii) A nucleation process of carbonates occurs in the cell wall of microorganisms. Based on the latter proposed mechanism, the role of microorganisms in creating an alkaline environment through various physiological activities is known. Under these circumstances, the bacterial surface plays an important role in the precipitation of carbonates due to the presence of various negatively charged groups at neutral pH, positive ions can bind to the bacterial surface favoring heterogeneous nucleation (Dhami, et al., 2013). The microbiological precipitation of minerals has several technological applications, such as the restoration of limestone monuments and statues, biocement production, improvement of soil quality and removal of soluble pollutants such as heavy metals and radioactive elements (Al-Thawadi, 2011). Additionally, this process promoted specifically by the ureolytic capacity of bacterial species also allows the removal of secondary ions such as calcium and magnesium present in seawater (Arias, et al., 2017). Furthermore, the precipitation of calcium carbonates mediated by ureolytic bacteria is widely described in the literature, mainly under the application of soil biocementation (Dick et al., 2006; Phillips, et al., 2013; Silva-Castro, et al., 2015). Other uses are related to carbon dioxide capture and remediation of soils and water (Dhami, et al., 2013; Achal, et al., 2015).

1.2.3.2 Different polymorphs and their effects in various calcium sources

Biomineralization can lead to produce different phases of $CaCO_3$ anhydrous polymorphs such as calcite, aragonite and vaterite, as well as hydrated crystalline phases such as monohydrocalcite ($CaCO_3 \cdot H_2O$) and hexahydrocalcite or ikaite ($CaCO_3 \cdot 6H_2O$) and amorphous calcium carbonate (Krumbein 1979; Hammes et al. 2003a; Wei et al. 2003; Chekroun et al. 2004; Xu et al. 2006; Chen et al. 2009; Sanchez-Navas et al. 2009; Gebauer et al. 2010; Dhami et al. 2013). Among these, calcite and vaterite are the most common polymorphs (Gonzalez-Munoz et al. 2010; Rodriguez-Navarro et al. 2007; Dhami et al. 2013, 2014). Vaterite is a minor, metastable and transitional phase during calcite formation (Tourney and Ngwenya 2009). Calcite is the most thermodynamically stable polymorph of $CaCO_3$ and the primary product of $CaCO_3$ in many MICPs (Spanos and Koutsoukos 1998; Stocks-Fischer

et al. 1999; Okwadha and Li 2010; Ganendra et al. 2014). In contrast, Rivadeneyra et al. (1996) reported that aragonite is the predominant crystal formed by *Deleya halophila*. Chen et al. (2009) found that $CaCO_3$ produced by Proteus mirabilis has an unusual morphology and structure, consisting of vaterite hollow spheres. Calcite and vaterite are different solid-state phases of $CaCO_3$. The precipitation of $CaCO_3$ by mixing concentrated Ca^{2+} and CO_3^{2-} solution involves at least three steps namely formation of amorphous calcium carbonate which is a form of $CaCO_3$ with low stability and high solubility, transformation of amorphous $CaCO_3$ into vaterite, and subsequent transformation of thermodynamically unstable vaterite into stable calcite (Spanos and Koutsoukos 1998; Wei et al. 2003; Shen et al. 2006; Hua et al. 2007). Pouget et al. (2009) have proposed the template controlled the initial stages of $CaCO_3$ formation i.e. before transformation of amorphous calcium carbonate into vaterite and calcite. The initial stages of $CaCO_3$ precipitation start with the formation of prenucleation clusters, aggregation of the clusters to form amorphous calcium carbonate nanoparticles and association of the nanoparticles with the template surface to initiate the amorphous calcium carbonate growth.

Different calcium sources induce crystal with different shapes, with a rhombohedral shape induced by calcium chloride being characteristic of the most stable form of $CaCO_3$ (calcite) (De Yoreo and Vekilov 2003; Favre et al. 2009; Gorospe et al. 2013). Other calcium sources also induced different shape of $CaCO_3$. For example, calcium acetate induces a lettuce like or lamellar shape, (a metastable form of $CaCO_3$) composed of vaterite, while calcium lactate and calcium gluconate induce a more complex form with packing that leads to growth of vaterite with a spherical shape (Tai and Chen 1998). The morphological differences in the crystal formation may be strain-specific, owing to differences in urease activity (Hammes et al. 2003a; Park et al. 2010). Alternatively, these differences could reflect the specific extracellular polymeric substance protein produced by different bacterial types controlling calcite or aragonite polymorph selection (Kawaguchi and Decho, 2002), because extracellular polymeric substance proteins may specifically bind Ca^{2+} and promote carbonate precipitation (Dhami et al. 2013b). The composition of the growth media or culture may also affect the crystal morphology because different bacterial species are able to precipitate different amounts, shapes and types of carbonate crystals from the same synthetic medium (Ferrer et al. 1988; Hammes and Verstraete 2002; Dhami et al. 2013b). Examination of the cells by electron microscopy reveals that calcium carbonate precipitation is closely associated with bacterial cells. Even though, many researchers have used different calcium sources for the induction of $CaCO_3$

precipitation, calcium chloride is the best source for induction of calcite precipitation (Achal and Pan 2014). The effects of different calcium salts on biocementation were investigated and blocks were formed in all samples treated using various calcium sources; however, the sand blocks collapsed after the Petridish demolded in the control samples, because dead cells were used (Gorospe et al. 2013). Our group has developed a simple method for testing impermeability to determine the efficiency of MICP. Specifically, the degree of impermeability was determined by measuring the migration distance of crystal violet. The activity of urease and the amount of $CaCO_3$ precipitation are based on several environmental factors. Indeed, many factors affect urease activity and calcium precipitation including bacteria type, bacteria cell concentrations, pH, temperature, urea and calcium concentrations (Hammes and Verstraete 2002; Mortensen et al. 2011; Ng et al. 2012; Qabany et al. 2012).

1.2.3.3 Isolation of ureolytic bacteria from various sources

The main task of the MICP technique is isolation and selection of potent urease producing bacteria. To promote ureolysis–driven calcite precipitation, the microorganisms should produce a sufficient amount of urease enzyme. Therefore, many investigators have isolated ureolytic microorganisms from various sources (Dejong et al. 2006; Hammes et al. 2003a; Achal and Pan 2014; Kang et al. 2014a). Ureolytic microorganisms that can induce CaCO3 precipitation have been studied for multiple applications such as remediation, consolidation and cementation (Ivanov and Chu 2008; De Muynck et al. 2010; Phillips et al. 2013). Hammes et al. (2003a) reported that $CaCO_3$ precipitating strains were isolated from garden and landfill soil from Ghent, Belgium. Achal et al. (2009a) developed a phenotypic mutant of *Sporosarcina pasterurii* by UV irradiation and compared it with the wild type strain MTCC 1761. The mutant strain (Bp-M3) was able to grow at higher pH (up to 11) than the wild type (up to 10) and to produce high urease activity and calcite precipitation. The increase in pH is very important to enhancement of the urease activity and calcium carbonate precipitation. The urease producing bacteria *Bacillus* sp. CR2 was isolated from mine tailing soil of Urumgi, Xinjiang, China (Achal and Pan 2014), and several *Sporosarcina* species were isolated from nursery garden soil at Tsinghwa University, China (Li et al. 2013). Positive strains were identified by the pink color formed upon hydrolysis of urea in urea test agar plates.

Dhami et al. (2013b) recently isolated the ureolytic bacterial strains from calcareous soil samples collected in Andhra Pradesh, India. Five positive strains (*B. megaterium, B. thuringiensis, B. cereus, B. subtilis* and *L. fusiformis*) were selected based on the urease activity, and calcite precipitation. However, *B. megaterium* produced highest urease activity

(690 U/ml), and calcite precipitation (187 mg/100 ml). Other urease producing bacteria were isolated from an abandoned express way and abandoned mining sites in Gangwondo, Korea (Kang et al. 2014a), four of which showed urease activity and calcite production. However, only two strains of *Lysinibacillus* sp. were able to produce high urease activity and calcite precipitation. The same group isolated another strain of urease producing bacteria, *Sporosarcina pasteurii* WJ-2 from abandoned express way sites, in Gangwondo, Korea (Unpublished data). Sarda et al. (2009) screened three different microorganisms for urease production and found that *B. pasteurii* could produce urease at levels approximately two-fold higher than other tested microorganisms. Some investigators have also revealed ureolytic activity in situ in natural soil and ground water systems (Nielsen et al. 1998; Fujita et al. 2008; Tobler et al. 2011). All bacteria could produce various amounts of urease and calcite precipitation, while some microorganisms could produce high levels of urease and were involved in the hydrolysis of urea (Achal et al. 2009a; Dhami et al. 2013b, 2014). The endospore forming bacteria *Sporosarcina pasteurii* ATCC 11859 and *B. megaterium* have been shown to produce high levels of urease and have therefore been extensively studied. The urease activity was determined by phenol-hypochloride assay (Natarajan 1995). One unit of urease is defined as the amount of enzyme hydrolyzing 1 µmol urea/ min. Bachmeier et al. (2002) investigated the role of nickel ions in the active site of the urease enzyme for its functional activity and the structural integrity of the enzyme. They also demonstrated recombinant transformation of the *B. pasteurii* urease gene to Escherichia coli HB101 containing pBU11 plasmid. However, the amount of calcite precipitation by recombinant strain *E. coli* HB101 was lower than that of the wild type (Bachmeier et al. 2002).

1.2.2.4 Recent status of MICP applications

The MICP process is an effective and eco-friendly technology that can be applied to solve various environmental problems, including remediation of heavy metals and radionuclides, bioconsolidation, biocement, CO_2 sequestration and other applications (De Muynck et al. 2010; Mitchell et al. 2010; Yoshida et al. 2010; Hamdan et al. 2011; Achal et al. 2012a). The MICP method is an alternative method for the production of several materials. The biominerals of calcium carbonate or calcium phosphate are involved in production of complex multifunctional composites with organic macromolecules at extreme temperature and pressure (Wakayama et al. 2005). Particularly, calcite formed by *Geobacillus thermoglucosidasius* has many advantages when applied as filler in rubber and plastics, fluorescent particles in stationary ink and stationary markers for western blotting and other biochemistry applications (Ling et al.

2009; Yoshida et al. 2010). Other alternative, MICP is able to produce a coating to seal polychlorinated biphenyls (PCBs) contaminated areas. Indeed, MICP coated areas showed no leaching and a reduction in permeability of 1–5 orders or magnitude (Okwadha and Li 2011). High concentrations of calcium ions in industrial wastewater are problematic because of the clogging of pipelines, boilers and heat exchangers through scaling or malfunctioning of aerobic and anaerobic reactors (Yu et al. 2001; Hammes et al. 2003). MICP is an alternative technology for removal of inorganic contaminants from the environment, and many researchers have reported the use of MICP methods for removal of calcium from industrial wastewater (Van Langerak et al. 1997; Hammes et al. 2003). Van Langerak et al. (1997) reported the removal of calcium from industrial wastewater using a fluidized sand bed calcification reactor that employed the alkalinity generated by microbes in a standard up-flow anaerobic sludge bed reactor. Using the biocatalytic calcification reactor, approximately 85–90 % (w/v) of the soluble calcium was precipitated as calcium carbonate and successfully removed through sedimentation in the treatment reactor (Hammes et al. 2003). Therefore, this is an effective, eco-friendly and simple method for removal of calcium from industrial wastewater.

Over the past 15 years, MICP has been tested for its potential as an innovative soil improvement technique for different purposes. While most of these tests were under laboratory conditions, the MICP technique has been proved to be suitable for use in applications such as strengthening loose sand, liquefaction control in saturated fine sand and fugitive dust control in desert areas (Montoya and Dejong, 2013). A few field trials of these applications were also reported. However, MICP has not demonstrated yet that it is as competitive as traditional mainstream technologies (i.e. able to achieve similar or better engineering effectiveness with sufficient safety margin and lower costs). Therefore, in order to fully realize the potential of MICP as a versatile technique for soil improvement applications, exploring its multi-functionality and upscaling its implementation in different areas will be important. Recently, an innovative bio- based granular geomaterial based on the MICP process has been developed, which can mitigate sediment resuspension as a result of wind erosion and enhance lake ecosystems by promoting aquatic plant growth (Hata, et al., 2019). In another case, MICP was found to have the potential to simultaneously immobilize heavy metals in a brownfield soil as well as strengthening the soil for construction purposes (Jiang, et al., 2019). Other multi-functional applications of MICP including shoreline protection (Salifu, et al., 2016), geological hazard mitigation (Jiang, et al., 2019), soil and water conservation, and pollution control for radionuclides are also under active research, though mostly at a preliminary stage. Nevertheless, more research effort is needed to develop multifaceted MICP protocols that could

address multidisciplinary engineering challenges by coupling soil engineering performance enhancement with ecological, environmental and carbon footprint benefits. The promising results on MICP feasibility for different applications now require that part of the effort is focused on the investigation of application approaches in the field.

1.3. Coastal erosion

Coastal erosion issues become more critical because coastal zones are optimal places for population concentration and the development of productive activities, such as, industry, transportation, tourism, etc. (Barragan and Andreis, 2015). Coastal erosion is a common problem affecting about 75% of the world's shorelines (Bird, 1987; Zhang et al., 2004; Pilkey and Cooper, 2014; Rangel-Buitrago, et al., 2018). Adger et al. (2005) indicated that close to 20% of the world population (1409 million inhabitants) reside less than 25 km from the coastline, and 40% (2818 million inhabitants) live less than 100 km inside a coastal strip representing approximately 25% of the world total surface. Coastal zone monitoring based on aerial data, satellite or field investigating is an important task in environmental protection and fundamental coastal management (Figure 1.4). Yogyakarta beaches were consisting of two different types of sands, whereas iron silica sand from Mt. Merapi volcanic sedimentary and calcareous sand from the coral reef and/or limestone formation in the eastern Yogyakarta. As a tourist destination, the beaches such as Parangtritis-Samas-Tisik-Pandansari (Silica sand - south central Yogyakarta) and also Krakal-Sadranan-Baron-Kukup-Drini-Pok Tunggal until Wediombo beaches (calcareous sand - south eastern Yogyakarta) has developed as an economic center in the coastal shoreline of Yogyakarta province.

The geomorphology of south Yogyakarta coastal area and their problems is explained in the appendixes A about the coastal drone mapping of Yogyakarta shoreline. As a potential economically growing area, the Yogyakarta coast has attracted over time more and more people to reside and has a good living condition. As a consequence, the growing number of people needs more space and starts to utilize the coast which creating vulnerable areas from coastal hazards despite the buffer zone of 200 m according to the spatial planning has been established. On the other hand, the south coast of Java has been suffered from geologic and climatologic events such as tsunami in July 2006 and storm-tidal wave, last moment is Oct 2018. Beach erosion also reported in some parts of Yogyakarta's south coast such as Samas beach and Parangtritis beach (Pujotomo, 2009). Those natural phenomena were reported to cause damages to infrastructure near the shore. The establishment of a buffer zone is one of several efforts commonly taken to reduce risk in the framework of coastal disaster risk management.

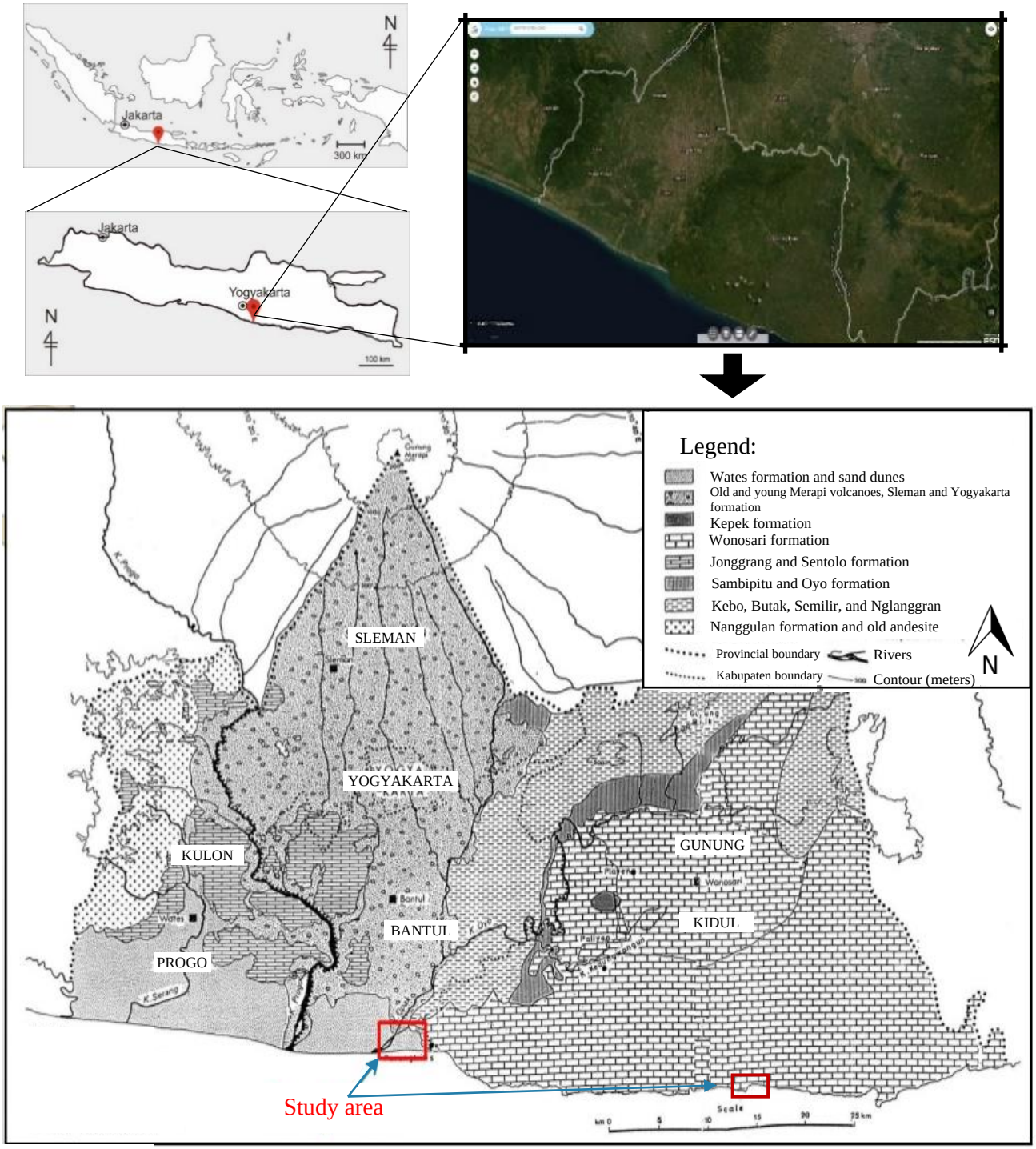


Figure 1.4. Simplified Geological Map of Yogyakarta, Indonesia (modify from Surono, et al, 1992).

Coastal zone management requires to the understanding of shoreline dynamic and consider the potential future hazard such as enhanced sea-level rise due to global warming phenomenon. Monitoring coastal changes over time needs a complete spatial-temporal data, which is difficult to find in Indonesia. The integration of multi-source spatial and temporal data such as topographic maps and also satellite imageries is considered to overcome the lack of data series availability (Marfai, et al., 2008). This study is focused on the understanding of Java South

coast characteristics particularly in Parangtritis beach and Krakal-Sadranan beach were beachrock were found, further studies were carried out to (i) identification of beachrock deposit occurrences in Krakal-Sadranan, Yogyakarta (ii) develop the biomineralization based on ureolytic bacteria from natural beachrock using calcareous and iron-silica sands, and (iii) explore biocementation for nearshore environments as an alternative technique for sand stabilization.

1.4 Current hardened structure erosion mitigation methods

Over the years, several mitigation measures have been used in various attempts to mitigate or prevent coastal erosion. While some of these measures are effective, each has its own negative consequences. These traditional shoreline stabilization techniques are discussed below:

1.4.1 Seawalls, bulkheads, and other wall structures

Seawalls, bulkheads, and other wall structures are the most common type of hard stabilization structure against beach erosion within the state of Florida and are used to protect shorelines from the impacts of normal wave action. Common building materials for these structures include timber, steel, rock, concrete, or polymers. However, these structures are not without their issues. First, under worst-case storm conditions, wall-type structures may overtop, which could lead to failure. After Hurricanes Irma and Matthew, the National Science Foundation (NSF) Geotechnical Extreme Events Reconnaissance (GEER) team noted that performance was significantly affected continuity in the sense that any “holes” or “gaps” in bulkheads tended to also lead to upland erosion and failure (Hudyma et al. 2018). Generally, when walls are installed, the beach on the shoreside of the structure will erode and, in some cases, shoreside beaches may be lost entirely. This may negatively affect beach-centric tourism environment or result in destruction of wildlife habitats (Bush, et al., 2004).

1.4.2 Breakwaters an alternative to wall-type structures are breakwaters.

While their primary purpose is wave attenuation, an added benefit to breakwaters in the context of beach protection is sediment accumulation between the beachfront and the breakwater. Two specific types of breakwaters that have become increasingly popular are fixed breakwaters and submerged breakwaters. An example of a submerged breakwater is an artificial reef, or a structure built on the seafloor. As more of these breakwater structures are

put into place, many of their disadvantages have become apparent. Fixed breakwaters are permanent structures that require continuous maintenance which can become expensive. In addition, fixed breakwaters are typically a displeasing sight to a popular shoreline, ultimately effecting the beachfront tourism industry. Alternatively, a submerged, artificial reef placed too close to the shoreline may result in shoreline erosion (Ranasinghe, 2006). While breakwaters can be best suited to protect port and harbor entrances from added silt build up, they provide little benefit as an erosion control method to a pre-existing shoreline.

1.4.3 Groins and jetties

In many coastlines of the United States, jetties and groins are sometimes used to prevent beach erosion. Groins are walls generally built perpendicular to the shoreline used to trap and hold sediment flowing in the long shore current. Jetties and groins are also built as T-shaped, Y-shaped, zigzag shaped, and angled from shore. They are typically placed in groin fields, which are multiple groins that extend like fingers away from shore (Dean, 2003). Materials used to build these structures include rock, concrete, wood, steel, and fabric bags filled with sand. They are intended to combat the problem of existing sediment erosion. In the state of Florida, these structures are typically found along the east coast. Many disadvantages exist with the placement of groins or groin fields. Updrift beaches are widened by this method, while downdrift beaches become starved of sediment. In addition, the entrapment of sediment on one side of the groin intensifies erosion on the other (Bush, et al., 2004).

1.4.4 Riprap and shore armoring

Riprap is another man-made shore stabilization technique used to armor a shoreline against wind and wave erosion and scour. Riprap is simply a method of layering rock across a threatened area to prevent further erosion. Typically, riprap is made of angular rock, rubble, or broken concrete slabs. Riprap can be strategically placed by hand or simply dumped in an area to form a revetment and protect from erosion and scour (Brown and Clyde, 1989). Generally, riprap revetments are designed to have an appropriate slope and rock size to adequately protect an area from erosion, typical slope ratios are 1:2 (vertical to horizontal) or 1:3. Layers of smaller stone or gravel are placed under and between the larger rock to help reinforcement. Like other traditional shoreline stabilization techniques, riprap also has some negative issues. Often, riprap projects along the coast are faced with ongoing repair and maintenance that become expensive and potentially problematic. Research has shown that fewer aquatic species and vegetation live in armored revetments than in natural coastal habitats (Massey, et al., 2017).

The limited vegetation degrades the wildlife and threatens the breeding areas for aquatic species. Due to the low coefficient of friction, riprap tends to increase the wave celerity in the water which ultimately increases erosion on adjacent shorelines and scour at the toe ends of the embankment making it a counterintuitive shore stabilization method (Brookes, 2018). Lastly, riprap has similar issues to wall-type structures in the sense that riprap often may replace beaches and negatively affect beach tourism.

1.4.5 Beach nourishment and dune benefits

As noted above, each method of structural beach protection has its disadvantages. In recent years, several communities have moved away from structural-type protection measures in favor of beach nourishment (Dean, 2003). This leaves sand dunes as the primary line of protection against erosion, upland flooding, and upland damage. Dunes are also excellent for the environment. Sand dunes are the primary location for sea turtle nesting and the home of many other wildlife species. Additionally, dunes and ongoing beach nourishment projects positively impact beach tourism. However, dunes are highly erodible and overall are very susceptible to failure during large-scale storm events. It would be beneficial if there were a sustainable, rapidly deployable mechanism that could be used to strengthen dunes to make them less susceptible to erosion and scour.

1.5 Objectives

The overall goal of this research was to quantify erodibility for MICP-treated specimens in terms of beach sand treatment against the erosion. Specimens were treated using an in-low syringes and surface-spray technique because under field conditions, such a technique would appear to be the most realistic way to spread MICP solutions onto dunes. Optimization testing was conducted both in terms of initial bacterial optical density and solution volume as a function of pore space. Investigating the beachrock mechanism and mimicking to developing artificial rock based on MICP will be presented in detail in Chapters 3 and 5, showed that specimens were fully treated with MICP method, but even under these conditions, the treatment samples were investigated under durability test based on wet-drying method to prove it will sustain for longer period. As such, under laboratory conditions, it is unlikely that a one-time MICP treatment of a dune system will significantly reduce erosion. In addition, through understanding the beachrock formation process, artificial rocks may be able to be formed at an accelerated speed of consolidation. Therefore, test pieces composed of sand cemented by MICP

were subjected to unconfined compressive strength (UCS) tests and observed by scanning electron microscopy (SEM). This study's aim was to evaluate the feasibility of using the unique and novel grout by exploiting ureolytic microbial adjustment activity in carbonate precipitation, respectively.

1.6 Scope and organization

The scope of this thesis is an investigation of different ground improvement techniques using biochemical methods. Chapter 2, Chapter 3 and Chapter 4 are described under investigated of natural beachrock sedimentary process toward mechanism and precipitation in natural processes within case study in Sumuide, Okinawa and Krakal-Sadranan, Yogyakarta, Indonesia. Chapter 5, Chapter 6, and Chapter 7 were mentioned under the soil improvement with MICP and as proposal to treat beach sand in-situ or ex-situ based on the research will described in Chapter 8. Last, the general summary of all this research were concluded in Chapter 9. Chapters of this thesis are as follows:

In Chapter 1, research background, objectives, and originality of thesis were described. Chapter 2 consisted with geophysical investigation of buried beachrock at Krakal-Sadranan beach, Yogyakarta, Indonesia. In Chapter 3 consisted of detail laboratory analysis toward beachrock sediment characteristics investigation. Other hand, Chapter 4 were established of ureolytic bacteria from Indonesian tropical shoreline which will compare between characteristic beachrock from Okinawa, Japan. Chapter 5 is consisting of beach sand treatment based on MICP process to mimic the natural beachrock, achievement almost similar to natural beachrock based on chemical compound and strength. Moreover, Chapter 6 is testing of durability based on MICP for coastal disaster countermeasures development. Chapter 7 consisted of cost reduction purposes using cheap chemical reagent from the culture media and also cement solution for MICP treatment and Chapter 8 is the proposal of the coastal prevention method based on ureolytic bacteria especially in Indonesia. The last, Chapter 9 summarized and provided a conclusion that may guide future work. This dissertation flowchart described in Figure 1.5.

1.7 Originality and usefulness of the study

The novelty of our research resides in the characterization of the ureolytic bacterial controlled in Natural Beachrock (case study: Krakal-Sadranan, Yogyakarta, Indonesia and

Sumuide, Okinawa, Japan) and the study of the biodiversity and distribution of such populations in harsh environmental conditions that prevails, and in calcareous-iron silica from local shoreline in Yogyakarta. Also, the native ureolytic bacteria isolated from beachrock will

Table 1.1 Research originality

Danjo and Kawasaki (2014, 2016)	*Pararhodobacter* sp. strain from local beachrock sedimentary from Sumuide, Gima, and Yomitan (Okinawa, Japan)
G. G. N. N. Amarakoon and Kawasaki (2016)	Development of sustainable ground improvement methods using biochemical techniques based on *Pararhodobacter* sp.
Nawarathna, et al. (2019)	Effect of chitosan (organic compound) to enhances MICP process using *Pararhodobacter* sp.
Nayanthara, et al. (2019)	MICP using native inland bacterium *Sporosarcina* sp., within effect of magnesium mineral for beach sand stabilization in nearshore area Sri Lanka.
This study	Lack of beachrock information in Indonesia concerning about distribution, mechanical properties, and sediment characteristics based on geology, chemical, mechanical, and biological perspective. Identification of sedimentary mechanism natural beachrock, Indigenous ureolytic bacteria strain from Indonesian beachrock and their efficiency of MICP biocement based on: • Magnesium-sodium mineral (achievement to natural beachrock) • Effect of carrageenan (red algae) organic compound to enhance strength of MICP • Biocementation using low-cost chemical compound to decreasing cost reduction Durability test “wetting-drying” of treatment sand using MICP method and cost reduction based on cheap chemical reagents.

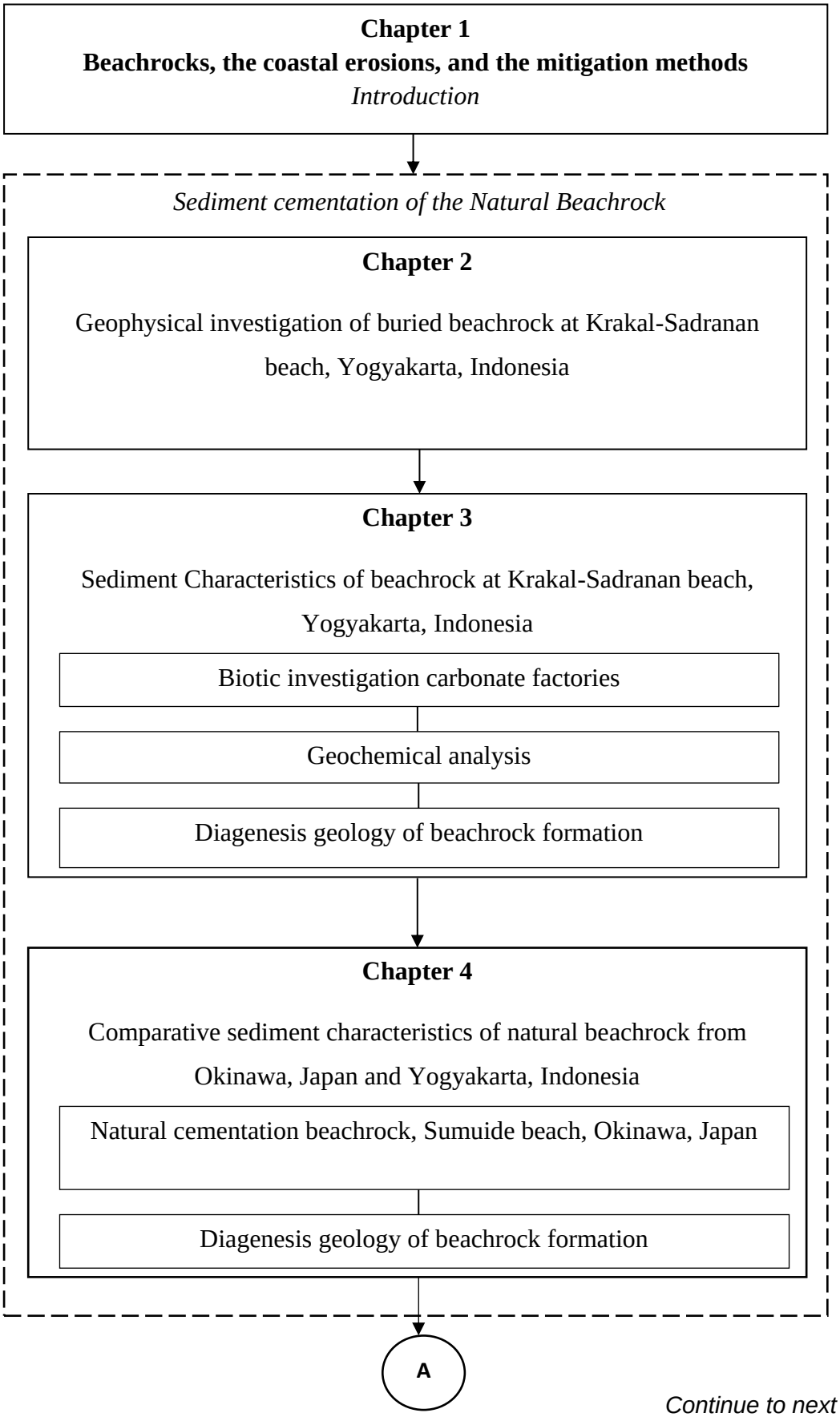
be used to bio-modify the soil. Furthermore, the significance of the research lies in the establishment of screening method to investigate the potentialities of ureolytic bacteria for their urease activity as well as to study the response of soil subjected to biomodification on small laboratory and field scales.

In this study, ureolytic bacteria as key role sedimentary of beachrock were deep investigated to develop artificial rocks based on microbial induce using native indigenous strain. The usefulness of this study from the viewpoint of effectiveness, sedimentary characteristics, and cost reduction may be one hint to promote this method as a large-scale practical application in the future. Furthermore, previous studies related to the MICP have been focused to obtain several MPa values of UCS. However, this study focused to obtain similar to natural beachrock and identify the durability of artificial rocks to mitigate the coastal disaster using biocementation.

1.8 Originality of the thesis

Many types of research as mentioned in the Section 1.3.1. were observed sand solidification with MICP method by using common ureolytic bacteria such as *Sporosarcina pasteurii* (formerly *Bacillus pasteurii*) and *Bacillus sphaericus*. From this research study, we introduced a new uearlytic bacteria for the MICP process. The bacterium was *Pararhodobacter* sp. which was found from Okinawa, Japan and local bacteria were isolated from Krakal-Sadranan beach whereas *Oceanobacillus profundus*, *Vibrio maritimus*, and *Pseudoalteromonas tetradonis.* It was originality of this research.

Moreover, previous researchers (Danjo and Kawasaki, 2016; Khan, et al., 2015) conducted solidification using *Pararhodobacter* sp. for marine purposes and they used artificial sea water for cultivation of bacteria and solidification process. However, in this research solidification with ureolytic bacteria was used for land usage whilst distilled water was introduced instead of artificial seawater. Also, another originality, we tried to find the reaction mechanism in microbial activity based on glucose complex and protein that assumed pathway of Ca^{2+} ion binding enzyme. The durability of materials after treated by MICP is conducted to clarify the long-term feasibility improvement with soaked in fresh water and also seawater to indicate this method are feasible in the shoreline areas. The cost reduction also investigated based on cheap chemical reagents from cultured media and cement solution for MICP treatment for economical feasibility of the MICP products. This will provide new knowledge about biotechnology and will greatly contribute to the development of environmental resource engineering.



Continue to next page

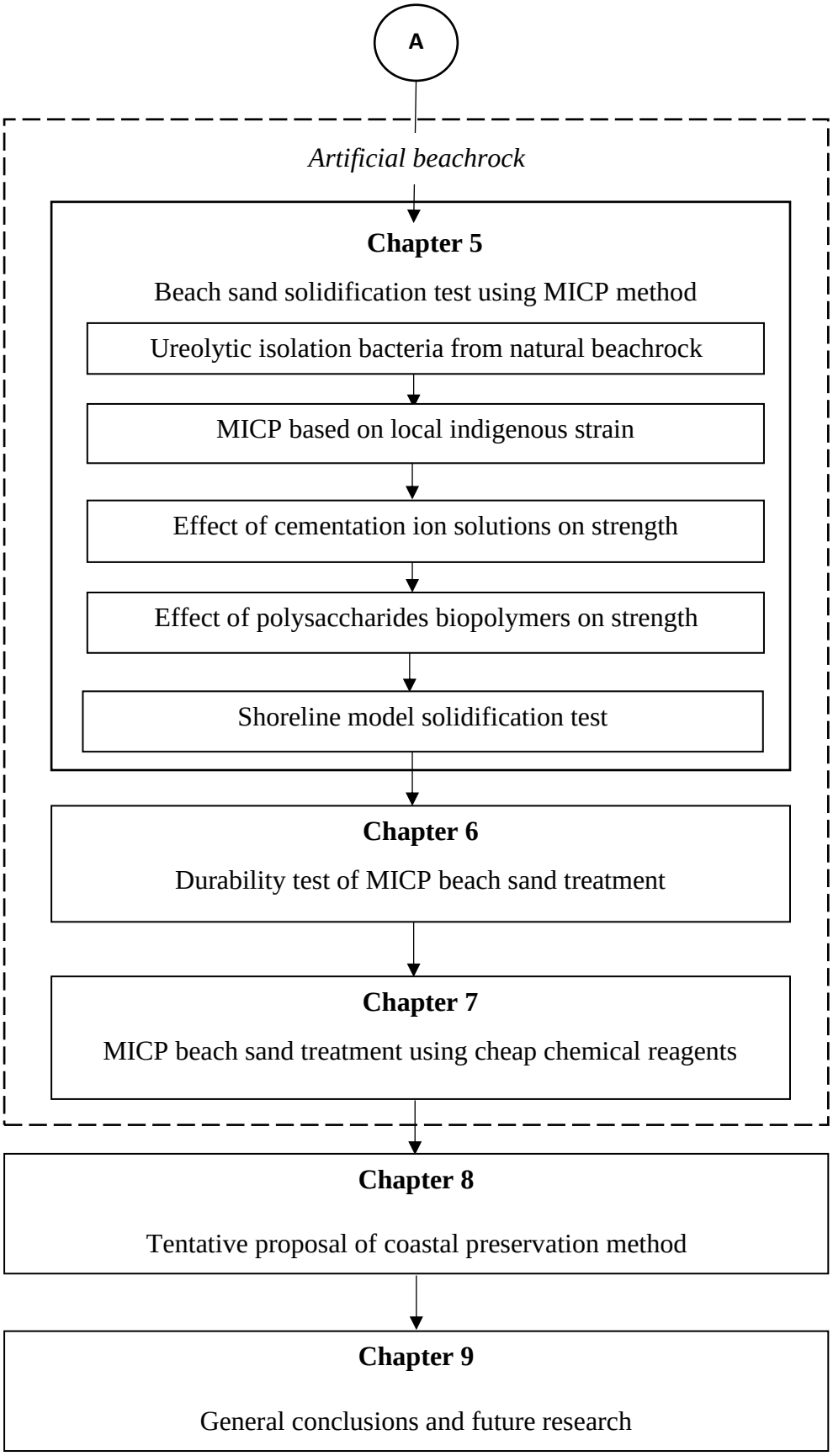


Figure 1.5. *Flow chart of this research*

References

Achal, V. and Pan, X., 2011. Characterization of urease and carbonic anhydrase producing bacteria and their role in calcite precipitation. Current microbiology, 62(3), pp.894-902.

Achal, V. and Pan, X., 2014. Influence of calcium sources on microbially induced calcium carbonate precipitation by Bacillus sp. CR2. Applied biochemistry and biotechnology, 173(1), pp.307-317.

Achal, V., Kumari, D. and Pan, X., 2011. Bioremediation of chromium contaminated soil by a brown-rot fungus, Gloeophyllum sepiarium. Research Journal of Microbiology, 6(2), pp.166-171.

Achal, V., Mukherjee, A., Basu, P.C. and Reddy, M.S., 2009. Strain improvement of Sporosarcina pasteurii for enhanced urease and calcite production. Journal of industrial microbiology & biotechnology, 36(7), pp.981-988.

Achal, V., Mukherjee, A., Kumari, D. and Zhang, Q., 2015. Biomineralization for sustainable construction–A review of processes and applications. Earth-science reviews, 148, pp.1-17.

Adger, W.N., Hughes, T.P., Folke, C., Carpenter, S.R. and Rockström, J., 2005. Social-ecological resilience to coastal disasters. Science, 309(5737), pp.1036-1039.

Al-Thawadi, S.M., 2011. Ureolytic bacteria and calcium carbonate formation as a mechanism of strength enhancement of sand. J. Adv. Sci. Eng. Res, 1(1), pp.98-114.

Alves, D. and Olívia Pereira, M., 2014. Mini-review: Antimicrobial peptides and enzymes as promising candidates to functionalize biomaterial surfaces. Biofouling, 30(4), pp.483-499.

Amarakoon, G.G.N.N. and Kawasaki, S., 2016. Factors affecting the improvement of sand properties treated with microbially-induced calcite precipitation. In Geo-Chicago 2016 (pp. 72-83).

Annamalai, S.K., Arunachalam, K.D. and Sathyanarayanan, K.S., 2012. Production and characterization of Bio Caulk by Bacillus pasteurii and its remediation properties with carbon nano tubes on concrete fractures and fissures. Materials Research Bulletin, 47(11), pp.3362-3368.

Arias, D., Cisternas, L.A. and Rivas, M., 2017. Biomineralization of calcium and magnesium crystals from seawater by halotolerant bacteria isolated from Atacama Salar (Chile). Desalination, 405, pp.1-9.

Arp, G., Reimer, A. and Reitner, J., 1999. Calcification in cyanobacterial biofilms of alkaline salt lakes. European Journal of Phycology, 34(4), pp.393-403.

Bachmeier, K.L., Williams, A.E., Warmington, J.R. and Bang, S.S., 2002. Urease activity in microbiologically-induced calcite precipitation. Journal of Biotechnology, 93(2), pp.171-181.

Bang, S.S. and Ramakrishnan, V., 2001, November. Microbiologically-enhanced crack remediation (MECR). In proceedings of the international symposium on industrial application of microbial genomes (pp. 3-13).

Barragán, J.M. and de Andrés, M., 2015. Analysis and trends of the world's coastal cities and agglomerations. Ocean & Coastal Management, 114, pp.11-20.

Beier, J.A., 1985. Diagenesis of Quaternary Bahamian beachrock; petrographic and isotopic evidence. Journal of Sedimentary Research, 55(5), pp.755-761.

Berner, R.A., 1971. Principles of chemical sedimentology.

Betzler, C., Brachert, T.C. and Nebelsick, J., 1997. The warm temperate carbonate province: a review of the facies, zonations, and delimitations. Courier Forschungsinstitut Senckenberg, 201, pp.83-99.

Binod, P., Palkhiwala, P., Gaikaiwari, R., Nampoothiri, K.M., Duggal, A., Dey, K. and Pandey, A., 2013. Industrial enzymes-present status and future perspectives for India.

Bird, E.C., 1994. Physical setting and geomorphology of coastal lagoons. Coastal lagoon processes, 60, pp.9-37.

Bird, E.C.F., 1987. The modern prevalence of beach erosion. Marine Pollution Bulletin, 18(4), pp.151-157.

Bosak, T. and Newman, D.K., 2005. Microbial kinetic controls on calcite morphology in supersaturated solutions. Journal of Sedimentary Research, 75(2), pp.190-199.

Braissant, O., Decho, A.W., Dupraz, C., Glunk, C., Przekop, K.M. and Visscher, P.T., 2007. Exopolymeric substances of sulfate-reducing bacteria: interactions with calcium at

alkaline pH and implication for formation of carbonate minerals. Geobiology, 5(4), pp.401-411.

Brandley, R.T. and Krause, F.F., 1997. Cool-water carbonates. SEPM (Society for Sedimentary Geology) Special Publication, 56, pp.365-390.

Bretzel, W., Schurter, W., Ludwig, B., Kupfer, E., Doswald, S., Pfister, M. and Van Loon, A.P.G.M., 1999. Commercial riboflavin production by recombinant Bacillus subtilis: down-stream processing and comparison of the composition of riboflavin produced by fermentation or chemical synthesis. Journal of Industrial Microbiology and Biotechnology, 22(1), pp.19-26.

Brookes, A., 2018. Alternative channelization procedures. In Alternatives in regulated river management (pp. 149-172). CRC Press.

Brown, S.A. and Clyde, E.S., 1989. Design of riprap revetment (No. FHWA-IP-89-016). United States. Federal Highway Administration.

Burne, R.A. and Chen, Y.Y.M., 2000. Bacterial ureases in infectious diseases. Microbes and Infection, 2(5), pp.533-542.

Bush, D.M., Longo, N.J., Neal, W.J., Lindeman, K.C., Pilkey, D.F., Esteves, L.S., Congleton, J. and Pilkey Jr, O.H., 2004. Living with Florida's Atlantic beaches: coastal hazards from Amelia Island to Key West. Duke University Press.

Cam, N., Benzerara, K., Georgelin, T., Jaber, M., Lambert, J.F., Poinsot, M., Skouri-Panet, F., Moreira, D., López-García, P., Raimbault, E. and Cordier, L., 2018. Cyanobacterial formation of intracellular Ca-carbonates in undersaturated solutions. Geobiology, 16(1), pp.49-61.

Cam, N., Georgelin, T., Jaber, M., Lambert, J.F. and Benzerara, K., 2015. In vitro synthesis of amorphous Mg-, Ca-, Sr-and Ba-carbonates: what do we learn about intracellular calcification by cyanobacteria?. Geochimica et Cosmochimica Acta, 161, pp.36-49.

Castanier, S., Le Métayer-Levrel, G. and Perthuisot, J.P., 1999. Ca-carbonates precipitation and limestone genesis—the microbiogeologist point of view. Sedimentary geology, 126(1-4), pp.9-23.

Chekroun, K.B., Rodríguez-Navarro, C., González-Muñoz, M.T., Arias, J.M., Cultrone, G. and Rodríguez-Gallego, M., 2004. Precipitation and growth morphology of calcium carbonate

induced by Myxococcus xanthus: implications for recognition of bacterial carbonates. Journal of Sedimentary Research, 74(6), pp.868-876.

Chen, X., Qian, X. and An, X., 2011. Using calcium carbonate whiskers as papermaking filler. BioResources, 6(3), pp.2435-2447.

Chua, T.E. and Garces, L.R., 1993. Regional efforts in the management of the coastal and marine environments in the ASEAN region.

Collins, L.B., France, R.E., Zhu, Z.R. and Wyrwoll, K.H., 1997. Warm-water platform and cool-water shelf carbonates of the Abrolhos Shelf, Southwest Australia.

Danjo, T. and Kawasaki, S., 2011, January. Property evaluation of beachrock based on field investigation in Okinawa Island, Japan. In 12th ISRM Congress. International Society for Rock Mechanics and Rock Engineering.

Danjo, T. and Kawasaki, S., 2013. A study of the formation mechanism of beachrock in Okinawa, Japan: Toward Making Artificial Rock. Int. J. of Geomate, 5(1), pp.633-638.

Danjo, T. and Kawasaki, S., 2014. Characteristics of beachrocks: a review. Geotechnical and Geological Engineering, 32(2), pp.215-246.

Danjo, T. and Kawasaki, S., 2014. Formation mechanisms of beachrocks in Okinawa and Ishikawa, Japan, with a Focus on Cements. Materials Transactions, pp.M-M2013844.

Danjo, T. and Kawasaki, S., 2016. Microbially induced sand cementation method using Pararhodobacter sp. strain SO1, inspired by beachrock formation mechanism. Materials Transactions, 57(3), pp.428-437.

Darwin, C., 1841. XXXVII. On a remarkable bar of sandstone off Pernambuco, on the coast of Brazil. The London, Edinburgh, and Dublin Philosophical Magazine and Journal of Science, 19(124), pp.257-260.

David, P., Panagiotis, T. and Konstantinos, A., 2009. Electrical resistivity tomography mapping of beachrocks: application to the island of Thassos (N. Greece). Environmental Earth Sciences, 59(1), p.233.

Davies, P.J. and Kinsey, D.W., 1973. Organic and inorganic factors in recent beach rock formation, Heron Island, Great Barrier Reef. Journal of Sedimentary Research, 43(1), pp.59-81.

Davies, P.J., Bubela, B. and Ferguson, J., 1978. The formation of ooids. Sedimentology, 25(5), pp.703-730.

De Muynck, W., De Belie, N. and Verstraete, W., 2010. Microbial carbonate precipitation in construction materials: a review. Ecological Engineering, 36(2), pp.118-136.

De Yoreo, J.J. and Vekilov, P.G., 2003. Principles of crystal nucleation and growth. Reviews in mineralogy and geochemistry, 54(1), pp.57-93.

Dean, R.G., 2003. Beach nourishment: theory and practice (Vol. 18). World Scientific Publishing Company.

DeJong, J.T., Fritzges, M.B. and Nüsslein, K., 2006. Microbially induced cementation to control sand response to undrained shear. Journal of Geotechnical and Geoenvironmental Engineering, 132(11), pp.1381-1392.

DeJong, J.T., Soga, K., Kavazanjian, E., Burns, S., Van Paassen, L.A., Al Qabany, A., Aydilek, A., Bang, S.S., Burbank, M., Caslake, L.F. and Chen, C.Y., 2014. Biogeochemical processes and geotechnical applications: progress, opportunities and challenges. In Bio-and Chemo-Mechanical Processes in Geotechnical Engineering: Géotechnique Symposium in Print 2013 (pp. 143-157). Ice Publishing.

Dhami, N.K., Mukherjee, A. and Reddy, M.S., 2016. Micrographical, minerological and nano-mechanical characterisation of microbial carbonates from urease and carbonic anhydrase producing bacteria. Ecological engineering, 94, pp.443-454.

Dhami, N.K., Reddy, M.S. and Mukherjee, A., 2013. Bacillus megaterium mediated mineralization of calcium carbonate as biogenic surface treatment of green building materials. World Journal of Microbiology and Biotechnology, 29(12), pp.2397-2406.

Dhami, N.K., Reddy, M.S. and Mukherjee, A., 2014. Synergistic role of bacterial urease and carbonic anhydrase in carbonate mineralization. Applied biochemistry and biotechnology, 172(5), pp.2552-2561.

Dick, J., De Windt, W., De Graef, B., Saveyn, H., Van der Meeren, P., De Belie, N. and Verstraete, W., 2006. Bio-deposition of a calcium carbonate layer on degraded limestone by Bacillus species. Biodegradation, 17(4), pp.357-367.

Dickinson, W.R., Burley, D.V. and Shutler Jr, R., 1999. Holocene paleoshoreline record in Tonga: geomorphic features and archaeological implications. Journal of Coastal Research, pp.682-700.

Douglas, S. and Beveridge, T.J., 1998. Mineral formation by bacteria in natural microbial communities. FEMS microbiology ecology, 26(2), pp.79-88.

Dupraz, C. and Visscher, P.T., 2005. Microbial lithification in marine stromatolites and hypersaline mats. Trends in microbiology, 13(9), pp.429-438.

Ehrlich, H.L. and Newman, D.K., 2009. Geomicrobiology of sulfur. Geomicrobiology,(Boca Raton, FL: Taylor & Francis), pp.439-489.

Erginal, A.E., Kıyak, N.G. and Öztürk, B., 2010. Investigation of beachrock using microanalyses and OSL dating: a case study from Bozcaada Island, Turkey. Journal of Coastal research, pp.350-358.

Favre, N., Christ, M.L. and Pierre, A.C., 2009. Biocatalytic capture of CO2 with carbonic anhydrase and its transformation to solid carbonate. Journal of Molecular Catalysis B: Enzymatic, 60(3-4), pp.163-170.

Ferrer, M.R., Quevedo-Sarmiento, J., Rivadeneyra, M.A., Bejar, V., Delgado, R. and Ramos-Cormenzana, A., 1988. Calcium carbonate precipitation by two groups of moderately halophilic microorganisms at different temperatures and salt concentrations. Current Microbiology, 17(4), pp.221-227.

Fujita, Y., Taylor, J.L., Gresham, T.L., Delwiche, M.E., Colwell, F.S., McLing, T.L., Petzke, L.M. and Smith, R.W., 2008. Stimulation of microbial urea hydrolysis in groundwater to enhance calcite precipitation. Environmental science & technology, 42(8), pp.3025-3032.

Ganendra, G., De Muynck, W., Ho, A., Arvaniti, E.C., Hosseinkhani, B., Ramos, J.A., Rahier, H. and Boon, N., 2014. Formate oxidation-driven calcium carbonate precipitation by Methylocystis parvus OBBP. Appl. Environ. Microbiol., 80(15), pp.4659-4667.

Gebauer, D., Gunawidjaja, P.N., Ko, J.P., Bacsik, Z., Aziz, B., Liu, L., Hu, Y., Bergström, L., Tai, C.W., Sham, T.K. and Edén, M., 2010. Proto-calcite and proto-vaterite in amorphous calcium carbonates. Angewandte Chemie International Edition, 49(47), pp.8889-8891.

Ghosh, P., Mandal, S., Chattopadhyay, B.D. and Pal, S., 2005. Use of microorganism to improve the strength of cement mortar. Cement and Concrete Research, 35(10), pp.1980-1983.

Ginsburg, I., 1953. The taxonomic status and nomenclature of some Atlantic and Pacific populations of yellowfin and bluefin tunas. Copeia, 1953(1), pp.1-10.

Gischler, E. and Lomando, A.J., 1997. Holocene cemented beach deposits in Belize. Sedimentary Geology, 110(3-4), pp.277-297.

Gischler, E., 2007. Beachrock and intertidal precipitates. Geochemical Sediments and Landscapes, pp.365-390.

Goddette, D.W., Paech, C., Yang, S.S., Mielenz, J.R., Bystroff, C., Wilke, M.E. and Fletterick, R.J., 1992. The crystal structure of the Bacillus lentus alkaline protease, subtilisin BL, at 1.4 Å resolution. Journal of molecular biology, 228(2), pp.580-595.

González-Muñoz, M.T., Rodriguez-Navarro, C., Martínez-Ruiz, F., Arias, J.M., Merroun, M.L. and Rodriguez-Gallego, M., 2010. Bacterial biomineralization: new insights from Myxococcus-induced mineral precipitation. Geological Society, London, Special Publications, 336(1), pp.31-50.

Gorospe, C.M., Han, S.H., Kim, S.G., Park, J.Y., Kang, C.H., Jeong, J.H. and So, J.S., 2013. Effects of different calcium salts on calcium carbonate crystal formation by Sporosarcina pasteurii KCTC 3558. Biotechnology and bioprocess engineering, 18(5), pp.903-908.

Gorospe, C.M., Han, S.H., Kim, S.G., Park, J.Y., Kang, C.H., Jeong, J.H. and So, J.S., 2013. Effects of different calcium salts on calcium carbonate crystal formation by Sporosarcina pasteurii KCTC 3558. Biotechnology and bioprocess engineering, 18(5), pp.903-908.

Goudie, A., 1969. Statistical laws and dune ridges in southern Africa. The Geographical Journal, 135(3), pp.404-406.

Groth, P. Schumann, L. Laiz, S. Sanchez-Moral, JC Cañveras, C. Saiz-Jimenez, I., 2001. Geomicrobiological study of the grotta dei cervi, Porto Badisco, Italy. Geomicrobiology Journal, 18(3), pp.241-258.

Hamdan, N., Kavazanjian Jr, E. and Rittmann, B.E., 2011. Sequestration of radionuclides and metal contaminants through microbially-induced carbonate precipitation. In Proc. 14th Pan American Conf. Soil Mech. Geotech. Engng, Toronto.

Hammes, F. and Verstraete, W., 2002. Key roles of pH and calcium metabolism in microbial carbonate precipitation. Reviews in environmental science and biotechnology, 1(1), pp.3-7.

Hammes, F., Boon, N., Clement, G., de Villiers, J., Siciliano, S.D. and Verstraete, W., 2003. Molecular, biochemical and ecological characterisation of a bio-catalytic calcification reactor. Applied microbiology and biotechnology, 62(2-3), pp.191-201.

Hammes, F., Boon, N., de Villiers, J., Verstraete, W. and Siciliano, S.D., 2003. Strain-specific ureolytic microbial calcium carbonate precipitation. Appl. Environ. Microbiol., 69(8), pp.4901-4909.

Hanor, J.S., 1978. Precipitation of beachrock cements; mixing of marine and meteoric waters vs. CO 2-degassing. Journal of Sedimentary Research, 48(2), pp.489-501.

Hata, T., Suetsugu, D., Kawachi, A. and Irie, M., 2019. Development of an eco-friendly bio-based granular geomaterial for the environmental restoration of Ichkeul Lake, Tunisia. Euro-Mediterranean Journal for Environmental Integration, 4(1), p.21.

Hedegaard, I.B., Deigaard, R. and Fredsøe, J., 1991. Onshore/offshore sediment transport and morphological modelling of coastal profiles. In Coastal Sediments (pp. 643-657). ASCE.

Hopley, D., 1986. Beachrock as a sea-level indicator. In Sea-level research (pp. 157-173). Springer, Dordrecht.

Hua, B., Deng, B., Thornton, E.C., Yang, J. and Amonette, J.E., 2007. Incorporation of chromate into calcium carbonate structure during coprecipitation. Water, air, and soil pollution, 179(1-4), pp.381-390.

Hudyma, N., Davies, M., Crowley, R., Ellis, T.N. and Miller, J., 2018, August. Microbially Induced Calcite Precipitation for the Improvement of Porous Building Stone. In 52nd US Rock Mechanics/Geomechanics Symposium. American Rock Mechanics Association.

Ibrahim, C.O., 2008. Development of applications of industrial enzymes from Malaysian indigenous microbial sources. Bioresource technology, 99(11), pp.4572-4582.

Ivanov, V. and Chu, J., 2008. Applications of microorganisms to geotechnical engineering for bioclogging and biocementation of soil in situ. Reviews in Environmental Science and Bio/Technology, 7(2), pp.139-153.

James, N.P., 1997. The cool-water carbonate depositional realm. Cool-water carbonate.

Jansson, C. and Northen, T., 2010. Calcifying cyanobacteria—the potential of biomineralization for carbon capture and storage. Current Opinion in Biotechnology, 21(3), pp.365-371.

Jha, B.K., Pragash, M.G., Cletus, J., Raman, G. and Sakthivel, N., 2009. Simultaneous phosphate solubilization potential and antifungal activity of new fluorescent pseudomonad strains, Pseudomonasaeruginosa, P. plecoglossicida and P. mosselii. World Journal of Microbiology and Biotechnology, 25(4), pp.573-581.

Jiang, N.J., Liu, R., Du, Y.J. and Bi, Y.Z., 2019. Microbial induced carbonate precipitation for immobilizing Pb contaminants: Toxic effects on bacterial activity and immobilization efficiency. Science of The Total Environment, 672, pp.722-731.

Jiang, N.J., Tang, C.S., Yin, L.Y., Xie, Y.H. and Shi, B., 2019. Applicability of microbial calcification method for sandy-slope surface erosion control. Journal of Materials in Civil Engineering, 31(11), p.04019250.

Jones, A. and Phillips, M., 2011. Introduction-disappearing destinations: current issues, challenges and polemics. Disappearing destinations: Climate change and future challenges for coastal tourism, pp.1-9.

Jonkers, H.M. and Schlangen, E., 2008, May. Development of a bacteria-based self healing concrete. In Proc. int. FIB symposium (Vol. 1, pp. 425-430).

Jørgensen, P.L., Tangney, M., Pedersen, P.E., Hastrup, S., Diderichsen, B. and Jørgensen, S.T., 2000. Cloning and sequencing of an alkaline protease gene from Bacillus lentus and amplification of the gene on the B. lentus chromosome by an improved technique. Appl. Environ. Microbiol., 66(2), pp.825-827.

Kang, C.H., Han, S.H., Shin, Y., Oh, S.J. and So, J.S., 2014. Bioremediation of Cd by microbially induced calcite precipitation. Applied biochemistry and biotechnology, 172(6), pp.2907-2915.

Kawaguchi, T. and Decho, A.W., 2002. A laboratory investigation of cyanobacterial extracellular polymeric secretions (EPS) in influencing CaCO3 polymorphism. Journal of Crystal Growth, 240(1-2), pp.230-235.

Kelletat, D., 2006. Beachrock as sea-level indicator? Remarks from a geomorphological point of view. Journal of Coastal Research, 2006(226), pp.1558-1564.

Khan, M.N.H., GGNN, A., Shimazaki, S. and Kawasaki, S., 2015. Coral sand solidification test based on microbially induced carbonate precipitation using ureolytic bacteria. Materials transactions, 56(10), pp.1725-1732.

Krumbein, W.E., 1979. Photolithotropic and chemoorganotrophic activity of bacteria and algae as related to beachrock formation and degradation (Gulf of Aqaba, Sinai). Geomicrobiology Journal, 1(2), pp.139-203.

Kubo, R., Kawasaki, S., Suzuki, K., Yamaguchi, S. and Hata, T., 2014. Geological exploration of beachrock through geophysical surveying on Yagaji Island, Okinawa, Japan. Materials Transactions, pp.M-M2013839.

Kuenen, P.H., 1950. Slump structures in the Waitemata Beds around Auckland. In Transactions of the Royal Society of New Zealand (Vol. 78, pp. 467-475).

Kumari, D., Qian, X.Y., Pan, X., Achal, V., Li, Q. and Gadd, G.M., 2016. Microbially-induced carbonate precipitation for immobilization of toxic metals. In Advances in applied microbiology (Vol. 94, pp. 79-108). Academic Press.

Langevin, E.T. and Bourque, J.A., Thermo Electron Web Systems Inc, 1992. Simultaneously controlled steam shower and vacuum apparatus and method of using same. U.S. Patent 5,149,401.

Lees, A. and Buller, A.T., 1972. Modern temperate-water and warm-water shelf carbonate sediments contrasted. Marine Geology, 13(5), pp.M67-M73.

Li, F., Wu, Y., Hutchins, D.A., Fu, F. and Gao, K., 2016. Physiological responses of coastal and oceanic diatoms to diurnal fluctuations in seawater carbonate chemistry under two CO 2 concentrations. Biogeosciences, 13(22).

Li, J., Margaret Oliver, I., Cam, N., Boudier, T., Blondeau, M., Leroy, E., Cosmidis, J., Skouri-Panet, F., Guigner, J.M., Férard, C. and Poinsot, M., 2016. Biomineralization patterns of intracellular carbonatogenesis in cyanobacteria: molecular hypotheses. Minerals, 6(1), p.10.

Li, M., Cheng, X. and Guo, H., 2013. Heavy metal removal by biomineralization of urease producing bacteria isolated from soil. International Biodeterioration & Biodegradation, 76, pp.81-85.

Lin, H., Suleiman, M.T., Brown, D.G. and Kavazanjian Jr, E., 2016. Mechanical behavior of sands treated by microbially induced carbonate precipitation. Journal of Geotechnical and Geoenvironmental Engineering, 142(2), p.04015066.

Ling, J., Huang, C.Z., Li, Y.F., Zhang, L., Chen, L.Q. and Zhen, S.J., 2009. Light-scattering signals from nanoparticles in biochemical assay, pharmaceutical analysis and biological imaging. TRAC Trends in Analytical Chemistry, 28(4), pp.447-453.

Lowenstam, H.A. and Weiner, S., 1989. On biomineralization. Oxford University Press on Demand.

Lyell, C., 1837. Principles of geology: being an inquiry how far the former changes of the earth's surface are referable to causes now in operation (Vol. 1). J. Kay, jun. & brother.

Marfai, M.A., King, L., Singh, L.P., Mardiatno, D., Sartohadi, J., Hadmoko, D.S. and Dewi, A., 2008. Natural hazards in Central Java Province, Indonesia: an overview. Environmental Geology, 56(2), pp.335-351.

Massey, W., 2017. Assessing the impact of riprap bank stabilization on fish habitat: A study of Lowland and Appalachian streams in Southern Québec (Doctoral dissertation, Concordia University).

McKenzie, R.M., 1971. The synthesis of birnessite, cryptomelane, and some other oxides and hydroxides of manganese. Mineralogical magazine, 38(296), pp.493-502.

McLean, R.F., 1967. Origin and development of ridge-furrow systems in beachrock in Barbados, West Indies. Marine Geology, 5(3), pp.181-193.

Meyer, D.L., Ausich, W.I., Bohl, D.T., Norris, W.A., Potter, P.E., Monty, C.L.V., Bosence, D.W.J., Bridges, P.H. and Pratt, B.R., 1995. Carbonate mud-mounds in the Fort Payne Formation (lower Carboniferous), Cumberland Saddle region, Kentucky and Tennessee, USA. Carbonate Mud-Mounds. Their Origin and Evolution, pp.273-287.

Mitchell, A.C., Dideriksen, K., Spangler, L.H., Cunningham, A.B. and Gerlach, R., 2010. Microbially enhanced carbon capture and storage by mineral-trapping and solubility-trapping. Environmental science & technology, 44(13), pp.5270-5276.

Mobley, H.L. and Hausinger, R.P., 1989. Microbial ureases: significance, regulation, and molecular characterization. Microbiology and Molecular Biology Reviews, 53(1), pp.85-108.

Molenaar, N. and Venmans, A.A.M., 1993. Calcium carbonate cementation of sand: a method for producing artificially cemented samples for geotechnical testing and a comparison with natural cementation processes. Engineering Geology, 35(1-2), pp.103-122.

Montoya, B.M. and Dejong, J.T., 2013. Healing of biologically induced cemented sands. Geotechnique Letters, 3(3), pp.147-151.

Monty, C.L., 1995. The rise and nature of carbonate mud-mounds: an introductory actualistic approach. Carbonate Mud-Mounds: Their Origin and Evolution, pp.11-48.

Morse, J.W. and Mackenzie, F.T., 1990. Geochemistry of sedimentary carbonates. Elsevier.

Mortensen, B.M., Haber, M.J., DeJong, J.T., Caslake, L.F. and Nelson, D.C., 2011. Effects of environmental factors on microbial induced calcium carbonate precipitation. Journal of applied microbiology, 111(2), pp.338-349.

Narayan, S., Nicholls, R.J., Clarke, D., Hanson, S., Reeve, D., Horrillo-Caraballo, J., Le Cozannet, G., Hissel, F., Kowalska, B., Parda, R. and Willems, P., 2014. The SPR systems model as a conceptual foundation for rapid integrated risk appraisals: Lessons from Europe. Coastal Engineering, 87, pp.15-31.

Natarajan, K.R., 1995. Kinetic study of the enzyme urease from Dolichos biflorus. Journal of chemical education, 72(6), p.556.

Nawarathna, T.H.K., Nakashima, K. and Kawasaki, S., 2019. Chitosan enhances calcium carbonate precipitation and solidification mediated by bacteria. International journal of biological macromolecules, 133, pp.867-874.

Neumeier, U., 1998. Tidal dunes and sand waves in deep outer-shelf environments, Bajocian, SE Jura, France. Journal of Sedimentary Research, 68(3), pp.507-514.

Neumeier, U., 1999. Experimental modelling of beachrock cementation under microbial influence. Sedimentary geology, 126(1-4), pp.35-46.

Neuweiler, F., d'Orazio, V., Immenhauser, A., Geipel, G., Heise, K.H., Cocozza, C. and Miano, T.M., 2003. Fulvic acid–like organic compounds control nucleation of marine calcite under suboxic conditions. Geology, 31(8), pp.681-684.

Ng, W.S., Lee, M.L. and Hii, S.L., 2012. An overview of the factors affecting microbial-induced calcite precipitation and its potential application in soil improvement. World Academy of Science, Engineering and Technology, 62(2), pp.723-729.

Nielsen, K.M., Bones, A.M., Smalla, K. and van Elsas, J.D., 1998. Horizontal gene transfer from transgenic plants to terrestrial bacteria–a rare event?. FEMS microbiology reviews, 22(2), pp.79-103.

Nolan, B.T., 1999. Nitrate behavior in ground waters of the southeastern USA. Journal of Environmental Quality, 28(5), pp.1518-1527.

Obst, M., Dynes, J.J., Lawrence, J.R., Swerhone, G.D.W., Benzerara, K., Karunakaran, C., Kaznatcheev, K., Tyliszczak, T. and Hitchcock, A.P., 2009. Precipitation of amorphous CaCO3 (aragonite-like) by cyanobacteria: a STXM study of the influence of EPS on the nucleation process. Geochimica et Cosmochimica Acta, 73(14), pp.4180-4198.

Okwadha, G.D. and Li, J., 2010. Optimum conditions for microbial carbonate precipitation. Chemosphere, 81(9), pp.1143-1148.

Okwadha, G.D. and Li, J., 2011. Biocontainment of polychlorinated biphenyls (PCBs) on flat concrete surfaces by microbial carbonate precipitation. Journal of environmental management, 92(10), pp.2860-2864.

Pandey, A. ed., 2011. Biofuels: alternative feedstocks and conversion processes. Academic Press.

Park, S.S., 2010. Effect of wetting on unconfined compressive strength of cemented sands. Journal of geotechnical and geoenvironmental engineering, 136(12), pp.1713-1720.

Pedone, V.A. and Folk, R.L., 1996. Formation of aragonite cement by nannobacteria in the Great Salt Lake, Utah. Geology, 24(8), pp.763-765.

Phillips, A.J., Gerlach, R., Lauchnor, E., Mitchell, A.C., Cunningham, A.B. and Spangler, L., 2013. Engineered applications of ureolytic biomineralization: a review. Biofouling, 29(6), pp.715-733.

Phillips, A.J., Lauchnor, E., Eldring, J., Esposito, R., Mitchell, A.C., Gerlach, R., Cunningham, A.B. and Spangler, L.H., 2013. Potential CO2 leakage reduction through biofilm-induced calcium carbonate precipitation. Environmental science & technology, 47(1), pp.142-149.

Pilkey, O.H. and Cooper, J.A.G., 2014. Are natural beaches facing extinction?. Journal of Coastal Research, 70(sp1), pp.431-436.

Pilkey, O.H. and Cooper, J.A.G., 2014. Are natural beaches facing extinction?. Journal of Coastal Research, 70(sp1), pp.431-436.

Pope, M.C., Fred Read, J., Bambach, R. and Hofmann, H.J., 1997. Late Middle to Late Ordovician seismites of Kentucky, southwest Ohio and Virginia: sedimentary recorders of earthquakes in the Appalachian basin. Geological Society of America Bulletin, 109(4), pp.489-503.

Pouget, E.M., Bomans, P.H., Goos, J.A., Frederik, P.M. and Sommerdijk, N.A., 2009. The initial stages of template-controlled CaCO3 formation revealed by cryo-TEM. Science, 323(5920), pp.1455-1458.

Pujotomo, M.S. and Sudibyakto, H.A., 2009, February. Coastal changes assessment using multi spatio-temporal data for coastal spatial planning Parangtritis Beach Yogyakarta Indonesia. ITC.

Qabany, A.A. and Soga, K., 2014. Effect of chemical treatment used in MICP on engineering properties of cemented soils. In Bio-and Chemo-Mechanical Processes in Geotechnical Engineering: Géotechnique Symposium in Print 2013 (pp. 107-115). ICE Publishing.

Ramachandran, S.K., Ramakrishnan, V. and Bang, S.S., 2001. Remediation of concrete using micro-organisms. ACI Materials Journal-American Concrete Institute, 98(1), pp.3-9.

Ranasinghe, R. and Turner, I.L., 2006. Shoreline response to submerged structures: a review. Coastal Engineering, 53(1), pp.65-79.

Rangel-Buitrago, N., Williams, A.T. and Anfuso, G., 2018. Hard protection structures as a principal coastal erosion management strategy along the Caribbean coast of Colombia. A chronicle of pitfalls. Ocean & Coastal Management, 156, pp.58-75.

Reitner, B., Herndl, G.J. and Herzig, A., 1997. Role of ultraviolet-B radiation on photochemical and microbial oxygen consumption in a humic-rich shallow lake. Limnology and oceanography, 42(5), pp.950-960.

Reitner, J. and Neuweiler, F., 1995. Supposed principal controlling factors of rigid micrite buildups. Mud Mounds: a Polygenic Spectrum of Fine-grained Carbonate Buildup. Facies, pp.62-64.

Reitner, J., Neuweiler, F. and Gautret, P., 1995a. Modern and fossil automicrites: implications for mud mound genesis. Facies, 32, pp.4-17.

Riding, R., 2006. Microbial carbonate abundance compared with fluctuations in metazoan diversity over geological time. Sedimentary Geology, 185(3-4), pp.229-238.

Rivadeneyra, M.A., Delgado, G., Soriano, M., Ramos-Cormenzana, A. and Delgado, R., 2000. Precipitation of carbonates by Nesterenkonia halobia in liquid media. Chemosphere, 41(4), pp.617-624.

Rodriguez-Navarro, C., Jimenez-Lopez, C., Rodriguez-Navarro, A., Gonzalez-Muñoz, M.T. and Rodriguez-Gallego, M., 2007. Bacterially mediated mineralization of vaterite. Geochimica et Cosmochimica Acta, 71(5), pp.1197-1213.

Rodriguez-Navarro, C., Jroundi, F., Schiro, M., Ruiz-Agudo, E. and González-Muñoz, M.T., 2012. Influence of substrate mineralogy on bacterial mineralization of calcium carbonate: implications for stone conservation. Appl. Environ. Microbiol., 78(11), pp.4017-4029.

Rodriguez-Navarro, C., Rodriguez-Gallego, M., Chekroun, K.B. and Gonzalez-Munoz, M.T., 2003. Conservation of ornamental stone by Myxococcus xanthus-induced carbonate biomineralization. Appl. Environ. Microbiol., 69(4), pp.2182-2193.

Russell, R.J. and McIntire, W.G., 1965. Southern hemisphere beach rock. Geographical Review, 55(1), pp.17-45.

Russell, R.J., 1962. Beach rock: geological observations.

Rutten, G.L., 2011. Interactions between beachrock formations and shoreline evolution. Case study: Togo.

Salifu, E., MacLachlan, E., Iyer, K.R., Knapp, C.W. and Tarantino, A., 2016. Application of microbially induced calcite precipitation in erosion mitigation and stabilisation of sandy soil foreshore slopes: a preliminary investigation. Engineering Geology, 201, pp.96-105.

Sánchez-Navas, A., Martín-Algarra, A., Rivadeneyra, M.A., Melchor, S. and Martín-Ramos, J.D., 2009. Crystal-growth behavior in Ca− Mg carbonate bacterial spherulites. Crystal Growth and Design, 9(6), pp.2690-2699.

Sánchez-Román, M., Romanek, C.S., Fernández-Remolar, D.C., Sánchez-Navas, A., McKenzie, J.A., Pibernat, R.A. and Vasconcelos, C., 2011. Aerobic biomineralization of Mg-rich carbonates: Implications for natural environments. Chemical Geology, 281(3-4), pp.143-150.

Sanz-Rubio, E., Sánchez-Moral, S., Cañaveras, J.C., Calvo, J.P. and Rouchy, J.M., 2001. Calcitization of Mg–Ca carbonate and Ca sulphate deposits in a continental Tertiary basin (Calatayud Basin, NE Spain). Sedimentary Geology, 140(1-2), pp.123-142.

Sarda, D., Choonia, H.S., Sarode, D.D. and Lele, S.S., 2009. Biocalcification by Bacillus pasteurii urease: a novel application. Journal of industrial microbiology & biotechnology, 36(8), pp.1111-1115.

Scheffers, A., Scheffers, S., Kelletat, D. and Browne, T., 2009. Wave-emplaced coarse debris and megaclasts in Ireland and Scotland: boulder transport in a high-energy littoral environment. The Journal of Geology, 117(5), pp.553-573.

Schlager, W., 1981. The paradox of drowned reefs and carbonate platforms. Geological Society of America Bulletin, 92(4), pp.197-211.

Schlager, W., 2005. Carbonate sedimentology and sequence stratigraphy (No. 8). SEPM Soc for Sed Geology.

Schmalz, R.F., 1971. Beachrock formation at Eniwetok Atoll. In Carbonate Cements (pp. 17-24). Johns Hopkins University Press Baltimore, Md.

Scoffin, T.P. and McLean, R.F., 1978. Exposed limestones of the northern province of the Great Barrier Reef. Philosophical Transactions of the Royal Society of London. Series A, Mathematical and Physical Sciences, 291(1378), pp.119-138.

Scoffin, T.P. and Stoddart, D.R., 1983. Beachrock and intertidal cements. Chemical Sediments and Geomorphology: precipitates and residua in the near-surface environment. Academic Press, London, pp.401-425.

Shen, J., Song, Z., Qian, X. and Yang, F., 2010. Carboxymethyl cellulose/alum modified precipitated calcium carbonate fillers: Preparation and their use in papermaking. Carbohydrate Polymers, 81(3), pp.545-553.

Shi, P., Xu, W., Ye, T., Yang, S., Liu, L., Fang, W., Liu, K., Li, N. and Wang, M., 2015. World atlas of natural disaster risk. In World Atlas of natural disaster risk (pp. 309-323). Springer, Berlin, Heidelberg.

Silva-Castro, G.A., Uad, I., Gonzalez-Martinez, A., Rivadeneyra, A., Gonzalez-Lopez, J. and Rivadeneyra, M.A., 2015. Bioprecipitation of calcium carbonate crystals by bacteria isolated from saline environments grown in culture media amended with seawater and real brine. BioMed research international, 2015.

Spanos, N. and Koutsoukos, P.G., 1998. Kinetics of precipitation of calcium carbonate in alkaline pH at constant supersaturation. Spontaneous and seeded growth. The Journal of Physical Chemistry B, 102(34), pp.6679-6684.

Stocks-Fischer, S., Galinat, J.K. and Bang, S.S., 1999. Microbiological precipitation of CaCO3. Soil Biology and Biochemistry, 31(11), pp.1563-1571.

Stoddart, D.R. and Cann, J.R., 1965. Nature and origin of beach rock. Journal of Sedimentary Research, 35(1), pp.243-247.

Strasser, A. and Davaud, E., 1986. Formation of Holocene limestone sequences by progradation, cementation, and erosion; two examples from the Bahamas. Journal of Sedimentary Research, 56(3), pp.422-428.

Strasser, A., Davaud, E. and Jedoui, Y., 1989. Carbonate cements in Holocene beachrock: example from Bahiret et Biban, southeastern Tunisia. Sedimentary Geology, 62(1), pp.89-100.

Surono, B.T. and Sudirno, I., 1992. Peta Geologi Lembar Surakarta-Giritontro. Jawa.(1408-3), Skala1, 100.

Tai, C.Y., Chen, F.B. and Chen, P.C., 1998. Control of polymorphism and morphology of calcium carbonate using a constant-composition method. In World Congress on Particle Technology 3 (p. 1998).

Thompson, R.C.A., 2017. Biology and systematics of Echinococcus. In Advances in parasitology (Vol. 95, pp. 65-109). Academic Press.

Thorne, C., Thorne, C.R., Evans, E.P. and Penning-Rowsell, E.C. eds., 2007. Future flooding and coastal erosion risks. Thomas Telford.

Tobler, D.J., Cuthbert, M.O., Greswell, R.B., Riley, M.S., Renshaw, J.C., Handley-Sidhu, S. and Phoenix, V.R., 2011. Comparison of rates of ureolysis between Sporosarcina pasteurii and an indigenous groundwater community under conditions required to precipitate large volumes of calcite. Geochimica et Cosmochimica Acta, 75(11), pp.3290-3301.

Tourney, J. and Ngwenya, B.T., 2009. Bacterial extracellular polymeric substances (EPS) mediate CaCO3 morphology and polymorphism. Chemical Geology, 262(3-4), pp.138-146.

Van Langerak, E.P.A., Hamelers, H.V.M. and Lettinga, G., 1997. Influent calcium removal by crystallization reusing anaerobic effluent alkalinity. Water Science and Technology, 36(6-7), pp.341-348.

Vousdoukas, M.I., Velegrakis, A.F. and Karambas, T.V., 2009. Morphology and sedimentology of a microtidal beach with beachrocks: Vatera, Lesbos, NE Mediterranean. Continental Shelf Research, 29(16), pp.1937-1947.

Vousdoukas, M.I., Velegrakis, A.F. and Plomaritis, T.A., 2007. Beachrock occurrence, characteristics, formation mechanisms and impacts. Earth-Science Reviews, 85(1-2), pp.23-46.

Wakayama, H., Hall, S.R. and Mann, S., 2005. Fabrication of CaCO 3–biopolymer thin films using supercritical carbon dioxide. Journal of Materials Chemistry, 15(11), pp.1134-1136.

Ward, W.C., 1975. Petrology and diagenesis of carbonate eolianites of northeastern Yucatan Peninsula, Mexico.

Warthmann, R., Van Lith, Y., Vasconcelos, C., McKenzie, J.A. and Karpoff, A.M., 2000. Bacterially induced dolomite precipitation in anoxic culture experiments. Geology, 28(12), pp.1091-1094.

Wei, H., Shen, Q., Zhao, Y., Wang, D.J. and Xu, D.F., 2003. Influence of polyvinylpyrrolidone on the precipitation of calcium carbonate and on the transformation of vaterite to calcite. Journal of Crystal Growth, 250(3-4), pp.516-524.

Wilson, J.L., 1975. Carbonate facies in geologic history: Berlin.

Wolf, K.H., 1965. Gradational sedimentary products of calcareous algae. Sedimentology, 5(1), pp.1-37.

Wong, L.S., 2015. Microbial cementation of ureolytic bacteria from the genus Bacillus: a review of the bacterial application on cement-based materials for cleaner production. Journal of Cleaner Production, 93, pp.5-17.

Xu, H., Ai, L., Tan, L. and An, Z., 2006. Stable isotopes in bulk carbonates and organic matter in recent sediments of Lake Qinghai and their climatic implications. Chemical Geology, 235(3-4), pp.262-275.

Yates, K.K. and Robbins, L.L., 1999. Radioisotope tracer studies of inorganic carbon and Ca in microbially derived CaCO3. Geochimica et Cosmochimica Acta, 63(1), pp.129-136.

Yoshida, N., Higashimura, E. and Saeki, Y., 2010. Catalytic biomineralization of fluorescent calcite by the thermophilic bacterium Geobacillus thermoglucosidasius. Appl. Environ. Microbiol., 76(21), pp.7322-7327.

Yu, H.Q., Tay, J.H. and Fang, H.H., 2001. The roles of calcium in sludge granulation during UASB reactor start-up. Water Research, 35(4), pp.1052-1060.

Zanuttigh, B. and Angelelli, E., 2013. Experimental investigation of floating wave energy converters for coastal protection purpose. Coastal Engineering, 80, pp.148-159.

Zhang, K., Douglas, B.C. and Leatherman, S.P., 2004. Global warming and coastal erosion. Climatic change, 64(1-2), p.41.

Zhu, X., Linham, M.M. and Nicholls, R.J., 2010. Technologies for climate change adaptation-Coastal erosion and flooding. Danmarks Tekniske Universitet, Risø Nationallaboratoriet for Bæredygtig Energi.

CHAPTER 2

Geophysical investigation of buried beachrock at Krakal-Sadranan beach, Yogyakarta, Indonesia

2.1 Introduction

The human evolution always coincides with environmental change, and human activities can be directly attributed to environmental degradation. Indonesia is the world's largest archipelagic state, consists of 18,108 islands where approximately 60% of the population lives within 50 km from the coast (Cribb and Ford, 2009a, b). Indonesia is an archipelago country whose coastline is the fourth largest in the world after the United States, Canada, and Russia respectively. As one of the countries with the longest coastline, Indonesian beaches have their quirks and issues. As compounding effects and conflicts arise in a complex, emergent and cross-scaled impact manner, a manifold of change drivers (e.g. climate change, urbanization, tourism development, and marine resource exploitation) may be at fault (Zhu, et al., 2010; Wilson, et al., 2011; Pilkey and Cooper, 2014). Beachrock (Figure 2.1) is an important feature of many tropical coastlines as it appears to have an anchoring effect for dynamic islands and provides protection from erosion. Yet, many things about its origin and properties remain unknown or debated hitherto. Outcrops of beachrock sediment are valuable records of the past climate of low-lying reef islands, despite the application beachrock sediment as an indicator of paleo-environment in the Pacific is still underdeveloped (Vousdoukas et al., 2007). Coastal zone monitoring based on aerial data, satellite or field investigating is an important task in environmental protection and fundamental coastal management. Datasets produced by UAVs have such a high spatial resolution of the characteristics and changes of the landscape, such as morphology, coastal zone, and beach morphological characteristics into two dimensions (2D) or three dimensions (3D) numerical models (Darmawan, et al., 2018). The beachrocks are sediments formed as a result of calcium carbonate cementation in coastal sediments especially around the tidal zone, generally found in the tropics and subtropics area and mostly warm seawater (Avcıoğlu et al., 2016). Beachrock is a crucial element in tropical coastal environments, mainly for its retaining effect on dynamic islands and its protecting properties that prevent erosion in coastlines (Vousdoukas et al., 2007; Danjo and Kawasaki, 2014). Beachrock studies are not only themed around its formation characteristics, but also on related topics such as ecology of beachrock process occurs at lower latitudes (as noted in Turkey,

Bangladesh, Scotland, Japan, Greece, the Great Barrier Reef of Australia, Sri Lanka, Bahamas Island, Brazil, South Africa, Indonesia and in Florida of the United States) (Danjo and Kawasaki, 2014; Daryono, et al., 2019). Linear beachrock outcrop on the continental shelf shows that it can promote the preservation and overstep of shoreline sediments during transgression, particularly during meltwater pulses (Cooper, et al., 2016).

Similarly, beachrocks in that area have also never been a subject of study in any of the past researches. The beachrocks found on Krakal-Sadranan Beach were spread locally, parallel to the coastline with a coverage of around 10-30 m^2. The most widely held theory of beachrock formation involves the deposition of $CaCO_3$ between coral sand and gravel by evaporation of seawater (Kubo, et al, 2014). There has been numerous domestic and foreign literature on beachrocks, but most only emphasized its geochemistry aspects. Meanwhile, its underground structure in particular, is not yet well understood. One of the few studies of this was by Psomiadis, who used electrical resistivity tomography to map the beachrock on the island of Thassos, Greece (David, et al., 2009). On a separate case, a direct current (DC) electrical survey

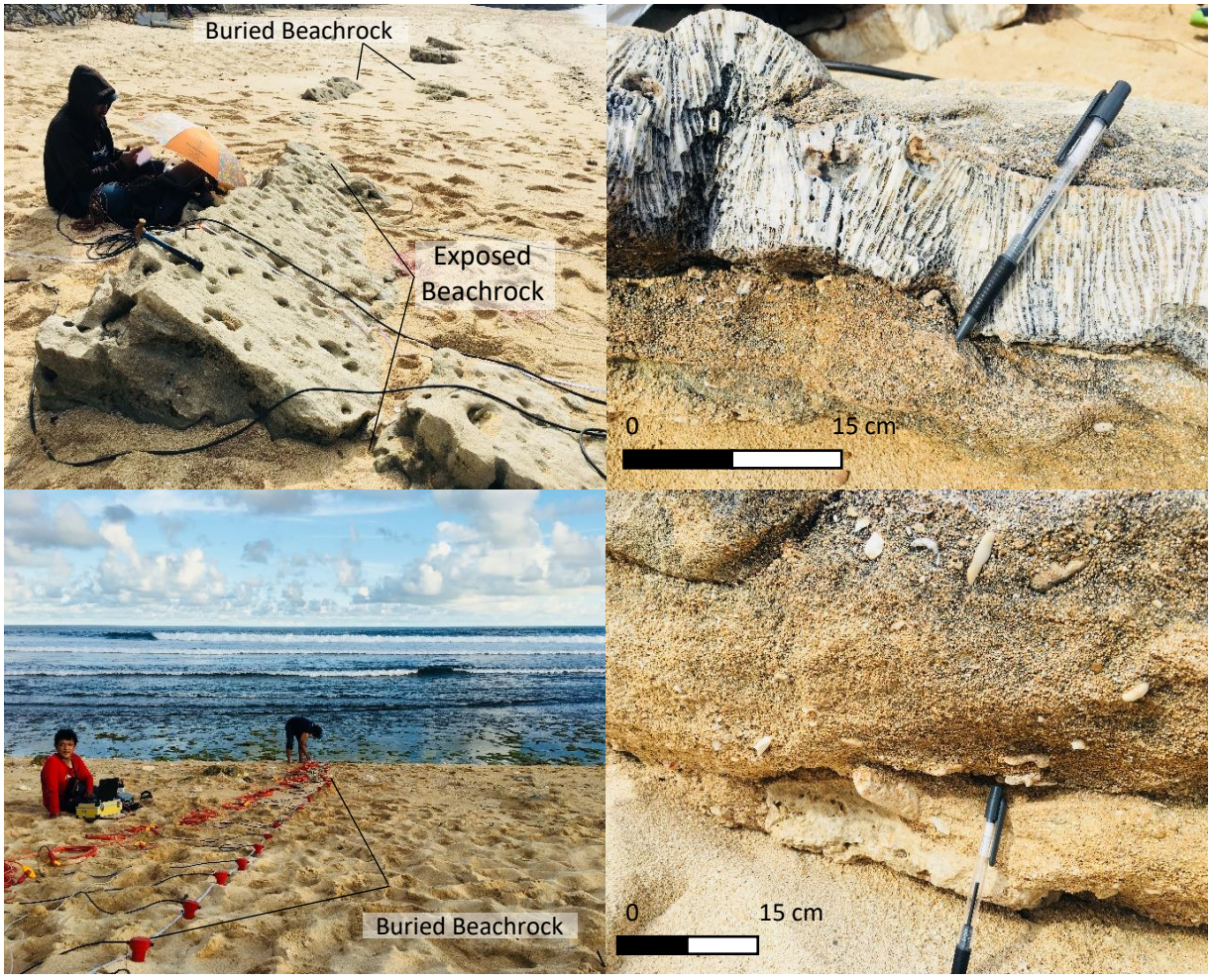


Figure 2.1. Beachrock deposits in Krakal-Sadranan, Yogyakarta, Indonesia.

and a seismic surface wave were conducted to obtaining the structure around the seashore to a depth of more than 10 m as the result (Kubo, et al., 2014). The geophysical measurement not only conclude the subsurface structure but within combination with unmanned aerial vehicle (UAV) drone also summarize the 3D model of subsurface and determine of beachrock deposition for more further tectonic propagation in Indonesia based on this deposit. The lack of reports in the tropical regions may be related to lack of relevant research. Beachrocks that are found in the Krakal-Sadranan Beach, Yogyakarta (Figure 2.1) are spread locally, parallel to the coastline and with a width of about 10-30 m^2. The south coast of Java has been known for large waves from the open Indian Ocean, causing a highly intensive process of abrasion, which made Krakal-Sadranan Beach a very intriguing subject to examine of its characteristics.

2.2 Regional geology

An understanding of the natural parameters and the interactions of beachrock requires an analysis of the genesis of all forms of beachrock. Figure 2.2 shown the stratigraphic of study area, included in the Wonosari - Punung Formation of the Surakarta sheet - Giritontro (Surono and Sudarno, 1992).

2.2.1 *Physiography*

Van Bemmelen (1949) divided eastern Java and Madura into 7 physiographic zones, namely the Southern Mountain Zone, Solo Zone, Kendeng Zone, Randublatung Zone, Rembang Zone, Alluvial Plain of North Java, and Quaternary Volcano. Of the seven zones, the zone most relevant to the research area is the Southern Mountains Zone. The Southern Mountains Zone is a block that is raised and tilted to the south. This zone stretches from Parangtritis Beach to the west to Blambangan Peninsula in the east. The Southern Mountains zone is bordered by complex swamps in the north and Indian Ocean in the south. The width of the South Mountain Zone is around 25 km (south of Blitar) to 55 km (south of Surakarta) (Van Bemmelen, 1949). Van Bemmelen (1949) divided the Southern Mountains Zone into 3 sub-zones, namely the North Subzone, Central Subzone, and the South Subzone. The North Subzone is a mountainous lane composed of strong-strength volcanic rocks, consisting of the Baturagung lane, the Stage lane, the Plopoh lane, and the Kambengan lane. Central Subzona is a plateau in the area of Wonosari and Baturetno. The South Subzona is composed of limestones that form the Kars landscape or commonly referred to as Gunung Sewu. The Gunung Sewu subzona is bordered in the south and is directly adjacent to the Indian Ocean. Meanwhile, Gunung Sewu Subzone in the north is bordered by Wonosari Basin, Baturetno Basin, and Stage

lane. The Sewu Mountain subzone is dominated by carbonates from the Wonosari-Punung Formation which form the hills of the southeast with the orientation of the southeast - west northwest. Referring to the zone division and subzone, the research area can be categorized in the Southern Mountain Subzone, southern part of Sewu Mountain.

2.2.2 *Stratigraphy*

According to Toha et al. (1994), the regional Southern Stratigraphy from the old to the young are Kebo-Butak Formation, Besole Formation, Mandalika Formation, Semilir Formation, Nglanggran Formation, Sambipitu Formation, Oyo Formation, Jaten Formation, Wuni Formation, Nampol Formation, Wonosari-Punung Formation and Kepek Formation (Figure 2.2). Referring to Toha et al. (1994) and on the regional geological map of Surakarta - Giritontro (Surono et al., 1992), rock formations associated with conditions on Sradanan Beach and its surroundings are the Wonosari - Punung Formation. This formation is composed of 2 facies, namely carbonate facies and clastic facies. Carbonate facies are composed of reef limestones, bioclastic limestones, sandstone limestone, and marl. Carbonate facies is deposited in the exposure environment at Middle Miocene - Late Miocene (N9 - N16). The clastic facies are composed of tuff-sandstones, side sandstones, siltstone and shale. Clastic facies of Late Miocene (N15) and deposited in external neritic metric (Sartono, 1964).

2.2.3 *Geological structure*

According to Sudarno (1997), the geological structure that developed in the Southern Mountains consists of 4 patterns, namely the Meratus pattern, Sundanese pattern, Javanese pattern, and Meratus antithetic pattern. The Meratus antithetic pattern is a group of geological structures that have a northwest-southeast orientation. These structures are mostly in the form of a deformed shear fault formed by compression forces at the age of Pliocene. While referring to the Surakarta - Giritontro map (Surono et al., 1992), no regional geological structure developed affected the study area.

2.2.4 *Geology of the research area*

The research area is located on the South coast of Java Island. When referring to the regional geological map of the Surakarta - Giritontro (Surono, et al. 1992) sheet (Figure 2.2), which has a scale of 1: 100,000, the study area is mapped as part of the Wonosari-Punung Formation. If you look at the position of the research area on the map, the landscape in the research area can be categorized as a coastal landscape. Whereas based on the geological

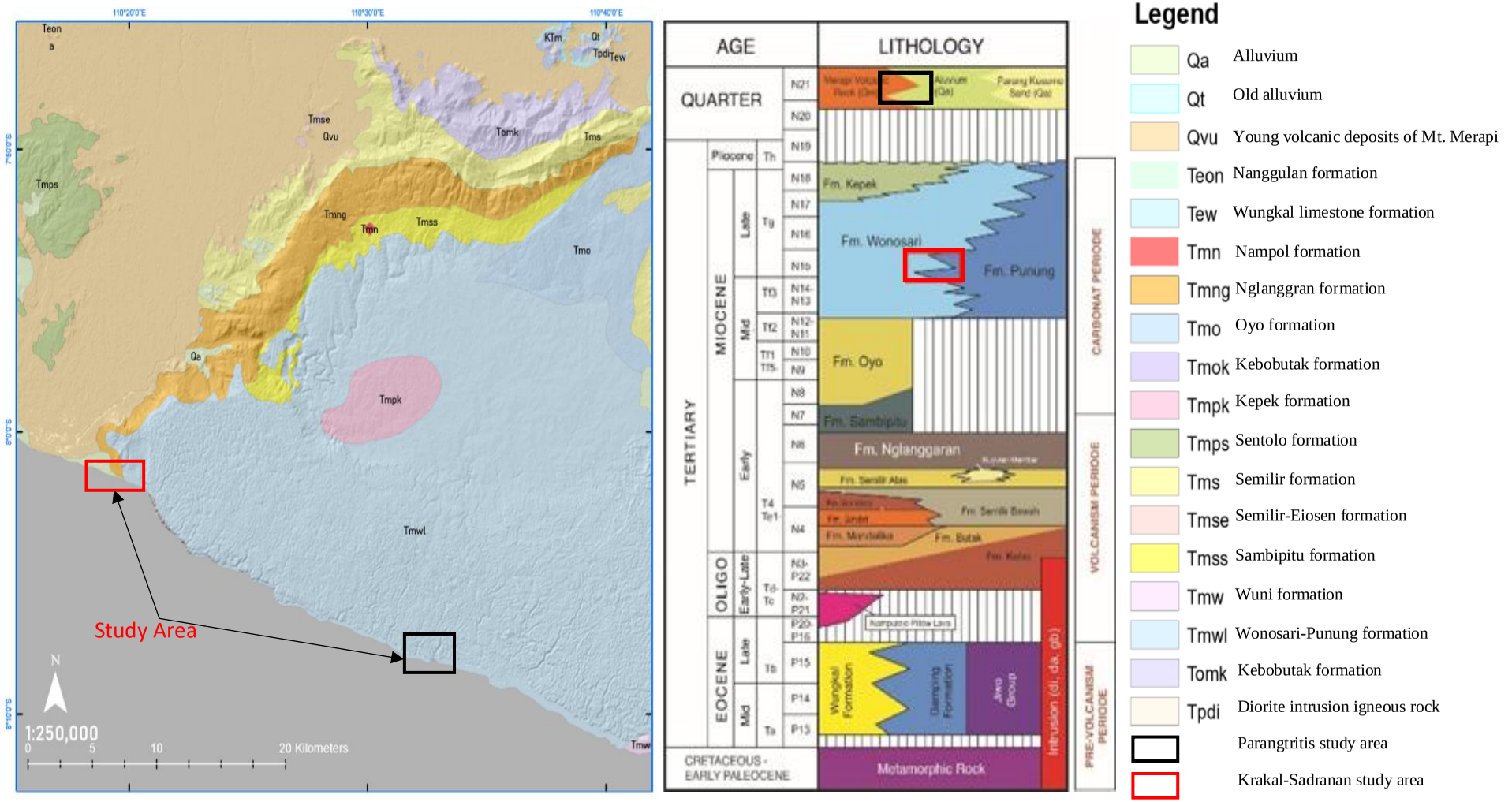


Figure 2.2. Geological map and stratigraphy of Yogyakarta, Indonesia.

structure patterns in Figure 2.2, no visible geological structure developed in the study area. Therefore, the landscape in the study area can be categorized as a coastal landscape. Whereas based on geological structure patterns from coastal geomorphology in South Java, there is no geological structure that develops in the study area (Verstappen, 2000). On other hand, Yogyakarta also consist by recent sedimentation of Merapi Volcano on the middle part (Graben Bantul) and several smaller parts in the form of Sentolo formation hill on the western part, Aluvium formation, Andecite (Baturagung), Semilir formation, Kepek, and Nglangran on the eastern part. Physiographycally, the landscape consists of the Merapi fluvio-volcanic plain, the Baturagung Mountain Range, the Sentolo Hills Range, Progo River plain and the shore plain. Bantul region which is consist of volcanic sedimentary is potential of coastal disaster then eastern part were consist (mostly) limestone formation. Blackish silica sands were consisting along the Parangtritis shoreline with the elevation of 0-35 m can be found especially in the southern part which bordered directly by Indian Ocean.

2.2.5 *Site study*

The Wonosari-Punung Formation has been the subject of many geological studies, including studies on the development of the Wonosari Formation in the Miocene era (Lokier, 2000), the reef facies of the Wonosari Formation (Siregar et al., 2004), the stratigraphic sequences and diagenesis of the Wonosari Formation carbonate rocks (Jauhari and Toha, 2005), the environmental deposition of carbonate rocks in the Wonosari Formation in the eastern region of Pacitan (Mukti et al., 2005), Puno-reef Punung (Premonowati et al., 2012), the red limestone Wonosari-Punung Formation in Ponjong area (Titisari and Atmoko, 2015; Atmoko et al., 2016), and the red limestones of Wonosari-Punung Formation on Siung beach (Titisari and Hendrawan, 2017). However, research on beachrocks found on the Sadranan Beach in the Wonosari-Punung Formation has never been the subject of a geological research. Beaches of Gunungkidul Regency, Province of Special Region Yogyakarta (Prov. DIY), Indonesia holds strong economic potentials for limestone mine deposits and as a tourist attraction. The karst beaches in the Gunung Kidul Regency, such as Sadranan Beach for one, have similarities in terms of geological conditions, methods, and geomorphologic processes beach formation. The characteristics of the Karst Mountains of South Beach indicate steep topography that rises to the east of Java Island (Drini Beach to Krakal to Sadranan). The coast of Sadranan has a slope with a steepness of ~12,33° with the tidal range of 12 meters that makes the sedimentary process in this coast thicker than the deeper slope. Grains of sediment along Krakal and Sadranan beaches are largely bright-colored along most of the coastline as a result

of the erosion of seabed being deposited on the beach. Composition of this sediment is mainly formed by coral, skeletal fragment, Foraminifera and Mollusca. Throughout the karst coast of the DIY Prov., Gunungkidul Regency the soil is derived from limestone bedrock, similar to the Mediterranean, i.e., the level of physical weathering is high (Daryono, et al., 2019). The research area is located on the south coast of Java Island. When referring to Surakarta's regional geological map - Giritontro (Surono, et al. 1992) with a scale of 1: 100.000, the study area is part of the Wonosari-Punung Formation (Figure 2.2). Therefore, the landscape in the study area can be categorized as a coastal landscape. Meanwhile, looking at the geological structure patterns of the coastal geomorphology in South Java, there is no geological structure that develops in the study area (Verstappen, 2000).

2.3 Objectives

This research will address: to (i) examine the underground structure of natural beachrock based on a geophysical survey, (ii) develop a 3D beachrock structure, and (iii) identify the physical and mechanical properties such as porosity, P wave velocity (Vp), S wave velocity (Vs), and strength characteristics of beachrock. To comprehend the underground structure with UAV drone photogrammetric overlay toward categorize the beachrock deposit as keyrole of beach propagation in the tropical-rapid weathering area, especially in term of tectonic plate and climate change. This research is considering beachrock as primary study to mimicking the natural countermeasures of coastal problem especially erosional impact for development in shoreline area.

2.4 Materials and methods

2.4.1 Field investigation

The field investigation was obtained from Krakal-Sadranan Beach area, Wonosari, Yogyakarta, Indonesia, within correlation check with regional geology control and sedimentary process in the section. The beachrock outcrops were found in the section and then divided into three sections (Figure 2.3). The first section (α) is located in the E 455900.11; S 9099654.13; there were three lines of both geophysical measurements conducted. The second section (β) is located in E 456041.31; S 9099631.61 and two lines of resistivity and surface seismic measurement in this section were conducted. The last section (γ) is in the E 456281.51; S 9099623.03 and conducted only one line in the outcrop of beachrock deposit. The azimuth

degree of this measurement in general are N334°E which is across to the shoreline beach and N164°E which is linear with the shoreline. The detailed location of this study is shown in the Table 2.1.

Table 2.1. Coordinates of survey line.

Conditions	α-location		
	Line-1	Line-2	Line-3
GPS (49L) (DC Resistivity) Electrode interval Line length	(455905.11 E; 9099638.01 S) – (455900.11 E; 9099654.13 S) 1 m 18 m	455914.28 E; 9099644.16 S) – (455847.36 E; 9099623.57 S) 1 m 70 m	455864.19 E; 9099624.79 S) – (455859.21 E; 9099641.04 S) 1 m 18 m
(Surface wave survey) Shot point Interval Line length	0.5 m 22 m	0.5 m 75 m	0.5 m 22 m
	β-location		γ-location
	Line-4	Line-5	Line-6
GPS (49L) (DC Resistivity) Electrode interval Line length	456041.31 E; 9099631.61 S) – (456042.79 E; 9099653.50 S)	456061.16 E; 9099644.31 S) – (456026.50 E; 9099645.36. S)	456281.51 E; 9099623.03 S) – (456275.66 E; 9099643.05 S)
	1 m 22 m	1 m 35 m	1 m 21 m
(Surface wave survey) Shot point Interval Line length	0.5 m 20 m	0.5 m 32 m	0.5 m 3 m

2.4.1.1 Drone photogrammetric data processing

Aerial photos were obtained from selected sites in Krakal–Sadranan Beach (Appendixes A). In this case, a GoPro HERO 6 camera attached to a DJI Phantom 3 and equipped with a 3D gimbal to minimize shaking was used for the drone photogrammetry. The Agisoft software was used to evaluate surface changes and conduct spatial analysis such as geomorphological surfaces of south Yogyakarta shoreline (Figure 2.3; Appendixes Figure A5; Appendixes Figure A7). Identification of the shoreline differences based on interactive 3D geospatial data find was conducted and compared with the literature information (Brown and Arbogast, 1999; Varela-González, et al., 2013). Further study may conclude the propagation of the intertropical shoreline based on beachrock role by comparing the data from this research with present geospatial data.

2.4.1.2 Geological identification

Fieldwork was carried out by making a ditch or horizontal section at several sections along the coastline in the study area (as deep as <1 m), extended laterally towards the sea, then sampled and mapped lithology facies in each ditch for analysis. In each section that has been

dug up, 19 samples were taken based on the horizontal and vertical position. Sampling were decided based on the presence of beachrock along the trench. Then, from each sampling point, lithology facies mapping was carried out based on rock composition on the samples taken. Laboratory analysis carried out in this study included petrographic analysis, which aimed to determine the texture and type of mineral constituent rocks. The section field investigation was obtained from Krakal-Sadranan Beach area, Wonosari, Yogyakarta, Indonesia, within correlation check with regional geology control and sedimentary process in the section. The study section is located around E 455900.11; S 9099654.13 to E 456281.51; S 9099623.03, 49 S Indonesia region. The azimuth degree of beachrock deposit, in general, are N334°E which is across to the shoreline beach and N164°E which is linear with the shoreline.

2.4.1.3 DC resistivity survey

Geophysical resistivity techniques are based on the Earth's response to the flow of electrical current to determine the rock body of beachrock based on resistivity behavior of rock and mineral. By applying these methods, an electrical current is passed through the ground and two potential electrodes allow us to record the resultant potential difference between them, giving us a way to measure the electrical impedance of a subsurface material. The beachrock body, in dimensional length and height will gave the assumption regarding the sedimentary process and this deposit works as natural wave barrier in the shoreline area. The apparent resistivity is then a function of the measured impedance (ratio of potential to current) and the geometry of the electrode array. Comprehensive overviews of resistivity methods are presented in Telford (1976) and Burger (1996).

The current flow lines and the equipotential lines will form an even more complex pattern as the current flow lines will bend at boundaries, where the resistivity change. Geoelectrical data are commonly expressed as apparent resistivity (Telford, 1976):

$$\rho_A = \frac{\Delta V}{I} K \qquad \text{(Eq. 2.1)}$$

where ΔV is the measured potential, I the transmitted current, and K the geometrical factor expressed as:

$$K = 2\pi \left[\frac{1}{|r_A - r_M|} - \frac{1}{|r_A - r_N|} - \frac{1}{|r_B - r_M|} + \frac{1}{|r_B - r_N|} \right]^{-1} \qquad \text{(Eq. 2.2)}$$

If there are two current (source) electrodes, the potential is the superposition of the effects from both. In a practical experiment (figure 2.4), one electrode, *A*, is the positive side of a current —

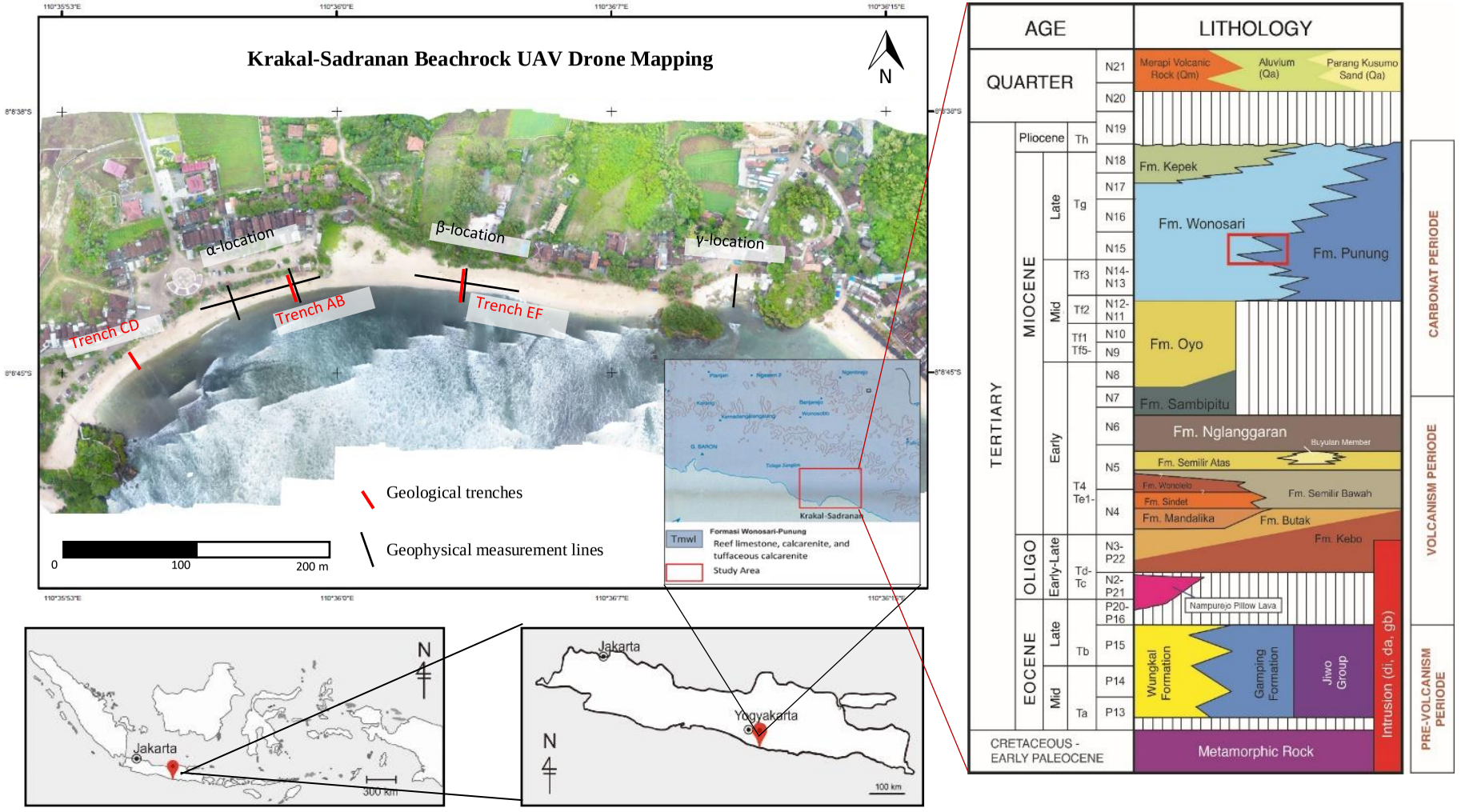


Figure 2.3. Location research area in Krakal-Sadranan, Yogyakarta, Indonesia.

source, and the other electrode, *B*, is the negative side. The current into each electrode is equal, but of opposite sign. For a practical survey, we need two electrodes to measure a potential difference. These are *M*, the positive terminal of the voltmeter (the one closest to the *A* current electrode), and N, the negative terminal of the voltmeter. The measured voltage is a potential difference (V_M - V_N) in which each potential is the superposition of the effects from both current sources. The apparent resistivity is defined so that it is equal to the true resistivity in a homogeneous half-space (Telford, 1976).

In this survey, we used *Syscal Junior (IRIS Instrument)* within a 1-meter space of electrode interval. The spikes as electrodes (about 5 mm in diameter and 15 cm in length) were driven with a hammer to a depth of about ~10 cm in the outcrop of beachrocks along the shoreline. There were 22 electrodes along line-1, 73 electrodes along line-2, and 21 electrodes along line-3 that represented α-section. As for β-section, it was described with line-4 within 26 electrodes and line-5 with 39 electrodes. However, γ-section was only represented by line-6 with 25 electrodes (Figure 2.4).

2.4.1.4 MASW (Multi Analysis of Seismic Surface)

The multichannel analysis of surface waves (MASW) method tries to utilize this dispersion property of surface waves for the purpose of Vs profiling in 1D (depth) or 2D (depth and surface location) format. Essentially, it is an engineering seismic method that deals with frequencies in a few tens of Hz (e.g., 3-30 Hz) recorded by using a multichannel (24 or more channels) recording system and a receiver array deployed over a few to a few hundred meters of distance (e.g., 2-200 m). The active MASW method generates surface waves actively through an impact source like a sledgehammer, whereas the passive method utilizes surface waves generated passively by cultural (e.g., traffic) or natural (e.g., thunder and tidal motion) activities. The investigation depth is usually shallower than 30 meters with the active method, whereas it can reach a few hundred meters with the passive method. The multichannel analysis of surface waves (MASW) method tries to utilize this dispersion property of surface waves for the purpose of Vs profiling in 1D (depth) or 2D (depth and surface section) format (Figure 2.4).

The equipment for analysis MASW and seismic refraction were identical, we used *Doremi Seismograph* (SARA Instrument) with 24 geophone channels in 2 wireline cables. This measurement utilized the same procedure as DC Electricity. Therefore, the resulting data can be compared and reinforced between one another. The geophones, 24 channels (4.5 Hz) were

deployed along each line (overlaying with resistivity line) at 0.5 m intervals. The source point is located 1.0 ~2.0 meter from the rear geophone in the direction against the movement. The ends of the survey lines were measured by shifting only the source point and also two-times recording in the start-ends lines, each line, both methods used active and passive seismic to minimize the noise from natural source or other factors. Assuming that the study site is multilayered, the dispersion curve of the phase velocity obtained in this survey were analyzed by 1D inversion technique using *SeismicImager* SW (OYO Corp., Japan).

2.4.1.5 Seismic refraction

One can study subsurface velocity and layer interface structure by analyzing the first arrival times of P-waves (longitudinal or compressional waves) at the surface of the earth. This technique is called seismic refraction. P-waves traveling through rock are analogous to sound waves traveling through air. The speed of a P-wave propagates through a medium depends on the physical properties (i.e. rigidity, density, saturation) and degree of homogeneity of the rock. From Snell's Law, a ray path is dependent on the wave velocities through different layers. In refraction seismology, the critical angle is the most important angle value to understand (Burger, 1996; Fowler 1990).

In this survey, the seismic refraction was conducted with the same instrument that as mentioned in the MASW methodology. The intervals obtained is the same as MASW methods and processed the data manual using *Microsoft Excel* based on Snell's Law calculation from the time arrival data (first break signal). Picking the first break (*GeoGiga Software*) is conducted to determine the propagation time received by each geophone from energy using seismic sources. Picking data is relatively tricky, especially for data whose noise level is high enough. The results are 2D layered data that represent subsurface model by using seismicity of rocks.

2.4.2 Laboratory tests

Further analysis, the beachrock sample will investigating inside laboratory to identify the rock properties and strength of the sedimentary mechanism as parameter to develop artificial beachrock. For laboratory tests, beachrock samples were gathered at two points: one about 0 m east from the western edge of the α-line (Sample 1), and the other between the β and γ-line of the beachrock outcrop (Sample 2). The samples were then brought to the laboratory and trimmed into rectangular parallelepipeds with a rock-cutting machine. Sample 1 was 3 cm

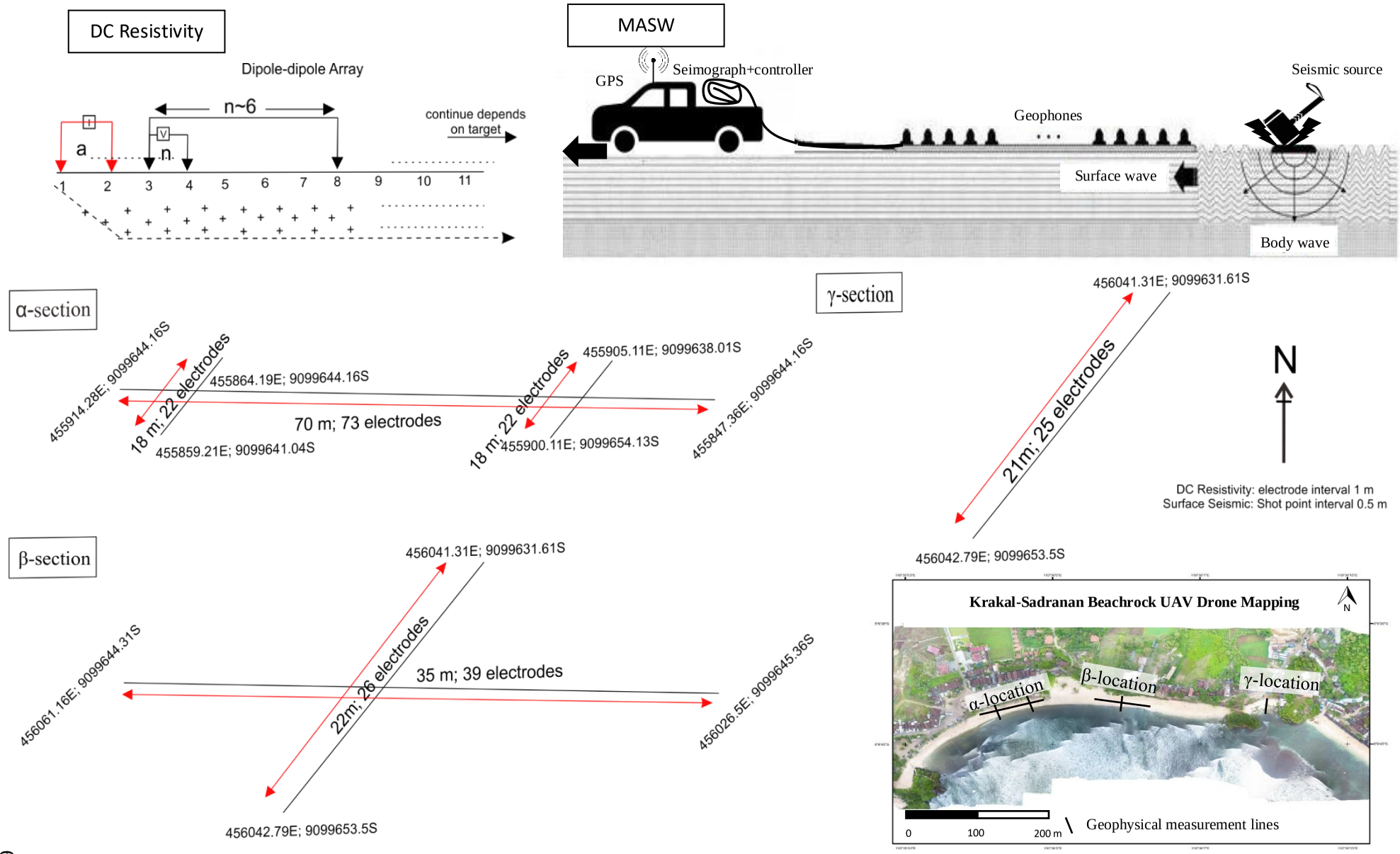


Figure 2.4. Schematic of acquisition plan.

diameter x 6 cm length and Sample 2 is the same size for coring. First, the specimens were soaked in artificial sea water (Aquamarin: Yashima Pure Chemicals Co., Japan) for 24 h in a vacuum. Then, the specimens were tested for P-wave velocity, S-wave velocity and mass during a natural evaporation at room temperature (25°C). Once the evaporation process slowed down, the tests were continued while the specimens were heated to and held at 40°C in a constant-temperature drying oven. Finally, tests were concluded with the specimens heated to 110°C for 24 h. Three times at each water content, the saturated density of the specimen was measured by the *Test Method for Bulk Density of Rock* and twice at each water content, the P- and S-wave velocities were measured (SonicViewer-SX; OYO Corp., Japan).

Compressional wave velocity (P-wave velocity) and shear wave velocity (S-wave velocity) were measured at room temperature and ambient pressure on cylindrical samples with a diameter of around 2.5 cm and a length of up to 3.5 cm cut from the blocks with frequencies of 500 kHz. The velocity of an ultrasonic wave in rock samples is related to its elastic coefficients, internal structure and density. Moreover analysis, the typical shear wave velocities of the soil states, ages, and behavior were compared to aid the design of the triaxial testing program. Target shear wave velocities, Vp and Vs, were chosen to represent the following different soil states, ages, and behavior of material (Montoya and DeJong, 2015; Feng and Montoya, 2017). Sample of beachrock from natural and artificial also identify the strength and stress with axial unconfined compression test (UCS).

2.5 Results

An understanding of the natural parameters and the interactions of characteristics beachrock requires an analysis of the genesis of all forms. An understanding of the natural parameters and the interactions of beachrock requires an analysis of the genesis of all forms of beachrock. Various case studies were conducted based on Krakal-Sadranan Beach rock samples, Yogyakarta, Indonesia. Final achievement for this research is establish the zonation of beachrock sediment deposit for keyrole of natural barrier and beach propagation in the tropical area.

2.5.1 Lithostratigraphy of Krakal-Sadranan beachrock

Lithostratigraphy and petrography analyses are important tools for the reconstruction of depositional environments and the interpretation of coastal evolution. The most common palaeontological analysis objects include mollusks, foraminifera skeletal fragments, mineral

and other rock fragments. Petrographic observations showed that Krakal-Sadranan beachrocks were composed by several compositions, namely skeletal fragments which were dominated by fossils of foraminifera *Baculogypsina sphaerulata*, calcite, aragonite minerals, micrite, and sparite cement, respectively. Identifications of rock sample shows that abundance of coarse coral sand size with the composition of limestone and skeletal fragments decreased at α-location. It could be assumed that the reducing of limestone and skeletal fragments in the western area of Sadranan beach is caused by intensive abrasion process, therefore no chance for the fragments to be deposited more. Calcareous sand deposit shows whitish yellow colour, grain size of 2 mm fragments and 1 mm matrix, subangular grain shape, unconsolidated, with thickness of 70 cm, respectively. It consists of limestone fragments, skeletal fragments dominated by *Baculogypsina sphaerulata*, and matrix of calcareous sand grain. In order to reconstruct the palaeoenvironmental changes in the study area, macrofossils were recorded and identified as well as Baculogypsina sphaerulata foraminifera (Figure 2.5). The detailed explanation of measurement stratigraphic is on Appendixes B1-B9.

2.5.1.1 Trench AB

It has coordinates of 455863 E/ 9099624 S with dimensions of 5 m in length, 1 m in width, and 1 m in depth. Stratigraphic columns that have been made in the Trench-AB (Figure 2.5) include stratigraphic columns for ABX_1 and ABX_2 samples (Appendix B1), stratigraphic columns for ABY_1 and ABY_2 samples (Appendix B2), and stratigraphic columns for ABZ_1 and ABZ_2 samples (Appendix B3).

(a) Stratigraphic columns for ABX_1 and ABX_2 samples (Appendix B1).

- Carbonate sand deposits (ABX_1)

  Whitish yellow, fragment 2 mm in size and 1 mm base mass, subangular, unconsolidated grain shape, and 80 cm thick. The identification of ABX_1 sample showed the composition of limestone fragments (30%) and fossil shell material (35%) which were dominated by *Baculogypsina sphaerulata*, limestone sand material (35%).

- Sparse biomicrite (Folk, 1962) (ABX_2)

  Whitish yellow, 4 mm fragment size and base mass <1 mm, subangular grain shape, open container, massive structure, about 20 cm in thickness. Identification of L-F samples showed the composition of limestone fragments (10%) and fossil shell material (20%),

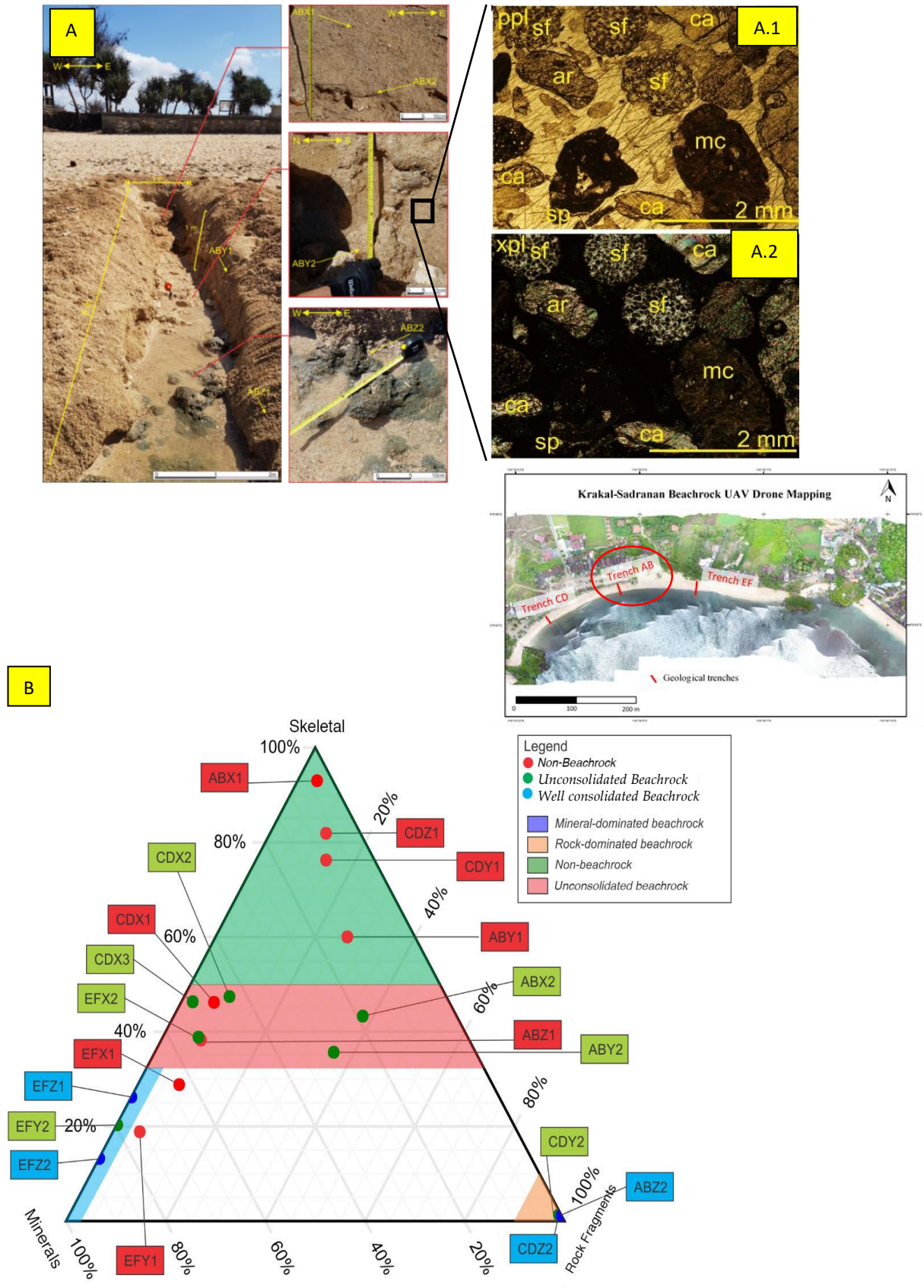


Figure 2.5. Stratigraphic of the Trench AB: (A) Petrographic on cross polarized nicol (XPL, A1) and plane polarized nicol (PPL, A2) with sf (skeletal fragment), mc (micrite), sp (sparite), ca (calcite) and ar (aragonite); (B) Degree of cementation based on composition of beachrock.

which were dominated by *Baculogypsina sphaerulata*, calcite minerals (30%) and limestone sand material (40%).

(b) Stratigraphic columns for ABY_1 and ABY_2 samples (Appendix B2):

- Carbonate sand deposits (ABY_1)

  Whitish yellow, fragment 2 mm in size and 1 mm base mass, subangular, unconsolidated, and 75 cm thick. The identification of ABY_1 sample showed the composition of limestone fragments (25%) and fossil shell material (45%) which were dominated by *Baculogypsina sphaerulata*, limestone sand material (30%).

- Sparse biomicrite (Folk, 1962) (ABY_2)

  Whitish yellow, fragment 4 mm and base mass <1 mm, subangular grain shape, open container, massive structure, about 25 cm in thickness. Identification of ABY_2 sample showed the composition of limestone fragments (15%) and fossil shell material (15%), which were dominated by *Baculogypsina sphaerulata*, calcite minerals (35%) and limestone sand material (35%).

(c) Stratigraphic columns for samples ABZ_1 and ABZ_2 samples (Appendix B3):

- Carbonate sand deposits (ABZ_1)

  Carbonate sand deposits show whitish yellow, 2 mm fragments and 1 mm matrix, subangular, unconsolidated grains with thickness of 70 cm. ABZ_1 samples were taken at these layers. The sample constituents are limestone fragments (30%) and fossil skeletal shell material (40%) which are dominated by *Baculogypsina sphaerulata*, limestone sand material (30%).

- Sparse biomicrite (Folk, 1962) (ABZ_2)

  The layer below the sand deposit has been well consolidated with a layer about 30 cm in thickness, showing whitish yellow, measuring 4 mm fragments and a base mass of less than 1 mm, subangular grain shape, open container, massive structure. In this layer ABZ_2 samples were taken. Identification of ABZ_2 samples showed samples composed of limestone fragments (10%) and fossil shell material (20%) which were dominated by fossils of foraminifera *Baculogypsina sphaerulata*, calcite minerals (40%) and limestone sand material (30%).

(d) Petrographic analysis trench AB

Petrographic observations showed that Krakal-Sadranan beachrocks were composed by several compositions, namely skeletal fragments which were dominated by fossils of foraminifera *Baculogypsina sphaerulata*, calcite, aragonite minerals, micrite, and sparite cement, respectively. Composition diagrams of all samples in the trench AB were categorized into three types of samples, namely non-beachrocks, unconsolidated beachrocks, and well-consolidated beachrocks. ABX_1 samples have shells > 80%; minerals and rock fragments <10%; and are classified as non-beachrocks. ABX_2 samples have 45% shell content, 20% minerals, and 40% rock fragments. Sample ABZ_2 samples have 2% shell content, 2% mineral content, and over 90% rock fragments.

2.5.1.2 Trench CD

The CD trench has coordinated of 455813 E/ 9099697 S, located on the west side of the trench AB, with dimensions of 5 m in length, 1 m in width, and 1 m in depth (Figure 2.6). Stratigraphic columns that have been made in CD trenches include stratigraphic columns for CDX_1, CDX_2 and CDX_3 samples (Appendix B4), stratigraphic columns for CDY_1 and CDY_2 samples (Appendix B5), and stratigraphic columns for CDZ_1 and CDZ_2 samples (Appendix B6).

(e) Stratigraphic columns for samples CDX_1, CDX_2 and CDX_3 samples (Appendix B4).

- Carbonate sand deposits (CDX_1 samples)
  Whitish yellow, 2 mm fragment size and 1 mm base mass, subangular, unconsolidated grain shape, with a thickness of 40 cm. The identification of CDX_1 samples showed the composition of limestone fragments (20%) and fossil shell material (35%) which were dominated by *Baculogypsina sphaerulata*, limestone sand material (45%).

- Sparse biomicrite (Folk, 1962) (CDX_2)
  Whitish yellow, 4 mm fragment size and base mass <1 mm, subangular grain shape, open container, massive structure, thickness of about 30 cm. Identification of L-L samples showed the composition of limestone fragments (15%) and fossil shell material (15%), which were dominated by *Baculogypsina sphaerulata*, calcite minerals (40%) and limestone sand material (30%).

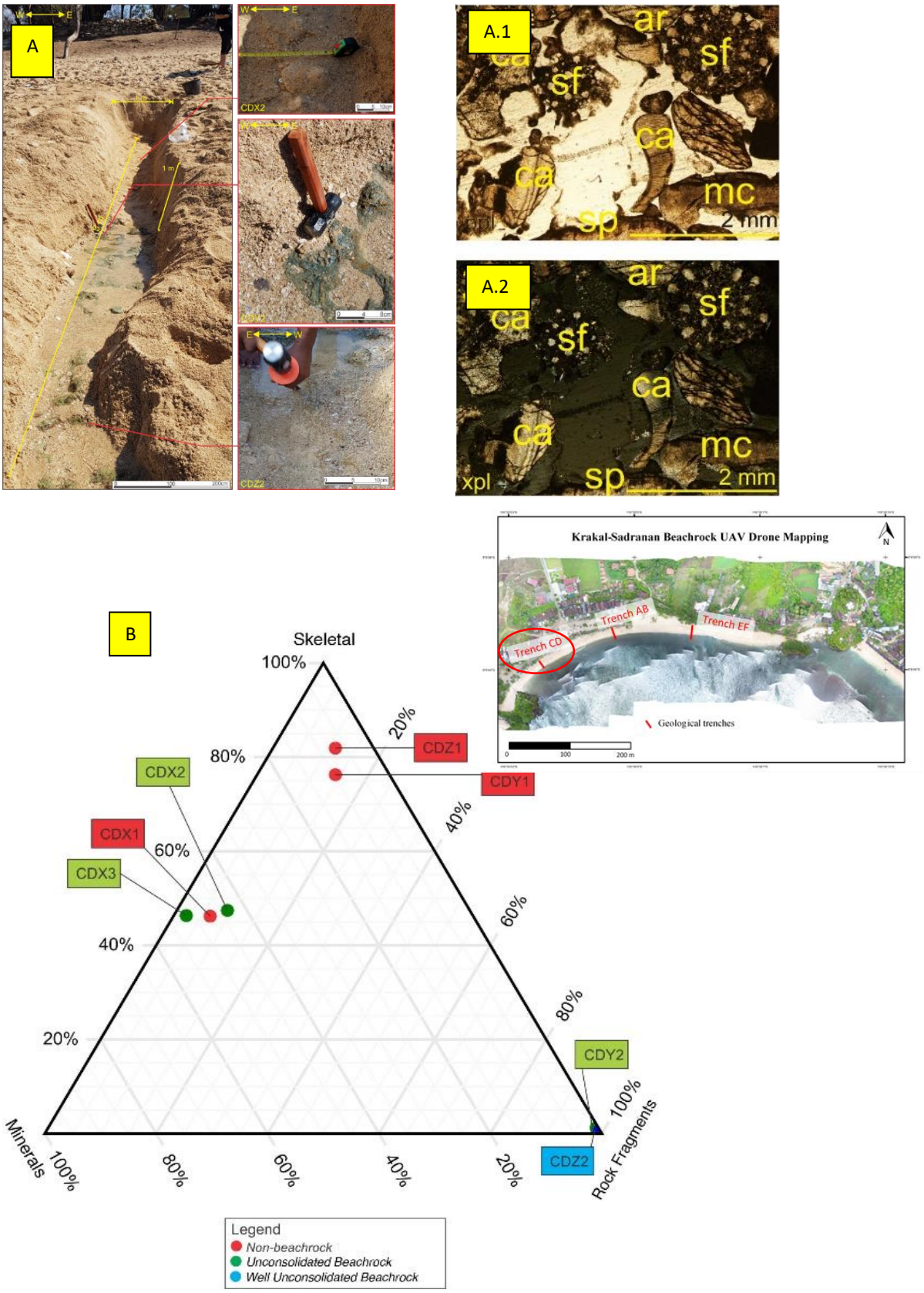


Figure 2.6. Stratigraphic of the Trench CD: (A) Petrographic on cross polarized nicol (XPL, A1) and plane polarized nicol (PPL, A2) with sf (skeletal fragment), mc (micrite), sp (sparite), ca (calcite) and ar (aragonite); (B) Degree of cementation based on composition of beachrock.

- Sparse biomicrite (Folk, 1962) (CDX_3)

  Whitish yellow, 4 mm fragment size and base mass <1 mm, subangular grain shape, open container, massive structure, thickness of about 30 cm. Identification of L-M samples showed the composition of limestone fragments (15%) and fossil shell material (15%), which were dominated by *Baculogypsina sphaerulata*, calcite minerals (30%) and limestone sand material (40%).

(f) Stratigraphic columns for CDY_1 and CDY_2 samples (Appendix B5)

- Carbonate sand deposits CDY_1 sample.

  Whitish yellow, 2 mm fragment size and 1 mm base mass, subangular, unconsolidated grain shape, with a thickness of 70 cm. Identification of CDY_1 samples showed the composition of limestone fragments (15%) and fossil shell material (45%) which were dominated by *Baculogypsina sphaerulata*, limestone sand material (40%).

- Sparse biomicrite (Folk, 1962) (CDY_2)

  Whitish yellow, 4 mm fragment size and base mass <1 mm, subangular grain shape, open container, massive structure, thickness of about 30 cm. The identification of CDY_2 samples showed the composition of fragments of limestone (10%) and fossil shell material (20%), which were dominated by *Baculogypsina sphaerulata*, calcite minerals (35%) and limestone sand material (35%).

(g) Stratigraphic columns for samples CDZ_1 and CDZ_2 samples (Appendix B6)

- Carbonate sand deposits CDZ_1 sample.

  Whitish yellow, 2 mm fragment size and 1 mm base mass, subangular, unconsolidated grain shape, 60 cm thick. Identification of CDZ_1samples showed the composition of limestone fragments (20%) and fossil shell material (40%) which were dominated by *Baculogypsina sphaerulata*, limestone sand material (40%).

- Sparse Biomicrite (Folk, 1962) (CDZ_2)

  Whitish yellow, 4 mm fragment size and base mass <1 mm, subangular grain shape, open container, massive structure, thickness of about 40 cm. Identification of CDZ_2 samples showed the composition of limestone fragments (10%) and fossil shell material (20%), which were dominated by *Baculogypsina sphaerulata*, calcite minerals (40%) and limestone sand material (30%).

(h) Petrographic analysis trench CD

Composition diagram of all samples in the trench CD were categorized into three types of samples, namely non-beachrock, unconsolidated beachrock, and well-consolidated beachrock. Samples of CDX_1, CDY_1, CDZ_1, have ~ 50% shell content, minerals and rock fragments <10% and are classified as non-beachrock. CDX_2 and CDX_3 samples have 45% shell content, 55% minerals and 10% rock fragments. CDY_2 and CDZ_2 samples have 2% shell content, 2% mineral content, and over 90% rock fragments.

2.5.1.3 Trench EF

The EF trench has coordinates 456025 E/ 9099647 S, located on the west side of the trench AB, with dimensions of 5 m in length, 1 m in width, and 1 m in depth (Figure 2.7). Stratigraphic columns that have been made in EF trenches include stratigraphic columns for EFX_1 and EFX_2 samples (Appendix B7), stratigraphic columns for EFY_1 and EFY_2 samples (Appendix B8), and stratigraphic columns for EFZ_1 and EFZ_2 samples (Appendix B9). This trenching is almost similar to trenching AB because it is assuming one formation. Dominated with carbonate sand deposits in the top within whitish yellow color, 2 mm fragments and 1 mm matrix, subangular, unconsolidated grains with a thickness of 70 cm. EFZ_1, EFY_1, and EFX_1 samples were taken at top of EF trenching layers. The sample constituents are limestone fragments, fossil skeletal shell materials which are dominated by *Baculogypsina sphaerulata* and limestone sand materials. Next, the beachrocks were then classified as Sparse Biomicrite (Folk, 1962) (EFZ_2, EFY_2, and EFX_2) whitish yellow color, measuring 4 mm fragments and a base mass of less than 1 mm, subangular grain shape, open container, massive structure. An identification of limestone fragments and fossil shell materials found a domination of foraminifera Baculogypsina sphaerulata, calcite minerals, and limestone sand materials.

2.5.2 Geophysics measurements

Geoelectrical data was processed based on resistivity value, true resistivity, and contrasts resistivity interpreted lithology of sub-surface and structural sub-surface geology, based on field acquisition in the α-, β-, and γ-section. Furthermore, the interpretation is carried out quantitatively by determining the rock resistivity according to the depth indicated by the results of refraction seismic processing. The resistivity section was derived from the measured data using 2D inversion technique. This method involves numerical calculation of the electric field

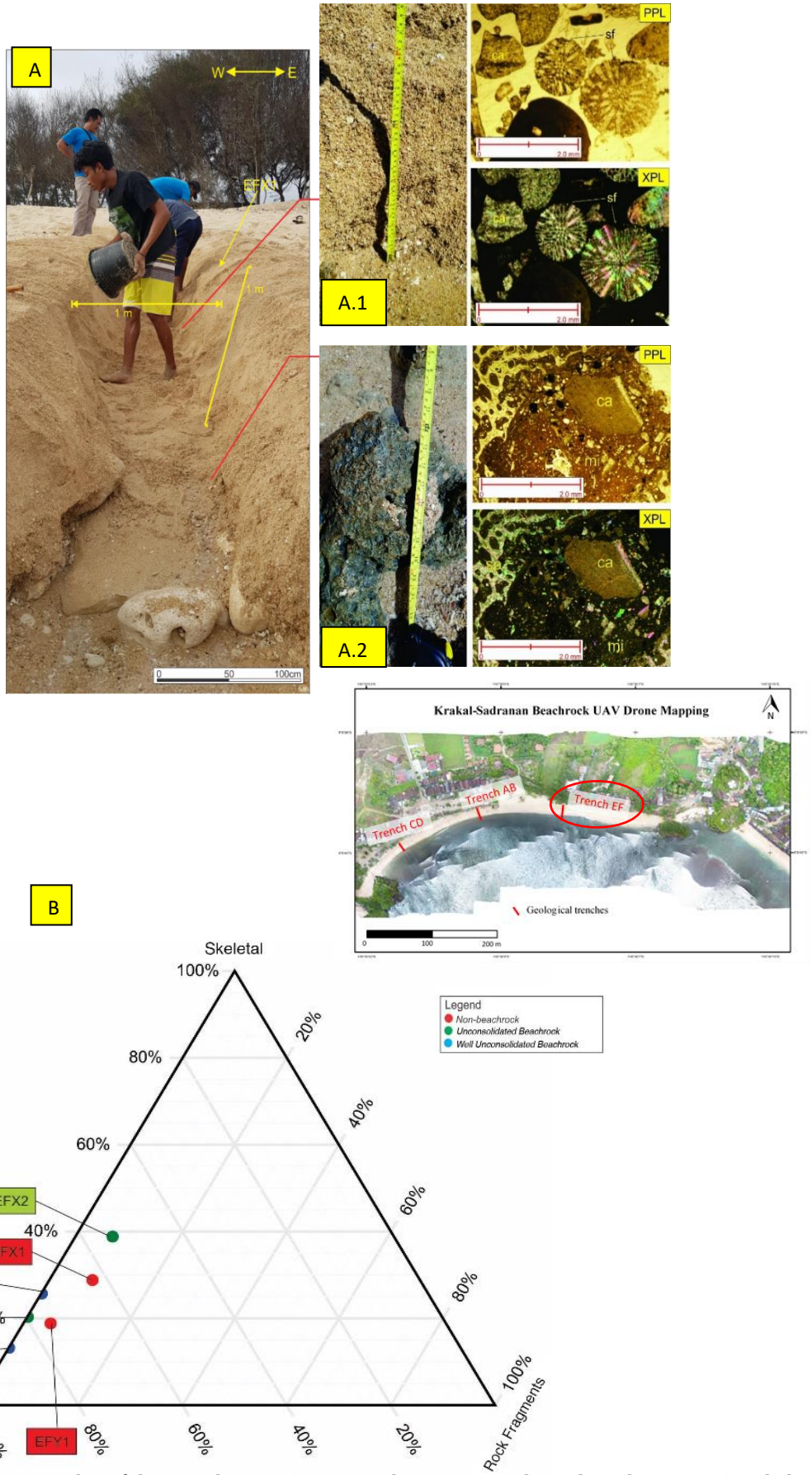


Figure 2.7. Stratigraphic of the Trench EF: (A) Petrographic on cross polarized nicol (XPL, A1) and plane polarized nicol (PPL, A2) with sf (skeletal fragment), mc (micrite), sp (sparite), ca (calcite) and ar (aragonite); (B) Degree of cementation based on composition of beachrock.

and constrained smoothing by a nonlinear least-squares method (Sasaki, 1992; Kubo, et al., 2014).

2.5.2.1 α-section

This section was constructed by three measurement lines, which were line-1, line-2, and line 3. The analysis data of this research were explained by each line to make it detailed and more comprehensible. The α-section (Figure 2.8) is a depth profile obtained from data processing. If the elastic waves that propagate in the Earth's medium meet the plane boundary with different elasticity and density, then reflection and refraction of the wave will occur. This high resistivity zone is a high resistivity anomaly, with resistivity values ranging from 27.6 – 78.7 Ωm. In this zone, the beachrock body is estimated. Based on the results of data processing that have been done, the depth of beachrock occurs from surface until 1-1.5 m and it solidifies un-uniform northward due to the proximity to a building foundation whose high resistivity is similar. From the dispersion curve of S-wave propagation that represented frequencies, phase velocity and amplitude was used. The graphic of S-velocity versus depth described that penetrating of source wave were propagated around ~4.5 m beneath the surface of beachrock within S-wave velocity around 500~600 m/s. In other word, toward reinforcing the thickness of beachrock, based on the results of data processing that has been done, v_1 is obtained for the first layer of 209.67 m/s with a depth of 1.5 m. Meanwhile, v_2 in the second layer obtained a value of 647.77 m/s. From the results of data processing, it is interpreted that natural beachrock has a thickness of 1-1.5m which is in the first layer.

2.5.2.2 β-section

This section was constructed by two measurement lines, which were line-4 and line-5. The data analysis of this research was explained by each line to make it more comprehensible and detailed. The β-section (Figure 2.9) is a depth profile obtained from data processing. If the elastic waves that propagate in the Earth's medium meet the plane boundary with different elasticity and density, then reflection and refraction of the wave will occur. Based on the results of data processing that has been done, the depth of beachrock occur from surface until ~2.5 m un-uniform. This high resistivity zone is a high resistivity anomaly, with resistivity values ranging from 27.6 - 78.7 Ωm. Based on the results of data processing that has been done, the depth of beachrock occur from surface until 1-1.5 m un-uniform that solid in the northern part because of the building concrete (Figure 2.9, a). From the dispersion, curve of S-wave propagation represented frequencies, phase velocity, and amplitude that were used. The graphic

of S-velocity versus depth described that penetrating of source wave were propagated around 2 m beneath the surface of beachrock. It is interpreted that natural beachrock has a thickness of 1-1.5 m which is in the first layer. Meanwhile, S-wave velocity in this section is 500~600 m/s. In other word, toward reinforcing the thickness of beachrock, based on the results of data processing, v_1 is obtained for the first layer of 230.27 m/s with a depth of 1.5-2 m (Figure 2.9, b), whereas v_2 in the second layer obtained a value of 500~600 m/s.

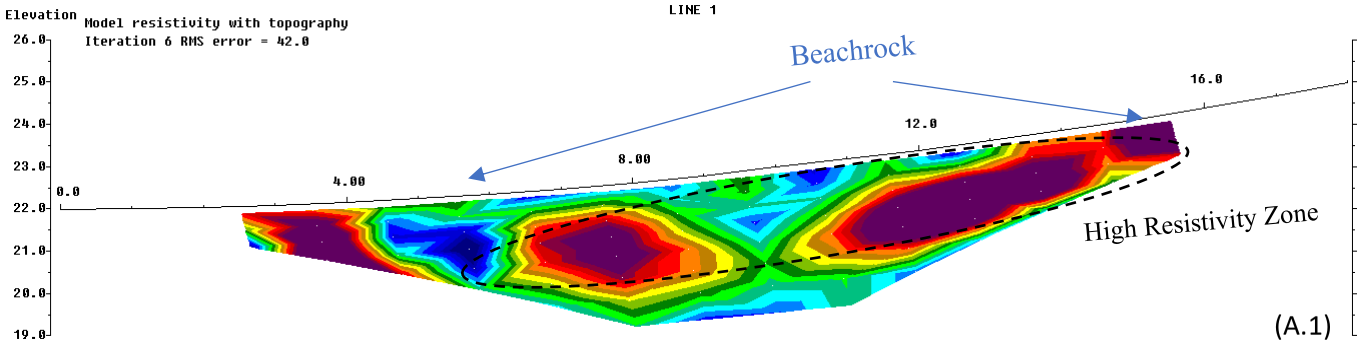
2.5.2.3 γ-section

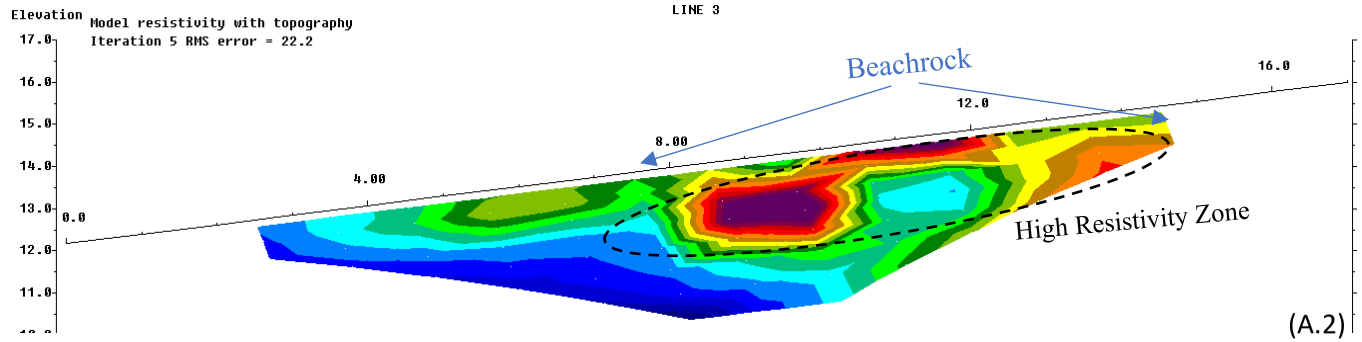
In this section, only one measurement line was constructed, which was line-6. The γ - section is a depth profile obtained from data processing. In this area (Figure 2.10), the outcrop of the beachrock is different to other sections. The outcrop found in this area is huge compared to other outcrops in other areas around 1~1.5 meters on the surface; we were assuming that beachrock may occur because of this section is in the bay and is protected naturally from topographic karst-hills. This area is an exception from deeply geological investigation because the existing condition, biota, and other factors are more complex than section α and β. This high resistivity zone is a high resistivity anomaly, with resistivity values ranging from 27.6 - 78.7 Ωm. Based on the results of data processing, the depth of beachrock occur from surface approximately until ~4 m within S-velocity below than 205 m/s. Because of the limited space, the distance between two consecutive geophone sensors (6 in total) was only 0.5 m in the surface of beachrocks.

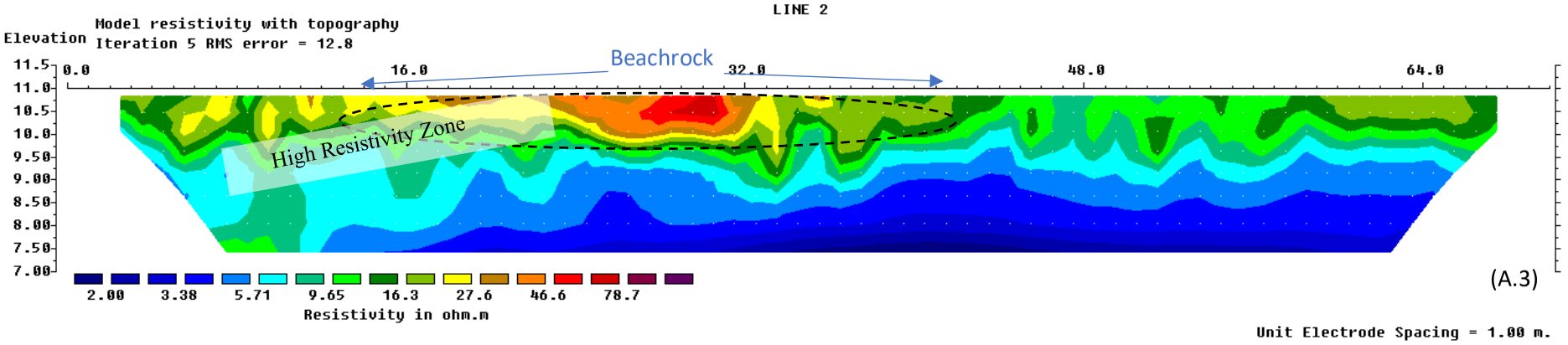
2.5.3 Three dimensional of subsurface model

The concept of 3D processing entails a combination of processing each line via the drone photogrammetric technique and overlaying digital elevation model data with using *ArcGIS*. The distance between lines was interpolated with the lines around it. The data input applied in3-D modeling has four parameters namely x, y, z, and n. Coordinates in UTM are labelled as x and y indicating the position of the north and east meters. The value of z as an elevation parameter is not depth because it follows the digital elevation model of topography and geophysics parameters such as of resistivity and surface wave values. This model uses *ArcGIS* and Rock Work to calculate the distribution of beachrock in the Krakal–Sadranan beach, Yogyakarta. The limitation of the value of resistivity and S-velocity taken also applies between 27.6-78.7 Ωm and a S-velocity value between 500-600 m/sec. Based on calculation,

A







Continue to next page

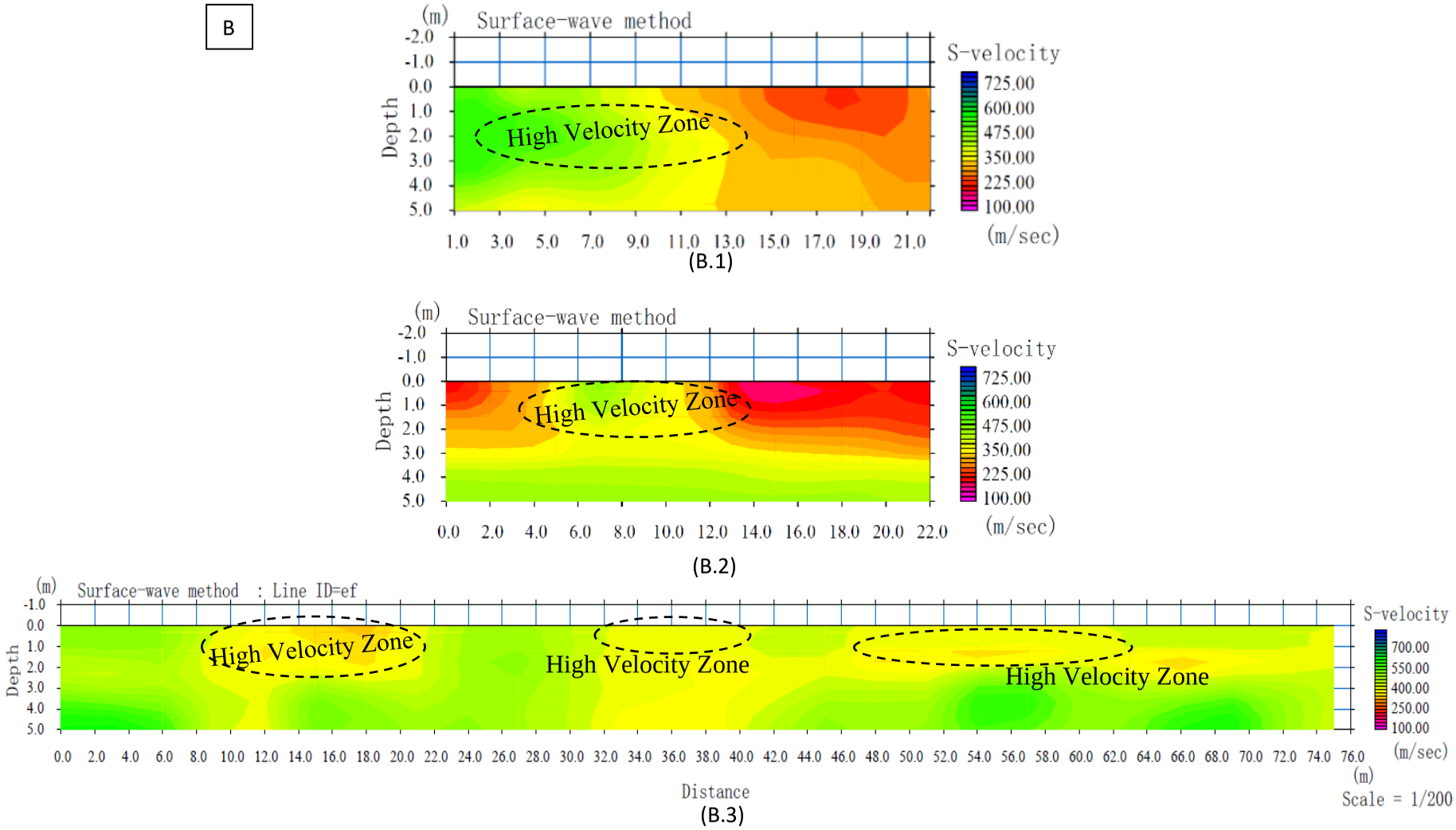


Figure 2.8. Electrical and multi analysis surface wave results of α-section. (A1) the resistivity of line 1, (B1) the MASW of line 1, (A2) the resistivity of line 3, (B2) the MASW of line 3, (A3) the resistivity of line 2, (B3) the MASW of line 2.

the α-section covers 210.5 m^3 of beachrock (Figure 2.11) while the β-section covers 76.9 m^3 (Figure 2.12).

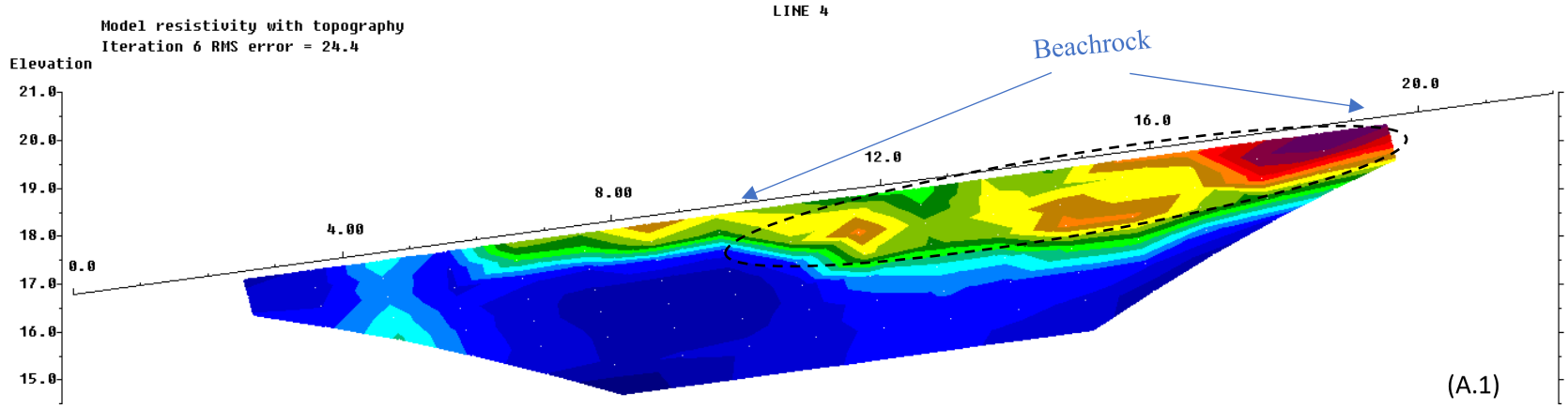
The wet density was 1.69 to 1.92 g/cm^3 (average 1.95 g/cm^3), porosity was 10 to 14 % (average 12.3%), S wave velocity was 2.3 to 2.92 km/s (average 2.66 km/s), and the P wave velocity was 3.35 to 4.41 km/s (average 4.18 km/s). The dynamic Poisson's ratio was 0.09 to 0.21 (average 0.16), respectively. Compared with the beach rock samples at other points shown in Table 2.2, these results show a lower porosity and higher values for both P wave velocity and S wave velocity compared to Okinawa, Japan samples (Danjo and Kawasaki, 2014). Figure 2.14 shows the results of comparing the properties of beach rocks with other rock types using existing data. The relationship between P-wave velocity and S-wave velocity for sedimentary rock samples in Japan (Suzuki, et al., 2013) and Indonesia in this research. It can be seen that the elastic wave velocity of the beachrock at this point (2B, 1A, 1C, 2C, 1B and 2A in the figure) show values similar to those of the early Paleogene until Cretaceous sedimentary rocks. It shown the beachrock distribution in Indonesia have a compacted crystallization than Japanese Okinawa beachrock, even though the pattern of beachrock samples from both sides were sedimented in the same characteristics (based on dynamic Poisson ration ~0.2) which mean it has a similar porosity. Based on the results, detail analysis of carbon dating is needed to prove the actual dating of beachrock in Indonesia as the most suitable approach for further analysis.

2.6 Discussions

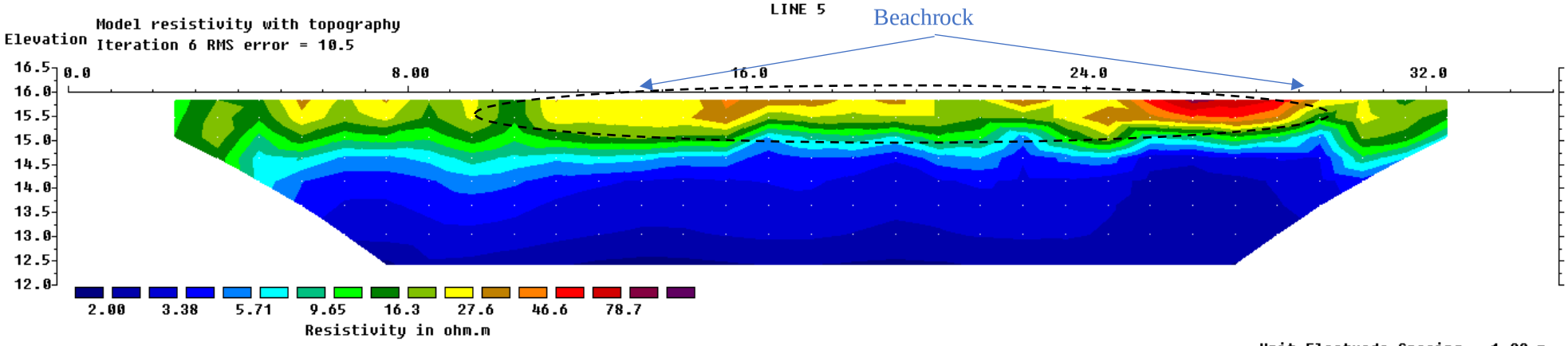
2.6.1 Beachrock characteristics

Beachrock is generally cemented in the tidal zone with high amounts of aragonite, HMC, and LMC. General carbonate cementation in the marine environment formed acicular-radial and spacious types of cement texture, whereas the tidal zone is indicated by aragonite or HMC. Meniscus and bridge cement indicate LMC composition (Vousdoukas et al., 2007; Mauz, et al., 2015). Krakal-Sadranan Beaches, Indonesia happens to have the same pattern, which is characteristics of cement solution are dominated by aragonite and calcite crystalline, soluble in water. In contrast, the cement product of beachrock evolution based on field investigation (from the sea to surface) is represented by aragonite crystalline that only occurs in the swash-zone area, due to aragonite mineral being easily dissolvable in fresh water from rain or land rich of

A



(A.1)



(A.2)

Continue to next page

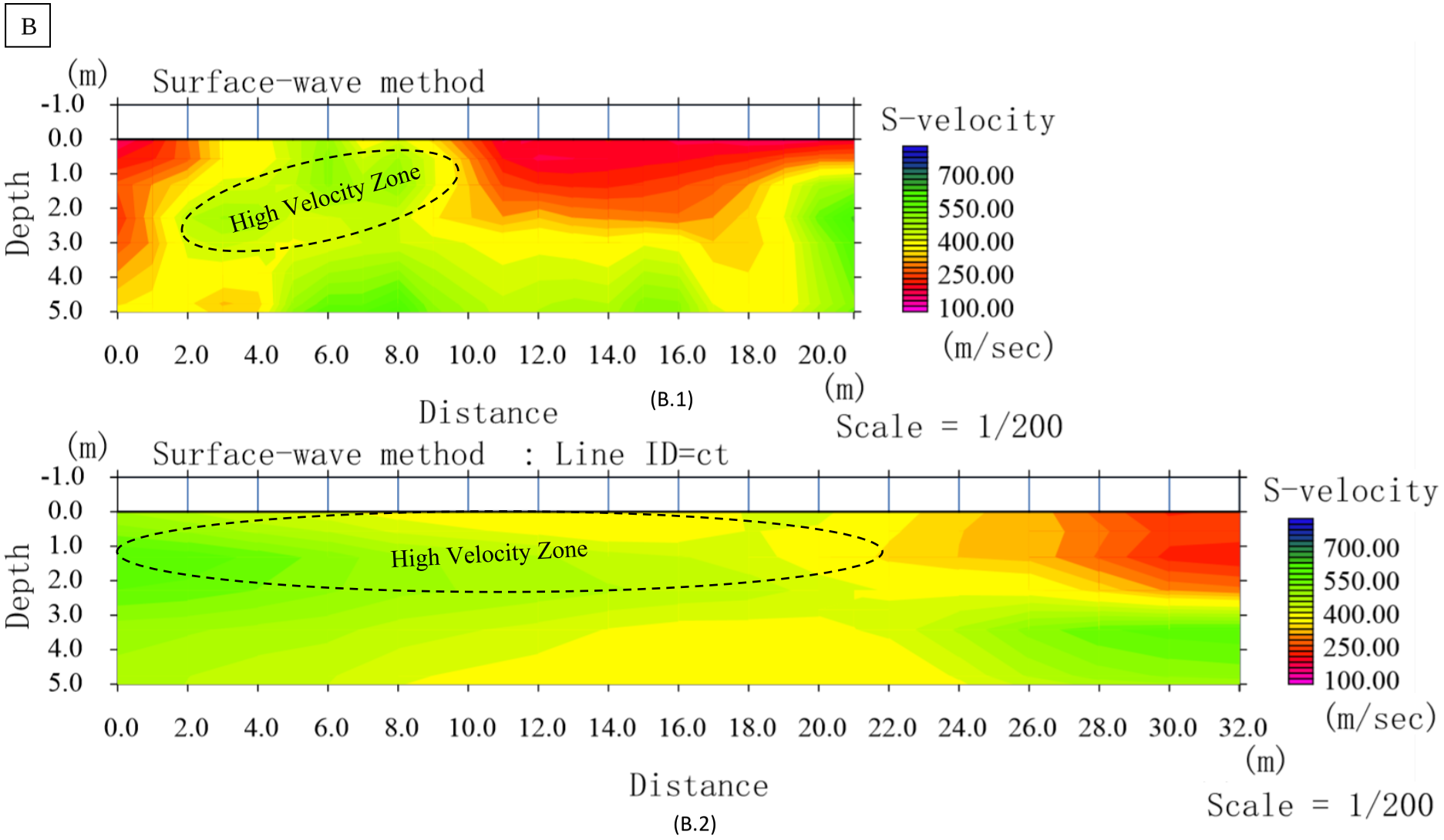


Figure 2.9. Electrical and multi analysis surface wave results of α-section. (A1) the resistivity of line 4, (B1) the MASW of line 4, (A2) the resistivity of line 5, and (B2) the MASW of line 5.

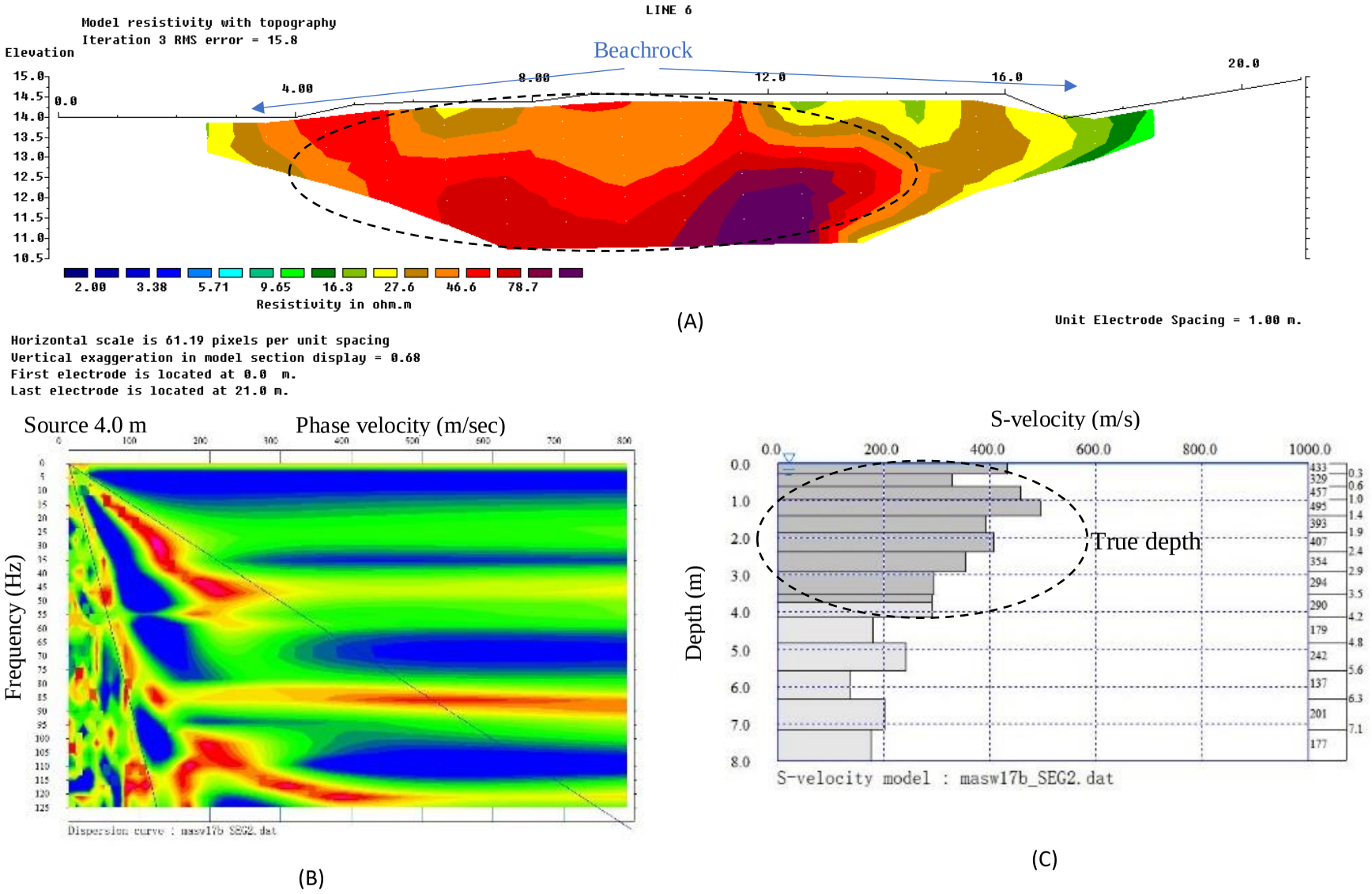


Figure 2.10. Electrical and multi analysis surface wave results of γ-section. (A) the resistivity of line 6, (B) the MASW of line 6, and (C) depth function for γ -section.

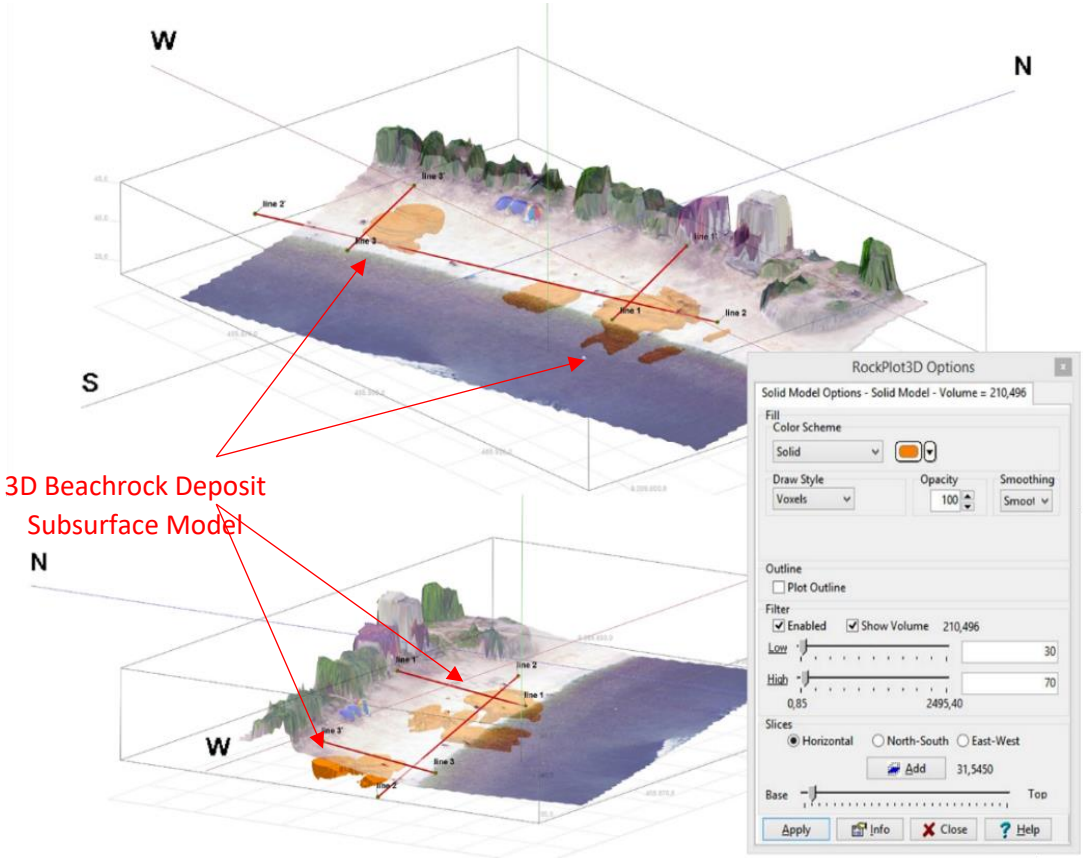


Figure 2.11. Three dimensional of beachrock model calculation based on geophysical statistical anomaly data from electrical resistivity and multi analysis surface wave of α-section.

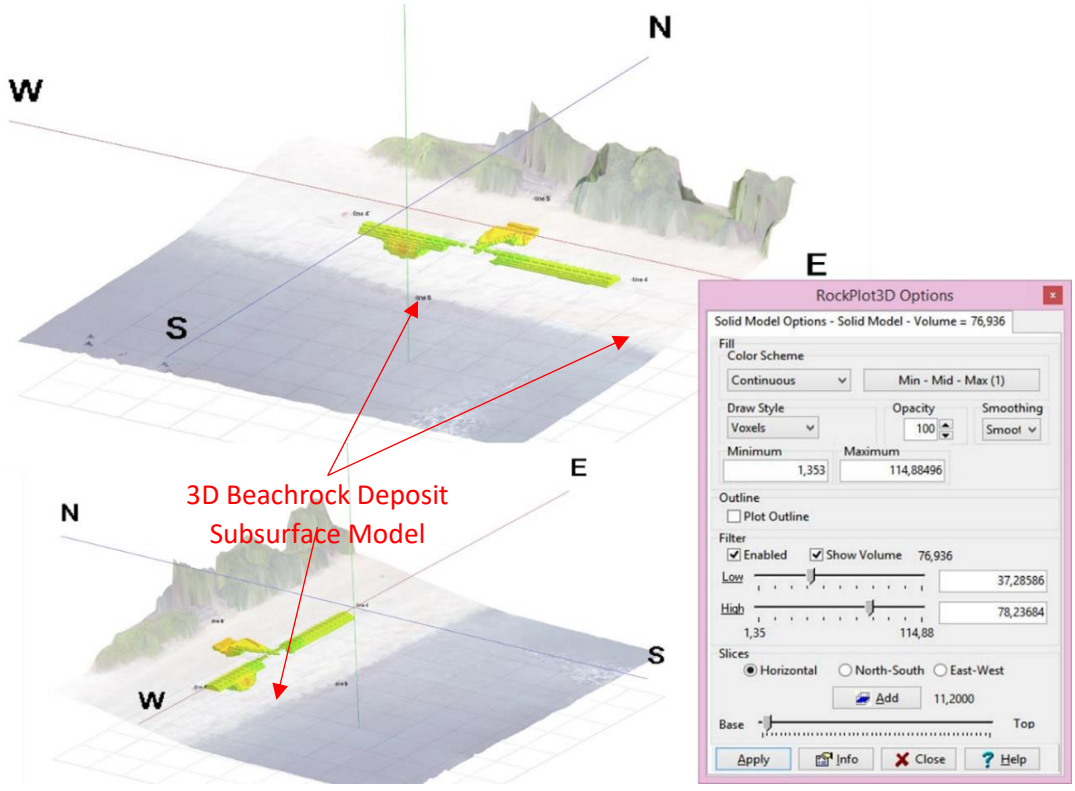


Figure 2.12. Three dimensional of beachrock model calculation based on geophysical statistical anomaly data from electrical resistivity and multi analysis surface wave of β-section.

Table 2.2. Comparison of the beachrock properties between Japan and Indonesia.

Sample	Japan Beachrock				Indonesia Beachrock					
	OK-A	OK-B	OK-C	OK-D	1-A	1-B	1-C	2-A	2-B	2-C
Saturated density (g/cm^3)	2.06	1.97	2.49	2.27	1.84	1.92	1.84	1.80	1.69	1.81
Porosity (%)	11.1	25.4	3.7	27	10.6	12.9	11.6	14.8	14.3	13.3
One axis compressive strength (MPa)	11.14	19.91	31.11	-	7.87	14.47	15.89	6.07	3.717	10.77
P wave velocity (km/s)	3.50	3.69	4.07	2.29	3.76	4.41	4.06	4.66	3.85	4.35
S wave velocity (km/s)	2.34	2.31	2.51	1.33	2.49	2.79	2.79	2.92	2.33	2.70
Dynamic Poisson ratio	0.096	0.178	0.193	0.245	0.11	0.16	0.09	0.18	0.21	0.19
Geological age (vBP)	1370	1250	2300	-	-	-	-	-	-	-

spars and micrite cement. Specific cement types are recognized as (i) acicular, fibrous, and bladed fabrics; (ii) radial fibrous and fascicular-optic fabrics; (iii) micro-and cryptocrystalline fabrics; (iv) equant spar, syntaxial overgrowth fabrics, scalenohedral calcites, peloidal fabrics and (v) non-carbonates. These types are incipient early marine cementation leading to a reduction in pore-space in near-seafloor sediments (Christ, et al., 2015). Krakal-Sadranan Beaches happen to follow the same pattern, which cement solution is characterized by domination of aragonite and calcite crystalline, soluble in water. In contrast, the cement product of beachrock evolution based on field investigation (from the sea to the surface) was represented by aragonite crystalline that only occurs in the swash-zone area, due to aragonite mineral being easily dissolvable in freshwater from rain or land rich of sparse and micrite cement.

2.6.2 Geophysical beachrock imagine

Beachrock body from the resistivity result of geophysical acquisition that reveals the beachrock outcrop in the range 0-70 m on the α-line is longest beachrock than that of its counterpart on the β-line, a result determined by comparing the resistivity sections of the α-line with those of the β-line. The distribution of the resistivity value of the zone on this track is divided into two zones, namely zones with low resistivity and high resistivity zones. This high resistivity zone is a high resistivity anomaly, with resistivity values ranging from 27.6 - 78.7 Ωm as it leads to the beachrock body characteristics with a thickness of 1-3 m at elevation 20-23 meters above from sea-level. In the zone with low resistivity, it is suspected that the zone is

a layer of sand saturated with sea water. In the case of the seismic surface-wave survey of the beachrock, there was a great difference between the S-wave velocity in the laboratory tests (about 2.6 km/s) and the S-wave velocity that had been assumed for detecting the beachrock in the field (about 0.6 km/s). The cause of this discrepancy is suspected due to the area of highest frequency (highest velocity) along the survey line which could not be detected, because the high frequencies had been attenuated by putting all the geophones on the beachrock. Toward reduce that noise because of attenuation frequency, the sensitive geophones be placed into holes made in the ground (buried into compacted coarse coral sand). Another reasons, the physical property of beachrock is not homogeneous in the site. The samples were probably picked up from a solidified part where was relatively easy to collect which affected of the S-wave velocity measured by laboratory tests is higher than that calculated by field data.

The geophysical prospecting, in which underground structures are surveyed without damaging the landscape can be an extremely effective way to study the distribution of beachrock especially in the tourism spot. This figure is a cross-section between geophysical data and the digital surface model drone to give an overall impression of geophysical surveying applied to geological exploration of beachrocks that is easily comprehensible (Radjawali and Pye, 2017; Darmawan, et al., 2018). The integrated study based on aerial photogrammetric with geophysics measurement gave better resolution and 3D image figure to reconstruct the sub-surface model based on physics parameter from acquisition geophysics.

2.6.3 Rock characteristic of natural beachrock

Shear wave velocity (S-wave) test results were used to develop a correlation to the precipitated calcite mass and this enables prediction of changes in porosity, density, and shear modulus during treatment (Weil et al. 2012). Shear wave velocity is used to nondestructively monitor the change in small-strain stiffness during shearing, which provides an indication of cementation degradation as a function of strain level. Because shear wave velocity is influenced by both the level of cementation and the change in effective mean stress during shearing, the normalized shear modulus is used to evaluate the degradation of cementation during shearing (Montoya and DeJong 2015). Biocementation in a change from a shear wave velocity of 140 m/s to an average of 600 m/s, compare with this research a shear wave around 510 m/s to 1330 m/s. Compression wave velocity (P-wave) measurements can be determined under different saturation conditions and used in combination with S-wave measurements to observe how the Poisson’s ratio evolved during treatment (Weil et al. 2012).

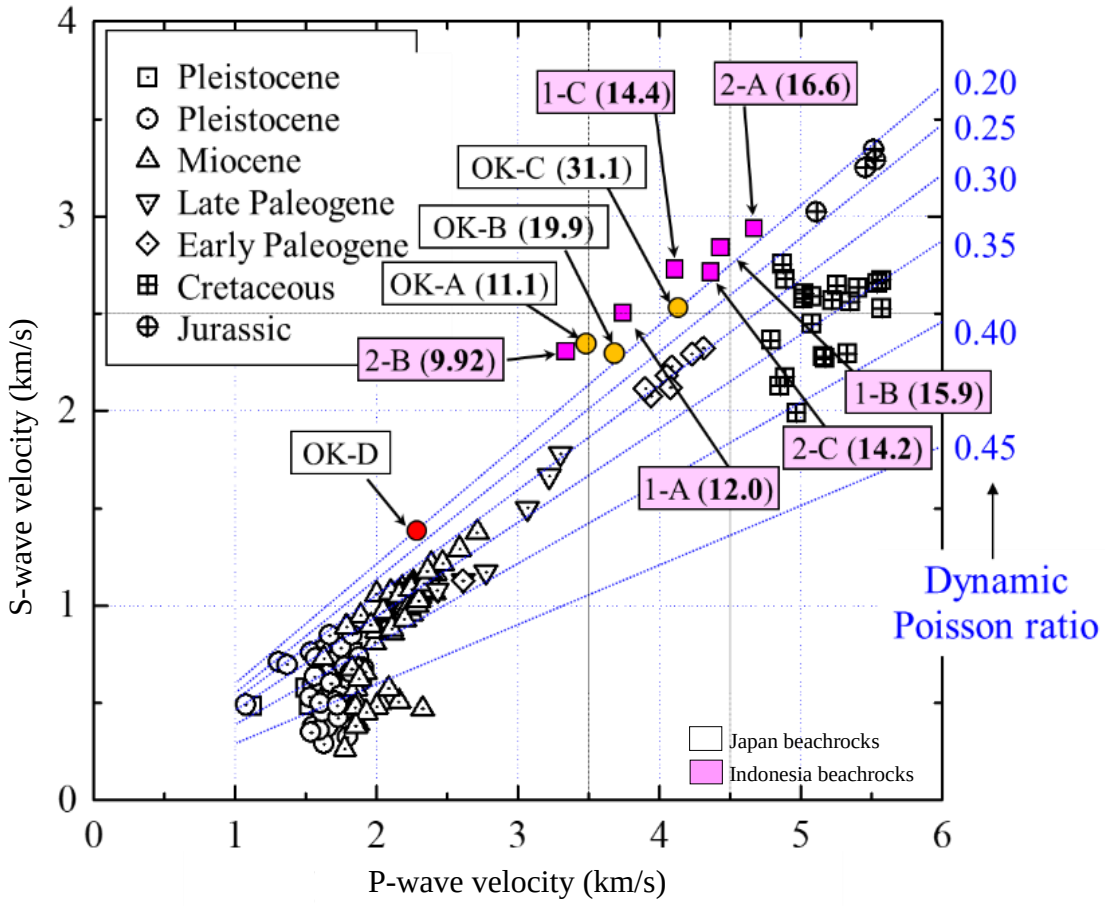


Figure 2.13. Comparison of the geophysical properties of the sedimentary rocks and beachrocks based on P-wave velocity and S-wave velocity

2.7 Conclusions

As a result of conducting electrical and surface wave surveys on sandy beaches, we found the following:

1. Beachrock were found in this area precipitated beneath beach sand which is wave erosional product and then solidify beneath that formation, floating, between limestone bedrock and beach sands formation based on greater value from resistivity and S-wave velocity in the formation layers.
2. Resistivity, thickness, and S-wave velocity of the beachrock increases as it gets closer to the coastline. The maximum thickness of the beachrock at this point is about 1 m (to be up to 3 m) based on calculations, the α-section covers 210.5 m^3 while the β-section covers 76.9 m^3 of beachrock deposit.

Therefore, the sufficient immersion and evaporation of seawater is an important condition for the solidification of sand to form a beachrock.

References

Atmoko, D.D., Titisari, A.D. and Idrus, A., 2016. Mineralogi dan Geokimia Batugamping Merah Ponjong, Gunungkidul, Daerah Istimewa Yogyakarta–Indonesia. RISET Geologi dan Pertambangan, 26(1), pp.55-67.

Avcıoğlu, M., Yiğitbaş, E. and Erginal, A.E., 2016. Beachrock formation on the coast of Gökçeada Island and its relation to the active tectonics of the region, northern Aegean Sea, Turkey. Quaternary international, 401, pp.141-152.

Brown, D.G., and Arbogast, A.F. 1999. Digital photogrammetric change analysis as applied to active coastal dunes in Michigan. Journal of Photogrammetric Engineering and Remote Sensing 65: 467-474.

Burger, H.R. 1996. Exploration Geophysics of the Shallow Subsurface. Prentice Hall. 489 pp.

Christ, N., Immenhauser, A., Wood, R.A., Darwich, K. and Niedermayr, A., 2015. Petrography and environmental controls on the formation of Phanerozoic marine carbonate hardgrounds. Earth-science reviews, 151, pp.176-226.

Cooper, J.A.G., Green, A.N., Meireles, R.P., Klein, A.H., Souza, J. and Toldo, E.E., 2016. Sandy barrier overstepping and preservation linked to rapid sea level rise and geological setting. Marine Geology, 382, pp.80-91.

Cribb, R. and Ford, M., 2009b. Indonesia as an archipelago: Managing islands, managing the seas. ISEAS-Yusof Ishak Institute.

Cribb, R.B. and Ford, M. eds., 2009a. Indonesia beyond the water's edge: managing an archipelagic state. Institute of Southeast Asian Studies.

Danjo, T. and Kawasaki, S., 2014. Characteristics of beachrocks: a review. Geotechnical and Geological Engineering, 32(2), pp.215-246.

Danjo, T. and Kawasaki, S., 2014. Formation mechanisms of beachrocks in Okinawa and Ishikawa, Japan, with a Focus on Cements. Materials Transactions, pp.M-M2013844.

Darmawan, H., Walter, T.R., Brotopuspito, K.S. and Nandaka, I.G.M.A., 2018. Morphological and structural changes at the Merapi lava dome monitored in 2012–15 using

unmanned aerial vehicles (UAVs). Journal of Volcanology and Geothermal Research, 349, pp.256-267.

Daryono, L.R., Titisari, A.D., Warmada, I.W. and Kawasaki, S., 2019. Comparative characteristics of cement materials in natural and artificial beachrocks using a petrographic method. Bulletin of Engineering Geology and the Environment, 78(6), pp.3943-3958.

David, P., Panagiotis, T. and Konstantinos, A., 2009. Electrical resistivity tomography mapping of beachrocks: application to the island of Thassos (N. Greece). Environmental Earth Sciences, 59(1), p.233.

Dewi Titisari, A. and Hendrawan, A., 2017, September. Genesa batugamping merah di daerah Siung dan sekitarnya, kecamatan Tepus dan Girisubo, kabupaten Gunungkidul. In proceeding, seminar nasional kebumian ke-10 peran penelitian ilmu kebumian dalam pembangunan infrastruktur di Indonesia 13–14 september 2017; Grha Sabha Pramana (In Bahasa).

Feng, K. and Montoya, B.M., 2017. Quantifying level of microbial-induced cementation for cyclically loaded sand. Journal of Geotechnical and Geoenvironmental Engineering, 143(6), p.06017005.

Folk, R.L., 1962. Spectral subdivision of limestone types.

Fowler, C.M.R., Fowler, C.M.R. and Fowler, M., 1990. The solid earth: an introduction to global geophysics. Cambridge University Press.

Jauhari, U. and Toha, B., 2005. High Resolution Sequence Stratigraphy and Diagenesis in Carbonate Rocks, Wonosari Formation, Yogyakarta: An Outcrop Analog for Modeling Chalky Limestone Reservoir Distribution.

Kubo, R., Kawasaki, S., Suzuki, K., Yamaguchi, S. and Hata, T., 2014. Geological exploration of beachrock through geophysical surveying on Yagaji Island, Okinawa, Japan. Materials Transactions, pp.M-M2013839.

Lokier, S.W., 2000. The Development of the Miocene Wonosari Formation, South Central Java.

Mauz, B., Vacchi, M., Green, A., Hoffmann, G. and Cooper, A., 2015. Beachrock: a tool for reconstructing relative sea level in the far-field. Marine Geology, 362, pp.1-16.

Montoya, B.M. and DeJong, J.T., 2015. Stress-strain behavior of sands cemented by microbially induced calcite precipitation. Journal of Geotechnical and Geoenvironmental Engineering, 141(6), p.04015019.

Mukti, M.M.R., 2005. Carbonate depositional environment and platform morphology of the Wonosari Formation in the area east of Pacitan. RISET Geologi dan Pertambangan, 15(2), pp.29-38.

Pilkey, O.H. and Cooper, J.A.G., 2014. Are natural beaches facing extinction?. Journal of Coastal Research, 70(sp1), pp.431-436.

Premonowati, P., Prastistho, B. and Firdaus, I.M., 2012. Allostratigraphy of Punung Paleoreef based on Lithofacies Distributions, Jlubang Area, Pacitan Region-East Java. Indonesian Journal on Geoscience, 7(2), pp.113-122.

Radjawali, I., Pye, O. and Flitner, M., 2017. Recognition through reconnaissance? Using drones for counter-mapping in Indonesia. The Journal of Peasant Studies, 44(4), pp.817-833.

Sartono, S., 1964. Stratigraphy and sedimentation of the easternmost part of Gunung Sewu, East Djawa (No. 1). Departemen Perindustrian Dasar/Pertambangan, Direktorat Geologi.

Sasaki, Y., 1992. Resolution of resistivity tomography inferred from numerical simulation 1. Geophysical prospecting, 40(4), pp.453-463.

Siregar, M.S., Kamtono, P. and Mukti, M.M., 2004. Reef facies of the Wonosari Formation, south of Central Java. RISET-Geologi dan Pertambangan, 14(1), pp.1-17.

Sudarno, I., 1997. Petunjuk Adanya Reaktifasi Sesar di Sekitar Aliran Sungai Opak, Perbukitan Jiwo dan Sisi Utara Kaki Pegunungan Selatan. Media Teknik, 19 (In Bahasa).

Surono, B.T. and Sudarno, I., 1992. Peta Geologi Lembar Surakarta-Giritontro, Jawa. Bandung: Pusat Penelitian dan Pengembangan Geologi.

Surono, B.T., Sudarno, I. and Wiryosujono, S., 1992. Geology of the Surakarta-Giritontro Quadrangles. Java: Bandung, Geological Research and Development Center, Indonesia, scale, 1(100,000), p.2.

Suzuki, K., Kawasaki, S., Kubo, R., Yamaguchi, S., and Hata, T. 2013. Geological structure of beachrock using electrical resistivity and surface wave surveys – Application to the coastal area of Yagaji Island in Nago-shi, Okinawa, Japan. SEGJ 128th, pp. 277-285.

Telford, W.M.L.P. and GELDART, L., P., SHERIFF, R, KEYS., D. 1976, Applied geophysics.

Titisari, A.D., Titisari, A.D., Atmoko, D.D. and Atmoko, D.D., 2015, October. Genesis of Ponjong Pink Limestone, Gunungkidul, Special Region of Yogyakarta–Indonesia (Genesa Batugamping Merah Muda Ponjong, Gunungkidul, Daerah Istimewa Yogyakarta-Indonesia). In proceeding, seminar nasional kebumian ke-8 Academia-Industry Linkage 15-16 Oktober 2015; Grha Sabha Pramana. Departmen Teknik Geologi (In Bahasa).

Toha, B., Resiwati, P., Sriyono, Soetoto, Rahardjo, W. and Pramumijoyo, S. (1994) Geology of Southern Mountain: A contribution (in Indonesia). In: Proceedings of geology and geotectonic of Java Island from Late Mesozoic – Quaternary, Teknik Geologi-UGM, Yogyakarta, 19-36.

van Bemmelen, R.W., 1949. General Geology of Indonesia and adjacent archipelagoes. The geology of Indonesia.

Varela-González, M., González-Jorge, H., Riveiro, B. and Arias, P. 2013. Performance testing of LiDAR exploitation software. Computers & geosciences, 54, pp.122-129.

Verstappen, H.T., 2000. Outline of the geomorphology of Indonesia: a case study on tropical geomorphology of a tectogene region: with a geomorphological map 1: 5,000,000 (No. 79). International Institute for Aerospace Survey and Earth Sciences.

Vousdoukas, M.I., Velegrakis, A.F. and Plomaritis, T.A., 2007. Beachrock occurrence, characteristics, formation mechanisms and impacts. Earth-Science Reviews, 85(1-2), pp.23-46.

Weil, M.H., DeJong, J.T., Martinez, B.C. and Mortensen, B.M., 2012. Seismic and resistivity measurements for real-time monitoring of microbially induced calcite precipitation in sand. Geotechnical Testing Journal, 35(2), pp.330-341.

Wilson, R.F., Turton, S.M., Jones, A. and Phillips, M., 2011. The impact of climate change on reef-based tourism in Cairns, Australia: adaptation and response strategies for a highly vulnerable destination. Disappear Destin: Climate Change Future Chall Coast Tour, pp.233-53.

Zhu, X., Linham, M.M. and Nicholls, R.J., 2010. Technologies for climate change adaptation-Coastal erosion and flooding. Danmarks Tekniske Universitet, Risø Nationallaboratoriet for Bæredygtig Energi.

CHAPTER 3

Sediment characteristics of beachrock at Krakal-Sadranan beach, Yogyakarta, Indonesia

3.1 Introduction

The precipitation of solid matter from dissolved substances in seawater occurs either abiotically (governed by inorganic thermodynamics and reaction kinetics) or biotically (as a metabolic consequence of living organisms). This process is primarily controlled by the biochemistry of organisms including algae, foraminifera, cyanobacteria, and corals but is also influenced by the marine conditions where they live. Beachrock (Figure 3.1) is a carbonate sedimentary product with an anchoring effect for dynamic islands and provides protection from erosion. The sedimentary characteristics of beachrock have been investigated; however, many things about its origin and properties remain unknown or are subject to debate. Outcrops of beachrock are valuable records of the past climate of the low-lying reef islands generally found in tropical and subtropical areas with generally warm seawater (Turner, 2005; Vousdoukas, 2007; Russell and McIntire, 1965; McLean, 2011; Avcioğlu, et al., 2016). Carbonate cement occurs as precipitation from interstitial seawater and or seawater waves (Ginsburg, 1953; Kelletat, 2006), coastal aquifers featuring the mixture of saltwater and freshwater (Moore, 1999), or at sea level due to CO_2 degassing (Vousdoukas, 2007), with biological activity as an additional agent (Neumeier, 1998). Indonesia's coastline is among the largest of any country, and Indonesian beaches face unique issues. Compounding effects and conflicts arise in a complex manner with emergent and cross-scaled impacts, including manifold potential change drivers (e.g., climate change, urbanization, tourism development, and marine resource exploitation) (Zhu, et al., 2010; Jones and Phillips, 2011; Pilkey and Cooper, 2014; Barragan and Andreis, 2015; Shi and Kasperson, 2015).

Beachrock in some areas has not yet been subjected to study. The beachrock found on Krakal-Sadranan Beach is distributed parallel to the coastline, with a coverage of around 10–30 m^2. The research area is located on a coastline that extends along the south of Java Island (the South Coast). It is included in the Wonosari-Punung Formation according to the regional geological map of the Surakarta-Giritontro sheet (van Bammelen, 1949). The authors chose this particular location due to the unexplored sedimentary and diagenesis beachrock in the area

around Krakal-Sadranan Beach, as well as the lack of records on beachrock occurrence. The aim of this study was to identify the ureolytic bacteria that induced the natural beachrock. This study serves as an initial exploration of beachrock sedimentary processes in the area and as a basis for future studies. These might include studies of the rocks' age based on carbon dating and the development of artificial beachrock using microbially induced carbonate precipitation (MICP) to resolve coastal erosion or other issues. As an initial step towards achieving this goal, native indigenous ureolytic strains were isolated from Indonesian beachrock and beach sand and their bioaugmentation potential.

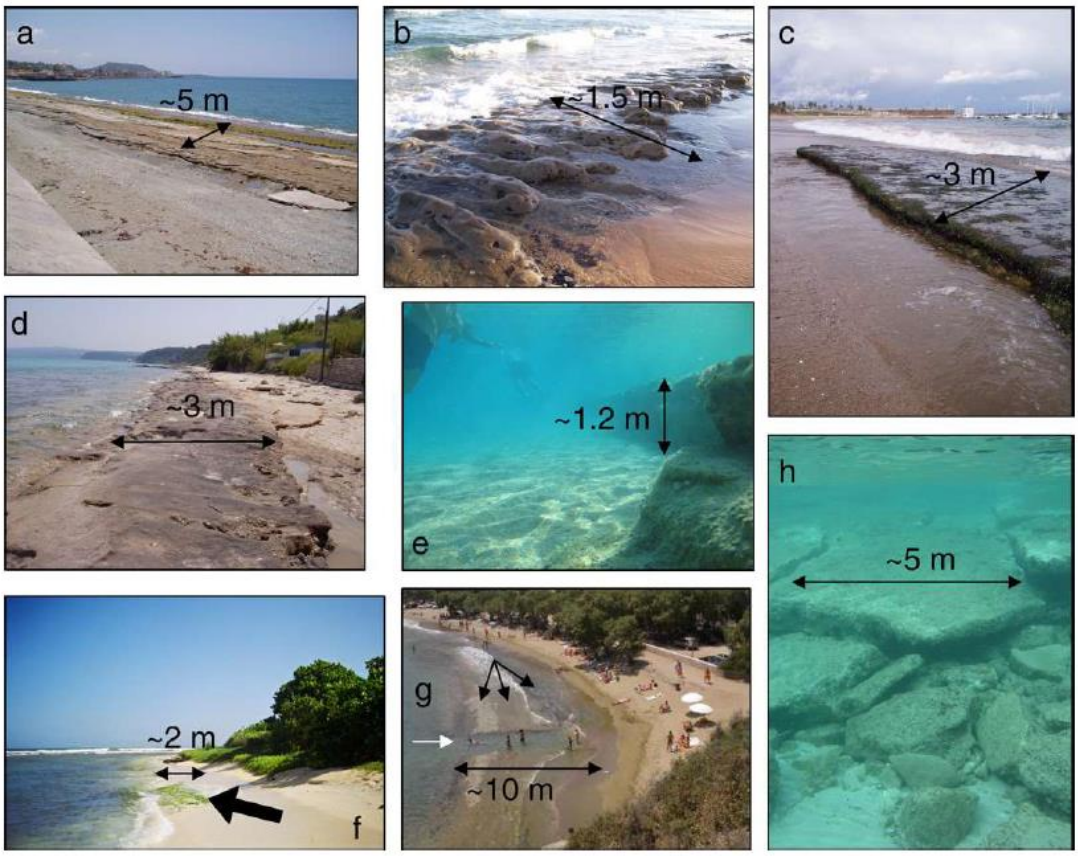


Figure 3.1. Beachrock: (a) Baracoa, Cuba; (b) Salvador, Brazil, (c) Barcelona, Spain; (d) Athitos, N. Greece; (e) Mykonos, Greece; (f) Morrocoy, Venezuela; (g) Sifnos, Greece; (h) Attica, Greece (Turner, 2005; Vousdoukas, 2007)

3.2 Objectives

Upon receiving more successful results for enhancing sedimentary of beachrock mechanism based on MICP treatment using a marine ureolytic bacterium for the desired engineering application. The lack of information about sediment in tropical area such as Indonesia was makes background why such research must be carried out. Further studies were carried out to (i) isolate a local strain of ureolytic bacteria from natural beachrock, (ii) optimize

the growth and enzymatic activity of the isolated strain, and (iii) explore the chemical compounds in the natural beachrock cementation material in nearshore environments as an alternative technique for sand stabilization.

3.3 Materials and methods

3.3.1 Sampling method

Fieldwork was carried out by extracting a horizontal sample at several locations along the coastline in the study area (less than or equal to 1 m near the surface) from June 2017 to December 2018. Each operation was conducted separately. At each location that was sampled, 19 samples were taken based on their horizontal and vertical positions. Sampling was conducted based on the presence of beachrock along the trench. Then, the lithostratigraphy of the samples was identified and beachrock samples were isolated. The field investigation was conducted in the Krakal-Sadranan Beach area, (Wonosari, Yogyakarta, Indonesia), within which the regional geology control and sedimentary processes were correlated. The study area was located around E 455900.11; S 9099654.13 to E 456281.51; S 9099623.03, 49 S Indonesia region. The azimuth of the beachrock deposits, in general, was at N334°E (crossing the shoreline beach) or N164°E (parallel with the shoreline). The ureolytic bacterial species were isolated from the coastal area of Krakal-Sadranan beach (Figure 2.3). The soil was sampled from each peripheral beachrock in Yoggyakarta, Indonesia. After screening, the bacterial species were identified by 16srDNA gene analysis. The genome extraction was done using 100 µL of Mighty Prep reagent taken into a 1.5 mL microtube. From the colonies on the plate, the cells were removed with a sterilized platinum loop, suspended in the microtube, heated at 95 ◦C for 10 minutes, and then centrifuged at 12000 rpm for 2 minutes. The supernatant of the suspension centrifuged was transferred to another tube and used as a template for PCR (polymerase chain reaction).

3.3.2 Laboratory analysis

3.3.2.1 Petrographic studies

In this study, beachrock types were grouped according to Folk’s classification of carbonate rocks (Folk, 1962) using five properties: grain size, chemically precipitated cements, textural maturity, miscellaneous transported constituents, and clan designation. Folk's fivefold name must be in the following format: (Grain size): (chemically precipitated cements) (textural maturity) (miscellaneous transported constituents) (clan designation). Samples of beachrock

that were brittle and poorly sorted were easy to break into pieces. Resin was added to such samples to solidify them, and they were cut to make thin sections for microscope slides. The collected samples were then examined in the laboratory using an optical petrographic microscope equipped for polarized light microscopy. The petrographic analysis was carried out at the Optical Geology Laboratory to assess the biostratigraphy of the samples.

3.3.2.2 Inductively coupled plasma-atomic emission spectroscopy and mass spectrometry (ICP-AES and MS)

Each prepared beachrock sample (10 g) was added to lithium metaborate/ lithium tetraborate flux, well mixed, and fused in a furnace at 1000 °C. Then, each sample was cooled and dissolved in 100 mL of 4% nitric acid and 2% hydrochloric acid for preparation and reduce of organic compound of samples. This solution was then analyzed using ICP-AES in the laboratory of ALS Canada Ltd. (North Vancouver, Canada). Major and trace elements were analyzed by ALS Canada Ltd. (North Vancouver, BC) using the ICP-AES and ICP-MS (method code ME-MS81L, iCAP 6000 Thermo Fischer Scientific) methods after aqua regia digestion (ARD) for combined whole rock analysis, trace elements by fusion and aqua regia digestion for the volatile trace elements, carbon and sulfur for combustion analysis, and several detection limit options for base metals. Four certified reference materials, ME-ICP06, OA-GRA05, ME-MS81, and TOT-ICP06, were measured using the same procedure as the samples for data calibration (Nichols, 2009). The loss on ignition (LOI) was determined using the gravimetric method. Each prepared beachrock sample (10 g) was placed in an oven at 1000 °C for one hour, cooled, and then weighed. The resulting material was then cooled and dissolved in an acid mixture containing nitric, hydrochloric, and hydrofluoric acids. Beachrock sample was consisted of ~90% of the organic compound of microbial carbonate precipitation therefore to eliminate the organic compound the samples have to dissolve in acid mixture. The normalization values for plotting the trace element concentration of the limestone samples are from the Average Phanerozoic Limestone (Martin, et al., 1994; Codie, et al., 1991), while Post-Archean Australian Shale (PAAS) normalization (Guimaraes, et al., 2013) was used for plotting major oxide and rare earth element (REE) concentrations in the samples (Rollinson, 2014).

3.3.2.3 X-Ray diffraction (XRD) and total organic carbon (TOC)

The research findings presented use geochemical analysis (XRD). This form of analysis is usually used when trying to determine mineral composition and the enrichment of elements

that can be found in the beachrock. Each sample finding for different locations represented a swash zone (intertidal, the narrow region of sediment between land and sea) in the different locations. In the XRD experimental analysis using a MiniFlex™ (Rigaku Co., Ltd., Tokyo, Japan), a natural beachrock sample was dried at 105°C and ground into powder manually. XRD scans were recorded from 5 to 80° 2θ, at rate of 20° per minute. The crystalline phases were identified using the International Center for Diffraction Data (ICDD) database and Match 3.4 (Putz and Brandenburg, 2015).

On other hand, since the evaluation process of these resources is essentially depending on the determination of total organic carbon (TOC), hence, an accurate and continuous evaluation of TOC is required. Direct measurement of TOC from core samples in the laboratory is accurate but it is costly and time consuming. On the other hand, the current practice of TOC estimation based on bulk density log alone or based on the conventional sonic (or density) logs and resistivity log using empirical correlations is fast but not accurate enough due to the assumptions implied in these correlations (Huang et al., 2015).Currently two proven techniques of estimating TOC from well-log data are used; these methods are: the Schmoker density log based technique (Schmoker, 1979, 1980) and *Δlog R* method (Passey et al.,1990). Schmoker correlation was developed for Devonian shale formation, Eq.3.1, based on treating the Devonian shale as a four-component system (matrix, interstitial pores, pyrite, and organic matter). He considered the total density of the formation as a function of the densities and fractional volumes of these four components, and setting the pyrite, organic matter and matrix densities of 5.0, 1.0, and 2.69 g/cm^3, respectively. The pyrite volume was assumed to increase linearly with the increase of the organic matter.

Based on these assumptions, Sckmoker derived Eq.3.1 to calculate the organic content in volume percent. TOC in wt% can be obtained by converting the volume to weight percent. There is a well-established correlation between wt% and volume percent for Devonian shale (Schmoker, 1979).

$$TOC(vol\%) = {(\rho_B - \rho)}/{1.378} \qquad \text{(Eq. 3.1)}$$

where TOC is the total organic carbon, ρ_B is the formation density in absence of organic matter (g/cm^3), ρ is the formation bulk density (g/cm^3). The major disadvantage of Schmoker method is that it assumes the formation bulk density and porosity are constant, and any change in the bulk density is due to presence or absence of low-density organic kerogen.

3.3.2.4 Algae taxonomy

Macroalgae can be divided into three divisions based on their primary pigment color: *Chlorophyta* (green algae), *Rhodophyta* (red algae), and *Phaeophyta* (brown algae) (Pratama, et al., 2015). Green algae are abundant in warm (trophic) waters and at least 12 genera of green algae were recorded (Romimohtarto, 2009). Algae were found in the intertidal zone of Krakal Beach and samples were collected by purposive random sampling. Each sample was taken completely from the substrate for identification. Samples taken by purposive random sampling from each quadrat plot were stored in Ziplock plastic bags. Then, samples were cleaned and photographed on millimeter block paper for identification. The identification results showed the seaweed diversity based on identification using the FAO Species Identification Guide for Fishery Purpose (Trono, 1998).

3.3.2.5 Isolation and identification of a suitable urease active bacterium

We hypothesized that there was likely to be a close biomineralization relationship between algae and other agents in microbial mats. Moreover, to identify the microbial activity, a 5.0 g sample of beachrock was mixed with 10 mL of autoclaved artificial seawater (Aquamarine, Yashima Drug Company, Osaka, Japan; Table 3.1), then diluted 10^1-10^4 times with artificial seawater. Next, 10 µL of each dilution was added to ZoBell2216E agar medium (for marine bacteria, pH 7.7) and NH_4-YE agar medium for inland bacteria (20 g/L yeast extract; 10 g/L di-ammonium sulfate $(NH_4)_2SO_4$; 0.13 M Tris buffer for pH 8.0), and 20 g/L agar amended to isolate micro bacteria resistant strains as target study of this research. To avoid contamination, every step of the investigation was conducted inside a clean-bench. After incubation at 35 °C for 3 d, about ~53 colonies from each location were isolated from the plates. A urease activity test was then conducted on the colonies to identify ureolytic bacteria. Each selected colony (diameter: 2–3 mm) was mixed with 20 mL of solution (20 mL/L cresol red solution, 0.4 g/L cresol red with distilled water, and 25 g/L $CO(NH_2)_2$ with distilled water) in a 20 mL bottle. The samples were then sealed, mixed by shaking, and then incubated at 45 °C for 2 h. To determine whether or not the colonies have urease activity, we observed the color of the solution after 2 h. There was a change in the cresol red, from yellow to purple as pH increased from 7.2 to 8.8.

Gene amplification (16S rRNA) and sequencing was carried out for selected ureolytic isolates. The analysis of the DNA sequences was performed using the DB-BA 12.0 and International Nucleotide Sequence Database created by the Techno Suruga Laboratory,

Shizuoka, Japan. The ureolytic bacteria isolated were identified using 16S rRNA sequence analysis. DNA extracts were amplified using two sets of primers targeting the region-specific 16S rRNA sequences for almost all bacterial 16S sequences: the F9 (5′-GAGTTTGATCCTGGCTCAG-3′) and R1451 (5′-AAGGAGGTGATCCAGCC-3′) primers. The PCR amplification cycle consisted of an initial denaturation step lasting 5 min at 94 °C, followed by 25 cycles lasting 1 min at 94 °C, 2 min at 60 °C, 1 min at 72 °C, and a final extension step of 30 min at 72 °C. The amplicons were separated through gel electrophoresis, and the resulting DNA bands were extracted and purified using the FastGene™ PCR extraction kit according to manufacturer instructions (Nippon Genetics Co., Ltd., Tokyo, Japan). The extracted DNA was sent to the Eurofins Genomics Laboratory (Eurofins Genomics, Tokyo, Japan) for sequencing. Subsequent phylogenetic analysis was conducted by TechnoSuruga Laboratory (TechnoSuruga Laboratory Company Ltd., Tokyo, Japan). The latter used the BLAST algorithm to find related sequences in the GeneBank Database, DNA Data Bank of Japan, and the European Molecular Biology Laboratory. PCR sequencing was conducted to identify the species of ureolytic bacteria isolated from the sites at Krakal-Sadranan.

Table 3.1. Composition of artificial seawater (Aquamarine, Japan)

Reagent	**(g/20 L)**
$MgCl_2 . 6H_2O$	222.23
$CaCl_2 . 2H_2O$	30.7
$SrCl_2 . 6H_2O$	0.85
KCl	13.89
$NaHCO_3$	4.02
KBr	2.01
H_3BO_3	0.54
NaF	0.06
NaCl	490.68
Na_2SO_4	81.88

3.3.2.6 Cultivation of bacteria and assessing the potential for microbial induced carbonate precipitation (MICP)

Standard media (ZoBell2216E for marine bacteria and NH_4-YE medium for land bacteria) were used for culturing under sterile aerobic conditions. Cells were precultured separately in 5 mL of each medium at 37 °C and 160 rpm for 24 h. One mL of the preculture was inoculated with 100 mL of the fresh medium and incubated under the same conditions. The microbial cell growth of the isolates was determined based on optical density at a wavelength of 600 nm (OD_{600}) using a UV–vis spectrophotometer (V-730, JASCO Corporation, Tokyo, Japan). Representative specimens were sampled at regular intervals of 24 h. Microbially induced calcium carbonate precipitation tests were conducted in 10 mL tubes to evaluate the feasibility of using isolated bacterial strains. Calcium chloride ($CaCl_2$) reagent was chosen as the calcium source, and 1 mL from equimolar concentrations (0.5 mol/L (M)) of $CaCl_2$ and urea solutions were used. One milliliter of the bacteria culture was added to the tube, and the total volume was adjusted to 10 mL using distilled water. Samples were then placed in a shaking incubator at 37 °C and shaken at 160 rpm for 48 h. Finally, the reaction mixtures were centrifuged, precipitates were collected, and the amount of precipitate formed by each isolate were gravimetrically compared. Based on the results, a single isolate was selected as the most suitable for further analysis.

3.4 Results

3.4.1 Stratigraphy of Krakal-Sadranan Beachrock

The studied samples were categorized as non-beachrock, unconsolidated beachrock, and well-consolidated beachrock, based on relative proportions of skeletal, mineral, and rock fragments and degree of cementation. Limestone sand with sparse biomicrite cement dominates most samples in the sampling/stratigraphic columns (e.g. EFX2 – see Appendixes B). Sample X2, for example, contains limestone fragments (30%), fossil shell 16 fragments (35%), and limestone sand (35%). Whereas the meniscus bridges inter- and intra-particle mainly consisted of calcite-aragonite calcium carbonate (Figure 3.2).

3.4.2 ICP – AES and -MS Analysis Data

Geochemically, enrichment of some major oxide concentrations such as calcium oxide (CaO) and magnesium oxide (MgO) shown in Table Appendixes C, indicates that the most

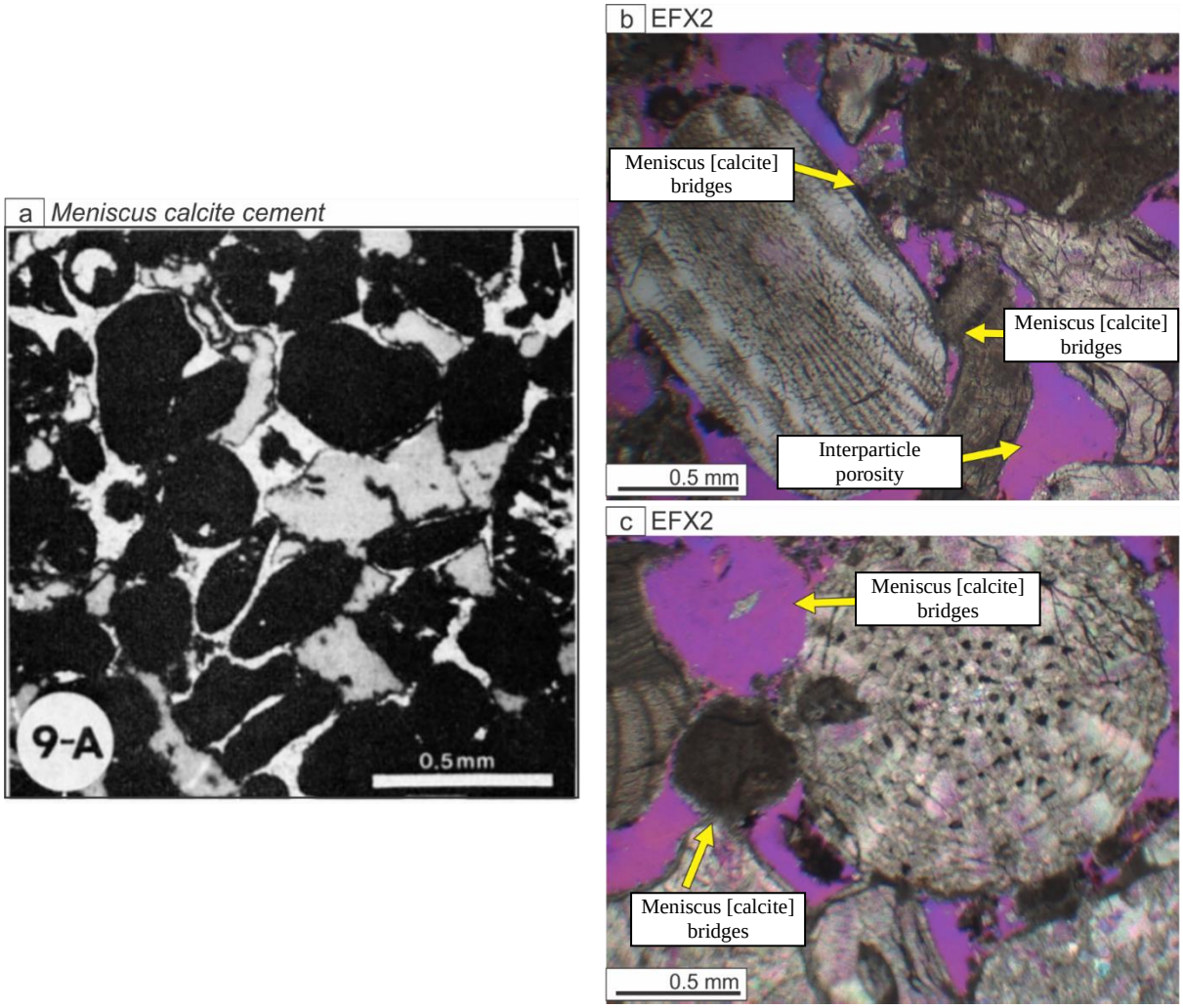


Figure 3.2. Petrography of beachrock samples from Krakal-Sadranan, Yogyakarta, Indonesia (a) the meniscus calcite cementation (Folk, 1962) and (b), (c) morphology of meniscus cement beachrock.

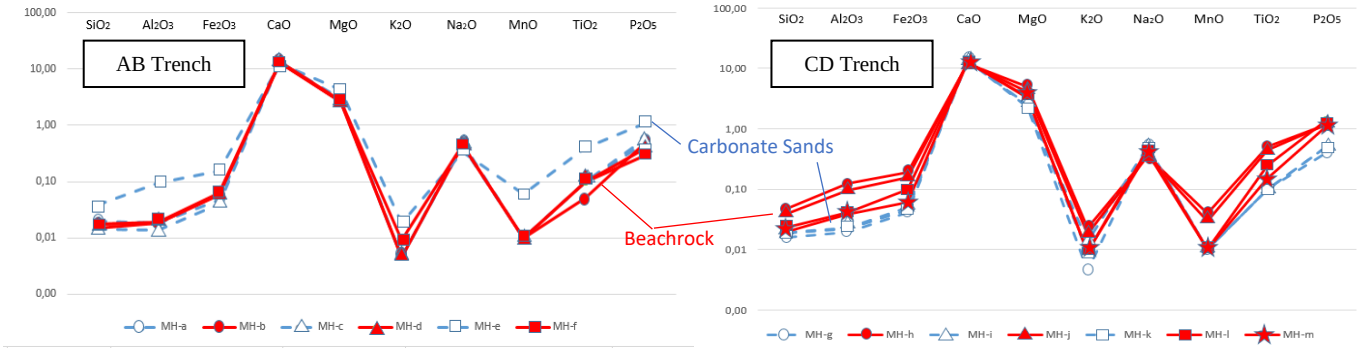
minerals were beachrocks. Furthermore, an increase of MnO concentration is directly proportional to beachrock changing to calcite dominant. Increasing MnO were found in samples that evaporated more intensely than beachrocks in the swash zone. The major oxide data from Table Appendixes C shows that beachrocks contain CaO concentration ranging from 43.7 – 49.9 wt.%, SiO_2 0.9 – 3.07 wt.%, Al_2O_3 0.26 – 2.38 wt.%, Fe_2O_3 0.26 – 1.25 wt.%, TiO_2 0.01 - 0.09 wt.%, and MnO 0.01 – 0.06 wt%. LOI (Loss on Ignition) in the samples of this study ranged from 41.80 - 44.80% (wt%) of CO_2 concentration, which when added to CaO, the concentration of $CaCO_3$ from the samples were greater than 90%, which concluded the samples to be classified as limestones, while ABX_1, CDY_2, and CDZ_2 samples are still classified as carbonaceous sedimentary rocks. Plotting of major oxide variation (x-axis) versus major oxide concentration of the sample on y-axis uses normalization from PAAS (Post-Archean Australian Shale; from Guimaraes et al., 2013). The plotting shows that CaO concentration of carbonate

sands is of a higher concentration than the beachrock samples (Figure 3.3, a). We observed a gradual decrease of the CaO concentration from the beachrocks in the swash zone to the carbonate sands in the land area. The CaO decrease was assumed to be on account of a nutrient deposit from the sea among the sedimentary processes that resulted in a decrease from the bottom to the top and linear from the land to the seashore (Porta, 2015; Avcioğlu, et al., 2016; Karkani, et al., 2016; Daryono et al., 2019).

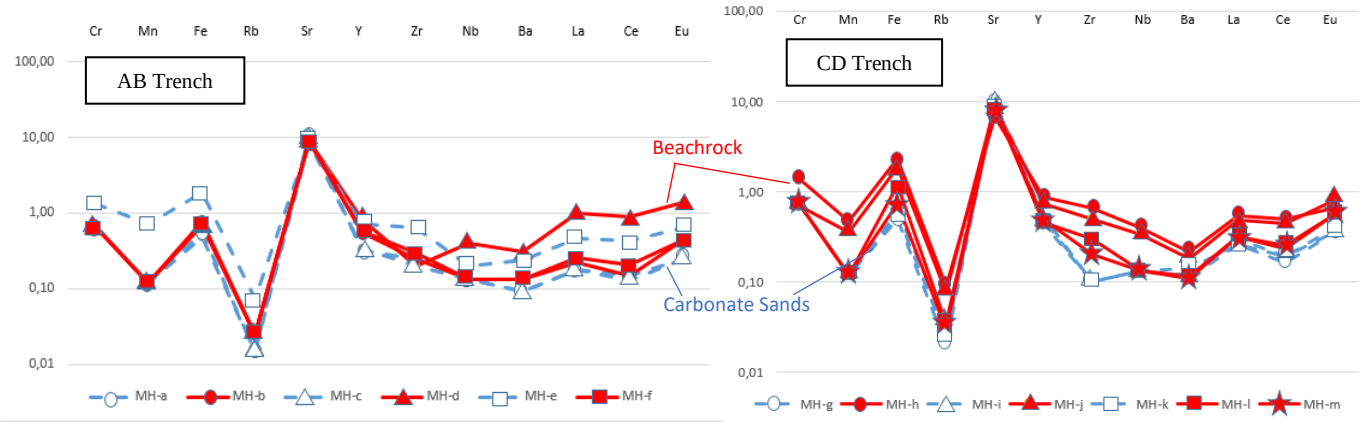
Figure 3.3 presents the concentration of quartz (SiO_2), magnetite (Fe_2O_3), and ilmenite (TiO_2) of the samples that displays the impurities of aggregate minerals in the beachrocks. The concentration of trace elements (Cr, Mn, Fe, Rb, Sr, Y, Zr, Nb, Ba, La, Ce, and Eu) including rare earth elements (REE) of the beachrock samples increased as it shifts from the land to the seashore as a mix of unconsolidated beachrocks-carbonaceous sands and beachrocks (Figures 3.3b, c). Note that the plotting of normalized trace element and rare earth element concentrations was only performed on those 13 samples from this study which are summarized as unconsolidated beachrocks-carbonate sands (ABX_1, ABY_1, ABZ_1, CDX_1, CDY_1, CDZ_1) and beachrocks (ABX_2, ABX_3, ABY_2, ABZ_2, CDX_2, CDY_2, CDZ_2) sample. Beachrock sedimentary is unique compared to other sedimentary rocks. Its characteristics do fit with the definition of a conglomerate with carbonate cement; however, most of the recent carbonate cementations are still classified as carbonate rocks or even young limestone. Geochemical evidence shows that beachrocks are rich of Sr elements, the complete opposite occurred to crust-mantle beachrocks found in Arabian gulf and limestones in the same location in Java Southern Mountain (Alshuaibi, et al., 2015; Atmoko, et al., 2018).

The rare earth element (REE) patterns of the various beachrocks vary consistently (Figure 3, c). However, all of the patterns in Figure 3.3,c showed depletion in light-REE (LREE) with respect to heavy-REE (HREE). All of the samples exhibited negative cerium (Ce) anomalies and positive Yttrium (Y) anomalies. In addition, the pattern of the normalized rare earth element concentration of the limestone samples showed consistency with seawater (Figure 3.3, c). Data of the seawater REE concentration was taken from Bolhar et al., (2004). A typical seawater REE profile is smooth and coherent with progressive enrichment in heavy REE with Ce negative anomaly and Y positive anomaly (Mauz, et al., 2015; Tostevin et al., 2016; Atmoko, et al., 2018). CaO, MgO and LOI (loss on ignition, i.e. mainly CO_2) represent the main components identified by chemical analyzes (Figure 3.3). This is in concordance with

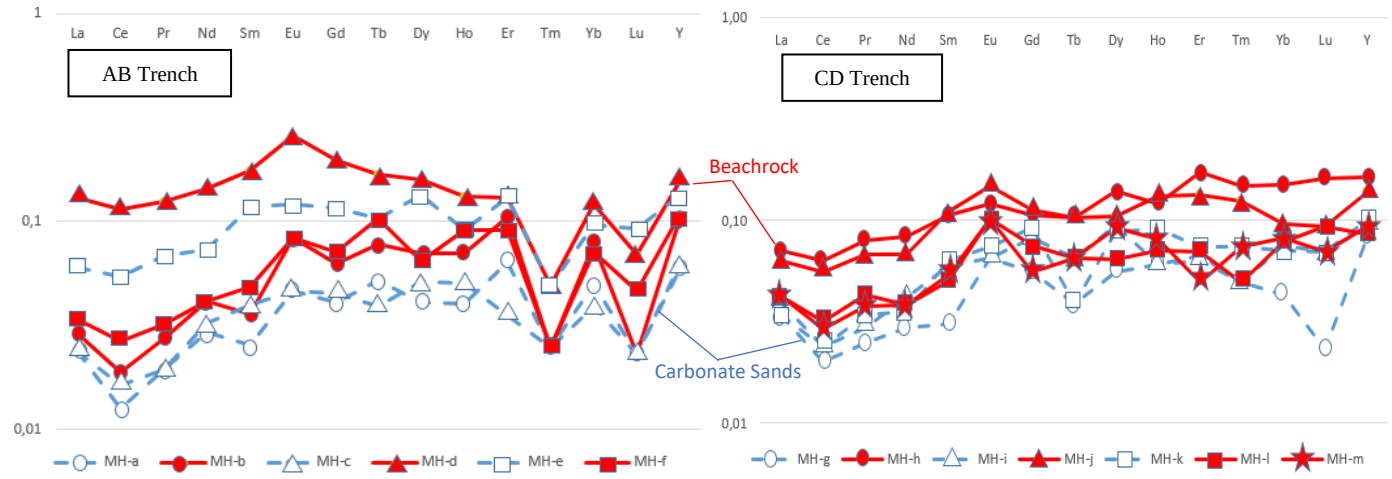
dominance of limestone-sand component in samples, and also suggest minor presence of Mg in the carbonate phase (i.e. magnesian calcite, or mixture of calcite and dolomite).



(a) Major Elements Normalization Based on PAAS



(b) Trace Elements Normalization Based on Average Phanerozoic Limestone



(c) REE Normalization Based on PAAS

Figure 3.3. Spider diagrams of beachrock elements analysis (a) PAAS (Post-Archean Australian Shale) normalized major oxide diagram for limestone samples of beachrock, (b) Trace element normalizing based on Average Phaenerozoic Limestone, (c) Rare elements analysis diagram of beachrock based on shale normalization.

3.4.3 X-Ray diffraction (XRD) and total organic carbon (TOC)

The results of XRD and TOC data processing in the show that there were several similarities in the mineral composition of each sample of carbonate and beachrock Sand Deposits. The minerals contained in each of the 13 samples that have been analyzed include calcite, aragonite, magnesium-calcite and a little quartz (SiO_2) (Figure 3.4, a). Then there is a little content of iron (Fe) and alumina (Al) in several samples, namely in the sample ABX_1, ABX_2, CDY_2, and CDX_2.

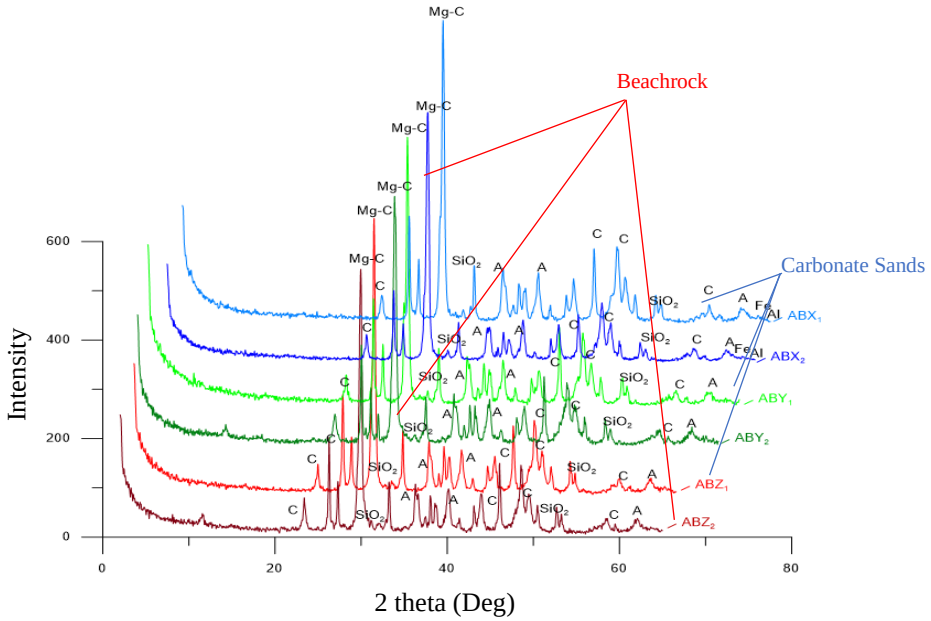


Figure 3.4. Graphic XRD (a) and total organic carbon (b) from Beachrock, Krakal-Sadranan, Yogyakarta. Within abbreviation Mg-C: Magnesium Calcite, C: Calcite; A: Aragonite; SiO_2: Silica; Fe: Iron; and Al: Alumina.

The TOC analysis yielded the organic carbon deposit supply during the sedimentary process of the beachrocks. The data showed that the supply deposit is mostly from the seawater deposition which is rich in carbon from biological activities. The TOC's from sample near the sea are ABZ_1, ABZ_2, CDZ_1, and CDZ_2 showed the highest amount of organic carbons which are 0.147%; 0.159%; 0.334%; and 0.218 % with the total carbon of 11.726%; 11.763%; 11.859%; 11.378%. Although the result of total organic carbon and total carbon (Figure 3.4, b) does not represent the ages of the sedimentary rocks, it still supports the fact that beachrocks are the aftermath of marine sedimentary dominant, which in turn also proves that carbon-rich components were more commonly found near sea, and less buried in the surface areas.

3.4.4 Biodiversity observations

3.4.4.1 Algae taxonomy

A total of six marine plant species were recorded across the six samples taken from the Krakal-Sadranan Beach. The recorded algal species included one species of green algae, one species of brown algae, and four species of red algae (Table 3.2). At macroscale, algae could be home to macrobenthos, microbenthos, and microorganisms surrounding beachrock or coral reef. In the end, those six species of algae were identified as being predominant in the Krakal-Sadranan Beach study area and of close proximity to the beachrock.

Table 3.2. Algae species taxonomy surrounded beachrock.

No.	**Location E 455900.11; S 9099654.13 until E 456281.51; S 9099623.03**					
	Division	Class	Ordo	Familia	Genus	Species Name
1.	Rhodophyta	Florideophyceae	Ceramiales	Rhodomelaceae	Laurencia	*Laurencia pappilosa (C. Agardh) Greville*
2.			Gelidiales	Gelidiaceae	Gelidium	*Gelidium corneum (Hudson) Lam.*
3.		Rhodophyceae	Gigartinales	Gigartinaceae	Gigartina	*Gigartina* sp
4.			Rhodymeniales	Rhodymeniceae	Rhodymenia	*Rhodymenia pseudopalmata (Lam.) P.Silva*
5.	Phaeophyta	Phaeophyceae	Fucales	Sargassaceae	Sargassum	*Sargassum duplicatum Bory*
6.	Chlorophyta	Chlorophyceae	Ulotrichales	Ulvaceae	Ulva	*Ulva Lactuca L.*

3.4.4.2 Isolation of indigenous ureolytic bacteria

The beachrock samples by the seashore and other outcrops found in Krakal-Sadranan were placed in sterile tubes and identify the urealytic bacteria's from inside of the rock samples. The bacteria inside the tubes were then diluted 10^1-10^4 times with artificial seawater. Next, 10 μL of each dilution was added to ZoBell2216E agar medium for marine bacteria. After incubation at 37 °C for 3 d, the bacterial colonies were isolated from one plate. Before the fieldwork, cells were cultured in ZoBell2216E and NH_4-YE media, which also contained 5.0 /L polypeptone (Nihon Seiyaku Co., Ltd., Tokyo, Japan), 1.0 g/L $FePO_4$ (Junsei Chemical Co., Ltd., Tokyo, Japan), and 1.0 g/L yeast extract (BD Bioscience Adv., Bioprocessing, Miami, Florida, USA). These were prepared with artificial seawater with pH 7.6–7.8, adjusted using 1 M NaOH (Fujita, et al., 2017).

After 72 h, medium-cultured colonies (aggregates of bacteria) were grown, and then counted to determine which plates were populated with 20–100 medium colonies, which had higher probability of being ureolytic bacteria. Using a sterilized toothpick, each colony from the selected medium was moved into its own medium for the next step, which was to select urease bacteria using a cresol red solution. Urease activity measured in a 10 mL solution was put into a polystyrene screw bottle. Furthermore, transfer a certain number of bacteria in solid medium using sterilized toothpick, then taken and added to a polystyrene screw bottle containing the urease activity measurement solution. The total potential urease bacteria found is less than 5% as the percentage ratio of ureolytic bacteria among the 527 colonies from the total number isolated from the rock samples. The diversity of microbes known in beachrock encompass three recognized ureolytic bacterial groups, most of which species are assorted microbial eukaryotes. The most frequently isolated 16S rDNA gene sequences include those from acid bacteria, Actinobacteria, and Chloroflexi (Oliver, et al., 2013; Elhadi, et al., 2004; Danjo and Kawasaki, 2014). The results of a homology search in the GenBank/DDBJ/EMBL, three group of bacteria that were highly homologous to the 16S rDNA nucleotide sequence of the species whereas *Oceanobacillus profundus*, *Vibrio maritimus*, and *Pseudoalteromonas tetradonis*. The strains in the 16S DNA gene sequences are shown in Figure 3.5. The *O. profundus* is a gram-positive species that are motile, aerobic, rod-shaped (0.2–0.4 μm) and classified as biosafety level 1 bacteria. The others, *V. maritimus* and *P. tetradonis* are gram-negative. The former are motile bacilli 1 μm wide and 1.5–4.0 μm, whereas the latter are strictly aerobic, motile with one polar flagellum, form either straight rods (or rod-shapes), 0.5–0.8 × 1.0-1.5 μm when in exponential growth phase. Even though *V. maritimus* and *P. tetradonis* are

classified as biosafety level 1, but further analysis of *Vibrio maritimus* caused it to be eliminated because of indicated pathogenic similarity to *Vibrio cholerae* (i.e., *V. cholerae*).

Samples code	Taxonomy result

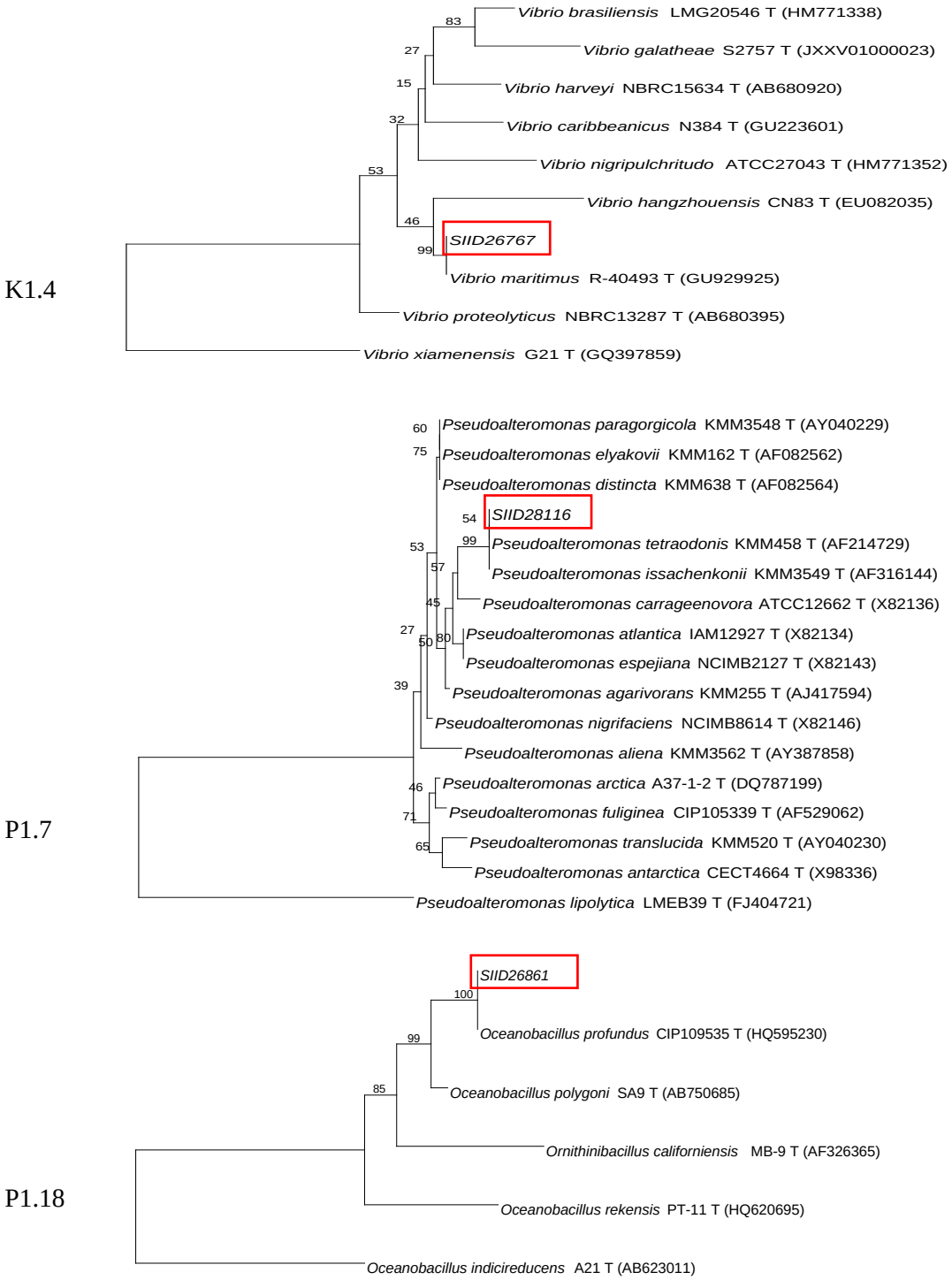


Figure 3.5. Phylogenetic tree based on 16S rDNA nucleotide sequence of *Vibrio maritimus*, *Psedoalteromonas tetradonis*, and *Oceanobacillus profundus (red-frame).*

3.4.4.3 Microbial population count and urease activity test

The cell concentration increased for 2 d and then reached the stationary phase. The urease activity of the cell culture increased with cell growth. Based on this result, the production of urease would be a growth-associated system. Considering microbial-based sand solidification, which should be sustained for relatively long duration for adequate solidification, the long-term stability of the enzyme would be advantageous in the MICP process (Danjo and Kawasaki, 2014). Even though the bacterial strains are considered biosafety level one (safe for the human body and environment), but some strains of *V. maritimus* are pathogenic (Kandianis, et al., 2008; Zhu and Dittrich, 2016; Almajed, et al., 2018) therefore for further research, only *O. profundus* and *P. tetradonis* were used to continue the deep research to develop the MICP method. The *P.tetradonis* were used to continue the deep research to develop the MICP method. The test tube precipitation test results are a good relative indication test tube precipitation test results are a good relative indication of the potential of each strain for sand solidification by MICP (Danjo and Kawasaki, 2014; Mwandira, et al., 2019; Marshall, et al., 2015; Arrieta, et al., 2017). This is because the improvement in strength is proportional to the amount of bio-precipitate formed. The results indicate that the strain belonging to *P. tetradonis* shows the highest performance for microbial induced carbonate precipitation and the weight of precipitate is approximately two times more than that from the others (Figure 3.6).

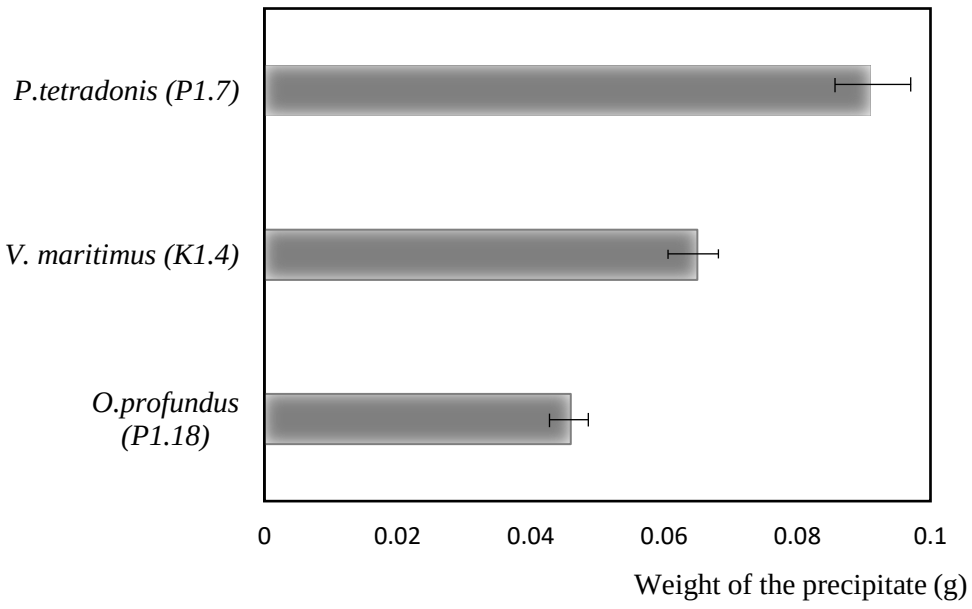


Figure 3.6. Microbial induced carbonate precipitation capacity of isolated strains.

3.5 Discussions

Beachrock is generally cemented in the tidal zone with a large amount of aragonite, high-magnesium calcite (HMC), and low-magnesium calcite (LMC). Carbonate cementation in the marine environment forms acicular-radial and spacious types of cement texture, whereas the tidal zone cement is indicated by aragonite or HMC. Meniscus bridge cement indicate LMC composition (Vousdoukas, 2007; Avcioğlu, et al., 2006; Danjo and Kawasaki, 2014; Daryono, et al., 2019). Beachrock found in Indonesia consisted of elements of calcium, magnesium, sodium, and phosphorus according to the oxide major ICP-data, which proved it dissimilar to those of limestone and/or other beachrock. Limestone generally consists of silica and carbonate. Meanwhile, beachrock from Kuwait, Arabia Gulf consists of silica and carbonate. (Karkani, et al., 2016; Porta, 2015). Hence, some authors have suggested that bacterial metabolism is related to the precipitation of rocks (Danjo and Kawasaki, 2014; van Paassen, et al., 2009; Almajed, et al., 2018) and that the end products lower the thermodynamic boundary for cement nucleation and increases the rates of the physicochemical processes involved (Bathurst, 1966). A technique for bio-cementation using microbial induced carbonate precipitation (MICP) for calcium carbonate precipitation could be biologically controlled or induced. Bacteria serve as a catalyst in urea hydrolysis through the generation of urease enzyme to form calcium carbonate cement (Mwandira, et al., 2019; Danjo and Kawasaki, 2014; Daryono, et al., 2018). Specific cement types are recognized as (i) acicular, fibrous, and bladed fabrics; (ii) radial fibrous and fascicular-optic fabrics; (iii) micro-and cryptocrystalline fabrics; (iv) equant spar, syntaxial overgrowth fabrics, scalenohedral calcites, and peloidal fabrics; and (v) non-carbonates. These types indicate incipient early marine cementation leading to a reduction in pore-space in near-seafloor sediments (Ng, et al., 2014). Krakal-Sadranan Beaches happen to follow the same pattern, in which the meniscus cement solution is characterized by domination by crystalline aragonite and magnesium-calcite, which are soluble in water.

3.5.1 Sediment characteristics

To summarize the petrographic analysis of all samples, the diagram splits the sedimentary beachrocks in this area into four zones: unconsolidated beachrocks; well-consolidated beachrocks; mineral-dominated beachrocks; and rock-dominated beachrocks. This lithofacies consists of samples with codes ABX_2, ABZ_2, CDY_2, CDZ_2, EFZ_1, EFX_2, EFY_2, and EFZ_2 classified as Sparse Biomicrite. Therefore, sample ABY_2, CDX_2, dan CDX_3 were classified as Packed Biomicrite. Sparse biomicrite has an allochem bioclastic texture of 0.04-10 mm grain

size. It is poorly sorted, open-packed, angular grain shape, and has relatively damaged fragment shape. The fossil pore is filled with micro calcite (sparse) and the presence of micrite (mud carbonate) and the dominant micrite little sparse and floating contact, the size of the fragments varies. Packed biomicrite has a bioclastic allochem texture of 0.04-10 mm grain size. Poor sorting, open container, angular grain shape, and relative fragment shape has been damaged. In the fossil pore filled with micro-calcite (sparse) and the presence of micrite (mud-carbonate) and the dominant micrite little sparse and floating contact, the size of the fragments varies. In this analysis, skeletal foraminifera dominated as a matrix that constructs the beachrock and recrystallization cement (micrite and sparse) that connected the grain material and the beachrock.

3.5.2 Post depositional diagenesis

The plotting results of trace element (Cr, Mn, Fe, Rb, Y, Ba, La, Ce, and Eu) concentration of the beachrock samples from this study exhibit enrichment trending from the land to seashore that assuming of marine nutrient for cementation process. In contrast, the Sr element shows the highest concentration in the beachrock and also carbonate sands (also assuming as unconsolidated beachrock (Figure 3.2, c). Azizi et al. (2014) and Nagendra and Nagarajan (2003) explained that Sr element depletion was an indicator of the diagenetic process on limestone. According to Azizi et al. (2014), the concentration of the Sr element in the limestone samples from Eastern Iran ranges from 121.14 to 191.13 ppm (mean = 159.12 ppm). The Sr values of these samples were higher than their limestone counterparts found in the same geological rock formation. In recent temperate carbonates, the Sr values ranged from 2690 to 4360, in contrast to the limestones with 1642 to 5007 ppm. The low content of Sr in comparison with the recent beachrocks was mainly due to permeation of freshwater that caused a removal during meteoric diagenesis of these carbonate cementation, as supported by Azizi et al. (2014) and Atmoko, et al. (2018). Furthermore, it was accelerated by prolonged diagenesis in an open system under the influence of meteoric water (Nagendra and Nagarajan, 2003). Based on the Sr concentration in the Wonosari-Punung limestone samples and by referring to studies of Nagendra and Nagarajan (2003), Azizi et al. (2014), Atmoko, et al. (2018), it could be interpreted that beachrock samples of this study with lower Sr content experienced more removal by freshwater during the diagenesis in comparison with carbonate sands (or close to unconsolidated beachrock) which is characterized by higher Sr content of ~3500 ppm. Involving freshwater on accelerating Sr depletion could suggest that the process of diagenesis might have occurred after the deposition of the beachrocks. Therefore, the Sr depletion of the

beachrocks suggests that the diagenetic process has not yet occurred in the phase after deposition.

3.5.3 Temperature and evaporation conditions

Figure 3.2 shows that beachrock and carbonate sand have relatively similar diagram patterns. However, when viewed in detail the concentration of REE on beachrock is relatively higher compared to carbonate sand. In addition, the anomaly of Tm elements negative for all depleted beachrock and carbonate sand samples. Dauphas and Pourmand (2015) explain that anomalies of negative Tm elements caused by high-temperature conditions (37°-50°C) cause an intensive evaporation and condensation process which reduces the elemental content of Tm. Therefore, it can be interpreted that the process of deposition of beachrock and carbonate sand in the study area is at a high temperature (37°-50°C) and under conditions of evaporation and condensation which is quite intensive.

3.5.4 Redox condition

Profiles of REE concentrations in the beachrock samples normalized by the PAAS (Post-Archaean Australian Shale) present a trend of the lowest value for the beachrock and carbonate sands near seashore then were found relative to the Figure 3.2, a Trench AB and CD. According to Schieber (1988), possible co-precipitation of REE in carbonates from seawater is much too small to account for the REE enrichment. Therefore, only the diagenetic REE enrichment has to be considered. Referring to tables of trace elements and REE (Table Appendixes C), it can be seen that beachrock samples have increased ∑REE, that is in ABY2 samples (24.03 ppm) and CDZ2 samples (14.30 ppm). Therefore, in samples of carbonate sand deposits have increased ∑REE in ABX1 samples (12.52 ppm) and CDX1 samples (6.56 ppm). Increased concentration of ∑REE, both heavy REE (Tb, Dy, Y, Ho, Er, Tm, Yb, and Lu) and light REE (La, Ce, Pr, Nd, Sm, Eu, and Gd) indicates that the condition of the beachrock deposition process is at oxidative environmental conditions. This can be supported by the result of the element ratio table (Table 3.3) showing that the value of Ce/ Ce* is less than 1. The Ce/ Ce* value less than 1 indicates a negative Ce anomaly. The negative Ce anomaly indicates that the beachrock deposition process originates from precipitation of seawater under oxidative conditions.

Table 3.3. Ratio of carbonate sands and beachrock in Krakal-Sadranan, Yogyakarta, Indonesia.

Trench	Name of rock	Element ratio				
		Sample	Mn*	Ce/ Ce*	Eu/ Eu*	Y/ Ho
AB	Carbonate sands	ABZ_1	0.45	-2.27	3.76	40
		ABY_1	0.51	-1.71	2.16	34
		ABX_1	0.71	-3.3	3.07	40
	Beachrock	ABZ_2	0.33	-1.63	3.1	40
		ABY_2	0.36	-3.36	6.2	32.3
		ABX_2	0.31	-2.5	2.02	32.22
CD	Carbonate sands	CDZ_1	0.49	-2.85	3.16	36.67
		CDY_1	0.41	-2.16	1.11	41.67
		CDX_1	0.45	-3.16	1.06	30.0
	Beachrock	CDZ_2	0.43	-3.57	8.9	36.67
		CDY_2	0.4	-4	1.0	28.46
		CDX_2	0.12	-4.63	2.24	32.85
		CDX3	0.32	-3.59	2.82	31.25

In addition, Table 3.3 shows the results of the calculation of a positive *Mn** value. A positive *Mn** value indicates the condition of the deposition process of carbonate rock in an oxidative environment. Machhour et al. (1994) and Bellanca et al. (1996) formulated Mn* as follow:

$$Mn^* = log\ [(Mn_{sample}/\ Mn_{shale})/\ (Fe_{sample}/\ Fe_{shale})] \quad \text{(Eq. 3.2)}$$

with Mn_{shale} and Fe_{shale} are 600 ppm and 46,150 ppm, respectively (Wedepohl, 1978).

The variations in the solubility of reduced manganese may lead to significant fractionation of these metals across the redox boundaries, where manganese tends to be incorporated under more oxygenated conditions above the redox boundary (e.g., Tribovillard et al., 2006; Madhavaraju and Lee, 2009; Piper and Calvert, 2009; Neumeister et al., 2016). Additionally, a study of Madhavaraju and Lee (2009) shows that positive Mn* values indicate an oxidative condition in beachrock deposition.

3.5.5 Terrigenous contaminant materials

Madhavaraju and Lee (2009) mentioned a method to interpret the source of rare earth elements using Eu anomaly $\{Eu/\ Eu^* = E_{uN}/\ (0.5*(Sm_N+Gd_N)\}$. The implementation of the

aforementioned formula on the beachrock samples of Krakal-Sadranan Beach showed that Eu anomaly of the samples ranged from 1.00 to 8.90 (Table 3.3). The value of Eu anomaly, which is higher than 1, means that the beachrocks have a positive Eu anomaly (Madhavaraju and Lee, 2009). Due to the result of Eu/ Eu* on the beachrock samples of the studied area being higher than 1, it indicates positive Eu anomalies. These positive Eu anomalies are shown by the REE plotting of PAAS -normalized on the beachrock samples from this study in the Figure 3.2 c, Trench AB and CD. A positive Eu anomaly indicates that the beachrock was affected by hydrothermal solutions (German et al., 1993; Kurian et al., 2008), intense diagenetic process (MacRae et al., 1992), plagioclase (feldspar) content (Nath et al., 1992), or input of aeolian sediment (Elderfield, 1988) close to recent limestone sedimentary (Atmoko, et al., 2018). In some cases, the terrigenous materials are characterized by the remain of plagioclase. The existence of feldspar (plagioclase) in beachrock samples, although in a very small quantity shows consistency with the positive Eu anomaly. The suggestion of the diagenetic process in the beachrock depositional environment is supported by values of Sr concentration, Mn*, contamination of terrigenous (clastic) materials in the limestone depositional environment is consistent with the suggestion of Ce/ Ce* values were in oxidative contamination with terrigenous material, as discussed previously. Therefore, in relation to the positive Eu anomaly, the Eu/ Eu* calculation, the presence of feldspar in the beachrock samples from the studied area conforms to previous studies (German et al.,1993; Kurian et al., 2008; MacRae et al.,1992), it can be interpreted that rare earth elements in the beachrock samples were possibly derived from a diagenetic process, terrigenous materials, and/or hydrothermal activity. As for the influence of the hydrothermal activity, it will be discussed later.

The interpretation of rare earth elements source can be further supported by Y/ Ho ratio as proposed by Bolhar et al. (2004). The calculation of the trace element ratios on the limestone samples yielded Y/ Ho ratios from 28.46 to 41.67 (Table 3.3). As terrestrial materials (i.e., felsic and basaltic crust) have a constant Y/ Ho ratio of ~26 and small admixtures of any contaminants, they are supposed to prove seawater-like Y/ Ho ratios of >44 (Bolhar, 2004). The limestones from the studied area showed high ratios of Y/ Ho (more than 26) by comparing to the Bolhar's ratios (2004). This may suggest that the limestone depositional environment was slightly contaminated by terrestrial material or had only small admixtures of any contaminants. The summary of mineralogy and geochemical characteristics of the various beachrocks from the study area and the interpretation of beachrock depositional environment and the source of trace elements are depicted in Table 3.4.

Table 3.4. Summary of deposition process affecting the limestone sand and beachrock at Krakal-Sadranan, Yogyakarta, Indonesia.

Condition	Limestone sands	*Beachrock*	Interpretation
Sr concentration	Raised (~3830 ppm)	Depleted (~3417 ppm)	*Beachrock* postdepositional diagentic alteration
Tm Anomaly	Negative	Negative	Higher temperature (37°C-50°C) and intensive evaporation
REE concentration	Raised (∑REE= 12,52 ppm)	Raised (∑REE = 24,03 ppm)	Oxidative Environment
Mn* = log [(Mn_{sample}/ Mn_{shale})/ (Fe_{sample}/ Fe_{shale})]	Mn* positive	Mn* positive	Oxidative Environment
Ce/Ce* value and Ce anomaly	Less 1	Less 1	Precipitation from seawater under oxidative conditions
Condition	Limestone sands	*Beachrock*	Interpretation
Eu/Eu* value and Eu anomaly	Positive anomaly with value >1	Positive anomaly with value >1	Terigenus material contamination
Y/Ho ratio	High ratio >26	High ratio >26	Terigenus material contamination

The multistage mineralization of the biota is also known as microbialites from marine activity. For example, successive stages of biocementation have been described in microbialites *Pararodhobacter* sp., and *Oceanobacillus profundus* sp., whereas ureolytic bacteria, aragonite nanograins are precipitated outside the cell wall of ureolytic bacteria and, later, the cell content was replaced by aragonite. Aragonite crystals formed outside and inside the cell wall are different in shape and size (Couradeau et al., 2013; Danjo and Kawasaki, 2014; Mwandira, et al., 2019). The reduction of porosity is greatest in this stage because low-Mg calcite completely fills some pores as the final stage of beachrock sediment, the evolution of aragonite crystals into calcite it might occur because of the pH and temperature dependence in the shoreline. In

the case of mineralized varieties, superficial crusts preserve as well as complicate the morphology of the organisms, whereas biomineralized fabrics within skeletal, mollusk and some thrombolites probably retain clearer details. In this environment, interference of the organic process by algae and microbial activities may accelerate the process (Riding, 1991; Henehan, et al., 2015; Arrieta, et al., 2017; Franchi, et al., 2018; Kishi, et al., 2018). The extent of vadose and freshwater diagenetic features indicates that more ancient beachrocks had occupied an inland position for a relatively long time.

3.5.6 Biotically controlled precipitation

The majority of carbonate material in modern oceans is precipitated as highly structured skeletons of organisms. Precipitation is primarily controlled by the biochemistry of the respective organisms (such as algae, foraminifera or corals); the organisms, in turn, are influenced by the conditions of the sea they live in, particularly light, temperature and water chemistry (for instance the degree of carbonate saturation of the sea water). To appreciate the effects of various environmental factors we need to recall the two fundamental types of metabolism. Autotrophic organisms nourish themselves by utilizing inorganic materials to synthesize their own living matter; heterotrophic organisms have to rely on organic material to do so. Autotrophic organisms among the carbonate producers are almost exclusively photo-autotrophic: they perform photosynthesis and thus depend on light for their livelihood. Some carbonate-secreting organisms are themselves heterotrophs but live in symbiosis with autotrophic algae. As a result, the system of host plus symbiont becomes autotrophic.

3.5.6.1 Light

This is arguably the most important control on skeletal carbonate precipitation because of the dominance of photoautotrophic organisms in carbonate production – at least in the Cenozoic. Photosynthesis is a complex, and only partly understood process. The basic reaction may be simplified as:

$$CO_2 + H_2O + \text{solar energy} \rightarrow HCHO + O_2 \qquad \text{(Eq. 3.3)}$$

where HCHO represents a simple summary formula for organic matter. The formula clearly illustrates the link between photosynthesis and carbonate chemistry. Photosynthesis extracts

CO_2 from the sea water, thus increasing its carbonate saturation and facilitating precipitation of carbonate minerals. For the organisms themselves, precipitation of $CaCO_3$ has the added advantage that potentially deleterious Ca^{2+} ions can be removed from the system and a protective skeleton can be constructed. The link between skeletal carbonate fixation, photosynthesis and light explain the decrease of skeletal carbonate production with water depth in tropical environments. Above sea level, carbonate production rapidly drops to zero in the supratidal zone and becomes negative in most terrestrial environments as carbonate material dissolves in rainwater and acidic soils. The euphotic zone is defined in the geologic record as the interval where abundant growth of photosynthetic, carbonate secreting benthos is possible. The zone of light saturation has not been defined in geological terms. Loosely speaking, it is the interval where light has no recognizable control on the rates of growth and calcification of organisms. The growth forms of corals indicate the zone of severe light limitation by a change from massive to platy colonies. In the light-saturated zone, corals indicate the presence of a very turbulent surface layer of the sea by dominance of branching growth forms.

3.5.6.2 Temperature

Rivals light in its effect on skeletal carbonate production. Generally, warmer is better, but there exist upper temperature limits for the various carbonate-secreting organisms. Thus, the temperature window of calcifying benthos is different for different organisms. Most hermatypic (i.e. symbiotic) corals function in the range of 20-30 °C. The upper temperature boundary sets important limits to carbonate production, particularly in restricted lagoons where temperatures frequently exceed 30 °C. The most important effect of temperature, however, is the global zonation of carbonate deposits by latitude. In spite of what has just been said about the importance of light, the boundary northern and southern limit of coral reefs, and thus the boundary of tropical and cool-water carbonates, in the modern oceans seems to be controlled by winter temperature rather than radiation. This indicates that as one moves poleward in the modern oceans, the temperature limit for hermatypic coral growth is reached before the light limit. In the past, this need not always have been the case. The temperature limit and the light limit may have shifted relative to one another during geologic history. The fairly stable position of 30-35 °C latitude for the boundary of Phanerozoic tropical carbonates may reflect the joint control by temperature and light.

3.5.6.3 Latitudinal zonation of skeletal production

Skeletal carbonate production changes very significantly with latitude. The differentiation into tropical and cool-water carbonates is widely applied and often further subdivided (Lees, 1975; Tucker and Wright, 1990; James and Kendall, 1992; James, et al., 1997). Tropical carbonates are dominated by photosynthetic organisms and usually include metazoan reefs, abundant green algae and larger foraminifera. Cool-water carbonates lack these deposit sand consist mainly of skeletal sand and gravel derived from molluscs, bryozoans, smaller foraminers and red algae. The contribution of photoautotrophs to cool-water carbonate production is limited to red algae that are normally not the dominant component. Consequently, the depth window of cool-water carbonate production is much wider. It should be noted that the zone of "tropical carbonates" reaches to 30-35 °C of latitude and thus extends from the humid tropics to the desert belt of the horse latitudes. The cool-water realm extends over several climate zones, reaching from the northern limit of the desert belt to the polar regions. The differences of the tropical and the cool-water realm are not restricted to the skeletal material. Cool-water carbonates also are distinct by the absence of mud, shallow reefs and oolitic sand shoals with early cementation. The lack of reefs and cemented shoals has fundamental implications for the depositional anatomy.

3.5.6.4 Nutrients

Contrary to common expectations, high-nutrient environments are unfavorable for many carbonate systems. Nutrients, to be sure, are essential for all organic growth, including that of carbonate-secreting benthos. However, the carbonate communities dominated by autotrophs, such as reefs, are adapted to life in submarine deserts. They can produce their organic tissue with the aid of sunlight from sea water with very low nutrient levels and are very efficient in recycling nutrients within the system. In high nutrient settings, the carbonate producers are outpaced by soft-bodied competitors such as fleshy algae, soft corals or sponges. Furthermore, the destruction of reef framework by bio-erosion increases with increasing nutrient supply.

3.5.6.5 Salinity

Varies relatively little in the open-marine environment. The effects of these subtle variations on carbonate production are not well known. Where access to the open ocean is

restricted, salinity varies greatly and significantly affects the diversity of the biota. The combined effects of salinity and temperature variations allow one to subdivide carbonate environments.

3.5.7 Ureolytic bacteria-controlled precipitation beachrock carbonate

The ureolytic bacteris identified and cultured from inside of natural beachrock samples. The sediment characteristic of meniscus bridge carbonate assuming came from micro-crystallization from the activity of ureolytic bacteria or also another microorganism. Based on petrographic analysis, were found enrichment of skeletal fragments and also algae (as fossils) which indicated this sedimentary controlled by microorganism in the shoreline areas. Further analysis of geochemical ICP-MS and -AES were found these beachrocks are moderately alkalo-tolerant bacteria, showing maximum growth and urease activity at an ambient temperature of 37 °C, which is compatible with the tropical climate prevailing in the target region. Microbial carbonate overriding environmental control is seen in the present day by localization of microbial carbonates in calcareous streams and springs and in shallow tropical seas, and in the past by temporal variation in the abundance of marine microbial carbonates. Only ~ 4.7% of ureolytic bacteria and algae precipitation, respectively, were assumed to be catalytic factors in beachrock precipitation. The beachrock of Krakal-Sadranan beach in the studied area can be categorized into non-beachrock, unconsolidated beachrock (similar to limestone sands), and well-consolidated beachrock consisting of mostly rock-mineral. Beachrock has a fairly consolidated feature and consists of a mixture of gravel-sized deposits of sand in the form of limestone fragments, calcite, and fossil minerals, and almost 50 % CaO content (carbonaceous).

The interpretation of the cerium anomaly can be used to determine the source of the REEs in this formation, indicating that the beachrock deposition processes originated from the precipitation of seawater under oxidative conditions. This can be interpreted as the beachrock derived from microbial process involving terrigenous materials under oxidative conditions. Beachrock of Krakal-Sadranan beach in the studied area can be categorized into non-beachrocks, unconsolidated beachrocks (or similar to carbonate sands), and well-consolidated beachrocks consisting of rocks-mineral dominated. The beachrock has a fairly consolidated feature, consists of a mixture of gravel-sized deposits of sand in the form of limestone fragments, calcite and fossil minerals, and almost 50% CaO content (carbonaceous). The

beachrocks showed the positive paleo-redox condition of calculation Mn* values (0.12 – 0.51), suggesting an oxidative environment. An increased concentration of total rare earth element (∑REE), both heavy REE (Tb, Dy, Y, Ho, Er, Tm, Yb and Lu) and light REE (La, Ce, Pr, Nd, Sm, Eu and Gd) signals that the beachrock deposition process happened at oxidative environmental conditions. The interpretation of cerium calculation can be used to determine the source of REE in this formation, a Ce/ Ce* and Eu/ Eu* value of less than 1 results in a negative Ce anomaly indicating that the beachrock deposition processes originated from the precipitation of seawater under oxidative conditions and it can be interpreted that beachrock derived from a diagenetic process, terrigenous materials, and/or hydrothermal activity. REE interpretation data of beachrock was done not have a correlation with ureolytic bacteria for further research MICP, however, these results of beachrock normalization REE have a unique pattern of carbonate sediment when comparing with limestone or another carbonate sedimentary. Based on this data, beachrock has to decrease REE from light to heavy element which is inconsistent with limestone precipitated. It is assuming beachrock still experience mechanical and chemical enrichment in its formation process (Atmoko, et al., 2018; Daryono, et al., 2020). Thus, the most favorable condition is to have the presence of oxygenated material contamination. Beachrock occurrence in an area depends on highly geological factors that contribute the matrix interior. Indonesian geological settings seem to be dominated by marine activities of the Pacific Ocean and may be labeled as oxidative conditions.

3.6 Conclusions

As a result of identification, the beachrock, we found the following:

1. Isolated strains of native bacteria belonging to *Psedoalteromonas tetradonis*, *Oceanobacillus profundus*, and *Vibrio maritimus* which have a potential for binding biocement based on MICP.
2. Classified as biotically controlled precipitation carbonate rocks and dominances with aragonite-HMC meniscus bridge binding skeletal fragment and also algae.
3. The major oxide results of the beachrock shown the characteristics sedimentary consisted with calcium oxide, magnesium oxide, sodium oxide, and phosphorus pentoxide for the cement material and/ or existing matrixes.
4. Beachrock precipitation of seawater under oxidative conditions with optimum temperature of sedimentation between 37 ~ 50 °C.

References

Almajed, A., Khodadadi Tirkolaei, H. and Kavazanjian Jr, E., 2018, Baseline Investigation on Enzyme-Induced Calcium Carbonate Precipitation. Journal of Geotechnical and Geoenvironmental Engineering, 144 (11), 04018081. https://doi.org/10.1061/(ASCE)GT.1943-5606.0001973.

Alshuaibi, A.A., Khalaf, F.I. and Al-Zamel, A., 2015, Calcareous thrombolitic crust on Late Quaternary beachrocks in Kuwait, Arabian Gulf. Arabian Journal of Geosciences, 8 (11), 9721-9732. https://doi.org/10.1007/s12517-015-1869-5.

Arrieta, N.; Iturregui, A.; Martínez-Arkarazo, I.; Murelaga, X.; Baceta, J.I.; de Diego, A.; Olazabal, M.Á.; Madariaga, J.M. Characterization of ferruginous cements related with weathering of slag in a temperate anthropogenic beachrock. Sci. Total Environ. 2017, 581, 49–65, doi:10.1016/j.scitotenv.2016.12.132.

Atmoko, D. D., Titisari, A. D., and Idrus, A., 2018, Geochemical Characteristics of Limestone of Wonosari-Punung Formation, Gunungkidul Regency, Yogyakarta, Indonesia. Indonesian Journal on Geoscience, 5 (2), 179-197. DOI: 10.17014/ijog.5.2.179-497

Avcıoğlu, M., Yiğitbaş, E. and Erginal, A.E., 2016. Beachrock formation on the coast of Gökçeada Island and its relation to the active tectonics of the region, northern Aegean Sea, Turkey. Quaternary international, 401, pp.141-152.

Avcioğlu, M., Yiğitbaş, E., and Erginal, A. E., 2016, Beachrock formation on the coast of Gökçeada Island and its relation to the active tectonics of the region, northern Aegean Sea, Turkey. Quaternary Int., 401, 141–152. https://doi.org/10.1016/j.quaint.2015.10.108.

Azizi, S. H. H., Shabestari, G. M. dan Khazaei, A., 2014, Petrography and Geochemistry of Paelocene-Eocene Limestones in the Ching-dar Syncline, Eastern Iran. Geoscience Frontiers, Vol. 5, 429-438. https://doi.org/10.1016/j.gsf.2013.08.002.

Bellanca, A., Claps, M., Erba, E., Masetti, D., Neri, R., Silva, I.P. and Venezia, F., 1996. Orbitally induced limestone/marlstone rhythms in the Albian—Cenomanian Cismon section (Venetian region, northern Italy): Sedimentology, calcareous and siliceous plankton distribution, elemental and isotope geochemistry. Palaeogeography, Palaeoclimatology, Palaeoecology, 126(3-4), pp.227-260.

Bolhar, R., Kamber, B. S., Moorbath, S., Fedo, C. M., Whitehouse, M. J., 2004, Characterisation of Early Archaean Chemical Sediments by Trace Element Signatures. Earth and Planetary Science Letters Vol. 222, 43-60. https://doi.org/10.1016/j.epsl.2004.02.016.

Condie, K.C., Wilks, M., Rosen, D.M. and Zlobin, V.L., 1991. Geochemistry of metasediments from the Precambrian Hapschan series, eastern Anabar Shield, Siberia. Precambrian Research, 50(1-2), 37-47. https://doi.org/10.1016/0301-9268(91)90046-D.

Couradeau, E., Benzerara, K., Gérard, E., Estève, I., Moreira, D., Tavera, R. and López-Garcıa, P., 2013. Cyanobacterial calcification in modern microbialites at the submicrometer scale.

Danjo, T.; Kawasaki, S. Formation Mechanism of Beachrock in Okinawa and Ishikawa, Japan, with a Focus on Cements. Mater. Trans. 2014, 55, 493–500.

Daryono, L.R., Titisari, A.D., Warmada, I.W. and Kawasaki, S., 2019. Comparative characteristics of cement materials in natural and artificial beachrocks using a petrographic method. Bulletin of Engineering Geology and the Environment, Vol. 78, 6, 1-16. https://doi.org/10.1007/s10064-018-1355-x.

Daryono, L.R., Nakashima, K., Kawasaki, S., Titisari, A.D. and Barianto, D.H., 2020. Sediment Characteristics of Beachrock: A Baseline Investigation Based on Microbial Induced Carbonate Precipitation at Krakal-Sadranan Beach, Yogyakarta, Indonesia. Applied Sciences, 10(2), p.520.

Dauphas, N. and Pourmand, A., 2015. Thulium anomalies and rare earth element patterns in meteorites and Earth: Nebular fractionation and the nugget effect. Geochimica et Cosmochimica Acta, 163, pp.234-261.

Elhadi, N.; Radu, S.; Chen, C.H.; Nishibuchi, M. Prevalence of potentially pathogenic Vibrio species in the seafood marketed in Malaysia. J. Food Prot. 2004, 67, 1469–1475.

Folk, R. L., 1962, Spectral subdivision of limestone types. W.E. Ham (Ed.), Classification of Carbonate Rocks, Am. Assoc. Pet. Geol., Mem., 1, pp. 62-84. DOI: https://doi.org/10.1306/M1357

Franchi, F., Bergamasco, A., Da Lio, C., Donnici, S., Mazzoli, C., Montagna, P., Taviani, M., Tosi, L. and Zecchin, M., 2018. Petrographic and geochemical characterization of the early

formative stages of Northern Adriatic shelf rocky buildups. Marine and Petroleum Geology, 91, pp.321-337.

Fujita, M., Nakashima, K., Achal, V. and Kawasaki, S., 2017. Whole-cell evaluation of urease activity of Pararhodobacter sp. isolated from peripheral beachrock. Biochemical engineering journal, 124, pp.1-5.

German, C.R., Hergt, J., Palmer, M.R. and Edmond, J.M., 1999. Geochemistry of a hydrothermal sediment core from the OBS vent-field, 21 N East Pacific Rise. Chemical Geology, 155(1-2), pp.65-75.

Ginsburg, R.N., 1953. Beachrock in south Florida. Journal of Sedimentary Research, 23(2), pp.85-92.

Guimaraes, J.T.F., Cohen, M.C.L., Franca, M.C., Silva, A.K.T.D., and Rodrigues, S.F.S., 2013. Mineralogical and Geochemical Influences on Sediment Color from Amazon Wetlands Analyzed by Visible Spectrophotometry. Acta Amazonica, 43 (3), p.331-342. DOI: 10.1590/ S0044-59672013000300009.

Henehan, M.J., Foster, G.L., Rae, J.W., Prentice, K.C., Erez, J., Bostock, H.C., Marshall, B.J. and Wilson, P.A., 2015. Evaluating the utility of B/C a ratios in planktic foraminifera as a proxy for the carbonate system: A case study of G lobigerinoides ruber. Geochemistry, Geophysics, Geosystems, 16(4), pp.1052-1069.

Huang, R., Wang, Y., Cheng, S., Liu, S. and Cheng, L., 2015. Selection of logging-based TOC calculation methods for shale reservoirs: A case study of the Jiaoshiba shale gas field in the Sichuan Basin. Natural Gas Industry B, 2(2-3), pp.155-161.

James, N.P., and Kendall, A.C. 1992. Introduction to carbonate and evaporite facies models. In Facies Models: Response to Sea-Level Changes, Walker, R. Pp.265-275.

James, N.P., Bone, Y., Hageman, S.J., Feary, D. and Gostin, V.A., 1997. Cool-water carbonate sedimentation during the terminal Quaternary sea-level cycle: Lincoln Shelf, southern Australia.

Jones, A., Phillips, M., 2011. Disappearing Destinations: Climate Change and the Future Challenges for Coastal Tourism. Cabi, London, 296 p.

Karkani, A., Evelpidou, N., Maroukian, H. and Kawasaki, S., 2016. Study of Beachrocks in East Attica. Bulletin of the Geological Society of Greece, Vol.50, 1, 434-440. http://dx.doi.org/10.12681/bgsg.11744.

Kelletat, D., 2006. Beachrock as sea-level indicator? Remarks from a geomorphological point of view. Journal of Coastal Research, 2006(226), pp.1558-1564.

Kishi, M., Kawai, M., Koyama, K.T.M., Nagao, N. and Toda, T., 2018. Enhancement of microalgal production through bacterial mineralization of ethylene glycol. Journal of Environmental Biology, 39(5), pp.725-731.

Kurian, S., Nath, B.N., Ramaswamy, V., Naman, D., Rao, T.G., Raju, K.K., Selvaraj, K. and Chen, C.T.A., 2008. Possible detrital, diagenetic and hydrothermal sources for Holocene sediments of the Andaman backarc basin. Marine Geology, 247(3-4), pp.178-193.

Lees, A., 1975. Possible influence of salinity and temperature on modern shelf carbonate sedimentation. Marine Geology, 19(3), pp.159-198.

Machhour, L., Philip, J. and Oudin, J.L., 1994. Formation of laminite deposits in anaerobic—dysaerobic marine environments. Marine Geology, 117(1-4), pp.287-302.

MacRae, N.D., Nesbitt, H.W. and Kronberg, B.I., 1992. Development of a positive Eu anomaly during diagenesis. Earth and Planetary Science Letters, 109(3-4), pp.585-591.

Madhavaraju, J. and Lee, Y.I., 2009. Geochemistry of the Dalmiapuram Formation of the Uttatur Group (Early Cretaceous), Cauvery basin, southeastern India: Implications on provenance and paleo-redox conditions. Revista Mexicana de Ciencias Geológicas, 26(2), pp.380-394.

Marshall, J.; Barnhart, A.; Butcher, A.; Freimuth, C.; Khaw, F.; Lafromboise, E.; Landeros, M.; Morrish, S.; Olson, E.; Ritzinger, B.; et al. Beachrock horizons of the Nicoya Peninsula, Costa Rica: Geomorphology, petrology, and neotectonic significance. In Proceedings of the Coastal Sediments, San Diego, CA, USA, 11–15 May 2015; doi:10.1142/9789814689977_0252.

Martin, T.D.; Brockhoff, J.T.; Creed, J.T. Method 200.7 Determination of Metals and Trace Elements in Water and WastesbyInductivelyCoupledPlasmaeatomicEmissionSpectrometryRevision4.4EMMCVersion,200.7e1,58; U. S. EPA: Washington, DC, USA, 1994.

Mauz, B., Vacchi, M., Green, A., Hoffmann, G., and Cooper, A., 2015, Beachrock: a tool for reconstructing relative sea level in the far-field. Marine Geology, Vol. 362, 1-16. https://doi.org/10.1016/j.margeo.2015.01.009.

McLean, R., 2011. Beachrock. Encyclopaedia of Coral Reefs. pp 107e111.

Moore, W.S., 1999, The subterranean estuary: a reaction zone of ground water and sea water. Marine Chemistry, Vol. 65, 1-2, 111-125. https://doi.org/10.1016/S0304-4203(99)00014-6.

Mwandira, W.; Nakashima, K.; Kawasaki, S.; Ito, M.; Sato, T.; Igarashi, T.; Chirwa, M.; Banda, K.; Nyambe, I.; Nakayama, S.; et al. Solidification of sand by Pb (II)-tolerant bacteria for capping mine waste to control metallic dust: Case of the abandoned Kabwe Mine, Zambia. Chemosphere 2019, 228, 17–25, doi:10.1016/j.chemosphere.2019.04.107.

Nagendra, R., and Nagarajan, R., 2003, Geochemical Studies of Shahabad Limestone (Younger Proterozoic), Bhima Basin, Karnataka. Indian Mineralogist, Vol. 36, 1, 13-23.

Neumeister, S., Algeo, T.J., Bechtel, A., Gawlick, H.J., Gratzer, R. and Sachsenhofer, R.F., 2016. Redox conditions and depositional environment of the Lower Jurassic Bächental bituminous marls (Tyrol, Austria). Austrian Journal of Earth Sciences, 109(2).

Nichols, G. Sedimentology and Stratigraphy; John Wiley & Sons: West Sussex, UK, 2009; p. 420.

Oliver, J.D.; Pruzzo, C.; Vezzulli, L.; Kaper, J.B. Vibrio species. In Food Microbiology; American Society of Microbiology: Washington, DC, USA, 2013; pp. 401–439.

Passey, Q.R., Creaney, S., Kulla, J.B., Moretti, F.J. and Stroud, J.D., 1990. A practical model for organic richness from porosity and resistivity logs. AAPG bulletin, 74(12), pp.1777-1794.

Pilkey, O.H., and Cooper, A., 2014, The Last Beach. Duke University Press, Durham, 256 p.

Piper, D.Z. and Calvert, S.E., 2009. A marine biogeochemical perspective on black shale deposition. Earth-Science Reviews, 95(1-2), pp.63-96.

Porta, G. D., 2015, Carbonate build-ups in lacustrine, hydrothermal and fluvial settings: comparing depositional geometry, fabric types and geochemical signature. Geological Society, London, Special Publications, Vol. 418, 1, 17-68. https://doi.org/10.1144/SP418.4.

Pratama, W.; Dewi, S.C.; Sari, I.Z.R.; Hardiyati, A.; Wajong, A.E. Distribution and Abundance of Macroalgae in Intertidal Zone of Drini Beach, Gunung Kidul, DIY. KnE Life Sci. 2015, 2, 514–515.

Putz, H. and Brandenburg, K., 2015. Match!-phase identification from powder diffraction. Crystal Impact Software.

Riding, R., 1991. Classification of microbial carbonates. In Calcareous algae and stromatolites (pp. 21-51). Springer, Berlin, Heidelberg.

Rollinson, H. R., 2014, Using geochemical data: Evaluation, Presentation, Interpretation. Routledge, London, 73 p.

Romimohtarto,K.;Juwana,S.BiologiLaut: IlmuPengetahuanTentangBiotaLaut;Djambatan: Jakarta,Indonesia, 2009.

Russell, R.J. and McINTIRE, W.G., 1965. Beach cusps. Geological Society of America Bulletin, 76(3), pp.307-320.

Schieber, J., 1988. Redistribution of rare-earth elements during diagenesis of carbonate rocks from the Mid-Proterozoic Newland Formation, Montana, USA. Chemical Geology, 69(1-2), pp.111-126.

Schmoker, J.W., 1979. Determination of organic content of Appalachian Devonian shales from formation-density logs: Geologic notes. AAPG Bulletin, 63(9), pp.1504-1509.

Schmoker, J.W., 1980. Organic content of Devonian shale in western Appalachian Basin. AAPG Bulletin, 64(12), pp.2156-2165.

Shi, P., and Kasperson, R., 2015, World Atlas of Natural Disaster Risk. Springer-Verlag, Berlin, Heidelberg, 368 p. DOI: 10.1007/978-3-662-45430-5.

Soon, N.W., Lee, L.M., Khun, T.C. and Ling, H.S., 2014. Factors affecting improvement in engineering properties of residual soil through microbial-induced calcite precipitation. Journal of Geotechnical and Geoenvironmental Engineering, 140(5), p.04014006.

Tostevin, R., Shields, G. A., and Tarbuck, G. M., 2016, Effective Use of Cerium Anomalies as a Redox Proxy in Carbonate-dominated Marine Settings. Elsevier: Chemical Geology Vol. 438, p.146-162. https://doi.org/10.1016/j.chemgeo.2016.06.027.

Tribovillard, N., Algeo, T.J., Lyons, T. and Riboulleau, A., 2006. Trace metals as paleoredox and paleoproductivity proxies: an update. Chemical geology, 232(1-2), pp.12-32.

Trono, G.C., Jr. Seaweed. In The Living Marine Resources of the Western Central Pacific. Volume 1. Seaweed, Corals, Bivalves, and Gastropods; Carpenter, K.E., Niem, V.H., Eds.; Food and Agriculture Organization of the United Nations: Rome, Italy, 1998; pp. 19–96.

Tucker, M.E. and Wright, V.P., 1990. Carbonate platforms: facies evolution and sequences. Int Ass Sed, 2, p.328.

Turner, R.J., 2005. Beachrock. Encyclopedia of coastal science. Kluwer Academic Publishers, The Netherlands, pp.183-186.

Van Bemmelen, R.W., 1949. General geology of Indonesia and adjacent archipelagoes. The geology of Indonesia, Government Printing House, The Hague, 732 p.

Van Paassen, L. A., Ghose, R., Van der Linden, T. J. M., Van der Star, W. R. L., and Van Loosdrecht, M. C. M., 2010, Quantifying biomediated ground improvement by ureolysis: Large-scale biogrout experiment. Journal of Geotechnical and Geoenvironmental Engineering, Vol. 136, 1721–1728. https://doi.org/10.1061/(ASCE)GT.1943-5606.0000382.

Van Paassen, L.A., Pieron, M., Mulder, A., Van der Linden, T.J.M., Van Loosdrecht, M.C.M., and Ngan-Tillard, D.J.M., 2009, Strength and deformation of biologically cemented sandstone. In Proceedings of the ISRM Regional conference EUROCK, Cavtat, Croatia, Oct. 29-31, p. 405-410. ISBN 978-0-415-80481-3.

Vousdoukas, M.I., Velegrakis, A.F. and Plomaritis, T.A., 2007. Beachrock occurrence, characteristics, formation mechanisms and impacts. Earth-Science Reviews, 85(1-2), pp.23-46.

Wedepohl, K.H., 1969. 1978. Handbook of geochemistry. An Arbor.

Zhu, X., Linham, M. M., and Nicholls, R. J., 2010, Technologies for Climate Change Adaptation - Coastal Erosion and Flooding. Roskilde: Danmarks Tekniske Universitet, Risø Nationallaboratoriet for Bæredygtig Energi. TNA Guidebook Series, University of Southampton, England, 167 p.

CHAPTER 4

Comparative characteristics of natural beachrock from Okinawa, Japan and Yogyakarta, Indonesia

4.1 Introduction

Marine seafloor sedimentary processes and the study of mechanism behaviors opens the door to many questions. Beachrock is among the recent seafloor sedimentary products that occurs on the shoreline as a carbonate compound and natural wave breaker. The terminology of beachrock is generally found in the tropical-subtopic zones that had warmer temperature climate. Beachrock studies have shown that the formation of the diachronic process occurs at lower latitudes. Thus far, beachrock deposit occurrences gave been noted in Turkey, Bangladesh, Scotland, Japan, Greece, the Great Barrier Reef of Australia, Sri Lanka, Bahamas Island, Brazil, South Africa, and in Florida in the United States (Danjo and Kawasaki, 2014; Khan and Kawasaki, 2016). Beachrock is cemented and rapidly forms in the areas as a recent carbonaceous deposit (Vousdoukas, et al., 2007; Desruelles et al., 2009; Mauz et al., 2015a; Ozturk et al., 2016; Karkani. et al., 2017; Kolaiti and Mourtzas, 2016).

Recent findings on beachrock are still debatable, as there are various issues still unresolved such as the geographical locations and the key processes that occur in the formation of beachrock from observations in the field. Some researchers have proposed intertidal formation (e.g., Neumeier, 1999; Vousdoukas et al., 2007; Desreulles et al., 2009; Mauz et al., 2015; Saitis, 2016) while other specific results of beachrock show sedimentary binding with an aragonitic composition cement occurring in the shallow marine zone, while low-magnesium calcite (LMC) indicates the supratidal zone, high-magnesium calcite (HMC), and also aragonite that indicates the shallow-marine zone (Stoddart and Cann, 1965a, b; Scholle and Ulmer-Scholle, 2003; Mauz, et al., 2015). However, learning from a natural analogy of the sedimentary process may yield valuable information to understand the genesis of beachrock on the basis of the cementation characteristics and sediment bedding information. The mineral composition of beachrock deposits is mainly $CaCO_3$ polymorphs, which are aragonite, LMC, and HMC. The dominance of calcium mineral compounds depends on physicochemical parameters, the genetic processes involved in them, and metabolic residual products of living organism activities (Calvet, et al., 2003; Kneale and Viles, 2004; Díez, et al., 2007).

Consequently, scientists in Japan have made an artificial “human-made” beachrock whose composition is similar to the natural beachrock in order to protect the shoreline from erosion. In addition, through understanding the beachrock formation process, artificial rocks may be able to be formed at an accelerated speed of consolidation (Danjo and Kawasaki, 2014; 2016; Khan, et al., 2016; Al Imran, et al., 2017; Daryono, et al., 2019; 2020). Several techniques and research practices have been put forward to identify beachrock formation whilst characterizing them. Petrographic analysis is an important method to identify specific aggregate minerals and understand petrogenesis interpretations with a focus on the structures, textures, and compositions of minerals inside rock samples.

4.2 Objectives

This study aims to investigate the cementation characteristics of natural beachrock from tropical shoreline Krakal-Sadranan, Indonesia and sub-tropic shoreline Okinawa, Japan (Figure 4.1), using biodiversity of microbial controlled sedimentation, petrographic measurement, and

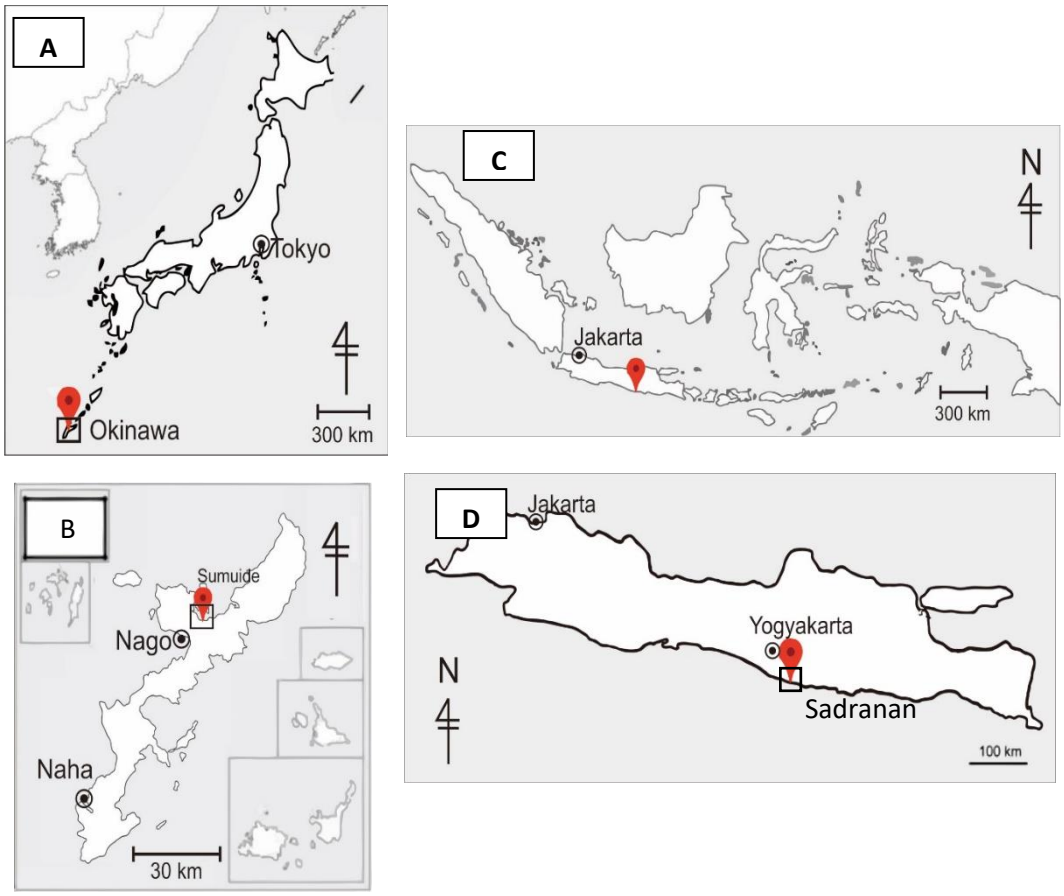


Figure 4.1. (A) Location map of Okinawa in Japan, (B) Research area in Sumuide, Okinawa island, (C) Location map of Indonesia, and (D) Locations Sadranan area.

geochemical for the additional analysis. In this research were explained ureolytic bacteria strain controlled from both locations within limitation of cultivation bacteria, such as temperature, pH, medium, and marine environment. A comparison of natural and their cementation characteristics are vital information when trying to decide the nature of beachrock with the focus is to compare the characteristic cementation process. In this chapter were discussed about sedimentary mechanism from Yogyakarta, Indonesia and Okinawa, Japan then bridging the technology to develop artificial beachrock based on ureolytic bacteria similar methods with Danjo and Kawasaki (2014; 2016) isolated from inner natural beachrock.

4.3 Methodology

The research was completed using geological research methods of identification of the sedimentary environment using petrographic analysis which included observations, physical characteristics, and data measurements using petrographic analysis and a geochemical approach (Potter, 1967; Pozo, et al., 2016; Ayinla, et al., 2017; Nabhan and Yang, 2018). This research was completed by observation and investigation from the geological field investigation on December 2015 in Okinawa, Japan and Sadranan, Yogyakarta on May, 2018-Dec, 2019. The identity of beachrock in the study area with an emphasis on the aspect of sedimentation and cementation.

4.3.1 Field work

A total of 12 natural beachrock samples were collected from Okinawa, Japan and Yogyakarta. Moreover, nine samples of artificial beachrock based on solidification tests of calcium carbonate into syringe-tubes were studied.

4.3.2 Petrographic analysis

The thin-section samples were collected at different zones from tidal to onshore locations to assess the degree of cementation and analyze under a microscope (Olympus CHA-P) to determine the carbonate-composition types of the cement and the characteristics of natural deposition. Qualitative analysis included an analysis of a thin section method with parallel and crossing Nicol polarizations microscope to identify the texture, structure, and composition of the thin-section samples. The point counting was conducted for classification of the composition fossils, matrixes of carbonate (cemented materials) and carbonate cementation (cement). The point-counting technique is based on grid lines from the microscope petrographic analysis, and statistical measurement with different angles of thin-section images.

Petrographic studies have attempted to define the underlying reason for the composition, cement materials, depositional environment, and the origin of clasts for beachrocks (Arrietta, et al., 2011; Christ, et al., 2015; Avcioğlu, et al., 2016; McCutcheon, et al., 2016).

4.3.3 Biodiversity microbial analysis

On the other hand, the important factors controlling calcium carbonate cementation of artificial beachrock are the chemistry of the seawater (the source of the cementing material); the physical conditions, in terms of hydraulic energy; sedimentary parameters such as permeability, texture, and composition of the sand; and an initial stabilizer of the loose sediment.

4.3.4.1 Isolation of ureolytic bacteria

The ureolytic bacterial species were isolated from the coastal area of Krakal-Sadranan beach, Indonesia and Sumuide, Okinawa, Japan (Figure 4.1). The soil was sampled from each peripheral beachrock. After screening, the bacterial species were identified by 16s DNA gene analysis. The genome extraction was done using 100 µL of Mighty Prep reagent taken into a 1.5 mL microtube. From the colonies on the plate, the cells were removed with a sterilized platinum loop, suspended in the microtube, heated at 95°C for 10 minutes, and then centrifuged at 12000 rpm for 2 minutes. The supernatant of the suspension centrifuged was transferred to another tube and used as a template for PCR (polymerase chain reaction). The bacteria inside tubes diluted 10^1-10^4 times with artificial seawater, after that 10mL of each dilution was added to ZoBell2216E agar medium for marine bacteria. After incubation at 30°C for 3 days, the bacteria colonies were isolated from one plate. Cells were cultured in ZoBell2216E medium, which contained 5.0 /L hipolypeptone (Nihon Seiyaku Co., Ltd., Tokyo, Japan), 1.0 g/L $FePO_4$ (Junsei Chemical Co., Ltd., Tokyo, Japan), and 1.0 g/L yeast extract (BD Bioscience Adv., Bioprocessing, Miami, FL., USA), prepared with artificial seawater with pH adjusted 7.6-7.8 using 1 M NaOH (Fujita, et al., 2017).

4.3.4.2 Microbial population count and urease activity test

Seawater, beachrock samples, and sand from both sites were collected in the sterile tubes and isolation for colonies hybrids. Subsequently, isolated colonies from nature sand adjacent to beachrock in Okinawa, Japan using ZoBell2216E medium containing Pararhodobacter sp., and Oceanisphaera sp., the time course of cell growth was determined based on the optical

density (OD) value 600nm by UV-vis spectrophotometer (V-730, Jasco International CO., Ltd., Tokyo, Japan for 14 days. The urease activity of bacterial cells was determined by monitoring ammonium ions generated in urea hydrolysis using the indophenol blue method based on Berthelot'sreaction in a water bath (Weatherburn, 1967; Natarajan, 1995). After bacterial cultivation for 48 hours, a bacterial suspension (1mL) (OD_{600}=1.0) was added to 0.1M phosphate buffer containing 0.1 M urea. Samples were then collected at intervals of 5 minutes (0, 5, 10, and 15 minutes) and passed through a 0.22 μm filter to remove cells. Next, 2 mL aliquot of the filtered sample was mixed with phenol nitroprusside reagent (4mL) (0.25 M phenol in 100 mL of deionized water containing 23 μM of sodium nitroprusside) and hypochlorite reagent (4mL) (0.05 M sodium hydroxide in 100 mL of deionized water containing 7.5 mL bleach (5% NaOCl)). Each reaction mixture was vortexed and then incubated at 60°C for 10 minutes. The amount of ammonium ion released because of urea hydrolysis was determined by referring to a previously prepared standard curve relating the absorbance at 630 nm to ammonium ion concentration (0-10 mg/L). Using this curve, one unit of urease activity (U) was fined as the amount of enzyme that would hydrolyze 1 μmol of urea per minute. The release of 2 μmol of ammonia is equivalent to the hydrolysis of 1 μmol of urea (Mwandira, et al., 2017).

4.4 Results

An understanding of the natural parameters and the interactions of beachrock requires an analysis of the genesis of all forms of beachrock. There is a lack of similarities in geology or geography but there are occurrences of outcrops of beachrock at 7° South latitude, where there is different climate, humidity, and source rocks compared to Indonesia which is mostly siliciclastic rocks. The beaches of Okinawa are at 26° North latitude. Invariably, there are advantages in comparing samples from different latitudes. In the following sections, one will find comparisons between the Japanese and Indonesian beachrocks, whilst also comparing the characteristics of both natural and artificial rocks.

4.4.1 Sumuide beachrock sample, Okinawa, Japan

4.4.1.1 Geology of Okinawa, East China Sea

The general geology of Ryukyu Island, Japan is summarized as a background to the discussion of the stratigraphy of the fossiliferous Tertiary and Quaternary rocks. The stratigraphic units are recognized as follows: the Shimajiri Formation, consisting of the

Yonabaru clay member (late Miocene) in the lower part of the exposed section, and the Shinzato tuff member (Miocene or Pliocene) in the upper part; and the Ryukyu Group, consisting of, in ascending order, the possibly contemporaneous Nakoshi sand (Pliocene) and Chinen sand (Pliocene), the Naha limestone (Pliocene), the Yontan limestone (Pliocene), and the Machinato limestone (Pliocene) (McNeil, 1960).

In Okinawa there is Group Formation that working on this geology system in Okinawa. Shinjimari Group, Ryukyu Group, Uchihana Formation, and Holocene deposits such as alluvial deposits, beach deposits, low- tide elevation (coral reef) and also reclaimed land. These ages were from Neogene, Quaternary, and the youngest is Holocene product include beachrock deposits. The Ryukyu Island form one of the island arcs of the western Pacific, extending from southern Japan to the northern end of Formosa. The convex side of the island faces the Philippine Sea and the shallow East China Sea lies behind them. The island of Okinawa lies about midway in the Ryukyu Island. The Ryukyu Archipelago is 1046 km long and it consists of 55 islands and islets with a total land area of 3090 km^2. Beachrock has formed had an average dip of 3.5° to the sea. The average altitude (above sea level) of the outcrops is 50 cm, with no evidence regarding the vertical position provided by a channeled coastline (Tokashiki and Aydan, 2010; Daryono, 2016).

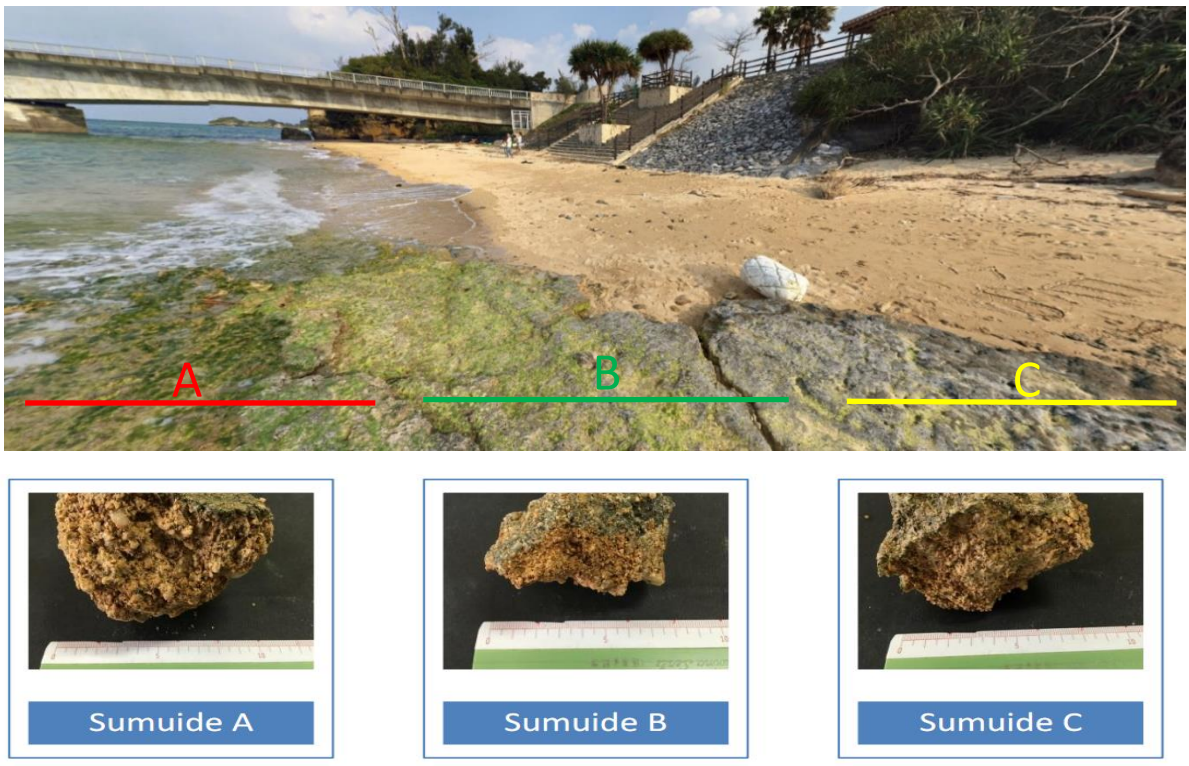


Figure 4.2. Sumuide beachrock sampling area, Okinawa, Japan.

Sample of natural beachrock from Okinawa was taken in Sumuide coast area, whereas three differences of sample that assumed fresh rocks and the weathered deposit (Figure 4.2). The megascopic scale of geology, Sumuide have a characteristic as uniform grain composition as material deposited. Solidified deposit and also non-solidified as beach sand deposit, rock fragments in Sumuide were dominance with shell and coral that formed relatives rounded with size 2 mm~2 cm grain sizes within carbonaceous cementation. In a sample from Sumuide A, the grain size of the fragments is relatively large, > 3 mm to 3 cm, with a brown color; however, it is not a compacted because of the lack of cement. Samples of beachrock Sumuide B have similar characteristics to those of Sumuide A. The main differentiation is the granule which are of dime size but have more pores. Samples of Sumuide C appear more compact when compared to those of Sumuide A and B, possibly due to rare exposure to waves of ocean currents. Therefore, the solidified version was seen as the process of carbonated precipitation.

4.4.1.2 Petrographic analysis result

Microscopic analysis of thin-section samples from Sumuide, Okinawa was conducted. During microscopic examinations, it was clear that the grains mostly consisted of calcite, quartz, and fragments which known as micritic cement HMC [(Ca, Mg) CO_3]. In addition, the cement can be found as a matrix which is composed of very fine sedimentary particles (5–20 m) and micritic HMC. During the sedimentary process of the experiment the organic materials may have been affected. The most impacted would have been grain sediments, as can be seen from the brownish color on their external surface. The textures can be characterized as micritic with interclass (Folk, 1959). The results found occurrences of lytic fragments in the formed quartz (metasedimentary) with many matrixes in the form of shell fragments and quartz or coral opaque varying with size, where the fabric is grain-supported. Micritic or mud carbonate filling contacts at carbonate or non-carbonate fragments produced mud during deposition. General pore of Sumuide samples were filled with intra-granular microsparite as the cement, which although the evolution in the dry zone as Sumuide C compacted then the Sumuide A sample because the fragments, pore size, and lytic partially due had increased to the large amount of cement. The name of the rock sample was based on the carbonate classification based on rock sedimentary particles in the carbonate rock or limestone which is composed of ooids, termed, oolitic limestone. The most widely used classifications are those of Folk (1959) and Dunham (1962), regarding beachrock samples from Okinawa assumed to be namely poorly sorted

intracrine (Folk, 1959) and lithoclast grainstone (Dunham, 1962) beachrock for samples Sumuide A and B, and for Sumuide C poorly sorted intramicrite (Folk, 1959) and lithoclast packestone (Dunham, 1962) beachrock (lithified). These differences in name classification are because of the different systems and cementation material inside beachrock from either the supratidal zone or intertidal zone (Daryono, 2016). Refer the appendixes D for further information about the petrographic of Okinawa beachrock.

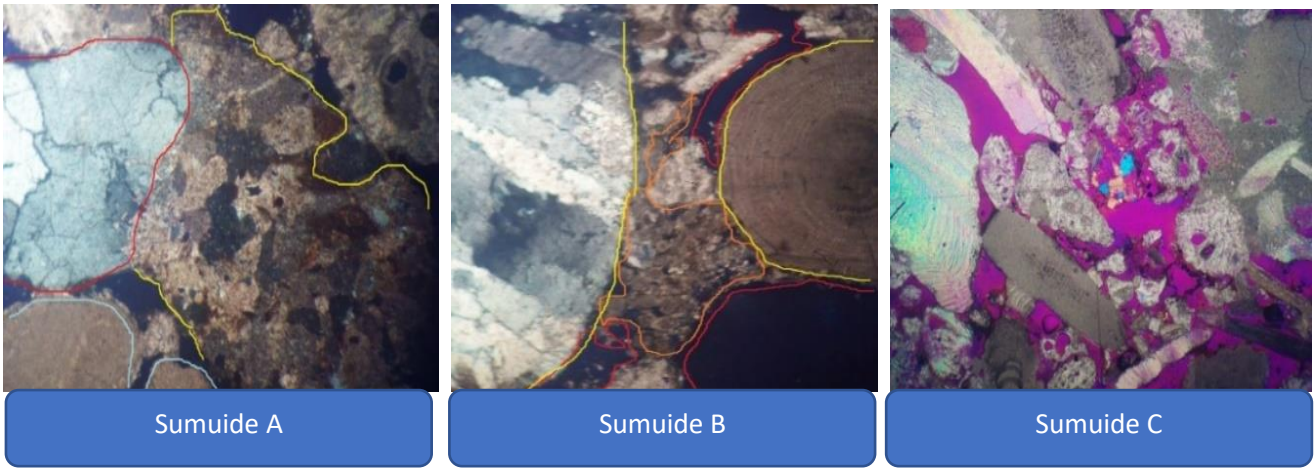


Figure 4.3. Sumuide beachrock cement vision using 100x (yellow pattern represented grain matrix and orange pattern represented cement).

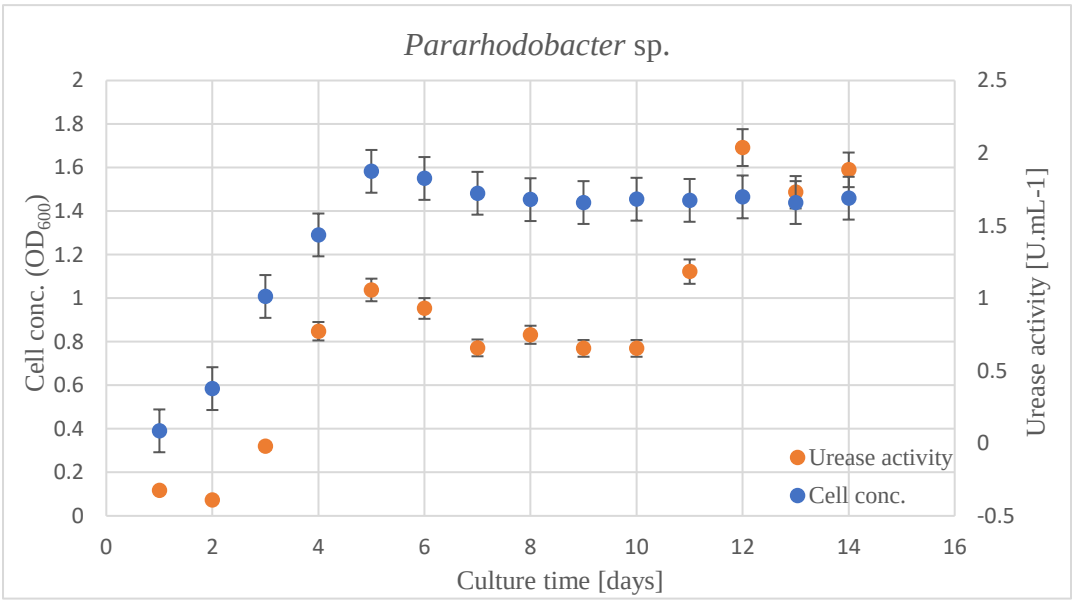
Figure 4.3 explains the cementation process of peloidal micritic cement, cement needles of aragonite, micritized granules, and the cover of micritic seen in the Sumuide beachrock, which is a product of diagenesis in the phreatic environment of the sea. This cementation mineral as micritization gathered on other materials such as coral, foraminifera, skeletons, and others as solid rock. The exclusive presence of aragonitic cement (needle aragonite and micritic cement peloidal) in rocks of sedimentary diagenesis indicates that the environment was mainly marine. However, the presence of cement in beachrock peloidal micritic was very significant as it presented that the micrite had played a vital role during the Sumuide beachrock sedimentary process. Whilst all of the aforementioned can be argued in terms of the origin of cement micritic peloidal, it remains uncertain. It can be suggested as precipitation occurring directly from seawater or it could just be a product of biological activity. The presence of microborings, however, may indicate that the micrites are also a product of biological activity. There is no direct evidence of the influence of meteoric water on beachrock sedimentation. Some have suggested that the process of diagenesis occurred much faster that meteoric; however, this is open to debate as both were subjected to weathering conditions during the sedimentary process.

4.4.1.3 Indigenous ureolytic bacteria from Okinawa, Japan

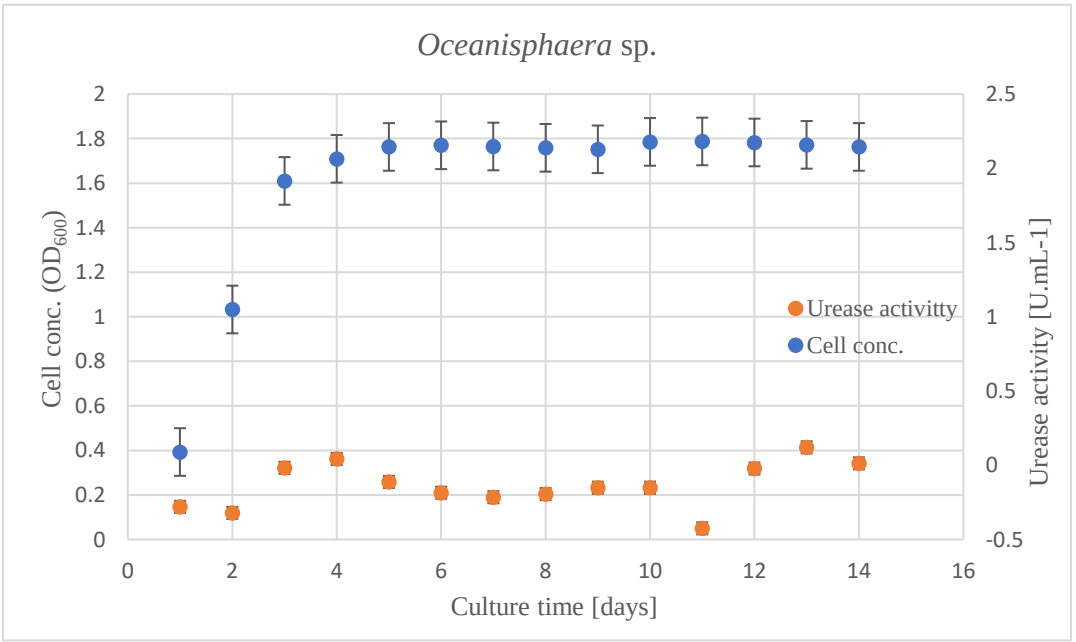
The results of isolated surface sand within assumption microbial enrichment then selected the ureolytic bacteria species only from Okinawa, Japan revealed that *Pararhodobacter* sp., that increased pH solution to the highest value for calcium carbonate beachrock. On other hand, in Japan also found beachrock deposits occurrences of silica mineral witch is Miyako-jima, Japan revealed *Oceanisphaera* sp. The P*ararhodobacter* sp., are Gram-negative, rod-shaped, aerobic, chemoorganotrophic bacteria, that are moderately halophilic with approximately 1 μm in diameter and 3 μm in length (Foesel, et al., 2011; Danjo and Kawasaki, 2016). Meanwhile, *Oceanisphaera* sp., had a spherical cell, 1.0-1.2 μm in diameter and motile by means of flagella. Gram-negative chemoorganotroph with absolute requirement for sodium ions, aerobic, moderately halophilic, and oxidase-catalase-positive (Romanenko, et al., 2003). Based on the research of Danjo and Kawasaki (2014), they analyzed the microorganism that worked on the precipitated solid and used urease bacteria for the microorganism reagent that is famous from an Okinawa sand sample termed *Pararhodobacter* sp. These types of species are strong during solidification at the laboratory scale because this species has the highest urease activity. This research tried to combine two species of urease bacteria, *Pararhodobacter* sp., and *Oceanisphaera* sp., (Miyakojima bacteria-silica deposits) to precipitate artificial beachrock.

The time course of cell growth and urease activity by *Pararhodobacter* sp., and *Oceanisphaera* sp., for 15 days are shown in Figure 4.4. Cell concentration increased up to 2 days and then reached stationary phase. The urease activity of the cell culture increased with cell growth. Based on this result, the production of urease would be a growth-associated system. Considering microbial-based sand solidification, which needs relatively long duration for adequate solidification, the long-term stability of the enzyme would be advantageous in the MICP process (Danjo and Kawasaki, 2016; Fujita, et al., 2017). The difference of temperature environment is shown in Figure 4.5, a for both species. High activity was obtained in the range temperatures of 30-70°C, within the maximum temperature of urase activity was obtained 70°C in this study. Most of urease molecule is known to be composed of protein subunits and the subunits of this urease would strongly bind each other to leads the high stability of urease during long-term cultivation (Mobley and Island, 1995; Balasubramanian and Ponnuraj, 2010; Fujita, et al., 2017). Urease activity under different pH is shown in Figure 4.5, b. The results showed with the maximum activity around pH 7.0 – 8.0. For this temperature and pH variations, the results were different with Fujita, et al. (2017), where he is mentioned the results of maximum temperature exponential increasing toward environment temperature of the buffer

solution and the method for urease activity measurement, he used ammonia meter of Tris/HCl buffer solution. Meanwhile, in this research, for measuring urease activity we used EDTA buffer solution for indophenol blue method then detect with colorimeter changing with optical density 630 nm. The results of Fujita, et al. (2017) and this research quite different but the pattern of bacterial growth and urease activity, especially for *Pararhodobacter* sp., is almost same (Daryono, 2016).

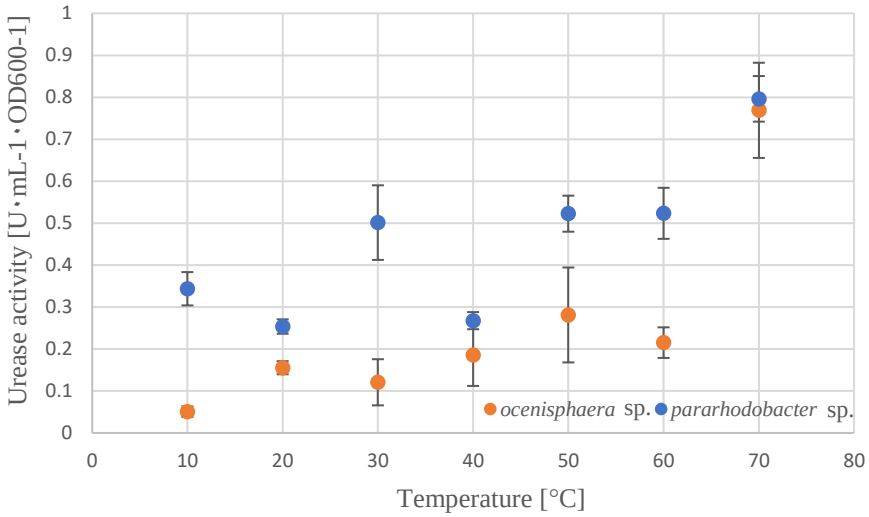


(a)

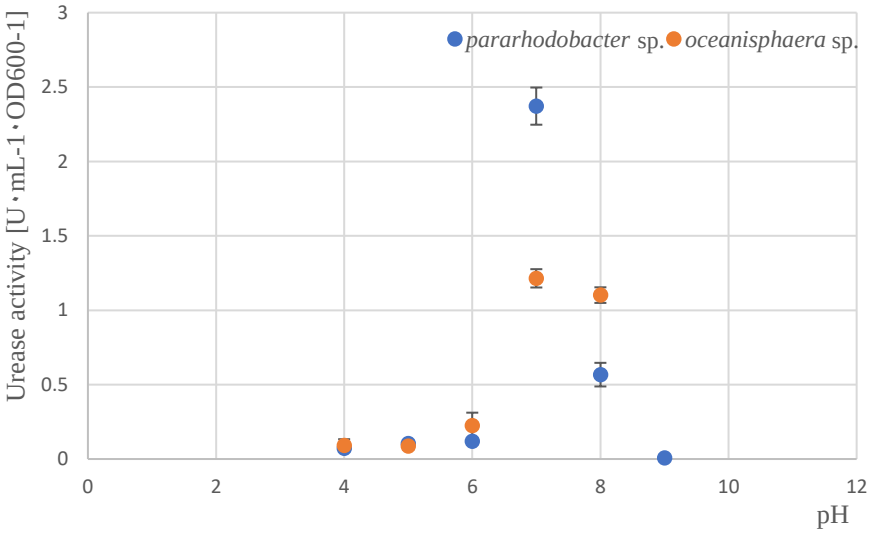


(b)

Figure 4.4. Cell growth and urase activity of *Pararodhobacter* sp. (a) and *Oceanisphaera* sp. (b).



(a)



(b)

Figure 4.5. Effect of reaction temperature on urease activity of the whole cell at pH 7 (a) and the effect of reaction pH on urease activity of the whole cell at 30°C (b). Experiment were conducted in triplicate: data represented the average of three experiments with error bars indicating the standard deviation.

4.4.1.4 Geophysical mapping of beachrock in Okinawa, Japan

Figure 4.6 shows the resistivity sections on both A- and B-lines. In Figure 4.7, (c) and (d2) show the resistivity sections on C- and D-lines, and (d1) shows the velocity section. The pink gridline in Figure 4.7 (d1) represents the areas of resistivity sections on the same lines. As will be shown below, the underground structure of beachrocks was detected by the DC electrical survey and the seismic surface wave survey. The higher resistivity areas (more than 4.0 Ωm) are observed at about 0–32 and 39–43 m (A-line), 38–42 and 62–88 m (B –line), 0-12 m (C-line), and 0–15 m (D-line) (Figs 4.5, 4.6 (c), (d1)). In the velocity sections of the D-line, the

near-surface areas showing the highest velocity (more than 325 m/s) are between about 12–14 m (Fig. 4.7 (d1)). As mentioned in Capture 3, the harder the rock, the higher both its resistivity and S wave velocity. The high velocity areas coincide relatively well with the high resistivity areas and the observed outcrops of beachrock (Fig. 4.7 (d1) and Capture 2). Furthermore, it was very likely able to detect the buried beachrocks. The examples are the surface areas at about 27–44.5 and 43–89 m on A- and B-lines, respectively. The area on the D-line is assumed to be between about 7.25–12 m because the resistivity of the higher surface area (more than 16 Ωm) between 0–4 m is too high in spite of not observing a beachrock outcrop, and this is due to the drying of sand by evaporation. The surface area be-tween 0-2 m on C-line is similar (Kubo, et al., 2014).

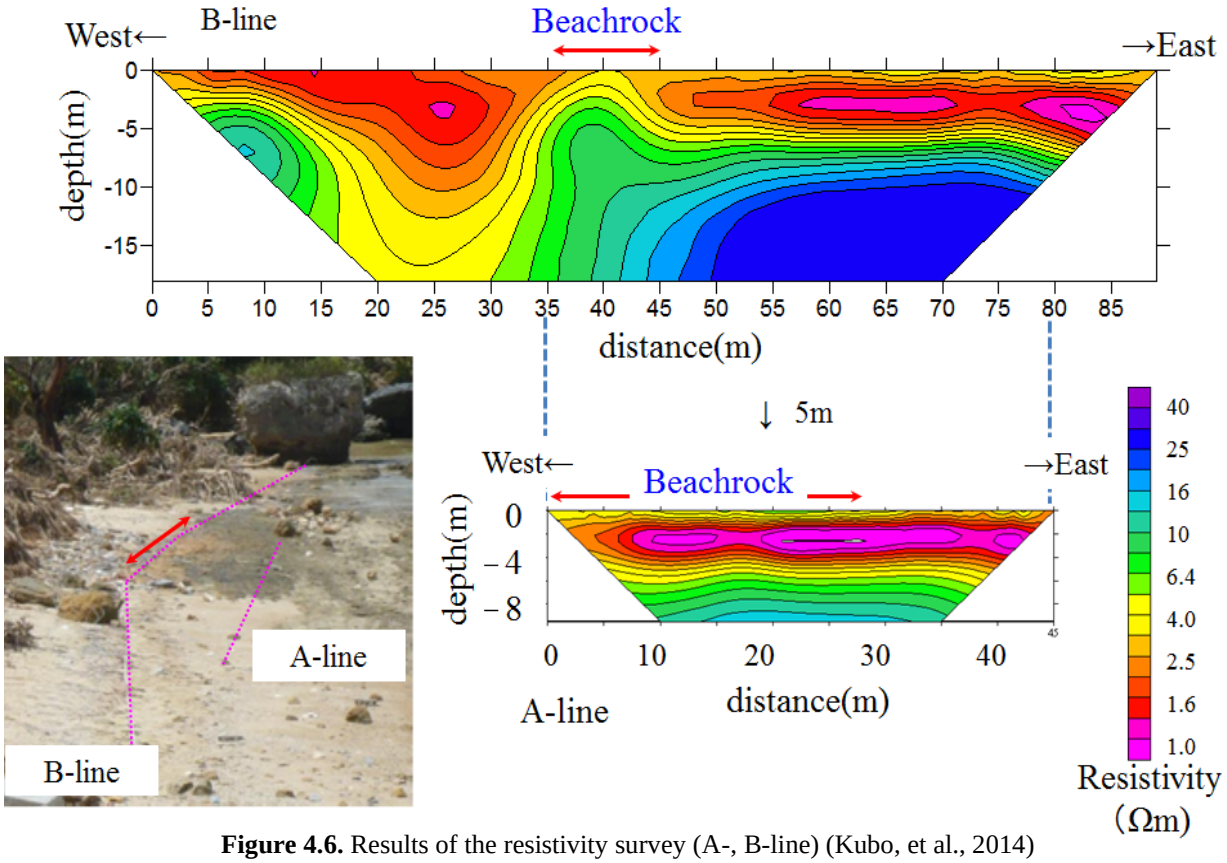


Figure 4.6. Results of the resistivity survey (A-, B-line) (Kubo, et al., 2014)

From the above, it is believed that the two surveys detected beachrocks. Likewise, it was assumed that the thickness of beachrock in this study area is about 1 m, its surface wave velocity is about 300–350 m/s, and its resistivity is about 4–40 Ωm. In the next location, it was assumed that the geological structure of this study area is as follows.

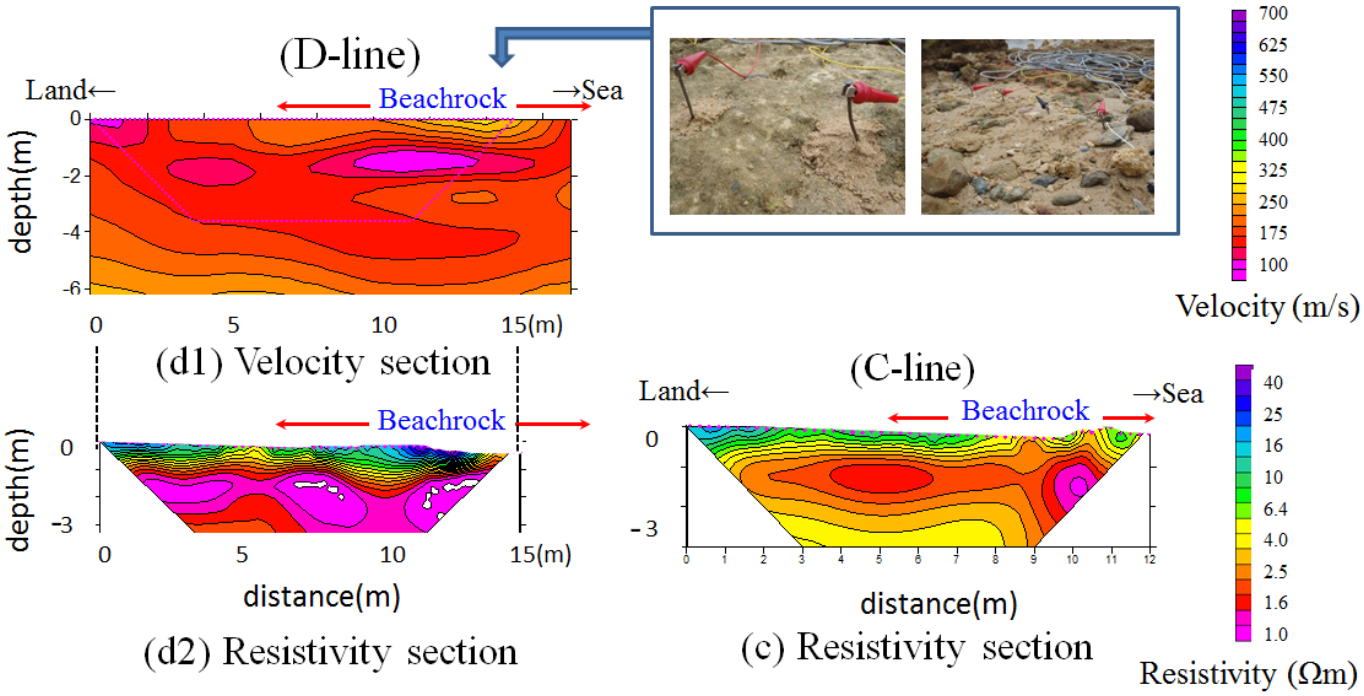


Figure 4.7. Results of velocity and resistivity survey (C-, D-line) (Kubo, et al., 2014).

4.4.2 Krakal-Sadranan beachrock sample, Yogyakarta, Indonesia.

4.4.2.1 Geology of Gunung Kidul Regency, Yogyakarta.

Beaches of Gunung Kidul Regency, Province of Special Region Yogyakarta, Indonesia have economic potential as limestone mine deposits and tourism. The karst beaches in Gunung Kidul Regency, Krakal-Sadranan beach to be exact, have similarities in terms of geological conditions, methods, and geomorphologic processes beach formation. The study area was located around E 455900.11; S 9099654.13 to E 456281.51; S 9099623.03, 49 S Indonesia region. However, for each of its shores, it is characteristically a coastal environment. The thin line of the characteristics of the environment are based purely on the shape of the beach and the diameter of the grains of sediment. This difference should also be noted as related to the condition of waves, ocean currents, temperature, salinity, and pH at each beach.

The characteristics of the karst mountains of south beach indicate that there is steep topography that rises to the east of Java Island. Continuing eastward hummocky valleys occur (Drini beach to Krakal to Sadranan). The coast of Krakal-Sadranan have a slope were steep ~12,33° with the tidal range of 12 meter that makes the sedimentary process in this coast were thickness than the deeper slope. The tidal reach of the littoral zone provides an opportunity for strong sea wave energies to erode the beach. The energy comes from crashing ocean waves

that break on the beach in the breaker zone that is not too far from the coastline. The result of the wave energy as well as the sharp, heterogenous rocks is the formation of an irregularly shaped beach at Krakal-Sadranan.

Throughout the karst coast of the Yogyakarta Special Prov., Gunung Kidul Regency the soil is derived from limestone bedrock, similar to the Mediterranean, i.e., the level of physical weathering is high. Grains of sediment along Krakal and Sadranan beaches are largely bright colored along most of the coastline as a result of the erosion of seabed being deposited on the beach. Composition of this sediment mainly formed by coral, skeletal fragment, Foraminifera and Mollusca. It is evident that the megascopic Sadranan beachrock has the same grain characteristics and the same grain composition as the non-solidified material along its beaches, with a dominance of shell fragments, corals, Foraminifera, and relatively anhedral-shaped grains varying from 2 mm to 4 cm. There is also carbonate cement. Figure 4.8 shows a sample of Krakal-Sadranan beachrock that has fragments of relatively large size (> 3 mm to 3 cm) with a grey to brownish grey color.



Figure 4.8. Sadranan beachrock sampling area, Yogyakarta, Indonesia.

4.4.2.2 Petrographic analysis result

The presence of different quartz crystals created an abundance of lytic fragments and more coral or shell-like fragments. The micrite or mud carbonate cement were filled the fragments showed that the cement formed during deposition, such as quartz, coral, and another

fragmented material. Whereas some of the opaque and quartz were formed as supported fabric (Figure 4.9).

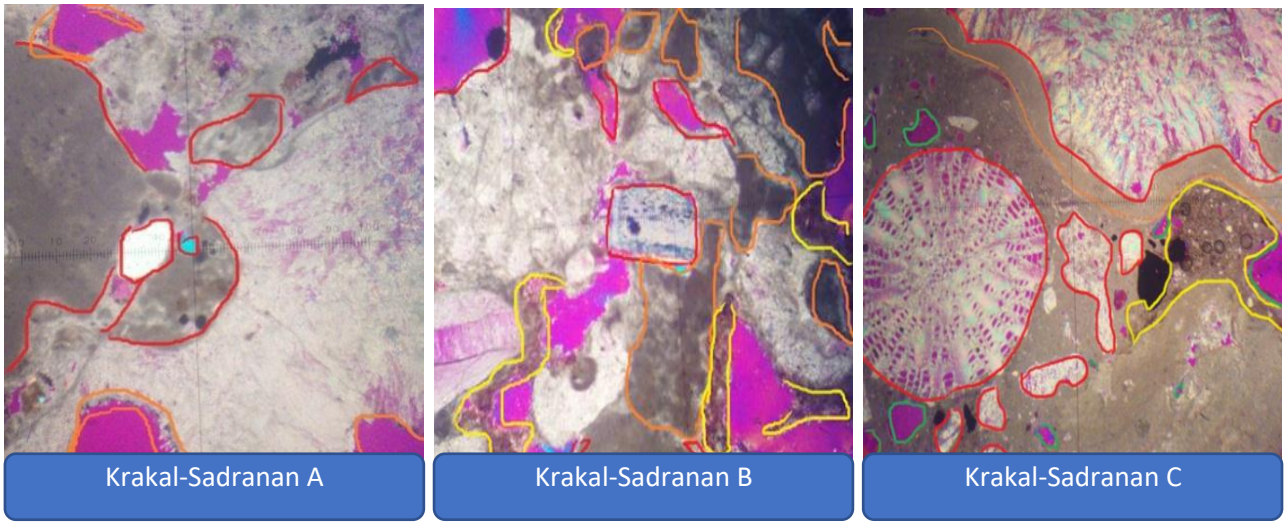


Figure 4.9. Sadranan beachrock cement vision using 100x (yellow pattern represented grain matrix and orange pattern represented cement).

Based on the analysis, the cementation mineral came from aragonite within needle crystalline fibrous, dark color micritized granules and cover a cryptocrystalline surrounded the fragments. This represented the Sadranan beachrock is a product of diagenesis in the phreatic environment of the sea sedimentation. The exclusive presence of aragonitic cement (needle aragonite and peloidal micrite cement) in rocks of the sedimentary diagenesis indicated that the coast occurred mainly within marine environments. The presence of cement found in the peloidal beachrock micrite cement is very significant, as it is a rare form of cement that can be found in rocks only along a coast, and therefore is very valuable. Research presenting some samples of cement showed gaps within the pores of the rocks, or an internal sedimentary intraparticle pore. The cement is comprised grains of round micritic and can be clearly observed in thin section which indicates that micrite played an important role in Sadranan beachrock cementation (Table 4.1).

In conclusion, it can be generalized that the Sadranan beachrock occurs mainly in sea conditions with different cements of the Sumuide sample, while the Sadranan sample is enriched in coral pores and pore-filling cement dominated by HMC. The names of the samples from Sadranan, Yogyakarta, are based on carbonate classification and are termed poorly sorted biomicrite (Folk, 1959) and bioclastic pack stone (Dunham, 1962) beachrock (lithified). In Sadranan, microorganism activities were the main source of material cemented inside the rock

compared to that of the Okinawa beachrock that formed from geochemical dissolution and reorganization followed by micritization of living organisms from the area.

Table 4.1. Percentage composition of beachrock

No	Composition type (%)	Name of samples					
		Sumuide A	Sumuide B	Sumuide C	KR-A	KR-B	KR-C
1.	Foraminifera	15.52	12.52	10.07	8.05	15.41	8.3
2.	Skeletal	16.88	14	46.91	32.17	32.17	33.67
3.	Coral	14	11.88	1.91	23.05	6.23	0
4.	Lithic	20.64	13.88	4.55	1.58	0	1.25
5.	Micrite	7.52	7.23	22.2	24.88	24.52	5.36
6.	Sparite	0.05	2.58	0	0	0	23.97
7.	Opaque	0.29	0.47	0.44	0.17	1.35	1.61
8.	Pores	14	18.11	11.39	8.41	17.88	24.19
9.	Quartz	10.11	18.23	2.5	1.17	0.88	0
10.	Others	0.94	1.05	0	0.47	1.52	1.61
TOTAL 100 %							

4.4.2.3 Indigenous ureolytic bacteria from Yogyakarta, Indonesia

The total potential urease bacteria found is less than 5% as the percentage ratio of ureolytic bacteria among the 527 colonies from the total number isolated from the rock samples. The diversity of microbes known in beachrock encompass three recognized ureolytic bacterial groups, most of which species are assorted microbial eukaryotes. The most frequently isolated 16S rDNA gene sequences include those from acid bacteria, Actinobacteria, and Chloroflexi (Janetzki, et al., 2015; Mauz, et al., 2015; Tostevin, et al., 2016). The results of a homology search in the GenBank/DDBJ/EMBL, three group of bacteria that were highly homologous to the 16S rDNA nucleotide sequence of the species whereas *Oceanobacillus profundus*, *Vibrio maritimus*, and *Pseudoalteromonas tetradonis*. The others, *V. maritimus* and *P. tetradonis* are gram-negative. The former are motile bacilli 1 μm wide and 1.5–4.0 μm, whereas the latter are strictly aerobic, motile with one polar flagellum, form either straight rods (or rod-shapes), 0.5–0.8 × 1.0-1.5 μm when in exponential growth phase. The bacteria expressed the highest urease activity after 48 h incubation, with only appreciable levels at 24 and 72 h. Cell concentration increased up to 2 days and then reached stationary phase.

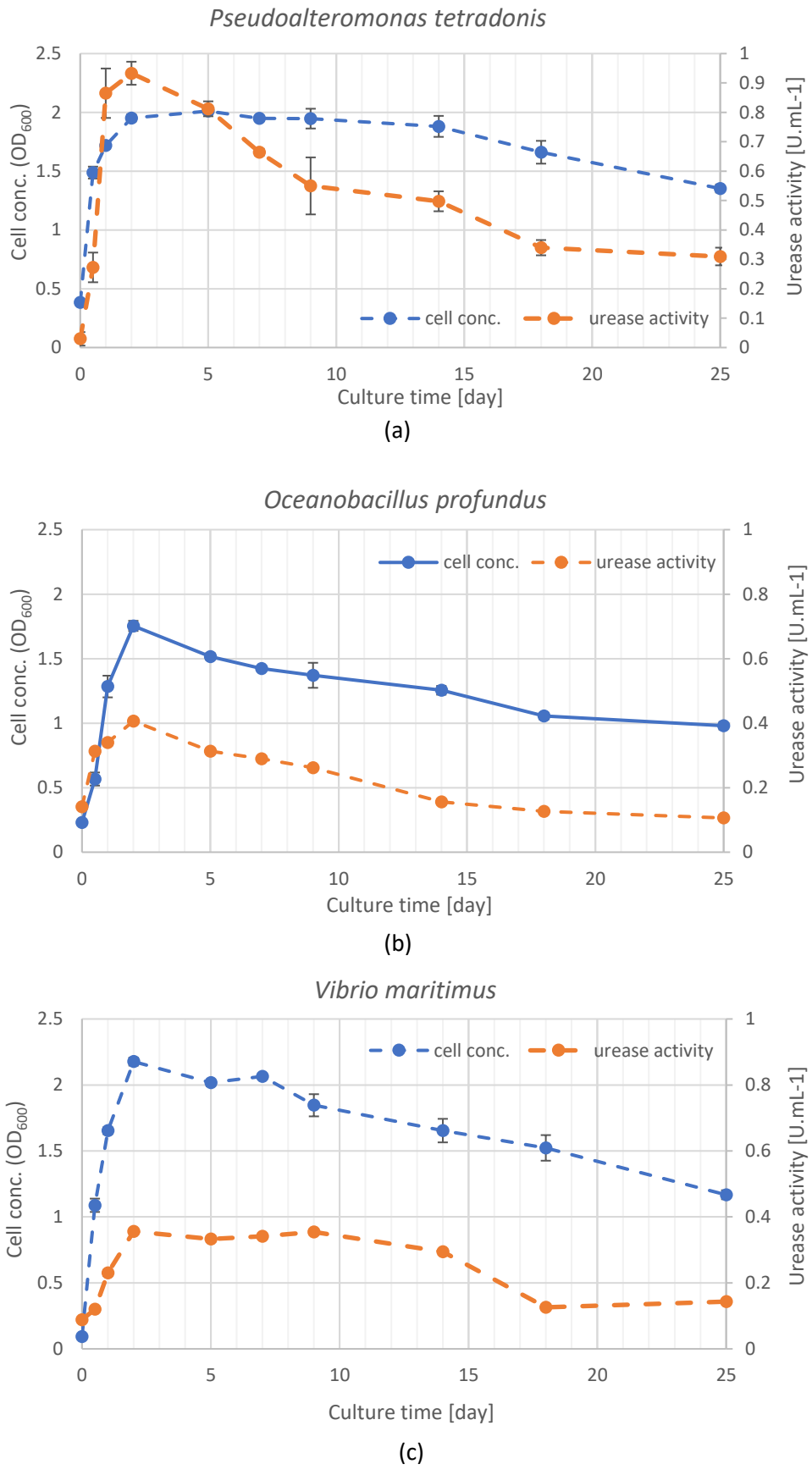


Figure 4.10. Cell growth and urase activity of *Pseudoalteromonas tetradonis* (a), *Oceanobacillus profundus* (b), and *Vibrio maritimus* (c)

The urease activity of the cell culture increased with cell growth. Based on this result, the production of urease would be a growth-associated system. The difference of temperature environment is shown in Figure 4.10, a for all of Indonesian species compared with *Pararhodobacter* sp. High activity was obtained in the range temperatures of 10-80 °C, within the maximum temperature of urase activity was obtained 80 °C in this study. Most of urease molecule is known to be composed of protein subunits and the subunits of this urease would strongly bind each other to leads the high stability of urease during long-term cultivation (Mobley and Island, 1995; Balasubramanian and Ponnuraj, 2010; Fujita, et al., 2017). Urease activity under different pH is shown in Figure 4.10, b. The results showed with the maximum activity around pH 2.0 – 13.0. For this temperature and pH variations, the results were different with Fujita, et al. (2017), where he is mentioned the results of maximum temperature exponential increasing toward environment temperature of the buffer solution and the method for urease activity measurement, he used ammonia meter of Tris/HCl buffer solution. Meanwhile, in this research, for measuring urease activity we used EDTA buffer solution for indophenol blue method then detect with colorimeter changing with optical density 630 nm. The results of Fujita, et al. (2017) and this research quite different but the pattern of bacterial growth and urease activity, especially for *Pararhodobacter* sp., is almost same. Indonesian ureolytic bacteria species proven have a higher activity then Okinawa species (*Pararhodobacter* sp.) which mean the possibility of developing beach sand using this bacteria strain in around tropical climate until room temperature is possible.

4.5 Discussions

Whilst the key aspect of mineral cementation is discussed, it is equally important to recognize the presence of aragonite primarily formed in a phreatic, low-marine, vadose environment. Aragonite formation has been related to the temperature of the solution; for example, the higher the solution temperature, the faster aragonite precipitates around calcite cement minerals (Burton and Walter, 1987) and the crystal form the cement takes is mostly fibrous. After this, the interplay between the different carbonate phases occurs in the cement, and the content of calcite, aragonite or Mg-calcite depends on the change in the water-table elevation, the temperature or the pressure, with a trend toward chemical stability. One of the most effective means to create a polymorph of calcite or dolomite is the infiltration of meteoric

water rich in dissolved CO_2, depleting the cement in Mg, Sr, and Na and enriching it in other elements.

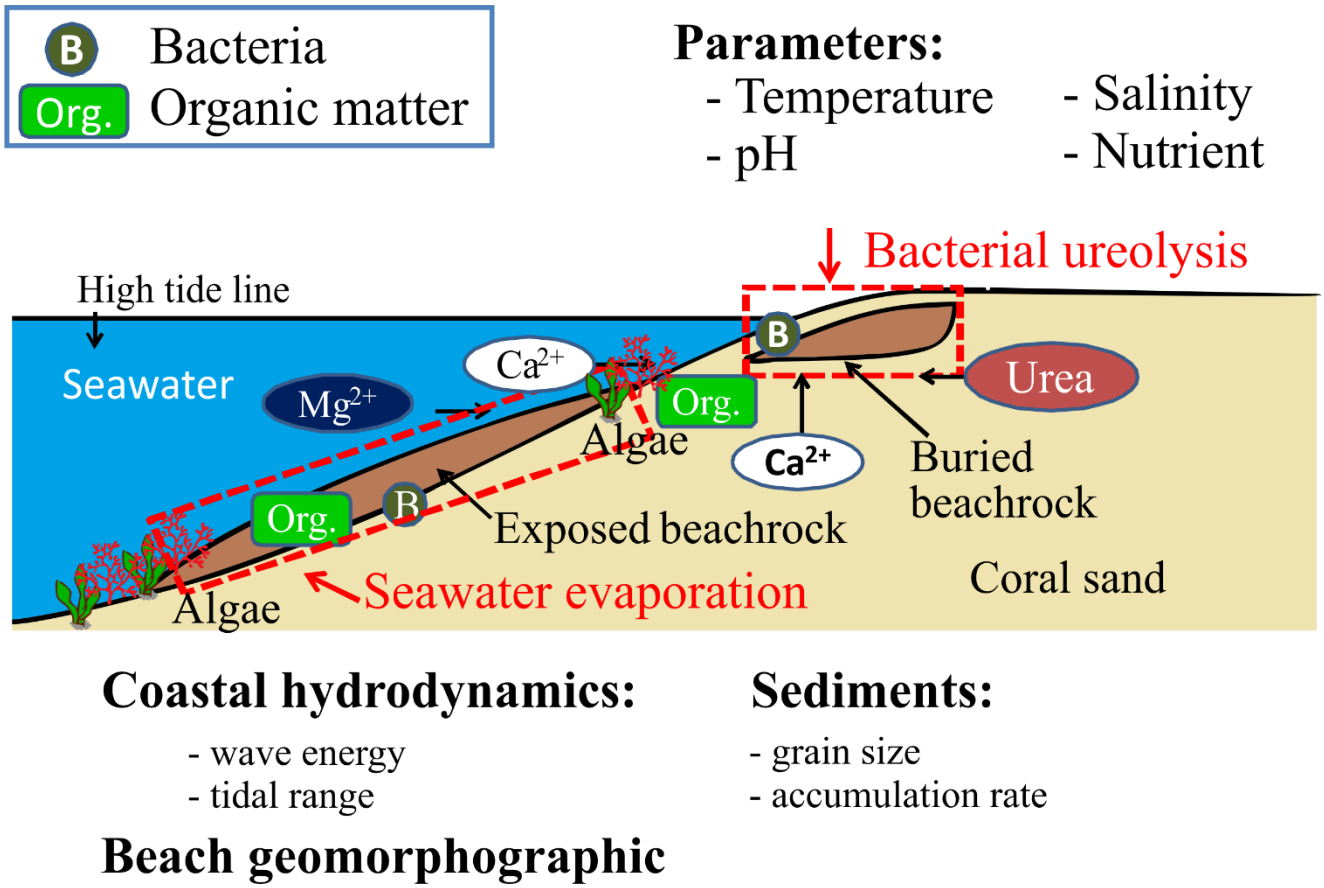


Figure 4.11. Illustration schemes of natural beachrock occurrences (after Danjo, 2014)

The main parameters of beachrocks sediments are pH, temperature, salinity, and nutrient from the sea (Figure 4.11). Other factors such as beach hydrodynamics, beach geomorphology, and also the formation of sediments from the coast. The pH, Temperature, salinity and nutrients in the surface layer of the sea are important controls on carbonate production. Their distribution is mainly governed by the latitudinal differences of solar radiation and by the patterns of surface circulation. The first-order trend is a decrease in temperature with increasing latitude and salinity maxima in the horse latitudes that correspond to the desert belts on land. From the horse latitudes, salinity decreases pole-ward and towards the equator where high rainfall dilutes the surface water. The effects of gyre circulation are more varied as outlined below high salinity because the gyre centers lie in the arid horse latitudes. In the equatorial belt, the opposed direction of the Coriolis force in the two hemispheres lead to surface divergence and gentle upwelling with moderately high nutrient levels. Upwelling and high rainfall lower the salinities.

4.5.1 Natural beachrock sedimentary

4.5.1.1 Cement characteristics

Thin-section analysis from all of the Okinawa samples present results in one direction; fossils are dominated by foraminifera and coral (skeletal grain particles), while other materials depend on the genesis of the source rock (opaque) that cemented from micritic and sparite. According to the theory of fossil marine paleontology, foraminifera are separated into two groups following their life strategy, namely planktonic and benthonic foraminifera. All benthic foraminifera occur in marine and neritic environmental zones, living largely in oligotrophic reefs and carbonate shoals and confined mainly to low-latitude areas. The prolific in nutrient-deficient of the nature, warm, shallow-water seas, often associated with coral reefs, an important key in producing carbonate sediment (Boudagher-Fadel, 2008). In general, the presence of benthic foraminifera (including larger foraminifera) indicates a warm environment, as the minimum water temperature tolerated by a living foram is 18 °C, while the maximum water depth at which they live is 35 m (Murray, 1973) as related to the photic zone.

Peloidal micrite cement, aragonite needled cementation, micritization, and micritic were covered on the thin sections. The analysis concluded that natural beachrock was a product of a diagenetic marine phreatic environment. The significant cost of aragonite cement (aragonite needled and micrite peloidal cement) for cementation of beachrock was a key factor in shoreline sedimentary diagenesis in the marine environmental system. It can be directly precipitated from sea water or be a by-product of biological activities. Beachrock is generally cemented in the tidal zone with high amounts of aragonite, HMC, and LMC (Daryono, 2016). General carbonate cementation in the marine environment formed acicular-radial and spacious types of cement texture whereas the tidal zone is indicated by aragonite or HMC. Meniscus and bridge cement indicate LMC composition (Scholes and Ulmer-Scholes, 2003; Vousdoukas et al., 2007; Mauz, et al., 2015; Avcioğlu, et al., 2016). Regarding the aforementioned cementation processed related to microbial activity, it is commonly referred to as biogenic cement. On the other hand, another author has suggested that the microbes of metabolic bacteria are related to the precipitation of rocks (Danjo and Kawasaki, 2016; Khan, et al, 2018; Tirkolaei, et al., 2018), and the end products lower the thermodynamic boundary for cement nucleation and increase the rates of the physicochemical processes involved (Kandianis, et al., 2008; Dupraz, et al., 2009). Bio-cementation using MICP technique of calcium carbonate

precipitation can occur by biologically controlled or induced (Lowenstan and Wiener, 1988; Daryono, 2016).

4.5.1.2 Geophysical properties of natural beachrock

Based on the results, analysis based on mineralogy, geochemical, and biodiversity of ureolytic bacteria approaches of both samples from Okinawa, Japan and Krakal-Sadranan, Indonesia have the same pattern which is the characteristics of cement solution were dominated with aragonite and calcite crystalline that soluble in the water. Beachrock found in both of those areas were precipitated beneath beach sand, which is a wave erosional product, and then solidified beneath that formation, floating between limestone bedrock and beach sands formation, based on a greater value from resistivity and S-wave velocity in the formation layers. The resistivity, thickness, and S-wave velocity of the beachrock increases as it gets closer to the coastline. The maximum thickness of the beachrock at this point is about 1 m based on calculations; the α-section covers 210.496 m^3, while the β-section covers 76,936 m^3 of beachrock deposit in Krakal-Sadrnan, Indonesia. In the other hand, Natural beachrock in Okinawa, Japan has the S-wave velocity was found to be about 350 m/s, and their resistivity was about 4–40 Ωm. Their thickness was about 1.0 m and had a tendency to become thicker closer to the sea. In order to solidify the sand, it is highly likely that it is important for the sand to be repeatedly immersed in seawater, resulting in repeated evaporation of the liquid (Suzuki, et al., 2013; Kubo, et al., 2014).

However, the mechanism of cement sedimentary not exactly the same because of the geomorphologic settlement Japan in Indonesia were different and source of mineral in Indonesia were close to volcanic activities that really active, especially Yogyakarta mountain activity which is famous of eruption every 4 years. Therefore, the temperature and pH in the tropic-subtropical area is the main role the interaction between microbial activity and chemical reaction proceed toward cementation of a beachrock. Cement product of beachrock evolution based on field investigation (area A, area B, and area C) is represented of aragonite crystalline only occur in the swash-zone area (mostly area A) because the aragonite mineral is really easy to soluble in the fresh water that came from rain or fresh water from land. This assumption does not only come from Japan or Indonesia studies but perhaps the cementation process is relatively same all around the world especially in the tropic-subtropic climate.

4.5.2 Indigenous ureolytic bacteria from natural beachrock

Furthermore, artificial beachrocks used microorganism activities significantly successfully and were noted as man-made especially from Indonesia species strains. The aragonite crystallization fibers formed between grain sand particles then interlocked with one another until the precipitate over time became a solid rock. The solidification experiment by using in-situ bacteria having urease activity and changing the composition of the solidification solution based on *Pararhodobacter* sp. (Danjo and Kawasaki, 2014). Since 2014, microbial treatment using *Pararhodobacter* sp., have a 75 published number of journals and proceedings. Hardening of a substrate using calcium carbonate as cement materials, using calcite and aragonite were valuable to consider how to make artificial beachrock. (Hata, et al., 2011; van Passen, et al., 2010; Danjo and Kawasaki, 2014; Khan, et al., 2018). Therefore, based on experiments of synthetic beachrock, it could mitigate erosion impacts in coastal areas subjected to problematic erosional damage based on bio-cementation technology is promising technology due to its suitability in an environment problem such as coastal erosional preventing development in the future especially of indigenous Indonesian local strain bacteria's.

Bacteria play a catalyzing role in urea hydrolysis through generation of urease enxyme to formed calcium carbonate cement (van Passen, 2009; Tirkolaei, et al., 2018; Al Thawadi, 2008). Specific cement types are recognized as (i) acicular, fibrous, and bladed fabrics; (ii) radial fibrous and fascicular-optic fabrics; (iii) micro-and cryptocrystalline fabrics; (iv) equant spar, syntaxial overgrowth fabrics, scalenohedral calcites, peloidal fabrics and (v) non-carbonates. These types are incipient early marine cementation leading to a reduction in pore-space in near-seafloor sediments (Christ, et al., 2015). Hydrolysis of urease bacteria as a result of increased total carbonate content through the production of dissolved inorganic carbon and a pH increase through the production ammonia. The species were isolated from Okinawa beachrock called *Pararodhobacter* sp., and *Oceanisphaea* sp., which are the *Pararhodobacter* sp., are Gram-negative, rod-shaped, aerobic, chemoorganotrophic bacteria, that are moderately halophilic with approximately 1 μm in diameter and 3 μm in length (Foesel, et al., 2011; Danjo and Kawasaki, 2016). Meanwhile, *Oceanisphaera* sp., had a spherical cell, 1.0-1.2 μm in diameter and motile by means of flagella. Gram-negative chemoorganotroph with absolute requirement for sodium ions, aerobic, moderately halophilic, and oxidase-catalase-positive (Romanenko, et al., 2003). On other hand, Indonesian ureolytic bacteria strain were found are *Oceanobacillus profundus*, *Vibrio maritimus*, and *Pseudoalteromonas tetradonis*. The others, *V. maritimus* and *P. tetradonis* are gram-negative. The former are motile bacilli 1 μm wide and

1.5–4.0 μm, whereas the latter are strictly aerobic, motile with one polar flagellum, form either straight rods (or rod-shapes), 0.5–0.8 × 1.0-1.5 μm when in exponential growth phase.

The differences between gram positive and gram-negative bacteria are primarily related to their cell wall composition. Gram positive bacteria have cell walls composed mostly of a substance unique to bacteria known as peptidoglycan, or murein. These bacteria stain purple after gram staining. Gram negative bacteria have cell walls with only a thin layer of peptidoglycan and an outer membrane with a lipopolysaccharide component not found in gram positive bacteria. gram negative bacteria stain red or pink after gram staining.

4.5.2.1 Gram positive bacteria

The cell walls of gram-positive bacteria differ structurally from the cell walls of gram-negative bacteria. The primary component of bacterial cell walls is peptidoglycan. Peptidoglycan is a macromolecule composed of sugars and amino acids that are assembled structurally like woven material. The amino sugar component consists of alternating molecules of N-acetylglucosamine (NAG) and N-acetylmuramic acid (NAM). These molecules are crosslinked together by short peptides which help give peptidoglycan strength and structure. Peptidoglycan provides protection for bacteria and defines their shape. The gram-positive cell wall has several layers of peptidoglycan. The thick layers of peptidoglycan help to support the cell membrane and provide a place of attachment for other molecules. The thick layers also enable gram positive bacteria to retain most of the crystal violet dye during gram staining causing them to appear purple (Figure 4.12). Gram positive cell walls also contain chains of teichoic acid that extend from the plasma membrane through the peptidoglycan cell wall. These sugar-containing polymers assist in maintaining cell shape and play a role in proper cell division. Teichoic acid helps some gram-positive bacteria to infect cells and cause disease.

Some gram-positive bacteria have an additional component, mycolic acid, in their cell walls. Mycolic acids produce a waxy outer layer that provides additional protection for mycobacteria, such as Mycobacterium tuberculosis. Gram positive bacteria with mycolic acid are also called acid-fast bacteria because they require a special staining method, known as acid-fast staining, for microscope observation. Pathogenic gram-positive bacteria cause disease by the secretion of toxic proteins known as exotoxins. Exotoxins are synthesized within the prokaryotic cell and released into the exterior of the cell. They are specific to certain bacterial

stains and can cause serious damage to body organs and tissues. Some gram-negative bacteria also produce exotoxins.

Gram positive cocci refer to gram positive bacteria that are spherically shaped. Two genera of gram-positive cocci noted for their role as human pathogens are *Staphylococcus* and *Streptococcus*. *Staphylococcus* are spherical in shape and their cells appear in clusters after they divide. *Streptococcus* cells appear as long chains of cells after division. Examples of gram-positive cocci that colonize the skin include *Staphylococcus epidermidis*, *Staphylococcus aureus*, and *Streptococcus pyogenes*. While all three are part of the normal human microbiota, they can cause disease under certain conditions. *Staphylococcus epidermidis* form thick biofilms and can cause infections associated with implanted medical devices. Some *Staphylococcus aureus* strains, such as methicillin-resistant *Staphylococcus aureus* (MRSA), have become resistant to antibiotics and can lead to the development of serious illness. *Streptococcus pyogenes* can cause strep throat, scarlet fever, and flesh-eating disease.

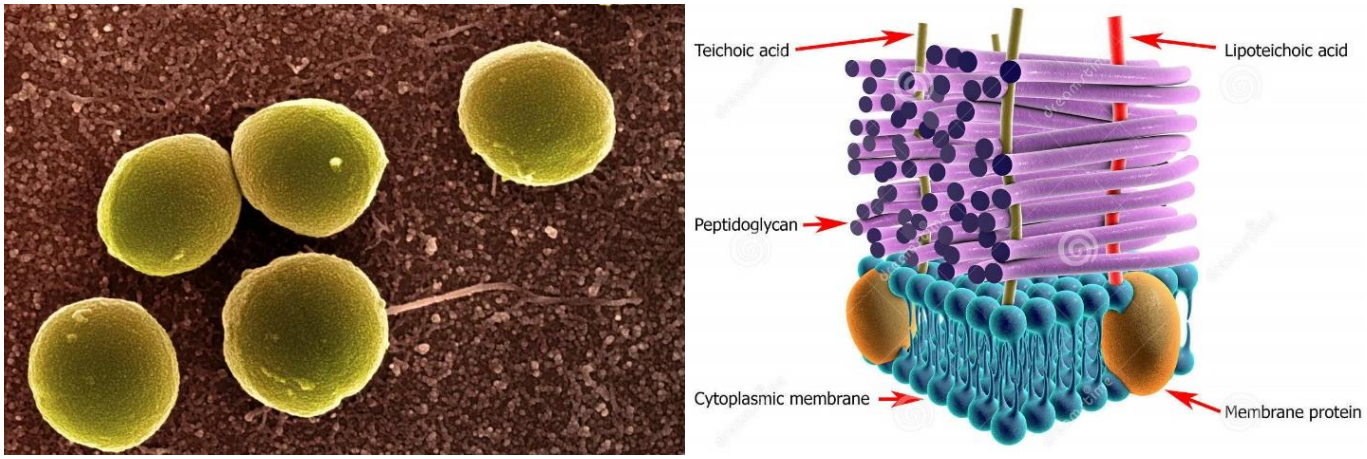


Figure 4.12. Illustration of gram-positive bacteria (after Bailey, 2020)

4.5.2.2 Gram negative bacteria

Like gram positive bacteria, the gram-negative bacterial cell wall is composed of peptidoglycan. However, the peptidoglycan is a single thin layer compared to the thick layers in gram positive cells. This thin layer does not retain the initial crystal violet dye but picks up the pink color of the counterstain during gram staining. The cell wall structure of gram-negative bacteria is more complex than that of gram-positive bacteria. Located between the plasma membrane and the thin peptidoglycan layer is a gel-like matrix called periplasmic space. Unlike in gram positive bacteria, gram negative bacteria have an outer membrane layer that is external

to the peptidoglycan cell wall. Membrane proteins, murein lipoproteins, attach the outer membrane to the cell wall (Figure 4.13). Another unique characteristic of gram-negative bacteria is the presence of lipopolysaccharide (LPS) molecules on the outer membrane. LPS is a large glycolipid complex that protects bacteria from harmful substances in their environment. It is also a bacterial toxin (endotoxin) that can cause inflammation and septic shock in humans if it enters the blood. There are three components of the LPS: Lipid A, a core polysaccharide, and an O antigen. The lipid A component attaches the LPS to the outer membrane. Attached to the lipid A is the core polyssaccharide. It is located between the lipid A component and the O antigen. The O antigen component is attached to the core polyssaccharide and differs between bacterial species. It can be used to identify specific strains of harmful bacteria.

Gram negative cocci refer to gram negative bacteria that are spherically shaped. Bacteria of the genus *Neisseria* are examples of gram-negative cocci that cause disease in humans. *Neisseria meningitidis* is diplococcus, meaning that its spherical cells remain in pairs after cell division. *Neisseria meningitidis* causes bacterial meningitis and can also cause septicemia and shock. Another diplococcus bacterium, *N. gonorrhoeae*, is the pathogen responsible for the sexually transmitted disease gonorrhea. *Moraxella catarrhalis* is a gram-negative diplococcus that causes ear infections in children, upper respiratory system infections, endocarditis, and meningitis. Gram negative coccobacillus bacteria have bacterial shapes that are in between spherical, and rod shaped. Bacteria of the genus *Haemophilus* and *Acinetobacter* are coccobacilli that cause serious infections. *Haemophilus* influenzae can cause meningitis, sinus infections, and pneumonia. *Acinetobacter* species cause pneumonia and wound infections.

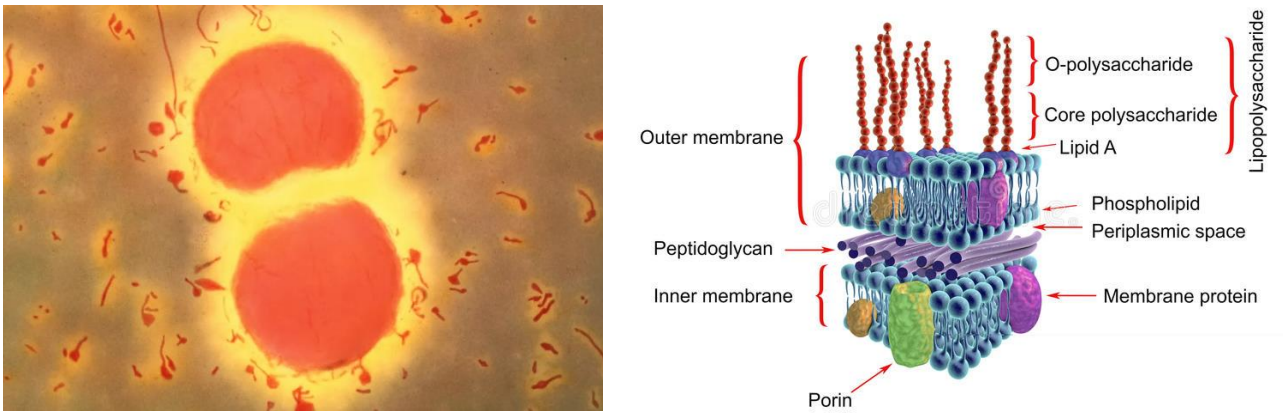


Figure 4.13. Illustration of gram-negative bacteria (after Bailey, 2020)

4.5.2.3 Gram positive versus gram negative bacteria

- Most bacteria can be broadly classified as gram positive or gram negative.
- Gram positive bacteria have cell walls composed of thick layers of peptidoglycan.
- Gram positive cells stain purple when subjected to a gram stain procedure.
- Gram negative bacteria have cell walls with a thin layer of peptidoglycan. The cell wall also includes an outer membrane with lipopolysaccharide (LPS) molecules attached.
- Gram negative bacteria stain pink when subjected to a gram stain procedure.
- While both gram positive and gram-negative bacteria produce exotoxins, only gram-negative bacteria produce endotoxins.
- Gram-negatives were commonly species strain were isolated from shoreline inside of beachrock rather than gram positive which dominant with in-land bacteria, but some of bacteria strain from shoreline also found as gram positive.

4.5.3 Sediment characteristics differences of Okinawa, Japan and Yogyakarta, Indonesia natural beachrock

Some of the differences between those two samples of beachrock not only from the characteristics but also the microbial which isolated inside the beachrock samples. Indonesian beachrock were found is categorize as *Biotically controlled precipitation* which have an enrichment of microbial activity such as algae, arthropods, and other foraminifera were represented the environment is rich of nutrient of another biotic organism rather than in the Okinawa site. Okinawa site is categorized as *Biotically induced precipitation.* Whichever, the environmental controls on microbial precipitation are less well known than those of skeletal precipitation. An important property of the microbial mode of precipitation is its near independence of light. Microbial precipitates may form in the photic zone or below, certainly to depths of 400 meters. On modern reefs, the microbial deposits are best developed in the forereef environment. However, stromatolites in the uppermost photic zone (e.g. Reid et al. 2000) and auto micrite in the interstices of coral framework (Camoin, et al. 1999) demonstrate that the microbial mode of carbonate fixation finds its niches even in the prime domains of skeletal production. An important chemical requirement is supply of alkalinity in the form of the anions HCO_3^- and CO_3^{2-}. A likely source of alkalinity is sulfate reduction combined with decay of organic matter in oxygen-deficient layers of the ocean such as the oxygen minimum of the thermocline (Schlager, 2005). The estimated water depth and organic-rich ambient

sediments of many mud mounds support this assumption. Whether temperature sets practically relevant limits for microbial carbonate precipitation is unclear. Mud mounds seem to be best developed in low latitudes. However, the paleo-latitude of many Paleozoic mounds is not well constrained and narrow latitudinal restriction is not to be expected with a production system that demonstrably functions at low light levels and in intermediate water depths, i.e.at temperatures significantly below tropical surface temperatures. To simplify the differences of natural beachrock from Japan and Indonesia were expressed in the table 4.2 in the below.

Table 4.2. Sedimentary characteristics differences of Okinawa natural beachrock, Japan and Yogyakarta, Indonesia natural beachrock

No.	Classification	Okinawa beachrock, Japan	Yogyakarta beachrock, Indonesia
1.	*Type of cementation*	Aragonite-HMC dominant with skeletal fragment	Aragonite-HMC dominant with *Baculogypsina sphaerulata*
2.	*Zone*	Tropic-Subtropics	Tropic
3.	*Geophysical properties*	S wave velocity ~350 m/s Resistivity around 4–40 Ωm	S wave velocity 400-600 m/s Resistivity around 9–78.7 Ωm
4.	*Thickness of beachrock*	Around 1 meter, respectively	Around 1.5~2 meters, respectively
5.	*Ureolytic bacteria strains*	*Pararhodobacter* sp.	*Oceanobacillus profundus*, *Vibrio maritimus*, and *Pseudoalteromonas tetradonis*
6.	*P-wave and S-wave comparison (see Figure 2.13)*	Identify sedimented around Early Paleogene until Miocene	Identify sedimented around Cretaceous until Late Paleogene
7.	*Optimum temperature*	50-60 °C	30-40 °C
8.	*Major oxide cement*	CaO, MgO, Al_2O_3, and SiO_2	CaO, MgO, Na_2O, and P_2O_5
9.	*pH*	7.2 ~ 8.8	7.2 ~ 8.8
10.	*UCS uniaxial strength*	3.4 ~ 28 MPa	3 ~ 16.4 MPa
11.	*Carbonate classification*	Biotically induced precipitate	Biotically controlled precipitate

6. Conclusions

The review analysis for both natural beachrock of Sumuide beach and Krakal-Sadranan beach are as good as the result sample obtained by the presence of either intraparticle or interparticle granules cement filling. On an average, the sample of natural beachrocks were very similar to Okinawa beachrock and Yogyakarta beachrock where this type of cement dominated by peloidal micritic and micritic dark granules that found in the same intertidal zone. Okinawa beachrock contained more lytic granules with fragments of quartz result material sediments there are predominantly with a fragment of coral shell, meanwhile Yogyakarta

beachrock was more sparite cement which had filling of pore interparticle, therefore that it appears more compact and lower porosity. Micritization proceed in beachrock of Okinawa or Yogyakarta is a product of diagenesis rock that formed on the phreatic environment of the sea within the presence of cement on the beachrock is peloidal micritic. To sum up, the origin of cement micritic peloidal is uncertain. It can be precipitated directly from seawater or it just be a product of biological activity. Beachrock of Okinawa were classified as *biotically induced precipitate*, because the organism sets the precipitation process in motion but organic influence on its course is marginal or absent. The reaction takes place outside the cell and the product is very similar, often indistinguishable, from abiotic precipitated. The majority of carbonate material in modern oceans is precipitated as highly structured skeletons of organisms were dominant in the cold water rather than tropical area. Whereas beachrock of Indonesia is *classified as biotically controlled precipitate* which the common precipitation were induced by microorganisms, mostly bacteria and cyanobacteria. Micrite is a major, often dominant component of these deposits. Microalgae as mats were found enrichment inside Indonesia beachrock site than Okinawa beachrock which mostly consist of skeletal shells.

References

Al Thawadi, S. 2008. High Strength In-situ Biocementation of Soil by Calcite Precipitating Locally Isolated Ureolytic Bacteria. Doctor Dissertation, Murdoch University, Australia.

Al Imran, M., Nakashima, K. and Kawasaki, S., 2017. Combination technology of geotextile tube and artificial beachrock for coastal protection. International Journal, 13(39), pp.67-72.

Arietta. N., Goienaga, N., Martinez-Azkarazo, I., Murelaga, X., Baceta, J. I., Sarmiento, A., and Madariaga, J. M. 2011. Beachrock Formation In Temperate Coastlines: Examples In Sand-gravel Beaches Adjacent To The Nerbioi-Ibaizabal Estuary (Bilbao, Bay of Biscay, North of Spain). Spectrochimica Acta Part A 80:55-65.

Avcioğlu, M., Yiğitbaş, E., and Erginal, A. E. 2016. Beachrock Formation On The Coast Of Gökçeada Island and Its Relation To The Active Tectonics Of The Region, Northern Aegean Sea, Turkey. Quaternary Int. 401, p.141-152.

Ayinla, H. A., Abdullah, W. H., Makeen, Y. M., Abubakar, M. B., Jaouro, A., Yandoka, B. M. S., and Abidin, N. S. Z. 2017. Petrographic and Geochemical Characteristization Of The

Upper Cretaceous Coal and Mudstones of Gombe Formation, Gongola sub-basin, Nortehn Benue Trough Nigeria: Implication For Organic Matter Preservation, Paleodepositional Environment And Tectonic Settings. Int. Journal of Coal Geology, v. 180, pp. 67-82. http://doi.org/10.1016/j.coal.2017.06.010.

Bailey, Regina. "Gram Positive vs. Gram Negative Bacteria." ThoughtCo, Feb. 11, 2020, thoughtco.com/gram-positive-gram-negative-bacteria-4174239.

Balasubramanian, A., and Ponnuraj, K. 2010. Crystal Structure of the First Plant Urease from Jack Bean: 83 years of journey its first crystal to molecular structure. J. Mol. Biol. 400, pp. 274-283.

Bäuerlein, E. 2003. Biomineralization Of Unicellular Organism: An Unusual Membrane Biochemistry for The Production of Inorganic Nano- and Microstructures. Angew. Chem. Int. 42, 614-641. Doi: 10.1002/anie.200390176.

Boudagher-Fadel, M. K. 2008. Evolution and Geological Significance of Larger Benthic Foraminifera. Departement of Earth Science, University College London: Elsevier, 560p.

Burton, E. A., and Walter, L. M. 1987. Relative Precipitation Rates of Aragonite and Mg Calcite from Seawater: Temperature Or Carbonate Ion Control? Geology 15, 111-114.

Christ, N., Immenhauser, A., Wood, R. A., Darwich, K., and Niedermayr, A. 2015. Petrography and Environmental Control On The Formation Of Phanerozoic Marine Carbonate Handgrounds. Earth-Science Reviews 151, p. 176-226.

Calvet, F., Cabrera, M. C., Carracedo, J. C., Mangas, J., Peréz-torrado, F. J., Recio, C., and Travé, A. 2003. Beachrock from the island of La Palma (Canary Island, Spain). Mar Geol 197: 75-93.

Díez, B., Bauer, K., and Bergman, B. 2007. Ephilithic Cyanobacterial Communities Of A Marine Tropical Beachrock (Heron Island, Great Barrier Reef): diversity and diazotrophy. Appl Environ Microbiol 73(11):3656-3668.

Danjo, T., and Kawasaki, S. 2014. Formation Mechanism of Beachrocks in Okinawa and Ishikawa, Japan, With a Focus on Cements. Materials Transaction Vol. 55: Japan, pp. 493-500.

Danjo, T., and Kawasaki, S. 2016. Microbially Induced Sand Cementation Method Using Pararhodobacter sp., Strain S01, Inspired by Beachrok Formation Mechanism. Materials Transaction Vol. 57: Japan, pp. doi:10.2320/matertrans.M-M2015842.

Desruelles, S., Fouache, E., Ciner, A., Dalongeville, R., Pavlopoulos, K., Kosun. E., Coquinot, Y., and Potdevin, J. L., 2009. Beachrock and Sea Level Changes since Middle Holocene: Comparison between the Insular Groups of Mykonos-Delos-Rheina (Cyclades, Greece) and the Southern Coast of Turkey. Glob. Planet. Chang. 66, 19-33.

Daryono, L. R. 2016. Comparison of natural beachrock and anthropogenic beachrock, case study: Okinawa-jima, Japan. Master's degree of Geological Engineering, Universitas Gadjah Mada, Indonesia.

Daryono, L.R., Titisari, A.D., Warmada, I.W. and Kawasaki, S., 2019. Comparative characteristics of cement materials in natural and artificial beachrocks using a petrographic method. Bulletin of Engineering Geology and the Environment, 78(6), pp.3943-3958.

Daryono, L.R., Nakashima, K., Kawasaki, S., Titisari, A.D. and Barianto, D.H., 2020. Sediment Characteristics of Beachrock: A Baseline Investigation Based on Microbial Induced Carbonate Precipitation at Krakal-Sadranan Beach, Yogyakarta, Indonesia. Applied Sciences, 10(2), p.520.

Dhami, N. K., Reddy, M. S., and Mukherjee, A. 2013. Biomineralization of Calcium Carbonate and Their Engineered Applications: A Review. Frontier In Microbiology.

Douglas, S., and Beveridge, T. J. 1998. Mineral Formation by Bacteria In Natural Microbial Communities. FEMS Microbiol. Ecol. 26, 79-88. Doi: 10.1111/j.1574-6941.1998.tb00494.x.

Dunham, R. J. 1962. Classification of Carbonate Rocks According To Depositional Texture. In: Ham, W. E. (ed.). Classification of Carbonate Rocks. American Association of Petroleum Geologist Memoir, p.108-121.

Dupraz, C., Reid, R. P., Braissant, O., Decho, A. W., Sean, N. R., and Visscher, L. K. 2009. Processes Of Carbonate Precipitation In Modern Microbial Mats. Earth-Sci. Rev. 96, pp. 141-162.

Foesel, B. U., Drake, H. L., and Schramm, A. 2011. Defluviimonas denitricans gen. nov., sp. nov., and Pararhodobacter aggregans gen. nov., sp. nov., non-phototrophic Rhodobacteraceae from the biofilter of a marine aquaculture. Systematic and Applied Microb. Jour. Vol 34, 498-502. http://doi.org/10.1016.j.syapm.2011.08.006.

Fujita, M., Nakashima, K., Achal, V., and Kawasaki, S. 2017. Whole-cell Evaluation of Urease Activity of Pararhodobacter sp., Isolated from Peripheral Beachrock. Biochem. Eng. J. 124, 1-5. http://dx.doi.org/10.1016/j.bej.2017.04.004.

Folk, R. L. 1959. Practical Petrographic Classification of Limestones. American Association of Petroleum Geologist Bulletin, v.43, p.1-38.

Hata, T., Tateno, N., and Abe, H. 2011. Jpn. Geotchnical J.6 (2011) 305-315 (in Japanese).

Kardianis, M. T., Fouke, B. W., Johnson, R. W., Veysey, J., and Inskeep, W. I. 2008. Microbial Biomass: A Catalys For CaCO3 Precipitation In Advection-dominated Transport Regimes. Bulletin of The Geological Society of Amerika 120, p. 442-450.

Karkani, A., Evelpidou, N., Vacchi, M., Morhange, C., Tsukamoto, S., Frechen, M., and Maroukian, H. 2017. Tracking Shoreline Evolution In The Central Cyclades (Greece) Using Beachrocks. Marine Geology 388, 25-37. http://dx.doi.org/10.1016/j.margeo.2017.04.009.

Klaus, Putz, H.B. 2017. Match! – Phase Identification from Powder Diffraction, Crystal Impact.

Khan, M. N. H., and Kawasaki, S. 2016. Formation of Artificial Beachrock Towards Inhibit of Coastal Erosion in Bangladesh: A Review. The 15th Asian Reg. Conference on Soil Mechanics and Geotechnical Engineering, Japan Geotechnical Society Special Publication. DOI:10.3208/jgssp.TC303-01.

Khan, M. N. H., and Kawasaki, S. 2018. Making Artificial Beachrock Through Bio-cementation: A Novel Technology to Inhibition of Coastal Erosion. Handbook of Environmental Materials Management. http://doi.org/10.1007/978-3-319-58538-3_38-1.

Kneale, D., and Viles, H. A. 2000. Beach Cement: Incipient $CaCO_3$- Cement Beachrock Development In The Upper Intertidal Zone, North Uist, Scotland. Sediment Geol 132:165-170.

Kolaiti, E., and Mourtzas, N. D. 2016. Upper Holocene Sea Level Changes In The West Saronic Gulf, Greece. Quant. Int. 401, 71-90.

Kubo, R., Kawasaki, S., Suzuki, K., Yamaguchi, S. and Hata, T., 2014. Geological exploration of beachrock through geophysical surveying on Yagaji Island, Okinawa, Japan. Materials Transactions, pp.M-M2013839.

Lowenstan, H. A., and Weiner, S. 1988. On Biomineralization. Oxford University Press, New York.

Mauz, B., Vacchi, M., Green, A., Hoffmann, G., and Cooper, A. 2015a. Beachrock: A Tool for Reconstructing Relative Sea Level in the Far-Field. Mar. Geol. 362, 1-16. http://dx.doi.org/10.1016/j.margeo.2015.01.009.

McCutcheon, J., Nothdurft, L. D., Webb, G. E., Paterson, D., and Southam, G. 2016. Beachrock Formation Via Microbial Dissolution and Re-precipitation Of Carbonate Minerals. Marine Geology 382, p. 122-135.

McNeil, F. S. 1960. The Tertiary and Quaternary Gastropoda of Okinawa. Prof. Paper, U.S. Geol. Surv, vol. 339, pp. 148.

Mobley, H. L. T., and Island, M. D. 1995. Molecular Biology of Microbial Ureases. Microbiol. Rev. 59, pp. 451-480.

Murray, J. W. 1973. Distribution and Ecology of Living Benthic Foraminifera. Heinemann, London, 274p.

Mwandira, W., Nakashima, K., and Kawasaki, S. 2017. Bioremediation of Lead-contaminated Mine Waste by Pararhodobacter sp., Based on the Microbially Induced Calcium Carbonate Precipitation Technique and Its Effects On Strength Of Coarse and Fine Grained Sand. Eco. Eng. 109, 57-64. http://dx.doi.org/10.1016/j.ecoleng.2017.09.011.

Nabhan, A. I., and Yang, W. 2018. Modern Sedimentary Facies, Depositional Environments, and Major Controlling Processes on an Arid Siliciclastic Coast, Al Qarmah, SE Red Sea, Saudi Arabia. Journal of African Earth Science, v. 140, pp. 9-28. http://doi.org/10.1016/j.jafrearsci.2017.12.014.

Natarajan, K. R. 1995. Kinetic Study of The Enzyme Urease from Dolichos biflorus. J. Chem. Educ. 72, 556-557. http://dx.doi.org/10.1021/ed072p556.

Nuemeier, U. 1999. Experimental Modelling of Beachrock Cementation under Microbial Influence. Sedimentary Geology. Vol. 126, pp. 35-46.

Ozturk, M. Z., Erginal, A. E., Kiyak, N. G., and Ozturk, T. 2016. Cement Fabrics and Optical Luminescence Ages of Beachrock, North Cyprus: Implications for Holocene Sea-level Changes. Quat. Int. 401, 132-140. http://dx.doi.org/10.2016/j.quaint.2015.03.024.

Potter, P. E. 1967. Sand Bodies and Sedimentary Environments: A Review. American Association of Petroleum Geologist, Bulletin, v. 51, pp. 337-365.

Pozo, M., Carretero, M. I., and Galán, E. 2016. Approach to the Trace Element Geochemistry of Non-Marine Sepiolite Deposits: Influence of the Sedimentary Environment (Madrid Basin, Spain). Applied Clay Science, v. 131, pp. 27-43. http://doi.org/10.1016/j.clay.2015.10.024.

Romanenko, L. A., Schumann, P., Zhukova, N. V., Rohde, M., Mikhailov, V. V., and Stakebrant, E. 2003. Oceanisphaera litoralis gen. nov., sp. nov., A Novel Halophilic Bacterium from Marine Bottom Sediments. Int. Jour. of Syst., and Evoluationary Microb., vol. 53, pp. 1885-1888. DOI 10.1099/ijs.0.02774-0.

Russell, R. J., and McIntire, W. G. 1965. Southern Hemisphere Beachrock. Geographical Review, 55, pp. 17-45.

Saitis, G., 2016. The Development of Beachrocks and Their Significance for the Coastal and Human Environment: Study of The Natural Formation and “In Viro” with the use of Bacteria, Area of Study: Corinth, Salamis (Greece) and Okinawa (Japan). Faculty of Geology and Geoenvironment, Natural and Kapodistrian, University of Athens: Greece.

Scholle, P. A., and Ulmer-Scholle, D. 2003. Cement and Cementation. In: Middleton, G. V. (ed.), Encyclopedia of Sediments and Sedimentary Rocks. Kluwer Academic Publishers, Dordrecht, The Netherlands, pp. 110-119.

Schlager, W., 2005. Carbonate sedimentology and sequence stratigraphy (No. 8). SEPM Soc for Sed Geology.

Stoddart, D. R., and Cann, J. R. 1965a. Nature and Origin of Beachrock. Journal of Sedimentary Petrology 35, 243-247.

Stoddart, D. R., and Cann, J. R. 1965b. Nature and Origin of Beachrock. Journal of Sedimentary Petrology 35 (1), 243-247.

Tirkolaei, H. K., Kavazanjian, E., van Passen, L., and DeJong, J. 2018. Bio-grout Materials: A Review. ASCE. http://doi.org/10.1061/9780784480793.001.

Tokashiki, N., and Aydan, O. 2010. The off-Okinawa Island earthquake of February 27th, 2010. Japan Society of Civil Engineering: Japan.

van Passen, L. 2009. Biogrout, Ground Improvement by Microbial Induced Carbonate Precipitation. Doctor Dissertation. Delft University of Technology, Netherlands.

van Passen, L., Daza, C., Staal, M., Sorokin, D., van der Zon, W., and van Loosdrecht, M. 2010b. Potential Soil Reinforcement by Microbial Denitrification. 1st Int. Conf. on Bio-Geo-Civil Engineering, 36(2), 168-175.

van Passen, L., Ghose, R., van der Linden, T., van der Star, W., and van Loosdrecht, M. 2010a. Quantifying Biomediated Ground Improvement by Ureolysis: Large-Scale Biogrout Experiment. J. Geotech. Geoenviron. Eng., 136(12), 1721-1728.

Vousdoukas, M.I., Velegrakis, A.F. and Plomaritis, T.A. 2007. Beachrock occurences, characteristics, formation mechanism and impacts. Earth-Science Review. Vol. 85, pp. 23-46.

Weatherburn, M. W. 1967. Phenol-hypochlorite Reaction for Determination of Ammonia. Anal. Chem. 39, 971-974. http://dx.doi.org/10.1021/ac60252a045.

CHAPTER 5

Beach sand solidification test using MICP method

5.1 Introduction

Present soil improvement applications comprise soil replacement, preloading for consolidation, chemical admixture, and grouting stabilization. These techniques are time-consuming, expensive, and environmentally harmful (DeJong et al. 2010). In addition, coastal erosion is a significant problem throughout the world. Breakwater construction is usedfor preventing coastal erosion. Production of cement, which is a major construction material for breakwater construction, is energy consuming and environmentally un-friendly. During the process of cement production, it releases a large amount of CO_2. In addition, the process is time consuming. Therefore, additional studies into discovery alternative techniques for soil improvement are vital to achieving optimum performance, economic viability, and environmental sustainability.

Biomineralization is a promising and environmentally innocuous technology to improve soil engineering properties. It naturally happens and is induced by nonpathogenic organisms that are native to the soil environment (DeJong et al. 2006). One common biomineralization process is microbially induced calcite precipitation (MICP), which can bond sand grains together and improve the engineering properties of sand. Improvement of soil mechanical properties by MICP is currently of particular interest to engineers, microbiologists, and has been demonstrated by several researchers at varying scales (DeJong et al. 2006; Whiffin et al. 2007; Van Paassen et al. 2010). The technique can alter soil characteristics to increase shear strength and stiffness, while maintaining adequate permeability (Burbank et al. 2011). The technique involves introducing aerobically cultivated bacteria with highly active urease enzyme into soil, harnessing the urease enzyme to catalyze the hydrolysis of urea to produce ammonium and carbonate ions. The produced microbially induced $CaCO_3$ precipitates bridge adjacent soil particles by cementing the soil grains together to form cemented sand illustrative of calcareous rock (DeJong et al. 2006).

The engineering properties of MICP-treated soil may vary because MICP is a complex biochemical process, which can be effected by many factors. The MICP contains two key steps, as above equations. The urea hydrolysis is mainly dependent on the concentration of ureolytic bacteria and the available substrate (e.g., urea), whereas calcite precipitation relates to available Ca^{2+} (Mortensen et al. 2011). In accordance with the growth of nutrient concentration and

incubation time, the $CaCO_3$ content increases. The particle size also has aneffect on MICP bonded soil. The efficiency of MICP is related to the permeability of the soil being sufficient to allow chemicals to flow to the bacteria and also the cement effect of $CaCO_3$ precipitation away particles (Mitchell and Santamarina 2005; Rebata-Landa 2007). Rebata-Landa (2007) showed a relation between grain size and $CaCO_3$ content, and maximum carbonate deposition observed on grains was approximately 100 μm in size. Qabany et al. (2012) also found well-graded and coralr sands had a higher rate of precipitation than finer and poorly graded soils.

5.2 Objective

In this chapter, we conducted a solidification test on local beach sand using the ureolytic bacteria isolated from the soil near beachrock in Krakal-Sadranan, Yogyakarta, Indonesia. The goal of this paper is to perform solidification of the specimen having an estimated unconfined compressive strength (UCS) of more than several MPa for soil improvement and preservation of *coastal* erosion and/or healing of coastal concrete structures, and investigate the influence of varies factors on engineering properties of treated soil catalyzed by Indonesian indigenous ureolytic bacteria.

A series of laboratory experiments conducted for identifying parameters which were affected for solidification of the sample. Syringe solidification method was used for the solidifying sample. Needle penetration test was conducted to obtain estimated UCS value and measured pH and Ca^{2+} concentration of the outlet solution.

5.3 Materials and methods

5.3.1 Sands

Physical properties of local beach sands which was used in the experiments are shown in Figure 5.1. The local beach sand used in the experiments was uniformly graded with a mean particle size of 0.9 mm for coral sand and 0.6 mm for fine sand. The sand was sterilized, and hand packed into a 50-mL syringe (mean diameter, D_{50} = 3 cm and height, h = 10 cm).

5.3.2 Bacteria

To identify the microbial activity, a 5.0 g sample of beachrock was mixed with 10 mL of autoclaved artificial seawater (Aquamarine, Yashima Drug Company, Osaka, Japan; see Table 3.1), then diluted 10^1–10^4 times with artificial seawater. Next, 10 μL of each dilution was added to ZoBell2216E agar medium (for marine bacteria, pH 7.7) and NH_4-YE agar medium for inland bacteria (20 g/L yeast extract; 10 g/L di-ammonium sulfate $(NH_4)_2SO_4$; 0.13 M Tris

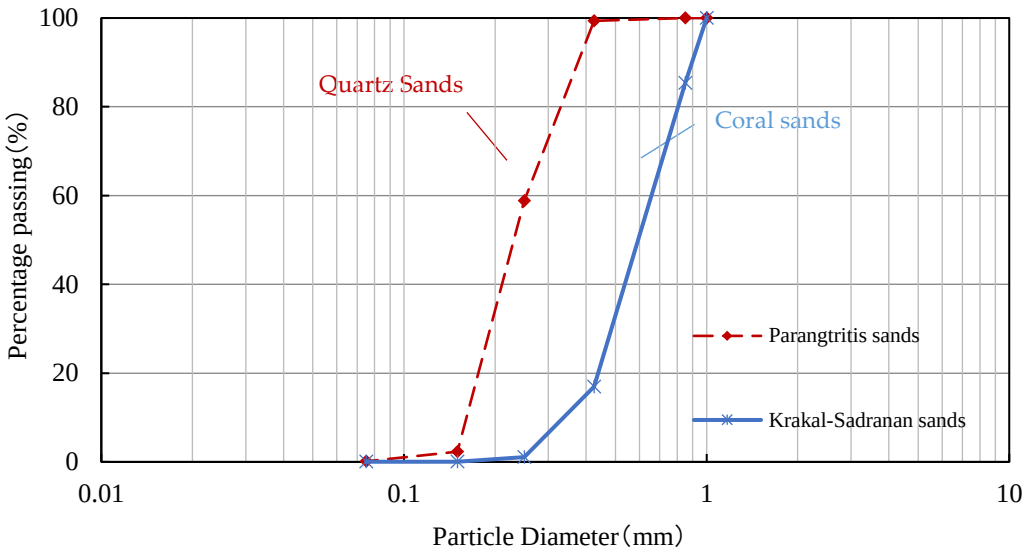


Figure 5.1. Particle size distribution of local beach sand from Yogyakarta south coast, Indonesia.

buffer for pH 8.0), and 20 g/L agar amended to isolate micro bacteria resistant strains as target study of this research. To avoid contamination, every step of the investigation was conducted inside a clean bench. After incubation at 35 °C for 3 d, about ~53 colonies from each location were isolated from the plates. A urease activity test was then conducted on the colonies to identify ureolytic bacteria. Each selected colony (diameter: 2–3 mm) was mixed with 20 mL of solution (20 mL/L cresol red solution, 0.4 g/L cresol red with distilled water, and 25 g/L $CO(NH_2)_2$ with distilled water) in a 20 mL bottle. The samples were then sealed, mixed by shaking, and then incubated at 45 °C for 2 h. To determine whether or not the colonies have urease activity, we observed the color of the solution after 2 h. There was a change in the cresol red, from yellow to purple as pH increased from 7.2 to 8.8. Cresol red solution, the composition of the urease activity measurement solution is shown in Table 5.1 and Table 5.2.

Table 5.1. The composition of the cresol red solution (per 100 mL, solvent: distilled water).

Cresol red (powder)	0.1 g
Ethanol (concentration 95%)	20 mL

Table 5.2. The composition of the urease activity measurement solution (per 100 mL, solvent: distilled water).

Urea	2.5 g
Cresol red solution	2 mL

1) A cresol red was added to the beaker containing 95% ethanol and dissolved by stirring.
2) It was transferred to the volumetric flask and filled up to a predetermined amount of distilled water to prepare a cresol red solution.
3) Distilled water to a beaker and stirred by adding urea, cresol red solution in this order.
4) Transferred to a volumetric flask and filled up to a predetermined amount of distilled water to produce a urease activity measurement solution.
5) Cresol red, discolored area is a pH indicator of 7.2 to 8.8, color and pH are raised to neutral to alkaline is discolored from yellow to purple.

5.3.2.1 Method for urease activity test

1) The state of the discoloration of the urease activity measurement solution is shown in Figure 5.2.
2) By the number of sample number +1 (control) providing a styrene screw bottle for 20 mL, it was dispensed the urease activity measurement solution by about 20 mL to each minute.
3) After isolation of the bacteria, taken out microorganisms were cultured for 24 hours from the incubator, it was added to each urease activity measured solution in a clean bench.
4) After stirring vertically about sealed to 20 times, allowed to stand in an incubator set at 45 °C, as compared to control the color change of after 2 hours, was measured the pH.

Since the urease activity measurement solution contains urea, when examined samples were ureolytic bacteria, progress in the hydrolysis of the urea in solution, pH of the solution is



Figure 5.2. Appearance of discoloration of the urease activity measurement solution (yellow is neutral, purple is alkaline).

increased. Along with this, because cresol red may change color to purple from yellow, differences in the color of the control, and the difference between the measured values of pH, it is possible to determine the presence and magnitude of urea resolution. The temperature of the incubator (45 °C) is to facilitate the action of microorganisms.

5.3.2.1 Genetic analysis of microorganisms

For strains discoloration was seen of the indicator in the urease activity test. The genetic analysis of microorganism is shown in Table 5.3 (Danjo, 2016).

Table 5.3. Genetic analysis of microorganisms.

DNA extraction	Achromopeptidase (Wako Pure Chemical Industries, Ltd., Osaka, Japan)
PCR amplification	PrimeSTAR HS DNA Polymerase (Takara Bio, Shiga)
Cycle sequencing	BigDye Terminator v3.1 Cycle Sequencing Kit (Applied Biosystems, CA, USA)
Use primer	PCR amplification: 9F, 1510R Sequence: 9F, 785F, 802R, 1510R
Sequence	ABI PRISM 3130 xl Genetic Analyzer System (Applied Biosystems, CA, USA)
Sequencing	ChromasPro 1.7 (Technelysium Pty Ltd., Tewantin, AUS)
BLAST homology search, and simple molecular phylogenetic analysis	*Software* Apollon 2.0 (Techno Suruga Lab., Shizuoka) *Database* Apollon DB-BA9.0 (Techno Suruga Lab., Shizuoka) International Nucleotide Sequence Database (GenBank / DDBJ / EMBL)

Gene amplification (16S rRNA) and sequencing was carried out for selected ureolytic isolates. The analysis of the DNA sequences was performed using the DB-BA 12.0 and International Nucleotide Sequence Database created by the Techno Suruga Laboratory, Shizuoka, Japan. The ureolytic bacteria isolated were identified using 16S rRNA sequence analysis. DNA extracts were amplified using two sets of primers targeting the region-specific

16S rRNA sequences for almost all bacterial 16S sequences: the F9 (5′-GAGTTTGATCCTGGCTCAG-3′) and R1451 (5′-AAGGAGGTGATCCAGCC-3′) primers. The PCR amplification cycle consisted of an initial denaturation step lasting 5 min at 94 °C, followed by 25 cycles lasting 1 min at 94 °C, 2 min at 60 °C, 1 min at 72 °C, and a final extension step of 30 min at 72 °C. The amplicons were separated through gel electrophoresis, and the resulting DNA bands were extracted and purified using the FastGene™ PCR extraction kit according to manufacturer instructions (Nippon Genetics Co., Ltd., Tokyo, Japan). The extracted DNA was sent to the Eurofins Genomics Laboratory (Eurofins Genomics, Tokyo, Japan) for sequencing. Subsequent phylogenetic analysis was conducted by TechnoSuruga Laboratory (TechnoSuruga Laboratory Company Ltd., Tokyo, Japan). The latter used the BLAST algorithm to find related sequences in the GeneBank Database, DNA Data Bank of Japan, and the European Molecular Biology Laboratory. PCR sequencing was conducted to identify the species of ureolytic bacteria isolated from the sites at Krakal-Sadranan.

The microorganism used was *Oceanobacillus profundus*, *Vibrio maritimus*, and *Pseudoalteromonas tetradonis*. The strains in the 16S DNA gene sequences are shown in Figure 3.5 (see Chapter 3). The *O. profundus* is a gram-positive species that are motile, aerobic, rod-shaped (0.2–0.4 μm) and classified as biosafety level 1 bacteria. The others, *V. maritimus* and *P. tetradonis* are gram-negative. The former are motile bacilli 1 μm wide and 1.5–4.0 μm, whereas the latter are strictly aerobic, motile with one polar flagellum, form either straight rods (or rod-shapes), 0.5–0.8 × 1.0–1.5 μm when in exponential growth phase. Even though *V. maritimus* and *P. tetradonis* are classified as biosafety level 1, but further analysis of Vibrio maritimus caused it to be eliminated because of similarity to *Vibrio cholerae* (i.e., *V. cholerae*). The bacteria were cultivated in ZoBell2216E media, which also contained 5.0/L hipolypeptone (Nihon Seiyaku Co., Ltd., Tokyo, Japan), 1.0 g/L $FePO_4$ (Junsei Chemical Co., Ltd., Tokyo, Japan), and 1.0 g/L yeast extract (BD Bioscience Adv., Bioprocessing, Miami, Florida, USA). These were prepared with artificial seawater with pH 7.6–7.8, adjusted using 1 M NaOH. After incubating aerobically at 30°C in a shaker at 160 rpm (revolutions/ min) for 72 hours, the bacteria and growth media were centrifuged at 5000 rpm for 10 min.

5.3.3 Ureolytic bacteria characteristics of Indonesian species in various culture condition

Standard media (ZoBell2216E for marine bacteria and NH_4-YE medium for land bacteria) were used for culturing under sterile aerobic conditions. Cells were precultured separately in 5 mL of each medium at 37 °C and 160 rpm for 24 h. One milliliter of the preculture was inoculated with 100 mL of the fresh medium and incubated under the same conditions. The

microbial cell growth of the isolates was determined based on optical density at a wavelength of 600 nm (OD_{600}) using a UV-vis spectrophotometer (V-730, JASCO Corporation, Tokyo, Japan). Representative specimens were sampled at regular intervals of 24 h. Microbially induced calcium carbonate precipitation tests were conducted in 10 mL tubes to evaluate the feasibility of using isolated bacterial strains. Calcium chloride ($CaCl_2$) reagent was chosen as the calcium source, and 1 mL from equimolar concentrations (0.5 mol/L (M)) of $CaCl_2$ and urea solutions were used. One milliliter of the bacteria culture was added to the tube, and the total volume was adjusted to 10 mL using distilled water. Samples were then placed in a shaking incubator at 37 °C and shaken at 160 rpm for 48 h. Finally, the reaction mixtures were centrifuged, precipitates were collected, and the amount of precipitate formed by each isolate were gravimetrically compared. Based on the results, a single isolate was selected as the most suitable for further analysis. In addition, the detail 16S rDNA (about 1500 bp) from the results of homology using Apollon DB-BA9.0 database showed the highest homology of homology 95.6%.

5.3.4 Cementation media

Cementation media was used to provide chemical compositions for ureolysis, including urea, $CaCl_2 \cdot 2H_2O$, NH_4Cl, $NaHCO_3$, and nutrient broth (Mortensen et al. 2011). Table 5.4 shows the chemical compositions of cementation media for bacteria experiments.

Table 5.4. Standard chemical compositions for cementation media.

Chemical	Chemical Concentration (g/L) – 0.5M Ca
Nutrient Broth (g)	3
NH_4Cl (g)	10
$NaHCO_3$ (g)	2.12
$(NH_4)_2CO$ (g)	30.03
$CaCl_2$ (g)	55.49

For the implementation of MICP for the desired application in nearshore environments, attention has to be paid to the fact that target treatment environments will consist of a considerable amount of magnesium and sodium ions. Therefore, a set of experiments were conducted incorporating both Ca^{2+}, Mg^{2+} and Na^{+} ions with various molar ratios from 0 to 1

(Table 5.5). The procedure to conduct precipitation test is same as above.

A solution of 5% carrageenan was obtained by dissolving the carrageenan powder in distilled water solution. *P.tetradonis* cells were added to a substrate solution containing urea (0.3 mol/L) and $CaCl_2$ (0.3 mol/L), in the presence or absence of carrageenan. The reaction mixture (10 mL) was shaken at 30°C and 160 rpm for 24 h. The samples were centrifuged (24°C, 14200×g,10 min) to separate the $CaCO_3$ precipitate from the supernatant. The precipitates were dried in an oven at 90°C for 24 h, and then the dry weights of the precipitates were determined. Experiments were conducted at various bacterial concentrations (OD_{600}= 0.01–0.1) in the presence (0.03%) or absence of carrageenan. The same reaction was conducted at various carrageenan concentrations (0–0.15%) with the bacterial concentration of OD_{600}= 0.1. All experiments were done in triplicate and mean value was plotted. Standard deviation was used to represent the error bars.

Table 5.5. Experimental conditions for precipitation carbonate

Test Case	Mg^{2+} (M)	Ca^{2+} (M)	Na^{+} (M)	Sum of ions	Urea (M)	Bacteria	Additional Information
1	0	0.5	0	0.5	0.5	O	
2	0.5	0	0	0.5	0.5	O	
3	0.25	0.25	0	0.5	0.5	O	Case 8 and 9 only added carrageenan polysaccharides
4	0	0.25	0.25	0.5	0.5	O	
5	0.25	0	0.25	0.5	0.5	O	
6	0.16	0.16	0.16	0.5	0.5	O	
7	0.25	0.2	0.05	0.5	0.5	O	
8	0.16	0.16	0.16	0.5	0.5	O	λ-Carrageenan
9	0.16	0.16	0.16	0.5	0.5	O	κ -Carrageenan
10	0.16	0.16	0.16	0.5	0.5	X	

5.4 Experimental method

5.4.1 Syringe solidification test

1) First, the pre-culture of bacterium *V. maritimus and P. tetradonis* sp. was shaken in with 100 mL ZoBell2216E medium for 2 days at 30° C, same protocol of bacterium *O. profundus* was shaken in with 100 mL NH_4-YE.
2) Then, 80 g of local beach sands from Yogyakarta province, Indonesia dried at 110ºC for more than 2 days, was placed in a 50 mL syringe.

3) Subsequently, 20 mL of a culture medium solution (ZoBell2216E and NH_4-YE solution) and 20 mL of the cementation media for consolidation (the compositions are shown in Table 5.5) were injected into the syringe and drained off leaving about 2 mL of solution above the top surface of the sand.
4) This solution for consolidation was then injected and drained once a day or once every two days and the curing period was 14 days.
5) Ca^{2+}, Mg^{2+} and Na^{+} ions concentration and pH value of outlet solution were measured.
6) The syringe solidification test is shown in Figure 5.3.

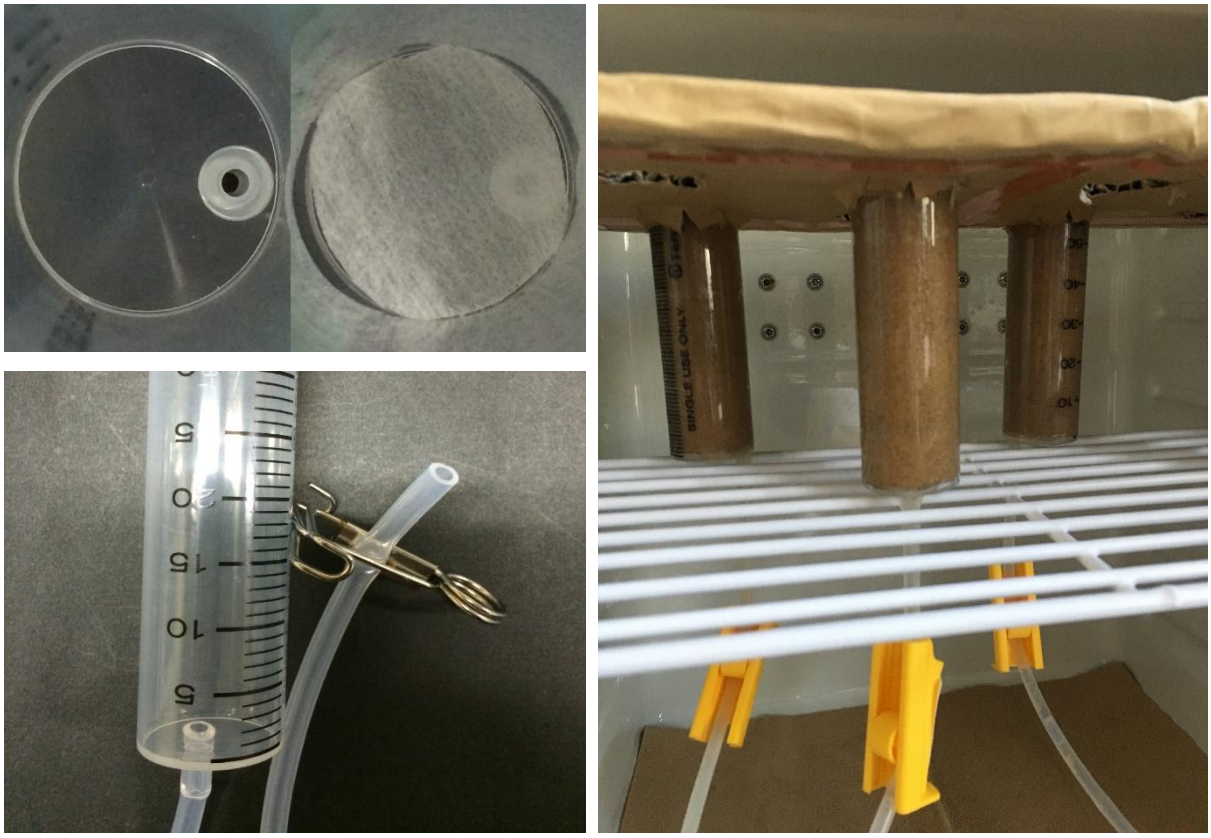


Figure 5.3. Syringe solidification test.

5.4.2 Beach slope model solidification test

1) First, the pre-culture of bacterium *P. tetradonis* was shaken in with 100 mL ZoBell2216E medium for 2 days at 30° C.
2) The bacteria and growth media were centrifuged at 5000 rpm for 10 min.
3) The slope model (13 × 10 × 10 cm) was filled with slope soil by five layers, and each layer was compacted evenly to a similar dry density used in column test. The gradient of the slope was resolved to the standard gradient of expressway cut slope in accordance with the road earthwork guidelines of Japan.

4) Two model of shoreline slope which cut slope 30° for the steep and 15° for the shallow shoreline slope. Then, 400 g of local beach coral sands from Yogyakarta province, Indonesia dried at 110ºC for more than 2 days.
5) Subsequently, 100 mL of a culture medium solution (ZoBell2216E solution) and 100 mL of the cementation media for consolidation (the compositions are shown in Table 5.5) were sprayed into the top surface of the treatment sand.
6) This solution for consolidation was then injected and drained once a day and the curing period was 14 days.
7) Ca^{2+} ions concentration and pH value of outlet solution were measured. Based on the pore volume of the soil below each grid, the injection volumes were estimated, and the rate of injection was 8–10 mL/min.
8) During the treatment, a grid-based injection method was performed. The slope surface was divided into 8 × 5 grids, each grid was 2 cm × 2 cm, and the solutions were injected on the surface of the slope and allowed to percolate under gravitational forces. The experimental arrangement of the shoreline slope solidification test is illustrated in Figure 5.4.

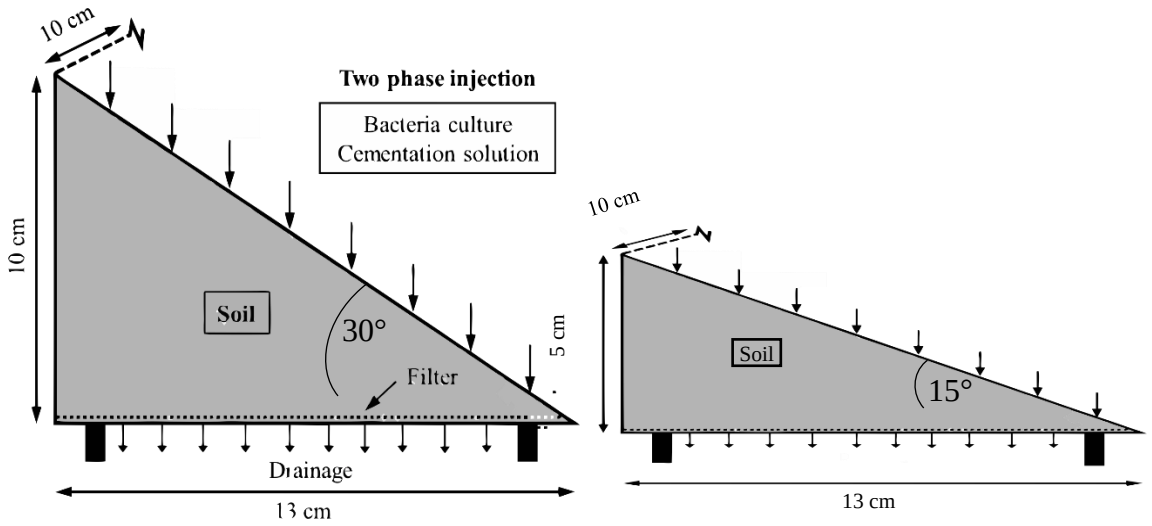


Figure 5.4. Schematic diagram of the experimental arrangement of beach slope model.

5.4.3 Needle penetration test

After 14 days of curing, the needle penetration inclination (N_p) values of each sample were measured using needle penetration device (SH-70, Maruto Testing Machine Company, Tokyo, Japan) and the UCS was estimated from N_p value. The N_P device consists of eight parts as

shown and described in Figure 5.5. Before testing, the surface, on which the test would be carried out, should be clean and smooth. The test doesn't require a specially prepared specimen. The N_P can be used in any direction both in the field and laboratory. Then by holding rather tightly the removable cap and the main body, the load is perpendicularly and slowly applied to the rock surface. If the test is carried out in the laboratory, the specimen should be fixed to prevent its movement during penetration. For weak and saturated rocks, the needle may be penetrated to a maximum depth of 10 mm. When this depth is reached, no more penetration could be applied, and the needle is slowly pulled out. Where the rock is hard and the penetration force has come up to 100 N before the needle penetrates for 10 mm, the needle is withdrawn. After the test is completed, the needle is slowly pulled out and the penetration load and penetration depth are read from the load scale (Fig.5.5, part 4) and the position of the presser on the penetration scale (Fig.5.5, part 3), respectively. The strength of the sample (*NPR value*) was calculated from the following equation (Eq. (5.1)).

$$NPR = F/D \qquad \text{Eq. (5.1)}$$

Where, F is the penetration load (N) and D is the depth of penetration (mm). The unit of *NPR* is N/mm. From the chart of *UCS-NPR* correlation, estimated UCS value was observed.

5.4.4 Experimental conditions

The local beach sand used in the experiments was uniformly graded with a mean particle size of 0.9 mm for coral sand and 0.6 mm for fine sand (Figure 5.1). The sand was sterilized, and hand packed into a 50-mL syringe (mean diameter, D_{50} = 3 cm and height, h = 10 cm). The bacterial suspension was injected first and allowed to stand in the column for 2 h; thereafter, solidification solution was injected. This was repeated every 24 h for a period of 14 d. In addition, two sets of biocementation experiments were conducted using conditions designed to mimic the possible conditions for in situ injection of treatment solutions. The first set of experiments involved using coral local sand of which the main content was skeletal shell carbonate. The other set of experiments involved the use of silica fine sand (fluvio-volcanic sand) of the Young Merapi deposit. In both injection conditions, 20 mL of cementation solution was left above the surface of the sand to mimic saturated conditions, and this procedure was called the immersed method. Control tests were also conducted following the same procedures but without the addition of bacterial cells. First, 100 mL ZoBell2216E medium solution (polypeptone 5.0 g/L, yeast extract 1.0 g/L, and $FePO_4$ 0.1 g/L with artificial seawater) was

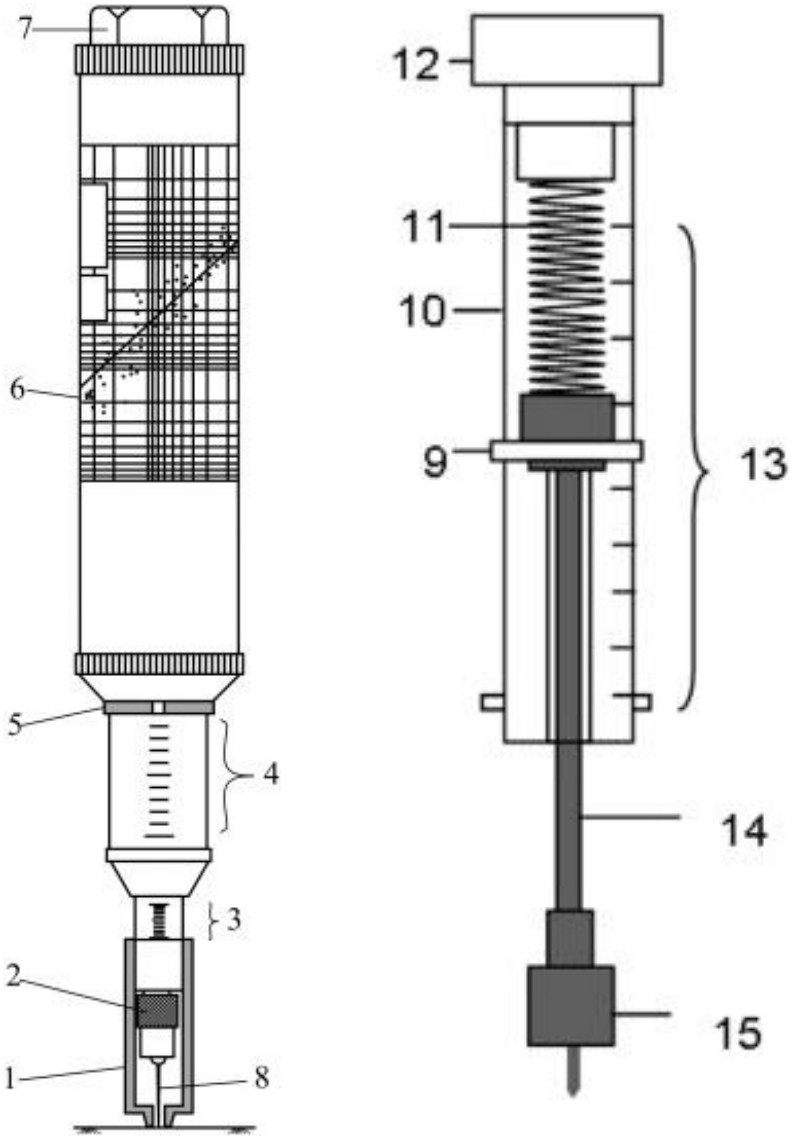


Figure 5.5 General view of the Maruto (left, from Erguler and Ulusay (2008)) and modified Eijkel kamp (right) penetrometers and their parts. (1) presser, (2) chuck, (3) penetration,(4)load scale,(5)load indication ring,(6)UCS–NPR correlation chart given by the manufacturer, (7) removable cap, (8) penetration needle produced according to the Japan Civil Engineering Society's guideline, (9) indicator ring, (10) penetrometer tube, (11) spring, (12) end cap, (13) scale, (14) extension rod, and (15) needle block.

inoculated with 0.1 g of the ureolytic bacterium isolated by the above test, then incubated at 37 °C with gentle shaking at 160 rpm for 3 d. Next, 80 g of coral sand and silica sand collected from the Yogyakarta south coast was dried at 110 °C for 2 d and then placed in a 50 mL syringe (diameter 3 cm). Subsequently, 16 mL (more than the estimated 14 mL initial pore volume in the sample) of bacterial culture and 20 mL of the cementation solution (Table 5.4) were sequentially added to the syringe and drained, leaving about 2 mL of solution above the surface of the sand (saturated condition). This solidification test was conducted for 14 cementation injections in 14 days. Toward considering the effect of conditions on the UCS of a specimen

who depend on the bacterial species, the particle size of the sand, cementation ions solutions and effect of the algae such as biopolymer product were investigating (as shown in Tables 5.5 and 5.6). The testing cases were summarized according to the investigation purpose.

Table 5.6. Purpose of conduction testing cases.

Case No.	Purpose – How to effect for the solidification
1, 2, 3, 4, 5, 6,	Effect of cementation ions solutions on coral sand
7, 8, 9	Effect of biopolymer algae product, λ- and κ -Carrageenan on coral sand
10, 11, 12	Effect of MICP using *P. tetradonis*, on coral sand for 14 days, 21 days and 28 days
13, 14, 15	Effect of MICP using *V. maritimus*, on coral sand for 14 days, 21 days and 28 days
16, 17, 18	Effect of MICP using *O. profundus*, on coral sand for 14 days, 21 days and 28 days
19, 20, 21	Effect of MICP using *P. tetradonis*, on fine silica sand for 14 days, 21 days and 28 days
22, 23, 24	Effect of MICP using *V. maritimus*, on fine silica sand for 14 days, 21 days and 28 days
25, 26, 27	Effect of MICP using *O. profundus*, on fine silica sand for 14 days, 21 days and 28 days
28, 29	Effect of MICP using *P. tetradonis*, on coral sand unsaturated treatment condition for 14 days and 21 days
30, 31	Effect of MICP using *V. maritimus*, on coral sand unsaturated treatment condition for 14 days and 21 days
32, 33	Effect of MICP using *O. profundus*, on coral sand unsaturated treatment condition for 14 days and 21 days
34, 35	Effect of MICP using *P. tetradonis*, on fine silica sand unsaturated treatment condition for 14 days and 21 days
36, 37	Effect of MICP using *V. maritimus*, on fine silica sand unsaturated treatment condition for 14 days and 21 days
38, 39	Effect of MICP using *O. profundus*, on fine silica sand unsaturated treatment condition for 14 days and 21 days

5.5 Results

5.5.1 Growth characteristics

The time course of cell growth and urease activity by *Oceanobacillus profundus*, *Vibrio*

maritimus, and *Pseudoalteromonas tetradonis* for 15 days are shown in Figure 4.10 (see Chapter 4). Cell concentration increased up to 2 days and then reached stationary phase. The urease activity of the cell culture increased with cell growth. Based on this result, the production of urease would be a growth-associated system. Considering microbial-based sand solidification, which needs relatively long duration for adequate solidification, the long-term stability of the enzyme would be advantageous in the MICP process (Danjo and Kawasaki, 2016; Fujita, et al., 2017).

5.5.2 Optimum pH and temperature condition

In the MICP biocementation technique, urease activity of enzyme activity is the key of role for bioindicator of artificial beachrock process success or not. The difference of temperature environment is shown in Figure 5.6 for those three species. High activity was obtained in the range temperatures of 10-80 °C, within the maximum temperature of urase activity was obtained 80 °C in this study. Most of urease molecule is known to be composed of protein subunits and the subunits of this urease would strongly bind each other to leads the high stability of urease during long-term cultivation (Mobley and Island, 1995; Balasubramanian and Ponnuraj, 2010; Fujita, et al., 2017).

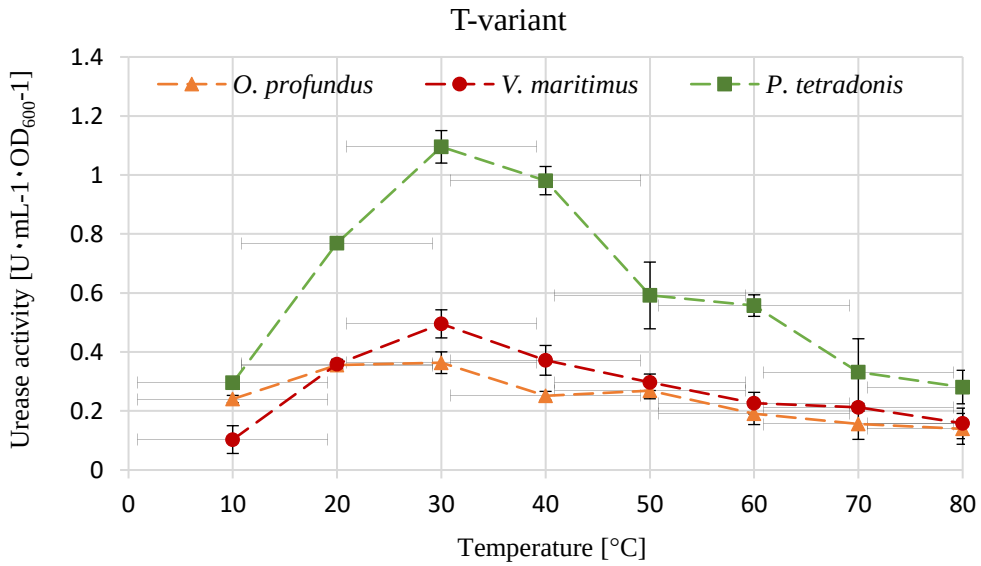


Figure 5.6. Effect of reaction temperature on urease activity of the whole cell at pH 7 (1 mM EDTA-disodium salt solution). Experiment were conducted in triplicate: data represented the average of three experiments with error bars indicating the standard deviation.

High activity was obtained in the range 10–80 ºC, but the maximum urease activity was obtained at 30-40 ºC in this study. Most of urease molecules are known to be composed of

protein subunits and the subunits of this urease bind strongly to each other. This leads to high stability of the urease during long-term cultivation (Fujita, et al., 2017; Danjo and Kawasaki, 2014; Daryono, et al., 2019). Urease activity under different pH is shown in Figure 5.7. The results showed with the maximum activity around pH 2.0 – 13.0. For this temperature and pH variations, the results were different with Fujita, et al. (2017), where he is mentioned the results of maximum temperature exponential increasing toward environment temperature of the buffer solution and the method for urease activity measurement, he used ammonia meter of Tris/HCl buffer solution. Meanwhile, in this research, for measuring urease activity we used EDTA buffer solution for indophenol blue method then detect with colorimeter changing with optical density 630 nm. The results of Fujita, et al. (2017) and this research quite different but the pattern of bacterial growth and urease activity, especially for *Pararodhobacter* sp., is almost same. The results of Fujita et al. (2017) and this research are quite different except for the patterns of bacterial growth and urease activity.

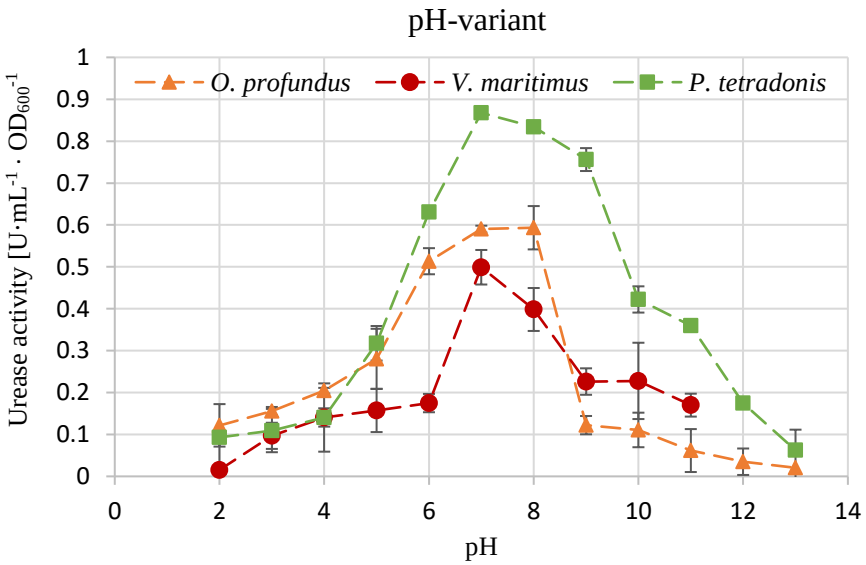


Figure 5.7. Effect of reaction pH on urease activity of the whole cell at 37°C 1 mM EDTA-disodium salt solution). Experiment were conducted in triplicate: data represented the average of three experiments with error bars indicating the standard deviation.

5.5.3 Effect of bacterial species on solidification test

The reactant and the bacterial cell concentration are two primary factors that govern the degree and the homogeneity of the strength increment over the treatment depth. The local strength of the sand specimens underwent different treatment conditions with respect to the aforementioned two parameters, which are illustrated in Figure 5.8. However, the cementation reagent contained equimolar concentrations of urea and $CaCl_2$ as in Ng et al., (2014). When

two samples injected with 0.5 M cementation solution were considered, it was clear that the specimen with bacteria injected twice showed significantly greater strength than that of the specimen injected with bacteria only once (at the beginning). According to previous records, it was deduced that higher concentrations of bacteria populations enhance the amount of $CaCO_3$ precipitate and, thus, the results of MICP treatment (Daryono, et al., 2019; 2020). Generally, bacteria play two key roles in the biocementation process: (i) catalysis of urea hydrolysis and (ii) provision of nucleation sites (Kandianis, et al., 2008). The initial investigations on urease activity of the isolated strain showed that enzymatic activity diminishes over time. Moreover, there are several other factors that could gradually inhibit the bacteria from performing their intended role as a catalyst for urea hydrolysis over the entire treatment time period. All the samples were strongly cemented and the estimated average (as well as individual) UCS values from two independent tests for all the cases were above 3 MPa.

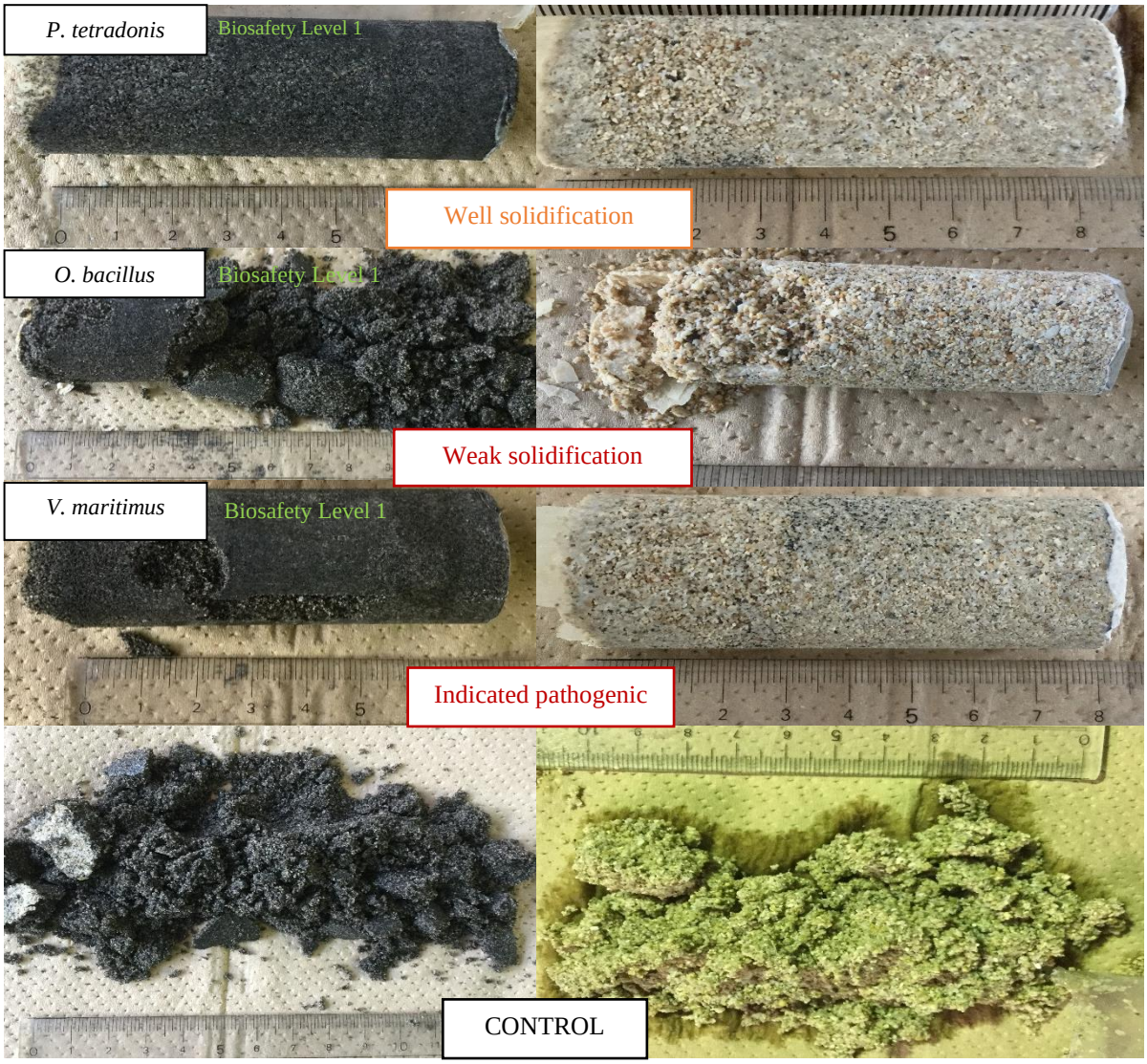


Figure 5.8. Microbial induced carbonate precipitation test using local strain ureolytic bacteria after 14 days treatment. Black sample (left) is silica sand from Parangtritis beach sand and white sample (right) is coral sand from Krakal-Sadranan beach sand.

5.5.4 Effect of bacterial population based on OD_{600} on solidification test

Figure 5.9 (a) shows that the estimated UCS of the sample increased with the increase of bacterial population. This finding indicates that bacteria plays a key role on MICP, i.e., (1) producing an enzyme to hydrolyze urea, and (2) acting as nucleation sites for the formation of calcium carbonate crystals (mainly calcite; Fujita et al. 2000). More bacteria in the solution can promote more enzymes and provides more nucleation sites for the MICP. The pH value in outlet solution was larger in high bacterial concentration sample than low bacterial

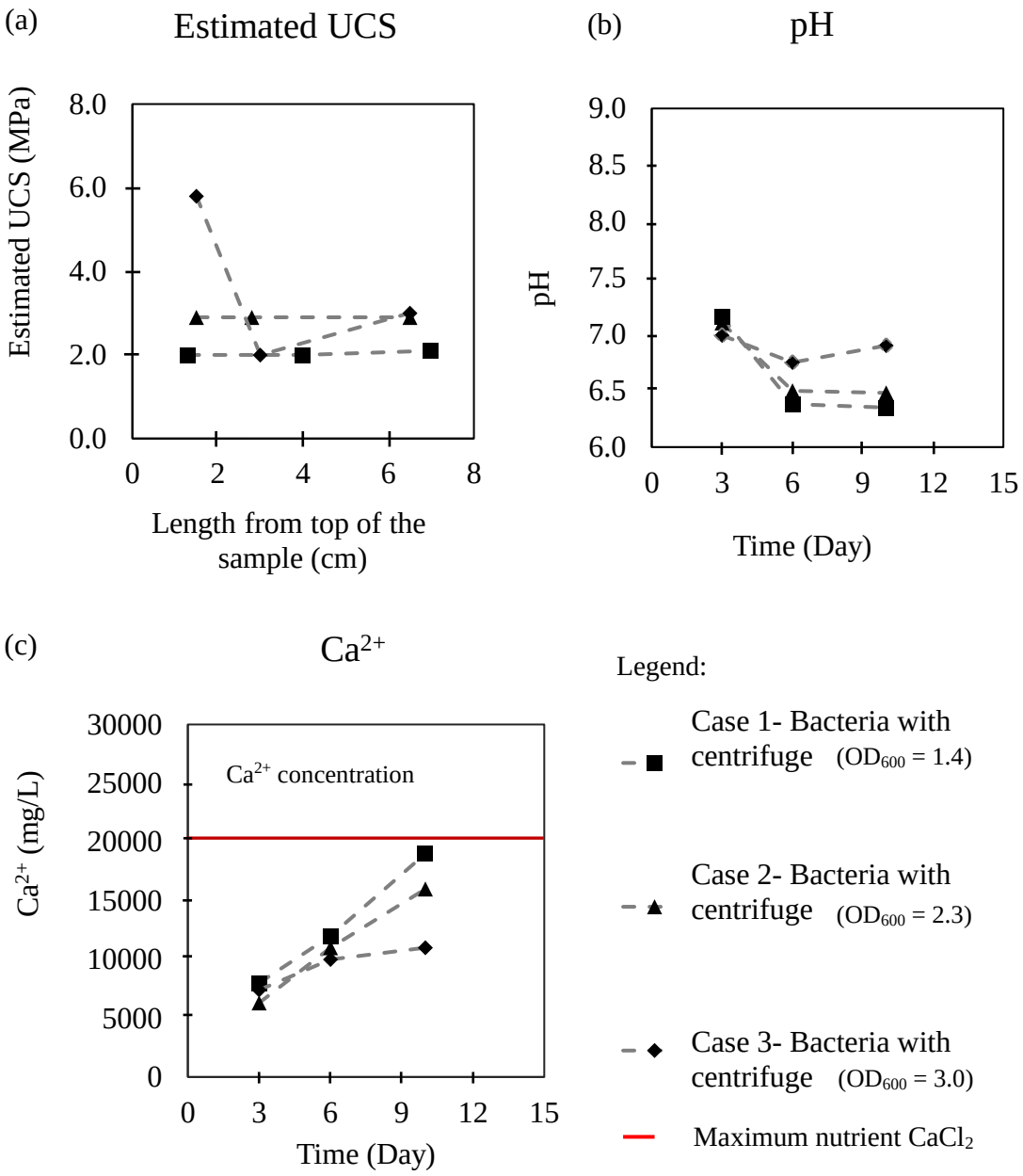


Figure 5.9. Results of MICP-treated sample catalyzed by *P. tetradonis* under different bacteria concentrations: (a) Estimated UCS value with the depth of the sample, (b) pH with time and (c) Ca^{2+} concentration with time.

concentration sample. Although pH value decreased with the time for all testing cases. The results of Ca^{2+} concentration in outlet solution were opposite to the results of pH value (Fig.5.9 (b) and 5.9 (c)).

Three different types of silica sand with three types of particle size were used MICP-treated soil catalyzed by *P. tetradonis* Fig.5.10 (a), 5.10 (b) and 5.10 (c) show that the solidified samples after catalyzed by *P. tetradonis* sp. for coral Krakal-Sadranan sand, fine silica Parangtritis fine sand, and glass beads, respectively.

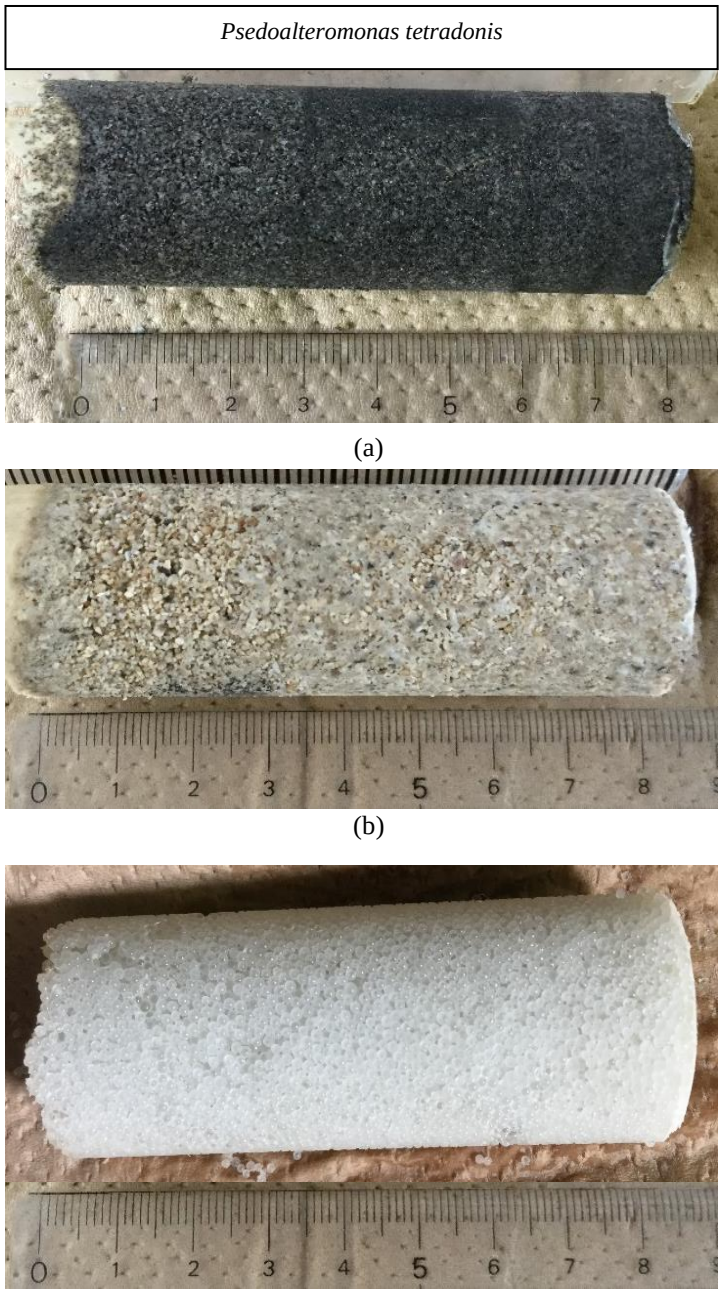


Figure 5.10. (a) Solidified sample with fine silica Parangtritis sand, (b) solidified sample with coral Krakal-Sadranan sand, and (c) solidified sample with glass beads

5.5.5 Effect of particle size and different sand samples on solidification test

The local beach sand used in the experiments was uniformly graded with a mean particle size of 0.9 mm for coral *Krakal-Sadranan* sand, 0.6 mm for silica *Parangtritis* fine sand, and microsphere glass beads varying from 0.25 mm to 0.6 mm in diameter. The sand was sterilized, and hand packed into a 50-mL syringe (mean diameter, D_{50} = 3 cm and height, h = 10 cm).

Figure 5.11 shows the estimated UCS value at the top, middle and bottom of the sample. From the results, estimated UCS value was larger in coral Krakal-Sadranan sand with 0.9 mm mean diameter than silica Parangtritis fine sand sample which has mean diameter 0.6 mm and estimated UCS value in glass beads sample with mean diameter 0.25 mm. The particle size of fine sand is small than other two samples. Due to the very small particle size, the penetration rate of cementation media can be low when compare with glass bead and coral Krakal-Sadranan sand samples. This reason may cause for decreasing the bacterial process. Then the hydrolysis process also getting slow. As a result of this, $CaCO_3$ precipitation decreasing and UCS value getting lower in fine sand sample than coral sand or glass bead sample. Therefore, the particle size of the sample was mainly affected for solidification of the sample.

5.5.6 Effect of cementation ion solutions on strength

The inherent properties of MICP bio-cement treatment of aragonite and calcite, such as specific gravity and Mohr hardness than those crystals. At the extreme, excessively high concentrations of magnesium and sodium where the molar ratio was 1.0, the magnesium resulted in a significant reduction in the unconfined compressive strength (UCS) using a soft rock penetrometer (SH-70, Maruto Testing Machine Company, Tokyo, Japan). In other hand, the sodium ions affect to accelerate the crystals amount production because of increased the salinity environment during MICP treatment test. It is clearly deducted that the strength declines in mainly due changed of the crystal morphology to a needle shaped crystal form with lower bonding capacity than that of the well-interweaved and cross-linked rhombohedral crystals produced in the absence of magnesium ion (Nawarathna, et al., 2018). However, the effect will be negligible in the target environment where naturally available Mg^{2+} is considerably lower compared to the concentration of Ca^{2+} supplied with the cement solution (Figure 5.12).

In the evaporitic environments, the dissolved cations are simultaneously concentrated through progressive of the evaporation seawater. Therefore, salinity is generally positively correlated with the saturation index of the carbonate minerals. However, in our experiments, the Na^+ and Cl^- concentrations increased independently of the concentrations of Ca^{2+} and Mg^{2+},

allowing the separate evaluation of the effect of salinity and the Mg^{2+} and Ca^{2+} ratio (Al Disi, et al.,2019). The effect of salinity and ionic strength on the incorporation of magnesium and sodium ions into the carbonate minerals are not fully resolved and existing studies show contrasting results. The observation that different minerals (i.e. calcium carbonate, high magnesium calcite, hydro magnesite) were formed simultaneously in the same pure culture is consistent with mineralization under the influence of heterogenic present in the bacterial cell walls. The relationship between the ionic strength and the Mg content in Mg-rich calcite obtained abiotically. Organic molecules with different cation-adsorption properties would indeed explain the occurrence of minerals with different morphologies and chemical compositions.

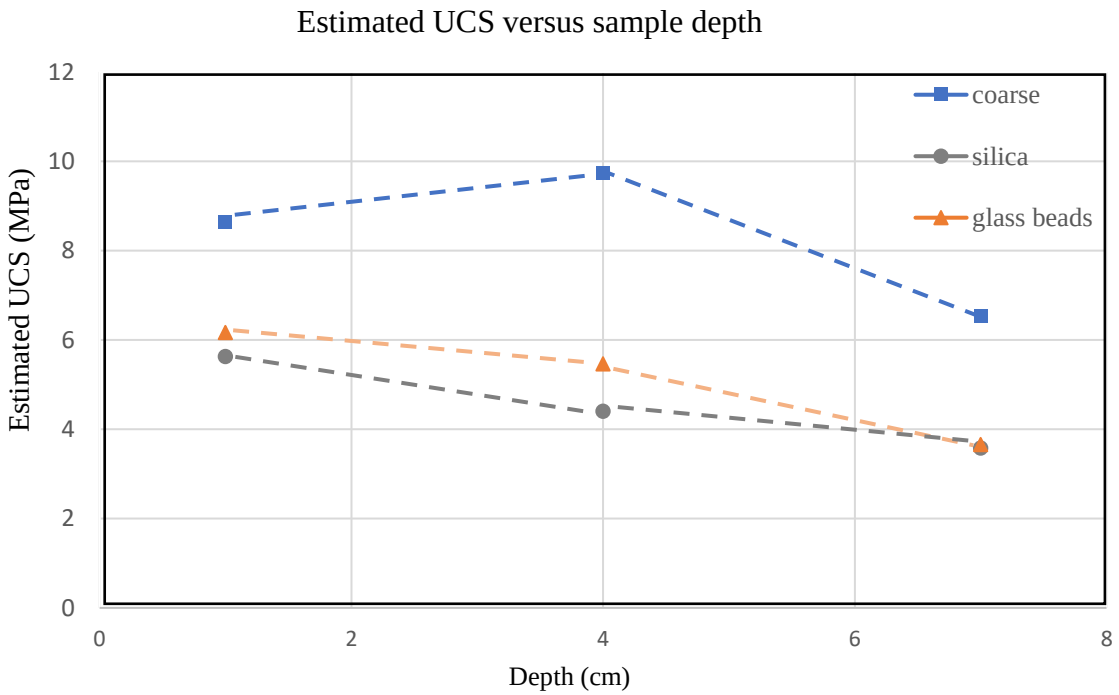


Figure 5.11. Estimated UCS value of MICP-treated sample catalyzed by *P.tetradonis* sp. under different particle size of sand samples.

Figure 5.13 shows the estimated UCS value at the top, middle and bottom of the sample. From the results, estimated UCS value was larger in coral Krakal-Sadranan sand with 0.9 mm mean diameter than silica Parangtritis fine sand sample which has mean diameter 0.6 mm. The particle size of fine sand is small than other two samples. Due to the very small particle size, the penetration rate of cementation media can be low when compare with coral Krakal-Sadranan sand samples. This reason may cause for decreasing the bacterial process. Then the hydrolysis process also getting slow. As a result of this, $CaCO_3$ precipitation decreasing and UCS value getting lower in fine sand sample than coral sand or glass bead sample. Therefore,

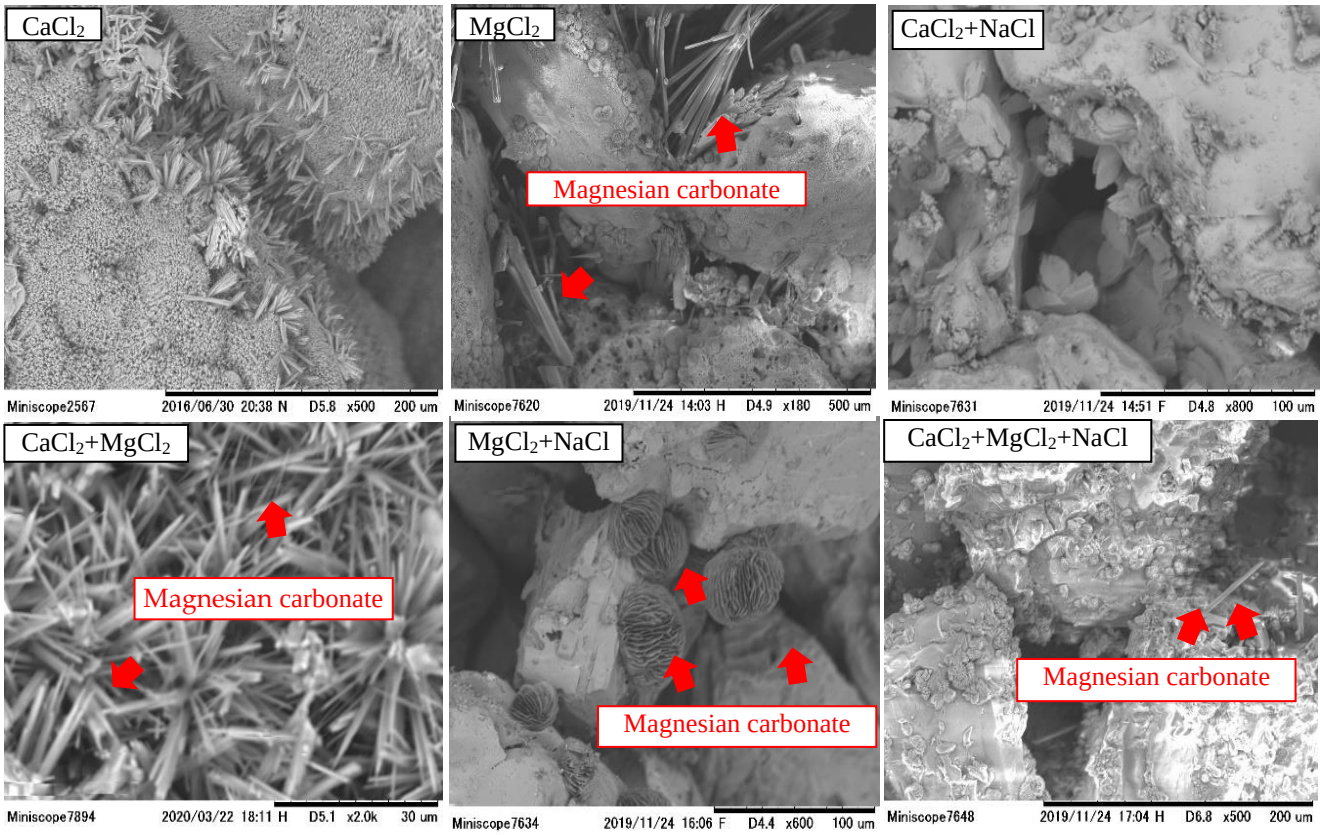


Figure 5.12. Ions dependencies of MICP precipitation test

the particle size of the sample was mainly affected for solidification of the sample. Based on the investigation results, it shown the higher strength of MICP process is dominant with calcium chloride then small amount of magnesium chloride and natrium chloride. The precipitation behavior of the microbial activity somehow is not representing of the cementation during treatment sands in the solidification test (Figure 5.14). The higher precipitation test of carbonate precipitation was express in the term of magnesium chloride mixed with natrium chloride rather than single ion solution, but the results of the solidification test is the opposite. Strength of the material treatment is not strong enough to cement the beach sands after 14 days. This phenomenon occurs because of magnesium chloride precipitation surrounding the apparatus test, in this case cylinder tube 10mL. Nucleation of urase hydrolysis between calcium ion and magnesium ion is different morphology of crystallization and behavior of crystal occurrences, which is shown in Figure 5.12 the calcium bonding crystal bridges between intra particle sands called *meniscus bridges* is solid and strong then magnesium carbonate that only precipitated surrounding the particles.

Based on that Figure 5.19, mineral composition was found have a generally formed vaterite, aragonite, calcite mineral, and other carbonate minerals complexes. Then using those

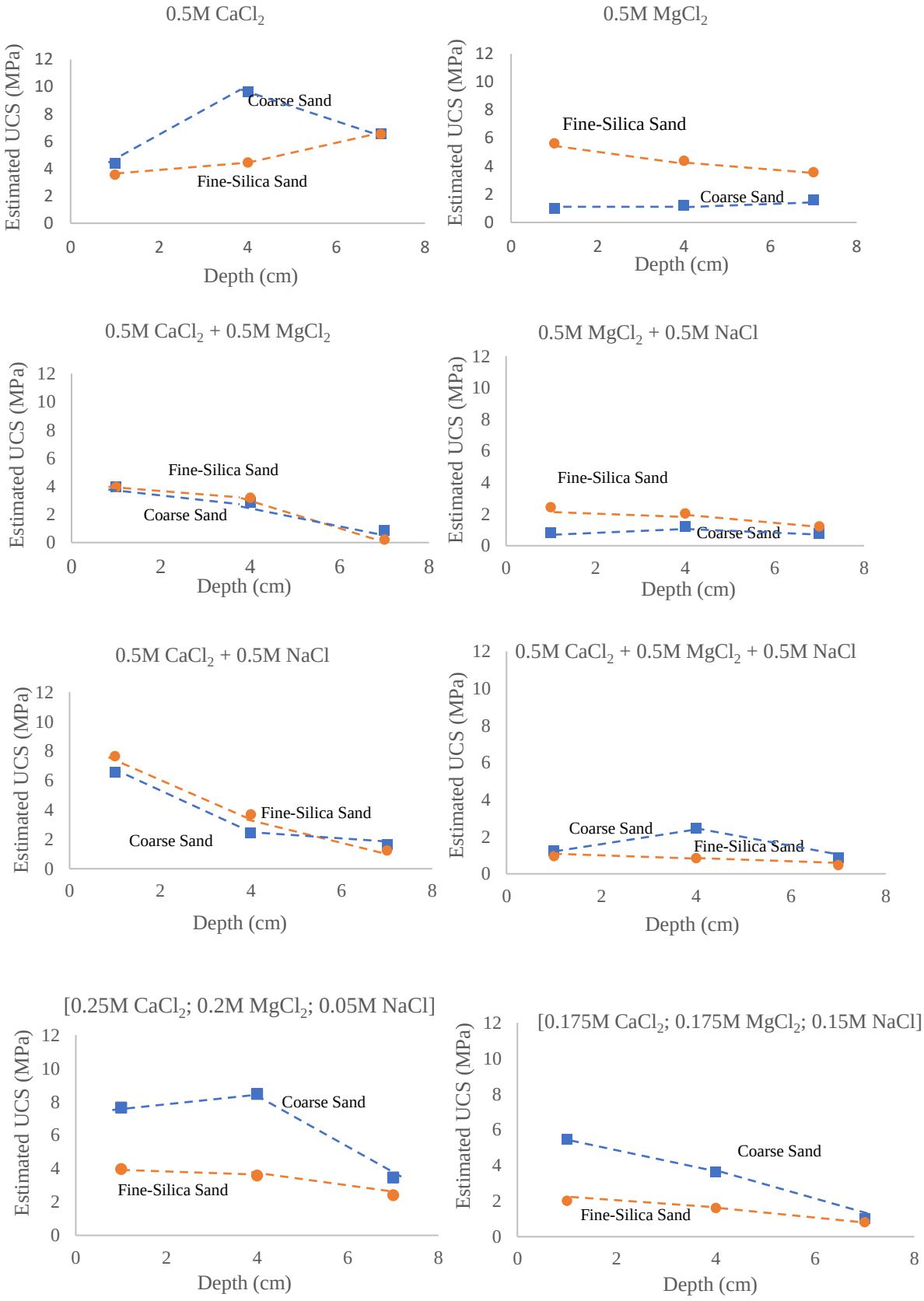


Figure 5.13. Estimated UCS value of MICP-treated sample catalyzed by *P.tetradonis* under different concentration of cement solution sand samples.

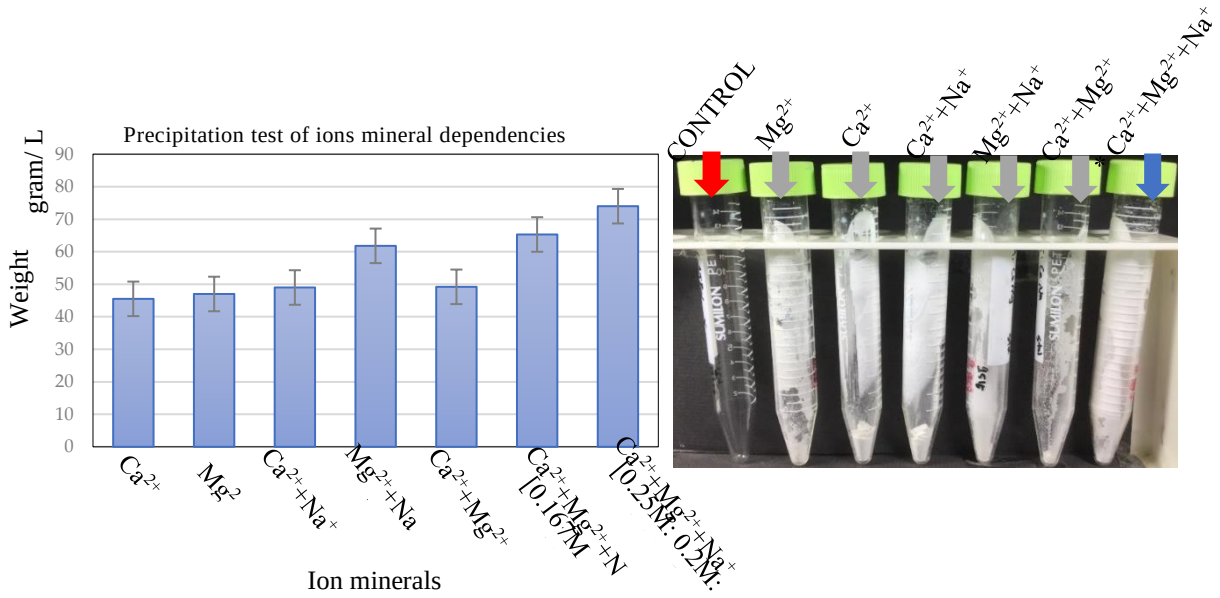


Figure 5.14. Precipitation test by *P. tetradonis* under different concentration of cement solution sand samples.

of these minerals, we tried to make a pattern from carbonate mineral which detected inside the treatment sand samples. The pattern will be presented differentiation graphic based on mineral parameters for eliminated diffraction wave in XRD analysis. The results shown of the treatment sands behavior based on ions solutions dependencies have an effect of mineralogy and crystallization intra-particles. The standard solution shown in table 5.4 will produce only vaterite, aragonite and calcite which depend on the temperature and pressure during treatment sands. Meanwhile, table 5.5 is representative of innovative carbonate solidification depends on the source of mineral ions and other factor such as micro algae to mimic the natural processes.

The metastable vaterite of calcium carbonate were usually occur in the low density and polymorphic forms. The crystal chemistry plays an important role in understanding the behavior of minerals, in term of reactivity and stability. Crystal growth processes, whether in the solid state or aqueous are influenced by arrangement of atoms in the crystal and constraints by coordination and bonding particles. The common rhombohedral carbonate was produced by MICP consist of calcite and dolomite, respectively. The structure of calcite is anhydrous such a single carbonate including magnesite ($MgCO_3$), siderite ($FeCO_3$) or rhodochrosite ($MnCO_3$). The differences of minerals were found in the XRD results because of the atomic structure of the CO_3 group as fairly rigid structural unit. Such a viewpoint is reinforced by consideration of the carbon-oxygen bond, which is generally regarded as strong covalent in character. The carbon-oxygen bond will be considerably stronger than any other molecule-oxygen bond typically found in carbonates. In calcite, for example, the carbon-oxygen bond strength using

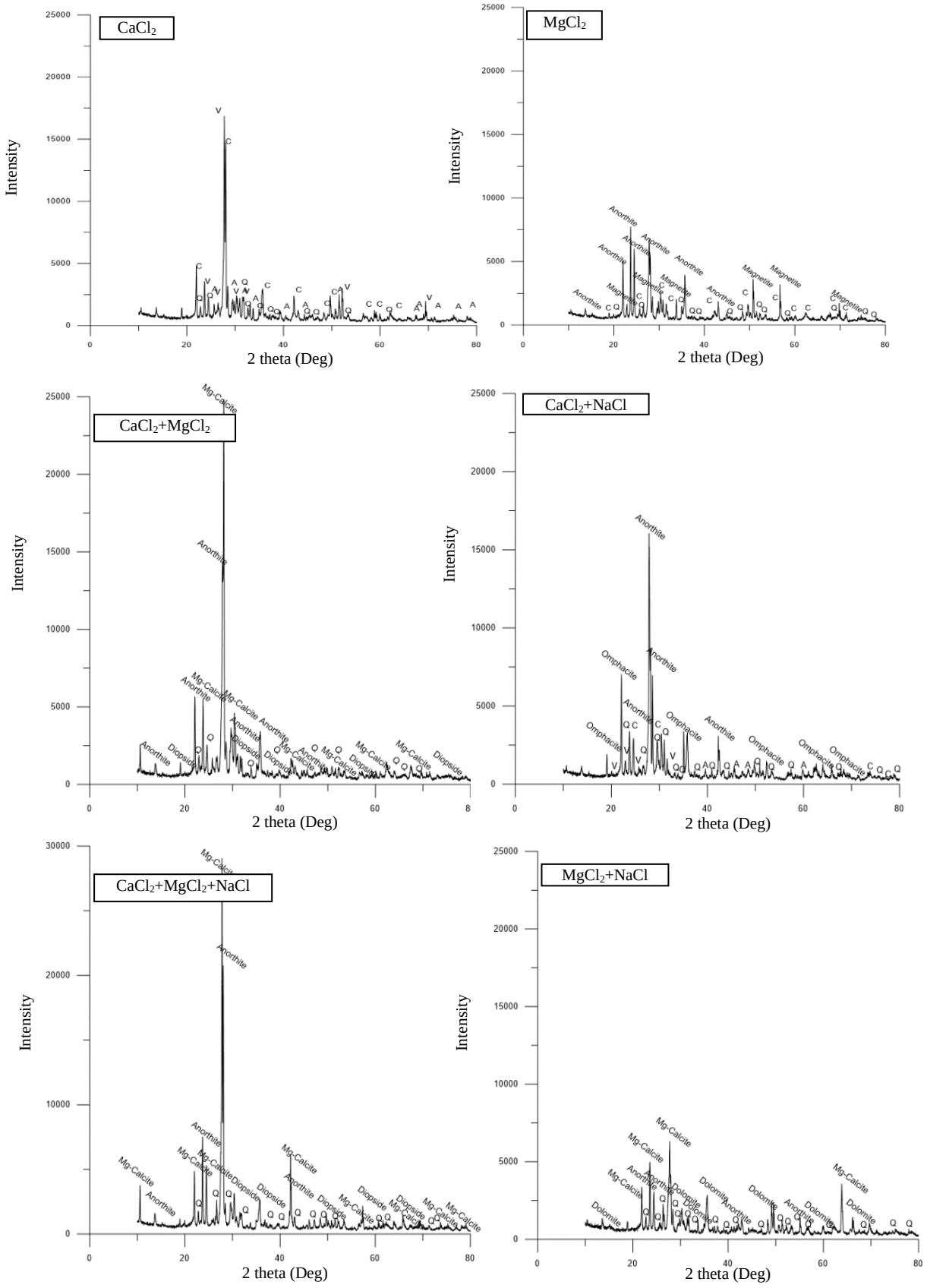


Figure 5.15. Graphic XRD analysis pattern using artificial beachrock. C: calcite; A: aragonite, Q; Quartz (SiO_2), V; Vaterite

empirical Brown-Shannon method which is approximately four times greater than for the calcium-oxygen bond. Same as the results SEM in Figure 5.12 the magnesium ions effect were bridging surrounded of the material it seems natural concept of beachrock the magnesium is sedimented after the deposition of vaterite-aragonite calcium carbonate were proven the meniscus bridge in the natural beachrock (Chapters 2-4) were overlay time to time and recrystallization commonly occur during the sediment process. The natural beachrock were mostly consist of magnesian calcite (high – low) depend on the sedimentary location which key role the natural beachrock can occur in the shore bay. Other minerals also found from XRD results such as Anorthite; Omphacite; Dolomite; and Diopsite that might effect of SiO_2 in the materials.

5.5.7 Effect of carrageenan biopolymer on strength of MICP

The results are consistent with our previous study using ionic polysaccharides as biopolymer carrageenan product. At higher cell concentrations, bacterial activity would be a dominant factor than the effect of the biopolymer (Nawarathna, et al., 2018). The precipitate with carrageenan was mainly composed of two components, precipitated $CaCO_3$ and the precipitated carrageenan hydrogel. Carrageenan is an ionic polysaccharide with *pKa* of approximately 2.8~4.9. Most of the polysaccharide inhibit $CaCO_3$ nucleation and growth, while basic polysaccharide promotes the growth and nucleation of crystals (Xie, et al., 2005). Carrageenan also promotes the $CaCO_3$ nucleation and growth. Interaction between the carrageenan and calcite is difficult to explain. The injection of the carrageenan simultaneously with the bacteria gave negative results in the solidification and it appears that carrageenan is mutualism symbiote for the bacteria to precipitation of $CaCO_3$.

The most important finding of this research is the positive effect of the carrageenan on sand solidification. By introducing carrageenan, well cemented sand specimens could be obtained, and the effect is clearer at higher concentrations. By introducing carrageenan, UCS of the top of the sample increased by ~40%, respectively, compared with the case without carrageenan. To achieve better cementation during the sand solidification, the pore spaces between the sand particles should be filled sufficiently by effective bridge between the sand particles (Polowczyk, et, al., 2016). This point-to-point intraparticle contact is very important to achieve higher strength (Harkes, et al., 2010). As mentioned before, carrageenan formed its hydrogel under the neutral conditions. This hydrogel helped to form better bridge between the sand particles. The higher carrageenan concentrations led to form thicker hydrogels, which

improved the formation of bridge. Hence, a better cementation and higher strength could be achieved.

Biopolymers are organic polymers produced by biological organisms which are categorized into three major classes: polynucleotides, polypeptides, and polysaccharides (Kalia and Averous, 2011). Of the three, polysaccharides are the most common biopolymer type used in various industry fields, including civil and construction engineering practices (Chang, et al., 2016). Generally, polysaccharide-type biopolymers are hydrophilic due to the abundant surface hydroxyl groups (OH^-), which mainly form viscous hydrogels in the presence of water (Dumitri, 2002; Clark and Ross-Murphy, 1987). The viscosity (or shear modulus) of biopolymer hydrogels varies based on the biopolymer-to-water content (Kulicke and Nottelmann, 1989; Imeson, 2010) and presence of counter-ions (alkali- or alkali earth metal ions) (Kirchmajer, et al., 2014; Izawa and Kadokawa, 2010), where the increase of both variables results in higher viscosity values of biopolymer hydrogels. Table 5.7 lists the typical characteristics of biopolymers considered for soil improvement (Hassan, et al., 2005; Daniel, et al., 2005; Wan, et al., 2004; Barrére, et al., 1986; Oliveira, et al., 2010; Imeson, 2012; Bacic, et al., 2009)

The strengthening mechanism of biopolymer is governed by the rheology of biopolymer hydrogels and the chemical (ionic-, hydrogen-) bonding between biopolymers and soil particles, where soil type becomes an important parameter (Chang, et al., 2018). Figure 5.16 shows the scanning electron microscopy (SEM) images of dried biopolymer treated coral soils, where mainly dehydrated biopolymer hydrogels form coats around electrically neutral silica-based particle surfaces (Chang, et al., 2012; 2016). The spherical crystals most probably could be vaterite. Vaterite is the least stable form of $CaCO_3$ with the highest solubility, so it precipitates first and then transforms into stable calcite, following the solution mediated transformation (Kralj, et al., 1997; Nawarathna, et al., 2018). Hence, the morphology change with the increase in the carrageenan concentration can be due to the conversion of themetastable phase of the crystals into a more stable form. Initially, both the vaterite and calcite phases precipitated simultaneously due to high solid content and limited diffusivity (Kosanovic, et al., 2011). Then, the metastable phase started to dissolve and re-precipitated upon the stable calcite crystals as shown in Figure 5.16(b). The dissolution of the vaterite starts when the supersaturation drops below the value of its solubility. It appears that carrageenan concentrations accelerate the conversion of the into a stable phase. Similarly, different polymorphisms and morphologies have been obtained by chemical precipitation of $CaCl_2$ and sodium carbonate (Na_2CO_3) under different experimental conditions. Parakhonskiy et al.

Table 5.7. Characteristics of biopolymers considered for soil improvement

Biopolymer	Chemical composition	Main characteristics	References	Applications
Cellulose	$(C_6H_{10}O_5)_n$	• The bond angles in the beta acetal linkage • Mostly a linear chain and water insoluble • Properties depend on the chain length	(Hassan, et al., 2005; Panarotto, et al., 2005)	Soil strengthening, erosion control and surface stabilization
Starch	$(C_6H_{10}O_5)_n$	• The alpha acetal linkage, starch-amylose actually forms a spiral much like a coiled spring. • Solubility in water depending on temperature • Used as viscosity thickeners and stabilizers	(Daniel, et al., 1994; Kulshreshtha, et al., 2017)	Soils strengthening, erosion control and surface stabilization
Chitosan *(cationic)*	$(C_6H_{11}NO_4)_n$	• Solubility increases with a decrease in pH • Cationic nature mainly binds with negatively charge surface • NH_3^+ amino group, positive charge	(Wan, et al., 2004; Latifi, et al., 2016)	Soils strengthening, erosion control and surface stabilization
Carrageenan λ and κ *(anionic)*	$(C_{24}H_{36}O_{25}S_2^{-2})_n$	• Kappa forms strong, rigid gels in the presence of potassium ions, and reacts with dairy proteins. • Kappa Carrageenan forms very firm and elastic gels. Lambda Carrageenan will not form a gel but can be used as a thickener. • SO_3^- sulfate group, negative charge	This research	Soils strengthening, erosion control and surface stabilization
Xanthan gum	$(C_{35}H_{49}O_{29})_n$	• Highly viscous and pseudoplastic rheology • Commonly used in drilling muds and soil treatment	(Barrare, et al., 1986; Nugent, et al., 2009; Orts, et al., 2007; Plank, et al., 2005; Bouazza, et al., 2009; Khachatoorian, et al., 2003; Smitha, et al., 2008; Chang, et al., 2016)	Soils strengthening, soil consistency control, erosion control and surface stabilization, soil hydraulic conductivity control, seismic resistance improvement
Gellan gum	$(C_{29}H_{43}O_{25})_n$	• Temperature depend viscosity variation (thermogelation) • Irreversible gel formation once cooled below 40°C	(Oliveira, et al., 2010; Im, et al., 2017; Smitha, et al., 2008)	Soils strengthening, erosion control and surface stabilization, soil hydraulic conductivity control, seismic resistance improvement
Agarose	$(C_{24}H_{38}O_{19})_n$	• Reversible gelation with heating and cooling • Most common gelling agent in food	(Imeson, et al., 2012; Zhan, et al., 2012)	Soils strengthening, soil hydraulic conductivity control, seismic resistance improvement
Curdlan	$(C_6H_{10}O_5)_n$	• Gel formation via heating in aqueous solutions • Applied to prevent material separation in concrete mixture	(Ivanov, et al., 2016; Bouazza, et al., 2009)	Soils strengthening, erosion control and surface stabilization

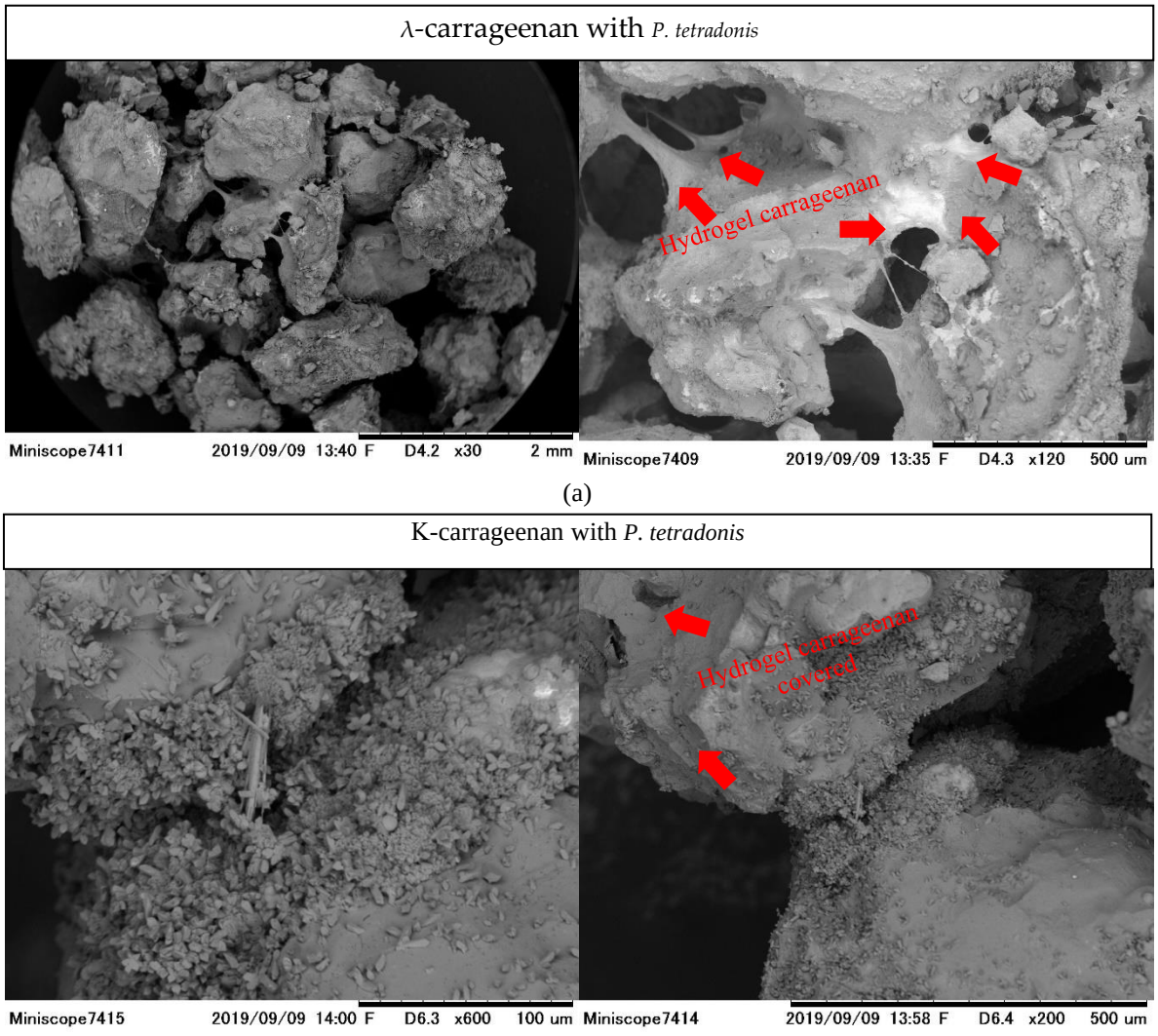


Figure 5.16. SEM image of $CaCO_3$ solidification test on coarse sand by *P. tetradonis* at (a) λ-carrageenan and (b) κ-carrageenan at concentration 0.5% carrageenan.

(2014) successfully obtained the isotropic (spherical and cubic) and anisotropic (elliptical and star-like) crystals by varying the salt concentration and slowdown the process by adding ethylene glycol. For saturated conditions, biopolymer hydrogels in pore spaces are reported to increase the apparent cohesion intercept with increasing biopolymer-to-water content, while the friction angle remains constant, regardless of biopolymer content. Thus, it seems that the biopolymer-to-water content and accompanying hydrogel viscosity become the main strengthening factors for coral soils.

The estimated UCS values for the solidified samples are shown in Figure 5.17. According to the measured UCS values, all of the sand specimens have strength in the range of 1–3 MPa. Hence, all specimens can be classified as strongly cemented according to the classification system proposed by Shafii and Clough (1982). In this classification system, the cemented soils

with UCS value between 1 and 3 MPa are classified as strongly cemented soil and a UCS value N3 are classified as soft rocks. For all the specimens, a higher strength could be achieved by the reinjection of bacteria after 7 days compared to the single injection. In the case of reinjection of bacteria 96% of strength increment was achieved for the top of the sample by adding carrageenan. Without carrageenan strength increment was around 50%. In previous studies found that amount of $CaCO_3$ precipitated is directly related to the measured UCS value. The formation of the larger size distorted-shape crystals with the increase in the carrageenan concentration may be due to the adsorption of the functional groups of the carrageenan onto the crystals surface.

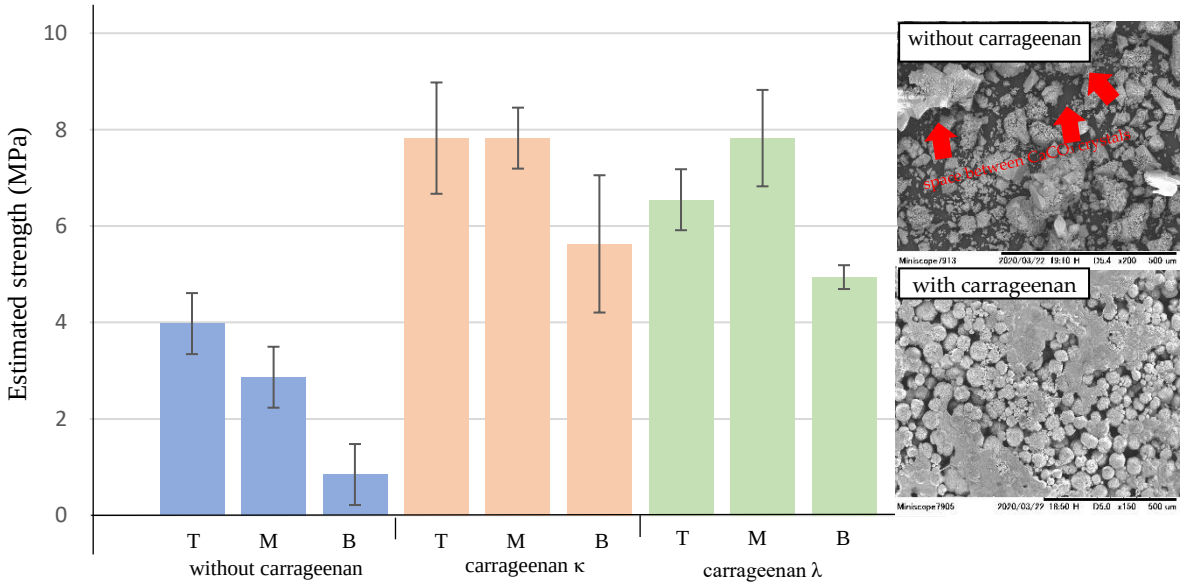


Figure 5.17. Estimated UCS values of solidification sand specimens at concentration 0.5% carrageenan.

5.5.8 Beach slope model solidification test

Beach slope model test is the scale-up version of soil column tests. Because the small columns are limited by confinement and boundary effects, the model test was additionally performed to demonstrate the feasibility of beach sand stabilization. After the 14 days of treatment, the shoreline slope was flushed with about 5 L of tap water to remove all soluble salts, followed by, slope specimen was carefully removed from the mold and submerged into the water bath to eliminate the uncemented aggregates. The cemented profile is presented in Figure 5.18.

The beach slope treatment sand based on MICP methods were successful to conduct especially for 15° of the shore bays. This is because of percolation sand treatment accumulated in the top and bottom level of the slope model. Figure 5.19 shown the 3D model of cementation

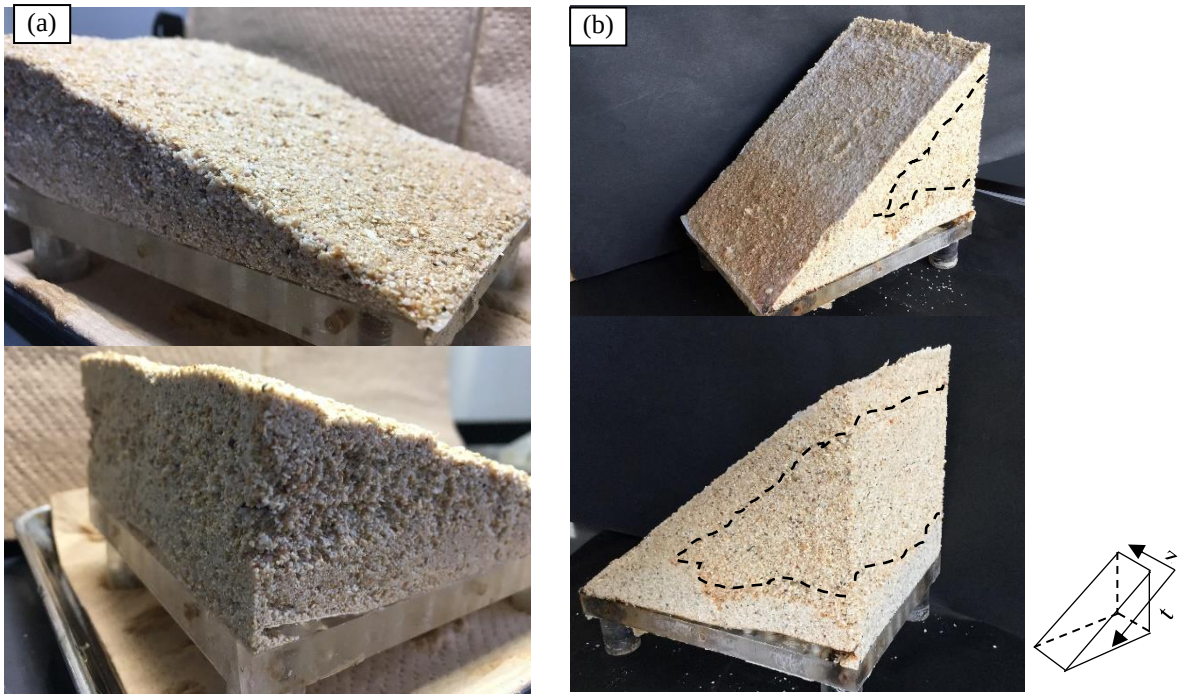


Figure 5.18. Profile of the cemented beach slope model (a) 15° and (b) 30°

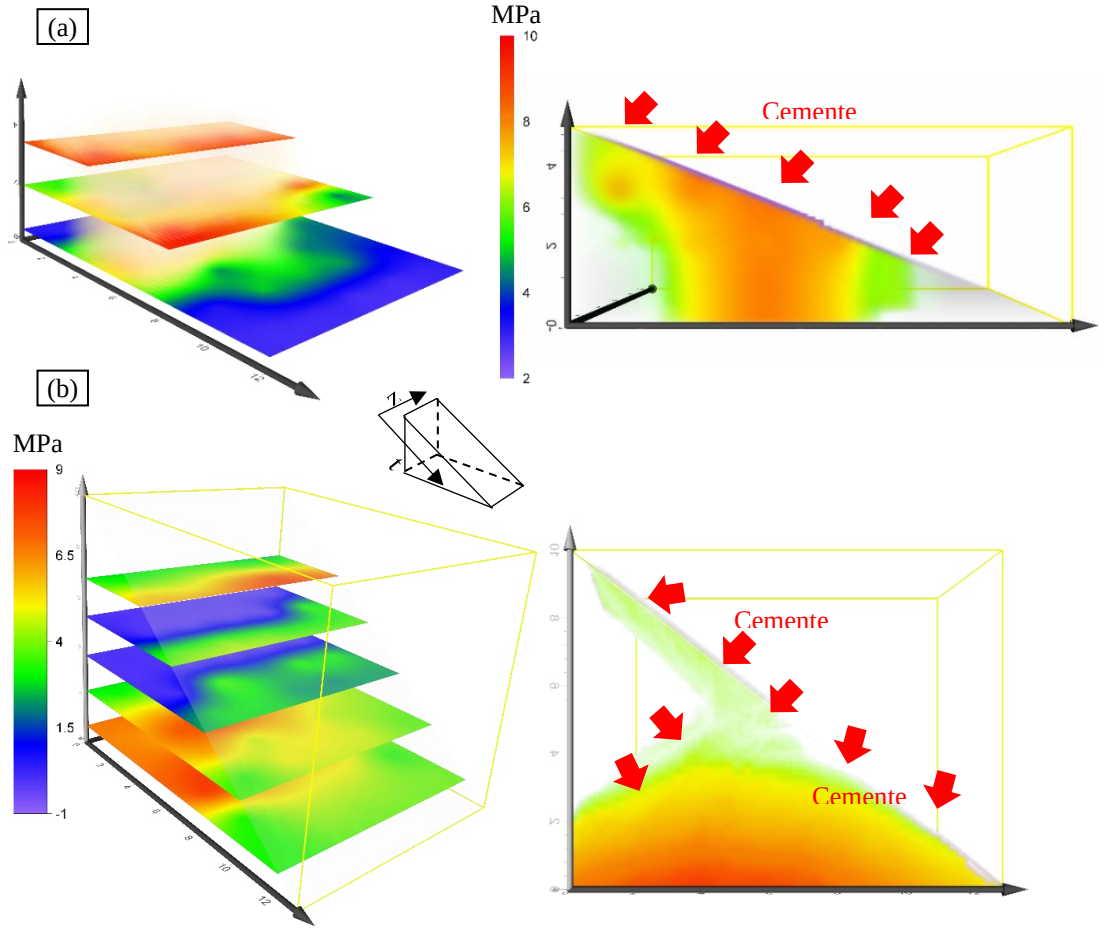


Figure 5.19. Estimated UCS 3D profile along the beach slope models (t-z axis) of the treated sands (measured by needle penetrometer), (a) 15° and (b) 30°

along the entire surface was achieved. However, cementation was not observed within the zone below the top slope (Figure 5.19, a), remained as untreated soil. The surface UCS was used as the indicator to evaluate the improvement of 15° beach slope, besides the UCS estimated by the treated sands based on needle penetration tests. Figure 5.19, b, the treated results of 30° beach slope which in the middle were not well solidified, compared the 15° beach slope. Because of the bio-cementation were occur and accumulated in the surface and bottom of the models. The bio-cemented slope surface had considerable estimated UCS between 2 and 8 MPa, and relatively lower estimated UCS values based on needle penetrometer test were obtained below the surface of the slope.

5.5.9 MICP of artificial rock properties

Natural beachrock were found in nature mostly consist of carbonate bridged material cementation, organic matter such as skeletal fragments and also other source of rock were consist depends on geological settling in that area. Therefore, artificial cement formed by mixing seawater and a solution containing $CO(NH_2)_2$ and $CaCl_2$ were injected into sand with culture bacteria as the solidification nutrient for cementation process (Cheng, et al., 2014). Fifteen MICP treated specimens were subjected to undrained shear under different loading paths including a mixture of both species, similar to the drained test series described previously. The test results indicate that as with the drained specimens, the total stress path influences the constitutive behavior of the cemented soil with small deviations in effective stress paths. A column solidification test was conducted for the purpose achieve strength in megapascal (MPa) which feasible as shoreline development method. A column solidification test is conducted over a period of 25 days owing to the accumulation of carbonate cement which might get clogged in the sample, under a 37°C curing temperature, and with injection of solidified solution at one-day intervals which results in a 0.5-M Ca^{2+} concentration of solidified solution. The results indicate that the UCS values increase with the decrease in particle size in the uniformly graded sands. The average UCS axial load (Figure 5.20) estimated close to the surface of fine sand and coral sands (D_{50} of 0.87 mm and 0.2 mm) are 2.87 MPa and 5.7 MPa respectively. This experiment was conducted in laboratory of rocks mechanics in the Engineering faculty, Hokkaido University using an Instron universal tester (manufactured by INSTRON, 5586). The UCS values and the calcium carbonate content of coral sand and fine silica sands reported herein are in a good agreement with the results reported by Cheng and

Cord-Ruwisch (2014). Basically, coral sands have high permeability that leads to the high liquid infiltration compared to the fine sands. In contrast, fine sand exhibits significant improvement in UCS with the depth, which could be due to the increased capillary effect along the sample depth. The higher capillary forces in fine sand tended to retain certain amount of cementation solutions close to particle contacts, resulting higher deposition of calcium carbonate and exhibiting higher UCS.

The results of the tests on bioclogging and biocementation (Table 5.8) can be monitored in real time using seismic velocity and resistivity measurements (Feng and Montoya, 2017; Phillips, et al., 2015). Shear wave velocity (S-wave) test results were used to develop a correlation to the precipitated calcite mass and this enables prediction of changes in porosity, density, and shear modulus during treatment (Weil, et al., 2012). Shear wave velocity is used to nondestructively monitor the change in small-strain stiffness during shearing, which provides an indication of cementation degradation as a function of strain level. Because shear wave velocity is influenced by both the level of cementation and the change in effective mean stress during shearing, the normalized shear modulus is used to evaluate the degradation of cementation during shearing (Montoya and DeJong, 2015). Biocementation in a change from a shear wave velocity of 140 m/s to an average of 600 m/s, compare with this research a shear wave around 510 m/s to 1330 m/s. Compression wave velocity (P-wave) measurements can be determined under different saturation conditions and used in combination with S-wave measurements to observe how the Poisson's ratio evolved during treatment (Whiffin, 2004). Permeability of the fractured rock after biotreatment decreased between 2 and 4 orders of magnitude and the sandstone core withstood three times higher well bore pressure than during the initial fracturing event showing that MICP is applicable for the bioclogging (biosealing) of the fractured rocks (Phillips, et al., 2015). Porosity is the amount of voids in a material. The porosity after MICP treatment have a porosity is larger than natural beachrock were found in the site study, additional measurement of tomography scan beneath sands particle were conducted to show the distribution of porosity of natural beachrock versus artificial rock based on MICP (Figure 5.20). The porosity content of beachrock (10-15%, approximately) in treatment sands significantly increases the number of particles in contact by bonding with the sand grains (30~45%) because of the meniscus bridge crystallization not intents precipitation as natural beachrock. It can be observed that the fine matrices content plays a very important role in support by enabling intermediate support to form bridges among the carbonate crystals that have grown in void spaces, thus, strengthening the force chain of the treated matrix. It should also be stated here that the MICP technique is limited due to the limited rate of

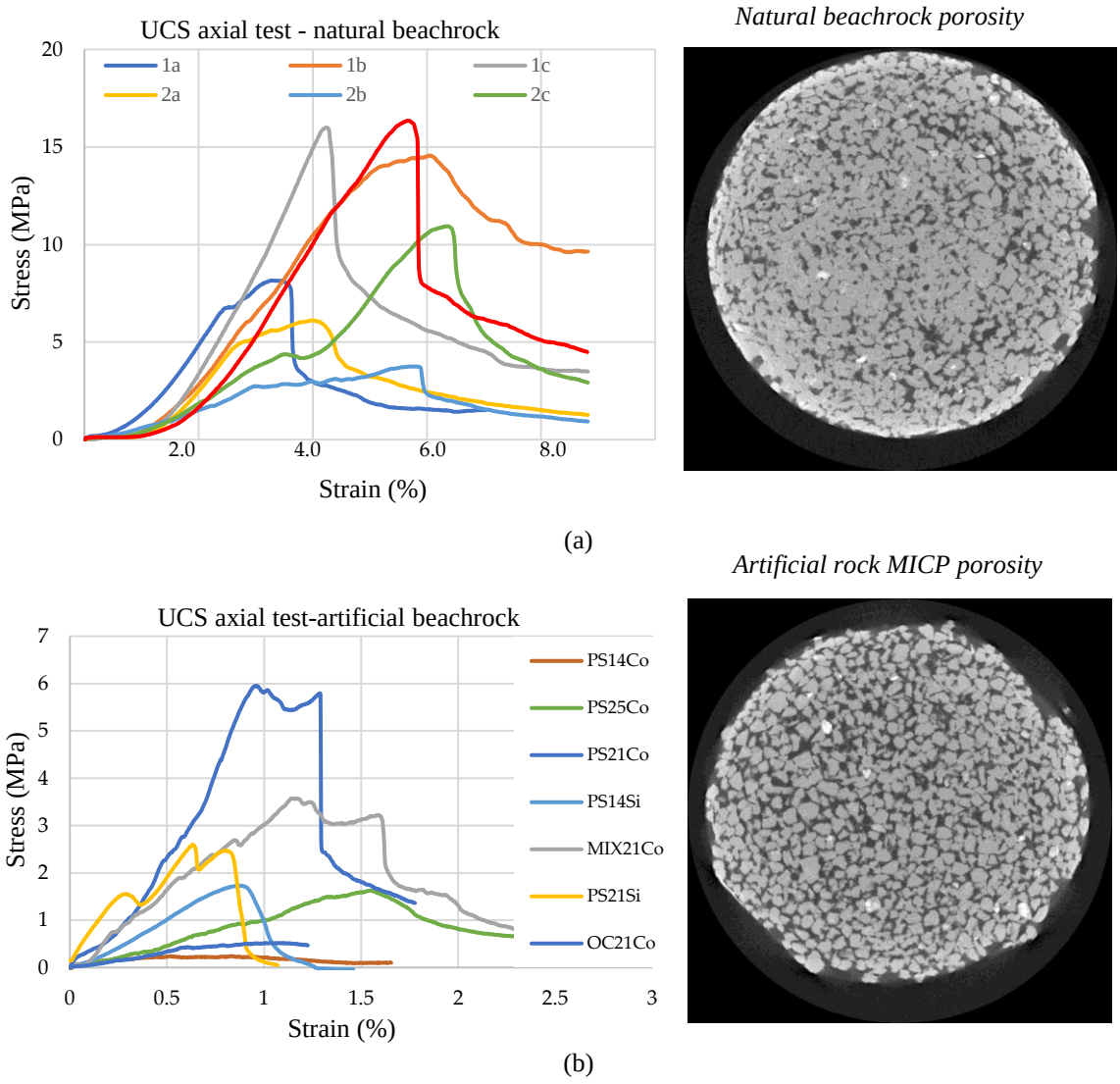


Figure 5.20 Comparison of the UCS axial load between (a) natural beachrocks and (b) artificial rock based on MICP method with x-ray chromatography scan images of porosity.

permeability that generally takes a much longer time to infiltrate the reactants (Mortesen, et al., 2011). Further, free passage of the bacteria might be inhibited due to the small pore throat size of fine soils (Cheng and Cord-Ruwisch, 2014) which mostly contain calcium carbonate compounds such as vaterite, aragonite and/ or calcite without magnesium mineral enrichment from the seawater supply (Russel and McIntire, 1965; Vousdoukas, et al., 2007; Daryono, et al., 2019).

5.6. Discussions

5.6.1 Uniformity of cementation

It is highly necessary to study uniformity of precipitated calcium carbonate along laterally (t-z axis) and vertically (x–y axis) in shoreline slope, as the MICP in soils is achieved by

Table 5.8. Rock properties of artificial beachrock using MICP method

Sample	Sand Type	Saturated density (g/cm^3)	Porosity (%)	Expectation strength (MPa)	P wave velocity (km/s)	S wave velocity (km/s)	Dynamic Poisson ratio
VB-14 Unsaturated	Quartz Silica Sands	1.60	37%	1.01	1.12	0.77	0.05
PS-14 Unsaturated		1.63	34%	2.33	1.20	0.84	0.01
MIX-14		1.56	30%	1.48	0.97	0.68	0.02
OC-21		1.56	38%	0.54	0.82	0.57	0.05
PS-14		1.53	30%	1.57	0.73	0.51	0.04
MIX-21		1.65	29%	3.19	1.00	0.69	0.06
PS-21		1.81	24%	3.73	1.78	1.24	0.02
PS-14 Unsaturated	Coral Limestone Sand	1.42	32%	2.40	1.31	0.88	0.09
PS-21 Unsaturated		1.74	28%	5.79	1.82	1.27	0.03
MIX-21		1.66	33%	3.20	1.94	1.33	0.05
OC-21		1.58	43%	1.78	1.07	0.72	0.07
PS-25		1.63	26%	1.39	1.68	1.13	0.09
PS-14		1.46	31%	1.58	1.04	0.73	0.01
PS-21		1.60	29%	2.46	1.48	1.01	0.07

biochemical injections. Before the measurements, it was anticipated that relatively a homogeneous cementation could be attained along the surface (t-z) by the injection method. However, Figure 5.18 and 5.19 suggests that the surface UCS increases along the distance (t) measured from the top slope, and the highest surface UCS was obtained near bottom slope. The average UCS at the bottom slope was about 7 MPa, whereas that of top is only 2 MPa. This variation along the surface could be attributed to the localization of bacteria cells. The consecutive injections of cementation solution (every 24 h) i.e. propagated flowlines would possibly transport the bacteria cells towards downslope, results increase in cell concentration in the direction of downslope; thus, more or less of the bacteria cells will in turn increase or decrease the cementation and UCS. The Precipitated carbonate profile is not uniform along the slope depth (x–y) similar to that observed in column specimens, suggesting higher calcium carbonate content near to the injection port. The spatial distribution of calcium carbonate generally follows the trend of microbe distributions along the specimen length/depth (Gowthaman, et al., 2019). As previously discussed, higher concentration of bacteria cells was

filtered at the top zone, leading to higher deposition of carbonate content near the injection surface. In order to confirm this postulation, soil samples were collected from three depths of slope after performing the biological injection, and the number of existing bacteria cells were measured by similar method used for isolation of bacteria. The measured locations are indicated clearly in Figure 5.4.

In addition, surface zone closest to the injection port is generally in exposure to higher concentrated reactants than the bottom zone (Whiffin, et al., 2007); therefore, higher carbonate content was precipitated at surface zone. It also has been reported that the amount of urease, precipitation rate and nutrient concentrations also have a great influence in carbonate distribution and must be maintained at their minimum to achieve a homogeneous cementation along the soil columns (Mortensen, et al., 2011; Cheng, et al., 2016). The measurements indicate that the slope beach sand consists of very small amount (0.22–0.25%) natural carbonate content. As reported by Mortensen et al. (2011), the soil particles consisted of carbonate content could provide ideal surfaces and nucleation sites for the additional precipitation of carbonate crystals. At the same time, the residual soil would consist of soil particles in broad range of shapes, irregularities and with varying surface roughness, which could provide additional effects in precipitation of carbonate. Future works should clearly address the effect of particle shapes and surface roughness to improve the understanding on the behavior of residual soils. The threshold calcium carbonate content required to provide measurable UCS of slope beach sand was found to be around 3%. The carbonate content reported herein is in a good agreement with the minimum carbonate content (3.5%, for the sand with D_{50} of 165μm) reported by Whiffin et al. (2007). Soil cemented below the threshold carbonate content exhibited an unsolidified loose matrix which was similar to the untreated soil. However, small carbonate crystals on the particle surface were evidenced through SEM analysis. At the same time, Feng and Montoya (2016) and Lin et al. (2018) have reported that the minimum carbonate content required to increase the strength of sands (D_{50} of 0.6 mm and 0.9 mm respectively) was around 1%. Actually, the threshold carbonate content of a soil is related to the number of particle contacts and grain size. Due to the increased number of particle contacts in slope beach sand, relatively a higher amount of threshold carbonate content (3%) (compared to that reported by Feng and Montoya (2016) and Lin et al. (2018)) was required to provide the measurable strength. Figure 5.21 presents a compilation of all UCS results obtained versus the measured calcium carbonate content. The UCS increases during MICP improvement as calcium carbonate precipitates and cements the soil particles, as a result of void space reduction. It is also clear that the UCS increases exponentially with the increase in calcium

carbonate content, similar to that reported in previous studies.

5.6.2 Field implication and associated limitations

To date, most of the studies of MICP have been extensively investigated under saturated or water-logged environmental conditions (Whiffin, et al., 2007; Lin, et al., 2016; van Paassen, et al., 2010; Feng, et al., 2017; Sivakumar, et al., 2019) , in which bacterial and cementation medias were injected to the specimen by a saturated flow with a constant flow rate using peristaltic pump. Pumping method has often resulted a heterogeneously cemented profile in soil columns, suggesting a higher precipitation level at the influent column. Recently, Li et al. (2018) have proposed a rotating soak method to promote the uniformity of cementation in specimen by facilitating more nutrition supply and air replenishment within the soil for effective bacterial performance. However, in the real field, it would be a challenge to maintain the saturated or submerged flow conditions during the treatment period, which requires hydraulic injection of cementation/ biological solutions, extraction of effluent solution and heavy machinery systems. Therefore, it is an essential to introduce alternative MICP approaches to produce carbonate cement with high efficacy with desirable cost minimization (Figure 5.21).

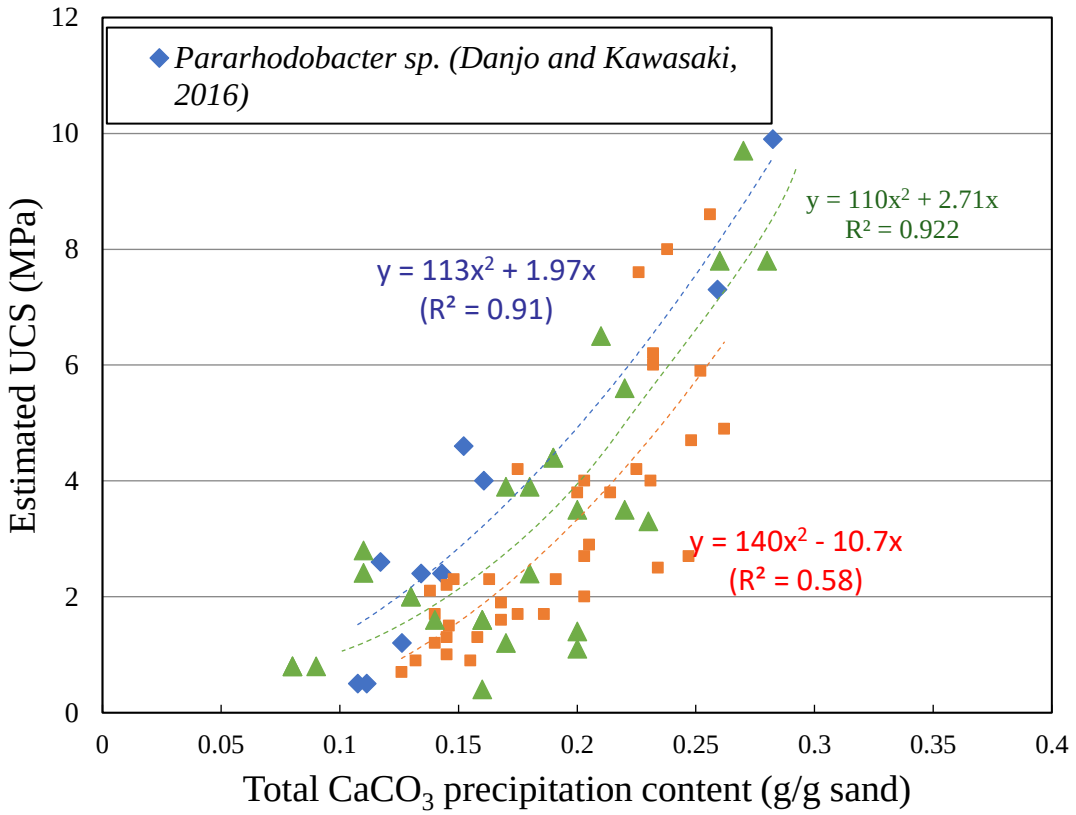


Figure 5.21. Relationship between estimated UCS versus calcium carbonate content of MICP comparing with previous study.

The simple surface percolation technique demonstrated in this study is more suitable for field application, which eliminates the destruction of existing soil structure and reduces the costs of required labor and machinery. However, it would be more effective, if the surface percolation is promoted to spraying instead of injections, which is left for the future work to be performed in the subsequent phase of this study. In civil engineering applications such as slope surface stabilizations, it is highly important to immobilize the ureolytic bacteria within the target surface zones, so that sufficient carbonate can be precipitated throughout the required zone. The experimental observations discussed in this paper suggest well immobilization of bacteria only within the surface zone, and the particle size distribution of slope soil limits the distribution of bacteria to more deeper depths. Therefore, it is appropriate to recommend the technique for slope surface stabilization i.e. stabilizing the slope by enhancing the surface cover condition of the slope and promoting high aggregate stability at the surface zone, which could be enabled against surface erosion. The results also indicate, treating the soil by surface percolation method could strengthen the soil significantly by forming more effective crystals at free-draining environmental conditions and can be highly applicable on unsaturated or partially saturated natural slopes and embankments. In the injection method investigated herein, grain size distribution highly governs the efficiency of MICP. Fine sands, well graded soils and soils consisting of certain number of fine particles have less permeability (compared to the coral soils) leading to low infiltration rate, that often increases the risk regarding local clogging. In order to avoid the risk of clogging, Whiffin et al. (2007) have suggested a faster injection/flow rates of reactants by allowing less reaction time along the path. Afterwards, Cheng and Cord-Ruwisch (2014) have reported the observation of non-clogged fine and coral sand columns treated under higher infiltration rates (7–28.5 cm/min). They have also reported that severe clogging occurred in fine sand when it was treated under low infiltration rate less than 0.25 cm/ min. Therefore, a moderate infiltration rate of 2–4 mL/min was maintained during the treatment period (no clogging occurred during the treatment).

5.6.3 Permeability of cemented specimens

Permeability was measured separately for the specimens treated using regular bacteria culture and segregated cell pellets by falling head method. Also, the permeability of the untreated soil was measured to investigate the reduction caused by the calcium carbonate precipitation. The permeability was significantly reduced (approximately by 90%) with the surface percolation technique irrespective of using regular culture or segregated cell pellets. However, a little more reduction was obtained in the specimen treated by using regular culture

due to higher deposition of calcium carbonate content as discussed in the previous section. Generally, the permeability of the specimen linearly decreases with increase in precipitated calcium carbonate content (Martinez et al., 2013). The results indicate that this surface percolation treatment technique was attributed to reduce the permeability in slope, which would help to control the infiltration of rainwater into the slope and enhance the surface sheet flow, and thus preserves the slope from failures. However, the reduction in infiltration of storm water might possibly result the water buildup on the bio-cemented stabilized slope surface, leading to additional overburden and sheet flow with high energy. Therefore, additional consideration regarding drainage is highly required. Facilitating the horizontal drains in slope is one of the feasible methods to lower the excess surface flow, and that can be easily implied in certain intervals (along the long edge) by using perforated metal or slotted plastic drainages.

5.7. Conclusions

The effects of the anionic polysaccharide carrageenan on $CaCO_3$ crystallization and sand solidification was analyzed by using the MICP method. It was found that chitosan has a positive effect on $CaCO_3$ crystallization and sand solidification. Higher amounts of the precipitate could be obtained upon carrageenan addition than without added. Carrageenan also precipitated as its hydrogel with the $CaCO_3$ crystals. Increase of the supersaturation in a reaction mixture by adding carrageenan leads to the formation of vaterite instead of calcite, which is the most common type of polymorphism in MICP. At lower bacterial concentrations, the precipitate consisted of good rhombohedral crystals and individual carrageenan hydrogel. However, the higher concentrations, distorted the crystal shape, and crystal agglomerates were produced. Carrageenan act as a template for the $CaCO_3$ crystals to nucleate due to adsorption of the Ca^{2+} ions onto hydrogel. In contrast, in the case of without chitosan bacteria cells themselves act as nucleation site for $CaCO_3$ crystals to nucleate and growth. Even though without carrageenan also $CaCO_3$ can nucleate and grow efficiently but process could be accelerated effectively by adding carrageenan. The higher carrageenan concentrations accelerate the conversion of metastable phase of vaterite into the stable phase of calcite. In addition, the carrageenan hydrogel assisted in the formation of better bridge between the sand particles. Hence, by adding carrageenan better cementation and strength could be achieved than the conventional method. Finally, carrageenan can be used to produce good organic-inorganic hybrid green materials, which can be used in a number of civil engineering applications. On other hand, the ions NaCl and $MgCl_2$ concentrations on MICP is higher than those of average seawater favor microbially mediated formation of Mg-rich carbonates, which are often considered as potential dolomite

precursors. Even though the process deemed to negatively affect the desired engineering properties of the treated specimens. It is clearly deduced that the strength decline is mainly due to the change in crystal morphology (rather than the quantity of precipitate) to a needle shaped crystal form with lower bonding capacity than that of the well-interweaved and cross-linked rhombohedral crystals produced in the absence of magnesium.

The effect of carbonate precipitation on the process of strengthening in slope soil was investigated by comparing the behavior of three uniformly graded sands. Microstructure of the soils treated by surface percolation shows the formation of effective crystals at particle contacts. Presence of fine content governs the behavior of residual slope soil significantly. It increases the number of particle contacts by bonding with the sand grains and participates in the force chain of the treated matrix. The fine content provides the matrix support effectively by facilitating intermediate supports to form bridges between carbonate crystals. However, grain size distribution tends to filter more bacteria at surface zone of slope, results high cementation at the surface level and relatively a long linear reduction in carbonate precipitation along the profile is observed. This preliminary investigation suggests that the technique can be implemented for stabilizing the slope by enhancing the cover condition of the slope, and the results obtained from this investigation would be highly beneficial to promote the study to the large scale.

References

A. Bacic, G.B. Fincher, B.A. Stone, Chemistry, biochemistry, and biology of (1–3)-[beta]-glucans and related polysaccharides, 1st, ed, Academic, Amsterdam,2009.

A. Bouazza, W. Gates, P. Ranjith, Hydraulic conductivity of biopolymertreated silty sand, Géotechnique 59 (1) (2009) 71–72.

A. Clark, S. Ross-Murphy, Structural and mechanical properties of biopolymer gels, Biopolymers, Springer, Berlin Heidelberg (1987) 57–192.

A. Imeson, Food stabilisers, thickeners and gelling agents, Wiley-Blackwell Pub., Chichester, U.K.; Ames, Iowa, 2010.

A.P. Imeson, Thickening and gelling agents for food, Springer Science & Business Media, 2012.

Amarakoon GGNN, Kawasaki S (2018) Factors affecting sand solidification using MICP with *Pararhodobacter* sp. Mater Trans 59:72–81. https ://doi.org/10.2320/mater trans .M-M2017 849

ASTM D2487–17 (2017) Standard practice for classification of soils for engineering

purposes (unified soil classification system). ASTM International, West Conshohocken

Bauerfeind P, Garner R, Dunn BE, Mobley HL (1997) Synthesis and activity of *Helicobacter pylori* urease and catalase at low pH. Gut 40:25–30

Bolleter WT, Bushman CJ, Tidwell PW (1961) Spectrophotometric determination of ammonia as indophenol. Anal Chem 33:592– 594. https ://doi.org/10.1021/ac601 72a03 4

Carlson, W.D., 1983. Polymorphs of $CaCO_3$ and the Aragonite-Calcite transformation. Reviews in Mineralogy, 11, pp.191-225.

Chen YYM, Anne Clancy K, Burne RA (1996) *Streptococcus salivarius* urease: genetic and biochemical characterization and expression in a dental plaque streptococcus. Infect Immun 64:585–592

Cheng L, Cord-Ruwisch R (2014) Upscaling effects of soil improvement by microbially induced calcite precipitation by surface percolation. Geomicrobiol J 31:396–406. https ://doi.

Cheng L, Cord-Ruwisch R, Shahin MA (2013) Cementation of sand soil by microbially induced calcite precipitation at various degrees of saturation. Can Geotech J 50:81–90. https ://doi.org/10.1139/cgj-2012-0023

Cheng L, Cord-Ruwisch R. 2014. Upscaling effects of soil improvement by microbially induced calcite precipitation by surface percolation. Geomicrobiol J 31:396–406. https ://doi. org/10.1080/01490 451.2013.83657 9

Cheng L, Shahin MA, Mujah D (2016) Influence of key environmental conditions on microbially induced cementation for soil stabilization. J Geotech Geoenviron Eng 143:04016083. https :// doi.org/10.1061/(asce)gt.1943-5606.00015 86

Chu J, Stabnikov V, Ivanov V (2012) Microbially induced calcium carbonate precipitation on surface or in the bulk of soil. Geomicrobiol J 29:544–549. https ://doi.org/10.1080/01490 451.2011.59292 9

Ciurli S, Marzadori C, Benini S et al (1996) Urease from the soil bacterium *Bacillus pasteurii*: immobilization on Ca- polygalacturonate. Soil Biol Biochem 28:811–817. https ://doi. org/10.1016/0038-0717(96)00020 -X

D. Mujah, M.A. Shahin, L. Cheng, State-of-the-art review of biocementation by microbially induced calcite precipitation (MICP) for soil stabilization, Geomicrobiol J. 34 (6) (2017) 524–537.

D.M. Kirchmajer, B. Steinhoff, H. Warren, R. Clark, M. in het Panhuis, Enhanced gelation properties of purified gellan gum, Carbohydr. Res. 388 (2014) 125–129.

Danjo T, Kawasaki S (2016) Microbially induced sand cementation method using *Pararhodobacter* sp. Strain SO1, inspired by Beachrock formation mechanism. Mater Trans

57:428–437. https ://doi.org/10.2320/mater trans .M-M2015 842

Daryono, L. R. 2016. Comparison of natural beachrock and anthropogenic beachrock, case study: Okinawa-jima, Japan. Published thesis. Master's degree of Geological Engineering, Universitas Gadjah Mada, Indonesia.

Daryono, L.R., Nakashima, K., Kawasaki, S., Titisari, A.D. and Barianto, D.H., 2020. Sediment Characteristics of Beachrock: A Baseline Investigation Based on Microbial Induced Carbonate Precipitation at Krakal-Sadranan Beach, Yogyakarta, Indonesia. Applied Sciences, 10(2), p.520.

DeJong JT, Martinez BC, Mortensen BM, et al (2009) Upscaling of bio-mediated soil improvement upscaling of bio-mediated soil improvement. In: 17th International conference on soil mechanics and geotechnical engineering. Netherlands, pp 2300–2303

DeJong JT, Mortensen BM, Martinez BC, Nelson DC (2010) Biomediated soil improvement. Ecol Eng 36:197–210. https ://doi. org/10.1016/j.ecole ng.2008.12.029

Feng K, Montoya BM (2016) Influence of confinement and cementation level on the behavior of microbial-induced calcite precipitated sands under monotonic drained loading. J Geotech Geoenviron Eng 142:04015057. https ://doi.org/10.1061/(ASCE) GT.1943-5606.00013 79

Feng, K. and Montoya, B.M. 2017. Quantifying level of microbial-induced cementation for cyclically loaded sand. Journal of Geotechnical and Geoenvironmental Engineering, 143(6), p.06017005.

Fujita M, Nakashima K, Achal V, Kawasaki S (2017) Whole-cell evaluation of urease activity of *Pararhodobacter* sp. isolated from peripheral beachrock. Biochem Eng J 124:1–5. https ://doi. org/10.1016/j.bej.2017.04.004

Fujita Y, Grant Ferris F, Daniel Lawson R et al (2000) Calcium carbonate precipitation by ureolytic subsurface bacteria. Geomicrobiol J 17:305–318. https ://doi.org/10.1080/78219 8884

Fukue M, Nakamura T, Kato Y (2001) A method for determining carbonate content for soils and evaluation of the results. Soils Found 49–2:9–12 (in Japanese)

Fukue M, Ono S-I, Sato Y (2011) Cementation of sands due to microbiologically-induced carbonate precipitation. Soils Found 51:83–93. https ://doi.org/10.3208/sandf .51.83

G.C. Barrére, C.E. Barber, M.J. Daniels, Molecular cloning of genes involved in the production of the extracellular polysaccharide xanthan by Xanthomonas campestris pv. campestris, Int. J. Biol. Macromol. 8 (6) (1986) 372–374.

Gat D, Ronen Z, Tsesarsky M (2016) Soil bacteria population dynamics following

stimulation for ureolytic microbial-induced $CaCO_3$ precipitation. Environ Sci Technol 50:616–624. https :// doi.org/10.1021/acs.est.5b040 33

Gomez MG, Martinez BC, DeJong JT et al (2015) Field-scale bio-cementation tests to improve sands. Proc Inst Civ Eng – Gr Improv 168:206–216. https ://doi.org/10.1680/grim.13.00052

Gowthaman S, Mitsuyama S, Nakashima K et al (2019) Biogeotechnical approach for slope soil stabilization using locally isolated bacteria and inexpensive low-grade chemicals: a feasibility study on Hokkaido expressway soil, Japan. Soils Found 59:484–499. https ://doi.org/10.1016/j.sandf .2018.12.010

H. Hassan, S. Al-Oraimi, R. Taha, Evaluation of open-graded friction course mixtures containing cellulose fibers and styrene butadiene rubber polymer, J. Mater. Civ. Eng. 17 (4) (2005) 416–422.

H. Izawa, J.-I. Kadokawa, Preparation and characterizations of functional ionic liquid-gel and hydrogel materials of xanthan gum, J. Mater. Chem. 20 (25) (2010) 5235–5241.

H.D. Shin, M.K. Son, B.R. Park, C.W. Son, H.J. Jang, Composition containing Beta-glucan for prevention and treatment of osteoporosis, in: D.D. Mckay (Ed.) Glucan Corporation, United States, 2004, p. 6.

I. Chang, A.K. Prasidhi, J. Im, G.-C. Cho, Soil strengthening using thermo gelation biopolymers, Constr. Build. Mater. 77 (2015) 430–438.

I. Chang, G.-C. Cho, Shear strength behavior and parameters of microbial gellan gum-treated soils: from sand to clay, Acta Geotech. (2018) 1–15.

I. Chang, G.-C. Cho, Strengthening of Korean residual soil with b-1,3/1,6-glucan biopolymer, Constr. Build. Mater. 30 (2012) 30–35.

I. Chang, J. Im, G.-C. Cho, Geotechnical engineering behaviors of gellan gum biopolymer treated sand, Can. Geotech. J. (2016) 1–13.

Ivanov, V. and Chu, J., 2008. Applications of microorganisms to geotechnical engineering for bioclogging and biocementation of soil in situ. Reviews in Environmental Science and Bio/Technology, 7(2), pp.139-153.

J. Daniel, R.L. Whistler, A.C.J. Voragen, W. Pilnik, Starch and other polysaccharides, VCH Verlagsgesellschaft mbH, Weinheim, Ullmann's Encyclopedia of Industrial Chemistry, 1994.

J. Im, A.T.P. Tran, I. Chang, G.-C. Cho, Dynamic properties of gel-type biopolymer-treated sands evaluated by Resonant Column (RC) tests, Geomechanics and Engineering 12 (5) (2017) 815–830.

J. Plank, Applications of biopolymers in construction engineering, Biopolymers Online, Wiley-VCH Verlag GmbH & Co. KGaA, 2005.

J.T. Oliveira, L. Martins, R. Picciochi, P.B. Malafaya, R.A. Sousa, N.M. Neves, J.F. Mano, R.L. Reis, Gellan gum: a new biomaterial for cartilage tissue engineering applications, J. Biomed. Mater. Res. Part A 93 (3) (2010) 852–863.

Jahns T (1992) Urea uptake by the marine bacterium Deleya venusta HG1. J Gen Microbiol 138:1815–1820. https ://doi.org/10.1099/00221 287-138-9-1815

L. Cheng, M. Shahin, Bacteria induced cementation for soil stabilization, in: Proceedings of the 19th International Conference on Soil Mechanics and Geotechnical Engineering, 2017, pp. 2371–2374.

Li C, Yao D, Liu S et al (2018) Improvement of geomechanical properties of bio-remediated Aeolian sand. Geomicrobiol J 35:132–140. https ://doi.org/10.1080/01490 451.2017.13387 98

Li H, Li C, Zhou T et al (2018) An improved rotating soak method for MICP-treated fine sand in specimen preparation. Geotech Test J 41:20170109. https ://doi.org/10.1520/GTJ20 17010 9

Lin H, Suleiman MT, Brown DG, Kavazanjian E (2016) Mechanical behavior of sands treated by microbially induced carbonate precipitation. J Geotech Geoenviron Eng 142:04015066-1–13.https ://doi.org/10.1061/(ASCE)GT.1943-5606.00013 83

M. McIntosh, B.A. Ston, V.A. Stanisich, Curdlan and other bacterial (1->3)-beta-D-glucans, Applied Microbiol. Biotechnol. 68 (2) (2005) 163–173.

M.W. Wan, I.G. Petrisor, H.T. Lai, D. Kim, T.F. Yen, Copper adsorption through chitosan immobilized on sand to demonstrate the feasibility for in situ soil decontamination, Carbohydr. Polym. 55 (3) (2004) 249–254.

Martinez BC, DeJong JT, Ginn TR et al (2013) Experimental optimization of microbial-induced carbonate precipitation for soil improvement. J Geotech Geoenviron Eng 139:587–598. https :// doi.org/10.1061/(ASCE)GT.1943-5606.00007 87

Mobley HL, Island MD, Hausinger RP (1995) Molecular biology of microbial ureases. Microbiol Rev 59:451–480

Montoya BM, DeJong JT, Boulanger RW (2013) Dynamic response of liquefiable sand improved by microbial-induced calcite precipitation. Géotechnique 63:302–312. https ://doi. org/10.1680/geot.sip13 .p.019

Montoya, B.M. and DeJong, J.T. 2015. Stress-strain behavior of sands cemented by microbially induced calcite precipitation. Journal of Geotechnical and Geoenvironmental

Engineering, 141(6), p.04015019.

Mortensen BM, Haber MJ, Dejong JT et al. 2011. Effects of environmental factors on microbial induced calcium carbonate precipitation. J Appl Microbiol 111:338–349. https ://doi.org/10.111 1/j.1365-2672.2011.05065.

Moyo CC, Kissel DE, Cabrera ML (1989) Temperature effects on soil urease activity. Soil Biol Biochem 21:935–938. https ://doi. org/10.1016/0038-0717(89)90083 -7

N. Latifi, S. Horpibulsuk, C.L. Meehan, M.Z. Abd Majid, M.M. Tahir, E.T. Mohamad, Improvement of problematic soils with biopolymer an environmentally friendly soil stabilizer, J. Mater. Civ. Eng. 29(2) (2016)04016204.

Nawarathna, T.H.K., Nakashima, K. and Kawasaki, S., 2019. Chitosan enhances calcium carbonate precipitation and solidification mediated by bacteria. International journal of biological macromolecules, 133, pp.867-874.

Omoregie AI, Khoshdelnezamiha G, Senian N et al (2017) Experimental optimisation of various cultural conditions on urease activity for isolated *Sporosarcina pasteurii* strains and evaluation of their biocement potentials. Ecol Eng 109:65–75. https ://doi. org/10.1016/j.ecole ng.2017.09.012

Omoregie AI, Palombo EA, Ong DEL, Nissom PM (2019) Biocementation of sand by *Sporosarcina pasteurii* strain and technicalgrade cementation reagents through surface percolation treatment method. Constr Build Mater 228:116828. https ://doi. org/10.1016/j.conbu ildma t.2019.11682 8

org/10.1080/01490 451.2013.8365794.

Osinubi KJ, Eberemu AO, Gadzama EW, Ijimdiya TS (2019) Plasticity characteristics of lateritic soil treated with *Sporosarcina pasteurii* in microbial-induced calcite precipitation application. SN Appl Sci 1:829. https ://doi.org/10.1007/s4245 2-019-0868-7

Panarotto, C.T., Cabral, A.R. and Lefebvre, G., 2005. Environmental, geotechnical, and hydraulic behaviour of a cellulose-rich by-product used as alternative cover material. Journal of environmental engineering and science, 4(2), pp.123-138.

Phang IRK, Chan YS, Wong KS, Lau SY (2018) Isolation and characterization of urease-producing bacteria from tropical peat. Biocatal Agric Biotechnol 13:168–175. https ://doi.org/10.1016/j. bcab.2017.12.006

Phillips, A.J., Eldring, J.J., Hiebert, R., Lauchnor, E., Mitchell, A.C., Cunningham, A., Spangler, L. and Gerlach, R. 2015. Design of a meso-scale high pressure vessel for the laboratory examination of biogeochemical subsurface processes. Journal of Petroleum Science and Engineering, 126, pp.55-62.

R. Khachatoorian, I.G. Petrisor, C.-C. Kwan, T.F. Yen, Biopolymer plugging effect: laboratory-pressurized pumping flow studies, J. Petrol. Sci. Eng. 38 (1–2) (2003) 13–21.

R.A. Nugent, G. Zhang, R.P. Gambrell, Effect of exopolymers on the liquid limit of clays and its engineering implications, Transp. Res. Rec. 2101 (2009) 34–43.

Reeder, R.J., 1983. Crystal chemistry of the rhombohedral carbonates. Reviews in Mineralogy, 11, pp.1-47.

Russell, R. J., and McIntire, W. G. 1965. Beach cusps. Geological Society of America Bulletin, Vol. 76, 3, 307-320. https://doi.org/10.1130/0016-7606(1965)76[307:BC]2.0.CO;2.

S. Dumitriu, Polymeric biomaterials, 2nd ed., Marcel Dekker Inc, New York, 2002.

S. Kalia, L. Averous, Biopolymers: Biomedical and Environmental Applications, Wiley, 2011.

S. Smitha, A. Sachan, Use of agar biopolymer to improve the shear strength behavior of sabarmati sand, Int. J. Geotech. Eng. 10 (4) (2016) 387–400.

Sensoy T, Bozbeyoglu NN, Dogan NM, et al (2017) Characterization of calcium carbonate produced by ureolytic bacteria (*Sporocarcina pasteurii* ATCC 6453 and Bacillus aerius U2) and effect of environmental conditions on production of calcium carbonate. In: 15th International conference on environmental science and technology. Rhodes, Greece

Soon NW, Lee LM, Khun TC, Ling HS (2014) Factors affecting improvement in engineering properties of residual soil through microbial-induced calcite precipitation. J Geotech Geoenviron Eng 140:04014006. https ://doi.org/10.1061/(ASCE)GT.1943-5606.00010 89

Stabnikov V, Naeimi M, Ivanov V, Chu J (2011) Formation of water-impermeable crust on sand surface using biocement. Cem Concr Res 41:1143–1149. https ://doi.org/10.1016/j.cemconres.2011.06.017

Ulusay R (2014) The ISRM suggested methods for rock characterization, testing and monitoring: 2007–2014. Springer, Berlin

van Paassen LA (2011) Bio-Mediated Ground Improvement: From Laboratory Experiment to Pilot Applications. Geo-frontiers 2011. American Society of Civil Engineers, Reston, pp 4099–4108

Van Paassen, L. A. et al., 2010. Quantifying Biomediated Ground Improvement by Ureolysis: Large-Scale Biogrout Experiment. J. Geotech. Geoenvirn. Eng. 136: 1721-1728.

Vousdoukas, M. I., Velegrakis, A. F., and Plomaritis, T. A. 2007. Beachrock occurrence, characteristics, formation mechanisms and impacts. Earth-Science Reviews, Vol. 85, 1–2, 23–46. https://doi.org/10.1016/j.earscirev.2007.07.002.

W.J. Orts, R.E. Sojka, G.M. Glenn, Biopolymer additives to reduce erosion induced soil losses during irrigation, Ind. Crops Prod. 11 (1) (2000) 19–29.

W.M. Kulicke, H. Nottelmann, Structure and Swelling of Some Synthetic, Semisynthetic, and Biopolymer Hydrogels, Polymers in Aqueous Media, American Chemical Society, Washington, DC, 1989, pp. 15-44.

Weil MH, DeJong JT, Martinez BC, Mortensen BM, Waller JT (2012) Seismic and resistivity measurements for real-time monitoring of microbially induced calcite precipitation in sand. ASTM Geotech Test J 35:1–12

Whiffin VS, van Paassen LA, Harkes MP (2007) Microbial carbonate precipitation as a soil improvement technique. Geomicrobiol J 24:417–423. https: //doi.org/10.1080/01490 450701 4365 05

Whiffin, V.S. 2004. Microbial $CaCO_3$ precipitation for the production of biocement (Doctoral dissertation, Murdoch University).

Yang Y, Zhu G, Wang G et al (2016) Robust glucose oxidase with a Fe_3O_4@C-silica nanohybrid structure. J Mater Chem B 4:4726– 4731. https ://doi.org/10.1039/c6tb0 1355d

CHAPTER 6
Durability test of MICP beach sand treatment

6.1 Introduction

For many decades, stability of slope soils is one of the serious concerns in the field of geotechnical Engineering. This is mainly because of the fact that sturdiness of most of the transportation structures is highly reliant on the stability of the slopes by which they are supported. During the construction of those structures (e.g. expressways, roads and railways), the natural slopes are modified in a way to fit the construction and design requirements, which often causes the clearance of vegetations and topographical amendments in natural slopes (Guerra et al., 2017; Zhang et al., 2018). Consequently, the slope surfaces become more vulnerable to the climatic measures and associated degradations, posing several risks regarding safety and sustainability. It is very clear that proper stabilization is essential to a slope to sustain its intrinsic characteristics against the varying nature and accompanied degradation processes. In the past, numerous methods were proposed and investigated to improve the cover condition of slopes. The most cost-effective and eco-friendliest method for stabilizing the slope is establishment of vegetation such as grass, weeds, plants and etc. (Chirico et al., 2013). The vegetation as an engineering material, serves as a crust layer between atmosphere and surface, enduring the slope from the direct contact of climatic measures such as rainfalls, snowfalls, etc. Also, their roots reinforce the surface, enhancing the stability of slope substrates.

However, to achieve the fullest benefits, it takes quite a long time, and the growth and survival of vegetation are limited to certain regions such as subarctic and arid zones (Jiang et al., 2019). Some of other methods widely in application stage are mechanical compactions, geosynthetic applications and chemical stabilizations (Gowthaman et al., 2019; Kumar and Das, 2018). Majority of these stabilization techniques utilize mechanical energy and artificial materials, both of which required substantial energy for manufacture and installation. Chemical grouts (such as cements, epoxy, acrylamide, phenoplasts, silicates, and polyurethane) are also found to be reliable, could enhance the surface by filling pore spaces and binding soil particles (Arya et al., 2018; DeJong et al., 2010). However, almost all these materials are reported to be toxic and hazardous, causing pollutions and influx of dangerous substances to the geo-environment; therefore, their applications to the field scale are extensively under the scrutiny of public policy (DeJong et al., 2010; Gowthaman et al., 2018). Confluence of these drawbacks in the conventional methods necessitates the exploration and development of new methods for

stabilizing the slope soil more effectively. As an emerging technique, MICP (microbial induced carbonate precipitation) has drawn substantial attentions in the past decade. MICP is a biochemical process which persuades the calcium carbonate bio-cement within the embedded soil matrix as a consequence of metabolic activity.

In the recent past, few studies have demonstrated that the MICP can be potentially applied to stabilize the slope soil (Gowthaman et al., 2019; Jiang et al., 2019). Similar to the conventional grouting techniques, MICP has also been proposed for surficial treatment (Gowthaman et al., 2019), which tends to promote the cover condition of the slope, so that to withstand various degradation processes. Rainfall induced surface erosion is one of the factors threatening the stability (Zhang et al., 2018). By investigating sets of MICP treated slope models, Jiang et al. (2019) have recently concluded that treating the slopes by 1 mol/L cementation solution would give optimum resistance against erosion induced by artificial rainfall. It is worth noting that despite of the considerable interests on MICP, the available information on the durability and performance are very limited. Processes of wetting-drying are also other serious concerns in Geotechnical Engineering, affecting the long-term performances. After the treatment, sooner or later, the slope surfaces are exposed to varying climates and environment conditions. During the rainfalls and subsequent evaporations, surfaces are subjected to periodical wetting-drying process (Tang et al., 2016), which might cause progressive damages in MICP surfaces. However, the effects of wetting-drying have not been extensively investigated in the past.

6.2 Objectives

In this chapter, we conducted after treatment test of solidification samples on local beach sand within statistical analysis of wetting-drying test. Therefore, the main objective of this study is to investigate the influence of variable wetting-drying cycles on the physical and mechanical characteristics of MICP treated slope beach sand, representing the erosion shoreline slope in the coastal area. The goal of this paper is to perform the durability of the specimen having an estimated unconfined compressive strength (UCS) of more than several MPa after wetting-drying cycles using fresh water and saltwater to compare the efficiency of treatment samples.

6.3 Research methodology

6.3.1 Beachrock and bacteria

The ureolytic bacterium, *Pseudoalteromonas tetradonis* isolated by Daryono, et al. (2019,

2020) from beachrock sample from Indonesia shoreline was used in this study due to its high urease activity which classified as gram-negative. The strain were motile bacilli 1 µm wide and 1.5–4.0 µm, aerobic, motile with one polar flagellum, rods (or rod-shapes) with 0.5–0.8 × 1.0–1.5 µm when in exponential growth phase was used in this study. Standard media (ZoBell2216E for marine bacteria medium) were used for culturing under sterile aerobic conditions. Cells were precultured separately in 5 mL of each medium at 37°C and 160 rpm for 24 h. One milliliter of the preculture was inoculated with 100 mL of the fresh medium and incubated under the same conditions.

The microbial cell growth of the isolates was determined based on optical density at a wavelength of 600 nm (OD_{600}) using a UV-vis spectrophotometer (V-730, JASCO Corporation, Tokyo, Japan). The local beach sand used in the experiments was uniformly graded with a mean particle size of 0.6 mm for fine sand, 0.9 mm for coral sands, Mizunami sands the standard laboratory sands with mean particle sizes (D_{50}) of 0.87 mm, and microsphere glass beads varying from 0.25 mm to 0.6 mm in diameter, respectively. The sands were sterilized, and hand packed into a 50-mL syringe (mean diameter, D_{50} = 3 cm and height, h = 10 cm). Figure 6.1 is shown the characteristic grain size distribution curves of the soils studied in this work and X-Ray diffraction data (Figure 6.2) of before the treatment with MICP. These XRD data will facilitate the comparison before and after beach sand treatment.

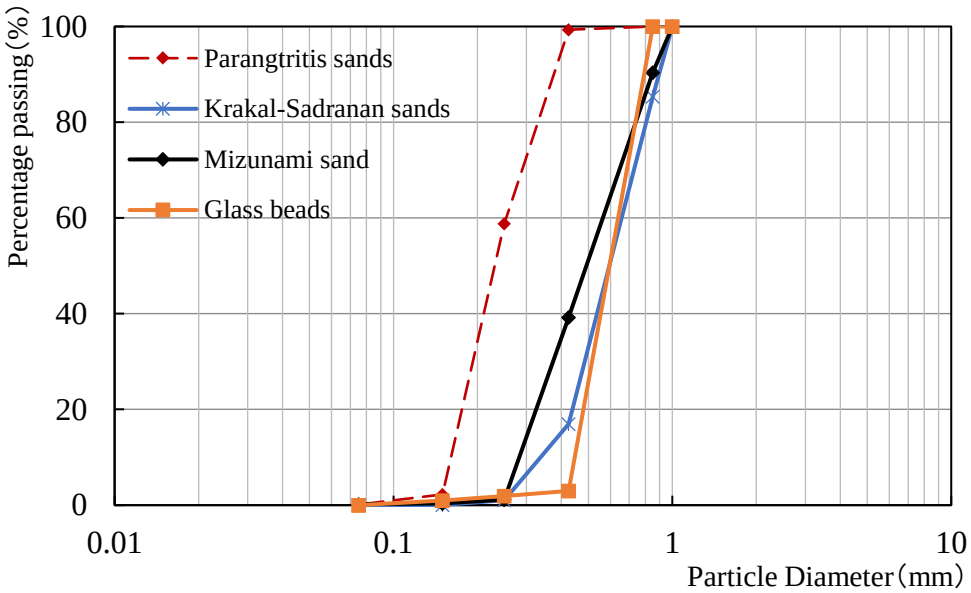


Figure 6.1. Grain size distribution curve of sands and local beach sands from Krakal-Sadranan site, Yogyakarta, Indonesia

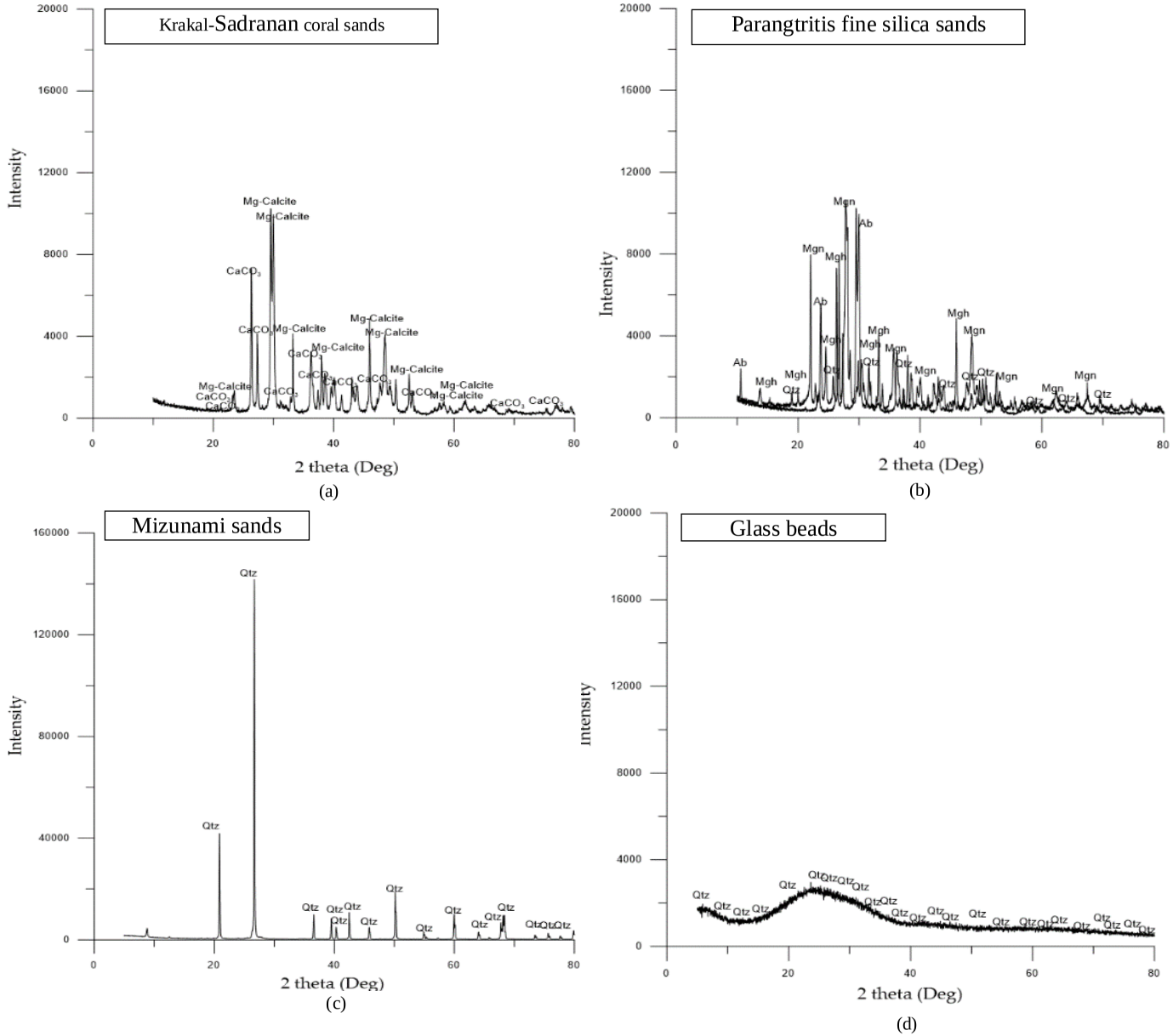


Figure 6.2. XRD pattern of (a) Krakal-Sadranan coral sands consist of $CaCO_3$ and Mg-Calcite; (b) Parangtritis sand with Ab (albite), Qtz (quartz), Mgh (maghemite), and Mgn (magnetite); (c) Mizunami sand consist of quartz; and (d) Glass beads with quartz consisted.

6.3.2 MICP treatment and reagents

The columns specimens were prepared using syringe molds (diameter of 3 cm, height of 6 cm) at a relative density of around 60%. As conceptually illustrated in Figure 6.3, the column specimens are considered to be simulating the slope surface (real field) to be treated. The MICP treatment was performed to the sand by using a simple two-phase surface percolation technique as proposed in the previous work (Cheng and Cord-Ruwisch, 2014). The MICP set up is also graphically depicted in Figure 6.3, together with the image of treated columns. At the first phase, the bacteria which had been cultivated in ZoBell2216E agar medium for marine bacteria and being incubated at 30 °C for 3 days. The cells cultured were ureolytic bacteria in ZoBell2216E media, which also contained 5.0/L hipolypeptone (Nihon Seiyaku Co., Ltd., Tokyo, Japan), 1.0 g/L $FePO_4$ (Junsei Chemical Co., Ltd., Tokyo, Japan), and 1.0 g/L yeast extract (BD Bioscience Adv., Bioprocessing, Miami, Florida, USA). These were prepared with artificial seawater with pH 7.6–7.8, adjusted using 1 M NaOH under shaking incubation (30°C, 160 rpm) were harvested at the OD_{600} of 1.8 – 2.6, and applied on the surface of the specimens to percolate under the gravitational and capillary forces. Around 2 – 3 hours were given to a better immobilization of bacteria cells with sand grains.

At the second phase, the cementation solution comprised of $CaCl_2$ (55.5 g/L), urea (60 g/L) and nutrient broth (6 g/L) was injected under the saturated conditions. The treatment was performed for 14 days, in which the cementation solution was injected every 24 hours. As the performance of the bacteria decrease gradually with the time (typically become insignificant after 14 days) (Martinez et al., 2013), the biological injection was once again performed after 7 days of the treatment. In this study, different treatment levels were achieved by controlling

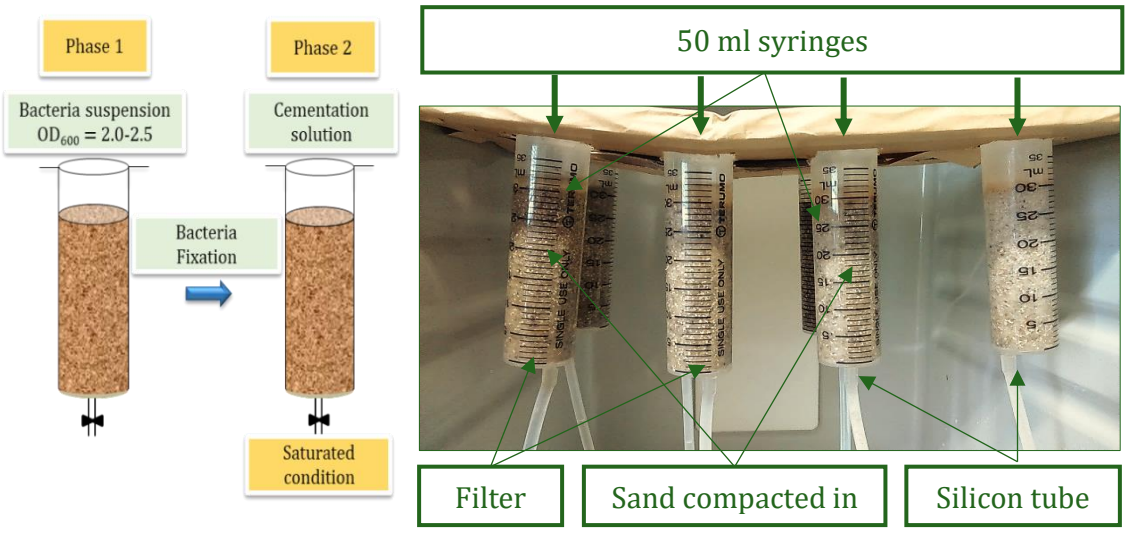


Figure 6.3. Conceptual illustration of MICP treatment by laboratory scale (columns specimens)

the number of cementation solution injections. Around 10, 15%, and 20%, of $CaCO_3$ (by weight) were achieved by 7, 14 and 21 injections of cementation solution respectively. The $CaCO_3$ content precipitated in the specimens were measured by typical acid washing method (Fukue et al., 2011), and the carbonate contents are presented as the ratio between the weight of precipitated carbonate and the weight of the uncemented dry soil. After the treatment process, the samples were rinsed with enough distilled water to remove the unreacted salts. Finally, the molds were cut, taken out, and carefully trimmed to make the surfaces flat and smooth before subjected to the wetting-drying experimentation. Two different sets of specimens treated identically were separately experimented for wetting-drying tests under salt-water and distilled water saturated.

6.3.3 Statistical analysis wetting-drying (WD) test

As there are no standards available for bio-cemented specimens, WD test was performed according to the standard suggested to the conventionally cemented soils (ASTM D559-03, 2003). During the wetting process, specimens were inundated at room temperature (25±1 °C) for 6 hours, followed by the oven dry at 70 ±1 °C for 48 hours (drying process). Specimens were subjected to the total number of twenty-one WD cycles.

6.3.4 XRD evaluation of specimens

Morphology of the precipitated $CaCO_3$ crystals before and after WD test was investigated by using scanning electron microscopy (SEM;Miniscope TM3000, Hitachi, Tokyo, Japan). X-ray diffraction (XRD; MiniFlex™, Rigaku Co., Ltd., Tokyo, Japan) analysis was conducted to identify the polymorphs of the precipitated $CaCO_3$.

6.3.5 Rock properties evaluation of specimens

During both WD experimentation, the physical and mechanical changes of specimens were determined by measuring mass loss and S-wave velocity (SonicViewer-SX: 5251, Japan). The uniaxial compressive strength (UCS) tests were performed to the specimens before and after subjected to the cyclic tests by using needle penetrometer (JGS 3431-2012, 2012). The needle penetration test is an International Society for Rock Mechanics (ISRM) recommended method for determining UCS of soft, weak to very weak rocks and cemented soil specimens.

6.4 Results and discussions

6.4.1 Aggregate stability

The physical damage during cyclic tests was evaluated by the mass loss of the specimens. The mass loss was carefully measured after every cycle with neither any structural damages nor considerable changes in temperature. Figure 6.4 shows the mass loss of the specimens subjected to cyclic WD action. The results suggest that the mass loss by the end of 21 WD cycles is less than 40% in all three levels of cementation, and the influence of precipitated calcium carbonate content against WD effects is likely to be not very significant. Case of WD based on distilled water is less than 25% in all three levels of cementation. It is clearly perceived that the degradation mechanisms of MICP specimens under WD cycles is different. During the WD test, regardless of cementation levels, rate of mass loss was high at the beginning (within couple of WD cycles) and remained relatively stable during subsequent cycles. This could possibly be attributed to the suspension of feeble deposits of calcium carbonates. During the MICP treatment, the calcium carbonate is precipitated in various forms such as primary bonds (strongly forms at particle contacts), individual crystals and accumulation (on the grain surface), amorphous and powdery deposits (Lin et al., 2016; Wang et al., 2019). In fact, these powdery bonds are often formed when the carbonates are deposited at its early stage of the crystallization. When the specimens are submerged during the wetting, the water penetrates the specimen and drives the powdery deposits to fall into suspension. This corrosion mechanism is similar to that reported to the calcarenite rocks (Ciantia, et al., 2015). The MICP treated soils have porous structure. In fact, the resultant stress acting on soil particles are distributed to the connections around them i.e. to the calcium carbonate bonds. When the acting tensile stresses exceed the maximum tensile strength of carbonate bonds, the bonds would start cracking. For the specimens cemented to ~10% carbonate, the bonds were weak, resulted the highest disintegration of aggregates (around 50%). But, for the specimens treated to 20% carbonate, the contact strength could be adequate to resist the stresses developed during WD, resulted negligible loss of aggregates (around 5%). But conversely, severe erodibility of MICP slope soil is evidenced under cyclic WD effects. However, the WD induced erosion could be controlled by treating the soil with appropriate quantity of calcium carbonate cement.

6.4.2 Mechanical characteristics

The influence of WD action on the mechanical behavior of MICP specimens was evaluated through S-wave velocity and UCS. Previous researchers have demonstrated that the S-wave velocity is a credible measure which can be used to assess particularly the particle connections

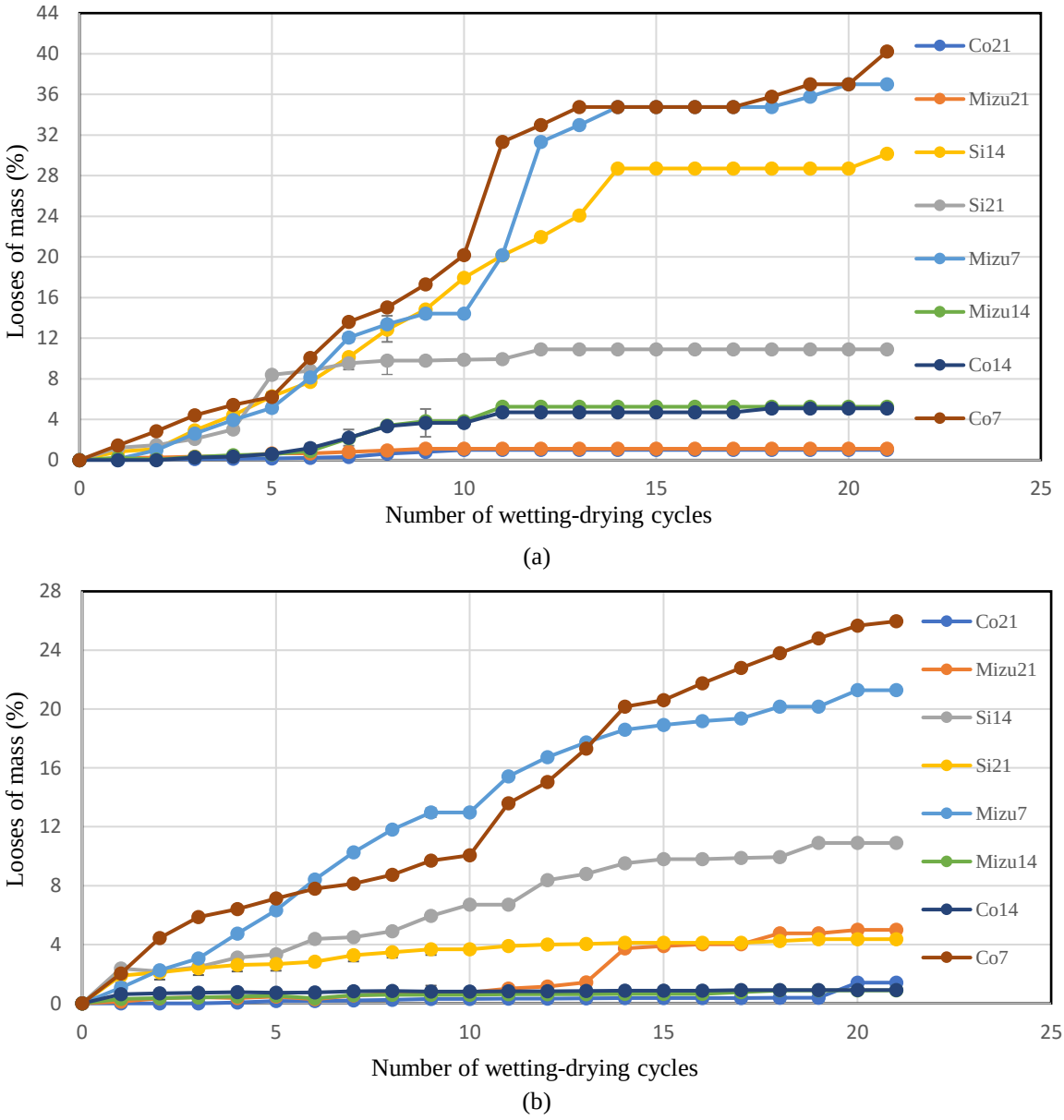


Figure 6.4. Average mass loss of the specimens subjected to WD cyclic treatments based on (a) saltwater and (b) distilled fresh water. With Co = coral sand; Si = silica sand; Mizu = Mizunami.

in MICP specimens (Feng and Montoya, 2017). Table 6.1 presents the S-wave velocity values of the specimens before and after subjecting to WD cycles. Overall, it can be seen that the S-wave velocity reduced significantly in both WD action, suggesting that particle connections have been deteriorated in both cases. It should be noted that the S-wave velocity of untreated slope soil ranges between 150 and 200 m/s (Gowthaman, et al., 2019). Meanwhile the natural beachrock in the shore bay ranges between 1330 to 2920 m/s (Daryono, et al., 2020). When the soil particles are connected by calcium carbonate bio-cement, the transmission of S-waves increases, leading to the increase in S-wave velocity values with respect to the level of cementation. However, when the connections are degraded and/or deformed under the both

cyclic treatments, the velocity values tended to decrease. The UCS measurements, illustrated in Figure 6.5, also show the similar tendency of S-wave velocity. It can be observed that the decrease in UCS values is lower when exposed to WD cycles under saltwater condition (red bars) compared to that under distilled water (grey bars). As explained in the previous section, the corrosion of powdery and weak deposits caused the mass loss, and that would also considerably affect the mechanical responses. Regardless of weak or strong, if the carbonates deposit at or near particle contacts, they contribute to the strengthening of MICP soil skeleton by supporting primary bonds.

When the suspension of those weak deposits occurs, there would be a weakening in primary chains in sand particles, leading to the decrease in UCS and S-wave velocities (Figure 6.5 and Table 6.1, respectively). Mechanical damage of MICP specimens appears to be higher under the exposure to WD cycles under saltwater condition. As explained in the previous section, when the porewater undergoes freezing process, uneven tensile stresses are developed around the soil particles, leading to the formation and the growth of microcracks. Consequently, the MICP skeleton gets weakened, could be able to withstand only lower compression stresses compared to that of unexperimented. In fact, the resistance to the WD damage depends on the porosity of the soil matrix. Higher porosity permits more and rapid transfer of water through the soil matrix, which could aid to prevent the damages WD effects. However, in the case of MICP, soils of less porosity i.e. fine-grained soils were more durable against the WD actions compared to that of coral-grained soils i.e. soils of higher porosity (Cheng et al., 2016). This is

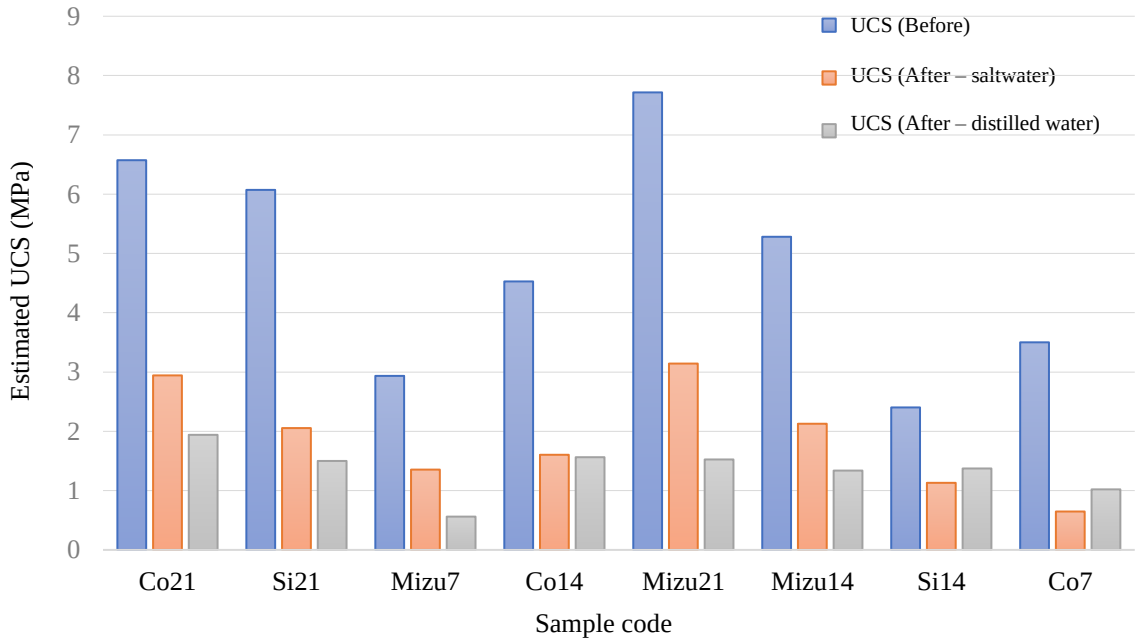


Figure 6.5. The variation of estimated UCS before and after the exposure of cyclic WD tests. With Co = coral sand; Si = silica sand; Mizu = Mizunami.

due to the fact that the number of contacts of each soil grain increase with the decrease in porosity. In the case of fine-grained soils, higher number of particle contact points facilitated to increased MICP bridges, which reduce the acting tensile stresses per connection, withstanding long WD cycles. The soil investigated herein also fine-grained soil. And, the specimens were investigated herein up to its possible optimum cementation level in order to assess the fullest feasibility. It also should be noted that when the specimens were treated over 20 – 23% by calcium carbonate, bio-clogging stage was frequently achieved similar to that reported by (Cheng and Cord-Ruwisch, 2014).

Table 6.1. The S-wave velocity values before and after subjected to WD test.

		21 WD cycles		
	Code sample	Before	After (saltwater)	After (distilled water
Average S-wave velocity (m/s)	Co21	1960	1355	1120
	Si21	1765	1135	960
	Mizu7	1200	932	600
	Co14	1440	1013	1000
	Mizu21	2090	1435	1000
	Mizu14	1970	1135	900
	Si14	1125	789	870
	Co7	1282	613	770

6.4.3 Strength deterioration ratio (SDR)

In order to better understand the effect of precipitated calcium carbonate content against mechanical degradation, SDR values under cyclic treatments are computed by using the following relationship (Eq. 6.1).

$$SDR = 1 - \frac{UCS_{(f)}}{UCS_{(i)}} \quad \text{(Eq. 6.1)}$$

SDR is the simplified measure, typically used to explain the deterioration of specimens exposed to cyclic treatments and had been broadly used by researchers for soft to hard rock materials (Hale and Shakoor, 2003; Khanlari and Abdilor, 2015). The $UCS_{(f)}$ represents the compressive strength at the end of the cyclic treatment and $UCS_{(i)}$ represents the compressive strength of virgin MICP specimens. The *SDR* varies between "0" and "1". A rating of "1" is allotted to the weakest specimen, reveals complete degradation at the end of the cyclic treatment. For the strongest specimens, which do not show any damages after the treatment, a rating value of "0" is allotted. The calculated *SDR* values of the samples subjected to cyclic WD cycles are plotted in Figure 6.6, together with the *SDR* values of various sandstones material obtained from the literature (Khanlari and Abdilor, 2015). The SDR_{WD} values of sandstones (subjected to 30 WD cycles) range between around 0.1 and 0.2. Comparatively, MICP specimens show higher

deterioration under WD cycles (SDR_{WD} of 0.53 – 0.82 for saltwater and 0.43 – 0.81 for distilled water), suggesting that MICP cemented soils are more susceptible than sandstones. It can also be seen that the SDR_{WD} values increase with the increase in calcium carbonate content. This can be explained by the high deposition of weaker carbonates at heavy treatment. As explained

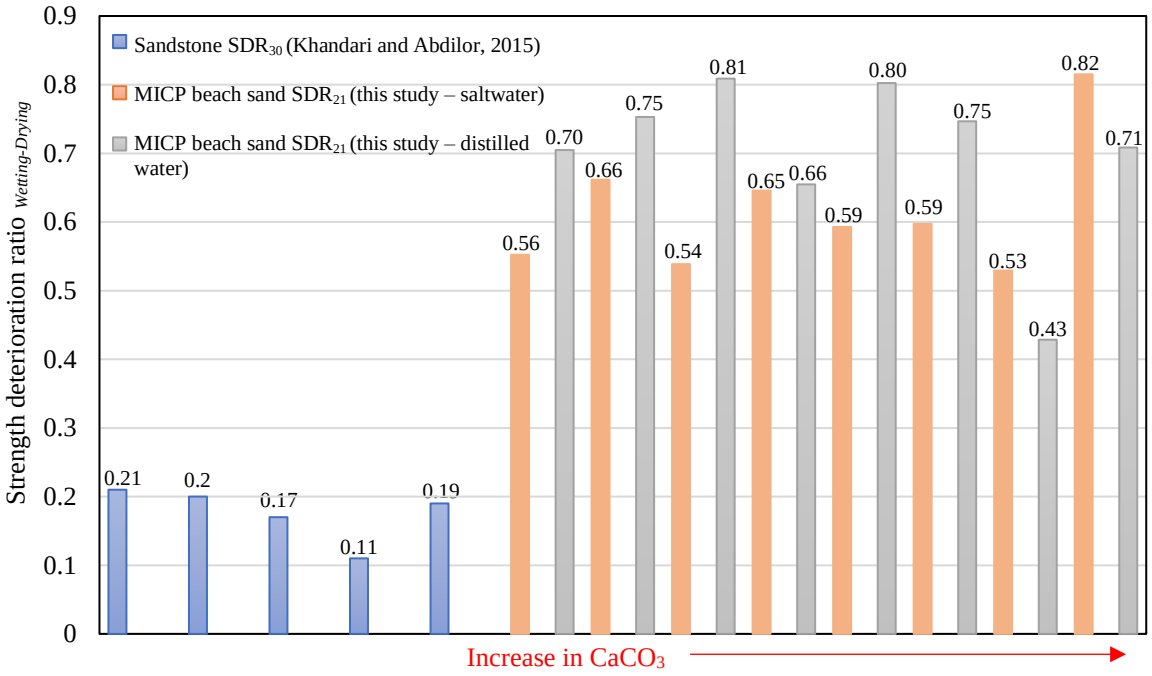


Figure 6.6. The variation of estimated UCS before and after the exposure of cyclic WD tests.

earlier, MICP treatment results the formation of both strong and weak carbonates. Longer treatment to achieve high cementation level not only strengthens the primary bonds, but also increase the deposition of weak and powdery carbonates. However, the WD effects cause the suspension and disintegration of such weak deposits which had been supporting the primary bonds. Moreover, as suggested by Li et al. (2019), the fatigue stresses developed during the cycles could also affect the mechanical responses. As the thermal expansion coefficients of calcium carbonate and slope soil are different, irregular internal stresses could be developed, which possibly led to the deformations in particle contacts and deteriorated the specimens. When the specimens are cemented heavily (~20% of $CaCO_3$), the particle connections become stronger, which provide significant resistance to the tensile stresses developed during the freezing of porewater. However, the formation of microcracks and ruptures at sand-calcium carbonate tended to decrease the mechanical behaviors of the MICP specimens.

The natural beachrock were mostly consist of magnesian calcite (high – low) depend on the sedimentary location which key role the natural beachrock can occur in the shore bay. Other minerals also found from XRD results such as Anorthite; Omphacite; Dolomite; and Diopsite

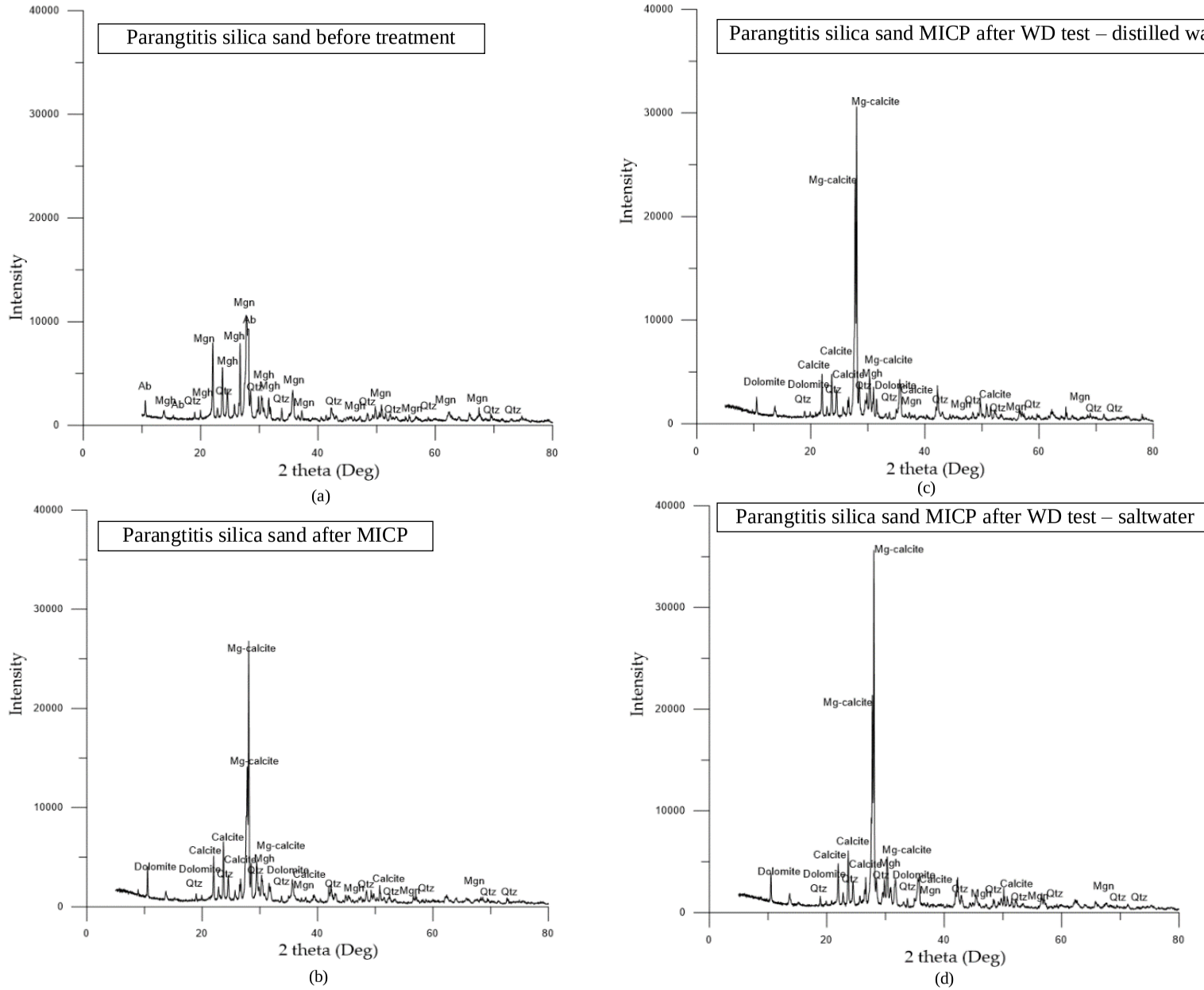


Figure 6.7. Graphic XRD analysis pattern using artificial beachrock (a) before MICP treatment, (b) after MICP treatment, (c) MICP treated after 21 WD cycle under distilled water, and (d) MICP treated after 21 WD cycle under saltwater. With Ab (albite), Qtz (quartz), Mgh (maghemite), and Mgn (magnetite).

that might effect of the SiO_2 in the materials. Figure 6.7 shown the XRD results of original silica sand, after MICP treatment, and after WD test for 21 cycles. The mineralogy inside the samples was found almost similar than before WD test was conducted, the significant difference especially strength of materials which is crystals bonding intra particles were loses than before because of WD cycle test. The higher damage was found in the fine material sands (11~28 %, respectively) with 0.6 mm, it is easily diluted in the water. Other results under different sand materials were similar as silica sands, which is not affect significantly the WD cycles for the mineralogy of the material (see Appendixes E for XRD results of other material). WD cycles might cause deionized of the calcium carbonate chain (reverse reactions of Eqs. 6.1 and 6.2) which came from the evaporation process of H_2O presence. Heavy damage found in the saltwater WD test because of H_2O ions and Na^+ (NaCl and Na_2SO_4) were found in the saltwater (Chierici and Fransson, 2009; Shahidzadeh-Bonn, et al., 2010) (Figure 6.8).

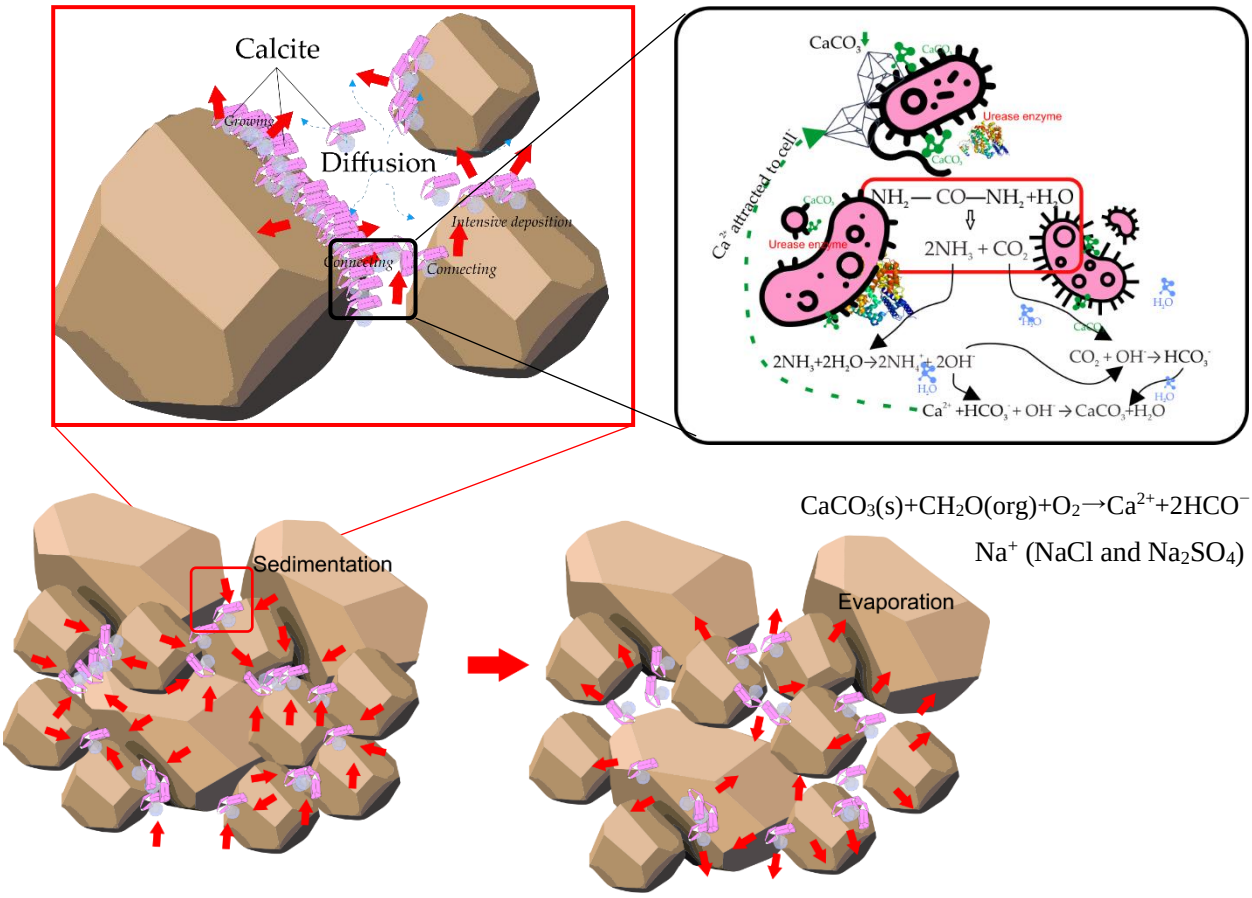


Figure 6.8. Illustration scheme of WD damages mechanism

The relationship between number of samples were shown in the Figure 6.9 regarding the estimated UCS versus calcium carbonate content of MICP using indigenous ureolytic bacteria were isolated from natural beachrock in Krakal-Sadranan, Indonesia. The samples was treated

with MICP period 7 days equal with the calcium carbonate content less than 0.15 g/ g sands materials, also for 14 days of curing MICP with the calcium carbonate content around 0.15 – 0.2 g/ g sand materials, and for the last 21 days of MICP treatment were consist with the calcium carbonate content more than 0.2 g/g sand materials. This total of the calcium carbonate content also can be mention as percentage of calcium carbonate based on gram of $CaCO_3$ ratio with original gram of sand materials.

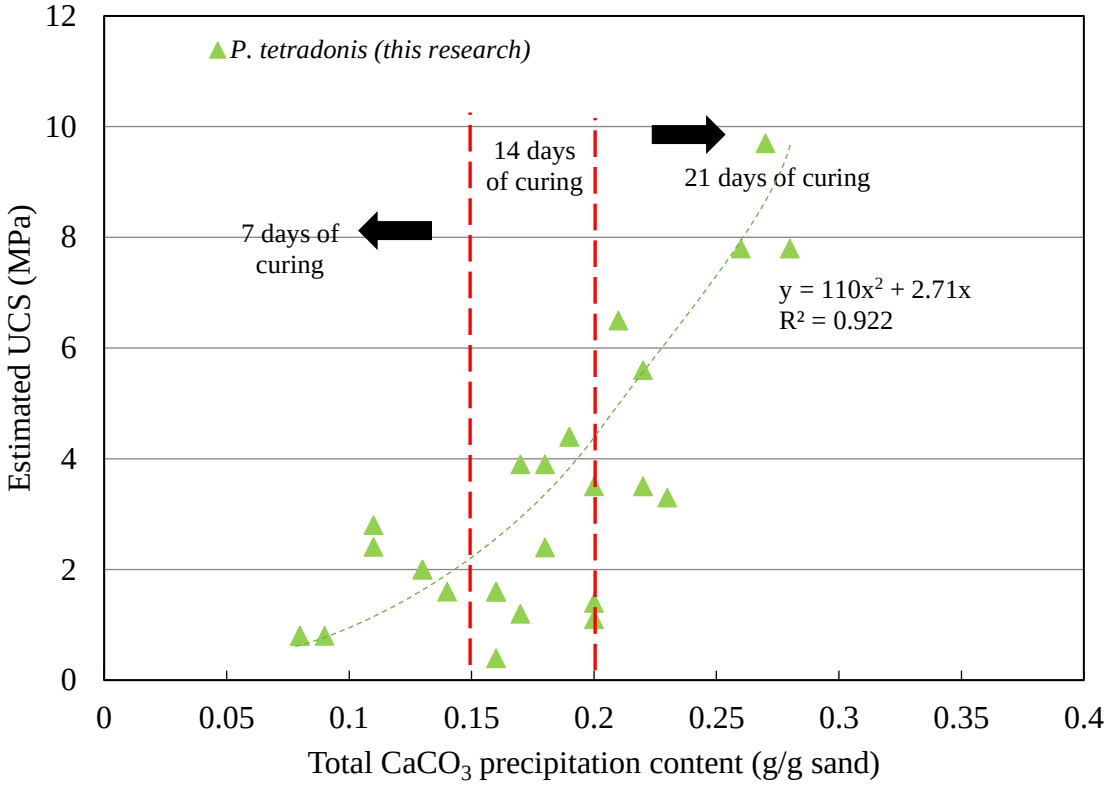


Figure 6.9. Relationship between estimated UCS versus calcium carbonate content of MICP treatment period

6.5 Conclusions

Experimental work presented in this paper investigated the physical and mechanical characteristics of MICP treated slope soil subjected to WD cyclic action. Based on the results, it can be concluded that the damages were higher to the specimens subjected to WD cycles under saltwater condition compared to those subjected to distilled WD cycles. The saltwater WD induced erosion is highly reliant on the level of cementation. The increase in precipitated calcium carbonate content substantially increased the aggregate stability of specimens under the exposure of WD cycles. On the other hand, the level of cementation was not significantly influencing the WD induced erosion, which is less than 40% for saltwater condition and less than 30% for distilled water condition. SDR values suggest that the MICP specimens

underwent severe degradation under saltwater WD cycles (over 40%). Comparatively, the reduction of UCS is low under WD cycles (between around 40 – 55%). Under both WD cycles, the strength deterioration likely to be in a relationship with the precipitated calcium carbonate content. The period of MICP treatment and source of sand material have a significant influence for durability after treated by MICP. Roughly hypothesis, the WD durability tested is represented the real-field implementation period indicated with wet-dry raining season. However, although, MICP for drowned system in the shoreline is necessarily deep investigation in the future to achieve sustainable and feasible material for against the coastal erosion problems. Minimum calcium carbonate content for ground improvement in the coastal areas should have a limit of no more than 15 % of the calcium carbonate cement material.

References

Achal, V., Kawasaki, S., 2016. Biogrout: A novel binding material for soil improvement and concrete repair. Front. Microbiol. 7.

Arya, I.W., Wiraga, I.W., Suryanegara, I.G.A.G., 2018. Effect of cement injection on sandy soil slope stability, case study: Slope in Petang district, Badung regency. J. Phys. Conf. Ser. 953.

ASTM D559-03, 2003. Standard Test Methods for Wetting and Drying Compacted Soil-Cement Mixtures. In: ASTM International, West Conshohocken, PA, West Conshohocken PA, United States.

Cheng, L., Cord-Ruwisch, R., 2014. Upscaling Effects of Soil Improvement by Microbially Induced Calcite Precipitation by Surface Percolation. Geomicrobiol. J. 31, 396–406.

Cheng, L., Shahin, M.A., Mujah, D., 2016. Influence of Key Environmental Conditions on Microbially Induced Cementation for Soil Stabilization. J. Geotech. Geoenvironmental Eng. 143, 04016083.

Chierici, M. and Fransson, A., 2009. Calcium carbonate saturation in the surface water of the Arctic Ocean: undersaturation in freshwater influenced shelves. Biogeosciences, 6(11).

Chirico, G.B., Borga, M., Tarolli, P., Rigon, R., Preti, F., 2013. Role of Vegetation on Slope Stability under Transient Unsaturated Conditions. Procedia Environ. Sci. 19, 932–941.

Ciantia, M.O., Castellanza, R., Crosta, G.B., Hueckel, T., 2015. Efects of mineral suspension and dissolution on strength and compressibility of soft carbonate rocks. Eng. Geol. 184, 1–18.

Daryono, L.R., Nakashima, K., Kawasaki, S., Titisari, A.D. and Barianto, D.H., 2020. Sediment Characteristics of Beachrock: A Baseline Investigation Based on Microbial Induced

Carbonate Precipitation at Krakal-Sadranan Beach, Yogyakarta, Indonesia. Applied Sciences, 10(2), p.520.

Daryono, L.R., Titisari, A.D., Warmada, I.W. and Kawasaki, S., 2019. Comparative characteristics of cement materials in natural and artificial beachrocks using a petrographic method. Bulletin of Engineering Geology and the Environment, 78(6), pp.3943-3958.

DeJong, J.T., Mortensen, B.M., Martinez, B.C., Nelson, D.C., 2010. Bio-mediated soil improvement. Ecol. Eng. 36, 197–210.

Feng, K., Montoya, B.M., 2017. Quantifying Level of Microbial-Induced Cementation for Cyclically Loaded Sand. J. Geotech. Geoenvironmental Eng. 143, 06017005.

Fukue, M., Ono, S.-I., Sato, Y., 2011. Cementation of Sands Due to Microbiologically Induced Carbonate Precipitation. Soils Found. 51, 83–93.

Gowthaman, S., Iki, T., Nakashima, K., Ebina, K., Kawasaki, S., 2019. Feasibility study for slope soil stabilization by microbial induced carbonate precipitation (MICP) using indigenous bacteria isolated from cold subarctic region. SN Appl. Sci. 1, 1480.

Gowthaman, S., Mitsuyama, S., Nakashima, K., Komatsu, M., Kawasaki, S., 2019. Biogeotechnical approach for slope soil stabilization using locally isolated bacteria and inexpensive low-grade chemicals: A feasibility study on Hokkaido expressway soil, Japan. Soils Found. 59, 484–499.

Gowthaman, S., Nakashima, K., Kawasaki, S., 2018. A state-of-the-art review on soil reinforcement technology using natural plant fiber materials: Past findings, present trends and future directions. Materials. 11, 553.

Guerra, A.J.T., Fullen, M.A., Jorge, M. do C.O., Bezerra, J.F.R., Shokr, M.S., 2017. Slope Processes, Mass Movement and Soil Erosion: A Review. Pedosphere 27, 27–41.

Hale, P.A., Shakoor, A., 2003. A laboratory investigation of the effects of cyclic heating and cooling, wetting and drying, and freezing and thawing on the compressive strength of selected sandstones. Environ. Eng. Geosci. 9, 117–130.

JGS 3431-2012, 2012. Japanese Standards and Explanations of Geotechnical and Geoenvironmental Investigation Methods, No. 1. In: JGS Publication (in Japanese), Tokyo, 426–432.

Jiang, N.-J., Tang, C.-S., Yin, L.-Y., Xie, Y.-H., Shi, B., 2019. Applicability of Microbial Calcification Method for Sandy-Slope Surface Erosion Control. J. Mater. Civ. Eng. 31, 04019250.

Khanlari, G., Abdilor, Y., 2015. Influence of wet–dry, freeze–thaw, and heat–cool cycles on the physical and mechanical properties of Upper Red sandstones in central Iran. Bull. Eng.

Geol. Environ. 74, 1287–1300.

Kumar, N., Das, D., 2018. Nonwoven geotextiles from nettle and poly (lactic acid) fibers for slope stabilization using bioengineering approach. Geotext. Geomembranes 46, 206–213.

Li, Y., Shi, T., Li, Y., Bai, W., Lin, H., 2019. Damage of magnesium potassium phosphate cement under dry and wet cycles and sulfate attack. Constr. Build. Mater. 210, 111–117.

Lin, H., Suleiman, M.T., Brown, D.G., Kavazanjian, E., 2016. Mechanical Behavior of Sands Treated by Microbially Induced Carbonate Precipitation. J. Geotech. Geoenvironmental Eng. 142, 04015066-1–13.

Martinez, B.C., DeJong, J.T., Ginn, T.R., Montoya, B.M., Barkouki, T.H., Hunt, C., Tanyu, B., Major, D., 2013. Experimental Optimization of Microbial-Induced Carbonate Precipitation for Soil Improvement. J. Geotech. Geoenvironmental Eng. 139, 587–598.

Shahidzadeh-Bonn, N., Desarnaud, J., Bertrand, F., Chateau, X. and Bonn, D., 2010. Damage in porous media due to salt crystallization. Physical Review E, 81(6), p.066110.

Tang, C.S., Wang, D.Y., Shi, B., Li, J., 2016. Effect of wetting-drying cycles on profile mechanical behavior of soils with different initial conditions. Catena 139, 105– 116.

van Paassen, L.A., Ghose, R., van der Linden, T.J.M., van der Star, W.R.L., van Loosdrecht, M.C.M., 2010. Quantifying Biomediated Ground Improvement by Ureolysis: Large-Scale Biogrout Experiment. J. Geotech. Geoenvironmental Eng. 136, 1721–1728.

Wang, Y., Soga, K., Dejong, J.T., Kabla, A.J., 2019. Microscale Visualization of Microbial-Induced Calcium Carbonate Precipitation Processes. J. Geotech. Geoenvironmental Eng. 145, 1–13.

Zhang, X., Hu, M., Guo, X., Yang, H., Zhang, Z., Zhang, K., 2018. Effects of topographic factors on runoff and soil loss in Southwest China. Catena 160, 394–402.

CHAPTER 7

MICP beach sand treatment using cheap chemical reagents

7.1 Introduction

Up to now, many studies have focused on MICP based soil stabilization in order to mitigate the potential of erodibility. Most of them have been performed based on a bioaugmentation strategy by introducing non-native ureolytic bacteria to the soil or sand. Among them, *Sporosarcina pasteurii* is the most researched bacterium: it enables a highly active urease enzyme associated with urea hydrolysis (Gomez et al., 2013). The solidification of sand using *S. pasteurii* allows for significant control of surficial sediment erosion (Bao et al., 2017; Salifu et al., 2016) and reduces hydraulic conductivity while increasing the confined compressive strength (Jiang and Soga, 2017; Whiffin et al., 2007). Also, *S. pasteurii* was shown to form an impermeable stiff crust with a thickness of 2.5 cm which increases resistance to erosion (Gomez et al., 2013). Cheng et al. (2014) reported that *Bacillus sphaericus* can enhance the strength of silica sand with relatively retained permeability when 10 mM urea concentrated artificial sea water was used as cementation solution.

Despite numerous attainable outcomes of this technology at laboratory-scale, MICP is still considered expensive for commercial implementation or field-scale applications (Mujah et al., 2017). One of the reasons is due to the nutrient medium used in the biotechnological process for bacteria cultivation (Achal et al., 2009). The use of laboratory-grade growth media (i.e. nutrient broth, yeast extract and tryptic soy broth) are a major cost factor for bacterial cultivation due to their high cost that can reach up to 60% of the total production cost (Kristiansen, 2006).To date, only limited studies in the literature have reported the use of alternative nutritional sources to cultivate ureolytic bacteria for MICP application. The use of waste materials such as chicken manure effluent, corn steep liquor, lactose mother liquor and activated sludge from agricultural, dairy and bakery industries have been the focus of alternative nutritional source (Achal et al., 2010, 2009; Cuzman et al.,2015a; Joshi et al., 2018; Whiffin, 2004; Yoosathaporn et al., 2016).These attempts are mostly performed to limit the economic challenges faced for cultivating ureolytic bacterial in large volume (Anbu et al.,2016). Irrespective of the promising findings which have been reported in the aforementioned studies for bacterial cultivation and also help minimize accumulative environmental wastes through recycling (Yoosathaporn et al., 2016). Unfortunately, most recent contemporary studies on MICP still make use of conventional growth media to grow

various ureolytic bacterial species.

However, the bio-augmentation of exogenous bacteria which have not been adapted to native environment is associated with uncertainties in bacterial survival and performance (Sensoy et al., 2017). On the other hand, a very few studies have been attempted to investigate the feasibility of bio-augmentation using indigenous bacteria (Danjo and Kawasaki, 2016; Khan et al., 2016; Stabnikov et al., 2011). Actually, bio-augmentation (the process includes the isolation of bacteria, culture enrichment, and supply back into the ground) conceptionally differs from bio-stimulation strategy in which the indigenous ureolytic bacteria are stimulated in situ. Danjo and Kawasaki (2016) and Khan et al. (2016) investigated the feasibility of artificial beach rock formation as the mitigation measure for coastal erosion by augmenting native *Pararhodobactor* sp. isolated from the native sand of Okinawa, Japan. Similarly, using native *Bacillus* sp. VS1, relatively impermeable biocemented crust (maximum flexural strength of 35.9 MPa; permeability of 1.6 10 7 m/s) has been achieved on the native sand surface for aquaculture pond construction (Stabnikov et al., 2011). The use of natively adapted bacteria is likely to be both more effective and more appropriate in regions with fluctuating cold climatic conditions, as the urease enzymes of most of the bacteria are temperature-sensitive and can readily be denatured by changes in the environmental temperature. However, due to the uneven presence of ureolytic bacteria in natural soil, stimulating the indigenous bacteria has been reported to result in diffuse zones of improvement with high variability even within the same region (Gomez et al., 2017). At the same time, augmentation has been shown to result in more uniform improvement on a more localized scale due to the reduction in soluble calcium concentrations transported to greater distances (Danjo and Kawasaki, 2016; Gomez et al., 2017). As this research aims for the uniform surface stabilization of slopes, the bioaugmentation of indigenous bacteria is likely to be the better choice among the strategies discussed above.

In fact, the feasibility of MICP does not depend on technical aspects regarding conditions of treatment alone but accompanies by economical and legislative issues as well. It has been reported that the discharging of vigorous chemicals and ammonium by-products to the soil-ecosystem in the MICP causes many harmful effects, and the subsequent removal of such harmful products must be taken into account (Soon et al., 2014). The cost of the required substances remains another contest in assessing the complete feasibility of the process (van Paassen et al., 2010). There are some suggestive drawbacks that can hinder the use of waste materials for MICP applications which includes: (i) limited quality control and processing (Williams et al., 2016); (ii) unavailability in localized regions; (iii) insufficient bulk quantity

(i.e. large volume) and (iv) transportation to site. Hence, there is a need to explore other types of nutrition sources which are easily accessible at low or no cost suitable for MICP application.

7.2 Objectives

The aim of this present study was to determine the feasibility of cultivating *P.tetradonis* strain in an economical food-grade yeast extract (Beer yeast and tempeh starter) medium and investigate its effect on bacterial production, urease activity and biocalcification. The performance of cheap chemical reagents was compared with laboratory-grade growth media, same protocol also conducted for cementation solution whereas laboratory-grade cementation solution with low-grade chemical reagents (snow melting agent and chalk powder extract). XRD analysis was further used to determine the elemental compositions and identify the polymorphs of $CaCO_3$ precipitates after biocalcification test. In the same way, we conducted after treatment test of solidification samples with low-grade chemicals treatment within statistical analysis of wetting-drying test to enhance the possibility of materials durability strength. Therefore, the influence of variable wet-dry cycles on the physical and mechanical characteristics of MICP treated slope beach sand, representing the erosion shoreline slope in the coastal area. The goal of this paper is to perform the efficiency of low-grade chemical solution and durability of the specimens in term of cost reduction the treatment soil/ sands.

7.3 Materials and methods

7.3.1 Ureolytic bacteria and cultivation

Ureolytic bacteria *P. tetradonis* isolated by Daryono, et al. (2020) from beachrock sample from Indonesia shoreline was used in this study due to its high urease activity. The bacterium was revived in Petri dishes containing sterile ZoBell2216E agar medium (for marine bacteria, pH 7.7). The Petri dishes were incubated at 30°C for 48 h under aerobic conditions and the grown colonies were subsequently sub-cultured until pure isolates were obtained. *P. tetradonis* are gram-negative specified with the former are motile bacilli 1 μm wide and 1.5–4.0 μm, whereas the latter are strictly aerobic, motile with one polar flagellum, form either straight rods (or rod-shapes), 0.5–0.8 × 1.0–1.5 μm when in exponential growth phase.

7.3.2 Culture medium

Is also called as *nutrient broth*, solution freed of all microorganisms by sterilization (usually in an autoclave, where it undergoes heating under pressure for a specific time) and containing

the substances required for the growth of microorganisms such as bacteria, protozoans, algae, and fungi. The medium may be solidified by the addition of agar. Some media consist of complex ingredients such as extracts of plant or animal tissue (e.g., peptone, meat extract, yeast extract); others contain exact quantities of known inorganic salts and one or more organic compounds (synthetic or chemically defined media).

7.3.2.1 Zobell2216 medium marine broth

Microorganisms in an aquatic environment may occur at all depths ranging from the surface region to the very bottom of the ocean trenches. The top layers and the bottom sediments harbor higher concentration of microorganisms (Pelezar, et al., 1977). Marine microorganisms are vital to ecological cycles because they form the foundations of many food chains (Alcamo, 2001). Zobell Marine Broth formulated by Zobell (1941), has a composition that mimics seawater (Lyman and Fleming, 1940) and thus helps the marine bacteria to grow abundantly. This medium has been used for the growth of marine bacteria (Sizemore and Stevenson, 1970; Weiner, et al., 1985). Zobell Marine Broth contains the nutrients, which are required for the growth of marine bacteria. These media have minerals as in seawater (Zobel, 1940) and peptone and yeast extract as the sources of nutrients for the marine bacteria as reported by Jones (1960). High amount of salt content is used to simulate seawater. Other minerals are used to mimic the mineral composition of seawater. The composition of Zobell2216 medium marine broth were described in the Table 7.1.

Table 7.1. Composition make culture medium

Composition (solvent by artificial seawater) for 1L Medium	
Chemical Compose	**Concentration Solution Unit**
Polypeptone	5.0 g/ L
Yeast extract	1.0 g/ L
$FePO_4$ Phospate Tetrahedraite	197 g/ L
Agar (solidify the medium)	15.0 g/ L

7.3.2.2 Beer yeast extract

Beer production is an important economic activity in many countries, especially in Japan. Consequently, plenty of beer yeasts, being the second major by-product from brewing industry, is generated and either thrown out or fed to livestock and fowl. This not only results in a series of environmental problems, but also causes an enormous waste of resources (Yang et al., 2006). In general, beer yeast is mainly composed of 48–55% protein, 23–28% carbohydrate, 6–8% RNA, 1% glutathione, and 2% vitamin B. Moreover, they are rich in P, K, Ca, Fe, P and Mg

(Liu et al.,2012). The detail composition of beer yeast is shown in the figure 7.1. The culture with this reagent made with 30 gr of beer yeast mixed into 1L of the artificial seawater solution (See table 5.1).

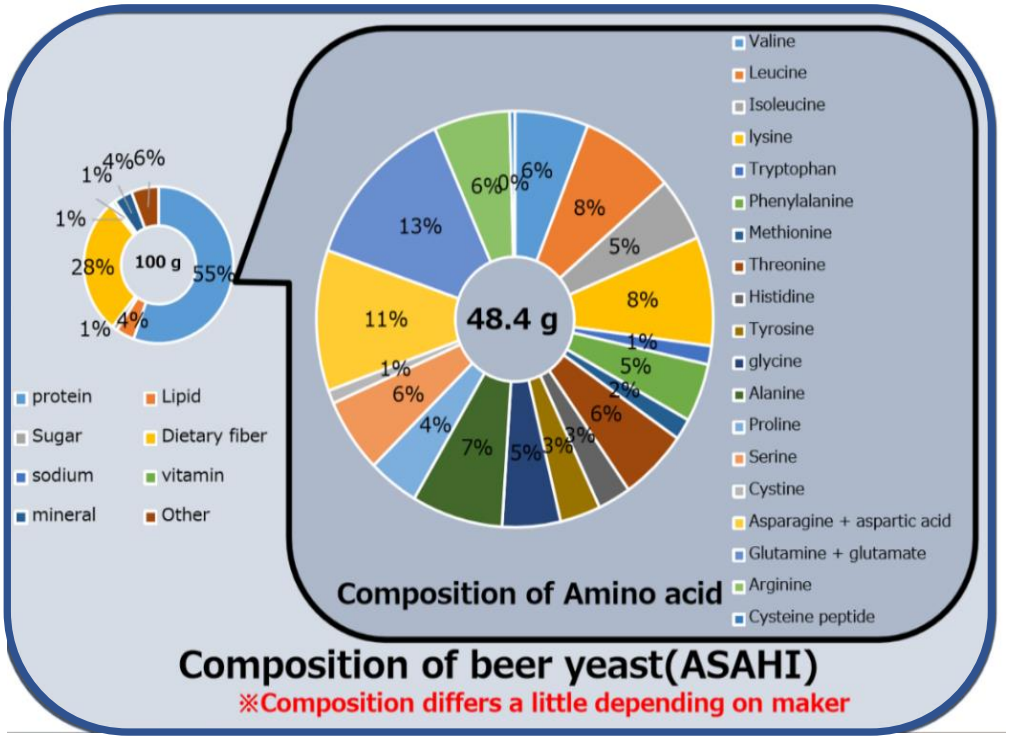


Figure 7.1. Beer yeast composition (Asahi Group Research & Development, 2019)

7.3.2.3 Tempeh starter

Tempeh (pronounced TEM-pay) is a mold-fermented soybean food. Occasionally other legumes, seeds, and cereal grains are also used along with soybeans. The mold fermentation results in a matrix of dense, cottony, mycelia in which cooked soybeans are embedded, forming a compact greyish-white cake. Tempeh possesses a pleasant aroma which can be described as nutty, cheesy, mushroom, etc. Tempeh is a popular fermented food of Indonesia. However, in the last two decades it has attracted the attention of the Western world, particularly North America. Tempeh starter is a dried mixture of live Rhizopus spores with substrate, which can be soybeans or rice. With most fermented food products, the starter to push the process in the desired direction. In the latter case there is a risk of contamination with other bacteria, a risk which increases with every successive batch. The same principle applies to tempeh fermentation: to produce good quality tempeh you need a tempeh starter with a very high count of desirable Rhizopus molds. The same protocol within this tempeh starter to made 1L liquid culture solution mixed with 30 gram of tempeh starter (Sivakumar, et al., 2019).

7.3.3 Nutrient cementation solution

The applicability of MICP technique under various complicated environments, attempt of using the technique to reinforce soil under sea environment was made recently (Harianto et al. 2013; Cheng, Shahin, and Cord-Ruwisch 2014; Cheng et al. 2014; Jiang et al. 2016). Cheng, Shahin, and Cord-Ruwisch (2014) and Cheng et al. (2014) proposed a novel approach to treat sandy soils under marine environments by modifying the promising MICP technique and using seawater as a calcium resource to facilitate the MICP process. Most studies using MICP involve feeding bacteria with nutrient cementation solution every several hours or day by injecting more nutrient cementation solution contained with urea into the soil, the enhancing of the hydrolysis of ureolytic bacteria. With a surface-spray technique like the one used during this study, the bacteria are being fed only once and consume urea until they either run out or die. Investigators hypothesized that it may be possible to use fewer bacteria than the 1:1 ratio, culture solution of the bacterium culture media with nutrient cementation solution. Presumably, under these conditions, there should be less competition for food, or more food per bacteria. As such, maybe with more food, each bacteria cell could live longer and produce more calcite over time.

7.3.3.1 Standard solution

The test liquid media used for chemical injections contained an equimolar amount of urea and calcium chloride, in addition to 3 g nutrient broth as a nutrient source for bacteria, 10 g ammonium chloride (NH_4Cl), and 2.12 g sodium bicarbonate ($NaHCO_3$) per litre of deionised water or artificial seawater for stabilization of the pH of the solution before injections. The 0.5M urea–calcium chloride concentrations were used in order to assess the effect permeability with cementation and nutrient solution-urea–calcium chloride concentration was added to this range for the strength tests. Chemical retention time in the samples (time between injections) was determined based on the conclusion of a previous study to ensure full chemical reaction (Al Qabany et al., 2012) and the retention times adopted were 24 h for the 0.5 M urea–calcium 200 chloride solutions, respectively. This was assuming that all injected urea and calcium chloride precipitated as calcium carbonate, which was verified by measuring the amount of precipitation. This was done by adding hydrochloric acid (HCl) and calculating the weight difference of the sample before and after dissolving the precipitated calcium carbonate.

7.3.3.2 Chalk powder extract

Chalk, either source of calcium carbonte product which contains more than 94% of calcium

carbonate (Lechtanski, 2000), and it can be dissolved using an acid liquid. In this study, distilled water mixed with acetic acid (CH_3COOH) which commonly found in the Walmart as vinegar diluted to 5% acidity was used (Choi, et al., 2016). The steps for making soluble calcium using chalk and vinegar are as follows. The crushed chalk was mixed with vinegar in a bottle and placed in a shaker for several days. Chang et al. (2014) suggested removing the membrane when using chalk to produce a calcium source. Table 7.2 shown the composition of nutrient solution with chalk powder extract

Table 7.2. Nutrient cementation solution of chalk powder extract with acetic acid.

Reagent	Content (g/L)
Nutrient broth	3.0
NH_4Cl	10.0
$NaHCO_3$	2.12
Urea	18.02
Chalk powder extract with acetic acid	1 L

7.3.3.3 Snow melting salt reagent

The winter wonderland is enchanting and fun, but it can also be dangerously slippery underfoot and on the road. Conveniently enough, chlorine chemistry provides a product that can reduce the risk of accidents on ice and snow. That product is the chemical compound calcium chloride, $CaCl_2$. Calcium chloride is a salt. Calcium chloride is commercially available under three different forms: two solid forms and one liquid. Calcium chloride can be bought in the form of flakes containing 77–80% of calcium chloride or granules containing 94% of calcium chloride. In its liquid form, it contains from 30% to 42% of calcium chloride per liter of solution, usually sold as 30% solution. Calcium chloride is also commonly used as an additive in swimming pool water as it increases the “calcium hardness” value for the water. Low calcium hardness values in pool water cause pool water to be corrosive on equipment, pumps, melt the snow and metal fittings. Other industrial applications include use as an additive in plastics, as a drainage aid for wastewater treatment, as an additive in fire extinguishers, as an additive in control scaffolding in blast furnaces, and as a thinner in “fabric softeners”. North American consumption in 2002 was 1,687,000 tons (3.7 billion pounds). A Dow chemical company manufacturing facility in Michigan produces about 35% of the total U.S. production of calcium chloride (Ropp, 2012). In term of nutrient cementation solutions for MICP treatment, the cementation solution (Table 7.3) were sequentially added to the syringe and drained of the sands to hardening the surface of bio-augmentation of the materials.

Table 7.3. Nutrient cementation solution of snow melting reagents (solvent in distilled water).

Reagent	Content (g/L)
Nutrient broth	3.0
NH_4Cl	10.0
$NaHCO_3$	2.12
Urea	18.02
Snow melting salt	33.3

7.3.4 Growth and pH profiles

Bacterial growth was assessed by measuring the OD which served as a biomass concentration indicator for ureolytic bacteria (Harkes et al., 2010). The OD was measured by using a spectrophotometer (Thermo Scientific™ GENESYS™ 20) at a wavelength of 600 nm. Before measurement of the OD, un-inoculated growth medium which served as blanks were used to calibrate the spectrophotometer. Three milliliters (3 mL) of the aliquot was sampled from the bacterial cultures and placed into clean 10mm cuvettes and the OD values were recorded. Additionally, a pH meter (SevenEasy™–Mettler Toledo) was used to measure the acidity or alkalinity of the bacterial culture in relation to the number of hydrogen ions (H^+) or hydroxyl ions (OH^-). The pH electrode was first calibrated with pH 4, 7 and 10 buffer solutions (Sigma-Aldrich) before immersing into the medium to obtain the respective pH values of the bacterial cultures after incubation.

7.3.5. Urease activity

Urease activity of the cultured bacterial cells was assessed at different pH and temperature levels following the indophenol method (Wei, et al., 2015; Novitsky, 1981) where ureolysis occurred directly by the bacterial cell in a solution. The collected sample solution (1 mL) from the cell culture was added to 100 mL of the stratum solution containing 0.3 M urea and 0.1 M EDTA (Basic Local Alignment Search Tool) buffer with phenol-nitroprusside. The reaction composition was stirred using a water bath and kept at a steady temperature and pH. At the sampling point, 10 mL solution was sampled and 0.1 mL of 10 M NaOCl was added to the solution to prevent quick enzymatic hydrolysis. The composed solution was incubated subsequently for 10 min at 50-60 °C. The urease activity test was carried out to evaluate the effect of the reaction solution conditions, by 48 h cultured cells at distinctive temperatures ranging from 10 to 60 °C, and the pH was 6, 7, and 8 (adding EDTA buffer solutions at 30 °C). The urase activity of bacterial their relationship to bacterial medium cultures was evaluated

(Figure 7.2).

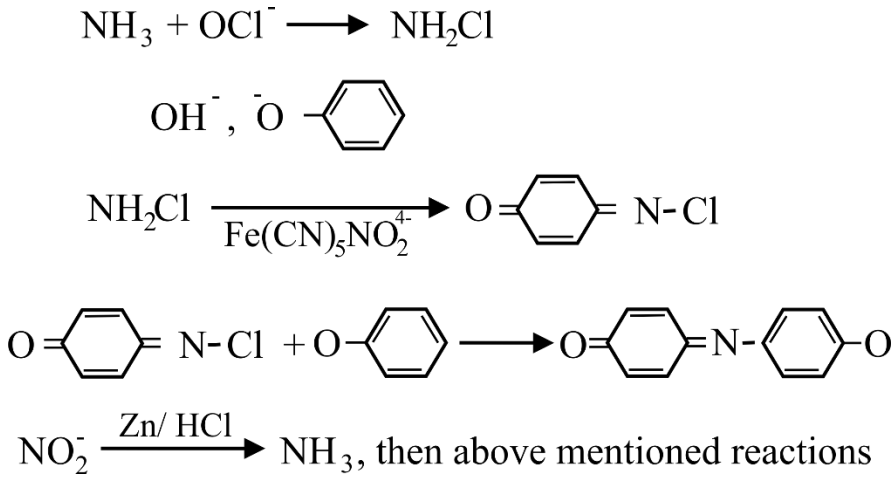


Figure 7.2. The reaction formula of the indophenol blue method.

7.3.6 Microbial $CaCO_3$ precipitation test

The *P. tetradonis* strains were cultured with a different culture with a controlled pH of 7.6–8.2, until the maximum cell growth was observed. The cell growth (OD_{600}) was measured by a UV-VIS spectrophotometer (V-730, JASCO Corporation, Tokyo, Japan). In the meantime, the standard nutrient solution (0.5 M $CaCl_2$), chalk powder extract, and snow-melting salt mixed with 0.5 M urea were put in a test tube up to 10 mL. The bacterial culture solution was centrifuged (12,000 rpm) for 10 min. The supernatant and cell pellets were divided and the bacterial cell concentration (OD_{600}) was adjusted using distilled water. The adjusted bacterial cell concentration was then added to the test tube and put in a shaker at 30°C for 48 h. Finally, the precipitation (white crystals) was observed and the precipitated crystals (centrifuged at 12,000 rpm for 10 min) was separated from the culture solution by a filter paper. Precipitated crystal tubes were kept in an oven drier for 24 h at 100°C and then the final weight was taken to calculate the total crystal precipitation amount.

7.3.7 Solidifications test

The local beach sand used in the experiments was uniformly graded with a mean particle size of 0.9 mm for coral sand and 0.6 mm for fine sand. The sand was sterilized, and hand packed into a 50-mL syringe (mean diameter, D_{50} = 3 cm and height, h = 10 cm). This was followed by gentle injection of bacteria and solidification solution, as illustrated in Figure 7.3. The bacterial suspension was injected first and allowed to stand in the column for 2 h; thereafter, solidification solution was injected. This was repeated every 24 h for a period of 14 d. In addition, two sets of biocementation experiments were conducted using conditions

designed to mimic the possible conditions for in situ injection of treatment solutions. The first set of experiments involved using coral local sand of which the main content was skeletal shell carbonate. The other set of experiments involved the use of iron-silica fine sand (fluvio-volcanic sand) of the Young Merapi deposit. In both injection conditions, 20 mL of cementation solution was left above the surface of the sand to mimic saturated conditions, and this procedure was called the immersed method. Control tests were also conducted following the same procedures but without the addition of bacterial cells. First, 100 mL bacteria medium solution (ZoBell2216E, beer yeast extract, and tempeh starter solution) was inoculated with 0.1 g of the ureolytic bacterium isolated by the above test, then incubated at 30 °C with gentle shaking at 160 rpm for 3 d. Next, 80 g of coral sand and silica sand collected from the Yogyakarta south coast was dried at 110 °C for 2 d and then placed in a 50 mL syringe (diameter 3 cm).

Subsequently, 16 mL (more than the estimated 14 mL initial pore volume in the sample) of bacterial culture and 20 mL of the nutrient cementation solutions (Laboratory-standard-grade; chalk powder extract, and snow melting salt reagent) were sequentially added to the syringe and drained, leaving about 2 mL of solution above the surface of the sand (saturated condition). This solidification test was conducted for 14 cementation injections in 14 d. In order to investigate the effect of different factors in solidification of soil, twelve cases were conducted. Each of them is clearly summarized in Table 7.4.

Table 7.4. Test condition for syringe solidification test

Case No.	Soil material	Culture solution	Cementation solution	Temperature (°C)	Test duration (days)
1	Coral sand	ZoBell2216E	Lab. Grade	30	14
2	Coral sand	ZoBell2216E	Snow melting salt	30	14
3	Coral sand	ZoBell2216E	Chalk extract	30	14
4	Coral sand	Beer yeast	Snow melting salt	30	14
5	Coral sand	Beer yeast	Chalk extract	30	14
6	Coral sand	Tempeh starter	Snow melting salt	30	14
7	Coral sand	Tempeh starter	Chalk extract	30	14
8	Fine silica sand	ZoBell2216E	Lab. Grade	30	14
9	Fine silica sand	ZoBell2216E	Snow melting salt	30	14
10	Fine silica sand	ZoBell2216E	Chalk extract	30	14
11	Fine silica sand	Beer yeast	Snow melting salt	30	14
12	Fine silica sand	Beer yeast	Chalk extract	30	14
13	Fine silica sand	Tempeh starter	Snow melting salt	30	14
14	Fine silica sand	Tempeh starter	Chalk extract	30	14

7.3.8 Needle penetration test

The local cementation strength of the specimens along the height of the column was examined in terms of estimated unconfined compressive strength (UCS) using a soft rock penetrometer (SH-70, Maruto Testing Machine Company, Tokyo, Japan). The needle of the device was penetrated into the sand specimens at three locations (1, 3, and 5 cm from the bottom of the column) and the penetration resistance (N) and penetration distance (mm) were simultaneously measured. From the results, a "penetration gradient" (N/mm) was determined, which was ultimately used to estimate UCS using Equation (7.1) where x is the penetration gradient and q_u is the UCS.

$$log(q_u) = 0.978\ log(x) + 2.621 \quad \text{(Eq. 7.1)}$$

The regression relation in Equation (7.1) has been developed by analyzing an adequate number of natural soft rock samples and cement based improved soils and confirmed by a correlation coefficient of 0.914.

7.3.9 Durability wetting-drying test

As there are no standards available for bio-cemented specimens, WD test was performed according to the standard suggested to the conventionally cemented soils (ASTM D559-03, 2003). During the wetting process, specimens were inundated at room temperature (25 ± 1 °C) for 6 hours, followed by the oven dry at 70 ± 1 °C for 48 hours (drying process). Specimens were subjected to the total number of fifty WD cycles.

7.4 Results and discussions

7.4.1 Culture medium

The growth and pH profiles of *P. tetradonis* which was studied up to 240 h at 30 °C in both beer yeast and tempeh starter medium yielded similar trends in relation to their respective OD, comparing with standard ZoBell2216E culture medium (Fig.7.3). Beer yeast culture had a constant growth rate of 0.04 h−1 and a doubling time of 1.696 in 12 h, while tempeh starter a constant growth rate of 0.05 h−1 and a doubling time of 24 h at the end of the growth study. Noteworthily, the maximum OD value (2.3) for beer yeast occurred at 120 h incubation period, while that of tempeh yeast occurred at 24 h incubation period with OD of 1.4. The pH profile of the ureolytic bacteria in both media showed a simultaneous increase towards alkaline level as the growth profile increased which is an indication of ureolysis process. The final pH values of the bacterial culture in beer yeast and tempeh starter medium were 8.16 and 8.0, respectively.

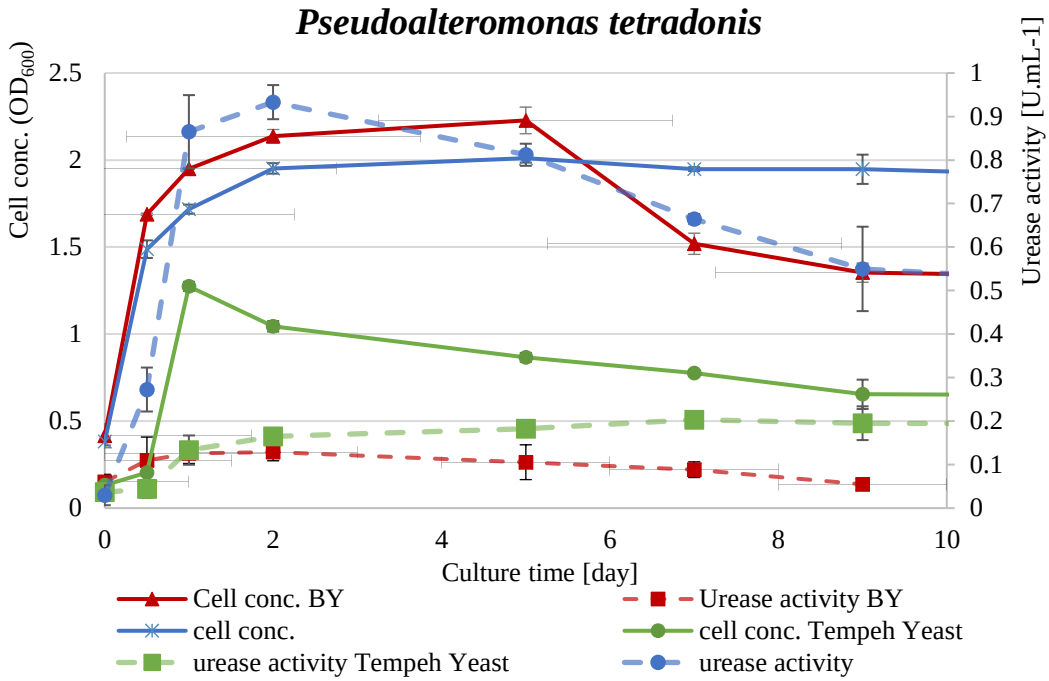


Figure 7.3. Cell growth and urase activity of *Pseudoalteromonas tetradonis* under different culture medium

The bacteria growth and urase activity still lower value compare with ZoBell2216E standard medium. There were noticeable slight differences between the growth profile of the ureolytic bacteria when grown beer yeast and tempeh starter, it is possible this could be influenced by the yeast extract components such as amino acid complexes additive present in the medium (Figure 7.4, after Anggriawan, 2017 and Munedata, 2020). Yeast extract typically contains abundant of amino acids, peptides, carbohydrates, salts, vitamins and minerals which are necessary for microbial cell cultivation (Li et al., 2011). Commercially manufactured yeast extract for bakery and cooking purposes often contains other ingredients such as flavoring agent in soup, snacks and canned foods for food industry containing (Milić et al., 2007). Nevertheless, the growth and pH profile showed that the ureolytic bacteria could adapt in the slow-cost media. In contrast to Zobell medium and beer's yeast, tempeh starter contains *Rhizopus* where the extract from the mushroom as a media material therefore that it needs to be sterilized first to avoid contamination from the effects of fungus or other organisms.

7.4.2 Nutrient cementation solution on precipitation test

7.4.2.1 Standard solution

A large community of bacteria has the ability to precipitate calcium carbonate through different mechanisms or pathways. MICP plays a significant role in the cementation of the earth's natural systems, such as caves, soils, sediments, etc. The Ca^{2+} concentrations (urea and

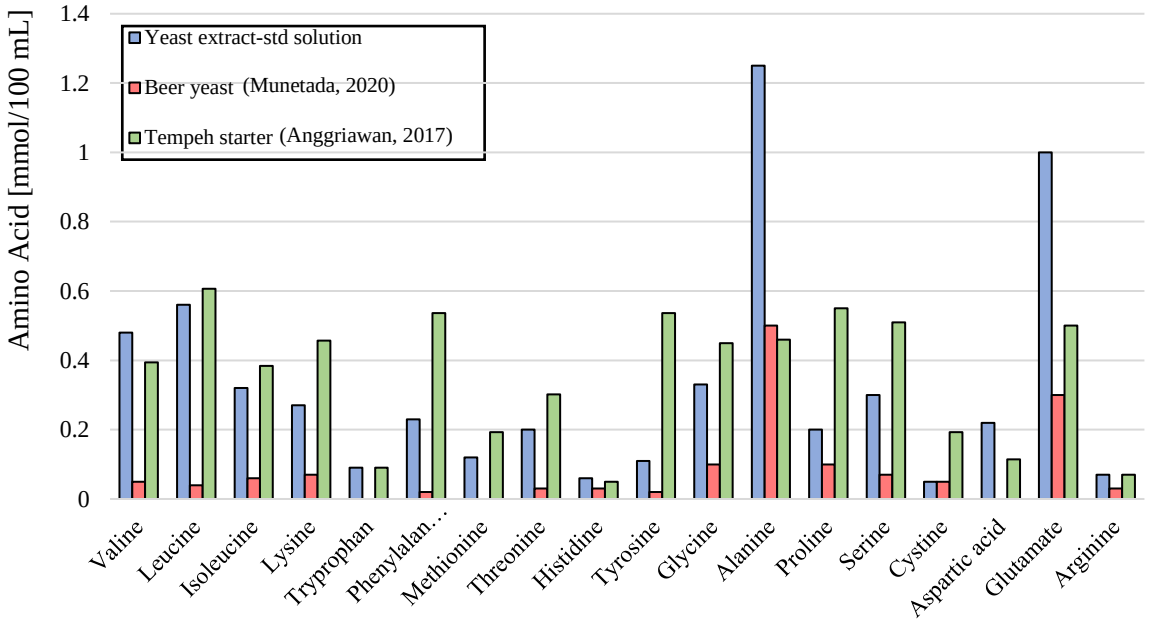


Figure 7.4. Amino acid content of each culture medium.

$CaCl_2$ concentrations) in the cementation solution pure product from FUJIFILM Wako Pure Chemical Corporation. The treatment conditions such as temperature and curing interval were selected based on simplification and efficiency of the sand cementation technique, as well as the environment around the beachrock. It was expected that temperature would affect bacterial growth and metabolism, injection interval, Ca^{2+} concentration, and test period would be correlated with the amount of $CaCO_3$ precipitation, and magnesium chloride and sodium chloride would stimulate the precipitation of magnesian calcite, which is the cement of beachrock in the area from which the bacteria were isolated. Moreover, the 0.5M Ca^{2+} concentration of the injectate (cementation solution) was about 20,000 ppm, respectively.

7.4.2.2 Chalk powder extract

The calcium concentrations of the soluble calcium solution made from chalk were measured using the ASTM D511-14 (ASTM 2014b) method and the results are shown in Fig.7.5. It can be seen that there is little difference in terms of production of soluble calcium between the use of chalk diluted solution. Intuitively, one would think the size of the powder made from eggshell will affect the production of soluble calcium. The results shown in Fig.7.5 were carried out using a chalk to vinegar ratio of 1:4 by weight. To check the effect of the chalk-to-vinegar ratio, tests with other chalk to vinegar ratios of 1:8 and 1:12 were also conducted. In general, a sufficient amount of vinegar should be used, but too much may not help in producing more soluble calcium. The data shown indicate that chalk to vinegar ratio of

1:8 appears to produce the highest calcium concentration. The data in all the tests in Fig.7.5 also show that the production of calcium reaches a peak in three days but the pH value still under acidic condition, after four days the chalk-vinegar solution became a neutral pH which safe to conduct further purposes. Thus, four days were taken as the duration for the production of calcium using chalk or chalk waste.

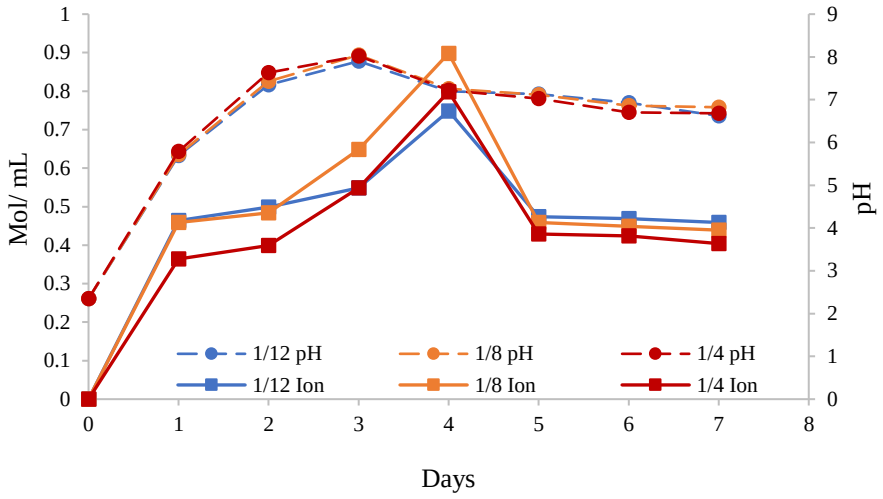


Figure 7.5. Influence of ratio of chalk powder to vinegar

Moreover, the Ca^{2+} concentration of 1:8 ratio cementation solution was about 14,000 ppm, respectively.

7.4.2.3 Snow melting

For low grade cementation solutions, the solidification effect of natural soil was investigated by incorporating commercially available low-grade chemicals. Basically, purity is the prime difference between standard pure chemicals and low-grade chemicals. The snow melting agent/de-icing salt consists of calcium (34.87%), chloride (61.89%), sodium (1.70%) and potassium (1.53%). The purity of calcium chloride is 74% in the de-icing salt commonly applied as bulk to melt the ice deposited on roads and pavements in winter seasons all over the world. The MICP feasibility of these low-grade chemicals was investigated since they are inexpensive and less harmful to the geo-environment than pure chemicals. Moreover, the Ca^{2+} concentration of the cementation solution was about 12,000 ppm, respectively.

7.4.3 Solidification tests

Natural beachrock were found in nature mostly consist of carbonate bridged material

cementation, organic matter such as skeletal fragments and also other source of rock were consist depends on geological settling in that area. Therefore, artificial cement formed by mixing seawater and a cementation solution (standard solution; snow melting; chalk powder) were injected into sand with culture bacteria as the solidification nutrient for cementation process (van Paassen, et al., 2010; Cheng and Cord-Ruwisch, 2014). Sixes MICP treated specimens were subjected to undrained shear under different loading paths including a mixture of both species, similar to the drained test series described previously. The test results indicate that as with the drained specimens, the total stress path influences the constitutive behavior of the cemented soil with small deviations in effective stress paths. A column solidification test was conducted for the purpose achieve strength in megapascal (MPa) which feasible as shoreline development method. A column solidification test is conducted over a period of 14 days owing to the accumulation of carbonate cement which might get clogged in the sample, under a 37°C curing temperature, and with injection of solidified solution at one-day intervals which results in a 0.5-M Ca^{2+} concentration of solidified solution, respectively. The local strength of the sand specimens underwent different treatment conditions with respect to the aforementioned two parameters, which are illustrated in Figure 7.6. However, the cementation reagent contained equimolar concentrations of urea and $CaCl_2$ as in Ng et al (2014).

7.4.4 MICP treated rock properties

The results indicate that the UCS values increase with the decrease in particle size in the uniformly graded sands. The average UCS axial load estimated close to the surface of fine sand and coral sands (D_{50} of 0.87 mm and 0.2 mm) are 2.87 MPa to 8 MPa, respectively. The UCS values and the calcium carbonate content of coral sand and fine sands reported herein are in a good agreement with the results reported by Cheng and Cord-Ruwisch (2014). The strength of materials based on standard solution is similar with chalk extract diluted with acetic acid, on other hand the lowest strength found in the treatment with snow melting reagent. Basically, coral sands have high permeability that leads to the high liquid infiltration compared to the fine sands. In contrast, fine sand exhibits significant improvement in UCS with the depth, which could be due to the increased capillary effect along the sample depth. The higher capillary forces in fine sand tended to retain certain amount of cementation solutions close to particle contacts, resulting higher deposition of calcium carbonate and exhibiting higher UCS. The results of the tests on bioclogging and biocementation (Table 7.5) can be monitored in real time using seismic velocity and resistivity measurements (Feng and Montoya, 2017; Phillips, et al.,



Figure 7.6 Beach sand treatment test using microbial induced carbonate precipitation after 14 days treatment. Sample with nigrescent color (left) is Quartz silica sand from Parangtritis beach and sample with whitish color (right) is carbonate coarse sand from Krakal-Sadranan beach sand.

2015). Shear wave velocity (S-wave) test results were used to develop a correlation to the precipitated calcite mass and this enables prediction of changes in porosity, density, and shear modulus during treatment (Cheng and Cord-Ruwisch, 2014). The XRD results of MICP treatment based on low-chemical compound were consist of calcite and magnesian-calcite, the detail of mineralogy were shown in the Appendixes F.

Shear wave velocity is used to nondestructively monitor the change in small-strain stiffness during shearing, which provides an indication of cementation degradation as a function of strain level. Because shear wave velocity is influenced by both the level of cementation and the change in effective mean stress during shearing, the normalized shear modulus is used to evaluate the degradation of cementation during shearing (Feng and Montoya, 2017). Biocementation in a change from a shear wave velocity of 140 m/s to an average of 600 m/s, compare with this research a shear wave around 690 m/s to 1330 m/s. Compression wave velocity (P-wave) measurements can be determined under different saturation conditions and used in combination with S-wave measurements to observe how the Poisson's ratio evolved during treatment (Phillips, et al., 2015). Further, free passage of the bacteria might be inhibited due to the small pore throat size of fine soils which mostly contain calcium carbonate

compounds such as vaterite, aragonite and/ or calcite without magnesium mineral enrichment from the seawater supply (Daryono, 2020; Russell and McIntire, 1965).

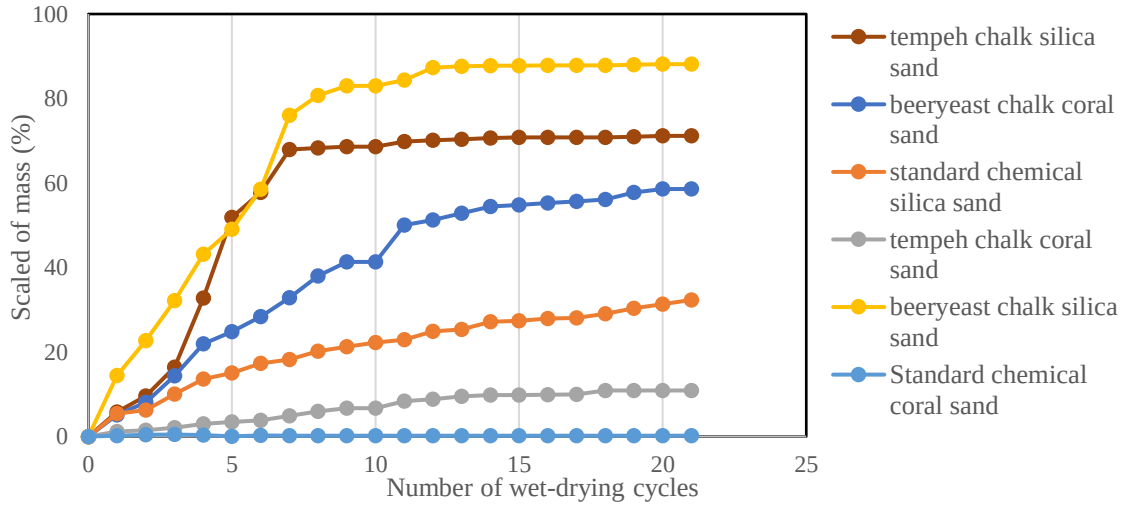
Table 7.5. Rock properties of artificial beachrock using MICP method

Sample	Cement solution	Sand Type	Saturated density (g/cm^3)	Porosity (%)	Expectation strength (MPa)	P wave velocity (km/s)	S wave velocity (km/s)	Dynamic Poisson ratio
ZoBell2216E	Std.		1.66	33%	3.20	1.94	1.33	0.05
ZoBell2216E	Snow melt	Quartz	1.60	29%	2.46	1.48	1.01	0.07
ZoBell2216E	Chalk ext.	Silica	1.81	24%	3.73	1.78	1.24	0.02
Beer yeast	Snow melt	Sands	1.65	29%	3.19	1.00	0.69	0.06
Beer yeast	Chalk ext.		1.63	34%	2.33	1.20	0.84	0.01
Tempeh starter	Snow melt		1.42	32%	2.40	1.31	0.88	0.09
Tempeh starter	Chalk ext.		1.56	30%	1.48	0.97	0.68	0.02
ZoBell2216E	Std.		1.63	26%	1.39	1.68	1.13	0.09
ZoBell2216E	Snow melt		1.42	32%	2.40	1.31	0.88	0.09
ZoBell2216E	Chalk ext.	Coral	1.60	29%	2.46	1.48	1.01	0.07
Beer yeast	Snow melt	Limestone	1.60	37%	1.01	1.12	0.77	0.05
Beer yeast	Chalk ext.	Sand	1.63	34%	2.33	1.20	0.84	0.01
Tempeh starter	Snow melt		1.60	29%	2.46	1.48	1.01	0.07
Tempeh starter	Chalk ext.		1.74	28%	5.79	1.82	1.27	0.03

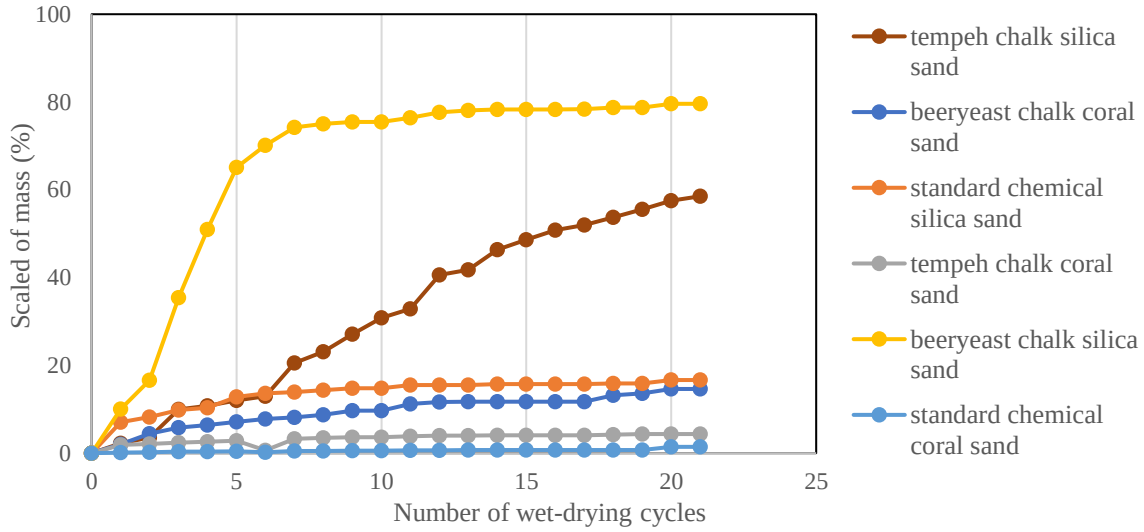
7.4.5 Durability wetting-drying test

The physical damage during cyclic tests was evaluated by the mass loss of the specimens. The mass loss was carefully measured after every cycle with neither any structural damages nor considerable changes in temperature. Fig. 7.7 shows the mass loss of the specimens subjected to cyclic WD action. The results suggest that the mass loss by the end of 21 WD cycles is more than 40% in chalk solution of cementation, and the influence of precipitated calcium carbonate content against WD effects is likely to be very significant compare the standard solution. This could possibly be attributed to the suspension of feeble deposits of calcium carbonates. During the MICP treatment, the calcium carbonate is precipitated in various forms such as primary bonds (strongly forms at particle contacts), individual crystals and accumulation (on the grain surface), amorphous and powdery deposits (Lin et al., 2016; Wang et al., 2019). In fact, these powdery bonds are often formed when the carbonates are deposited at its early stage of the crystallization. When the specimens are submerged during the wetting, the water penetrates the specimen and drives the powdery deposits to fall into suspension. This corrosion mechanism is similar to that reported to the calcarenite rocks

(Ciantia, et al., 2015). The low-chemical crystal bonding was not stronger than standard solution, the WD test shown heavy damage of feeble deposits of calcium carbonates. The evaporate of sodium and calcium ions during saturated cycles was caused the damage bonding of the crystals, deionized of Ca^{2+} ions and water.



(a)



(b)

Figure 7.7. Average mass loss of the specimens subjected to WD cyclic treatments based on (a) saltwater and (b) distilled fresh water.

7.4.6 Cost feasibility of low-grade chemicals in MICP

The same amount of $CaCO_3$ precipitation, the UCS of soil treated using low-grade chemicals was significantly higher than that of pure chemicals. This result is contrary to previous understanding that a higher $CaCO_3$ content can contribute higher strength for a soil treated under the same conditions (van Paassen et al., 2010; Whiffin et al., 2007). During the

MICP process, precipitated carbonate crystals deposit at particle contacts, coat the exposed surface of soil particles, fill the voids and provide a matrix to support to the soils, as was clearly explained by Lin et al. (2016). Using shear wave velocity measurements, it has been proven that the distribution of $CaCO_3$ at the particle contacts of MICP treated specimens can vary at the equivalent precipitated $CaCO_3$ content (Feng and Montoya, 2017; Qabany et al., 2011; Weil et al., 2012). Thus, the strength response is governed by not the average $CaCO_3$ precipitated, but the effective $CaCO_3$ precipitated at the particle contacts (Feng and Montoya, 2017), and the amount of effective $CaCO_3$ is influenced by the number of bacteria attached at particle contact during treatment (DeJong et al., 2010). Moreover, Cheng et al. (2014) reported that crystals formed under the unfavorable bacterial condition were inadequate and incapable of efficiently forming effective bridges at particle contacts. In this study, although the precipitated crystal content is low in the specimen treated using low-grade chemicals, crystals were driven to support the soil matrix effectively and contributed higher UCS compared to the soil treated using pure chemicals.

However, the matrix supporting mechanism is not clear toward the cost differences, a detailed cost comparison was performed based on the market price of reagents (in Japan), and the results are presented in Table 7.6. The total reagent cost of the 14 days of MICP treatment for the 1 m^3 soil using pure chemicals and low-grade chemicals is estimated as 13.134 USD for the former and 1647 to 2144 USD for the latter, which is a 25-fold difference. The difference price is depending on the solution were used, chalk powder extract has a 500 USD higher price than snow melting reagent but stronger results of the cementation product. As well as resulting in an 83.6%~ 87.5% cost reduction, the approach improves the strength significantly. Considering the economic aspects of this soil improvement technique, Ivanov and Chu (2008) gave a raw material cost estimate for microbial grouting of US \$0.5/m^3 to US \$9.0/m^3, while the total cost of the MICP treatment (i.e., material, equipment, and installation) in saturated soils was reported to range from US \$25/m^3 to US \$75/m^3 (DeJong, et al., 2013). However, similar studies (Cheng and Cord-Ruwisch, 2012) have shown that materials and costs can be reduced through more effective cementation, while Karol (2003) reported that the cost of placement for chemical grouting can be a major part of the total cost. Apart from the greenhouse effect associated with the production of cement, the cost of producing materials needed in biogrout is far cheaper when compared with the cost of cement production (Naeimi and Haddad, 2018; Suer, et al., 2009). The MICP technique is based on natural processes that require less energy; it can be carried out at ambient temperature, beneath existing structures without disturbing them, and can allow improvement over a large area. Studies (van Paassen,

et al., 2010; Martinez, et al., 2013; Achal and Pan, 2011; Osinubi, et al., 2017; Chiet, et al., 2016) have also shown that MICP treatment of soil results in a substantial increase in its strength, stiffness, and dilative behavior, resulting in improved geotechnical properties of the soil in order to solve several engineering problems. This would certainly be a considerable advantage for future industrial level MICP advancements.

Table 7.6. Cost comparison between pure chemicals and low-grade solutions in the MICP treatment of $1m^3$ natural sand (after Gowthaman, et al., 2019)

Reagents	**Pure Chemicals**			
	Substance	Required amount (kg)	Unit price (JPY/kg)	Price (JPY)
Cementation solution	Urea (Wako Chem.)	64.3	1580	101572
	$CaCl_2$	118.9	5600	666000
	Nutrient Broth	6.4	36600	235286
Culture solution	Yeast extract	7.14	34580	246902
	Artificial seawater	357	434	154938
Estimation		TOTAL		1404697
				(13134 USD)
Reagents	**Low-grade reagents I**			
	Substance	Required amount (kg)	Unit price (JPY/kg)	Price (JPY)
Cementation solution	Urea (fertilizer)	64.3	150	9643
	Chalk powder+acetic acid	118.9	572	68010.8
	Tempeh starter	6.4	500	3200
Culture solution	Tempeh starter	7.15	500	3575
	Artificial seawater	357	434	154938
Estimation		TOTAL		239366.8
				(2222 USD)
Reagents	**Low-grade reagents II**			
	Substance	Required amount (kg)	Unit price (JPY/kg)	Price (JPY)
Cementation solution	Urea (fertilizer)	64.3	150	9643
	Snow melting	118.9	124	14747
	Tempeh starter	6.4	500	3200
Culture solution	Tempeh starter	7.15	500	3575
	Artificial seawater	357	434	154938
Estimation		TOTAL		186103
				(1728 USD)

**prices are subject to change*

7.5 Conclusions

In this research study, the feasibility of using the emerging MICP technique for the stabilization of natural soil/sand in order to mitigate the erosion potential of beach slope was investigated. Sand samples treated under different conditions were subjected to a needle penetration test and WD test for durability of the materials. Introducing low-grade chemicals rather than laboratory-grade pure chemicals resulted in a remarkable enhancement in strength. The UCS value was similar value obtained while using pure chemicals. This innovative alternation amounts to an 83~87% reduction in the material cost and allows the leaching of harmful chemicals to be avoided. There was a relationship between the surface strength of the treated samples and the global average calcium carbonate content precipitated in samples of slope. However, the durability results of the low-grade chemical show that it has huge damage when treated for 21 cycles of WD test, it is shown the bonding particles of biocement was not as stronger as treated with pure standard chemical solutions. Future research related to the enhancement of the low-grade chemical is necessary for suitable products in the long-term application. It can be used as a strategy for the prevention of beach slope erosion and promises to be an economically feasible alternative after the appropriate scale-up experimentations and environmental impact analysis are complete.

References

Achal, V. and Pan, X., 2011. Characterization of urease and carbonic anhydrase producing bacteria and their role in calcite precipitation. Current microbiology, 62(3), pp.894-902.

Achal, V., Mukherjee, A., Basu, P.C., Reddy, M.S., 2009. Lactose mother liquor as an alternative nutrient source for microbial concrete production by Sporosarcina pasteurii. J. Ind. Microbiol. Biotechnol. 36, 433–438. https://doi.org/10.1007/s10295-008-0514-7.

Achal, V., Mukherjee, A., Reddy, M.S., 2010. Biocalcification by Sporosarcina pasteurii using corn steep liquor as the nutrient source. Ind. Biotechnol. 6, 170–174. https://doi.org/10.1089/ind.2010.6.170.

Alcamo E.I.,2001, Fundamentals of Microbiology, 6th Ed., Jones AND Barlett Publishers

Anbu, P., Kang, C.H., Shin, Y.J., So, J.S., 2016. Formations of calcium carbonate minerals by bacteria and its multiple applications. Springerplus 5, 1–26. https://doi.org/10.1186/s40064-016-1869-2 Australia.

Anggriawan, R. 2017. Microbiological and Food Safety Aspects of Tempeh Production in Indonesia. Published dissertation. Doctoral degree in the International Ph.D. Program for

Agricultural Sciences in Göttingen (IPAG), Georg-August-University Göttingen, Germany.

Bao, R., Li, J., Li, L., Cutright, T.J., Chen, L., 2017. Effect of microbialinduced calcite precipitation on surface erosion and scour of granular soils proof of concept. J. Transp. Res. Board 2657, 10–18 https://doi.org/https://doi.org/10.3141/2657-02.

Cheng L, Cord-Ruwisch R. 2014. Upscaling effects of soil improvement by microbially induced calcite precipitation by surface percolation. Geomicrobiol J 31:396–406. https ://doi. org/10.1080/01490 451.2013.83657 9

Cheng, L. and Cord-Ruwisch, R., 2012. In situ soil cementation with ureolytic bacteria by surface percolation. Ecological Engineering, 42, pp.64-72

Cheng, L., Shahin, M.A., Addis, M., Hartanto, T., Elms, C., 2014. Soil stabilisation by Microbial-Induced Calcite Precipitation (MICP): investigation into some physical and environmental aspects. In: 7th International Congress on Environmental Geotechnics. Melbourne,

Chiet, K.T.P., Kassim, K.A., Chen, K.B., Martula, U., Yah, C.S., Arefnia, A., 2016. Effect of reagents concentration on biocementation of tropical residual soil. IOP Conf. Ser. Mater. Sci. Eng. 136. https://doi.org/10.1088/1757-899X/136/1/012030.

Choi, S.G., Wu, S. and Chu, J., 2016. Biocementation for sand using an eggshell as calcium source. Journal of Geotechnical and Geoenvironmental Engineering, 142(10), p.06016010.

Ciantia, M.O., Castellanza, R., Crosta, G.B., Hueckel, T., 2015. Efects of mineral suspension and dissolution on strength and compressibility of soft carbonate rocks. Eng. Geol. 184, 1–18.

Cuzman, O.A., Rescic, S., Richter, K., Wittig, L., Tiano, P., 2015a. Sporosarcina pasteurii use in extreme alkaline conditions for recycling solid industrial wastes. J. Biotechnol. 214, 49–56. https://doi.org/10.1016/j.jbiotec.2015.09.011.

Danjo, T., Kawasaki, S., 2016. Microbially induced sand cementation method using Pararhodobacter sp. strain SO1, inspired by Beachrock formation mechanism. Mater. Trans. 57, 428–437. https://doi.org/ 10.2320/matertrans.M-M2015842.

Daryono, L.R., Nakashima, K., Kawasaki, S., Titisari, A.D. and Barianto, D.H., 2020. Sediment Characteristics of Beachrock: A Baseline Investigation Based on Microbial Induced Carbonate Precipitation at Krakal-Sadranan Beach, Yogyakarta, Indonesia. Applied Sciences, 10(2), p.520.

DeJong, J.T., Mortensen, B.M., Martinez, B.C., Nelson, D.C., 2010. Biomediated soil improvement. Ecol. Eng. 36, 197–210. https://doi.org/ 10.1016/j.ecoleng.2008.12.029.

DeJong, J.T., Soga, K., Kavazanjian, E., Burns, S., Van Paassen, L.A., Al Qabany, A.,

Aydilek, A., Bang, S.S., Burbank, M., Caslake, L.F. and Chen, C.Y., 2014. Biogeochemical processes and geotechnical applications: progress, opportunities and challenges. In Bio-and Chemo-Mechanical Processes in Geotechnical Engineering: Géotechnique Symposium in Print 2013 (pp. 143-157). Ice Publishing.

Feng, K. and Montoya, B.M., 2017. Quantifying level of microbial-induced cementation for cyclically loaded sand. Journal of Geotechnical and Geoenvironmental Engineering, 143(6), p.06017005.

Gomez, M.G., Anderson, C.M., Graddy, C.M.R., DeJong, J.T., Nelson,D.C., Ginn, T.R., 2017. Large-scale comparison of bioaugmentation and biostimulation approaches for biocementation of sands. J.Geotech. Geoenviron. Eng. 143, 4016124. https://doi.org/10.1061/(ASCE)GT.1943-5606.0001640.

Gomez, M.G., DeJong, J.T., Martinez, B.C., Hunt, C.E., DeVlaming, L. A., Major, D.W., Dworatzek, S.M., 2013. Bio-mediated soil improvement field study to stabilize mine sands. In: Proceedings of GeoMontreal, Montreal, Canada.

Gowthaman, S., Mitsuyama, S., Nakashima, K., Komatsu, M. and Kawasaki, S., 2019. Biogeotechnical approach for slope soil stabilization using locally isolated bacteria and inexpensive low-grade chemicals: A feasibility study on Hokkaido expressway soil, Japan. Soils and Foundations, 59(2), pp.484-499.

Ivanov, V. and Chu, J., 2008. Applications of microorganisms to geotechnical engineering for bioclogging and biocementation of soil in situ. Reviews in Environmental Science and Bio/Technology, 7(2), pp.139-153.

Jiang, N.-J., Soga, K., 2017. The applicability of microbially induced calcite precipitation (MICP) for internal erosion control in gravel–sand mixtures. Ge´otechnique 67, 42–55. https://doi.org/10.1680/jgeot.15.P.182.

Jones, 1960, Bact. Proc. Pg. 36 (A29)

Joshi, S., Goyal, S., Reddy, M.S., 2018. Corn steep liquor as a nutritional source for biocementation and its impact on concrete structural properties. J. Ind. Microbiol. Biotechnol. https://doi.org/10.1007/s10295-018-2050-4.

Karol, R.H., 2003. Chemical grouting and soil stabilization revised and expanded (Vol. 12). Crc Press.

Khan, M.N.H., Shimazaki, S., Kawasaki, S., 2016. Coral sand solidification test through microbial calcium carbonate precipitation using Pararhodobacter sp. Int. J. Geomate 11, 2665–2670.

Kristiansen, B., 2006. Process economics. In: Ratledge, C., Kristiansen, B. (Eds.), Basic

Biotechnology. Cambridge University Press, Cambridge, pp. 271–286. https://doi.org/10.1017/CBO9780511802409.013.

Lechtanski, V. L. (2000). “Calcium carbonate content of eggshell.” Inquirybased experiments in chemistry, Oxford, New York, 159–165.

Li, M., Liao, X., Zhang, D., Du, G., Chen, J., 2011. Yeast extract promotes cell growth and induces production of polyvinyl alcohol-degrading enzymes. Enzym. Res. https://doi.org/10.4061/2011/179819.

Lin, H., Suleiman, M.T., Brown, D.G., Kavazanjian, E., 2016. Mechanical Behavior of Sands Treated by Microbially Induced Carbonate Precipitation. J. Geotech. Geoenvironmental Eng. 142, 04015066-1–13.

Liu, M., Zhang, M., Lin, S., Liu, J., Yang, Y. and Jin, Y., 2012. Optimization of extraction parameters for protein from beer waste brewing yeast treated by pulsed electric fields (PEF). Afr J Microbiol Res, 6, pp.4739-4746.

Lyman J. and Fleming R. H., 1940, J. Mar. Res. 3:134.

Martinez, B.C., DeJong, J.T., Ginn, T.R., Montoya, B.M., Barkouki, T.H., Hunt, C., Tanyu, B. and Major, D., 2013. Experimental optimization of microbial-induced carbonate precipitation for soil improvement. Journal of Geotechnical and Geoenvironmental Engineering, 139(4), pp.587-598.

Milić, T.V., Rakin, M., Šiler-Marinković, S., 2007. Utilization of baker's yeast (Saccharomyces cerevisiae) for the production of yeast extract: Effects of different enzymatic treatments on solid, protein and carbohydrate recovery. J. Serb. Chem. Soc. 72, 451–457. https://doi.org/10.2298/JSC0705451V.

Mital, B.K. and Garg, S.K., 1990. Tempeh—technology and food value. Food Reviews International, 6(2), pp.213-224.

Mortensen BM, Haber MJ, Dejong JT et al. 2011. Effects of environmental factors on microbial induced calcium carbonate precipitation. J Appl Microbiol 111:338–349. https ://doi.org/10.111 1/j.1365-2672.2011.05065.

Mujah, D., Shahin, M.A., Cheng, L., 2017. State-of-the-art review of biocementation by Microbially Induced Calcite Precipitation (MICP) for soil stabilization. Geomicrobiol. J. https://doi.org/10.1080/01490451.2016.1225866.

Munetada, S. 2020. Proposal for preservation technology of highway slopes in Hokkaido using MICP method. Published thesis. Master’s degree of the Graduate School of Engineering, Hokkaido University and Kyushu University, Japan.

Naeimi, M. and Haddad, A., 2018, May. Investigation on the environmental impact of soil

improvement techniques: comparison of cement grouting and biocement. In GeoShanghai International Conference (pp. 483-490). Springer, Singapore.

Ng, W., Lee, M., Hii, S., 2012. An overview of the factors affecting microbial-induced calcite precipitation and its potential application in soil improvement. World Acad. Sci. Eng. Technol. 62, 723–729.

Oliveira, P.J.V., Freitas, L.D., Carmona, J.P.S.F., 2016. Effect of soil type on the enzymatic calcium carbonate precipitation process used for soil improvement. J. Mater. Civ. Eng. 29, 1–7. https://doi.org/10.1061/(ASCE)MT.1943-5533.0001804.

Osinubi, K.J., Eberemu, A.O., Ijimdiya, S.T., Yakubu, S.E. and Sani, J.E., 2017, September. Potential use of B. Pumilus in microbial-induced calcite precipitation improvement of lateritic soil. In Proceedings of the 2nd symposium on coupled phenomena in environmental geotechnics (CPEG2), session: clean-ups, paper (Vol. 64, pp. 1-6).

Pelczar M.J..Jr., Reid R.D., Chan E.C.S., 1977, Microbiology, 4th Edi, Tata McGraw-Hill Publishing Company Ltd,New Delhi

Phillips, A.J., Eldring, J.J., Hiebert, R., Lauchnor, E., Mitchell, A.C., Cunningham, A., Spangler, L. and Gerlach, R. 2015. Design of a meso-scale high pressure vessel for the laboratory examination of biogeochemical subsurface processes. Journal of Petroleum Science and Engineering, 126, pp.55-62.

Qabany, A.A., Mortensen, B., Martinez, B., Soga, K. and DeJong, J., 2011. Microbial carbonate precipitation: correlation of S-wave velocity with calcite precipitation. In Geo-Frontiers 2011: Advances in Geotechnical Engineering (pp. 3993-4001).

Ropp, R.C., 2012. Encyclopedia of the alkaline earth compounds. Newnes.

Russell, R. J., and McIntire, W. G. 1965. Beach cusps. Geological Society of America Bulletin, Vol. 76, 3, 307-320. https://doi.org/10.1130/0016-7606(1965)76[307:BC]2.0.CO;2.

Salifu, E., MacLachlan, E., Iyer, K.R., Knapp, C.W., Tarantino, A., 2016. Application of microbially induced calcite precipitation in erosion mitigation and stabilisation of sandy soil foreshore slopes: a preliminary investigation. Eng. Geol. 201, 96–105. https://doi.org/10.1016/j.enggeo.2015.12.027.

Sensoy, T., Bozbeyoglu, N.N., Dogan, N.M., Bozkaya, O., Akyol, E., 2017. Characterization of calcium carbonate produced by ureolytic bacteria (Sporocarcina pasteurii ATCC 6453 and Bacillus aerius U2) and effect of environmental conditions on production of calcium carbonate. In: 15th International Conference on Environmental Science and Technology. Rhodes, Greece.

Sizemore R. K. and Stevenson L. H., 1970, Appl. Microbiol., 20:991.

Soon, N.W., Lee, L.M., Khun, T.C., Ling, H.S., 2014. Factors affecting improvement in engineering properties of residual soil through microbial-induced calcite precipitation. J. Geotech. Geoenviron. Eng.140, 4014006. https://doi.org/10.1061/(ASCE)GT.1943-5606.0001089.

Stabnikov, V., Naeimi, M., Ivanov, V., Chu, J., 2011. Formation of waterimpermeable crust on sand surface using biocement. Cem. Concr. Res.41, 1143–1149. https://doi.org/10.1016/j.cemconres.2011.06.017.

Suer, P., Hallberg, N., Carlsson, C., Bendz, D. and Holm, G., 2009. Biogrouting compared to jet grouting: environmental (LCA) and economical assessment. Journal of Environmental Science and Health Part A, 44(4), pp.346-353.

van Paassen, L.A., Ghose, R., van der Linden, T.J.M., van der Star, W.R.L., van Loosdrecht, M.C.M., 2010. Quantifying biomediated ground improvement by ureolysis: large-scale biogrout experiment. J. Geotech. Geoenviron. Eng. 136, 1721–1728. https://doi.org/10.1061/(ASCE) GT.1943-5606.0000382.

Wang, Y., Soga, K., Dejong, J.T., Kabla, A.J., 2019. Microscale Visualization of Microbial-Induced Calcium Carbonate Precipitation Processes. J. Geotech. Geoenvironmental Eng. 145, 1–13.

Warnock., D.W. 2015. Manual of Clinical Microbiology, 11th Edition. Vol. 1.

Weil, M.H., DeJong, J.T., Martinez, B.C. and Mortensen, B.M., 2012. Seismic and resistivity measurements for real-time monitoring of microbially induced calcite precipitation in sand. Geotechnical Testing Journal, 35(2), pp.330-341.

Weiner R. M., Segall A. M. and Colwell R. R., 1985, Appl. Environ. Microbiol., 49:83.

Whiffin, V.S., 2004. Microbial $CaCO_3$ Precipitation for the Production of Biocement (Ph. D. Thesis). 1–162. http://researchrepository.murdoch.edu.au/399/2/02Whole. pdf⟩.

Whiffin, V.S., Van Paassen, L.A. and Harkes, M.P., 2007. Microbial carbonate precipitation as a soil improvement technique. Geomicrobiology Journal, 24(5), pp.417-423.

Williams, S.L., Kirisits, M.J., Ferron, R.D., 2016. Optimization of growth medium for Sporosarcina pasteurii in bio-based cement pastes to mitigate delay in hydration kinetics. J. Ind. Microbiol. Biotechnol. 43, 567–575. https://doi.org/10.1007/ s10295-015-1726−2.

Yang, C.Z., LI, Y., Ruan, N., Mou, D.H. and Kang, M.L., 2006. Study and applications of technology about breaking yeast cell wall [J]. Food Science and Technology, 7.

Yoosathaporn, S., Tiangburanatham, P., Bovonsombut, S., Chaipanich, A., Pathom-aree, W., 2016. A cost-effective cultivation medium for biocalcification of Bacillus pasteurii KCTC 3558 and its effect on cement cubes properties. Microbiol. Res. 186–187, 132–138.

https://doi.org/10.1016/j.micres.2016.03.010.

Zobell C. E., 1940, J. Marine Research, 3:134

CHAPTER 8

Tentative proposal of coastal prevention method

8.1 Introduction

The multidisciplinary research between geotechnical engineers and microbiologists has paved a way into a new frontier of knowledge called geobiology. This realization came to provide engineers opportunities to consider soil as a living ecosystem rather than an inert construction material. The use of microorganisms as a potential catalyst in soil biocementation was first suggested by Whiffin (2004) and Mitchell and Santamarina (2005). Since then, countless research has advanced considerably high in this field. In recent years, conducting interdisciplinary research shows a strong capability in dealing with some hot and critical issues. With the development of interdisciplinary cooperation among biological engineering, chemical engineering and civil engineering, microbial induced carbonate precipitation (MICP) technique has been widely used in various engineering applications, such as evolution of water resources and rehabilitation of old buildings. In addition, this method has been applied to ground improvement as well. For example, Zhou, Luo, and Wang (1997) found that the physical and chemical changes of organic matter and micro-organisms induced by the environmental change will have an impact on the properties of geomaterials. Xu, Zhang, and Zhou (2009) extracted carbonate mineralization bacteria and polysaccharide of the adhesive bacteria from soils to improve the related engineering properties of silty soils. Al-Thawadi (2008) and Burbank et al. (2011) isolated the original ecological urease-producing bacteria that provide bacteria species for the application of MICP technique. The bacteria were then used to improve the geotechnical properties of sandy soils successfully. In addition, the broad application of MICP technique and the potential benefits of the microbial reinforced soils attract more scholars to participate in this research area (Mujah, Shahin, and Cheng 2017).

The feasibility of MICP does not depend on technical aspects regarding conditions of treatment alone but accompanies by economical and legislative issues as well. It has been reported that the discharging of vigorous chemicals and ammonium by-products to the soil ecosystem in the MICP causes many harmful effects, and the subsequent removal of such harmful products must be taken into account (Soon et al., 2014). The cost of the required substances remains another contest in assessing the complete feasibility of the process (van Paassen et al., 2010). The previous chapter was concern about nutrition sources that are easily accessible at low or no cost suitable for MICP application. The results were remarkable in the

low-cost reagents, not only for culture medium but also for the cementation solution based on snow melting or chalk powder extract. However, this product has a heavy damage to the durability test based on the wetting-drying method compared with the standard chemical solution.

8.2 Objectives

In this chapter, the goal is to propose of the prevention method based on MICP by indigenous ureolytic bacteria. The bacteria strains were isolated from the natural of beachrock along the shoreline in Krakal-Sadranan, Yogyakarta south coast, Indonesia. Future research related to the enhancement of the low-grade chemical is necessary for suitable products in the long-term application. Moreover, envisioned applications, potential advantages and limitations of MICP in beach sand improvement are presented and addressed. The current challenges and future work on biocementation by MICP are also outlined.

8.3 Materials and methods

One of the most emerging and promising biological soil improvement techniques, i.e. MICP or biocementation, is reviewed and discussed in some detail.

MICP is a biologically driven calcium carbonate (calcite or $CaCO_3$) precipitation technology, which includes the following two mechanisms of biologically controlled and biologically induced $CaCO_3$ precipitation. In the biologically controlled mechanism, the organism controls the nucleation and growth of the mineral particles, and independently synthesizes minerals in a form that is unique to the species regardless of the environmental conditions. Hence, several factors key role of the mechanism MICP were succeeded or not such as ureolytic bacteria, culture media, cementation solution, sand, and treatment sand condition.

8.3.1 Ureolytic bacteria

Microbial activities can change the appearance of soil/sand and increase its ability to withstand applied forces/loads by precipitating calcite, which binds soil particles (Sari, 2015). According to Reichle (1977), microbes constitute between 70% and 85% of the living component within soil systems, but a good understanding of their metabolic rate is essential to forecast correctly how microorganisms will act under different conditions (Epelde, et al., 2008). The number of organisms in kjbkjba single kilogram of soil at the surface is between 109 and 1012 (Mitchell and Santamarina, 2005; Umar, et al., 2016). It was reported by Dejong and his research team (2014) that a gram of soil could be home to 1012 bacteria, and over 106

bacteria could be present in a single gram of poorly graded soil. Yargicoglu and Reddy (2015) also reported approximately 109 cells within a gram of soil. Research has shown that microorganisms, especially bacteria, are linked to the formation of carbonate minerals, as they also play an important role in carbon cycling (Hamdan, et al., 2011). Bacteria can differ in shape; they can be rod like, almost round or spiral, and the range of their cell thickness is between 0.5 and 3 μm (DeJong, et al., 2013, 2014; Umar, et al., 2016; Soon, et al., 2012). Their thickness can be reduced under stress settings to around 0.2 μm; they reproduce by fission naturally. Bacteria can withstand unfavorable conditions, and at low to elevated acidity or salinity some are spore-forming organisms, allowing them to withstand/survive in harsh conditions such as high pressures of several hundred bar and equally at temperatures from below the freezing to above the boiling point of water (Madigan, et al., 2008).

Microorganisms, in general, can reproduce very rapidly by fission, and their growth rate is exponential. The generation (reproduction) time for bacteria is 10 min, but 1 h is typically used; For example, starting with bacteria with a reproduction time of 1 h under an ideal condition, they could multiply to 224. With this high reproduction rate, microbial activity can be anticipated everywhere. In soil pore fluid, bacteria with size of 1 μm could reach approximately 108 bacteria/ml (Mitchell and Santamaria, 2005). The presence of microorganisms in the soil may not cause any harm to the soil environment, as the majority are native species of the soil. The ureolytic bacterium, *Pseudoalteromonas tetradonis* isolated by Daryono, et al. (2019, 2020) from beachrock sample from Indonesia shoreline was used in this study due to its high urease activity which classified as gram-negative. The strain were motile bacilli 1 μm wide and 1.5–4.0 μm, aerobic, motile with one polar flagellum, rods (or rod-shapes) with 0.5–0.8 × 1.0–1.5 μm when in exponential growth phase was used in this study. Standard media (ZoBell2216E for marine bacteria medium) were used for culturing under sterile aerobic conditions. Cells were precultured separately in 5 mL of each medium at 37°C and 160 rpm for 24 h. One milliliter of the preculture was inoculated with 100 mL of the fresh medium and incubated under the same conditions. The microbial cell growth of the isolates was determined based on optical density at a wavelength of 600 nm (OD_{600}) using a UV-vis spectrophotometer (V-730, JASCO Corporation, Tokyo, Japan).

Urease, a member of the hydrolases group, is a nickel-containing metalloenzyme that catalyzes the hydrolysis of urea into ammonia and carbonate, initiating the reaction chain of the calcium carbonate precipitation described above (Hwang, et al., 2013). Meanwhile, carbonic anhydrase, like urease, plays a vital role in the MICP process, but it still needs more detailed studies on how it works at MICP. Carbonic anhydrase is also a metalloenzyme, but

during stage 9 uses zinc in the catalytic nodes with carbon dioxide (CO_2) and bicarbonate (HCO_3^-). In the carbonic anhydrase pathway, after the production of bicarbonate, hydrogen ions (H^+) promote the precipitation of calcium carbonate in the form of calcite plus the output of water and carbon dioxide (Jiménez-López, et al., 2017). Hwang et al. (2013) reported the action of carbonic anhydrase in biomineralization and the fact that the morphology of calcium carbonate (calcite) depends on the constant pressure of CO_2 and the addition of polymers that affect the growth and nucleation of the precipitate. The $CaCO_3$ precipitated in the presence of carbonic anhydrase can take three forms: ellipsoidal, polygonal, or rhombohedron. The same process in the absence of carbonic anhydrase only precipitates $CaCO_3$ in the form of a rhombohedron, a less rigid morphology. The activities of urease are interdependent and guide the stages of calcite precipitation (Fig.8.1). The activity of urease depends on the incorporation of nickel in its nucleation site, which is regulated by the chemical reaction between carbon dioxide and bicarbonate catalyzed (Wong, 2015). The characteristics of the ion's nucleation site define the morphology of the calcium carbonate precipitates such as calcite, vaterite, or other metastable polymorphs which may not only enzyme dependency but also the source of minerals. The polymorph of calcium carbonate which has different stability due to its micromorphology proceeds in different reactivities with the surface of its environment. Calcite, for example, is thermodynamically stabilized and has a hexagonal-rhombohedral crystal structure; aragonite is metastable and has an orthorhombic crystalline structure, usually in the form of a needle; and vaterite (precursor to calcite and aragonite) is a metastable hexagonal crystalline structure in spherulitic or disc-like form. This identification of the formation of structures and the level of reactivity of precipitated calcium carbonate is vital to define whether this procedure is a potential bioremediation technique for aquifer contamination (Portugal, et al., 2020).

8.3.2 Culture media

The solution freed of all microorganisms by sterilization (usually in an autoclave, where it undergoes heating under pressure for a specific time) and containing the substances required for the growth of microorganisms such as bacteria, protozoans, algae, and fungi. The medium may be solidified by the addition of agar. Some media consist of complex ingredients such as extracts of plant or animal tissue (e.g., peptone, meat extract, yeast extract); others contain exact quantities of known inorganic salts and one or more organic compounds (synthetic or chemically defined media). In this research, the author used Zobell2216 medium marine broth as a standard medium for cultivated bacteria, beer yeast extract which yeast is mainly composed

of 48–55% protein, 23–28% carbohydrate, 6–8% RNA, 1% glutathione, and 2% vitamin B. Moreover, they are rich in P, K, Ca, Fe, P and Mg (Liu et al.,2012), and tempeh starter, the mold fermentation results in a matrix of dense, cottony, mycelia in which cooked soybeans are embedded, forming a compact greyish-white cake which possesses a pleasant aroma that can be described as nutty, cheesy, mushroom, etc. Tempeh is a popular fermented food in Indonesia. Within this medium, the results were interesting results that might be implemented in Indonesia with this medium which is cheap, can be found everywhere, and high urease activity around 0.5 unit/mL, respectively.

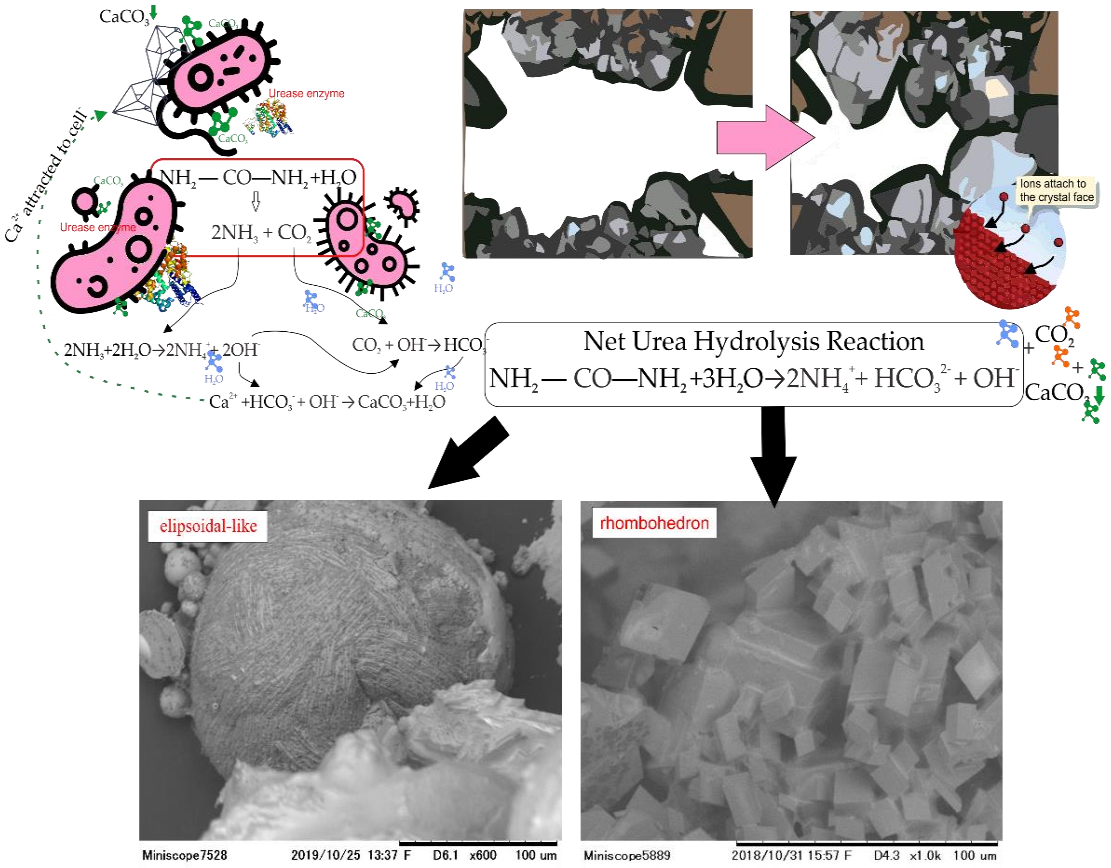


Figure 8.1. Schematic illustration of MICP process of urease activity.

The differences between standard medium and low-cost medium not only based on the economic aspect but also considered by the urease activity of the medium. The beer yeast, for example, is easy to find in Japan or another country but not in the southeast Asia, especially Indonesia. Based on this culture and market demanded of the products, tempeh starter is mutual symbiont between microorganism bacteria and fungi whereas Rhizopus molds it's proven success to replaceable of the standard medium to cultivated ureolytic bacteria. The comparison of the medium, mostly consists of the amino acid inside the solution (see fig.7.4) and also price

comparison at the price of the tempeh starter with standard Zobell2216 medium is 69:1 cheaper of tempeh yeast (see table 7.6).

8.3.3 Cement solution

In the MICP protocols, the cementation solution certainly provides the basic chemicals for MICP process (as urea and Ca^{2+} source). Sometimes, it also includes components like pH stabilizer ($NaHCO_3$), a carbon source or nutrients (nutrient broth, yeast) to maintain the bacteria. Concentration of cement solution refers to the concentration of urea and Ca^{2+} in the cement solution. It is an important parameter when designing a MICP protocol (DeJong et al., 2013). Many authors have conducted laboratory experiments by using different concentrations of cement solution (either equimolar or non-equimolar concentrations of urea and Ca^{2+}, usually < 2 M) to different soils, and tried to find out the optimal concentration for their experimental conditions. Even though the low-chemical crystal bonding was not stronger than the standard solution it's still a feasible solution to reduce the cost of production. The WD test of low-chemical reagents shown heavy damage to feeble deposits of calcium carbonates. The evaporate of sodium and calcium ions during saturated cycles was caused by the damage bonding of the crystals, deionized Ca^{2+} ions and water. It means the low-chemical reagent is working well to treat the soil/sand in the dry area, such as biogrouting for liquefaction countermeasures. In this case of coastal prevention, future research related to the enhancement of the low-grade chemical is necessary for suitable products in the long-term application.

The efficiency of $CaCO_3$ crystals formation is believed to be affected by various cementation solution concentrations. This is attributed to the fact that more homogeneous $CaCO_3$ crystals distribution along the sand matrix is usually observed at lower cementation solution concentration. On the other hand, the precipitated $CaCO_3$ crystals at higher cementation solution concentration are usually randomly formed in the soil voids due to the faster precipitation induced by the higher cementation solution concentration (Okwadha and Li 2010). The $CaCO_3$ formation was also found to be more effective at lower cementation solution concentration. For example, Al Qabany and Soga (2013) conducted an experiment using sand samples treated under different cementation reagents of 0.1, 0.25, 0.5 and 1 M urea-calcium chloride solution and found that the treated sand with lower reagent concentration gave higher strength compared to that treated with higher reagent concentration. The lower concentration led to more homogeneous $CaCO_3$ crystals formation at the particle contact points which contributed to the strength improvement with minimum soil disturbance and permeability reduction. This is consistent with the findings of Ng et al. (2014) who claimed

that biocementation was found to be more effective on the residual soil treated with 0.5 M cementation reagent compared to that treated with 1 M cementation reagent. Cheng et al. (2014) even produced biocemented sand columns using low concentration of Ca^{2+} source (i.e. 10 mM) from seawater; however, a greater number of injections were required to achieve the same amount of $CaCO_3$ crystals precipitation when lower cementation reagent concentration was used.

8.3.4 Soil/ sand

Soil/ sand properties, such as density, grading, saturation, have a vital impact on bio-treatment efficiency. Studying soils with different characteristics are beneficial to understand the use of MICP in various sites. Soil/sand samples preparation should consider the aim of the research. Studying the effect of soil characteristics makes the protocol more feasible and efficient in varying conditions of geological sites. Some of these parameters are considered below.

8.3.4.1 Density

Density of sand has a great impact on its mechanical behavior. The density state is also characterized by the relative density *Dr*, calculated by:

$$D_r(\%) = \frac{e_{max} - e}{e_{max} - e_{min}} \quad \text{(Eq. 8.1)}$$

where e_{max}, e_{min} represent the standardized maximum and minimum void ratios, and e, the actual void ratio of the sand. For similar MICP treatments, increasing density (40%, 70%, 80%) resulted in a reduction of $CaCO_3$ production and an increase in strength (Rowshanbakht et al., 2016). Bahmani et al. (2017) conducted a series of experiments with various soil densities (1.86, 1.93, 2.11, 2.23, 2.36 gr/cm3, corresponding to relative densities of 0%, 17%, 56%, 78%, 100%). Results indicated that the treated soil sample with a density of 2.11 gr/cm^3 had the highest value of stiffness and compressive strength. It shows that the highest density does not necessarily lead to the highest strength. Rowshanbakht et al. (2016) used poorly graded silica sand (D_{max} = 0.4 mm, C_u = 1.46, C_c =0.83, D_{50} = 0.2 mm) with no shape description, Bahmani et al. (2017) used poorly graded angular to sub-angular quartz grains (D_{max} = 1 mm, C_u = 2.2, C_c = 0.77, D_{50} = 0.18 mm). Both of them used ASTM Standards. The results obtained by Rowshanbakht et al. (2016) and Bahmani et al. (2017) are conflicting, maybe because Bahmani used a sand with a higher fines content (20% < 0.1 mm) whereas, in the study of Rowshanbakht et al., the fines content (<0.1 mm) was 1%. When the relative density increases from 56% to

higher values, the smaller pore throats inhibited the transport of bacteria, thereby decreasing the efficiency of MICP.

Gao et al. (2019) used Ottawa sand (ASTM poorly graded round quartz sand), with grain sizes ranging from 0.2 to 0.5 mm, and a mean size of 0.36 mm, similar with fine silica from Parangtritis in this research. For loose (D_r = 30%) and medium dense (D_r = 50%) sands, a light bio-treatment gave a strength improvement comparable to, or exceeding, that of untreated dense sand (D_r = 90%) (Gao et al., 2019). Xiao et al. (2019) applied cyclic loadings to MICP-treated calcareous sand (angular, with no fines, D_{10} = 0.19 mm, D_{50} = 0.38 mm) and untreated sand with different relative densities (10%, 50%, 80%) and different degrees of bio-cementation. From this research, the fine particle size (Parangtritis silica sand D_{50} of 0.2 mm) and coral sands (Krakal-Sadranan D_{50} of 0.87 mm) were successfully treated with MICP, fine material it will rapid cementation period rather than coral beach sand because of bonding particle intraparticle smaller and less of pores. Comparing treated and untreated sands, with the same increment in dry unit weight, they showed that treated sand samples had gained a larger increase in cyclic resistance, which indicates that the MICP treatment method is more efficient in promoting cyclic resistance of calcareous sand than densification.

8.3.4.2 Particle size

Many studies have been carried out using sands (e.g. Ottawa silica sand, Fontainebleau sand) with grain diameters smaller than 2mm (Choi et al., 2016; Gao et al., 2019; Hamdan et al., 2013; O'Donnell & Kavazanjian, 2015; Zhao et al., 2014). Under the consideration of free passage of bacteria, as well as limit of injectability in-situ, very fine grains are usually not used. For example, DeJong et al. (2006) used Ottawa 50–70 sand to represent loose natural deposit, which is sufficient for the bacteria in the size range of 1–3 mm. Bahmani et al. (2017) used a soil with a particle size ranged between 50 and 400 mm, which was sufficient for the transportation of bacteria. Hataf and Jamali (2018) tried to determine the maximum fine content (i.e. in a clay with low plasticity) that did not influence the effect of MICP. For that, a fine-grained soil (100% finer than 75 mm, 25.6% finer than 2 mm) and a coral-grained soil (0.4mm–5 mm) were mixed at different percentages, and consolidated drained direct shear tests were carried out before and after the MICP treatment. Results showed that the higher the fine content, the lower the strength increase due to MICP. A fine content up to 20% did not affect the efficiency of MICP. Few studies include larger grains in soil preparation. However, in the study of Mahawish et al. (2018), Pakenham Blue Metal (Old Basalt) coral grain (2.36–16 mm) and relatively fine grains (0.075–9.5 mm) were mixed at different percentages to conduct

column cementation experiments. As a result, in comparison with other groups of materials, materials with 25% fine grains resulted in a better distribution of $CaCO_3$ and a relatively higher value of unconfined compressive strength.

8.3.5 Treatment sand condition

In order to ensure a successful ground improvement by MICP, the introduction and retention of ureolytic bacteria or urease enzyme inside the soil matrix is crucial. The retained bacteria can induce $CaCO_3$ precipitation through the supply of injecting a cementation solution. Improper bacteria retention could lead to the bacteria being flushed away or detached by a subsequent injection of the cementation solution, leading to uneven distribution of bacteria and resulting in non-uniform $CaCO_3$ precipitation and strength within the biocemented soil. Figure 8.2 is shown the conceptual design of coastal prevention with the MICP method of this entire research.

8.3.5.1 pH and temperature

pH and temperature have a direct bearing on the growth and urease activity of the bacteria. *P. tetradonis* is sensitive to pH and temperature during the cementation process as some studies have shown (Kim et al., 2018; Sun et al., 2019). pH and temperature also have an impact on the equilibria of dissolution and precipitation during the MICP process. Here we mainly talk about the influence of microbial activity caused by these parameters. pH has a crucial biochemical effect on the activity of urease produced by *P. tetradonis* (Whiffin, 2004; Daryono, et al., 2020a, 2020b). Optimal pH for bacteria growth and urease activity is not the same. For the cultivation of the bacteria, the optimal pH is around 9, while the optimum pH for urease activity is usually near neutral for *P. tetradonis* (Mobley et al., 1995; Daryono, et al., 2020a, 2020b). According to Whiffin (2004), pH in the range of 6.25–7.7 gives a urease activity higher than 40 mM urea/min and the maximum (around 43 mM urea/min) occurs around pH = 7. Cheng et al. (2014) found that pH lower than 3.5 and higher than 9.5 is averse to the cementation process. During the MICP process, Stocks-Fischer et al. (1999) determined that MICP starts at pH = 8.3, and its rate increases up to pH 9 of the *S.pasteurii* strain. Kim et al. (2018) studied the effect of the pH (in the range of 6–10) of a urea-$CaCl_2$ solution and found that pH = 7 was the optimal condition for biocementation. Temperature affects microbial growth and urease activity. Bahmani et al. (2017) studied the urease activity of *S. pasteurii* at different temperatures (10, 15, 21, 35, 50, 60, and 80 °C), and found that urease activity increased with temperature up to an optimum temperature of 60 °C. Another researcher, Fujita

et al., (2017) and Daryono, et al., (2020a) was conducted the study of urease activity of ureolytic bacteria from beachrock at different temperatures. During the process of cultivation of bacteria, the optimal temperature for different strains of P. tetradonis to reach the maximum specific urease activity is 30°C to 40°C, record from the geochemical analysis were mentioned beachrock occurred at 37 °C (Daryono, et al., 2020a; 2020b). Cheng et al. (2014) found that increasing temperature could increase the production of calcite; however, the strength was smaller than that obtained at room temperature. For the cementation of relatively coral materials (1–3 mm), the moderate temperature of 20 °C was optimal (Mahawish et al., 2018). In Sun et al. (2019) study, 30 °C resulted in the highest rate of $CaCO_3$ precipitation. Kim et al. (2018) studied the influence of temperatures between 20 and 50 °C and found that 20, 25, 30 °C were the optimal temperatures for different strains.

8.3.5.2 Marine environment

Most previous studies regarding the MICP improved soils were performed on granular sandy soils under simple ionic environment in freshwater (Mujah, Shahin, and Cheng 2017). However, there could be many different ions existing in practice. For example, ionic concentrations of K^+, Na^+, Ca^{2+}, Mg^{2+}, Cl^-, SO_3^{2-}, and HCO_3^{2-} in seawater are much higher than those in freshwater. Due to the difference of sedimentation environment, the mechanism of using urease producing micro-organisms to improve dredged sediments under marine environment is different from that for sandy soils (Li, Chu, and Whittle 2016). To validate the applicability of MICP technique under various complicated environments, attempt of using the technique to reinforce soil under sea environment was made recently (Harianto et al. 2013; Cheng, Shahin, and Cord-Ruwisch 2014; Cheng et al. 2014; Jiang et al. 2016). Cheng, Shahin, and Cord-Ruwisch (2014) and Cheng et al. (2014) proposed a novel approach to treat sandy soils under marine environments by modifying the promising MICP technique and using seawater as a calcium resource to facilitate the MICP process. It is found that the amount of microbial induced $CaCO_3$ was the highest under alkaline condition and the lowest under acidic condition. In addition, the unconfined compressive strength of treated specimen under neutral condition can reach 300 kPa, which was greater than that under acidic and alkaline conditions. The results also reveal that the strength of sand columns can be significantly increased by the MICP technique from repeated treatment using seawater. The application of MICP technique using seawater can possibly offer a cost-effective and sustainable way to improve ground under marine and coastal environments for sustainable development.

8.3.5.3 Injection mode and rates

Injection methods are quite different from one study to another. Mixing the bacteria and cement solution before injection gives rise to an instant reaction, producing $CaCO_3$ precipitation and bacteria flocculation immediately. This injection method is appropriate for the treatment of coral sand materials (van Paassen, 2009) that need higher reaction rates and larger amounts of precipitates. And it is also used in surface stabilization, because it only needs to cement the soil to a limited depth. Because this method needs less injection time, it makes the process easier and reduces cost in real works. In recent studies, this method has been improved to prevent the occurrence of an immediate reaction by prolonging the lag period of the reaction. It has been applied successfully to lab column experiments, either by lowering concentration of bacteria and adjusting the initial pH of the mixture to pH = 4 (Cheng et al., 2019), or by refrigerating the bacteria and cement solution at low temperature (4 °C) before mixing (Xiao, et al., 2019). Another method is two-phase injection (by first injecting the bacterial cell solution followed by the cement solution). This method is expected to prevent clogging and give a more homogeneous distribution of $CaCO_3$ crystals (Whiffin, et al., 2007). It is widely used by many researchers.

For strengthening soil surface, injection is usually realized by surface percolation. For ground improvement, Whiffin, et al. (2007) used 0.35 L/h (for a column 5m long, ϕ=66 mm), Mortensen et al. (2011) used 10 mL/min (column: 100/50mm long, ϕ=50 mm), Cheng, et al., (2013) used1 L/h (column: 160mm long, ϕ=55 mm). They all obtained good cementation results in their samples of various sizes (<1 mm) with the mentioned injection rates. To make the results clearer, seepage velocity (the velocity through the bulk of the porous medium) is calculated using the following equation to unify the units, $v = Q/A$, where v is the seepage velocity (m/day), Q is the total volume flowing through the corresponding cross-sectional area per time unit (m^3/day), A is the cross-section area of the flow (m^2). The results are 2.5 m/ day, 7.3 m/day and 10.1 m/day for Whiffin et al., (2007), Mortensen, et al., (2011) and Cheng et al., (2013), respectively. Whiffin, et al., (2007) concluded that relatively low flow rates (<10 m/day) were desirable. However, if the urea hydrolysis is quite fast, to prevent clogging near the inlet, a higher injection rate is expected to deliver precipitates to further locations.

8.4 Sustainability to the environment

Applying MICP for soil improvement results in a significant change in indigenous microbial populations. While this is unavoidable as part of the MICP process, the potential risk to the ecological balance must be properly assessed. Recent studies have started to investigate

microbial dynamics during MICP implementation (Gat, et al., 2016), but a complete life-cycle analysis from an ecological perspective is not yet available and the capability of MICP-treated soil to sustain life (i.e. as habitats for organisms) is not known. Traditionally, terrestrial ecologists view ecological restoration as an indispensable part of an engineered land system. This perspective, unfortunately, is often ignored in geotechnical design practice (DeJong, et al., 2015). Meanwhile, the most popular ureolysis process to achieve MICP generates ammonia as a by-product, which could cause harm to different environments. Thus, researchers might consider utilizing alternative greener bio-mineralization processes. For example, the microbial iron reduction process is responsible for the formation of coastal and continental shelf sediments in geological history. Hydroxyapatite, which can be synthesized through bio-mineralization, has been exploited in medical science for bone grafting and bone building. Currently, it is not clear whether these alternative bio-mineralization processes are technically feasible for soil improvement applications and, therefore, effective collaborations among geochemists, biomaterial scientists and engineers are required. Moreover, ongoing MICP research and development efforts have overlooked possible long-term deterioration of MICP-treated soils. Although researchers have recently started to look into the dissolution of formed precipitates as a result of evolving bio-geochemical processes (Gat, et al., 2016), the degradation of engineering performance has not been fully evaluated over long time scales and under severe adverse environments. In addition, further efforts are needed to lower the energy requirements of MICP technique, as the currently used nutrient media and multi-treatment regime are both high in embodied energy. This can be potentially achieved by optimizing the raw materials and technological process so as to make it an energy-saving soil improvement method.

8.4.1 Biosafety risk of indigenous ureolytic microorganisms

There is popular construction biotechnology that is based on “stimulation of indigenous (native) microorganisms” (Burbank, et al., 2011; 2012; Gomez, et al., 2017; Hammes, et al., 2003; Kiasari, et al., 2018; Rajasekar, et al., 2017). This technology is based on opinion that there will be no harm for people and environment if native microorganisms of soil are used. However, it is well known that soil microbial community is concentrated in the upper layer of 10–30 cm of fertile soil and there is almost no microbial activity in soil deeper than a few meters from the soil surface, as well as in the cracks of the rocks, or in the desert sand (Ivanov, 2015; Ivanov and Stabnikov, 2017). Therefore, construction biotechnology with indigenous microorganisms is applicable only for the upper layer of soil, which is fertilized by urea and

therefore containing a lot of urease-producing microorganisms. Soil microbial community is very complex and there will be obviously present ureolytic indigenous microorganisms because urea is released into environment by mammals. An addition of urea to soil will increase its pH and stimulate growth of indigenous alkaliphilic ureolytic bacteria. Additionally, soil will be enhanced by amino acids and carbohydrates due to lysis of soil non-alkaliphilic microorganisms. Due to these processes, the soil community of indigenous microorganisms will be replaced by enrichment culture of alkaliphilic halotolerant microorganisms with undefined biosafety risk. The short-list of soil-born alkaliphilic halotolerant pathogens include bacteria *B. anthracis* causing deadly disease anthrax, *Clostridium tetani* causing tetanus, *Clostridium perfringens* causing gas gangrene, *B. cereus* causing gastroenteritis, *Listeria monocytogenes* causing meningitis, *Burkholderia pseudomallei* causing melioidosis, fungi *Blastomyces dermatitidis* causing blastomycosis, and fungi *Coccidioides* associated with alkaline, saline sandy soils and causing pneumonia (Baumgardner, 2012; Ivanov, 2015; Ivanov and Stabnikov, 2017). Therefore, it is not safe to stimulate growth of indigenous urease producing soil microorganisms because even the high pH and salinity of soil do not prevent growth of both "native" ureolytic and non-ureolytic pathogenic microorganisms. Enhancement of soil with pathogens during MICP could cause infections due to direct contact of the workers with soil or spread of microbial pathogens into environment with the soil dust and the MICP effluent.

8.4.2 Biosafety risk of pure bacterial cultures

A major point for the use of pure bacterial culture for MICP is biosafety requirements for cultivation of cells, production and storage of biocement, its injection into or spraying onto soil, persistence of introduced microorganisms in soil, effect of introduced microorganisms on human and environment, and fate of these microorganisms in environment. It requires expensive studies that will complicate use of living bacterial cells in construction biotechnologies. Additionally, a lot of formal approvals and permissions are needed for release of living bacteria in environment (Ball, 2015). Therefore, to eliminate the point of biosafety at all and to avoid obtaining of approvals for industrial scale MICP, the new technology of MICP was proposed. The main point of this technology is the use of dead but urease active cells of urease-producing bacteria (Ivanov and Stabnikov, 2017). The best treatment of bacterial cells was incubation in 0.5% solution of the surfactant sodium dodecyl sulfate (SDS) for 2 h. This treatment killed all cells of micrococci *Yaniella* sp. but decreased urease activity of bacterial suspension just from 4.9 to 3.2 mM of hydrolyzed urea/min. SEM showed only the remainders

of cell wall of *Yaniella* sp. cells after this incubation. However, biomass of alkali tolerant, halophilic, ureolytic Gram-positive micrococci was killed by surfactant but enzyme urease remains still active. The dead bacterial biomass with urease activity is just a chemical matter

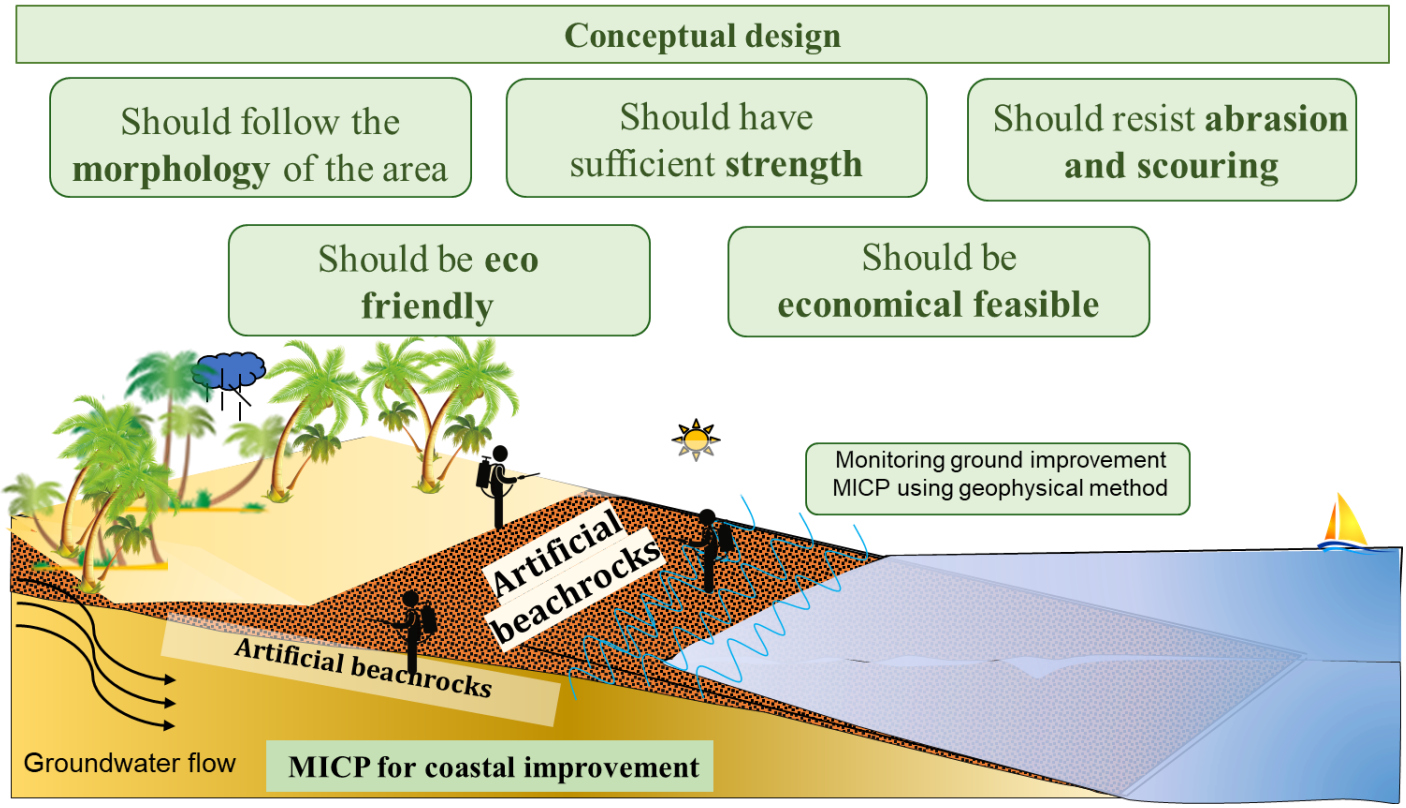


Figure 8.2. Conceptual design of coastal prevention with MICP method

and will not require biosafety risk evaluation.

Similar treatment did not kill all cells of *S. pasteurii*, probably because of the presence of spores, which are more resistant to the surfactants than the vegetative cells. Bioclogging with dead but urease active cells of *Yaniella* sp. urease decreased the hydraulic conductivity of sand from 5.2·10−4 m/s to 7.7·10−9 m/s (Stabnikov, et al., 2016). Probably, biomass of culture collection strains, for example *Yaniella halotolerans* DSM 15476 or *Yaniella* flava DSM 16377 from Group Risk 1, also can be used for bioclogging/ biocementation after growth in the medium with urea and killing cells by surfactants. There may be another hypothetical way to increase biosafety of MICP with any pure culture. It could be selection and use of psychrophilic, alkaliphilic, halotolerant microorganisms for biocementation with optimum temperature for growth about 15–20 °C and maximum temperature 25 °C, so that these microorganisms will die at temperature 30 °C (Ivanov, 2015).

Therefore, they will be not dangerous for humans with temperature 36.6 °C. Psychrophilic microorganisms with optimum temperature for growth 20 °C and their urease could be more

suitable for underground geotechnical works than mesophilic microorganisms with optimum temperature for growth of 30 °C because underground temperature in sites deeper than 20 m from surface is about 10–15 °C in Europe, North America, and north of Asia, and 20–25 °C in the tropical zone. Psychrophilic microorganisms could be also useful for the soil surface bioclogging/biocementation during spring and autumn seasons in Europe, North America and north of Asia, where only 3 months of the summer season are suitable for the soil biotreatment using mesophilic microorganisms. Psychrophilic microorganisms were not studied for use in construction biotechnology yet, but they are used in industrial biotechnology (Banerjee, et al., 2016). This research was concluded the three urrolytic bacteria strain from local beachrock in Krakal-Sadranan, whereas one of them is same genus with *Vibrio cholera* and indicated it have a pathogenic strain even though it is biosafety level 1.

8.4.3 Undesired byproducts

Soil improvement using MICP is a novel and innovative technique compared with the conventional methods that have been in use for environmental applications. Undesired byproducts (e.g., ammonium, ammonia, hydrogen sulfite, nitrite, nitrous oxide, and carbon dioxide) generated during the various MICP processes may pose environmental and health risks (Reeburgh, 2007; Erşan, et al., 2005; Hommel, et al., 2016; Paul, et al., 2017; González-Muñoz, et al., 2010; De Muynck, 2013). For example, ammonium (the byproduct of ureolysis) is very costly to treat in groundwater. van Paassen (2010) reported that, if an incomplete reaction occurs during denitrification (a method used in MICP), greenhouse gases such as nitrite and nitrous oxide will be produced. Solomon, et al., (2007) reported that nitrous oxide has an atmospheric lifespan of 114 years and is a dominant greenhouse gas, having a 300- fold greater potential for global warming effects compared with carbon dioxide. Another undesired byproduct of the MICP process is the toxic and combustible H_2S gas released by sulfate-reducing bacteria, which results in many environmental and health issues (Kirk, et al., 2015). However, undesired byproducts can be mitigated by: (1) identifying other strategies or techniques to prevent their generation, (2) using the byproducts for other applications nearby, or (3) adopting treatments to eliminate the byproducts (Zhu and Dittrich, 2016).

8.4.4 Nonuniform injection of microbes and cementation reagents

The presence of microorganisms, sufficient nutrients, and cementation reagents in a soil medium is required for the beneficial application of the MICIP technique (Zhu and Dittrich, 2016). Dejong, et al., (2014) reported that both the nutrients and cementation reagents can

rapidly be exhausted due to: (1) the flow rates through the soil medium being too fast for reaction to occur, (2) nutrients not being provided in sufficient quantity, or (3) nutrients being exhausted over time. To overcome some of these challenges, studies (Barkouki, et al., 2011; Martinez, et al., 2012; 2013; Rowshanbakht, et al., 2016; Inagaki, et al., 2011) have been conducted to determine or optimize the quantities of injection of the microbes, nutrients, and cementation reagents. Some of the reported findings of the studies are: (1) The stop-flow injection method is preferred over continuous and recirculation methods of injection, as it provides an even and more uniform distribution of calcite when compared with the other two methods, which either result in greater filling of voids near the injection points or flushing of some of the microbes, preventing their participation in the precipitation process; (2) A maximum of two-thirds of the pore volume should be used as the injection volume for the microbes, nutrients, and cementation reagents (Rowshanbakht, et al., 2016): (3) It is recommended that a maximum of one-third of the pore volume should be used for the injection of microbes, an approach that yielded positive results with tropical residual soils (Osinubi, et al., 2018; 2019)

8.4.5 Limitations of microbes

Most MICP laboratory studies have been carried out under nutrient-rich conditions (Lauchnor, et al., 2013), while in practical applications, such as soil reinforcement, metal remediation, repair of cracks in concrete, etc., such conditions are quite rare. Furthermore, microbes may be exposed to unfavorable conditions such as high pH, high temperature and pressure, desiccation, evaporation, oxygen and nutrient deficiency, salt concentration, etc. in the field. Field conditions limit the bacterial strains within the soil, which is a requirement for MICP to occur. Although several reported field studies were conducted at high pressure, most bacteria used in MICP have been cultured at ambient temperature and pressure (Okyay, et al., 2015). However, it is difficult for bacteria cultured in the ambient temperature range of 20–37 °C to survive or maintain their microbial activities at a temperature of 120 °C (Kumar, et al., 2011). Finally, better understanding of fundamental, multifunctional and sustainable characters of MICP requires an extensive deployment of monitoring facilities. Thanks to recent advances in monitoring technologies, we now have the capabilities to obtain more timely and refined data. Researchers could seek solutions from interdisciplinary technological breakthroughs such as sensors for multi-physical measurements, robotics for automated real-time data collection and artificial intelligence (AI) tools for establishing robust predictive models (Osinubi, et al., 2020).

8.5 Conclusions

To sum up of this research, except the durability factor, Table 8.1 were describing the formula for ground improvement in the shoreline area.

Table 8.1. Formula for MICP treatment of beach sand solidification test.

Item	Condition	Amount
Bacteria strain	Ureolytic bacteria isolated from beachrock (gram-negative for marine bacteria and gram-positive for inland bacteria)	Optimum ratio is between 1:3 to 1:4 of bacteria versus material
Environment Condition	Marine environment (mostly oxidative environment)	pH 7 to 8 with temperature 30 ~ 40 ℃
Culture media	Inexpensive material such as beer yeast or tempeh starter was possible to substitute industrial pure chemical standard	Approximal 7.15 kg of tempeh fungi to treat 1 meter3 beach sand
Cement solution	Inexpensive material such as chalk extract or another calcium carbonate waste is feasible to enhance similar amount concentration with the pure chemical standard	118.9 kg to treat 1 $meter^3$ of material
Soil/ sands type	1. Density Based on the experiment results, the fine silica sand D_{50} of 0.2 mm and coarse coral D_{50} of 0.87 mm. 2. Particle size Coarse grain (2.36 -16mm) to relative fine grains (0.075-9.5mm).	Optimum ratio is between 1:3 to 1:4 of bacteria versus material. Beach coral sand will have strong bonding rather than silica sand material.
Injection mode and rates	Optimum injection is separately between culture media and cement solution, for the column syringe test the culture media can be injected once per week bur for beach slope every injection/ spraying the culture media and cement solution in the difference valves.	Ratio 1:5 between 1 of crude-culture media into 5 of the cement solutions
Principle MICP	By injection of spraying in the surface of the ground (separately)	
Beach slope stability	Optimum condition to treat it have a limit slope degree maximum is 15°, steep slope it might percolate of the MICP reaction only in the bottom of target	

Improved engineering properties of MICP-treated soil or sands, including strength, stiffness, permeability, and liquefaction resistance, are carefully reviewed. Influence factors of MICP technique, modeling of MICP process, and engineering applications are examined.

Finally, limitation and cost analyses of the technique are discussed. Some recommendations have also been provided for future development. Urea hydrolysis is the most preferred $CaCO_3$ precipitation mechanism because it can be easily controlled and possesses about 90% of $CaCO_3$ production efficiency in a short period of time. The most favorable bacteria for soil biocementation come from, but not limited to, highly urease active bacteria (e.g. *Psedoalteromonas tetradonis*). It is vital to know the effective mechanism of $CaCO_3$ precipitation because it translates to a lower cost of MICP treatment and achieves strong material in the long-term periods. In return, this can pave the way into possible commercialization of the technique in the near future. Some important key factors of the MICP determined to include ureolytic bacteria, culture media, cement solution, soil/sand, and treatment sand condition such as pH and also temperature during the treatment. The treated reason based on local indigenous bacteria because for real implementation the treatment condition factor could be eliminate based on their natural condition.

References

Al Qabany A, Soga K. 2013. Effect of chemical treatment used in micp on engineering properties of cemented soils. Geotechnique 63(4):331–339.

Al-Thawadi, S. 2008. High strength in-situ biocementation of soil by calcite precipitating locally isolated ureolytic bacteria. Western Australia: Murdoch University.

Amini Kiasari, M., Pakbaz, M.S. and Ghezelbash, G.R., 2018. Increasing of soil urease activity by stimulation of indigenous bacteria and investigation of their role on shear strength. Geomicrobiology Journal, 35(10), pp.821-828.

Bachmeier, K.L., Williams, A.E., Warmington, J.R. and Bang, S.S., 2002. Urease activity in microbiologically-induced calcite precipitation. Journal of Biotechnology, 93(2), pp.171-181.

Bahmani, M., Noorzad, A., Hamedi, J. and Sali, F., 2017. The role of bacillus pasteurii on the change of parameters of sands according to temperatur compresion and wind erosion resistance. Journal CleanWAS, 1(2), pp.1-5.

Ball, A.S., 2015. The intentional release of micro-organisms into the environment: challenges to commercial use. In Biosafety and the environmental uses of micro-organisms: conference proceedings, OECD Publishing, Paris (pp. 115-126).

Banerjee, R., Halder, A. and Natta, A., 2016. Psychrophilic microorganisms: Habitats and exploitation potentials. Eur J Biotechnol Biosci, 4, pp.16-24.

Barkouki, T.H., Martinez, B.C., Mortensen, B.M., Weathers, T.S., De Jong, J.D., Ginn,

T.R., Spycher, N.F., Smith, R.W. and Fujita, Y., 2011. Forward and inverse bio-geochemical modeling of microbially induced calcite precipitation in half-meter column experiments. Transport in Porous Media, 90(1), p.23.

Burbank, M. B., T. J. Weaver, T. L. Green, B. C. Williams, and R. L. Crawford. 2011. Precipitation of calcite by indigenous microorganisms to strengthen liquefiable soils. Geomicrobiology Journal 28 (4):301–312. doi:10.1080/01490451.2010.499929

Burbank, M.B., Weaver, T.J., Williams, B.C. and Crawford, R.L., 2012. Urease activity of ureolytic bacteria isolated from six soils in which calcite was precipitated by indigenous bacteria. Geomicrobiology Journal, 29(4), pp.389-395.

Cheng, L. and Cord-Ruwisch, R., 2012. In situ soil cementation with ureolytic bacteria by surface percolation. Ecological Engineering, 42, pp.64-72.

Cheng, L., Cord-Ruwisch, R. and Shahin, M.A., 2013. Cementation of sand soil by microbially induced calcite precipitation at various degrees of saturation. Canadian Geotechnical Journal, 50(1), pp.81-90.

Cheng, L., Shahin, M.A. and Chu, J., 2019. Soil bio-cementation using a new one-phase low-pH injection method. Acta Geotechnica, 14(3), pp.615-626.

Cheng, L., Shahin, M.A. and Cord-Ruwisch, R., 2014. Bio-cementation of sandy soil using microbially induced carbonate precipitation for marine environments. Géotechnique, 64(12), pp.1010-1013.

Choi, S.G., Wang, K. and Chu, J., 2016. Properties of biocemented, fiber reinforced sand. Construction and building materials, 120, pp.623-629.

Daryono, L.R., Nakashima, K., Kawasaki, S., Titisari, A.D. and Barianto, D.H., 2020a. Sediment Characteristics of Beachrock: A Baseline Investigation Based on Microbial Induced Carbonate Precipitation at Krakal-Sadranan Beach, Yogyakarta, Indonesia. Applied Sciences, 10(2), p.520.

Daryono, L.R., Nakashima, K., Kawasaki, S., Suzuki, K., Suyanto, I. and Rahmadi, A., 2020b. Investigation of Natural Beachrock and Physical–Mechanical Comparison with Artificial Beachrock Induced by MICP as a Protective Measure against Beach Erosion at Yogyakarta, Indonesia. Geosciences, 10(4), p.143.

Daryono, L.R., Titisari, A.D., Warmada, I.W. and Kawasaki, S., 2019. Comparative characteristics of cement materials in natural and artificial beachrocks using a petrographic method. Bulletin of Engineering Geology and the Environment, 78(6), pp.3943-3958.

De Muynck, W., Verbeken, K., De Belie, N. and Verstraete, W., 2013. Influence of temperature on the effectiveness of a biogenic carbonate surface treatment for limestone

conservation. Applied microbiology and biotechnology, 97(3), pp.1335-1347.

Dejong, J. T., Proto, C., Kuo, M., and Gomez, M. 2014. Bacteria, bio-films and invertebrates… the next generation of geotechnical engineers. In: Proceedings of geo-congress 2014: technical papers, ASCE, Geotechnical Special Publication, vol 234, pp 3959–3968

DeJong, J., Tibbett, M. and Fourie, A., 2015. Geotechnical systems that evolve with ecological processes. Environmental earth sciences, 73(3), pp.1067-1082.

DeJong, J.T., Soga, K., Kavazanjian, E., Burns, S., Van Paassen, L.A., Al Qabany, A., Aydilek, A., Bang, S.S., Burbank, M., Caslake, L.F. and Chen, C.Y., 2014. Biogeochemical processes and geotechnical applications: progress, opportunities and challenges. In Bio-and Chemo-Mechanical Processes in Geotechnical Engineering: Géotechnique Symposium in Print 2013 (pp. 143-157). Ice Publishing.

Epelde, L., Becerril, J. M., Hernández-Allica, J., Barrutia, O., and Garbisu, C. 2008. Functional diversity as indicator of the recovery of soil health derived from Thlaspi caerulescens growth and metal phytoextraction. Appl Soil Ecol 39(3):299–310. https ://doi. org/10.1016/j.apsoi l.2008.01.005

Erşan, Y.Ç., De Belie, N. and Boon, N., 2015. Microbially induced CaCO3 precipitation through denitrification: an optimization study in minimal nutrient environment. Biochemical Engineering Journal, 101, pp.108-118.

Fujita, M., Nakashima, K., Achal, V. and Kawasaki, S., 2017. Whole-cell evaluation of urease activity of Pararhodobacter sp. isolated from peripheral beachrock. Biochemical engineering journal, 124, pp.1-5.

Gao, Y., Hang, L., He, J. and Chu, J., 2019. Mechanical behaviour of biocemented sands at various treatment levels and relative densities. Acta Geotechnica, 14(3), pp.697-707.

Gat, D., Ronen, Z. and Tsesarsky, M., 2016. Soil bacteria population dynamics following stimulation for ureolytic microbial-induced CaCO3 precipitation. Environmental science & technology, 50(2), pp.616-624.

Gomez, M.G., Graddy, C.M., DeJong, J.T., Nelson, D.C. and Tsesarsky, M., 2018. Stimulation of native microorganisms for biocementation in samples recovered from field-scale treatment depths. Journal of Geotechnical and Geoenvironmental Engineering, 144(1), p.04017098.

González-Muñoz, M.T., Rodriguez-Navarro, C., Martínez-Ruiz, F., Arias, J.M., Merroun, M.L. and Rodriguez-Gallego, M., 2010. Bacterial biomineralization: new insights from Myxococcus-induced mineral precipitation. Geological Society, London, Special Publications, 336(1), pp.31-50.

Hamdan, N., Kavazanjian Jr, E. and O'Donnell, S., 2013, September. Carbonate cementation via plant derived urease. In Proceedings of the 18th International Conference on Soil Mechanics and Geotechnical Engineering (pp. 2-6).

Hamdan, N., Kavazanjian, J., Rittman, B.E., and Karatas, I. 2011. Carbonate mineral precipitation for soil improvement through microbial denitrification. In: Proceedings of geo-frontiers 2011: advances in geotechnical engineering, Dallas TX, ASCE, Geotechnical Special Publication, vol 211, pp 3925–3934

Hammes, F., Boon, N., de Villiers, J., Verstraete, W. and Siciliano, S.D., 2003. Strain-specific ureolytic microbial calcium carbonate precipitation. Appl. Environ. Microbiol., 69(8), pp.4901-4909.

Harianto, T., Hamzah, S., Nur, S.H., Abdurrahman, M.A., Latief, R.U., Fadliah, I. and Walenna, A., 2013, September. Biogrouting stabilization on marine sandy clay soil. In The 7th International Conference on Asian and Pacific Coasts (Vol. 848, p. 52).

Hataf, N. and Jamali, R., 2018. Effect of fine-grain percent on soil strength properties improved by biological method. Geomicrobiology journal, 35(8), pp.695-703.

He, J., Chu, J. and Liu, H., 2014. Undrained shear strength of desaturated loose sand under monotonic shearing. Soils and Foundations, 54(4), pp.910-916.

Hommel, J., Lauchnor, E., Gerlach, R., Cunningham, A.B., Ebigbo, A., Helmig, R. and Class, H., 2016. Investigating the influence of the initial biomass distribution and injection strategies on biofilm-mediated calcite precipitation in porous media. Transport in Porous Media, 114(2), pp.557-579.

Hwang, E.T., Gang, H. and Gu, M.B., 2013. CO2 bioconversion using carbonic anhydrase (CA): effects of PEG rigidity on the structure of bio-mineralized crystal composites. Journal of biotechnology, 168(2), pp.208-211.

Inagaki, Y., Tsukamoto, M., Mori, H., Sasaki, T., Soga, K., Qabany, A.A. and Hata, T., 2011. The influence of injection conditions and soil types on soil improvement by microbial functions. In Geo-Frontiers 2011: Advances in Geotechnical Engineering (pp. 4021-4030).

Ivanov, V. and Stabnikov, V., 2017. Bioclogging and biogrouts. In Construction Biotechnology (pp. 139-178). Springer, Singapore.

Ivanov, V., 2015. Environmental microbiology for engineers. CRC press.

Jiang, N.J., Yoshioka, H., Yamamoto, K. and Soga, K., 2016. Ureolytic activities of a urease-producing bacterium and purified urease enzyme in the anoxic condition: Implication for subseafloor sand production control by microbially induced carbonate precipitation (MICP). Ecological engineering, 90, pp.96-104.

Jiménez-López, C., Rodriguez-Navarro, C., Piñar, G., Carrillo-Rosúa, F.J., Rodriguez-Gallego, M. and Gonzalez-Muñoz, M.T., 2007. Consolidation of degraded ornamental porous limestone stone by calcium carbonate precipitation induced by the microbiota inhabiting the stone. Chemosphere, 68(10), pp.1929-1936.

Kim, G., Kim, J. and Youn, H., 2018. Effect of temperature, pH, and reaction duration on microbially induced calcite precipitation. Applied Sciences, 8(8), p.1277.

Kirk, G.J., Versteegen, A., Ritz, K. and Milodowski, A.E., 2015. A simple reactive-transport model of calcite precipitation in soils and other porous media. Geochimica et Cosmochimica Acta, 165, pp.108-122.

Kumar, K., Dasgupta, C.N., Nayak, B., Lindblad, P. and Das, D., 2011. Development of suitable photobioreactors for CO2 sequestration addressing global warming using green algae and cyanobacteria. Bioresource technology, 102(8), pp.4945-4953.

Lauchnor, E.G., Schultz, L.N., Bugni, S., Mitchell, A.C., Cunningham, A.B. and Gerlach, R., 2013. Bacterially induced calcium carbonate precipitation and strontium coprecipitation in a porous media flow system. Environmental science & technology, 47(3), pp.1557-1564.

Li, B., Chu, J. and Whittle, A., 2016. Biotreatment of fine-grained soil through the bioencapsulation method. In Geo-Chicago 2016 (pp. 25-32).

Liu, M., Zhang, M., Lin, S., Liu, J., Yang, Y. and Jin, Y., 2012. Optimization of extraction parameters for protein from beer waste brewing yeast treated by pulsed electric fields (PEF). Afr J Microbiol Res, 6, pp.4739-4746.

Madigan, M. T., Martinko, J. M., Dunlap, P. V., and Clark, D. P. 2008. Brock biology of microorganisms, 12th edn. Benjamin Cummings, San Francisco

Mahawish, A., Bouazza, A. and Gates, W.P., 2018. Effect of particle size distribution on the bio-cementation of coral aggregates. Acta Geotechnica, 13(4), pp.1019-1025.

Martinez, B.C., 2012. Up-scaling of microbial induced calcite precipitation in sands for geotechnical ground improvement. University of California, Davis.

Martinez, B.C., DeJong, J.T., Ginn, T.R., Montoya, B.M., Barkouki, T.H., Hunt, C., Tanyu, B. and Major, D., 2013. Experimental optimization of microbial-induced carbonate precipitation for soil improvement. Journal of Geotechnical and Geoenvironmental Engineering, 139(4), pp.587-598.

Mitchell, J.K., and Santamarina, J.C. 2005. Biological considerations in geotechnical engineering. J Geotech Geoenviron Eng 131(10):11222–11233. https ://doi.org/10.1061/(ASCE)1090-0241(2005)131:10(1222)

Mortensen, B.M., Haber, M.J., DeJong, J.T., Caslake, L.F. and Nelson, D.C., 2011. Effects

of environmental factors on microbial induced calcium carbonate precipitation. Journal of applied microbiology, 111(2), pp.338-349.

Mujah, D., Shahin, M.A. and Cheng, L., 2017. State-of-the-art review of biocementation by microbially induced calcite precipitation (MICP) for soil stabilization. Geomicrobiology Journal, 34(6), pp.524-537.

Ng WS, Lee ML, Tan CK, Hii SL. 2014. Factors affecting improvement in engineering properties of residual soil through microbial-induced calcite precipitation. J Geotech Geoenviron Eng 140(5):04014006. doi: 10.1061/(ASCE)GT.1943-5606.0001089.

Okwadha GD, Li J. 2010. Optimum conditions for microbial carbonate precipitation. Chemosphere 81(9):1143–1148.

Okyay, T.O. and Rodrigues, D.F., 2015. Biotic and abiotic effects on CO2 sequestration during microbially-induced calcium carbonate precipitation. FEMS microbiology ecology, 91(3), p.fiv017.

Osinubi, K.J., Eberemu, A.O., Ijimdiya, T.S., Yakubu, S.E., Gadzama, E.W., Sani, J.E. and Yohanna, P., 2020. Review of the use of microorganisms in geotechnical engineering applications. SN Applied Sciences, 2(2), pp.1-19.

Osinubi, K.J., Sani, J.E., Eberemu, A.O., Ijimdiya, T.S. and Yakubu, S.E., 2018, October. Unconfined compressive strength of Bacillus Pumilus treated lateritic soil. In The International Congress on Environmental Geotechnics (pp. 410-418). Springer, Singapore.

Osinubi, K.J., Yohanna, P., Eberemu, A.O. and Ijimdiya, T.S., 2019, October. Evaluation of hydraulic conductivity of lateritic soil treated with Bacillus Coagulans for use in waste containment applications. In The International Congress on Environmental Geotechnics (pp. 401-409). Springer, Singapore.

Paul, V.G., Wronkiewicz, D.J. and Mormile, M.R., 2017. Impact of elevated CO2 concentrations on carbonate mineral precipitation ability of sulfate-reducing bacteria and implications for CO2 sequestration. Applied geochemistry, 78, pp.250-271.

Portugal, C.R.M., Fonyo, C., Machado, C.C., Meganck, R. and Jarvis, T., 2020. Microbiologically Induced Calcite Precipitation biocementation, green alternative for roads–is this the breakthrough? A critical review. Journal of Cleaner Production, p.121372.

Rajasekar, A., Moy, C.K. and Wilkinson, S., 2017, May. Stimulation of indigenous carbonate precipitating bacteria for ground improvement. In IOP Conference Series: Earth and Environmental Science (Vol. 68, No. 1, p. 012010). IOP Publishing.

Reeburgh, W.S., 2007. Oceanic methane biogeochemistry. Chemical reviews, 107(2), pp.486-513.

Reichle, D. E. 1977. The role of soil invertebrates in nutrient cycling. Ecol Bull 25:145–156

Rowshanbakht, K., Khamehchiyan, M., Sajedi, R.H. and Nikudel, M.R., 2016. Effect of injected bacterial suspension volume and relative density on carbonate precipitation resulting from microbial treatment. Ecological engineering, 89, pp.49-55.

Sari, Y. D. 2015. Soil strength improvement by microbial cementation. Mar Georesour Geotechnol 33(6):567–571. https ://doi. org/10.1080/10641 19X.2014.95323 4

Solomon, S., Manning, M., Marquis, M. and Qin, D., 2007. Climate change 2007-the physical science basis: Working group I contribution to the fourth assessment report of the IPCC (Vol. 4). Cambridge university press.

Soon, N. W., L. M. Lee, T. C. Khun, and H. S. Ling. 2013. Improvements in engineering properties of soils through microbial-induced calcite precipitation. KSCE Journal of Civil Engineering 17 (4):718–728. doi:10.1007/s12205-013-0149-8

Soon, N., Lee, L., Khun, T., and Ling, H. 2012. An overview of the factors affecting microbial-induced calcite precipitation and its potential application in soil improvement. Int J Civ Environ Struct Constr Archit Eng 6(2):188–194

Stabnikov, V., Ivanov, V. and Chu, J., 2016. Sealing of sand using spraying and percolating biogrouts for the construction of model aquaculture pond in arid desert. International Aquatic Research, 8(3), pp.207-216.

Stocks-Fischer, S., Galinat, J.K. and Bang, S.S., 1999. Microbiological precipitation of CaCO3. Soil Biology and Biochemistry, 31(11), pp.1563-1571.

Sun, X., Miao, L., Tong, T. and Wang, C., 2019. Study of the effect of temperature on microbially induced carbonate precipitation. Acta Geotechnica, 14(3), pp.627-638.

Thomas O'Donnell, S. and Kavazanjian Jr, E., 2015. Stiffness and dilatancy improvements in uncemented sands treated through MICP. Journal of Geotechnical and Geoenvironmental Engineering, 141(11), p.02815004.

Umar, M., Kassim, K. A., Tiong, K., and Chiet, P. 2016. Biological process of soil improvement in civil engineering: a review. J Rock Mech Geotech Eng. https ://doi.org/10.1016/j.jrmge .2016.02.004

Van Paassen, L. A., C. M. Daza, M. Staal, D. Y. Sorokin, W. van der Zon, and M. C. M. van Loosdrecht 2010. Potential soil reinforcement by biological denitrification. Ecological Engineering 36 (2):168–175. doi:10.1016/j.ecoleng.2009.03.026

Van Paassen, L.A., 2009. Biogrout, ground improvement by microbial induced carbonate precipitation [Ph. D. thesis]. Delft University of Technology, Delft, The Netherlands.

Whiffin, V. 2004. $CaCO_3$ precipitation for the production of biocement. Doctoral dissertation, Murdoch Univ., Perth, Western Australia.

Whiffin, V.S., Van Paassen, L.A. and Harkes, M.P., 2007. Microbial carbonate precipitation as a soil improvement technique. Geomicrobiology Journal, 24(5), pp.417-423.

Wong, L.S., 2015. Microbial cementation of ureolytic bacteria from the genus Bacillus: a review of the bacterial application on cement-based materials for cleaner production. Journal of Cleaner Production, 93, pp.5-17.

Xiao, P., Liu, H., Stuedlein, A.W., Evans, T.M. and Xiao, Y., 2019. Effect of relative density and biocementation on cyclic response of calcareous sand. Canadian Geotechnical Journal, 56(12), pp.1849-1862.

Xu, Z. Y., L. Zhang, and J. Zhou. 2009. Effect of microorganisms on some engineering properties of silt. Journal of Civil, Architectural & Environmental Engineering 31 (2):80–84 (in Chinese).

Yargicoglu, E.N., and Reddy, K. R. 2015. Review of biological tools and their applications in geoenvironmental engineering. Rev Environ Sci Biotechnol 14:161–194. https ://doi.org/10.1007/s1115 7-014-9358-y

Zhao, Q., Li, L., Li, C., Li, M., Amini, F. and Zhang, H., 2014. Factors affecting improvement of engineering properties of MICP-treated soil catalyzed by bacteria and urease. Journal of Materials in Civil Engineering, 26(12), p.04014094.

Zhou, F. Q., H. X. Luo, and Y. S. Wang. 1997. The effect of microbes on some geotechnical engineering properties. Rock and Soil Mechanics 18 (2):17–22 (in Chinese).

Zhu, T. and Dittrich, M., 2016. Carbonate precipitation through microbial activities in natural environment, and their potential in biotechnology: a review. Frontiers in bioengineering and biotechnology, 4, p.4.

CHAPTER 9
General conclusions and future research

9.1 Summary of work presented and main conclusions

This research investigated the natural beachrock and identify the durability of artificial rocks to mitigate coastal disaster using biocementation which are environment-friendly and economic feasible techniques for ground improvement. Biochemical methods introduced in this thesis. Furthermore, previous studies related to the MICP have been focused to obtain several MPa values of UCS. However, this study focused to mimic the natural beachrock and identify the durability of artificial rocks to mitigate the coastal disaster using biocementation. It consists of two major sections, which are:

1) Sedimentation mechanism and the properties of natural beachrock
2) Beach sand improvement with microbial induced carbonate precipitation (MICP) of the indigenous local bacteria from beachrock

In Chapter 1, research background, objectives and originality of thesis were described. A comprehensive literature review was carried out on various aspects related to natural coast rock processes and the stability of the MICP process was considered.

Chapter 2 consisted of geophysical investigation of the buried beachrock at Krakal-Sadranan beach, Yogyakarta, Indonesia. The objective was to evaluate the feasibility of constructing artificial beachrocks using natural materials (e.g., microbes, sand, shell, pieces of coral, and seaweed etc.) within a short time, and to propose the method as a novel strategy for coastal protection. Beachrock were found in this area in precipitated beneath beach sand which is wave erosional product and then solidify beneath that formation, floating, between limestone bedrock and beach sands formation based on greater value from resistivity and S wave velocity in the formation layers. The field survey on natural beachrocks suggests that both resistivity and shear wave velocity were higher in the deeper deposits compared to the underlying unconsolidated sand layer within a depth of approximately 1.5 m and covering an area of 210.5 m^3 for the α-section and 76.9 m^3 for the β-section of beachrock deposit.

Chapter 3 consisted of detail laboratory analysis toward beachrock sediment characteristics investigation. The beachrock was also examined to determine the depositional conditions and distribution of rare earth elements. An increased concentration of total rare earth elements, both heavy rare earth elements (terbium, dysprosium, yttrium, holmium, erbium, thulium, ytterbium, and lutetium) and light rare earth elements (lanthanum, cerium, praseodymium,

neodymium, samarium, europium, and gadolinium) indicate that the beachrock deposition process happened under oxidative environmental conditions. This study proposes the novel use of ureolytic bacteria in a depositional environment for carbonate control of a sedimentary process for the development of artificial rock to mitigate coastal erosion. Isolated strains of native bacteria association to *Psedoalteromonas tetradonis*, *Oceanobacillus profundus*, and *Vibrio maritimus* were identified and cultured. These moderately alkalo-tolerant bacteria were showing maximum growth and urease activity at an ambient temperature of 37 °C (based on geochemistry results), which is compatible with the tropical climate prevailing in the target region. Microbial carbonate overriding environmental control is seen in the present day by localization of microbial carbonates in calcareous streams and springs and in shallow tropical seas, and in the past by temporal variation in the abundance of marine microbial carbonates. Only ~4.7% of ureolytic bacteria and algae precipitation, respectively, were assumed to be catalytic factors in beachrock precipitation. The beachrock of Krakal-Sadranan beach in the studied area can be categorized into non-beachrock, unconsolidated beachrock (similar to limestone sands), and well-consolidated beachrock consisting of mostly rock-mineral. Beachrock has a fair consolidated feature and consists of a mixture of gravel-sized deposits of sand in the form of limestone fragments, calcite, and fossil minerals, and almost 50% CaO content (carbonaceous). The interpretation of the cesium anomaly can be used to determine the source of the REEs in this formation, indicating that the beachrock deposition processes originated from the precipitation of seawater under oxidative conditions. This can be interpreted as the beachrock derived from microbial process involving terrigenous materials under oxidative conditions. Thus, the most favorable condition is to have the presence of oxygenated material contamination. Beachrock occurrence in an area depends on highly geological factors that contribute the matrix interior. Indonesian geological settings seem to be dominated by marine activities of the Pacific Ocean and may be labeled as oxidative conditions.

Chapter 4 were determined of ureolytic bacteria from Indonesian tropical shoreline which will compare between characteristic beachrock from Okinawa, Japan. Okinawa beachrock contained more lytic granules with fragments of quartz result material sediments there are predominantly with a fragment of coral shell, meanwhile Yogyakarta beachrock was more like sparite cement which had filling of pore interparticle, therefore that it appears more compact and lower porosity. Micritization proceed in Okinawa beachrock or Yogyakarta is a product of diagenesis rock that formed on the phreatic environment of the sea within the presence of cement on the beachrock occur peloidal micritic. To conclude, the origin of cement micritic peloidal is uncertain. It can be precipitated directly from seawater or it just be a product of

biological activity. Okinawa beachrock were classified as *biotically induced precipitates*, because the organism sets the precipitation process in motion but organic influence on its course is marginal or absent. The reaction takes place outside the cell and the product is very similar, often indistinguishable, from abiotic precipitates. The majority of carbonate material in modern oceans is precipitated as highly structured skeletons of organisms were dominant in the cold water rather than tropical area. Whereas Indonesia beachrocks is *classified as biotically controlled precipitates* which commonly the precipitation is induced by microorganisms, mostly bacteria and cyanobacteria. Micrite is a major, often dominant component of these deposits. Microalgae as mats were found enrichment inside Indonesia beachrock site than Okinawa beachrock which mostly consist of skeletal shells.

Chapter 5 consisted of beach sand treatment based on MICP process to mimic the natural beachrock, achievement identical with natural beachrock based on chemical compound and strength. The results revealed that the bacteria could effectively mineralize the calcium carbonate between 30 to 40 ℃, showing in more robust performance under tropical conditions. Natural beachrock and artificial beachrock bore similar results following the MICP process examining properties such as chemical compounds, meniscus carbonate bridges, and rock properties. However, the strength and porosity of artificial bedrocks were significantly different from those of natural beachrocks which intensified carbonate precipitation processes. The results of the sand solidification test in the laboratory showed that treated sand achieved unconfined compressive strength of up to around 6 MPa, determined after a treatment period of 14 days under optimum conditions. The calcium carbonate crystals which found in this research were amorphic condition which has an orthorhombic, rhombohedron, hexagonal, and spherical geometry of the calcium carbonate complexes. By adding biopolymer polysaccharides, the reaction leads the crystallization formation of vaterite instead of calcite which common type of polymorphism in MICP without changing the morphology of the crystals (anionic polysaccharides). On other hand, the ions NaCl and $MgCl_2$ concentrations on MICP is higher than those of average seawater favors microbially mediated formation of Mg-rich carbonates, which are often considered as potential dolomite precursors. Even though the process deemed to negatively affect the desired engineering properties of the treated specimens. It is clearly deduced that the strength decline is mainly due to the change in crystal morphology (rather than the quantity of precipitate) to a needle shaped crystal form with lower bonding capacity than that of the well-interweaved and cross-linked rhombohedral crystals produced in the absence of magnesium.

Chapter 6 delivers the testing of durability based on MICP for coastal disaster countermeasures development. Experimental work presented in this paper investigated the physical and mechanical characteristics of MICP treated slope soil subjected to WD cyclic action. Based on the results, it can be concluded that the damages were higher to the specimens subjected to WD cycles under saltwater condition compared to those subjected to distilled WD cycles. The saltwater WD induced erosion is highly reliant on the level of cementation. The increase in precipitated calcium carbonate content substantially increased the aggregate stability of specimens under the exposure of WD cycles. On the other hand, the level of cementation was not significantly influencing the WD induced erosion, which is less than 40% for saltwater condition and less than 30% for distilled water condition. SDR values suggest that the MICP specimens underwent severe degradation under saltwater WD cycles (over 40%). Comparatively, the reduction of UCS is low under WD cycles (between around 40 – 55%). Under both WD cycles, the strength deterioration likely to be in a relationship with the precipitated calcium carbonate content.

Chapter 7 consisted of cost reduction purposes using inexpensive chemical reagent from the culture media and cement solution for MICP treatment. Sand samples treated under different conditions were subjected to a needle penetration test and WD test for durability of the materials. Introducing low-grade chemicals rather than laboratory-grade pure chemicals resulted in a remarkable enhancement in strength. The UCS value was similar value obtained while using pure chemicals. This innovative alternation amounts to an 83% up to 87% reduction in the material cost and allows the leaching of harmful chemicals to be avoided. However, the durability results of the low-grade chemical show that it has huge damage when treated for 21 cycles of WD test, it is shown the bonding particles of biocement was not as strong as treated with pure standard chemical solutions. Further investigation is needed to achieve sustainable MICP material by mixing solution ratio with standard material for coastal development. Inexpensive material could be an alternative solution for inland biocementation and also maintenance of the material.

Chapter 8 is the proposal of the coastal prevention method based on ureolytic bacteria especially in Indonesia. The most favorable bacteria for soil biocementation come from, but not limited to, highly urease active bacteria (e.g. *Psedoalteromonas tetradonis*). It is vital to know the effective mechanism of $CaCO_3$ precipitation because it translates to a lower cost of MICP treatment and achieves strong material in the long-term periods. In return, this can pave the way into possible commercialization of the technique in the near future. Some important key factors of the MICP determined to include ureolytic bacteria, culture media, cement

solution, soil/sand, and treatment sand condition such as pH and temperature during the treatment.

Overall, the results of this study were contributed to the application of a new technique for soil improvement and bio-stimulation. Therefore, to summaries of this research were described in this chapter including suggestions for the next future research regarding MICP treatment in the coastal areas. For obtaining the achievement of a uniformly homogenous sample and getting several MPa of average strength from the solidified sample, the small size of lab model tests was conducted as described in this chapter. The result obtained from each chapter point out that the solidification using indigenous ureolytic bacteria strain for MICP method and stand as promising techniques for beach slope improvement.

9.2 Suggestions for future works in MICP method

The field of biocementation involves multidisciplinary research at the confluence of geotechnical engineering, microbiology, ecology, and chemical engineering. Despite the fact that several types of surface improvement research fields have developed main sets of data and interpretations, currently, no study has yet attempted to determine the optimum MICP process in terms of the cost and factors involved, for potential commercial implementation.

9.2.1 Froude similarity of upscale MICP

Specific challenges ahead to MICP upscaling include controlling the flow and transport through heterogeneous media, dynamic movement of sedimentary transport the treated material, the permanence of the mixing technique, and the Froude similarity prototype example are necessarily needed to minimize the failure of treated material especially in the coastal area.

9.2.2 Hydrodynamic test and wave erosion test of beach treatment by MICP

Testing methods by using model for artificial beachrock against the marine environment system such as hydrodynamic test and wave erosion test. After treatment of the prototype example are necessarily needed to minimize the failure of treated material.

9.2.3 Further research for durability of saltwater resistance

Further study should be carried out to develop methods that could extract Ca from waste material or to reduce the usage of urea and broaden the scope of MICP applications, not just in terms of strengthening and improving soils but also harnessing the soil's ability to self-heal using the premixed microorganisms in the soil matrix. One method to use chalk waste and

agriculture by-products (vinegars-acetic acid or folic acid) to produce biogrout to remove the need for calcium chloride or other types of calcium. However, the durability of long-term MICP product especially for marine environment which have a fully saturated condition. Inexpensive material has a Ca^{2+} ion similar to a pure standard from industrial products but the durability wetting-drying tests shown the material is not resistant with the water and saltwater. The sodium and H_2O ions evaporated the meniscus bridge of calcium carbonate crystals. The mixing composition of cement solution will achieve to develop water-resistant materials in the next future research.

APPENDIXES A

Coastal drone mapping of Yogyakarta shoreline

A.1 Introduction

Unmanned Aerial Vehicles (UAVs) technology nowadays were effective for monitoring of large area and existing of infrastructure, farm mapping, or other purposes. With recent advances in aerial data acquisition technologies from UAVs (Harwin and Lucieer,2012; Turner et al., 2012), it is now possible to capture high-resolution rock surface images and analyses geological structures within those data sets digitally. Very large digital data sets can be collected rapidly, covering significant surface areas with centimeter-scale resolution. Photogrammetry is a technique that captures 3D information of features from two or more photographs of the same object, obtained from different angles (Donovan and Lebaron, 2009; Haneberg, 2008; Behan, 2010). In particular, structure from motion, is a photogrammetric technique, where the camera positions and orientation are solved automatically, in contrast to conventional photogrammetry where a priori knowledge of these parameters is required (Goesele, et al.,2007; Vasuki, et al., 2014). The UAV survey equipment and data processing methods are now readily available and suitable for use by coastal engineers, managers and scientists. At its core, UAVs use autonomous flight technology combined with recent advances in computer vision techniques, to extend the very familiar and already extensive use of aerial photogrammetry applied to coastal surveying (Turner, et al., 2016; Warren, et al, 2018; Cawood, et al., 2017).

Coastal erosion issues become more critical because coastal zones are optimal places for population concentration and the development of productive activities, such as, industry, transportation, tourism, etc. (Barragan and Andreis, 2015). Coastal erosion is a common problem affecting about 75% of the world's shorelines (Bird, 1985; Zhang et al., 2004; Pilkey and Cooper, 2014; Rangel-Buitrago, et al., 2018). Adger et al. (2005) indicated that close to 20% of the world population (1409 million inhabitants) reside less than 25 km from the coastline, and 40% (2818 million inhabitants) live less than 100 km inside a coastal strip representing approximately 25% of the world total surface. Coastal zone monitoring based on aerial data, satellite or field investigating is an important task in environmental protection and fundamental coastal management. Datasets produced by UAV's have such a high spatial resolution that characteristics and changes of the landscape, such as morphology, coastal zone, and beach morphological characteristics into two dimensions (2D) or three dimensions (3D) numerical models (Yastikli, et al., 2013; Mancini, et al., 2013; Nex and Remondino, 2014; Topouzelis, et al., 2015). However, a coastline is defined as the line that forms the boundary between the land and the sea, the detection of a coastline in high resolution includes recognizing several discontinuities. For the proper study of a coastal areas, the four typical beach zones should be examined. These beach zone

include the swash zone, beach face, wrack line, and berm (Papakonstantinou, et al., 2016). The movement of the shoreline position due to accretion or erosion is a great concern in coastal zone management. Morton (1977) after Moran (2004) stated that mapping shoreline changes and predicting future shoreline positions have to be an important scientific and coastal management objective. Therefore, the accurate measures of the historic shoreline position and prediction of future locations are essential for coastal planning and management. In this research were explained only measurement of UAV to identifying into 3D elevation model and classifying of the area toward beachrock investigation in Krakal-Sadranan beach area, beachrock as a key for coastal propagation mapping identification outcome for final result.

A.1.1 Problem statement

Yogyakarta beaches were consisting of two different types of sands, whereas iron silica sand from Mt. Merapi volcanic sedimentary and calcareous sand from the coral reef and/or limestone formation in the eastern Yogyakarta. As a tourist destination, the beaches such as Parangtritis-Samas-Tisik-Pandansari (Silica sand - south central Yogyakarta) and also Krakal-Sadranan-Baron-Kukup-Drini-Pok Tunggal until Wediombo beaches (Calcareous sand - south eastern Yogyakarta) has developed as an economic center in the coastal shoreline of Yogyakarta province (Figure A.1). As a potential economically growing area, the Yogyakarta coast has attracted over time more and more people to reside and has a good living condition. As a consequence, the growing number of people needs more space and starts to utilize the coast which creating vulnerable areas from coastal hazards despite the buffer zone of 200 m according to the spatial planning has been established.

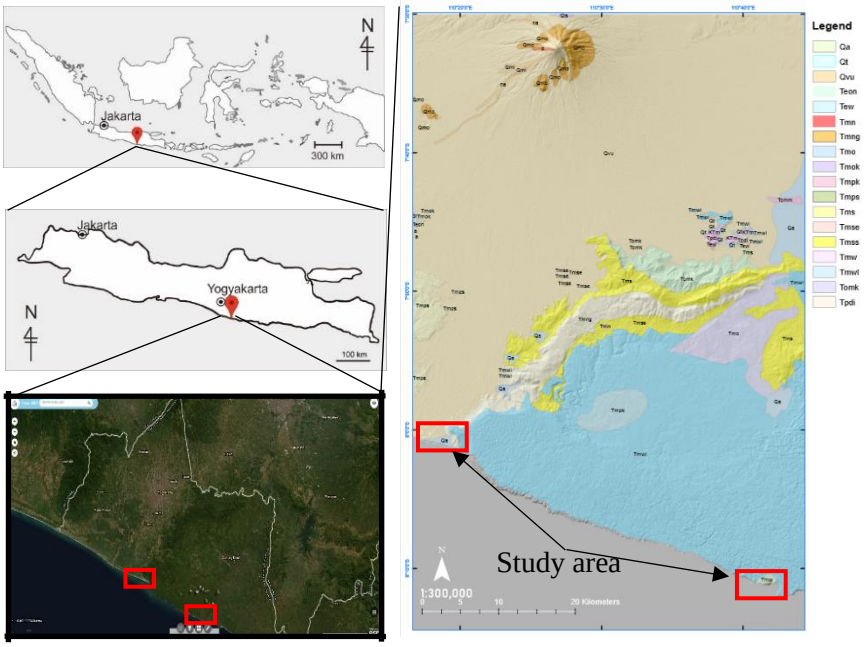


Figure A.1. Simplified geological map of Yogyakarta, Indonesia.

On the other hand, the south coast of Java has been suffered from geologic and climatologic events such as tsunami in July 2006 and storm-tidal wave, last moment is Oct 2018. Beach erosion also reported in some parts of Yogyakarta's south coast such as Samas beach and Parangtritis beach (Tijaya, 2008; Pujotomo, 2009). Those natural phenomena were reported to cause damages to infrastructure near the shore. The establishment of a buffer zone is one of several efforts commonly taken to reduce risk in the framework of coastal disaster risk management. Coastal zone management requires to the understanding of shoreline dynamic and consider the potential future hazard such as enhanced sea-level rise due to global warming phenomenon. Monitoring coastal changes over time needs a complete spatial-temporal data, which is difficult to find in Indonesia. The integration of multi-source spatial and temporal data such as topographic maps and also satellite imageries is considered to overcome the lack of data series availability (Marfai and King, 2007). This study is focused on the understanding of Java South coast characteristics particularly in Parangtritis beach and Krakal-Sadranan beach were beachrock were found, further studies were carried out to (i) identification of beachrock deposit occurrences in Krakal-Sadranan, Yogyakarta (ii) develop the biomineralization based on ureolytic bacteria from natural beachrock using calcareous and iron-silica sands, and (iii) explore biocementation for nearshore environments as an alternative technique for sand stabilization.

A.1.2 Overview of Beach Sediment

The beach system includes the dry (subaerial) beach, the wet beach (swash or intertidal zone), the surf zone, and the nearshore zone lying beyond the breakers (Short, 2006). Mostly the nearshore zone is defined as the area beginning from the low-water line extending seaward. The surf zone is part of the nearshore zone. The subaerial beach has a gentle seaward slope, typically with a concave profile, and extends from the low-water mark landward to a place where there is a change in material or physiography (such as a dune, bluff, or cliff, or even a sea wall) or to the line of permanent vegetation marked by the limit of highest storm waves or surge. If the area beginning from the low-water line is regarded, the profile is not concave when looking to a beach with a certain tidal range. The dry beach is concave, but at low water when including the wet beach, the morphology switches from a concave beach (dry part) to a convex beach (wet part). Nearshore bars and troughs (in the subtidal domain) are often present in the surf zone, but are obscured by waves and surf, as is the always submerged nearshore zone (Short, 2006). Beach morphology refers to the shape of the beach, surf, and nearshore zone. The beach per se contains numerous morphological– processual subunits such as berms, storm ridges (e.g., Pethick, 1984; Hesp, 1988; Komar, 1998; Davis and FitzGerald, 2009), cusps, beach face, shoreface (e.g., Swift et al., 1985), plunge step (Davis and Fox, 1971), scarp, etc.

A.1.2.1 Parangtritis beach

The geological formation in Bantul region are formed by recent sedimentation of Merapi Volcano on the middle part (graben Bantul) and several parts were form of Sentolo formation hill on the western part consist of alluvium, andesite (Baturagung), Semilir formation, Kepek and Nglanggran formation on the eastern Yogyakarta (Figure 1.4 – see chapter 1). Physiographical, the landscape consists of the Mt. Merapi fluvio-volcanic plain, the Baturagung mountain range, the Sentolo hills, Progo river plain and the shore plain. The elevation between 0 – 35 m above mean sea level which bordered directly by the Indian Ocean. Most of the beach topography is almost flat and gradually steeper toward the west near Opak river. Landward of the beach, one finds large areas with sand dune of several types such as barchan and longitudinal dunes (Bronto, 1989; Pujotomo, 2009).

A.1.2.2 Krakal-Sadranan beach

Beaches of Gunungkidul Regency, Province of Special Region Yogyakarta (Prov. DIY), Indonesia have economic potential as limestone mine deposits and tourism. The karst beaches in Gunungkidul Regency, Sadranan Beach to be exact, have similarities in terms of geological conditions, methods, and geomorphologic processes beach formation. The characteristics of the Karst Mountains of South Beach indicate that there is steep topography that rises to the east of Java Island. Continuing eastward hummocky valleys occur (Drini Beach to Krakal to Sadranan). The coast of Sadranan have a slope were steep ~12,33° with the tidal range of 12 meter that makes the sedimentary process in this coast were thickness than the deeper slope. Grains of sediment along Krakal and Sadranan beaches are largely bright colored along most of the coastline as a result of the erosion of seabed being deposited on the beach. Figure 1.4 (see chapter 1) is described the composition of this sediment mainly formed by coral, skeletal fragment, Foraminifera and Mollusca. Throughout the karst coast of the DIY Prov., Gunungkidul Regency the soil is derived from limestone bedrock, similar to the Mediterranean, i.e., the level of physical weathering is high (Daryono, et al., 2019).

A.1.3 Coastal disaster

According to the Indonesian disaster management bill, disaster is defined as an event or series of events that threaten or disturb community life caused by natural, non-natural, or human factors that bringing losses of properties even the lives of the community. Coastal disasters caused by the coastal dynamic that damaging the coastal environment. Coastal dynamic understanding is the changes by the interaction of seven factors that operate interactively and interdependently, whereas called astrodynamics, aerodynamic, hydrodynamic, morphodynamic, eco dynamic, and anthropodynamic (Marfai and Permana, 2014). The coastal disaster classified into (1) Natural Disaster which consists of

storm waves, tidal waves, tsunami, marine erosion, and sedimentation; (2) Non-natural Disaster which consist of coastal structures failures, coastal spatial planning failure, deprived of coastal ecosystem and coast; (3) Social Disaster such as social conflict and crime. To alleviate the consequences of being threatened by coastal disasters, the mitigation effort should be considered. Indonesia Disaster Management Bill defined mitigation as a series to reduce disaster risk utilizing structural or physical development of the building capacity. Further, the bill described that mitigation consists of spatial planning, building code, and community building capacity through education, information, and training.

A.1.1.4 Oceanography of the Java south coast

Yogyakarta beaches were directly facing Indian Ocean and therefore subjected to Indian Ocean's high waves energy. Data derived from US Navy Marine Climate Atlas of the World Vol. 3 Indian Ocean (1976) reported by JICA (1988) cited in Triatmojo (1999), based on 120-year statistic pointed out that wave from south direction with 1-2 m in height has dominated about 20% of waves occurrences (shown in Table A.1).

Table A.1. Wave height in Indian Ocean (Levitus, et al., 1994)

Wave height	**Percentage (%) of occurrences**		
H (m)	Southeast	South	Southwest
0 – 1	4.67	3.02	2.54
1 – 2	9.89	20.27	7.79
2 – 3	4.48	7.54	5.07
> 3	0.56	1.89	1.13

South and southeast waves in relation to general orientation of the shoreline has generated alongshore currents toward the west direction. Indications of this area that material deposited in the mouth of Opak river form coastal gradation to the west direction. The pattern of surface current along the south coast of Java has been recorded by Wyrtki (1961) in Pujotomo (2009), showing that during the months December – June surface current is directed to the east while during August – October it changed to the west. Tide pattern in South Yogyakarta coast is mixed predominantly semidiurnal type. This type of tide has high and low tides twice a day. Water level between successive high tides separated approximately by 12-hour time period. Figure A.2 is described the tide pattern in Yogyakarta, Java south coast which is mixed-predominantly semidiurnal.

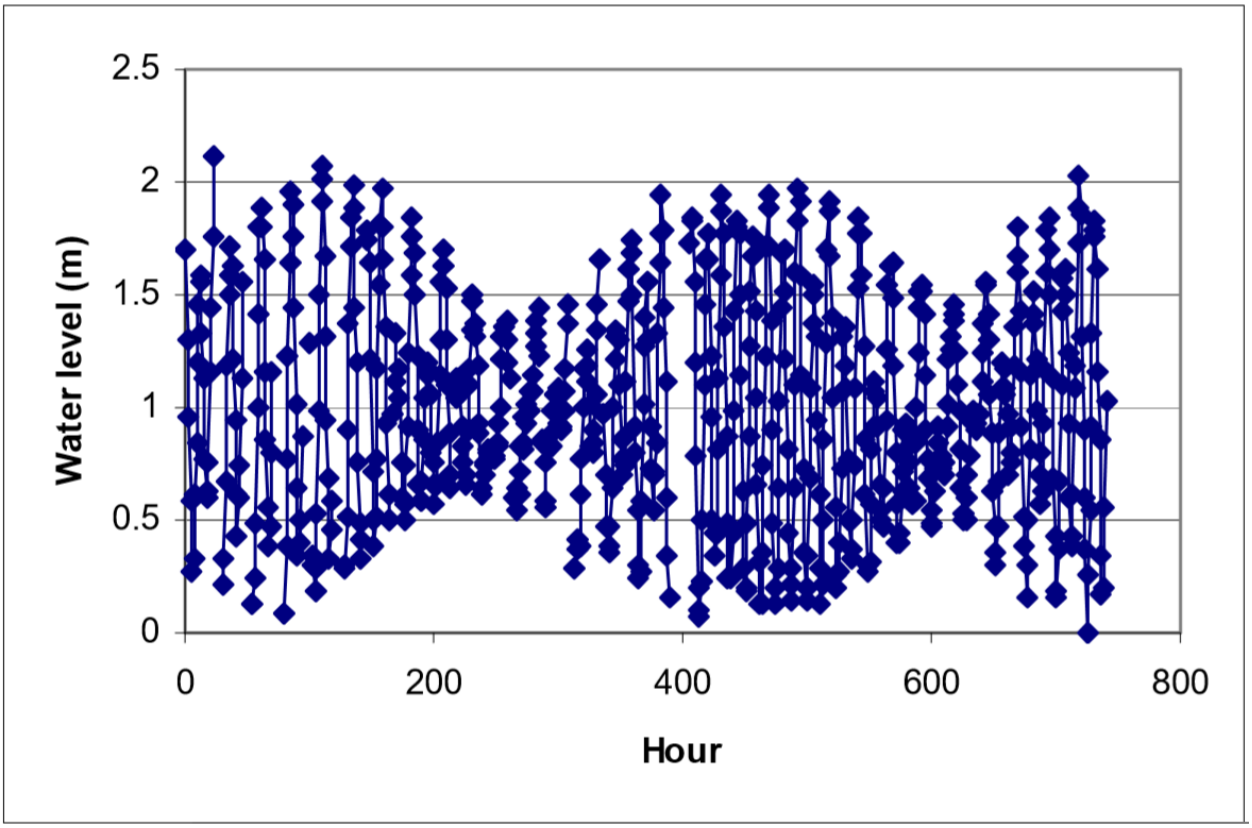


Figure A.2. Tide pattern of South Yogyakarta coast (Sadeng tide gauge station)

A. 2 Materials and methods

A.2.1 UAV photogrammetric data

Photogrammetry is a science of performing measurements from photographs. The key problem is to find a 3D position of points of a scene from overlapping images. Normally, site measured by UAS cannot be taken with one photo, so it demands that the pictures are taken with proper forward and side overlap so that they can be later processed. This process is based on collinearity condition, in which a line originates from central projection of a camera and goes through a point in sensor plane (on the image) to the object point in the ground coordinate system. The intersection of many lines determines the location of three-dimensional points of a scene.

Image orientation and camera calibration are essential for reconstructing metric model from images. They can be achieved by two approaches: classical photogrammetric workflow or computer vision (CV) technique. The former relies on known camera positions and resolves the model by triangulation. If the camera positions are unknown, the solution is to place a set of reference markers with known 3D coordinates, identify them manually in the images and use re-sectioning to get camera positions. The challenges with the acquisition of data using a UAV on coastal zone environmental parameter such as

wind and cloud coverage. The UAV photogrammetry in this case we used DJI Phantom 3 which carried a GoPro HERO 7 camera and 3D gimbal to reduce shaking. The lens of the GoPro camera was replaced with a distortion-free lens to reduce the lens distortion effect. In this context, aerial photos were obtained from selected sites aiming to a) study and map in detail particular shoreline features and b) facilitate the reconstruction of the coastal environment. The details specification of the photogrammetric measurement using UAV are given in Table A.2. Three locations were selected for Krakal-Sadranan beach with corresponding aerial photographs. In order to carry out the aerial photography at each site, it was necessary to locate a wide flat space for the take-off and landing of the UAV. Using special software, the desired area to cover is defined, along with required ground resolution and image overlap, and a full flight plan is generated with flight lines.

Table A.2. Specification of unmanned aerial vehicle (UAV) drone

Characteristic	Detail description	Specifications
UAV	Flying height	80 m
	Relative total flight time	20 min
	Coverage area	1 km^2
	Estimated speed	2 m/s
	Auto pilot	No
	Distance from launch pad	10 m
	Size	11.4” x 11.4” x 7.7”
Sensor	Camera	GoPro 6
		12 MP/ 30 fps Burst Time Lapse
	Touch Display	2 inches with pinch zoom
	GPS	Provided
	Waterproof	33 ft to 10 m
	Video modes	4K40/ 1440p120/ 1080p240
	Image dimension	4096 x 3072
	Focal length (mm)	2.77
	Number of images	359
	Images overlay	90%
	Error tie points (pixels)	1.47
	Format	Jpg
	Pixel size (μm)	1.597 x 1.957
	Angular field of view	Horizontal: 49.1°
		Vertical: 58.5°
Survey	Ground sampling distance (m/ pix)	0.034

A.2.2 Photogrammetric data processing

We generated 3D dense point clouds representing the digital terrain and photomosaic of Krakal-Sadranan beach using the structure from motion and multi view stereo (SfMMVS) workflows (Szeliski, 2010). The workflow consists of 3 main processing steps. First, the same ground features are detected and matched in different camera perspectives; then, a three-dimensional (3D) scene structure is reconstructed by solving the intrinsic and extrinsic orientation parameters of the camera and generating a sparse point cloud. In the last step, a 3D dense point cloud is produced by calculating a depth map for each camera frame using the MVS image-matching algorithm (Carrivick et al., 2016).

Automatic aerial triangulation (AAT) to determine the orientation of the captured images usually is the first step of photogrammetric evaluation. Commercially software systems to solve this task are available for more than a decade (Tang et.al., 1997). As a central component, these systems contain image matching tools for the generation of tie points. The required automatic measurement is usually realized at sufficient accuracy and reliability by a combination of standard feature and intensity based matching approaches. Primitives suitable for image matching are extracted in a first step, while in a second step their correspondences are determined by some similarity and consistency measures (Förstner, 1993). In order to efficiently transfer the extracted feature points to the respective neighbor images, usually a priori information is additionally integrated in order to speed up the required search effort. For this purpose, the respective image overlap is provided from the so-called block configuration. By these means, suitable search areas can be defined, which considerably speeds up the matching step. For standard aerial image flights this block configuration is usually derived from the respective camera stations as provided from GPS measurements. In principle, camera orientation can additionally be used, if for example measured by an integrated GPS/inertial system. However, for block configuration of photogrammetric flights with large format cameras, the assumption of nadir views is usually sufficient. This initial guess holds especially true if the camera is mounted in a stabilized platform. An addition problem for block configuration results from the fact that the consumer cameras used for aerial image collection have a much smaller format footprint than digital airborne cameras. Both high flight dynamics and relatively small image footprint result in considerable deviations in mutual image overlaps. As a consequence, standard assumptions and implications used during standard AAT do not hold true anymore. This will frequently aggravate the successful block configuration and thus hinder processing of UAV imagery by such software tools.

A.2.3 Digital elevation models and volume calculations

High-resolution DEMs were used to analyze the surface of the lava dome before and after the six-explosion episode and to calculate the losses and gains in volume. We measured the length, width, and depth of the main fissure by creating cross-section profiles of the beachrock in Krakal-Sadranan beach,

Yogyakarta. For the volume calculations, we first delineated the loss and gain areas based on the results of topography change calculations. Then, we cropped the DEMs in the loss and gain areas. By applying the cut and fill tool in the ArcGIS software, we obtained the values of the lost and gained volumes in the identified cell areas.

A.2.4 Processing software

To evaluate surface changes and differences in the beaches and dunes, spatial analysis was conducted using Pix4D mapper and Agisoft software. This software is a validated analysis tool for interactive 3D geo-spatial processing (Varela-González et al., 2013), which allows for a surface comparison between surveys and provides information regarding spatial variation (Brown and Arbogast, 1999). This software allows for the draping of DSMs with orthophotos, thereby improving analysis and integrating the 3D assessment from DSMs with 2D data to clearly identify seasonal changes, beach land use, or vegetation cover above dunes (Gonçalvez and Henriques, 2015). This process was performed for each segment.

Pix4D Mapper was used in post processing of the data as the most suitable tool among all Pix4D products for terrain mapping. While creating a new project, user can set two different coordinate systems, one for centers of images and the second one for Ground Control Points and output products. Geolocation of images can be imported straight from EXIF or coordinates of photos can also be acquired for example from flight logs from UAV and imported into the software from *.txt file. After creating a project, processing is restricted to 3 steps, that are followed one after another and each creates some output products (Pix4D, 2017). Agisoft Photo Scan is a stand-alone software package created and developed by Russian company Agisoft LCC founded in 2006. It is designed to cope with photogrammetric computer vision projects such as area mapping or 3D object digitization task. It found its application in field where digital photogrammetry is a fast and low-cost tool. There are numerous examples of using the software in archaeology for excavation documentation, in 3D scanning for video games or cultural heritage for conservation and documentation (Tokarczyk & Kwiatek, 2015). However, the most important application for this thesis is its topography reconstruction and mapping.

A.2.5 Beach/dune surface changes

To evaluate surface changes and differences in the beaches and dunes, spatial analysis was conducted using Arc-Gis software. This software is a validated analysis tool for interactive 3D geo-spatial processing (Varela-González et al., 2013), which allows for a surface comparison between surveys and provides information regarding spatial variation (Brown and Arbogast, 1999). This software allows for the draping of DSMs with orthophotos, thereby improving analysis and integrating

the 3D assessment from DSMs with 2D data to clearly identify seasonal changes, beach land use, or vegetation cover above dunes (Gonçalvez and Henriques, 2015). The high resolution of DSMs allowed for the representation of beach and dune spatial changes using a 0.5 m color scale within the ranges of <+4 m to >− 4 m. Regarding of the beachrock formation as a key to identify the beach zonation in this area, whereas beachrocks have proven particularly useful in the absence of other sea level indicators or when coupled with other available sea level indicators (e.g. Erginal et al., 2012; Stattegger et al., 2013; Mourtzas et al., 2014). In the past decades a number of studies have taken place regarding beachrocks (e.g. Guilcher, 1969; Sanlaville, 1970; Dalongeville, 1984). Hopley (1986) was the first to provide a methodological synthesis on the use of beachrocks as sea level indicators with particular guidelines, and further stated that beachrocks should be used in conjunction with other types of evidence, particularly in macrotidal areas. Furthermore, the potential of beachrocks as a useful record of shore position has been suggested by Semeniuk and Searle (1987), while Cooper (1991) suggested they may preserve former shoreline morphology and alignment. Based on the cement characteristics and sediment bedding information, a reliable of sea level changes may be achieved, by defining the position of a beachrock and transforming it into an index point (Mauz et al., 2015).

A.3 Results

A.3.1. Parangtritis beach

A.3.1.1 Geomorphology

Parangtritis beach stretches along approximately 7 km in east-west direction, started from cliff in east to the Opak river mouth in the west. According to Sunarto (2008) Parangtritis is classified as a depositional coast. Parangtritis also can divided into two landforms whereas coastal lowland and coastal



Figure A.3. 3D view of Parangtritis (Google earth)

highland. Parangtritis coastal lowland is characterized by sandy volcanic beach, while coastal highland is marked by limestone cliff coast and andesite cliff coast. The beach profile in the coastal lowland shows the existence of foreshore, backshore, and dune. Parangtritis beach grain size distribution gradually change in diameter from east to west (Bronto, 1989; Pujotomo, 2009). At the east part, the beach has relatively fine sand and gentle slope while in the west part, grain size is relatively coarse and steep slope. Near the mouth Opak river and surroundings, very coarse sand to gravel were found which is interfere from the river sedimentation source (Figure A.3).

A.3.1.2 Shoreline changes analysis

Shoreline change is analyzed statistically using ArcGIS software which is the powerful option software for analyzing shoreline change data. These options are, for example, shoreline change envelope (SCE), net shoreline movement (NSM), end point rate (EPR), and linear regression (LRR). SCE and NSM provide a shoreline distance at each transect; however, their results do not include information on the rate at which the shoreline changes. SCE calculates the greatest distance between all shorelines without factoring in the year of the shoreline, while NSM represents a total distance between the oldest and the most recent shoreline, i.e. 2006 and 2015, respectively. EPR and LRR provide the rate of shoreline change at each transect. EPR is the distance of shoreline shift divided by the time elapsed between the 2006 and 2015 shorelines. Meanwhile, LRR is determined by fitting a least squares regression line to all shoreline points for a particular transect. Even though LRR uses all available shorelines and provides a statistically robust analysis, it is susceptible to outlier effect. Therefore, this research uses EPR to analyze the rate of shoreline change. In NSM and EPR, positive values refer to accretion, while negative values indicate erosion.

The 1995 shoreline data is used as a baseline because the shoreline data from the existing high-resolution imagery (2006–2015) did not meet the requirements for the baseline, i.e. the baseline should be established adjacent to the series of shoreline positions and cannot place entirely onshore or offshore with respect to the other shorelines. Furthermore, 29 transects spaced at 50-meter intervals along the shoreline stretch 100 meters landward and perpendicularly to the baseline (Mutaqin, 2017). The rate of shoreline change (meter/year) is obtained technically by dividing the distance of shoreline displacement (meters) by the time elapsed between the years of satellite images used in the analysis (years). Table 2 shows the rate of shoreline change, as measured using EPR, in South Yogyakarta coastal area in 2006–2015. A zero lowest rate in 2006–2015, found at transect number 23, does not represent any shoreline movement because the result of SCE at the same transect shows that the greatest distance between the shorelines is 41.0 m. The zero lowest rate is caused by one variable used in EPR, i.e. the very short distance of shoreline movement (< 0.5 m) at transect number 23 (Figure A.4). In general, the average

rate of shoreline change is negative (−2.3 m/year), which corroborates the result of NSM that states erosion as a more likely trend of shoreline change in the research area in 2006–2015.

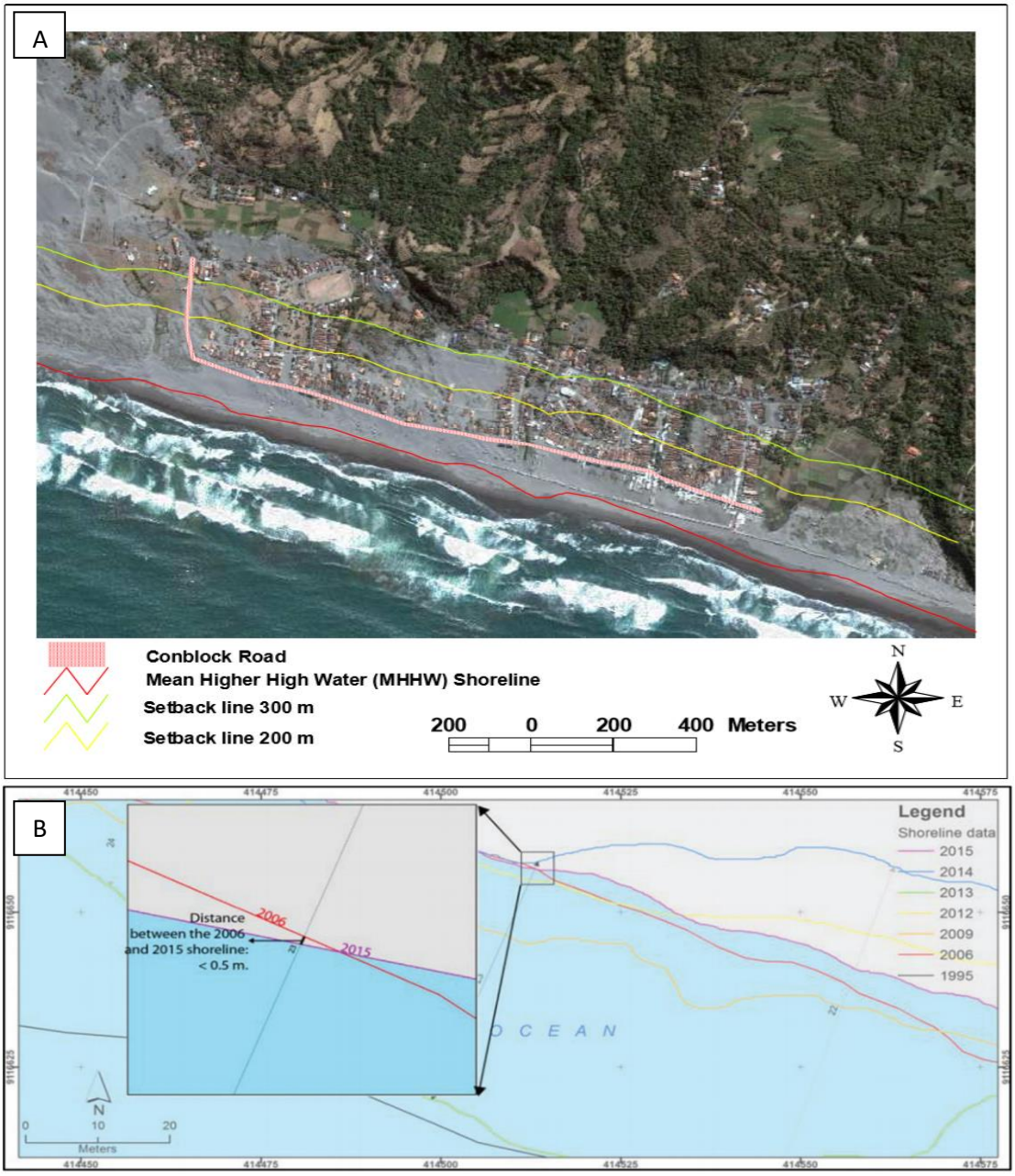


Figure A.4. Shoreline change on Yogyakarta south coast since 1995-2015 (modified from Pujotomo, 2009 and Mutaqin, 2017), (A) propagation in the Parangtritis area and (B) Samas beach area.

A.3.2 Krakal-Sadranan beach

A.3.2.1 Geomorphology

The geomorphological of this research area (Figure A.5) divided based on morphographic, morphogenesis and morphometry. Morphographic by determining the shape of the land that seen of the field appearance, including plains, hills, mountains and others. Morphometry with the value of the regional geomorphological aspects in the form of slope, altitude, slope length and roughness relief.

Morphogenesis by determining the processes that become the cause of the morphology that exists in the mapping area. This research area is in the form of a karst landscape and a beach, namely the karst hill, the karst valley and the coast. While the morphometry is related to the slope and point slope height. The slope is one of the controlling factors that influence mass movement in determining the susceptibility zone of mass movement. From the results of the analysis of the geomorphological data of the study area with an approach. The geomorphology of the study area is divided into five geomorphological units which are the Kars sloping hill unit, the steep Kars hill unit, the steep Kars hill unit, the Kars valley unit, and the beach unit.

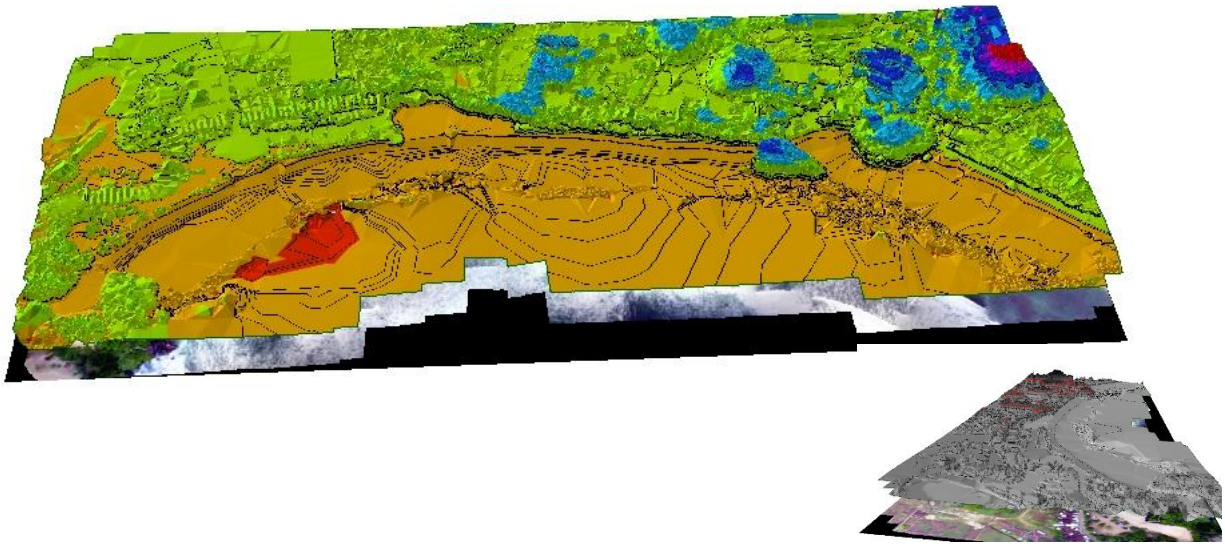


Figure A.5. 3D view of digital elevation model Krakal-Sadranan beaches, Yogyakarta

A.3.2.2 Straightness density

The geological structure is one of the controlling factors that cause the occurrence of mass movements. This lineament density is in the form of lineaments that exist in the area of research identified based on appearance on the map contour and digital elevation model (DEM). The use of this straightness density is because it is difficult for the discovery of clear structures in the field. The straightness pattern that is around the research area is southwest-northeast and southeast-northwest. The classification of the density of this structure is based on the classification according to Baskoro and Rifai (2015) where the number of lineages per 1 km^2 is calculated. The division of lineament density is based on the number of straightness in the research area. The research area is divided into three parts with a width of 500 meters each part. In western research, the area has 4 straightness were shown in table A.3. In the study area, the middle section has 9 lineaments. In the eastern area of the study has 5 lineaments. From the amount of straightness, therefore, this research area is divided into three units of

lineament density that is, the unit density is very rare with 4 straightness, the unit density is sparse with 5 straightness, and medium density unit with 9 straightness (Figure A.6).

Table A.3. Interval class of straightness density

No.	Number of Straightness per 1 km^2	Classification
1	1 – 4	Very rare
2	5 – 8	Rare
3	9 – 12	Moderate
4	13 – 16	Often
5	17 – 20	Very often

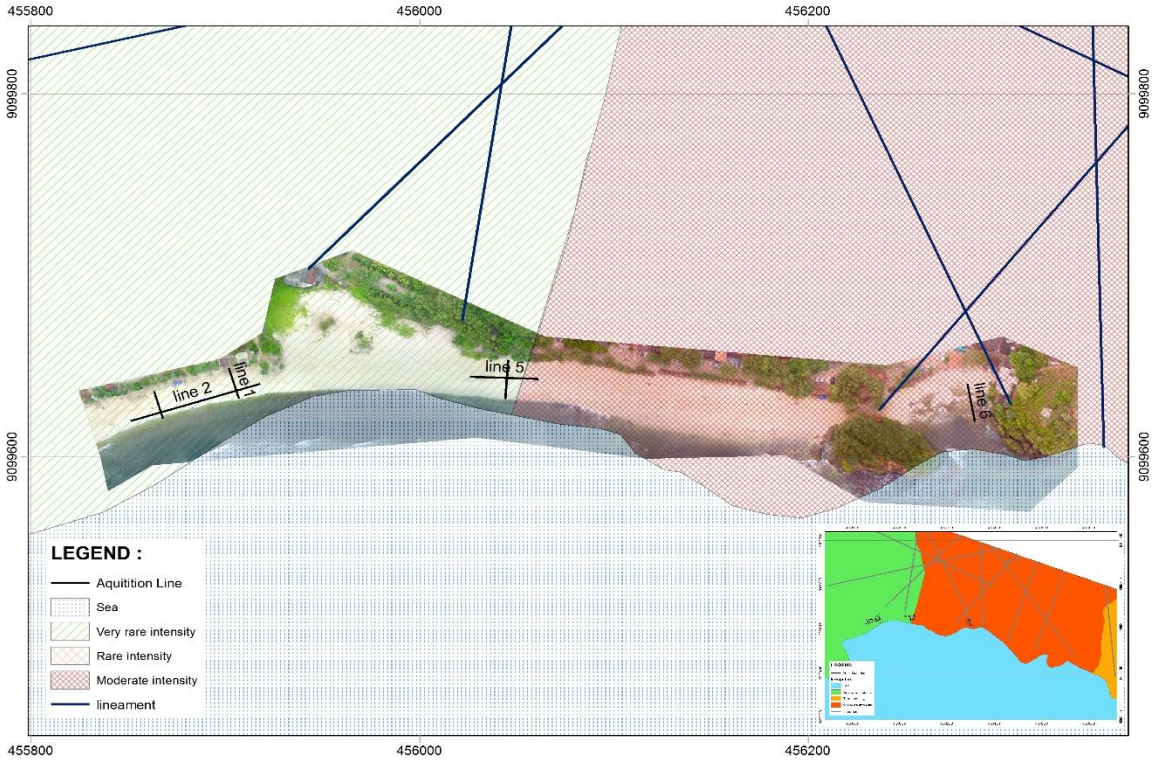


Figure A.6. Straightness density lineament of Krakal-Sadranan beach overlay with UAV photogrammetric.

A.3.2.3 Zonation of beachrock deposit

A broader counter-mapping movement had been developed through the 1990s as a response to two decades of industrial timber exploitation and the Indonesian government's superseding of customary forest rights through official planning and mapping efforts (Peluso 1995). It was conducted by local activists with assistance from international organizations and sometimes government agencies. Counter-mapping tended to delineate and formalize claims to forest territories and resources that certain communities or villages had traditionally managed by using sketch maps (Peluso 1995). The automatic

aerial triangulation (AAT) method which is used to determine the orientation of captured images is usually the first step of a photogrammetric evaluation. Commercial software systems to solve this task have been available for more than a decade (Tang et.al., 1997; Szeliski, 2010; Carrivick et al., 2016). As a central component, these systems contain image matching tools for the generation of tie points. The required automatic measurement is usually realized at sufficient accuracy and reliability by a combination of standard features and intensity-based matching approaches. The first step of image marching has extracted the data which is the primitive's suitable step, and then for a second step are determined by similarity and consistency measures from the data (Förstner, 1993). To efficiently transfer the extracted feature points to the respective neighbor images, usually, a priori information is additionally integrated in order to speed up the required search effort. For this purpose, the respective image overlap is provided from the so-called block configuration. By these means, suitable search areas can be defined, which considerably speeds up the matching step.

The gap between technologies also promotes this method that is applicable to support the acceleration of data procurement because it offers many advantages, including the ease of operation and low operational cost. Due to the main vehicle used for acquiring aerial photo data, UAV is relatively cheap (Radjawali, I. and O. Pye. 2017). The risk of flying UAV for aerial mapping is also very small such as the risk of falling, misconduct, safety factor, and others. Compared to the conventional photogrammetric method, UAV method is more effective, especially in small mapping areas. The constraints of this method are the inability to covers large mapping area. The battery endurance of the UAV is limited, so it takes several flight missions to cover the whole area. Strong wind and wireless interference are also limiting the flexibility of UAV mobilization. The highest resolution of coastal mapping with this method to identify the distribution of beachrock and classify the zonation of beachrock might be powerful enough to conduct further researches such as coastal propagation in the tropical country, paleo-tsunami based on beachrock, and perhaps disaster mitigation in the coastal area especially in Indonesia. Based on the image processing, we classified the shoreline as coarse sand, fine sand, seawater, wet sand (swash zone), and shoreline itself. The distribution of a beachrock seems to only occur in the fine-sand zone that is represented by white-cream color for the α- and β-location. On the other hand, the γ-location is only dominant with the beachrock (purple color) whereas the distribution of this rock well sediment is in this bay only (Figure A.7).

To evaluate surface changes and differences in the beaches and dunes, spatial analysis was conducted using Agisoft software. This software is a valid analysis tool for interactive 3D geo-spatial processing (Varela-González et al., 2013), which allows a surface comparison among surveys and provides information regarding spatial variation (Brown and Arbogast, 1999). This software allows for the draping of DSMs with orthophotos, thereby improving analysis and integrating the 3D assessment from DSMs with 2D data to identify seasonal changes, beach land use, or vegetation cover above dunes (Gonçalvez and Henriques, 2015). This process was performed for each segment. The measurement

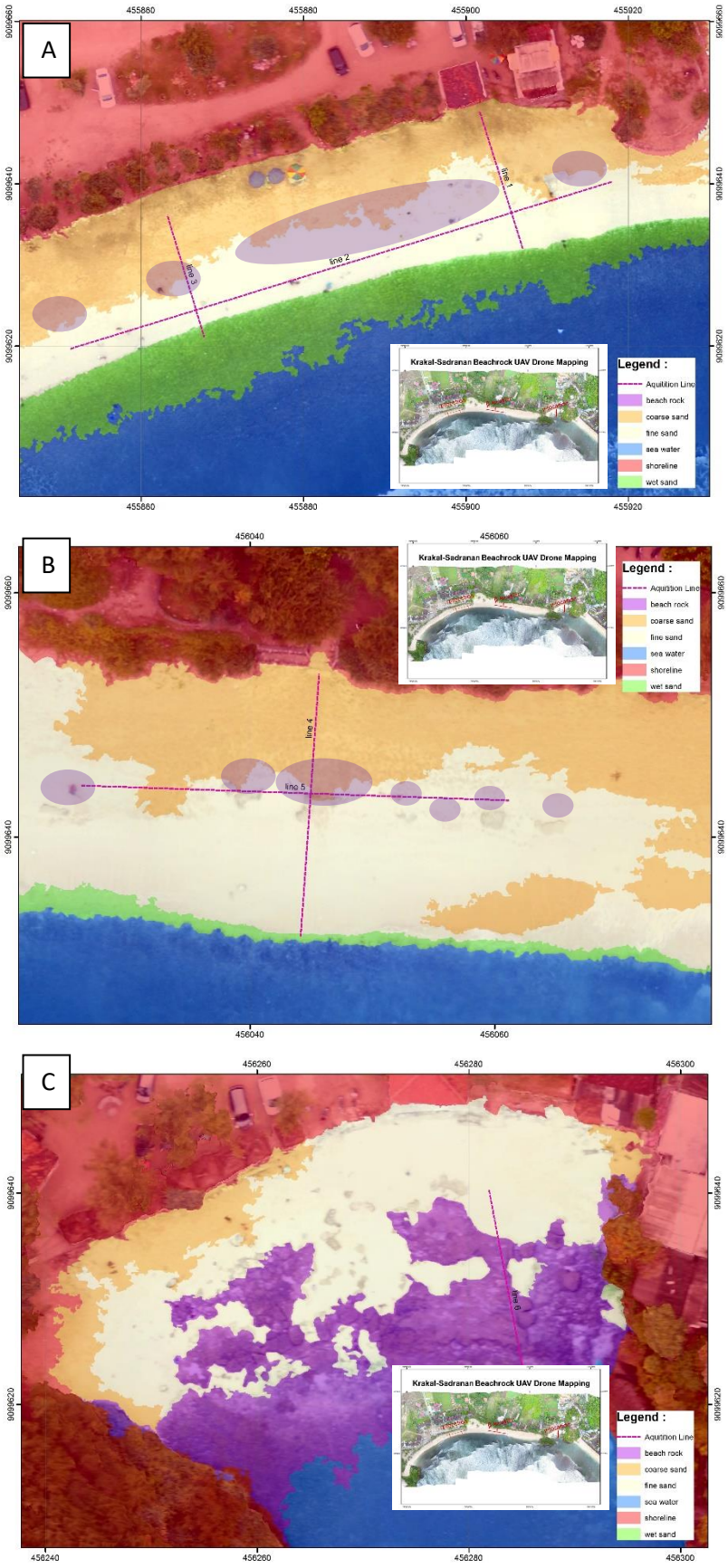


Figure A.7. Beachrock zonation in Krakal-Sadranan beaches, Yogyakarta (A) α-location (B) β-location and (C) γ-location.

location is represented by beachrock sedimentary deposit which is the same location the geophysical measurement will be conducted to identify the sub-surface structure of beachrock body. Ultimate goals of UAV photogrammetric and geophysical measurement for the 3D cross-section model of beachrock body will explain more detail in Chapter 3.

A.4 Discussions

Coastal dynamics is a natural process that occurs as a result of seasonal weather variability and hydro-oceanographic factors. However, at certain times, it has a destructive nature that potentially damages public facilities and infrastructures and leads to environmental damage. Aside from tsunami, shoreline change is one of the major issues on the southern coast of Java Island in Indonesia. In the last 20 years, shoreline change in Southern Yogyakarta coastal area has been a concern of the local government since it caused severe impacts on the environment and human activity, and from an economic aspect. Based on the analysis results, during the period 2006–2015 coastal erosion has occurred in Parangtritis with an average shoreline distance of −20.0 m and at an average rate of −2.3 m/year. The coastal erosion is influenced by several factors, some of which are wave activity, sediment material, coastal protection, and landuse. The predominant factor of the coastal dynamics is wave activity. Wave is one of the forces that cause sediment erosion and transport in coastal areas. Waves that arrive on a coast are generated by winds that transfer their energy into the water. Wind measurements on August 27, 2013 and June 2–6, 2014 present a temporal variation of wind speeds. For example, the wind speed on June 5, 2014 was 5.1 m/s in the morning, which then increased linearly in the afternoon (8.6 m/s) and in the evening (12.4 m/s). In dry season, the waves in Parangtritis are normally classified as swells and constructive waves; however, in extreme weather (e.g. storms), the energy of wind and wave increases. Consequently, a destructive wave is formed. Destructive waves have a weak swash but strong backwash that is powerful enough to remove sediment material at the coast. The coast is eroded away over time. Several previous extreme conditions that led to destructive waves in low-land coastal area such as Parangtritis to the west of Yogyakarta coast. There were no casualties; however, various losses and damages were caused to buildings, coastal vegetation, and public facilities. In July 2011, the access road to the beach eroded up to 20 m and the distance between the fish auction place and the beach was diminished by up to 150 m. The destructive wave that occurred in April 2012 with a height of 5–7 m resulted in a number of inundated stalls and many fishermen securing their boats and nets. In September 2013 and June 2016, due to the high waves Disaster Relief Agency of Bantul urged people to evacuate and avoid activities near the beach.

The local government provides a new location for stalls that are threatened and damaged by coastal erosion. However, the stall owners refuse to relocate and prefer to stay in the affected area rather than leave to the new location. Interviews to stall owners reveal that this preference is provoked by the

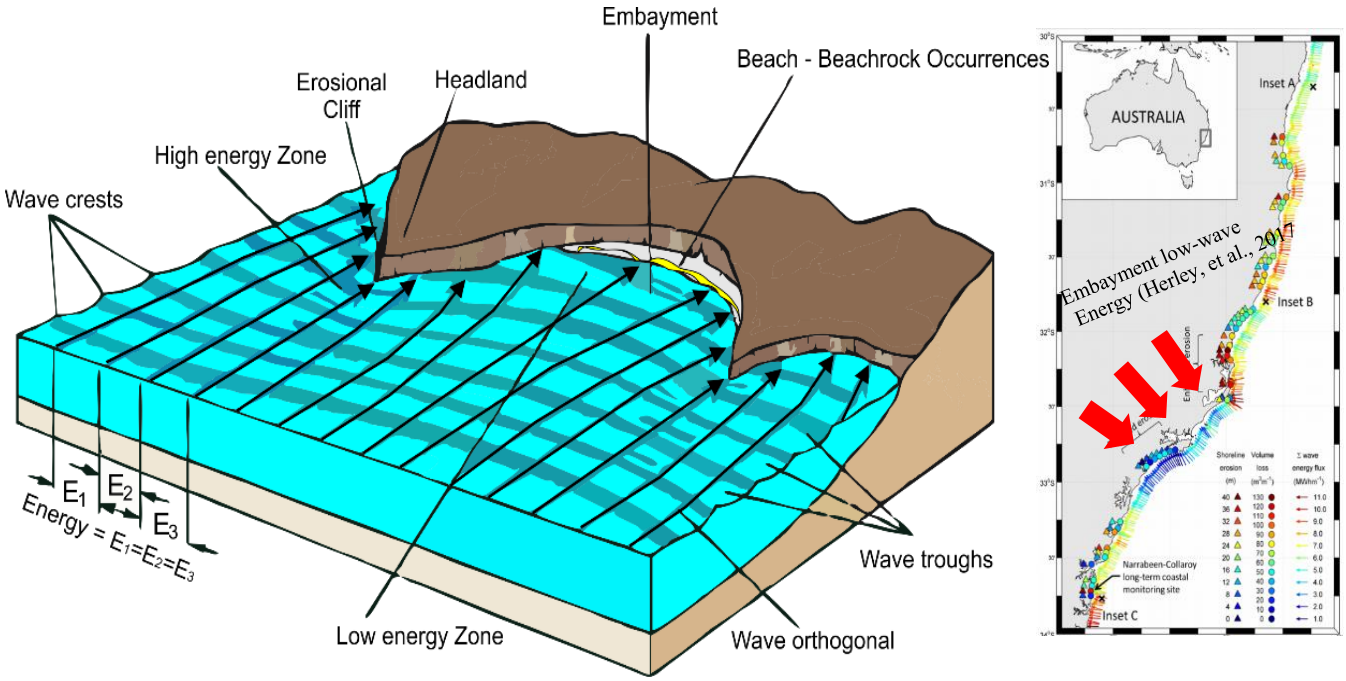


Figure A.8. Morphology of beachrock occurrences schemes (modified from Stull, 2000; Harley, et al., 2017)

inconvenience of moving to another place especially because the new location is far from the beach. They associate the far location from tourist attraction with a decreased number of buyers. Furthermore, they perceive coastal erosion as a non-daily phenomenon that only occurs in extreme weather. Coastal erosion reduces the income of the stall owners and causes the local people who no longer own a stall or a building in Parangtritis to change their livelihood and convert their farmland to fishpond. Based on the trend of shoreline change and its impact on the environment and human life, prevention and mitigation measures generated from information on the existing disaster, as well as integrated coastal planning and management have to be implemented immediately through structural mitigation or non-structural mitigation. Furthermore, public awareness and community participation also play an important role in reducing the risk of coastal erosion. Accurate information, training, and public dissemination will be helpful in increasing community awareness of disaster.

On other hand, beachrock occurrences only formed in the high-land coastal area especially in the eastern South Yogyakarta coastal were consist of coarse limestone sand. The high-land coastal area has a natural barrier more intense than low-land coastal that mostly open area, deep slope, and lack of cliff barrier which mean the wave reflection from Indian Ocean does not decrease the energy and speed. Figure A.8 is represented of wave reflection scheme of beachrock occurrences. The cliff morphology and high-land coastal type is significant factor of beachrock might be occur in Yogyakarta, Indonesia. Deep investigation regarding chemical compound and environment diagenesis will be describe in Chapter 4.

A.5 Conclusions

South Yogyakarta coast has very dynamic coastal areas whose average distance and rate of shoreline change) were −20.0 m and −2.3 m/year in the last 9 years (2006–2015), respectively. Instead, the eastern Yogyakarta coast system which consists of coarse limestone is difficult to measure erosional degree because of natural wave breaker also beachrock occurrences in several locations. Due to the severe impacts of shoreline change, coastal mitigation efforts that factor in the dynamics of coastal processes have to be implemented immediately through structural mitigation, non-structural mitigation, and the improvement of public awareness and community participation in the research area. Beachrock could be one of the optional for coastal countermeasures for high tidal and marine erosion however beachrock occurrences still debatable based on geomorphology, geology settling and also the sedimentary process. Future research for this experiment to deeper investigates beachrock to develop coastal mitigation.

References

Adger, W.N., Hughes, T.P., Folke, C., Carpenter, S.R. and Rockström, J., 2005. Social-ecological resilience to coastal disasters. Science, 309(5737), pp.1036-1039.

Barragán, J.M. and de Andrés, M., 2015. Analysis and trends of the world's coastal cities and agglomerations. Ocean & Coastal Management, 114, pp.11-20.

Baskoro, A.A. and Rifa'i, I.A., 2015. Pemetaan Risiko Tanah Longsor di Kecamatan Samigaluh Kabupaten Kulon progo (Doctoral dissertation, Universitas Gadjah Mada – In Bahasa).

Behan, A., 2010. Digital photogrammetry: A practical course. The Photogrammetric Record, 132(25), pp.476-477.

Bird, E.C.F., 1985. Coastline changes. A global review.

Bronto, S., 1989. Volcanic geology of Galunggung, west java, Indonesia.

Brown, D.G. and Arbogast, A.F., 1999. Digital photogrammetric change analysis as applied to active coastal dunes in Michigan. Photogrammetric Engineering and Remote Sensing, 65, pp.467-474.

Carrivick, J.L., Smith, M.W. and Quincey, D.J., 2016. Structure from Motion in the Geosciences. John Wiley & Sons.

Cawood, A.J., Bond, C.E., Howell, J.A., Butler, R.W. and Totake, Y., 2017. LiDAR, UAV or compass-clinometer? Accuracy, coverage and the effects on structural models. Journal of Structural Geology, 98, pp.67-82.

Cooper, J.A.G., 1991. Beachrock formation in low latitudes: implications for coastal evolutionary models. Marine Geology, 98(1), pp.145-154.

Dalongeville, R. and Sanlaville, P., 1984. Essai de synthèse sur le beach-rock. MOM Éditions, 8(1), pp.161-167.

Daryono, L.R., Titisari, A.D., Warmada, I.W. and Kawasaki, S., 2019. Comparative characteristics of cement materials in natural and artificial beachrocks using a petrographic method. Bulletin of Engineering Geology and the Environment, 78(6), pp.3943-3958.

Davis Jr, R.A. and FitzGerald, D.M., 2009. Beaches and coasts. John Wiley & Sons.

Davis Jr, R.A. and Fox, W.T., 1971. Beach and Nearshore Dynamics in Eastern Lake Michigan (No. WMU-1). Western Michigan Univ. Kalamazoo.

Donovan, J. and Lebaron, A., 2009, January. A comparison of photogrammetry and laser scanning for the purpose of automated rock mass characterization. In 43rd US Rock Mechanics Symposium & 4th US-Canada Rock Mechanics Symposium. American Rock Mechanics Association.

Erginal, A.E., 2012. Beachrock as evidence of sea-level lowstand during the classical period, Parion antique city, Marmara Sea, Turkey. Geodinamica Acta, 25(1-2), pp.96-103.

Förstner, W., 1993. A future of photogrammetric research. NGT geodesia, 93(8), pp.372-383.

Goesele, M., Snavely, N., Curless, B., Hoppe, H. and Seitz, S.M., 2007, October. Multi-view stereo for community photo collections. In 2007 IEEE 11th International Conference on Computer Vision (pp. 1-8). IEEE.

Gonçalves, J.A. and Henriques, R., 2015. UAV photogrammetry for topographic monitoring of coastal areas. ISPRS Journal of Photogrammetry and Remote Sensing, 104, pp.101-111.

Guilcher, A., 1969. Pleistocene and Holocene sea level changes. Earth-Science Reviews, 5(2), pp.69-97.

Haneberg, W.C., 2008. Using close range terrestrial digital photogrammetry for 3-D rock slope modeling and discontinuity mapping in the United States. Bulletin of Engineering Geology and the Environment, 67(4), pp.457-469.

Harwin, S. and Lucieer, A., 2012. Assessing the accuracy of georeferenced point clouds produced via multi-view stereopsis from unmanned aerial vehicle (UAV) imagery. Remote Sensing, 4(6), pp.1573-1599.

Hesp, P., 1988. Morphology, dynamics and internal stratification of some established foredunes in southeast Australia. Sedimentary Geology, 55(1-2), pp.17-41.

Hopley, D., 1986. Beachrock as a sea-level indicator. In Sea-level research (pp. 157-173). Springer, Dordrecht.

Komar, P.D., 1998. Beach processes and sedimentation.

Kwiatek, K. and Tokarczyk, R., 2015. Immersive photogrammetry in 3D modelling. Geomatics and Environmental Engineering, 9(2).

Levitus, S., Boyer, T.P. and Antonov, J.I., 1994. World ocean atlas 1994. Volume 5, Interannual variability of upper ocean thermal structure.

Mancini, F., Dubbini, M., Gattelli, M., Stecchi, F., Fabbri, S. and Gabbianelli, G., 2013. Using unmanned aerial vehicles (UAV) for high-resolution reconstruction of topography: The structure from motion approach on coastal environments. Remote Sensing, 5(12), pp.6880-6898.

Marfai, M.A. and King, L., 2007. Monitoring land subsidence in Semarang, Indonesia. Environmental geology, 53(3), pp.651-659.jj

Marfai, M.A. and Permana, K., 2014. Erosi dan Sedimentasi Kawasan Pesisir Jepara refer from Sunarto, Marfai, MA, & Setiawan, MA, Geomorfologi dan Dinamika Pesisir Jepara, pp.39-76 (In Bahasa).

Mauz, B., Vacchi, M., Green, A., Hoffmann, G. and Cooper, A., 2015. Beachrock: a tool for reconstructing relative sea level in the far-field. Marine Geology, 362, pp.1-16.

Moran, C.A.A., 2004. Spatio-temporal analysis of Texas shoreline changes using GIS Technique (Doctoral dissertation, Texas A & M University).

Morton, R.A., 1977. Historical shoreline changes and their causes, Texas Gulf Coast (1).

Mourtzas, N.D., Kissas, C. and Kolaiti, E., 2014. Archaeological and geomorphological indicators of the historical sea level changes and the related palaeogeographical reconstruction of the ancient foreharbour of Lechaion, East Corinth Gulf (Greece). Quaternary International, 332, pp.151-171.

Mutaqin, B.W., 2017. Shoreline changes analysis in Kuwaru coastal area, Yogyakarta, Indonesia: an application of the Digital Shoreline Analysis System (DSAS). International Journal of Sustainable Development and Planning, 12(7), pp.1203-1214.

Nex, F. and Remondino, F., 2014. UAV for 3D mapping applications: a review. Applied geomatics, 6(1), pp.1-15.

Papakonstantinou, A., Topouzelis, K. and Pavlogeorgatos, G., 2016. Coastline zones identification and 3D coastal mapping using UAV spatial data. ISPRS International Journal of Geo-Information, 5(6), p.75.

Peluso, N.L., 1995. Whose woods are these? Counter-mapping forest territories in Kalimantan, Indonesia. Antipode, 27(4), pp.383-406.

Pethick, J.S., 1984. An introduction to coastal geomorphology. Dept. of Geography, Univ. of Hull.

Pilkey, O.H. and Cooper, J.A.G., 2014. The last beach. Duke University Press.

Pix4D, S.A., 2017. Pix4Dmapper 4.1 User Manual. Pix4D SA: Lausanne, Switzerland.

Pujotomo, M.S. and Sudibyakto, H.A., 2009, February. Coastal changes assessment using multi spatio-temporal data for coastal spatial planning Parangtritis Beach Yogyakarta Indonesia. ITC.

Radjawali, I. and Pye, O., 2017. Drones for justice: inclusive technology and river-related action research along the Kapuas. Geographica Helvetica, 72(1), p.17.

Rangel-Buitrago, N., de Jonge, V.N. and Neal, W., 2018. How to make integrated coastal erosion management a reality. Ocean & Coastal Management, 156, pp.290-299.

Sanlaville, P., Dalongeville, R., Bernier, P. and Evin, J., 1997. The Syrian coast: a model of Holocene coastal evolution. Journal of Coastal Research, pp.385-396.

Semeniuk, V. and Searle, D.J., 1987. Beach rock ridges/bands along a high-energy coast in Southwestern Australia: Their significance and use in coastal history. Journal of Coastal Research, pp.331-342.

Short, A.D., 2006. Australian Beach System: Nature and Distribution. Journal of Coastal Research, pp.11-161.

Stattegger, K., Tjallingii, R., Saito, Y., Michelli, M., Thanh, N.T. and Wetzel, A., 2013. Mid to late Holocene sea-level reconstruction of Southeast Vietnam using beachrock and beach-ridge deposits. Global and Planetary Change, 110, pp.214-222.

Swift, D.J., Niederoda, A.W., Vincent, C.E. and Hopkins, T.S., 1985. Barrier island evolution, middle Atlantic shelf, USA Part I: Shoreface dynamics. Marine Geology, 63(1-4), pp.331-361.

Szeliski, R., 2010. Computer vision: algorithms and applications. Springer Science & Business Media.

Tang, L.Q., Chassapis, C. and Manoochehri, S., 1997. Optimal cooling system design for multi-cavity injection molding. Finite Elements in Analysis and Design, 26(3), pp.229-251.

Topouzelis, K., Papakonstantinou, A. and Pavlogeorgatos, G., 2015. Coastline change detection using UAV, Remote Sensing, GIS and 3D reconstruction. In 5th Int. Conf. Environ. Manag. Eng. Plan. Econ. SECOTOX Conf..

Triatmodjo, B., 1999. Teknik pantai. Beta Offset, Yogyakarta, 397 (In Bahasa).

Trijaya, D. W. 2008. Abrasi pantai Samas semakin mengkhawatirkan. http://okezone.com (In Bahasa)

Turner, D., Lucieer, A. and Watson, C., 2012. An automated technique for generating georectified mosaics from ultra-high resolution unmanned aerial vehicle (UAV) imagery, based on structure from motion (SfM) point clouds. Remote sensing, 4(5), pp.1392-1410.

Turner, I.L., Harley, M.D. and Drummond, C.D., 2016. UAVs for coastal surveying. Coastal Engineering, 114, pp.19-24.

Varela-González, M., González-Jorge, H., Riveiro, B. and Arias, P., 2013. Performance testing of LiDAR exploitation software. Computers & geosciences, 54, pp.122-129.

Vasuki, Y., Holden, E.J., Kovesi, P. and Micklethwaite, S., 2014. Semi-automatic mapping of geological Structures using UAV-based photogrammetric data: An image analysis approach. Computers & Geosciences, 69, pp.22-32.

Warren, M., Paton, M., MacTavish, K., Schoellig, A.P. and Barfoot, T.D., 2018. Towards visual teach and repeat for GPS-denied flight of a fixed-wing UAV. In Field and Service Robotics (pp. 481-498). Springer, Cham.

Wyrtki, K., 1961. Physical oceanography of the Southeast Asian waters (Vol. 2). University of California, Scripps Institution of Oceanography.

Yastıklı, N., Bagci, I. and Beser, C., 2013. The processing of image data collected by light UAV systems for GIS data capture and updating. International Archives of the Photogrammetry, Remote Sensing and Spatial Information Sciences, 7, p.W2.

Zhang, R.S., Shen, Y.M., Lu, L.Y., Yan, S.G., Wang, Y.H., Li, J.L. and Zhang, Z.L., 2004. Formation of Spartina alterniflora salt marshes on the coast of Jiangsu Province, China. Ecological Engineering, 23(2), pp.95-105.

APPENDIXES B

Appendix B.1. Measurement Stratigraphy and Petrographic Analysis of ABX_1 and ABX_2 samples

MEASURED STRATIGRAPHY

SCALE : 1:10

Date : 9 Juli 2018
Trenching AB
L = 5m, W= 1m, D= 80 cm

Location / Section : Krakal-Sadranan Beach / MS 3
Coordinate : 455865/9099626

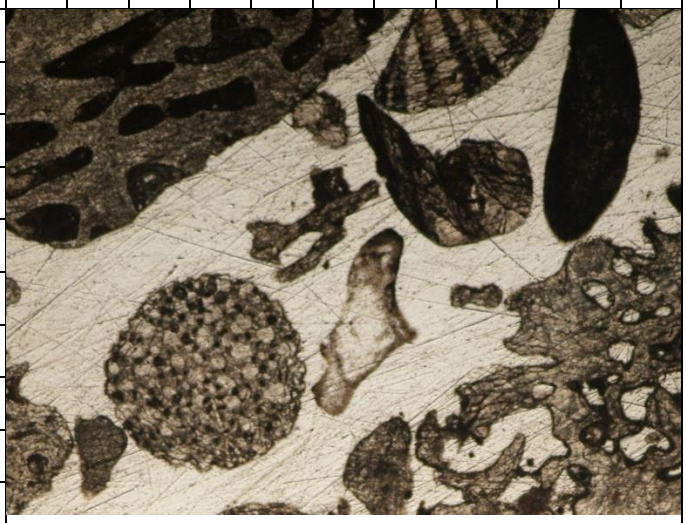
LEGEND

Carbonaceous Sandstone
Sparse Biomicrite
Sampling Points
Massive Structure
Skeletal Fragment

COORDINATE	THICKNESS	LITHOLOGY	SEDIMENTARY STRUCTURE	STRIKE DIP	DESCRIPTION	SAMPLE NUMBER	PHOTO NUMBER	PHOTO
	0 cm							
					Whitish yellow, sized 2 mm fragments and base mass 1 mm, the shape of sub-angular grain, not-consolidated. Quartz composition fragments(30%) and fossil shell material (40%), a basic mass of coarse sand material (30%). Rock name: Carbonated sand deposits	ABX1		
	80 cm	?		N280°E / 27°	Whitish yellow, sized 4 mm fragment and base mass <1 mm, sub-angular grain shape, open packed. Massive structure. The composition of fragments: Quartz (10%) and skeletal fossil (40%), the base mass of calcite (20%) and fine sand material (30%). Rock name: Sparse Biomicrite (Folk, 1962)	ABX2		

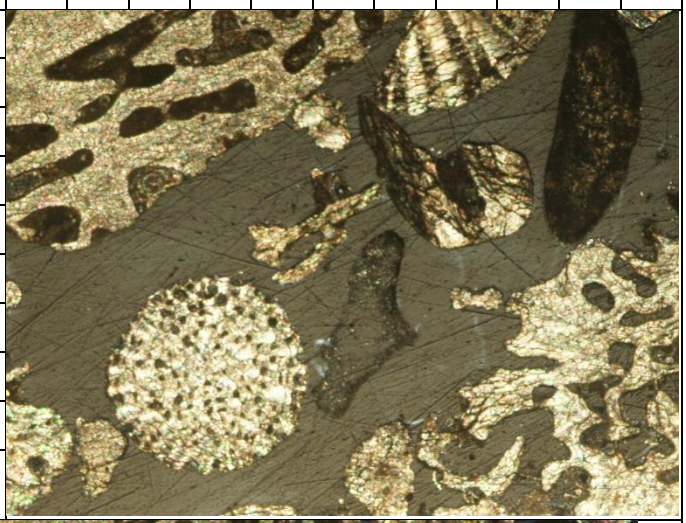
Sample: ABX$_2$	**Name**: Sparse Biomicrite (Folk, 1962); Beachrock
Location: Trench AB, Krakal-Sadranan beach	455865/ 9099626

PPL	1	2	3	4	5	6	7	8	9	10	11
A											
B											
C											
D											
E											
F											
G											
H											
I											
J											



100 µm

XPL	1	2	3	4	5	6	7	8	9	10	11
A											
B											
C											
D											
E											
F											
G											
H											
I											
J											

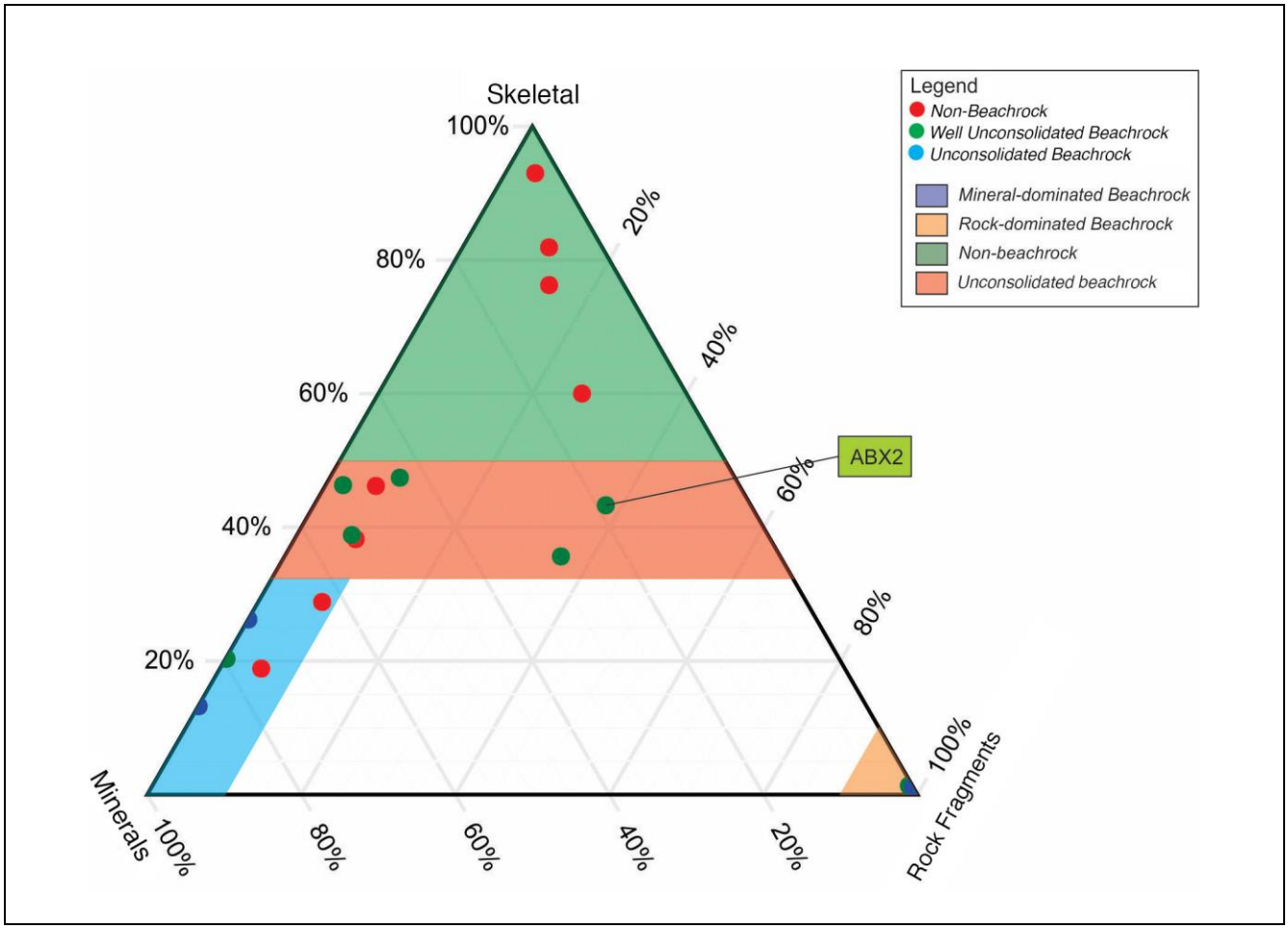




(XPL within gips chip)

Texture:
Allochem bioclastic with the grain size 0,04-10 mm. Bad sorted, open packed, angular grain shape and fragments relatively damaged. Microcalcite (Sparitee) cementation found re-crystallization inside fragment, micrite (mud carbonate), less spars with floating contact matrix, and variative fragment size.

Main composition:
- **Coral Fragment [10%]** with size 0,5 - 4 mm (C3).
- **Skeletal Fragment [30%]:** matrix fragment with random size and aragonite mineral (G3, B7, D8).
- **Micrite [30%]:** Clay grainsize when occurred in depositional process. Size <0,04 mm whereas smooth aggregate between matrix fragments. Brown color shown there is erosional process and weathered from this section (D3).
- **Spars [30%]:** microcalcite cement (G9).


Skeletal
100%
80%
60%
40%
20%
Minerals
Rock Fragments
ABX2
Legend
Non-Beachrock
Well Unconsolidated Beachrock
Unconsolidated Beachrock
Mineral-dominated Beachrock
Rock-dominated Beachrock
Non-beachrock
Unconsolidated beachrock

Appendix B.2. Measurement Stratigraphy and Petrographic Analysis of ABY_1 and ABY_2 samples

MEASURED STRATIGRAPHY

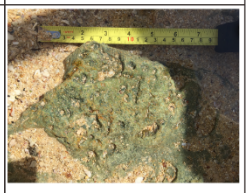
SCALE : 1:10

Date : 9 Juli 2018
Trenching AB
L = 5m, W= 1m, D= 1m

Location / Section : Krakal-Sadranan Beach / MS 1
Coordinate : 455863/9099624

LEGEND

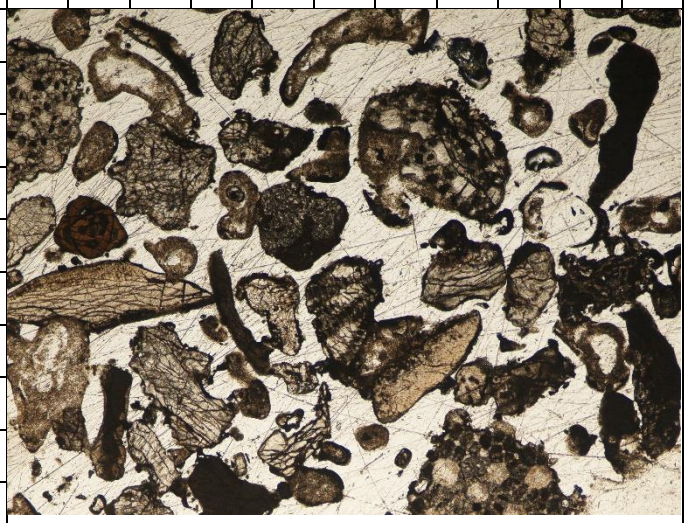
Carbonaceous Sandstone
Sparse Biomicrite
Sampling Points
Massive Structure
Skeletal Fragment

COORDINATE	THICKNESS	LITHOLOGY	SEDIMENTARY STRUCTURE	STRIKE/ DIP	DESCRIPTION	SAMPLE NUMBER	PHOTO NUMBER	PHOTO
	Surface							
	0 cm				Whitish yellow, sized 2 mm fragments and base mass 1 mm, the shape of sub-angular grain, not-consolidated, with a thickness of 70 cm. MH-a sample identification shows the composition of limestone fragments (30%) and skeletal fossil (40%) dominated by *Baculogypsina Sphaerulata*, limestone sand material(30%). Rock name: Carbonated sand deposits	ABY1		
	-70 cm	?		$\frac{N280^0E}{27^0}$	Whitish yellow, sized 4 mm fragment and base mass <1 mm, sub-angular grain shape, open packed, massive structure, thickness around 30 cm. MH-b sample identification shows the composition of the fragment limestone (10%) and skeletal fossil (20%), which is dominated by *Baculogypsina Sphaerulata*, mineral calcite (40%) and sand material limestone (30%). Rock name: Sparse Biomicrite (Folk, 1962)	ABY2		

Sample: ABY$_2$	**Name:** Packed Biomicrite (Folk, 1962); Beachrock
Location: Trench AB, Krakal-Sadranan beach	455862 / 9099622

PPL

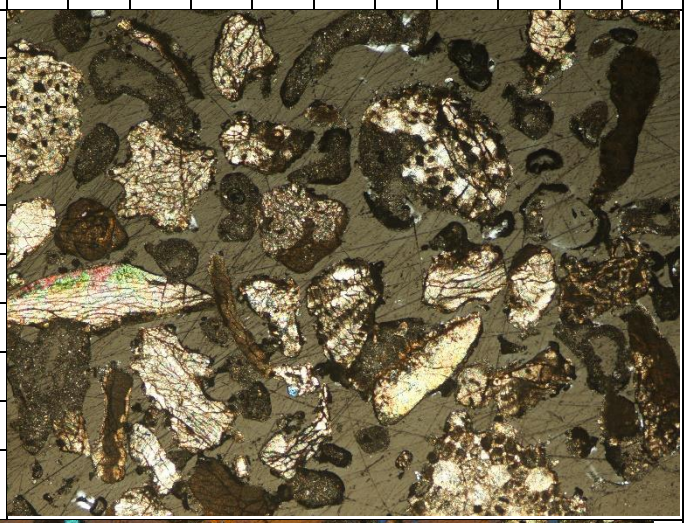
	1	2	3	4	5	6	7	8	9	10	11
A											
B											
C											
D											
E											
F											
G											
H											
I											
J											

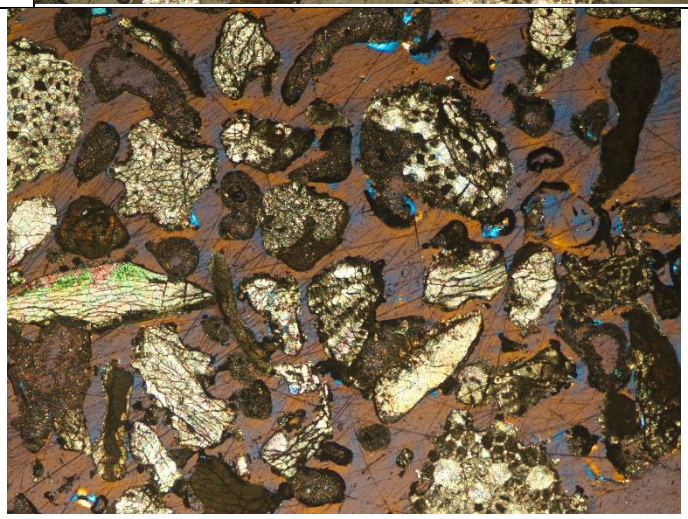


100 µm

XPL

	1	2	3	4	5	6	7	8	9	10	11
A											
B											
C											
D											
E											
F											
G											
H											
I											
J											





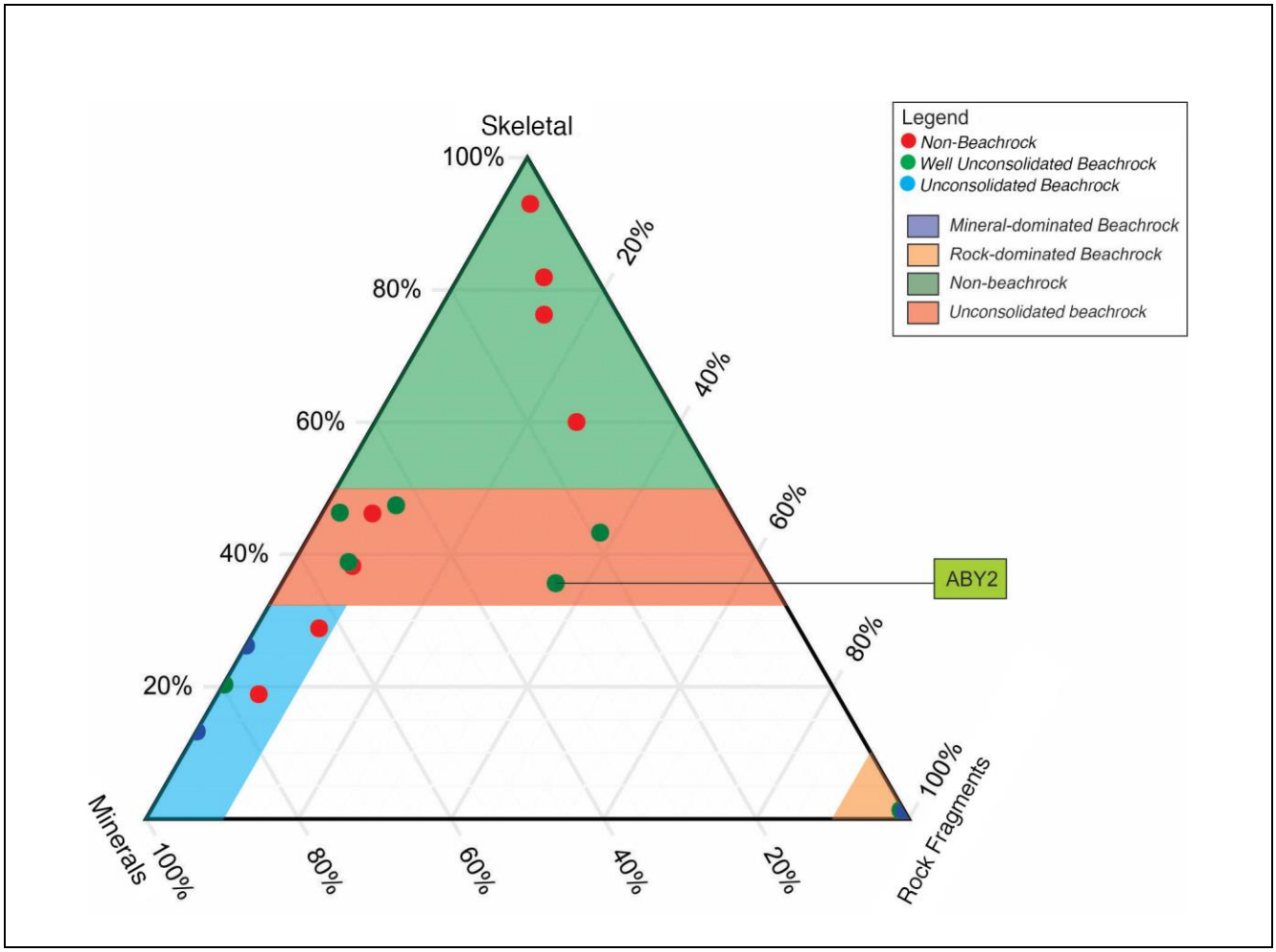
(XPL within gips chip)

Texture:

Allochem bioclastic with the grain size 0,04-10 mm. Bad sorted, open packed, angular grain shape and fragments relatively damaged. Microcalcite (sparite) cementation found re-crystallization inside fragment, micrite (mud carbonate), less spars with floating contact matrix, and variative fragment size.

Main composition:

- **Coral Fragment [30%]** with size 0,5 - 4 mm (C3).
- **Skeletal Fragment [35%]:** variation size with aragonite mineral (B1, C8).
- **Micrite [25%]:** Clay grainsize when occurred in depositional process. Size <0,04 mm whereas smooth aggregate between matrix fragments. Brown color shown there is erosional process and weathered from this section (C7).
- **Sparite [10%]:** microcalcite cement (E5).


Skeletal
100%
80%
60%
40%
20%
Minerals
Rock Fragments
ABY2
Legend
Non-Beachrock
Well Unconsolidated Beachrock
Unconsolidated Beachrock
Mineral-dominated Beachrock
Rock-dominated Beachrock
Non-beachrock
Unconsolidated beachrock

Appendix B.3. Measurement Stratigraphy and Petrographic Analysis of ABZ_1 and ABZ_2 samples

MEASURED STRATIGRAPHY

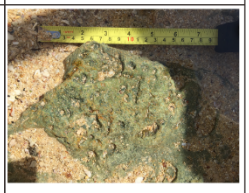
SCALE : 1:10

Date : 9 Juli 2018
Trenching AB
L = 5m, W= 1m, D= 1m

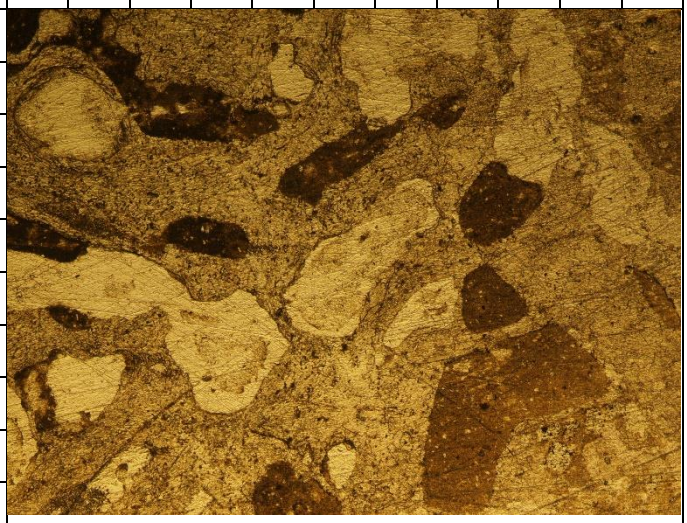
Location / Section : Krakal-Sadranan Beach / MS 1
Coordinate : 455863/9099624

LEGEND

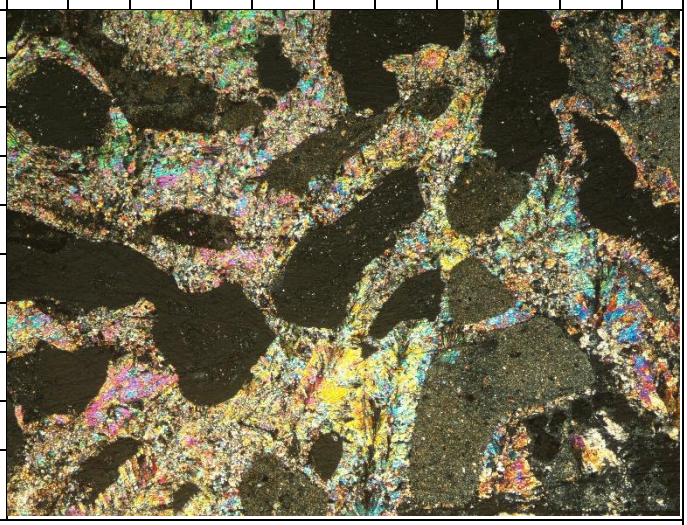
Carbonaceous Sandstone
Sparse Biomicrite
Sampling Points
Massive Structure
Skeletal Fragment

COORDINATE	THICKNESS	LITHOLOGY	SEDIMENTARY STRUCTURE	STRIKE/ DIP	DESCRIPTION	SAMPLE NUMBER	PHOTO NUMBER	PHOTO
	Surface							
	0 cm				Whitish yellow, sized 2 mm fragments and base mass 1 mm, the shape of sub-angular grain, not-consolidated, with a thickness of 70 cm. MH-a sample identification shows the composition of limestone fragments (30%) and skeletal fossil (40%) dominated by *Baculogypsina Sphaerulata*, limestone sand material(30%). Rock name: Carbonated sand deposits	ABZ1		
	-70 cm	?		$\frac{N280^0E}{27^0}$	Whitish yellow, sized 4 mm fragment and base mass <1 mm, sub-angular grain shape, open packed, massive structure, thickness around 30 cm. MH-b sample identification shows the composition of the fragment limestone (10%) and skeletal fossil (20%), which is dominated by *Baculogypsina Sphaerulata*, mineral calcite (40%) and sand material limestone (30%). Rock name: Sparse Biomicrite (Folk, 1962)	ABZ2		

Sample: ABZ_2	**Name:** Sparse Biomicrite (Folk, 1962); Beachrock
Location: Trench AB, Krakal-Sadranan beach	455863/ 90099624

PPL	1	2	3	4	5	6	7	8	9	10	11
A											
B											
C											
D											
E											
F											
G											
H											
I											
J											

100 µm

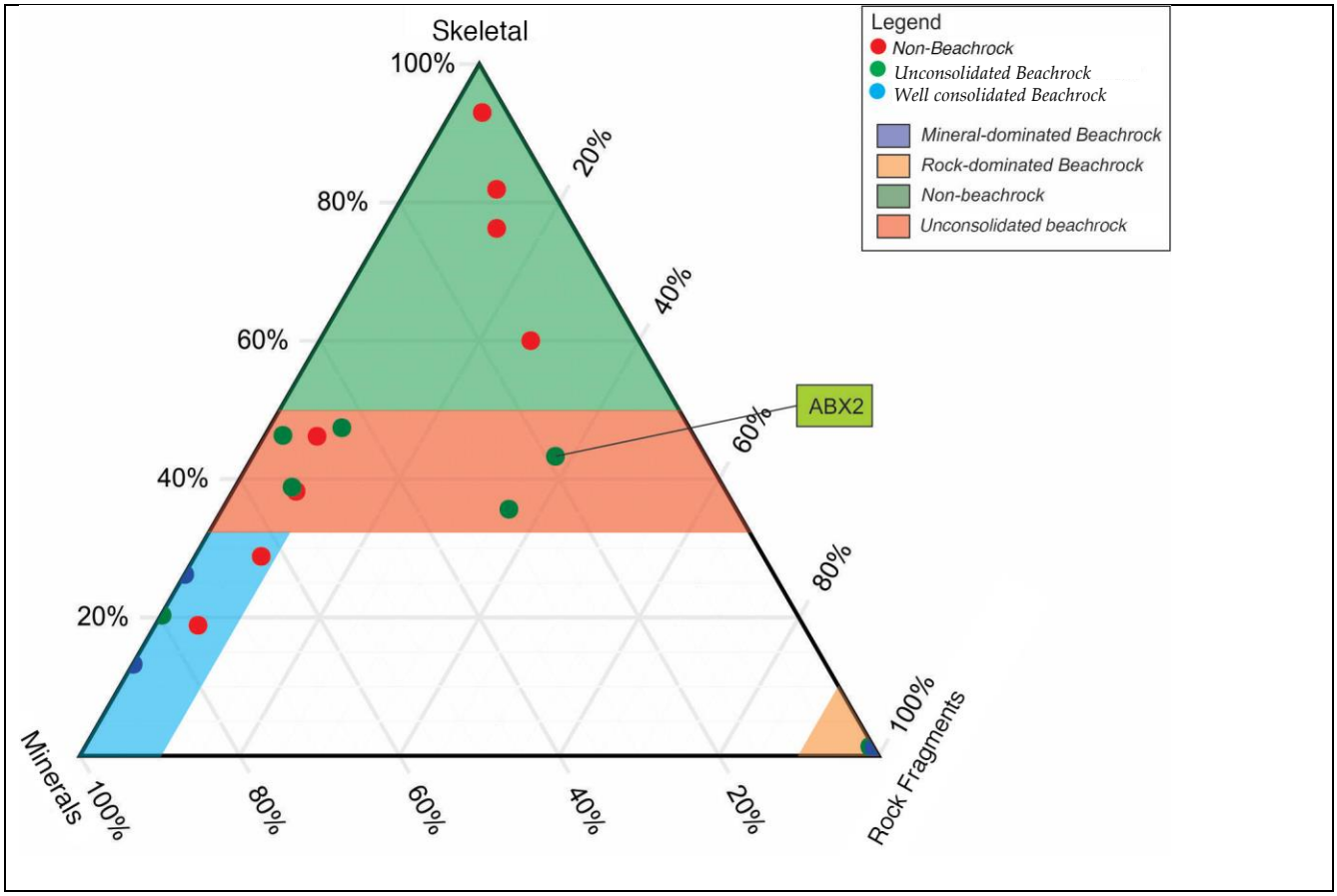
XPL	1	2	3	4	5	6	7	8	9	10	11
A											
B											
C											
D											
E											
F											
G											
H											
I											
J											

Texture:

Allochem bioclastic with the grain size 0,04-10 mm. Bad sorted, open packed, angular grain shape and fragments relatively damaged. Microcalcite (Sparite) cementation found re-crystallization inside fossil fragment, micrite (mud carbonate), less spars with floating contact matrix, and variative fragment size.

Main composition:

- **Coral Fragment [10%]** with size 0,5 - 4 mm (C3).
- **Skeletal Fragment [30%]: %]:** matrix fragment with random size and aragonite mineral
- **Micrite [30%]:** Clay grainsize when occurred in depositional process. Size <0,04 mm whereas smooth aggregate between matrix fragments. Brown color shown there is erosional process and weathered from this section (D5).
- **Sparite [30%]:** microcalcite cement (G9).


Skeletal
100%
80%
60%
40%
20%
Minerals
Rock Fragments
ABX2
Legend
Non-Beachrock
Unconsolidated Beachrock
Well consolidated Beachrock
Mineral-dominated Beachrock
Rock-dominated Beachrock
Non-beachrock
Unconsolidated beachrock

Appendix B.4. Measurement Stratigraphy and Petrographic Analysis of CDX_1, CDX_2 and CDX_3 samples

MEASURED STRATIGRAPHY

SCALE : 1:10

Date : 9 Juli 2018
Trenching CD
L = 5m, W= 1m, D= 70 cm

Location / Section : Krakal-Sadranan Beach / MS-6
Coordinate : 455807/9099603

LEGEND

Carbonaceous Sandstone
Sparse Biomicrite
Sampling Points
Massive Structure
Skeletal Fragment

COORDINATE	THICKNESS	LITHOLOGY	SEDIMENTARY STRUCTURE	STRIKE DIP	DESCRIPTION	SAMPLE NUMBER	PHOTO NUMBER	PHOTO
	0 cm				Whitish yellow, sized 2 mm fragments and base mass 1 mm, the shape of sub-angular grain, not-consolidated. Quartz composition fragments(30%) and skeletal fossil (40%), a basic mass of coarse sand material (30%). Rock name: Carbonated sand deposits	CDX1		
	40 cm			$\frac{N280^0E}{27^0}$	Whitish yellow, sized 4 mm fragment and base mass <1 mm, sub-angular grain shape, open packed. Massive structure. The composition of fragments: Quartz (20%) and skeletal fossil (40%), a base mass of calcite (20%) and fine sand material (20%). Rock name:Sparse Biomicrite (Folk, 1962)	CDX2		
	70 cm	?		$\frac{N280^0E}{27^0}$	Whitish yellow, sized4 mm fragment and base mass <1mm, subangular grain shape, packedOpen. Massive structure. The composition of fragmentsQuartz (10%) and shell materialfossil (40%), a base mass of calcite (25%)and fine sand material (25%).Rock name:Sparse Biomicrite (Folk, 1962)	CDX3		

Sample: CDX_2	**Name:** Packed Biomicrite (Folk, 1962); Beachrock
Location: Trench CD, Krakal-Sadranan beach	455807/ 9099603

PPL	1	2	3	4	5	6	7	8	9	10	11
A											
B											
C											
D											
E											
F											
G											
H											
I											
J											

100 µm

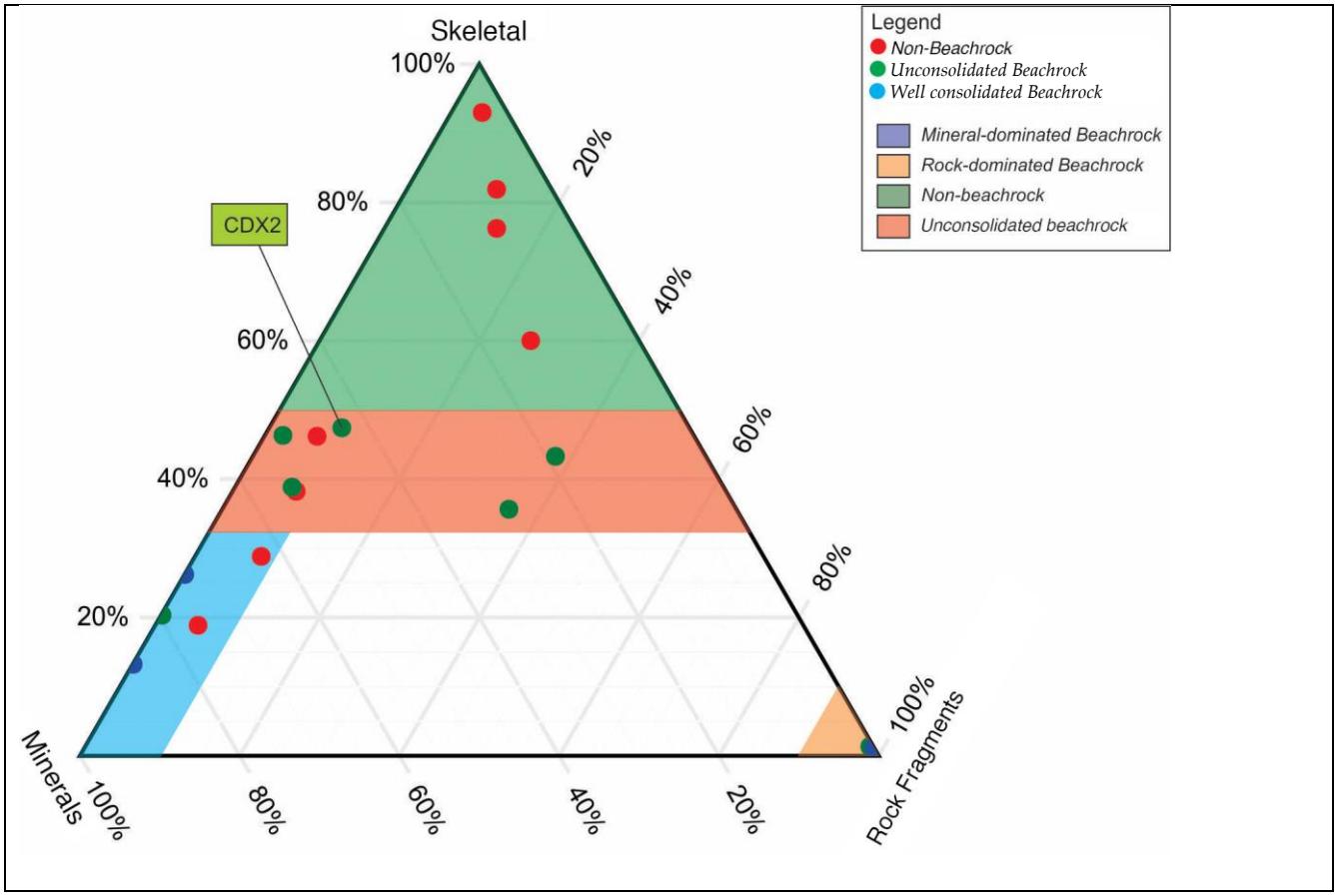
XPL	1	2	3	4	5	6	7	8	9	10	11
A											
B											
C											
D											
E											
F											
G											
H											
I											
J											

Texture:

Allochem bioclastic with the grain size 0,04-10 mm. Bad sorted, open packed, angular grain shape and fragments relatively damaged. Microcalcite (Sparite) cementation found re-crystallization inside fossil fragment, micrite (mud carbonate), less spars with floating contact matrix, and variative fragment size.

Main composition:

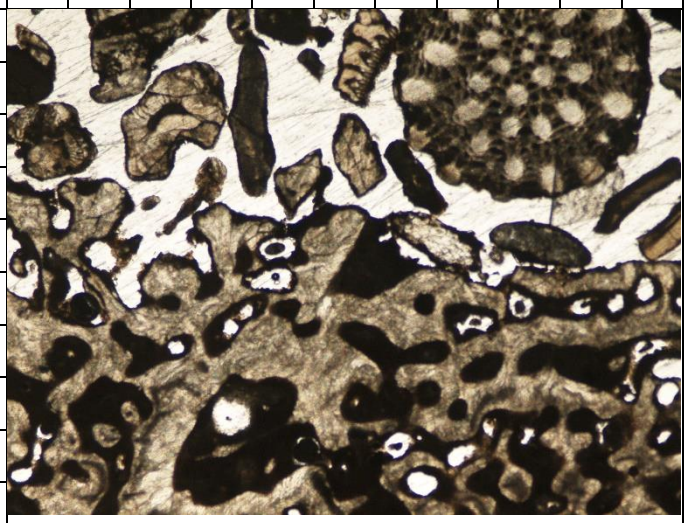
- **Coral Fragment [10%]:** with size 0,5 - 4 mm (G3)
- **Skeletal Fragment [40** matrix fragment with variation random size and aragonite mineral (I7)
- **Micrite [10%]:** Clay grainsize when occurred in depositional process. Size <0,04 mm whereas smooth aggregate between matrix fragments. Brown color shown there is erosional process and weathered from this section (H1).
- **Sparite [40%]:** microcalcite cement (G1).


Skeletal
100%
80%
60%
40%
20%
CDX2
Minerals
Rock Fragments
Legend
Non-Beachrock
Unconsolidated Beachrock
Well consolidated Beachrock
Mineral-dominated Beachrock
Rock-dominated Beachrock
Non-beachrock
Unconsolidated beachrock

Sample: CDX_3	**Name:** Packed Biomicrite (Folk, 1962); Beachrock
Location: Trench CD, Krakal-Sadranan beach	455807/ 9099603

PPL

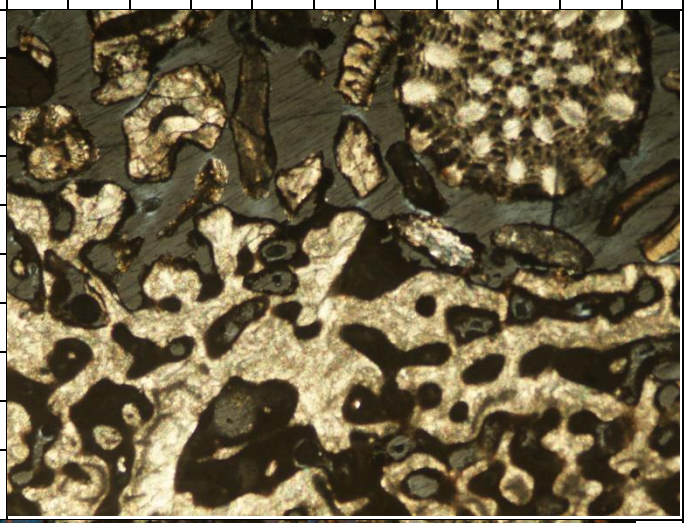
	1	2	3	4	5	6	7	8	9	10	11
A											
B											
C											
D											
E											
F											
G											
H											
I											
J											

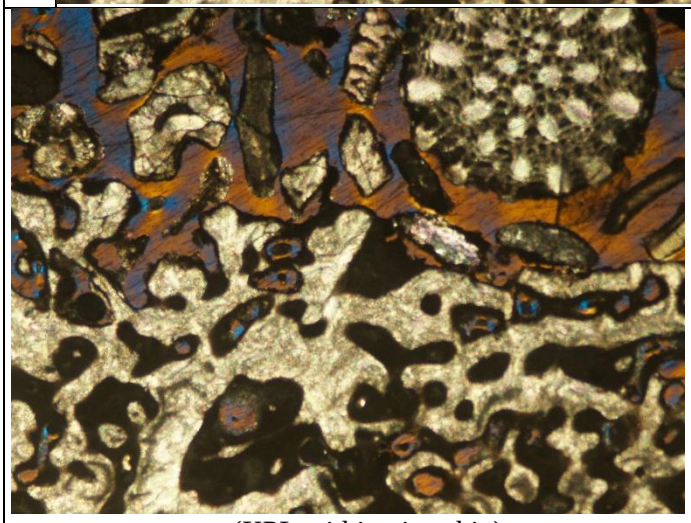


100 µm

XPL

	1	2	3	4	5	6	7	8	9	10	11
A											
B											
C											
D											
E											
F											
G											
H											
I											
J											





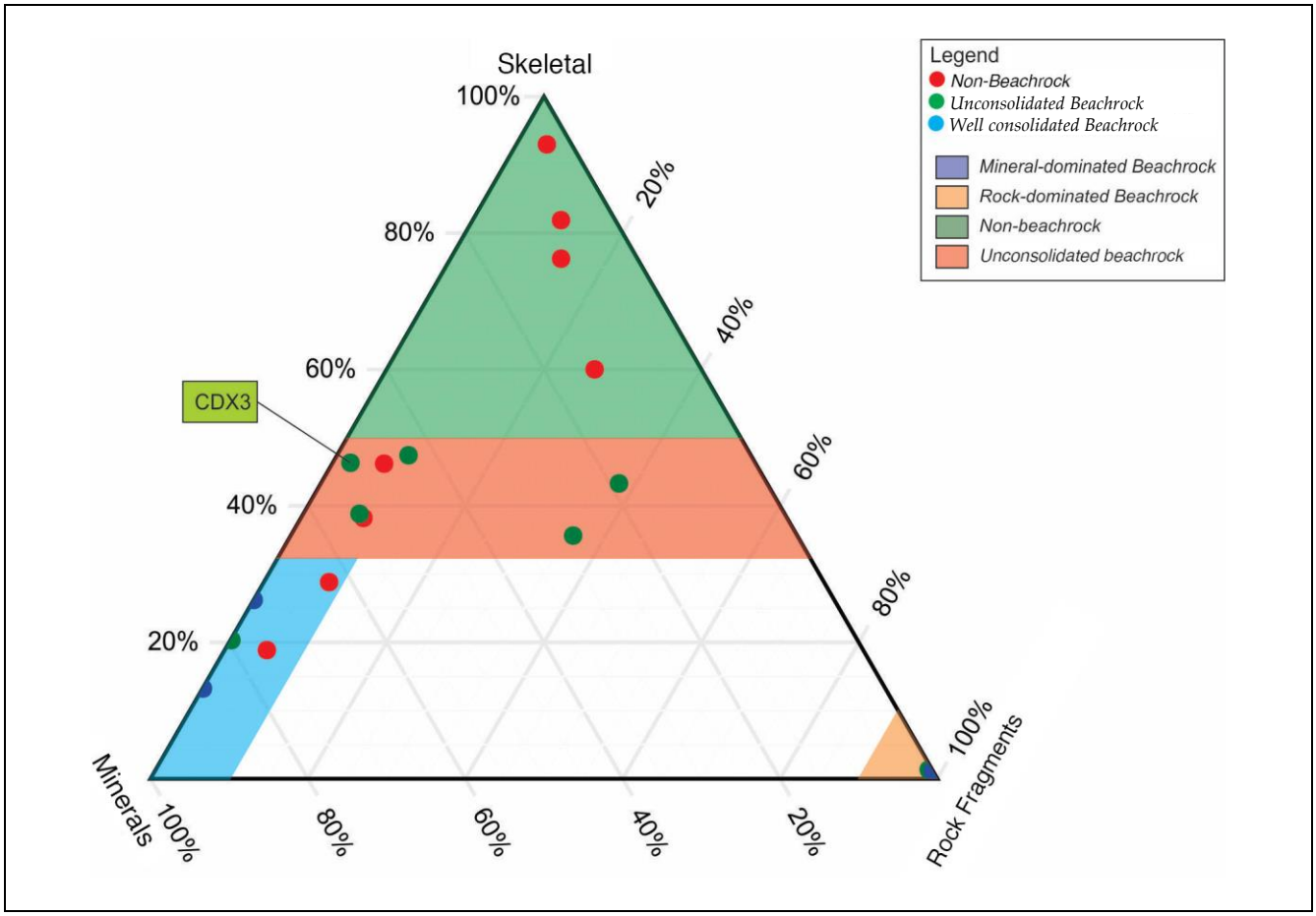
(XPL within gips chip)

Texture:

Allochem bioclastic with the grain size 0,04-10 mm. Bad sorted, open packed, angular grain shape and fragments relatively damaged. Microcalcite (Sparite) cementation found re-crystallization inside fossil fragment, micrite (mud carbonate), less spars with floating contact matrix, and variative fragment size.

Main composition:

- **Coral Fragment [20%]:** with size 0,5 - 4 mm (G5)
- **Skeletal Fragment [40%]:** matrix fragment with variation random size and aragonite mineral (C9)
- **Micrite [10%]:** Clay grainsize when occurred in depositional process. Size <0,04 mm whereas smooth aggregate between matrix fragments. Brown color shown there is erosional process and weathered from this section (F6).
- **Sparite [20%]:** microcalcite cement (G1).
- **Calcite Mineral [10%] (D6)**


Skeletal
100%
80%
60%
40%
20%
CDX3
Minerals
Rock Fragments
Legend
Non-Beachrock
Unconsolidated Beachrock
Well consolidated Beachrock
Mineral-dominated Beachrock
Rock-dominated Beachrock
Non-beachrock
Unconsolidated beachrock

Appendix B.5. Measurement Stratigraphy and Petrographic Analysis of CDY_1, and CDY_2 samples

MEASURED STRATIGRAPHY

SCALE : 1:10

Date : 9 Juli 2018
Trenching CD
L = 5m, W= 1m, D= 70 cm

Location / Section : Krakal-Sadranan Beach / MS-5
Coordinate : 455880/9099690

LEGEND

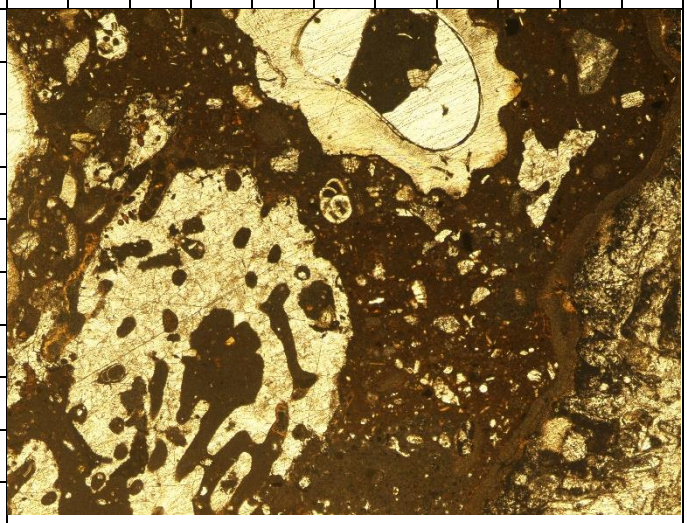
Carbonaceous Sandstone
Sparse Biomicrite
Sampling Points
Massive Structure
Skeletal Fragment

COORDINATE	THICKNESS	LITHOLOGY	LIMESTONE: mud, wacke, pack, grain, float, rud / MUD: clay, silt / SAND: vf, f, m, c, vc / GRAVEL: grain, peb, cob, boul	SEDIMENTARY STRUCTURE	STRIKE DIP	DESCRIPTION	SAMPLE NUMBER	PHOTO NUMBER	PHOTO
	0 cm								
						Whitish yellow, sized2 mm fragments and base mass 1mm, the shape of sub-angular grain, not-consolidated. Quartz composition fragments(30%) and skeletal fossil (40%), a basic mass of coarse sand material(30%). Rock name: Carbonated sand deposits	CDY1		
	70 cm	?			N280°E / 27°	Whitish yellow, sized 4 mm fragment and base mass <1 mm, sub-angular grain shape, open packed. Massive structure. The composition of fragments Quartz (10%) and skeletal fossil (30%), the base mass of calcite (30%) and fine sand material (30%). Rock name: Sparse Biomicrite (Folk, 1962)	CDY2		

Sample: CDY_2	**Name:** Sparse Biomicrite (Folk, 1962); Beachrock
Location: Trench CD, Krakal-Sadranan beach	455880/ 9099690

PPL

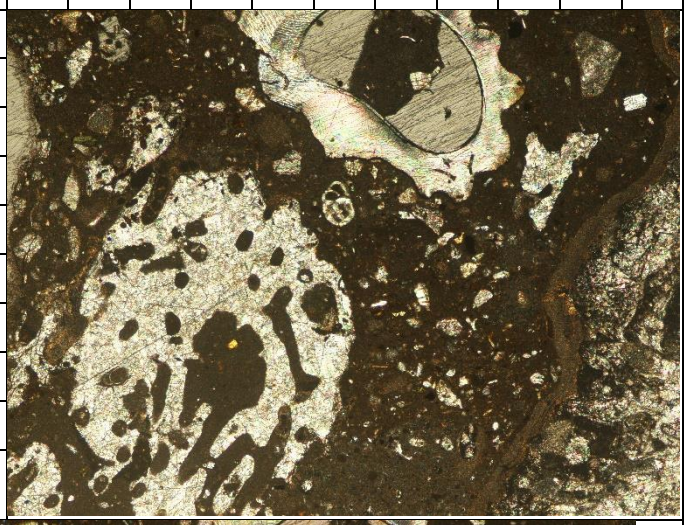
	1	2	3	4	5	6	7	8	9	10	11
A											
B											
C											
D											
E											
F											
G											
H											
I											
J											

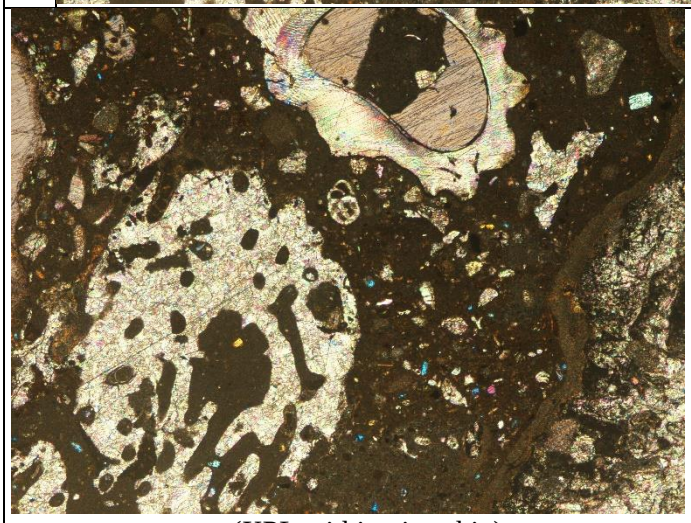


100 µm

XPL

	1	2	3	4	5	6	7	8	9	10	11
A											
B											
C											
D											
E											
F											
G											
H											
I											
J											





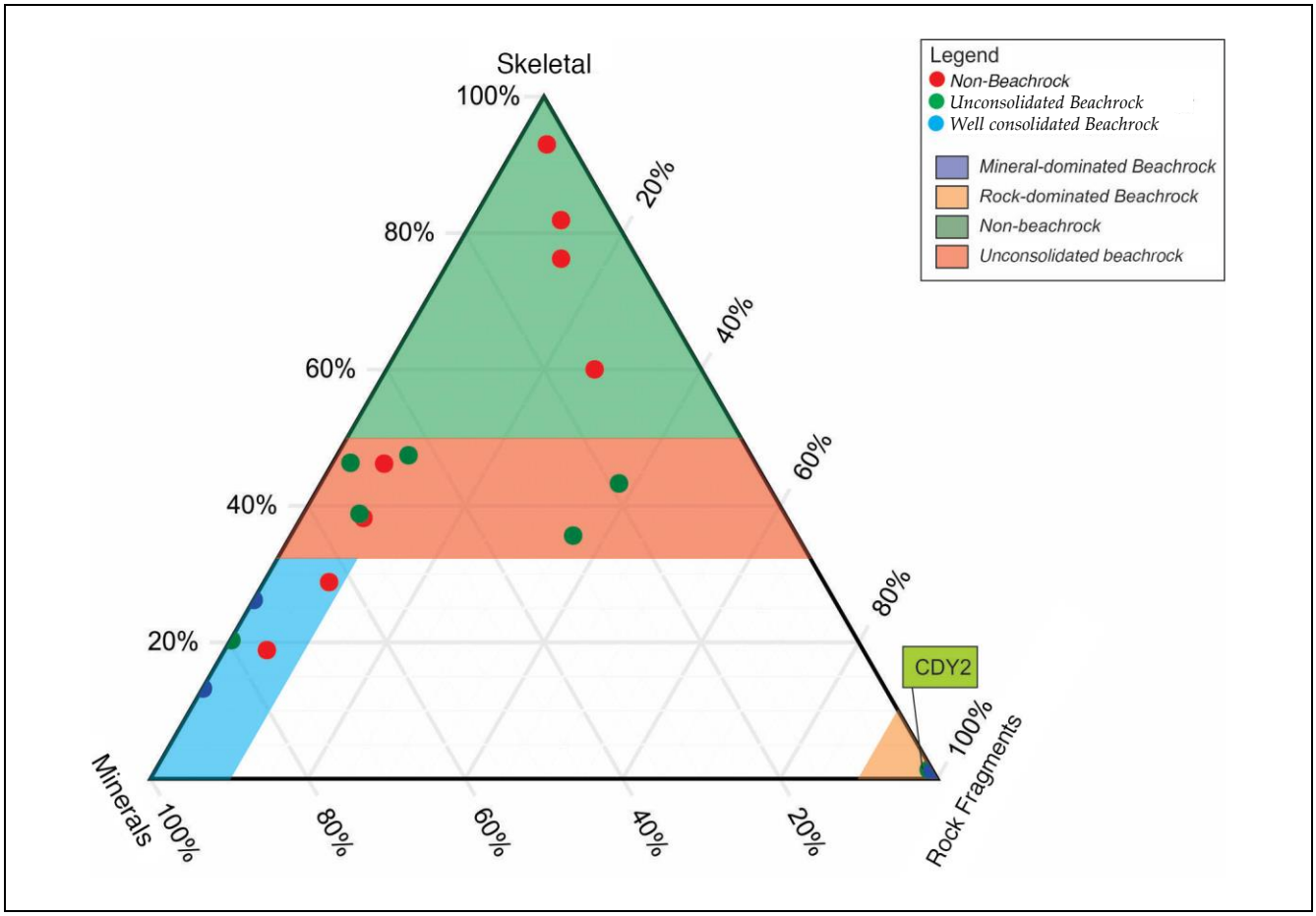
(XPL within gips chip)

Texture:

Allochem bioclastic with the grain size 0,04-10 mm. Bad sorted, open packed, angular grain shape and fragments relatively damaged. Microcalcite (Sparite) cementation found re-crystallization inside fossil fragment, micrite (mud carbonate), less spars with floating contact matrix, and variative fragment size.

Main composition:

- **Fragmen koral [10%]:** with size 0,5 - 4 mm (F4)
- **Skeletal Fragment [10%]:** matrix fragment with variation random size and aragonite mineral (D6)
- **Micrite [40%]:** Clay grainsize when occurred in depositional process. Size <0,04 mm whereas smooth aggregate between matrix fragments. Brown color shown there is erosional process and weathered from this section (G4).
- **Sparite [30%]:** microcalcite cement (F10).
- **Calcite Mineral [10%]**


Skeletal
100%
80%
60%
40%
20%
20%
40%
60%
80%
100%
Minerals
Rock Fragments
CDY2
Legend
Non-Beachrock
Unconsolidated Beachrock
Well consolidated Beachrock
Mineral-dominated Beachrock
Rock-dominated Beachrock
Non-beachrock
Unconsolidated beachrock

Appendix B.6. Measurement Stratigraphy and Petrographic Analysis of CDZ_1, and CDZ_2 samples

MEASURED STRATIGRAPHY

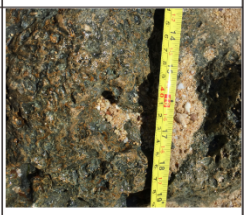
SCALE : 1:10

Date : 9 Juli 2018
Trenching CD
L = 5m, W= 1m, D= 1m

Location / Section : Krakal-Sadranan Beach / MS-4
Coordinate : 455813/9099597

LEGEND

Carbonaceous Sandstone
Sparse Biomicrite
Sampling Points
Massive Structure
Skeletal Fragment

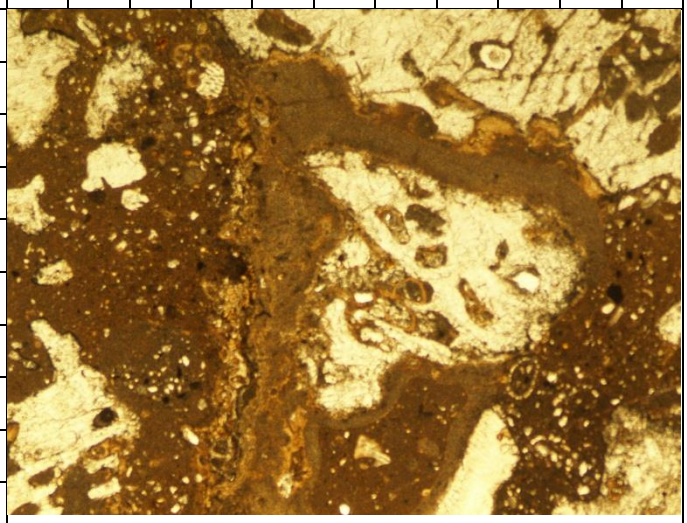
COORDINATE	THICKNESS	LITHOLOGY	SEDIMENTARY STRUCTURE	STRIKE DIP	DESCRIPTION	SAMPLE NUMBER	PHOTO NUMBER	PHOTO
	Surface							
	0 cm				Whitish yellow, sized 2 mm fragments and base mass 1 mm, the shape of sub-angular grain, not-consolidated, the thickness of 60 cm. Identification MH-g samples show the composition limestone fragments (20%) and skeletal fossil (40%)domination by *Baculogypsina Sphaerulata* limestone sand materials (40%). Rock name: Carbonated sand deposits	CDZ1		
	-60 cm	?		N280°E / 27°	Whitish yellow, sized 4 mm fragment and base mass <1mm, sub-angular grain shape, open packed, massive structure, thickness around ~30 cm. MH-h sample identification show the composition of stone fragments limestone (10%) and skeletal fossil (20%) are dominated by *Baculogypsina Sphaerulata*, mineral calcite (40%) and limestone sand material(30%). Rock name: Sparse Biomicrite (Folk, 1962)	CDZ2		

Sample: CDZ_2

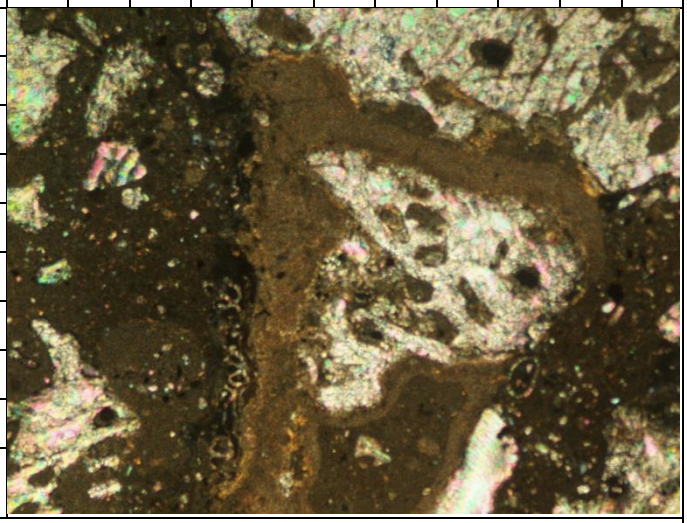
Name: Sparse Biomicrite (Folk, 1962); Beachrock

Location: Trench CD, Krakal-Sadranan beach

455813 / 9099597

PPL	1	2	3	4	5	6	7	8	9	10	11
A											
B											
C											
D											
E											
F											
G											
H											
I											
J											

100 µm

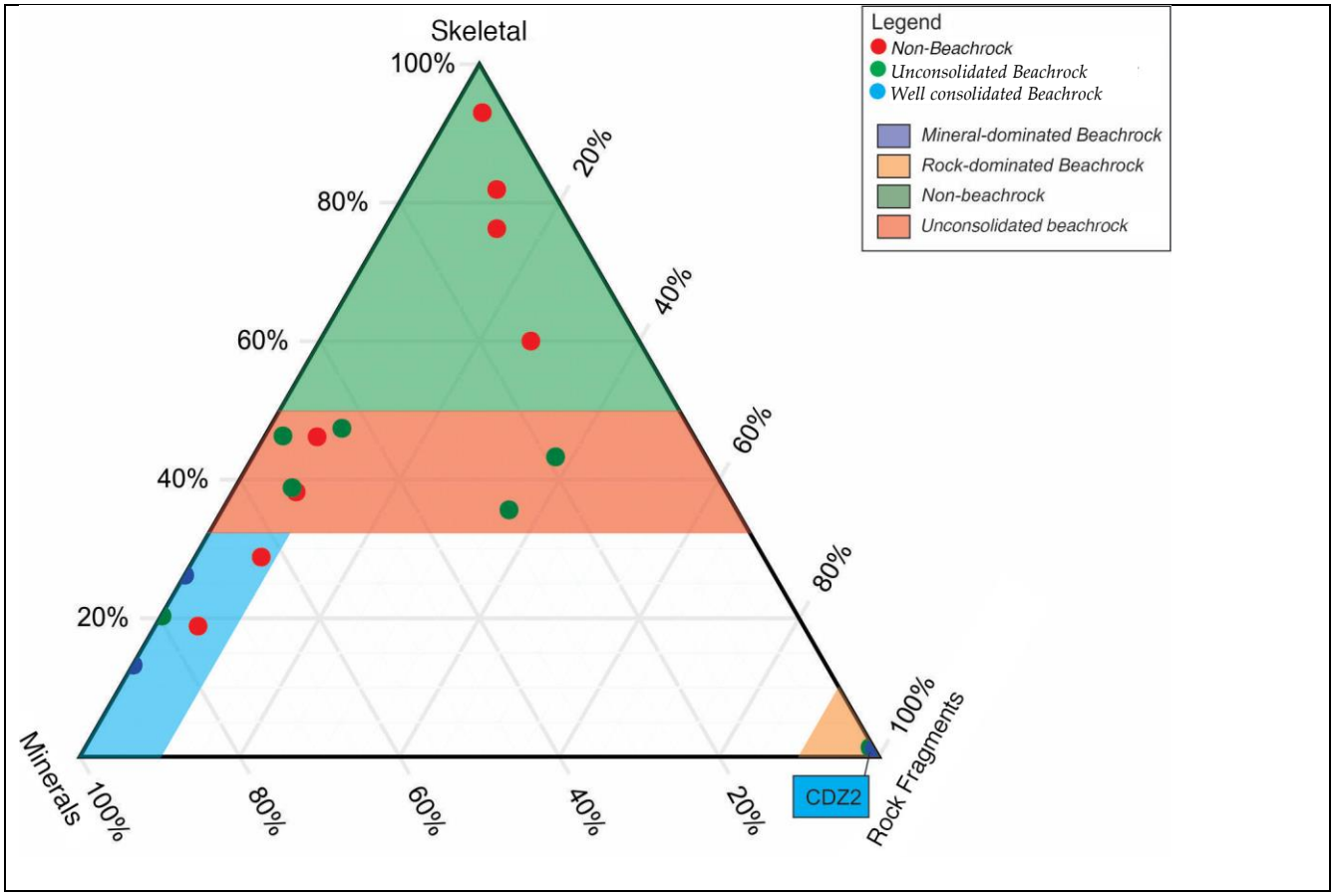
XPL	1	2	3	4	5	6	7	8	9	10	11
A											
B											
C											
D											
E											
F											
G											
H											
I											
J											

Texture:

Allochem bioclastic with the grain size 0,04-10 mm. Bad sorted, open packed, angular grain shape and fragments relatively damaged. Microcalcite (Sparite) cementation found re-crystallization inside fossil fragment, micrite (mud carbonate), less spars with floating contact matrix, and variative fragment size.

Main composition:

- **Coral Fragment [15%] %]:** with size 0,5 - 4 mm (C11).
- **Skeletal Fragment [10%]:** matrix fragment with variation random size and aragonite mineral (E6).
- **Micrite [45%]:** Clay grainsize when occurred in depositional process. Size <0,04 mm whereas smooth aggregate between matrix fragments. Brown color shown there is erosional process and weathered from this section (F2).
- **Sparite [20%]:** microcalcite cement (I1).
- **Calcite Mineral [10%] (J8)**


Skeletal
100%
80%
60%
40%
20%
Minerals
Rock Fragments
CDZ2
Legend
Non-Beachrock
Unconsolidated Beachrock
Well consolidated Beachrock
Mineral-dominated Beachrock
Rock-dominated Beachrock
Non-beachrock
Unconsolidated beachrock

Appendix B.7. Measurement Stratigraphy and Petrographic Analysis of EFX_1, and EFX_2 samples

MEASURED STRATIGRAPHY

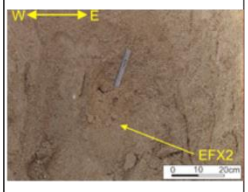
SCALE : 1:10

Date : 9 Juli 2018
Trenching EF
L = 5m, W= 1m, D= 80 cm

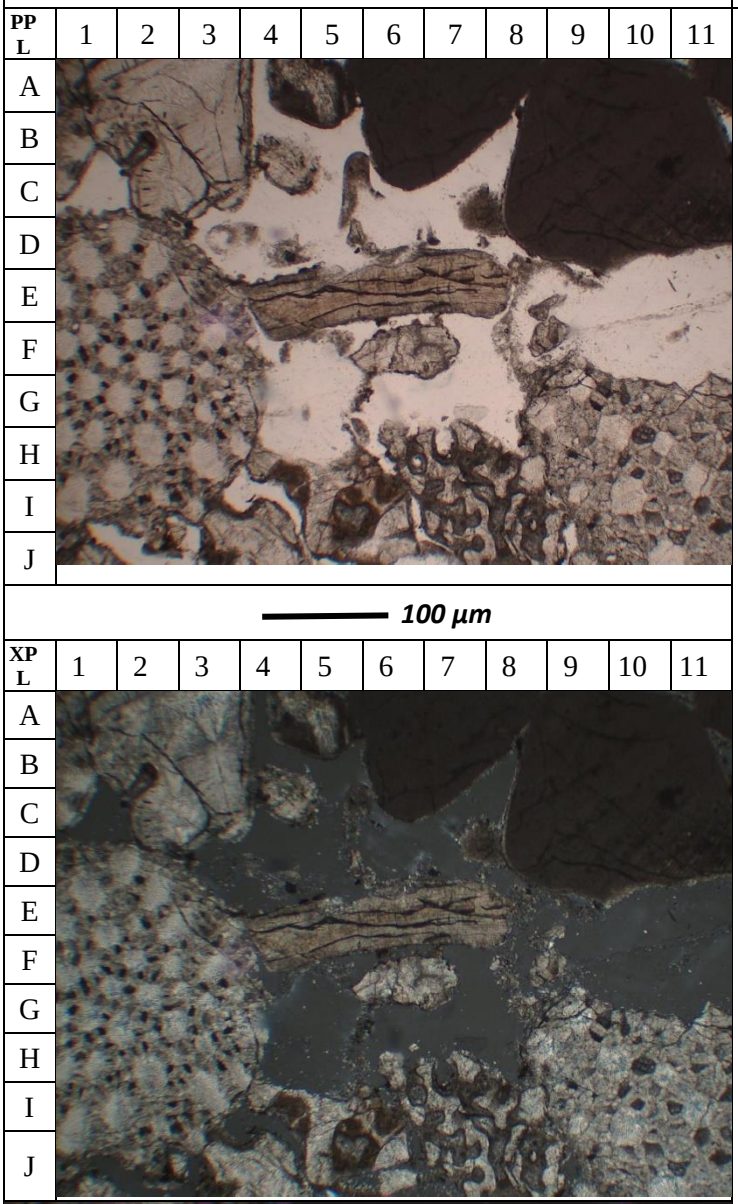
Location / Section : Krakal-Sadranan Beach / MS 7
Coordinate : 456028/9099620

LEGEND

Carbonaceous Sandstone
Sparse Biomicrite
Sampling Points
Massive Structure
Skeletal Fragment

COORDINATE	THICKNESS	LITHOLOGY	LIMESTONE (mud, wackestone, packstone, grainstone, floatstone, rudstone) / MUD (clay, silt) / SAND (vf, f, m, c, vc) / GRAVEL (grain, peb, cob, boul)	SEDIMENTARY STRUCTURE	STRIKE DIP	DESCRIPTION	SAMPLE NUMBER	PHOTO NUMBER	PHOTO
	0 cm					Whitish yellow, sized 2 mm fragments and base mass 1 mm, the shape of sub-angular grain, not-consolidated. Quartz composition fragments(30%) and fossil shell material (40%), a basic mass of coarse sand material (30%). Rock name: Carbonated sand deposits	EFX1		
	80 cm	?			N280°E / 27°	Whitish yellow, sized 4 mm fragment and base mass <1 mm, sub-angular grain shape, open packed. Massive structure. The composition of fragments: Quartz (10%) and skeletal fossil (40%), the base mass of calcite (20%) and fine sand material (30%). Rock name: Sparse Biomicrite (Folk, 1962)	EFX2		

Sample: EFX$_2$	**Name:** Sparse Biomicrite (Folk, 1962); Beachrock
Location: Trench EF, Krakal-Sadranan beach	456021/ 9099640



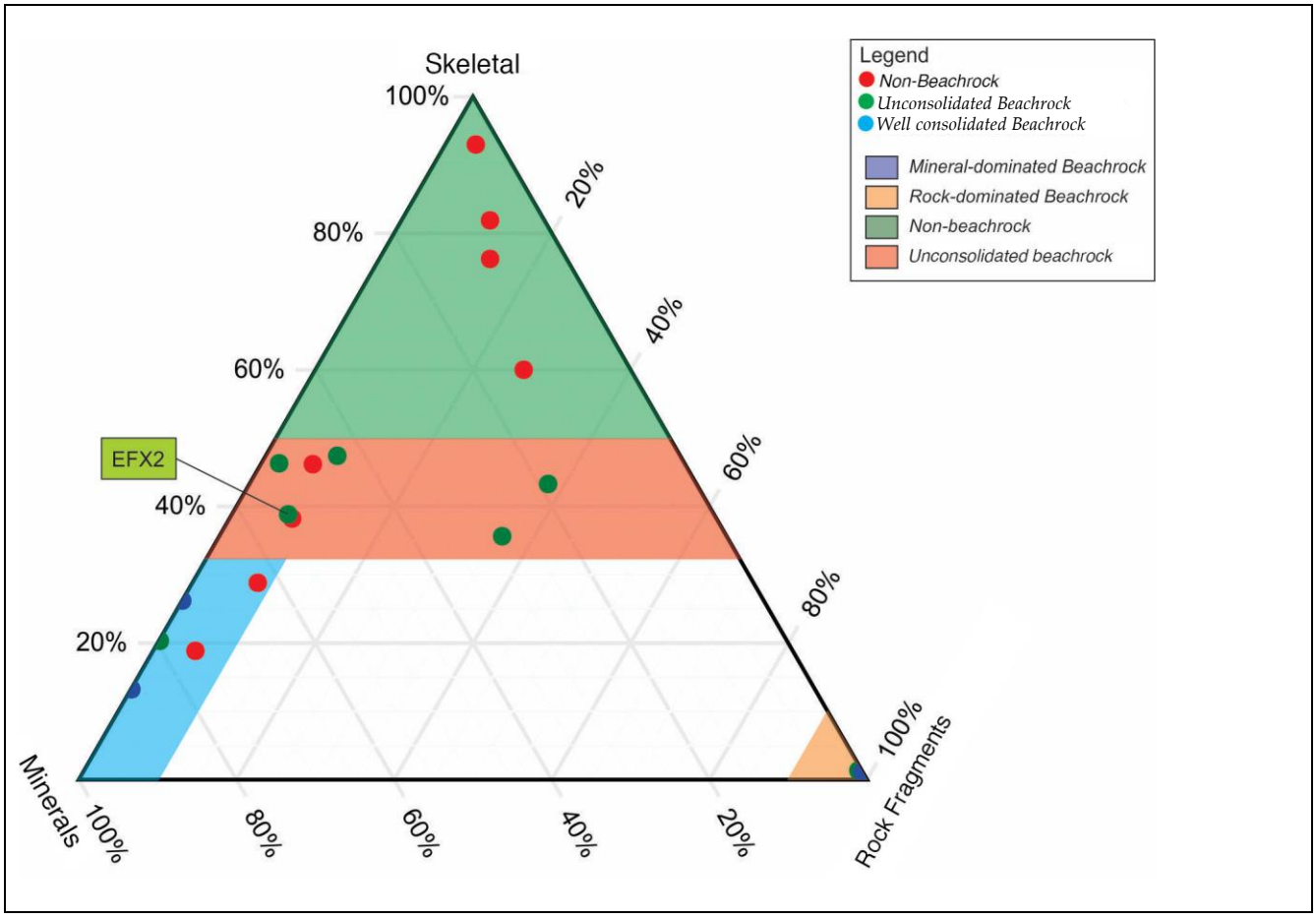
(XPL within gips chip)

Texture:

Allochem bioclastic with the grain size 0,04-10 mm. Bad sorted, open packed, angular grain shape and fragments relatively damaged. Microcalcite (Sparite) cementation found re-crystallization inside fossil fragment, micrite (mud carbonate), less spars with floating contact matrix, and variative fragment size.

Main composition:

- **Coral Fragment [20%]** with size 0,5 - 4 mm (J6).
- **Skeletal Fragment [20%]:** matrix fragment with variation random size and aragonite mineral (G2).
- **Micrite [20%]:** Clay grainsize when occurred in depositional process. Size <0,04 mm whereas smooth aggregate between matrix fragments. Brown color shown there is erosional process and weathered from this section (I4).
- **Sparite [30%]:** microcalcite cement (C2).
- **Calcite Mineral [10%] (C10)**


Skeletal
100%
80%
60%
40%
20%
EFX2
Minerals
Rock Fragments
Legend
Non-Beachrock
Unconsolidated Beachrock
Well consolidated Beachrock
Mineral-dominated Beachrock
Rock-dominated Beachrock
Non-beachrock
Unconsolidated beachrock

Appendix B.8. Measurement Stratigraphy and Petrographic Analysis of EFY_1, and EFY_2 samples

MEASURED STRATIGRAPHY

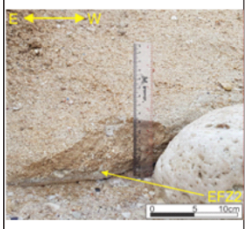
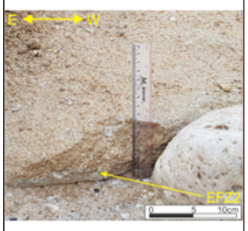
SCALE : 1:10

Date : 9 Juli 2018
Trenching AB
L = 5m, W= 1m, D= 1m

Location / Section : Krakal-Sadranan Beach / MS 1
Coordinate : 455863/9099624

LEGEND

Carbonaceous Sandstone
Sparse Biomicrite
Sampling Points
Massive Structure
Skeletal Fragment

COORDINATE	THICKNESS	LITHOLOGY	LIMESTONE (mud, wacke, pack, grain, float, rud; MUD, SAND, GRAVEL; clay, silt, vf, f, m, c, vc, grain, peb, cob, boul)	SEDIMENTARY STRUCTURE	STRIKE/ DIP	DESCRIPTION	SAMPLE NUMBER	PHOTO NUMBER	PHOTO
	Surface								
	0 cm					Whitish yellow, sized 2 mm fragments and base mass 1 mm, the shape of sub-angular grain, not-consolidated, with a thickness of 70 cm. MH-a sample identification shows the composition of limestone fragments (30%) and skeletal fossil (40%) dominated by *Baculogypsina Sphaerulata*, limestone sand material(30%). Rock name: Carbonated sand deposits	EFY1		
	-70 cm	?			$\frac{N280^0E}{27^0}$	Whitish yellow, sized 4 mm fragment and base mass <1 mm, sub-angular grain shape, open packed, massive structure, thickness around 30 cm. MH-b sample identification shows the composition of the fragment limestone (10%) and skeletal fossil (20%), which is dominated by *Baculogypsina Sphaerulata*, mineral calcite (40%) and sand material limestone (30%). Rock name: Sparse Biomicrite (Folk, 1962)	EFY2		

Sample: EFY$_2$	**Name:** Sparse Biomicrite (Folk, 1962); Beachrock
Location: Trench EF, Krakal-Sadranan beach	456024 / 9099638

PPL

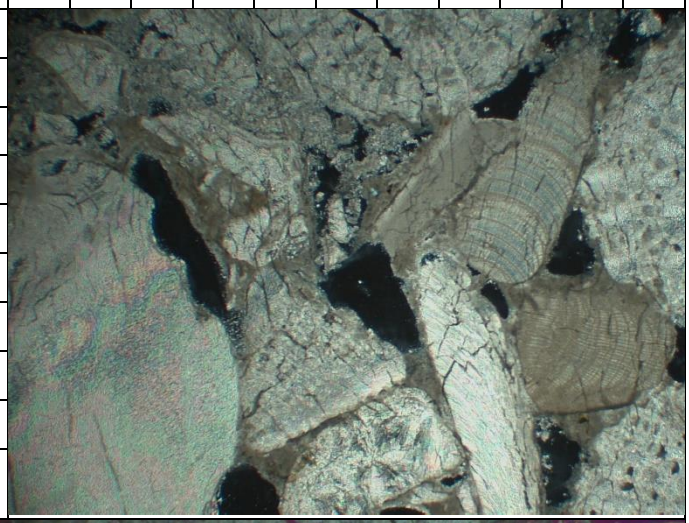
	1	2	3	4	5	6	7	8	9	10	11
A											
B											
C											
D											
E											
F											
G											
H											
I											
J											

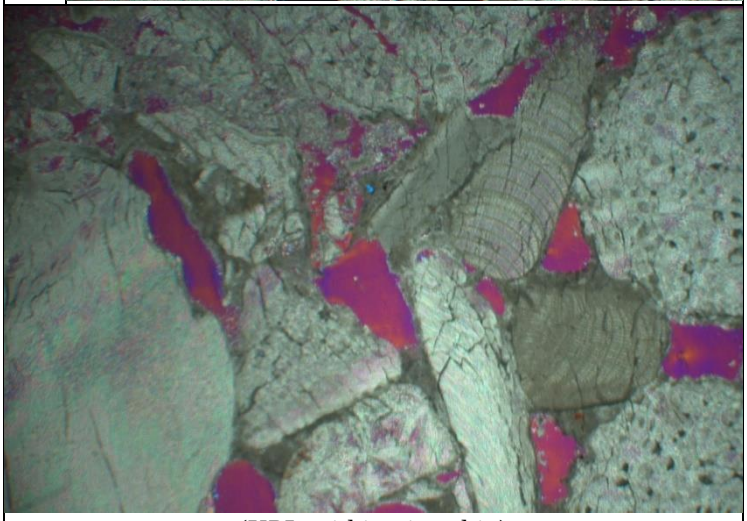


100 µm

XPL

	1	2	3	4	5	6	7	8	9	10	11
A											
B											
C											
D											
E											
F											
G											
H											
I											
J											





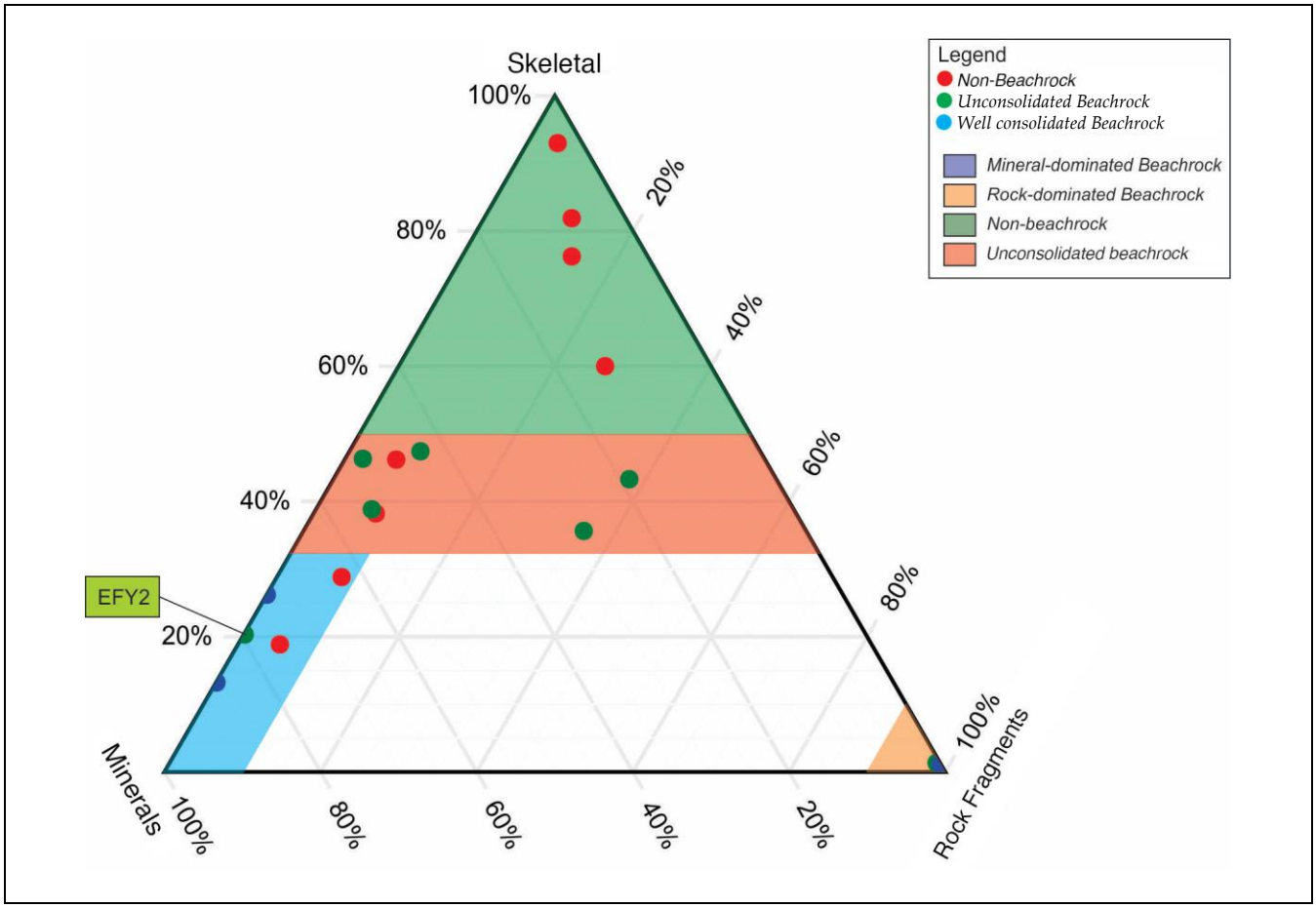
(XPL within gips chip)

Texture:

Allochem bioclastic with the grain size 0,04-10 mm. Bad sorted, open packed, angular grain shape and fragments relatively damaged. Microcalcite (Sparite) cementation found re-crystallization inside fossil fragment, micrite (mud carbonate), less spars with floating contact matrix, and variative fragment size.

Main composition:

- **Coral Fragment [5%]** with size 0,5 - 4 mm (J6).
- **Skeletal Fragment [25%]:** matrix fragment with variation random size and aragonite mineral (G2).
- **Micrite [30%]:** Clay grainsize when occurred in depositional process. Size <0,04 mm whereas smooth aggregate between matrix fragments. Brown color shown there is erosional process and weathered from this section (I4).
- **Sparite [30%]:** microcalcite cement (C2).
- **Calcite Mineral [10%] (F2)**


Skeletal
100%
80%
60%
40%
20%
Minerals
Rock Fragments
EFY2
Legend
Non-Beachrock
Unconsolidated Beachrock
Well consolidated Beachrock
Mineral-dominated Beachrock
Rock-dominated Beachrock
Non-beachrock
Unconsolidated beachrock

Appendix B.9. Measurement Stratigraphy and Petrographic Analysis of EFZ_1, and EFZ_2 samples

MEASURED STRATIGRAPHY

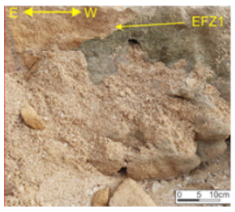
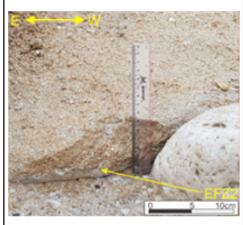
SCALE : 1:10

Date : 9 Juli 2018
Trenching EF
L = 5m, W= 1m, D= 1m

Location / Section : Krakal-Sadranan Beach / MS 7
Coordinate : 456028/9099620

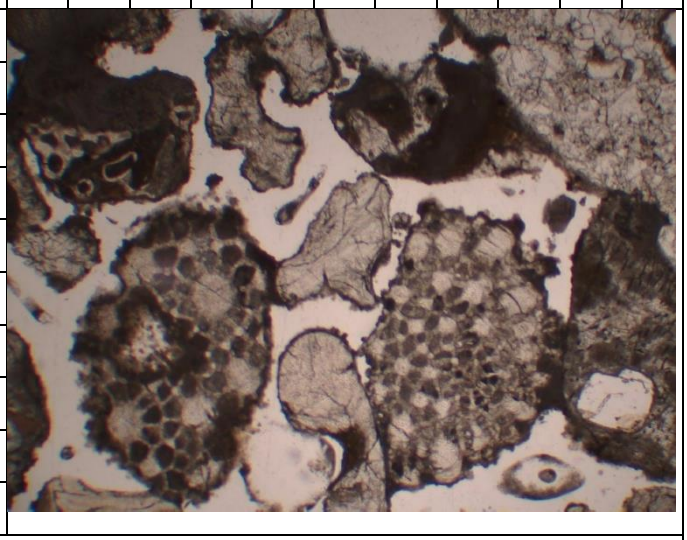
LEGEND

Carbonaceous Sandstone
Sparse Biomicrite
Sampling Points
Massive Structure
Skeletal Fragment

COORDINATE	THICKNESS	LITHOLOGY	SEDIMENTARY STRUCTURE	STRIKE/ DIP	DESCRIPTION	SAMPLE NUMBER	PHOTO NUMBER	PHOTO
	Surface							
	0 cm				Whitish yellow, sized 2 mm fragments and base mass 1 mm, the shape of sub-angular grain, not-consolidated, with a thickness of 70 cm. MH-a sample identification shows the composition of limestone fragments (30%) and skeletal fossil (40%) dominated by *Baculogypsina Sphaerulata*, limestone sand material(30%). Rock name: Carbonated sand deposits	EFZ1		
	-70 cm	?		$\frac{N280^0E}{27^0}$	Whitish yellow, sized 4 mm fragment and base mass <1 mm, sub-angular grain shape, open packed, massive structure, thickness around 30 cm. MH-b sample identification shows the composition of the fragment limestone (10%) and skeletal fossil (20%), which is dominated by *Baculogypsina Sphaerulata*, mineral calcite (40%) and sand material limestone (30%). Rock name: Sparse Biomicrite (Folk, 1962)	EFZ2		

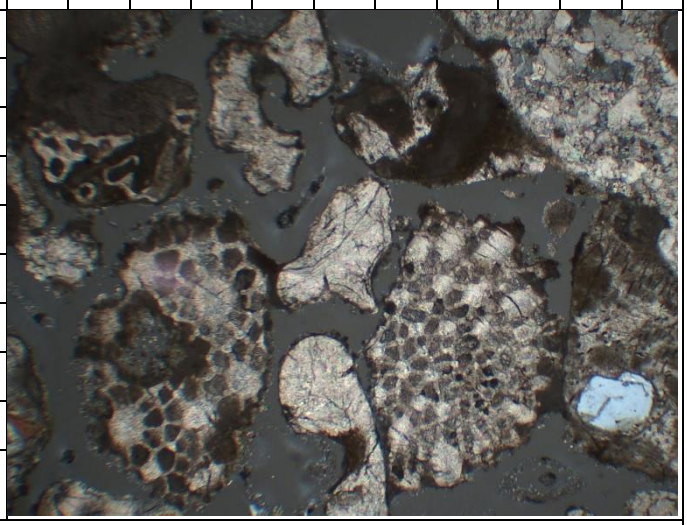
Sample: EFZ$_1$	**Name:** Sparse Biomicrite (Folk, 1962); Beachrock
Location: Trench EF, Krakal-Sadranan beach	456025/ 9099647

PPL	1	2	3	4	5	6	7	8	9	10	11
A											
B											
C											
D											
E											
F											
G											
H											
I											
J											



100 µm

XPL	1	2	3	4	5	6	7	8	9	10	11
A											
B											
C											
D											
E											
F											
G											
H											
I											
J											

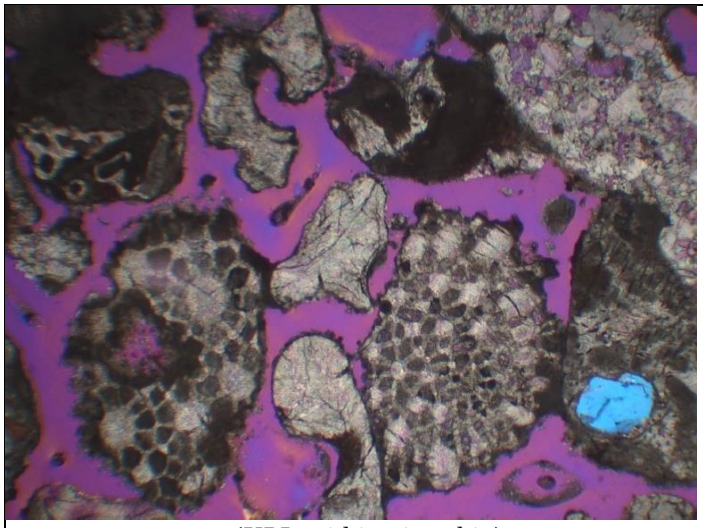


Texture:

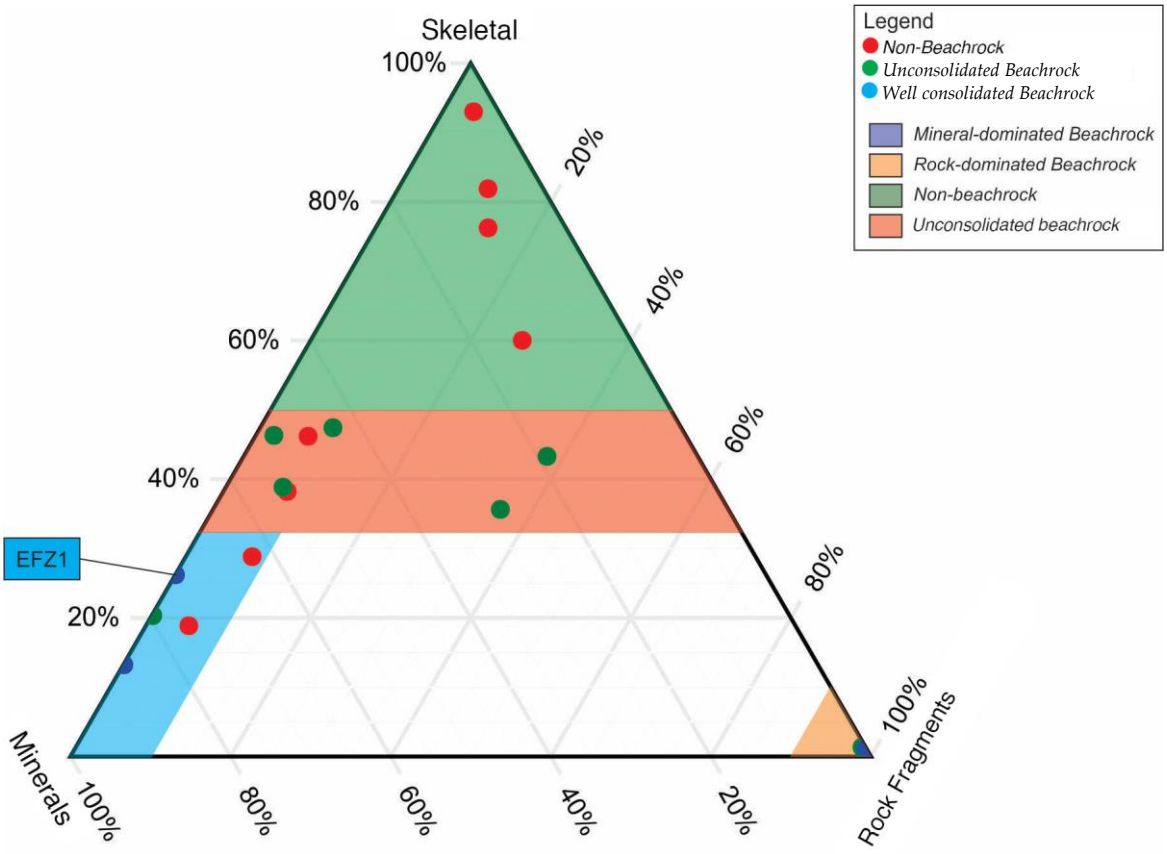
Allochem bioclastic with the grain size 0,04-10 mm. Bad sorted, open packed, angular grain shape and fragments relatively damaged. Microcalcite (Sparite) cementation found re-crystallization inside fossil fragment, micrite (mud carbonate), less spars with floating contact matrix, and variative fragment size.

Main composition:

- **Coral Fragment [10%]** with size 0,5 - 4 mm (D2).
- **Skeletal Fragment [10%]:** matrix fragment with variation random size and aragonite mineral (H7).
- **Micrite [40%]:** Clay grainsize when occurred in depositional process. Size <0,04 mm whereas smooth aggregate between matrix fragments. Brown color shown there is erosional process and weathered from this section (H5).
- **Sparite [30%]:** microcalcite cement (C8).
- **Calcite Mineral [10%] (F5)**

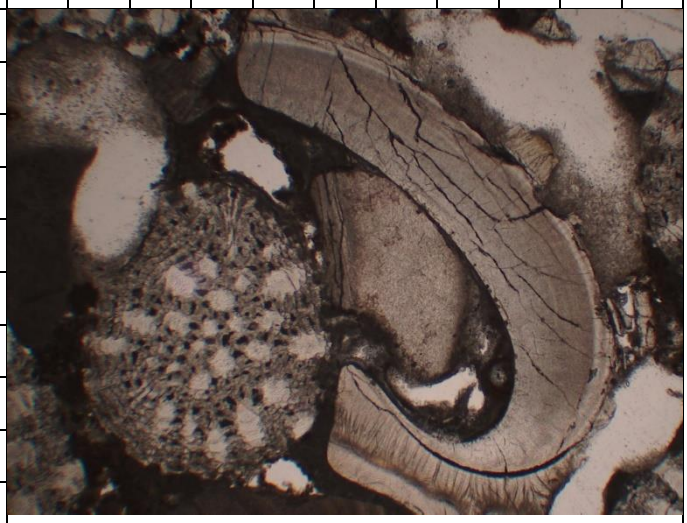


(XPL within gips chip)



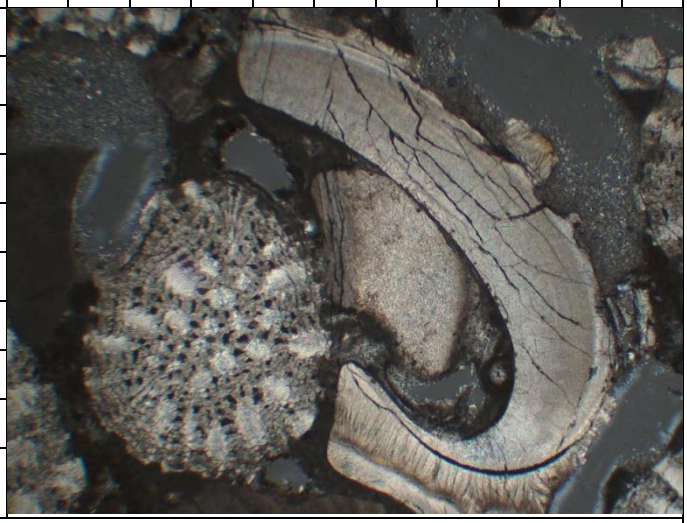
Sample: EFZ2	**Name:** Sparse Biomicrite (Folk, 1962); Beachrock
Location: Trench EF, Krakal-Sadranan beach	456025 / 9099647

PPL	1	2	3	4	5	6	7	8	9	10	11
A											
B											
C											
D											
E											
F											
G											
H											
I											
J											



100 µm

XPL	1	2	3	4	5	6	7	8	9	10	11
A											
B											
C											
D											
E											
F											
G											
H											
I											
J											

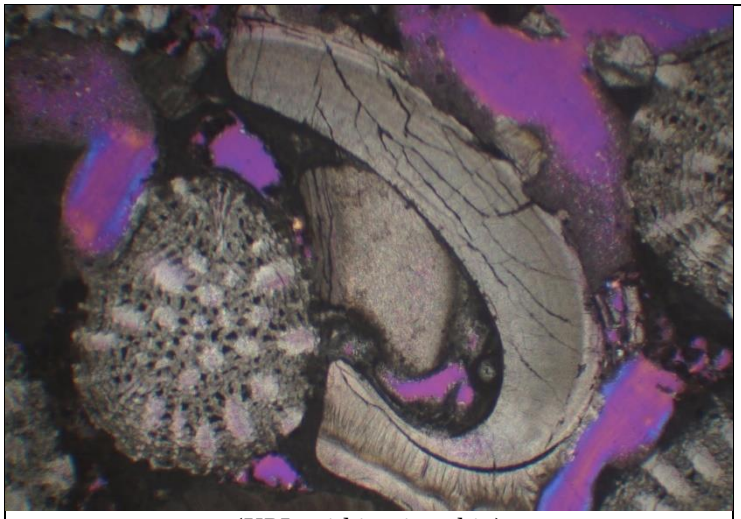


Texture:

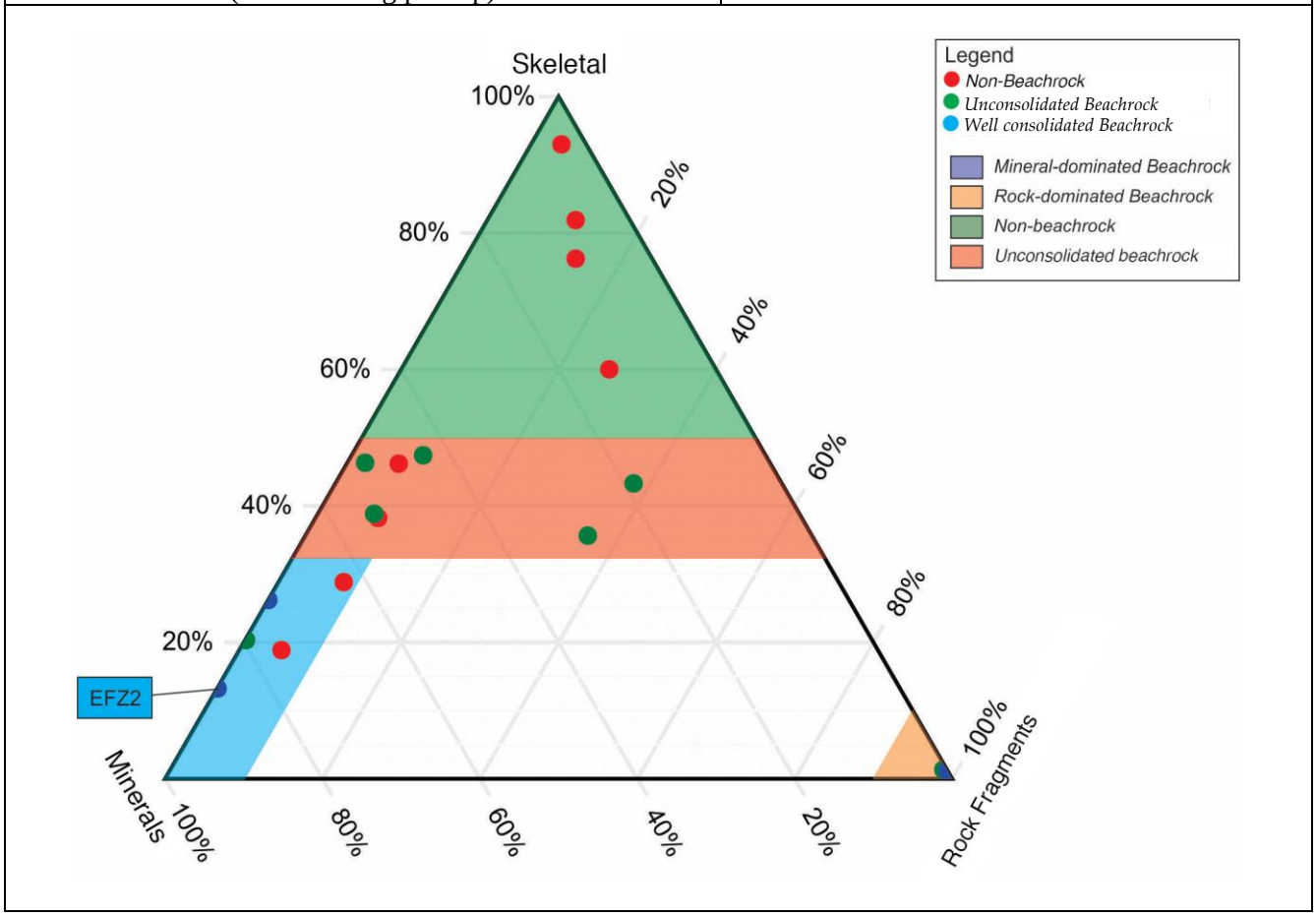
Allochem bioclastic with the grain size 0,04-10 mm. Bad sorted, open packed, angular grain shape and fragments relatively damaged. Microcalcite (Sparite) cementation found re-crystallization inside fossil fragment, micrite (mud carbonate), less spars with floating contact matrix, and variative fragment size.

Main composition:

- **Coral Fragment [15%]** with size 0,5 - 4 mm
- **Skeletal Fragment [20%]:** matrix fragment with variation random size and aragonite mineral (G4, F9).
- **Micrite [35%]:** Clay grainsize when occurred in depositional process. Size <0,04 mm whereas smooth aggregate between matrix fragments. Brown color shown there is erosional process and weathered from this section (F10).
- **Sparite [20%]:** microcalcite cement (F7).
- **Calcite Mineral [10%] (D9)**



(XPL within gips chip)



APPENDIXES C

Appendixes Table C. Standart normalization rare earth element (REE) results concentration for sediment. The major element of beachrock (ppm), trace element result (in ppm), and REE of beachrock (in ppm).

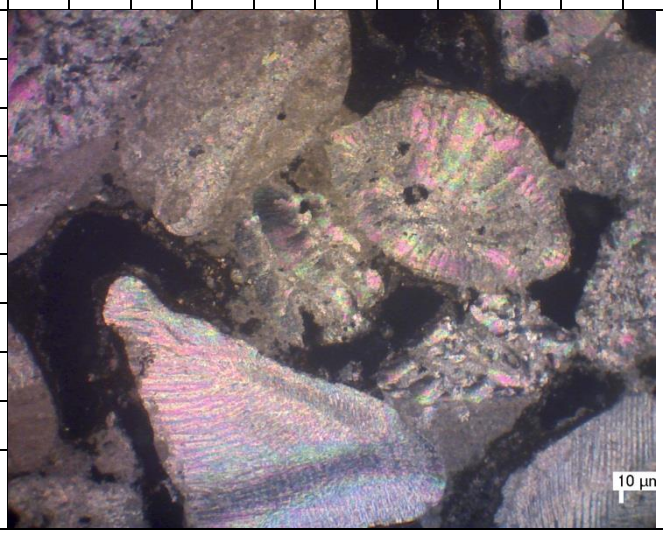
Element	AB.major elements (ppm)						CD.major elements (ppm)							Beachro Crust Ty (AlShuai et al., 2015)
	Sampel						Sampel							
	ABZ2	ABZ1	ABY1	ABY2	ABX1	ABX2	CDZ1	CDZ2	CDY1	CDY2	CDX1	CDX2	CDX3	
	Beachrock	Carbonate Sands	Carbonate Sands	Beachrock	Carbonate Sands	Beachrock	Carbonate Sands	Beachrock	Carbonate Sands	Beachrock	Carbonate Sands	Beachrock	Beachrock	
SiO_2	12400	11000	9000	9400	23900	10900	10100	30700	12400	25400	11900	14700	12600	72100
Al_2O_3	3400	3400	2600	3500	18100	3600	3700	23800	4300	18300	4200	7700	7400	20100
Fe_2O_3	3000	3900	2600	3700	10100	4100	2700	12500	3300	10100	3000	6400	4000	10200
CaO	495000	485000	486000	486000	451000	491000	499000	437000	493000	454000	498000	474000	474000	49320(
MgO	30600	31700	35600	31100	50500	32400	26900	58900	30000	48300	29400	38400	40500	20100
K_2O	100	100	100	100	400	200	100	500	300	400	200	200	200	6900
Na_2O	6300	5700	5600	5800	4400	5900	6800	4600	6500	4600	5800	6000	5300	8000
MnO	100	100	100	100	600	100	100	400	100	300	100	100	100	-
TiO_2	200	100	200	200	800	200	200	1000	200	900	200	500	300	2400
P_2O_5	500	500	600	400	1100	300	400	1200	500	1200	500	1400	1100	1000
Loss of Ignition	445000	446000	447000	448000	426000	445000	441000	418000	442000	425000	441000	439000	441000	351000
	AB.trace elements (ppm)						CD.trace elements (ppm)							
Chromium	10.00	10.00	10.00	10.00	20.00	10.00	10.00	20.00	10.00	10.00	10.00	10.00	10.00	-
Manganese	77.00	77.00	77.00	77.00	460.00	77.00	77.00	308.00	77.00	231.00	77.00	77.00	77.00	-
Iron	2100.00	2730.00	1820.00	2590.00	7070.00	2870.00	1890.00	8750.00	2310.00	7070.00	2100.00	4480.00	2800.00	-
Rubidium	0.30	0.50	0.30	0.50	1.50	0.50	0.40	1.80	0.70	1.50	0.50	0.70	0.60	-
Strontium	4360.00	3570.00	3500.00	3530.00	3490.00	3540.00	4010.00	2690.00	3830.00	3590.00	3790.00	3460.00	3540.00	-
Yttrium	1.60	2.80	1.70	4.20	3.60	2.90	2.20	4.40	2.50	3.70	2.70	2.30	2.50	-
Zirconium	5.00	5.00	4.00	4.00	13.00	6.00	2.00	13.00	2.00	10.00	2.00	6.00	4.00	-
Niobium	0.20	0.20	0.20	0.60	0.30	0.20	0.20	0.60	0.20	0.50	0.20	0.20	0.20	-
Barium	7.90	11.20	8.00	26.70	20.10	11.20	9.30	18.10	9.80	15.20	12.00	9.70	9.20	-
	AB.REE (ppm)						CD.REE (ppm)							
Lanthanum	0.90	1.10	0.90	5.00	2.30	1.30	1.30	2.70	1.50	2.40	1.30	1.60	1.60	-
Cerium	1.50	1.50	1.30	9.10	4.30	2.10	1.60	5.00	1.90	4.40	1.90	2.50	2.30	-
Praseodymium	0.17	0.24	0.17	1.10	0.60	0.28	0.22	0.70	0.26	0.60	0.30	0.38	0.33	-
Neodymium	1.00	1.40	1.10	4.90	2.50	1.40	1.00	2.80	1.40	2.30	1.20	1.30	1.30	-
Samarium	0.14	0.20	0.22	0.97	0.65	0.27	0.17	0.59	0.33	0.61	0.35	0.28	0.30	-
Europium	0.05	0.09	0.05	0.28	0.13	0.09	0.07	0.13	0.07	0.16	0.08	0.11	0.11	-
Gadolinium	0.19	0.29	0.21	0.92	0.54	0.33	0.26	0.49	0.38	0.52	0.43	0.35	0.26	-
Terbium	0.04	0.06	0.03	0.13	0.08	0.08	0.03	0.08	0.05	0.08	0.03	0.05	0.05	-
Dysprosium	0.19	0.33	0.24	0.74	0.63	0.30	0.26	0.65	0.44	0.49	0.41	0.30	0.43	-
Holmium	0.04	0.07	0.05	0.13	0.09	0.09	0.06	0.12	0.06	0.13	0.09	0.07	0.08	-
Erbium	0.18	0.30	0.10	0.37	0.37	0.26	0.19	0.49	0.18	0.38	0.21	0.20	0.14	-
Thulium	0.01	0.01	0.01	0.02	0.02	0.01	0.02	0.06	0.02	0.05	0.03	0.02	0.03	-
Ytterbium	0.14	0.22	0.11	0.34	0.27	0.20	0.12	0.42	0.21	0.27	0.20	0.22	0.23	-
Lutetium	0.01	0.01	0.01	0.03	0.04	0.02	0.01	0.07	0.03	0.04	0.03	0.04	0.03	-

APPENDIXES D

Petrography analysis of Okinawa beachrock

<table>
<tr><td colspan="12">Code D.1: YOMITAN A</td><td>Name: Biomicrite (folk 1959) pack stone (dunham,1962) beachrock (lithified)</td></tr>
<tr><td colspan="12">Location : YOMITAN ,OKINAWA</td><td>N26°23’45.7” E127° 43’13.2”</td></tr>
<tr><td>PPL</td><td>1</td><td>2</td><td>3</td><td>4</td><td>5</td><td>6</td><td>7</td><td>8</td><td>9</td><td>10</td><td>11</td><td rowspan="12"><u>Texture and Description</u>
Bioclastic with grain size clay to granule (0.02-7mm). Bad sorted with shape of grain particle angular-sub rounded, but within altered remains fossil fragment. Open fabric grain supported, dominated by foraminifera, coral and lithic. There is found matrix micro quartz (part of lithic aggregate) inside re-microcrystalline fossils and also micrite (mud carbonate). Shell fragment aragonite (0,5-4 mm) with micrite domination and little sparite, fossils founded point contact re-worked, floating, and shown imbricate process, variated fragment sized.

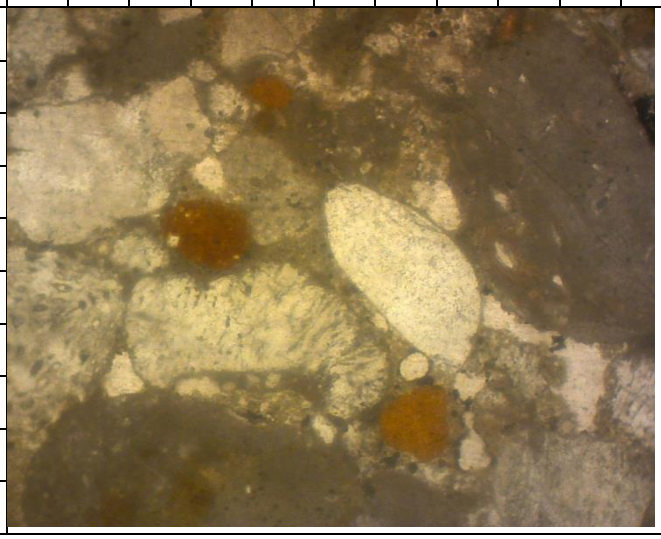
<u>Main Compositions</u>

➢ Big Foraminifera [15%]: as fragment Ø 2-5 mm (C7-F9) with uncleaned shaped, surrounding with mud carbonate (micrite).
➢ Coral Fragment [10%] as a fragment with variation sized between 0,5-5 mm
➢ Shell Fragment [20%]: as a part of fragment with variation grain size and composition aragonite (G3-J7).
➢ Micrite [15%]: dark color organic micrite as clay grain size that occur from depositional, Grain size <0,04mm whereas grain particles fragment as smoothed aggregate, acicular shaped with dominant smooth tabular. Some</td></tr>
<tr><td>A</td><td colspan="10" rowspan="10"> 
100 µm</td></tr>
<tr><td>B</td></tr>
<tr><td>C</td></tr>
<tr><td>D</td></tr>
<tr><td>E</td></tr>
<tr><td>F</td></tr>
<tr><td>G</td></tr>
<tr><td>H</td></tr>
<tr><td>I</td></tr>
<tr><td>J</td></tr>
<tr><td>XPL</td><td>1</td><td>2</td><td>3</td><td>4</td><td>5</td><td>6</td><td>7</td><td>8</td><td>9</td><td>10</td><td>11</td></tr>
<tr><td>A</td><td colspan="10" rowspan="10">  </td></tr>
<tr><td>B</td></tr>
<tr><td>C</td></tr>
<tr><td>D</td></tr>
<tr><td>E</td></tr>
<tr><td>F</td></tr>
<tr><td>G</td></tr>
<tr><td>H</td></tr>
<tr><td>I</td></tr>
<tr><td>J</td></tr>
<tr><td colspan="12">Note :
o Thickness of thinsection >0.03 mm (± 0.04mm), make a difficult to observed the matrixs.</td></tr>
</table>

<table>
<tr><td></td><td>of part with brownie color represented weathering process.
➢ Pore [30%]: as pores inside the rock because of interparticle grain contacted and intraparticle fossil, really rare with cement material (sparite).
➢ Lithic (quartz) [10%]: as a lithic fragment and matrix with size <0,3mm whereas birefringence ordo 1, anhedral. Matrix sub angular (0,1- 0,5 mm).
Assessor Compositions [< 1%]:
➢ Opaque: as lithic that filled inside fossil with size <0,1 mm, magnetite?</td></tr>
<tr><td colspan="2">Microfacies :
Assuming as intertidal zone sedimentary and spray zone coasts</td></tr>
<tr><td colspan="2">Diagenesis characteristics:
Dominant by compaction process ,first phase lithification, cemented</td></tr>
<tr><td colspan="2">Pore system:
Interparticle and intra particle (Choquette and pray 1970)</td></tr>
<tr><td colspan="2">Interpretation:
Shell fragment dominant with aragonite and coral whereas mud carbonate (micrite) filled non-carbonate lithic cavity that have a high pores. Interparticle type and intra particle high permeability not much as strong enough based on grain particle contact.</td></tr>
</table>

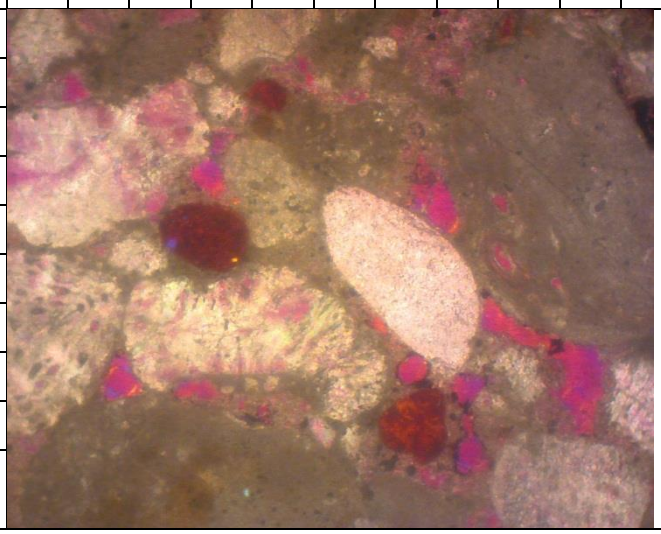
Code D.2: YOMITTAN B	**Name**: Biomicrite (folk 1959) pack stone (dunham,1962) beachrock (lithified)
Location : YOMITAN ,OKINAWA	N26°23'45.7" E127° 43'13.2"

PPL	1	2	3	4	5	6	7	8	9	10	11
A											
B											
C											
D											
E											
F											
G											
H											
I											
J											



100 µm

XPL	1	2	3	4	5	6	7	8	9	10	11
A											
B											
C											
D											
E											
F											
G											
H											
I											
J											



Texture and Description

Bioclastic allochem with grain size clay to sand (0,02-20mm). Bad sorted with shape of grain particle angular-sub rounded, but within altered remains fossil fragment. Open fabric grain supported, dominated by foraminifera, coral and lithic. There is found matrix micro quartz (part of lithic aggregate) inside re-microcrystalline fossils and also micrite (mud carbonate). Shell fragment aragonite (0,5-4 mm) with micrite domination and little sparite, fossils founded point contact re-worked, floating, and shown imbricate process, variated fragment sized.

Main Compositions

- **Foraminifera [15%]:** as a fragment Ø 2-5 mm (F1-H3) with uncleaned shaped, surrounding with mud carbonate (micrite).
- **Coral Fragment [10%]** as a fragment with variation sized between 0,5-4 mm
- **Shell Fragment [15%]:** as a part of fragment with variation grain size and composition aragonite

<table>
<tr>
<td>Note :
o Thickness of thinsection >0.03 mm (± 0.04mm), make a difficult to observed the matrixs.</td>
<td>➢ Micrite [25%]: as clay grain size that occur from depositional, Grain size <0,04mm whereas grain particles fragment as smoothed aggregate, several found with brownie color represented weathered process.
➢ Pore [15%]: as pores inside the rock because of interparticle grain contacted and intraparticle fossil, really rare with cement material (sparite).
➢ Lithic (quartz) [10%]: as a lithic fragment and matrix with size <0,3mm whereas birefringence ordo 1, anhedral. Matrix sub angular (0,1- 0,5 mm).

Assessor Compositions [< 5%]:
➢ Opaque: as lithic muscovite fragment with grain size <0,1 mm.</td>
</tr>
<tr>
<td colspan="2">Microfacies :
Assuming as intertidal zone sedimentary and spray zone coasts</td>
</tr>
<tr>
<td colspan="2">Diagenesis characteristics:
Dominant by compaction process ,first phase lithification, cemented</td>
</tr>
<tr>
<td colspan="2">Pore system:
Interparticle and intra particle (Choquette and pray 1970)</td>
</tr>
<tr>
<td colspan="2">Interpretation:
Shell fragment dominant with aragonite and coral whereas mud carbonate (micrite) filled non-carbonate lithic cavity that have a high pores. Interparticle type and intra particle high permeability not much as strong enough based on grain particle contact, Amount of micrite is bigger than Yomitan A sample.</td>
</tr>
</table>

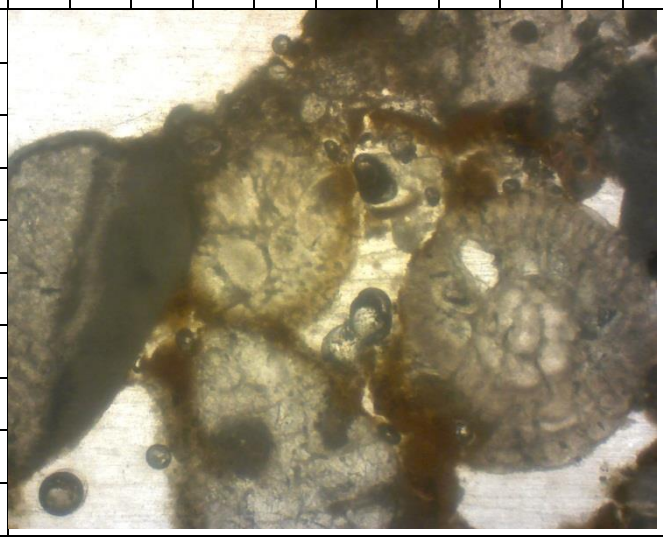
Code D.3: YOMITTAN C

Name: Biomicrite (folk 1959) pack stone (dunham) beachrock(lithified)

Location : YOMITAN ,OKINAWA

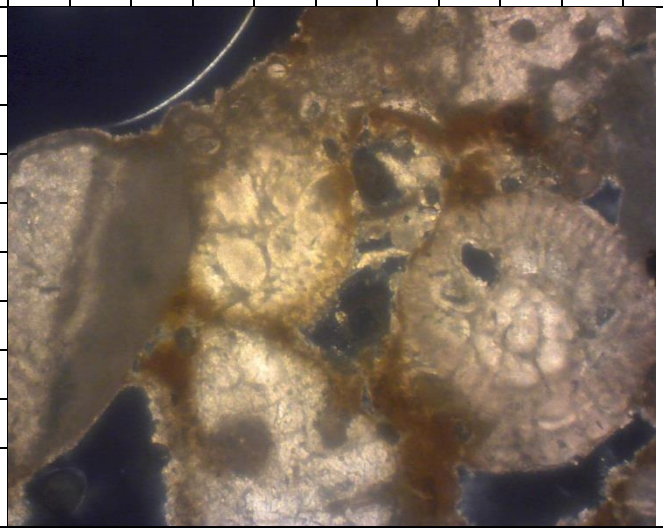
N26°23'45.7" E127° 43'13.2"

PPL	1	2	3	4	5	6	7	8	9	10	11
A											
B											
C											
D											
E											
F											
G											
H											
I											
J											



100 µm

XPL	1	2	3	4	5	6	7	8	9	10	11
A											
B											
C											
D											
E											
F											
G											
H											
I											
J											



Note :

- Thickness of thinsection >0.03 mm (± 0.04mm), make a difficult to observed the matrixs.

Texture and Description

Grain size clay to granule (0,03 – 14mm). Bad sorted with shape of grain particle angular-sub rounded, but within altered remains fossil fragment. Open fabric grain supported, dominated by foraminifera, coral and lithic. There is found matrix micro quartz (part of lithic aggregate) inside re-microcrystalline fossils and also micrite (mud carbonate). Shell fragment aragonite (0,5-5 mm) with micrite domination and little sparite, fossils founded point contact re-worked, floating, and shown imbricate process, variated fragment sized between 0,1-7 mm.

Main Compositions

- **Foraminifera [15%]:** as a fragment Ø 2-5 mm (F8-I10) with uncleaned shaped, surrounding with mud carbonate (micrite) and also point contact between grained particles.
- **Coral Fragment [10%]** as a fragment (A8-B10) with variation sized between 0,2-5 mm.
- **Shell Fragment [15%]:** as a part of **f**ragment with variation sized of aragonite dominant.
- **Micrite [25%]:** as clay grain size that occur from depositional, Grain size <0,04mm whereas grain particles fragment as smoothed aggregate, some of part with a brownies color represented weathering process
- **Sparite [10%]:** as a smooth tabular micro calcite that filled pores between grain particle (>0,04mm)
- **Pore [15%]:** as pore inside the rock sample because of interparticle grain contacted and intraparticle fossil, really rare with cement

	material (sparite). Only several part of particle size are connected. ➢ **Lithic (quartz) [4%]:** as a lithic fragment and matrix with size <0,3mm whereas birefringence ordo 1, anhedral. Matrix sub angular (0,1- 0,5 mm). **Assessor Compositions [< 1%]:** ➢ **Opaque**: as lithic whereas muscovite fragment with size <0,1 mm.

Microfacies : Assuming as intertidal zone sedimentary and spray zone coasts
Diagenesis characteristics: Dominant by compaction process ,first phase lithification, cemented
Pore system: interparticle and intra particle (Choquette and pray 1970)
Interpretation: Shell fragment dominant with aragonite, foraminifera, and coral whereas mud carbonate (micrite) filled non-carbonate lithic cavity pores. Interparticle type and intra particle low permeability not much as strong enough based on grain particle contact, Amount of micrite is bigger than Yomitan B sample.

Code D.4: YOMITTAN D

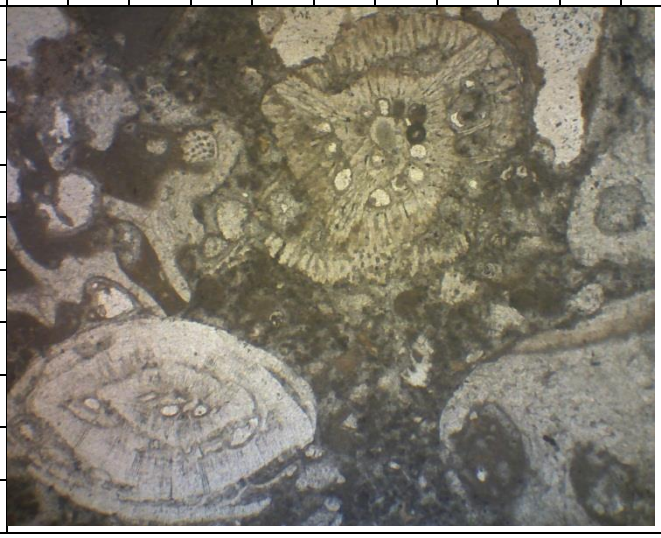
Name: Biomicrite (folk 1959) pack stone (dunham) beachrock (lithified)

Location : YOMITAN ,OKINAWA

N26°23'45.7" E127° 43'13.2"

PPL

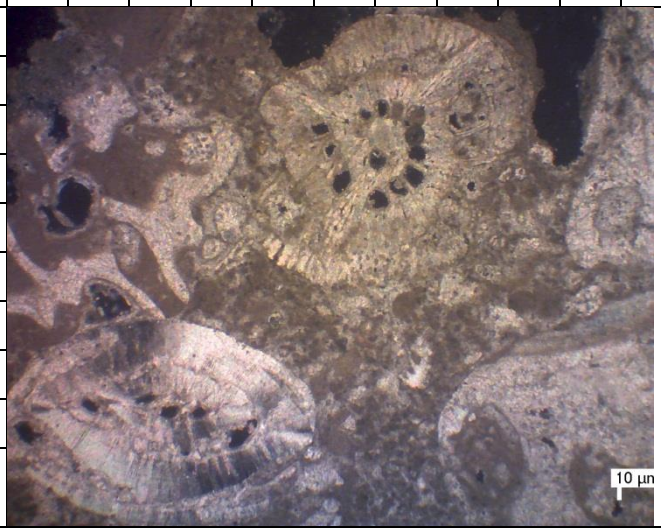
	1	2	3	4	5	6	7	8	9	10	11
A											
B											
C											
D											
E											
F											
G											
H											
I											
J											



100 µm

XPL

	1	2	3	4	5	6	7	8	9	10	11
A											
B											
C											
D											
E											
F											
G											
H											
I											
J											



Note :

- Thickness of thinsection >0.03 mm (± 0.04mm), make a difficult to observed the matrixs.

Texture and Description

Grain size clay to granule. Bad sorted with shape of grain particle angular-sub rounded, but within altered remains fossil fragment. Open fabric grain supported, dominated by foraminifera, coral and lithic. There is found matrix micro quartz (part of lithic aggregate) inside re-microcrystalline fossils and also micrite (mud carbonate). Shell fragment aragonite (0,5-5 mm) with micrite domination and little sparite, fossils founded point contact re-worked, floating, and shown imbricate process, variated fragment sized between 0,1-5 mm.

Main Compositions

- **Foraminifera [15%]:** as a fragment Ø 2-5 mm (F8-I10) with uncleaned shaped, surrounding with mud carbonate (micrite) and also point contact between grained particles.
- **Coral Fragment [10%]** as a fragment (A8-B10) with variation sized between 0,2-5 mm.
- **Shell Fragment [15%]:** as a part of **f**ragment with variation sized of aragonite dominant.
- **Micrite [25%]:** as clay grain size that occur from depositional, Grain size <0,04mm whereas grain particles fragment as smoothed aggregate, some of part with a brownies color represented weathering process
- **Sparite [10%]:** as a smooth tabular micro calcite that filled pores between grain particle (>0,04mm)
- **Pore [15%]:** as pore inside the rock sample because of interparticle grain contacted and intraparticle fossil, really rare with cement

	material (sparite). Only several part of particle size are connected. ➢ **Lithic (quartz) [4%]:** as a lithic fragment and matrix with size <0,3mm whereas birefringence ordo 1, anhedral. Matrix sub angular (0,1- 0,5 mm). **Assessor Compositions [< 1%]:** ➢ **Opaque** : as lithic whereas muscovite fragment with size <0,1 mm.
Microfacies : Assuming as intertidal zone sedimentary and spray zone coasts	
Diagenesis characteristics: Dominant by compaction process ,first phase lithification, cemented	
Pore system: interparticle and intra particle (Choquette and pray 1970)	
Interprets: Shell fragment dominant with aragonite, foraminifera, and coral whereas mud carbonate (micrite) filled non-carbonate lithic cavity pores. Interparticle type and intra particle low permeability not much as strong enough based on grain particle contact, Amount of micrite and sparite is bigger than the other samples.	

Code D.5: GIMA A

Name: biomicrite (folk 1959) pack stone (dunham,1962), beachrock (lithified)

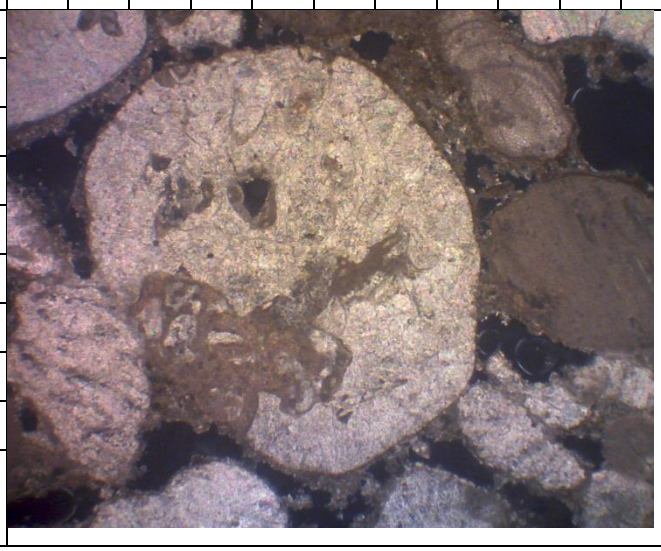
Location : GIMA ,OKINAWA

N26°25'2.8"; E127°42'48.9"

PPL	1	2	3	4	5	6	7	8	9	10	11
A											
B											
C											
D											
E											
F											
G											
H											
I											
J											



XPL	1	2	3	4	5	6	7	8	9	10	11
A											
B											
C											
D											
E											
F											
G											
H											
I											
J											



Note :

- Thickness of thinsection >0.03 mm (± 0.04mm), make a difficult to observed the matrixs.

Texture and Description

Grain size clay to granule (0.03-7mm), with shape of grain particle angular-sub rounded, but within altered remains fossil (relatively). Open fabric grain supported, dominated by big foraminifera. High pores inside fossils recrystallized with micro-calcite and also mud carbonate. Shell fragment aragonite (0.5-2mm) with micrite domination and little sparite, fossils founded reworked and not strong solidification yet.

Main Compositions

- **Big Foraminifera [35%]:** as mega-phenocryst Ø 1 – 3.2 mm (F8-G10) with uncleaned shaped, surrounding with mud carbonate (micrite) and also point contact between grained particles.
- **Coral Fragment [15%]** as a fragment with variation sized between 0,5-3mm
- **Micrite [15%]:** dark color organic micrite as clay grain size that occur from depositional, Grain size <0,04mm whereas grain particles fragment as smoothed aggregate, acicular shaped with dominant smooth tabular.
- **Sparite [5%]:** as cement filled by calcite.
- **Pore [20%]:** as pore inside the rock because of interparticle grain contacted and intraparticle fossil, really rare with cement material (sparite). Only several part of particle size are connected.

Assessor Compositions [< 1%]:

- **Opaque**: as lithic that filled inside fossil with size <0,1 mm, magnetite (?)

	Analysis : Not strong connection between grain particle and some of it still floated (mud carbonate) or maybe point contact, dominant by micrite from depositional process with minimum altered remains fossil. Assuming because of strong sea wave
Microfacies : Assuming as intertidal zone sedimentary	
Diagenesis characteristics: Dominant by compaction process ,first phase lithification, cemented	
Pore system: interparticle and intra particle (Choquette and pray 1970)	

Code D.6: GIMA B

Name: biomicrite (folk ,1959), Pickstone (dunham,1962), beachrock (lithified)

Location : GIMA ,OKINAWA

N26°25'2.8"; E127°42'48.9"

PPL	1	2	3	4	5	6	7	8	9	10	11
A											
B											
C											
D											
E											
F											
G											
H											
I											
J											



100 µm

XPL	1	2	3	4	5	6	7	8	9	10	11
A											
B											
C											
D											
E											
F											
G											
H											
I											
J											



Note :

- Thickness of thinsection >0.03 mm (± 0.04mm), make a difficult to observed the matrixs.

Texture and Description

Grain size 0.03-10 mm with angular-sub rounded shaped with altered remains fossil. Open grain supported fabric, dominant big foraminifera. Pores found not so much than sample A, inside the fossil are filled by micro calcite and micrite (mud carbonate). Shell fragment aragonite (0.5 - 4 mm) with micrite dominant, less sparite and a little altered remain fossils. More strong lithified than Gima A, within convex concave contact between particles shown imbricate process, size of grain particles more variation than before but bigger than Gima A sample.

Main Compositions

- **Big Foraminifera [30%]:** as mega-phenocryst Ø 2-5 mm (A7-G11) with uncleaned shaped, surrounding with mud carbonate (micrite).
- **Coral Fragment [10%]** as a fragment with variation sized between 0,5-2 mm
- **Shell Fragment [20%]:** as matrixes but smaller with variation size.
- **Micrite [15%]:** dark color organic micrite as clay grain size that occur from depositional, Grain size <0,04mm whereas grain particles fragment as smoothed aggregate, acicular shaped with dominant smooth tabular.
- **Sparite [5%]** as cement filled by calcite.
- **Pore [20%]:** as pores inside the rock because of interparticle grain contacted and intraparticle fossil, really rare with cement material (sparite).

.

Assessor Compositions [< 1%]:

	➢ **Opaque** : as lithic that filled inside fossil with size <0,1 mm.
Microfacies : Assuming as intertidal zone sedimentary	
Diagenesis characteristics: Dominant by compaction process ,first phase lithification, cemented	
Pore system: Interparticle and intra particle (Choquette and pray 1970)	
Interpretation: Stronger solidified than Gima A whereas convex concave contact between grain particles (mud carbonate), micrite dominant when depositions process with minimum altered because of strong wave impact.	

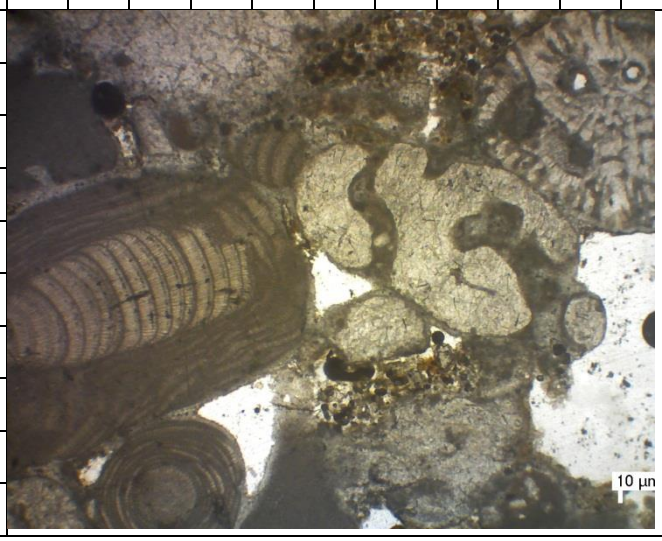
Code D.7: GIMA C

Name: biomicrite (folk 1959) pack stone (dunham) beachrock (lithified)

Location : GIMA ,OKINAWA

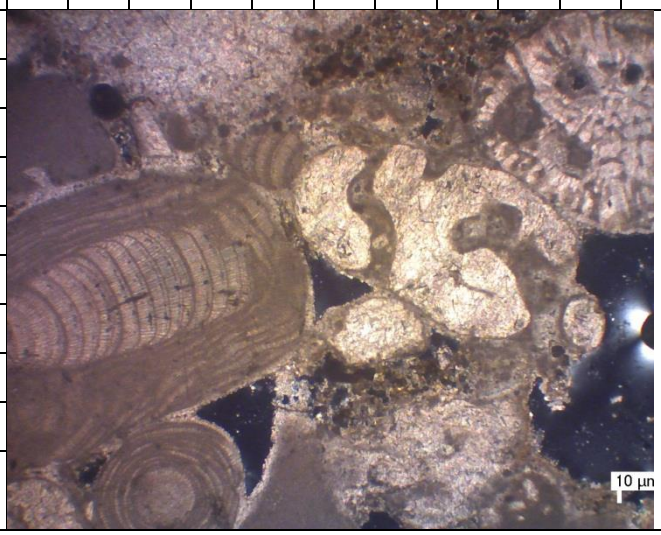
N26°25'2.8"; E127°42'48.9"

PPL	1	2	3	4	5	6	7	8	9	10	11
A											
B											
C											
D											
E											
F											
G											
H											
I											
J											



100 µm

XPL	1	2	3	4	5	6	7	8	9	10	11
A											
B											
C											
D											
E											
F											
G											
H											
I											
J											



Note :

- Thickness of thinsection >0.03 mm (± 0.04mm), make a difficult to observed the matrixs.

Texture and Description

Grain size clay to granule (0,03-7mm), with shape of particle angular-sub rounded and fossils is little bit broke (relatively). Open grain supported fabric, dominant coral fragment. Pores size are small, with inside fossils filled by micro calcite and micrite (mud carbonate). Grain shell particle are from aragonite (0,5-5 mm) dominant with micrite and less sparite altered remain fossils are solidified really strong with concave convex contact between particles and cemented uniform shown imbricate process. Fragment size are variations but bigger than Gima A with uncleaned the contact limit degree.

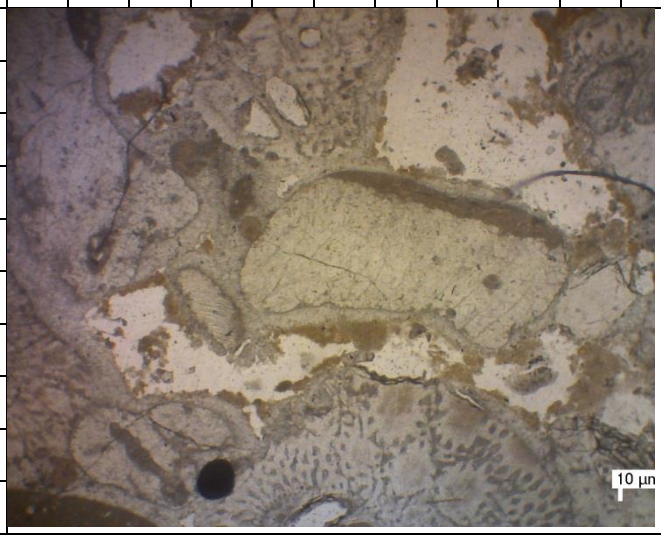
Main Compositions

- **Big Foraminifera [20** as mega-phenocryst Ø 2-5 mm (A9-D11) with uncleaned shaped, surrounding with mud carbonate (micrite).
- **Coral Fragment [30%]** as a fragment with variation sized between >0,5 cm, some of fossil changed to be calcite.
- **Shell Fragment [20%]:** as an aragonite fragment (D6-G9) but more smaller size of particle grain but variated.
- **Micrite [25%]:** dark color organic micrite as clay grain size that occur from depositional, Grain size <0,04 mm whereas grain particles fragment as smoothed aggregate, acicular shaped with dominant smooth tabular.
- **Sparite [5%]:** as a cement that filled by micro calcite with tabular shaped surrounding the fragments.

	➢ **Pore [10%]:** as a pore inside the rock because of interparticle grain contacted and intraparticle fossil, really rare with cement material (sparite). **Assessor Compositions [< 10%]:** ➢ **Opaque**: as a lithic that filled inside fossils with size <0,1 mm. ➢ **Quartz**: as a matrix (0,1mm) anhedral
Microfacies : Assuming as intertidal zone sedimentary and spray zone coasts	
Diagenesis characteristics: Dominant by compaction process ,first phase lithification, cemented	
Pore system: interparticle and intra particle (Choquette and pray 1970)	
Interpretation: More compacted better than Gima A and B samples which have convex concave contact between grain particles (mud carbonate), dominant with micrite based on depositional process riches altered remain fossils but some of fossils are broken (uncleaned shape) because of strong tidal wave. Grain size coral fragments bigger than Gima A and B samples.	

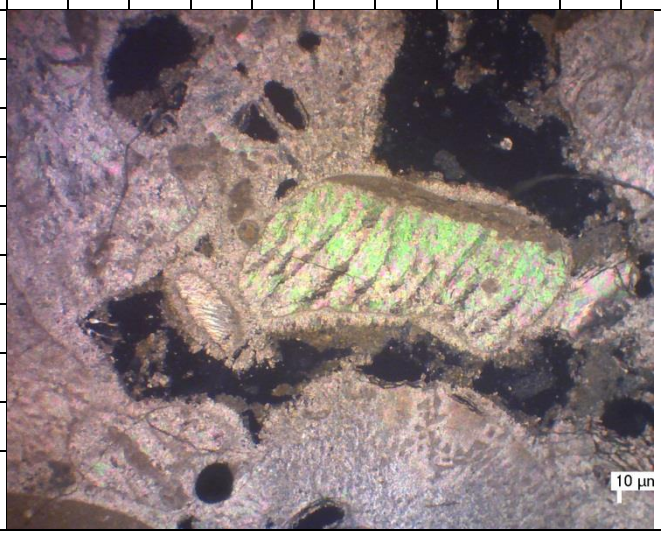
Code D.8: GIMA D (Weathered)	**Name**: biomicrite (folk 1959) pack stone (dunham) beachrock (lithified)
Location : GIMA ,OKINAWA	N26°25'2.8"; E127°42'48.9"

PPL	1	2	3	4	5	6	7	8	9	10	11
A											
B											
C											
D											
E											
F											
G											
H											
I											
J											



100 µm

XPL	1	2	3	4	5	6	7	8	9	10	11
A											
B											
C											
D											
E											
F											
G											
H											
I											
J											



Note :

- Thickness of thinsection >0.03 mm (± 0.04mm), make a difficult to observed the matrixs.

Texture and Description

Grain size clay to granule), with shape of grain particle angular-sub rounded and the fossils is little bit broke (relatively). Open fabric grain supported, dominated by coral fragment. Pores size are small, with inside fossils filled by micro calcite and micrite (mud carbonate). Shell fragment aragonite (0,5-5 mm) with micrite domination and little sparite, altered remain fossils really strong compacted with concave convex contact between particles and cemented uniform shown imbricate process. Fragment size are variations but bigger than Gima A.

Main Compositions

- **Big Foraminifera [20%]:** as mega-phenocryst Ø 2-5 mm (A4-C6), uncleaned shaped surrounding with mud carbonate (micrite)
- **Coral Fragment [30%]** b as a fragment with variation sized between >0,5 cm, some of fossils changed to be calcite.
- **Shell Fragment [20%]:** as an aragonite fragment (D6-G9) but smaller within variation sized.
- **Micrite [30%]:** as clay grain size that occur from depositional, Grain size <0,04mm whereas grain particles fragment as smoothed aggregate, acicular shaped with dominant smooth tabular, the color of rock more brownies because weathered process.
- **Sparite [5%]:** as a cement filled by calcite.
- **Pore [10%]:** as pore inside the rock because of interparticle grain contacted and

	intraparticle fossil, really rare with cement material (sparite). . **Assessor Compositions [< 5%]:** ➢ **Opaque**: as a lithic with filled inside fossils, size <0,1 mm ➢ **Quartz**: as a matrix (0,1mm) anhedral
Microfacies : Assuming as intertidal zone sedimentary and spray zone coasts	
Diagenesis characteristics: Dominant by compaction process ,first phase lithification, cemented	
Pore system: interparticle and intra particle (Choquette and pray 1970)	
Interpretation: More compacted better than Gima A and B samples which have convex concave contact between grain particles (mud carbonate), dominant with micrite based on depositional process riches altered remain fossils but some of fossils are broken (uncleaned shape) because of strong tidal wave. Grain size coral fragments bigger than Gima A and B samples.	

Analysis samples GIMA A, GIMA B and GIMA C

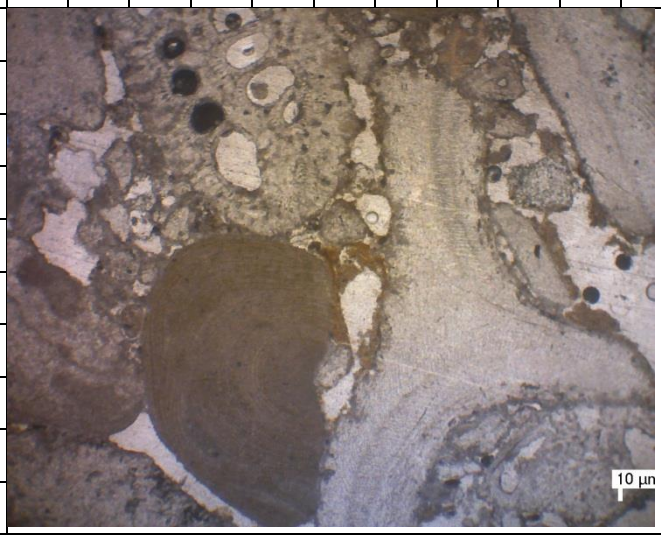
Sample Gima A more sparite filled crystallize better than Gima B with grain size particle smaller and pores much more than Gima B. Gima B have a little calcite and also aragonite (shell) whereas cement aggregate is, mud carbonate less than Gima A. Gima C sample much more compacted than the others maybe based on contact precipitated calcium more intense and found big amount of cement micrite. In sample Gima C found more foraminifera fragments, altered remain fossils became log Mg Carbonate from aragonite.

Code D.9: SUMUIDE A

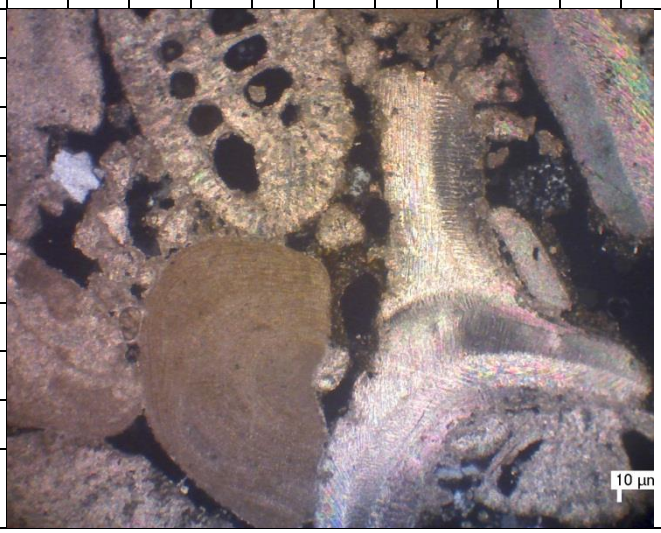
Name: intra micrite (folk ,1959) pack stone (dunham,1962), beachrock(lithified)

Location : SUMUIDE ,OKINAWA

N26°40'43.8" E128°00'44.6"

PPL	1	2	3	4	5	6	7	8	9	10	11
A											
B											
C											
D											
E											
F											
G											
H											
I											
J											

100 µm

XPL	1	2	3	4	5	6	7	8	9	10	11
A											
B											
C											
D											
E											
F											
G											
H											
I											
J											

Note :

- Thickness of thinsection >0.03 mm (± 0.04mm), make a difficult to observed the matrixs.

Texture and Description

Grain size clay to granule. Bad sorted with shape of grain particle angular-sub rounded, but within altered remains fossil fragment. Open fabric grain supported, dominated by foraminifera, coral and lithic. There is found matrix micro quartz (part of lithic aggregate) inside re-microcrystalline fossils and also micrite (mud carbonate). Shell fragment aragonite (0,5-4 mm) with micrite domination and little sparite, fossils founded point contact re-worked, floating, and shown imbricate process, variated fragment sized.

Main Compositions

- **Big Foraminifera [15%]:** as a fragment Ø 2-5 mm (F3-J6) with uncleaned shaped, surrounding with mud carbonate (micrite)
- **Coral Fragment [10%]** as a fragment with variation sized between 0,5-2 mm
- **Shell Fragment [30%]:** as a part of **f**ragment with variation sized of aragonite dominant (B7-H11).
- **Micrite [15%]:** as clay grain size that occur from depositional, Grain size <0,04mm whereas grain particles fragment as smoothed aggregate, some of part with a brownies color represented weathering process
- **Sparite [3%]:** as a micro calcite cement that filled pore.
- **Pore [20%]:** as pore inside the rock sample because of interparticle grain contacted and intraparticle fossil, really rare with cement material (sparite).

	➢ **Lithic (quartz)[15%] :** as a lithic fragment and matrix with size (D2) 0,3 mm whereas birefringence ordo 1, anhedral. Matrix sub angular (0,1- 0,5 mm). **Assessor Compositions [< 1%]:** ➢ **Opaque**: as lithic filled the fossils with size <0,1 mm, magnetite (?)
Microfacies : Assuming as intertidal zone sedimentary and spray zone coasts and spray zone coasts	
Diagenesis characteristics: Dominant by compaction process ,first phase lithification, cemented	
Pore system: interparticle and intra particle (Choquette and pray 1970)	
Interpretation: Aragonite shell fragment and lithic (as quartz-metasedimentary) are dominant whereas depositional process, micrite (mud carbonate) filled cavity pores of non-carbonate lithic between grain particles.	

Code D.10: SUMUIDE B

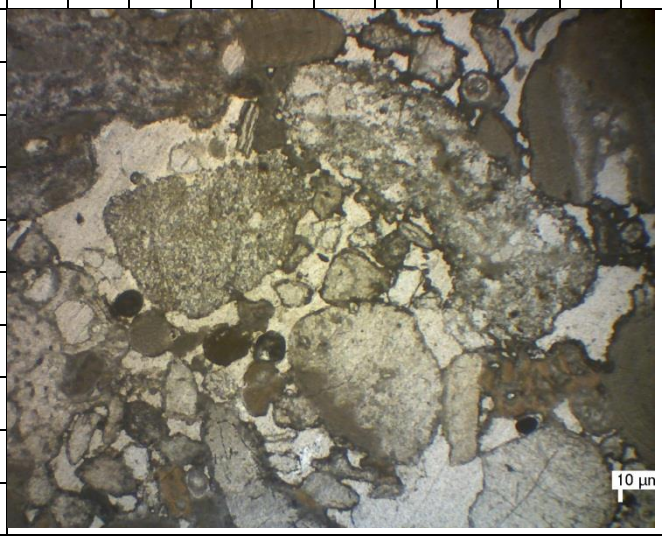
Name: Intra micrite (folk 1959) pack stone (dunham,1962), beachrock (lithified)

Location : SUMUIDE ,OKINAWA

N26°40’43.8” E128°00’44.6”

PPL

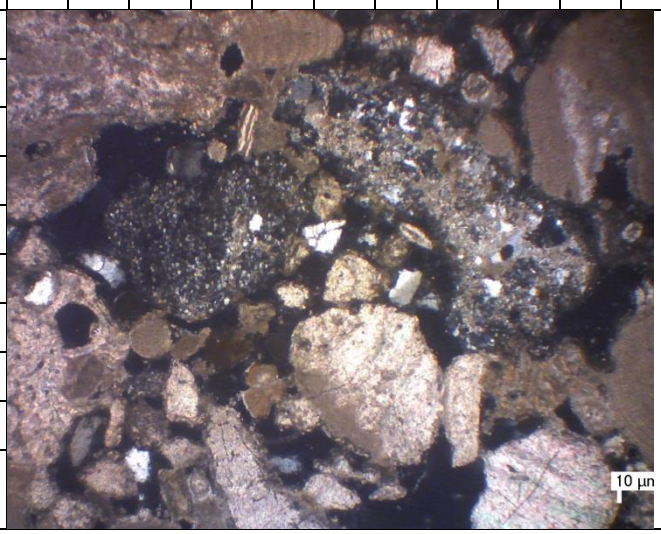
	1	2	3	4	5	6	7	8	9	10	11
A											
B											
C											
D											
E											
F											
G											
H											
I											
J											



100 µm

XPL

	1	2	3	4	5	6	7	8	9	10	11
A											
B											
C											
D											
E											
F											
G											
H											
I											
J											



Note :

- Thickness of thinsection >0.03 mm (± 0.04mm), make a difficult to observed the matrixs.

Texture and Description

Grain size clay to granule (0.03-10mm). Bad sorted with shape of grain particle angular-sub rounded, but within altered remains fossil fragment. Open fabric grain supported, dominated by foraminifera, coral and lithic. There is found matrix micro quartz (part of lithic aggregate) inside re-microcrystalline fossils and also micrite (mud carbonate). Shell fragment aragonite (0.5-5 mm) with micrite domination and little sparite, fossils founded point contact re-worked, floating, and shown imbricate process, variated fragment sized.

Main Compositions

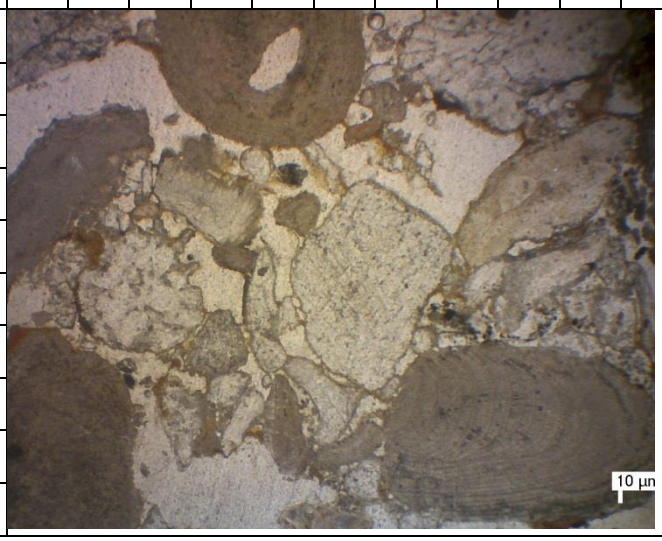
- **Big Foraminifera [15%]:** as a fragment Ø 2-5 mm (F3-J6) with uncleaned shaped, surrounding with mud carbonate (micrite).
- **Small Foraminifera [5%]:** Benthonic biserial with low mg carbonate (calcite) composition.
- **Coral Fragment [10%]** as a fragment with variation sized between 0,5-5 mm, unaltered fossil remains.
- **Shell Fragment [15%]:** as a part of **f**ragment with variation sized of aragonite dominant (I9-J10).
- **Micrite [15%]:** as clay grain size that occur from depositional, Grain size <0,04mm whereas grain particles fragment as smoothed aggregate, some of part with a brownies color represented weathering process
- **Sparite [5%]:** as a smooth tabular micro calcite that filled pores between grain particle.

<table>
<tr><td></td><td>➢ Pore [20%]: as pore inside the rock sample because of interparticle grain contacted and intraparticle fossil, really rare with cement material (sparite). Only several part of particle size are connected.
➢ Lithic (quartz) [20%]: as a lithic fragment and matrix with size (F1) 0.3mm whereas birefringence ordo 1, anhedral.
➢ Matrix: as quartz mineral or part of micro-shell and coral.

Assessor Compositions [< 5%]:
➢ Opaque: as filled lithic inside the fossils with size <0,1 mm.</td></tr>
<tr><td colspan="2">Microfacies :
Assuming as intertidal zone sedimentary and spray zone coasts</td></tr>
<tr><td colspan="2">Diagenesis characteristics:
Dominant by compaction process ,first phase lithification, cemented</td></tr>
<tr><td colspan="2">Pore system:
interparticle and intra particle (Choquette and pray 1970)</td></tr>
<tr><td colspan="2">Interpretation:
Aragonite shell fragment and lithic (as quartz-metasedimentary) are dominant whereas depositional process, micrite (mud carbonate) filled cavity pores of non-carbonate lithic between grain particles. Size of grain particles is bigger and much more amount better than Sumuide A sample, so there is found a lot of matrix’s but not really strong compact between contact fragments.</td></tr>
</table>

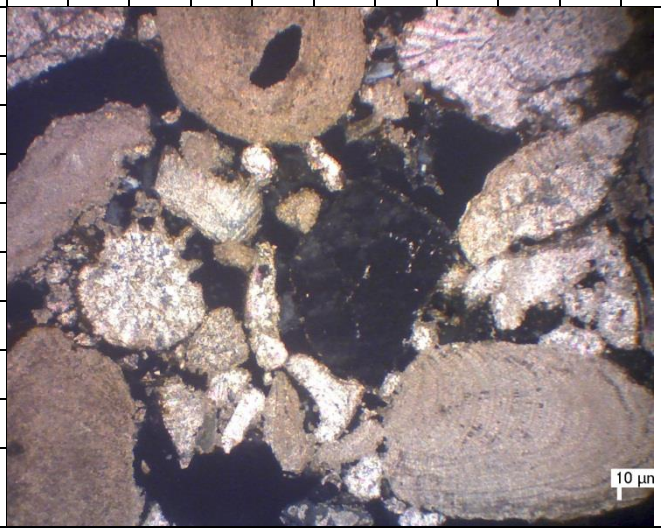
Code D.11: SUMUIDE C	**Name**: Intra micrite (folk 1959) pack stone (dunham,1962) beachrock (lithified)
Location: SUMUIDE, OKINAWA	N26°40’43.8” E128°00’44.6”

PPL	1	2	3	4	5	6	7	8	9	10	11
A											
B											
C											
D											
E											
F											
G											
H											
I											
J											



100 µm

XPL	1	2	3	4	5	6	7	8	9	10	11
A											
B											
C											
D											
E											
F											
G											
H											
I											
J											



Note :

- Thickness of thinsection >0.03 mm (± 0.04mm), make a difficult to observed the matrixs.

Texture and Description

Grain size clay to granule (0.02-9mm). Bad sorted with shape of grain particle sub-angular rounded, but within altered remains fossil fragment. Open fabric grain supported, dominated by foraminifera, coral and lithic. There is found matrix micro quartz (part of lithic aggregate) inside re-microcrystalline fossils and also micrite (mud carbonate). Shell fragment aragonite (0.4-5 mm) dominant with micrite and foraminifera fossil altered convex concave contact between grain particles, sized of particles are variated.

Main Compositions

- **Big Foraminifera [15%]:** as a fragment Ø 2-5 mm with uncleaned shaped, surrounding with mud carbonate (micrite).
- **Small Foraminifera [5%]:** Benthonic biserial with low mg carbonate (calcite) composition.
- **Coral Fragment [10%]** as a fragment with variation sized between 0,5-5 mm, filled by calcite.
- **Shell Fragment [15%]:** as a part of **f**ragment with variation sized of aragonite dominant. (D9-E11).
- **Micrite [20%]:** as clay grain size that occur from depositional, Grain size <0,04mm whereas grain particles fragment as smoothed aggregate, some of part with a brownies color represented weathering and erosion process.
- **Sparite [5%]:** as a micro calcite lithic that filled intra particles with tabular shaped.

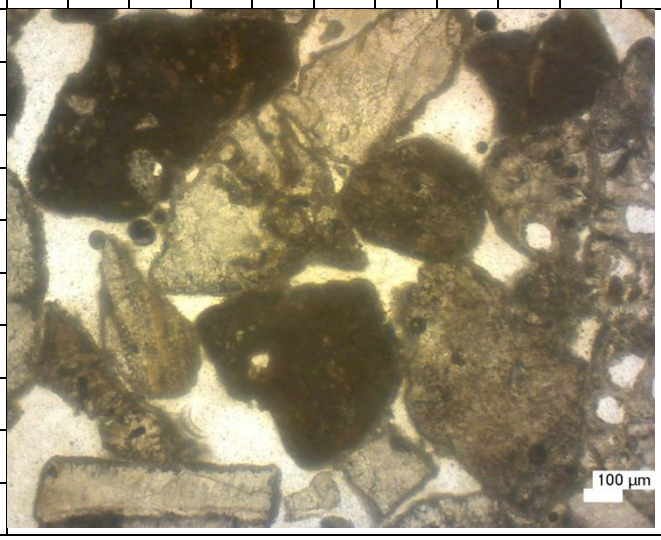
	➢ **Pore [15%]:** as pore inside the rock sample because of interparticle grain contacted and intraparticle fossil, really rare with cement material (sparite). ➢ **Lithic (quartz) [20%]:** as a lithic fragment (E6) and matrix with size 0,3mm whereas birefringence ordo 1, anhedral. ➢ **Matrix:** as quartz mineral or part of micro-shell and coral. **Assessor Compositions [< 5%]:** **Opaque**: as filled lithic inside the fossils with size <0,1 mm.
Microfacies: Assuming as intertidal zone sedimentary and spray zone coasts	
Diagenesis characteristics: Dominant by compaction process, first phase lithification, cemented	
Pore system: interparticle and intra particle (Choquette and pray 1970)	
Interpretation: Aragonite shell fragment and lithic (as quartz-metasedimentary) are dominant whereas depositional process, micrite (mud carbonate) filled cavity pores of non-carbonate lithic between grain particles. Inter particles and intraparticle less pores are impermeable because of amount of matrix's and contact between grain particles are not too strong.	

Analysis Samples Sumuide A, B, and C

Sumuide samples is different with another location because lithic fragment that found in this deposit is quartz mineral (metasedimentary) and amount of matrix such as shell, coral, opaque and quartz with variated grain size. Grain supported fabric micrite (mud carbonate) refilled contact limit degree between carbonate fragment and also non carbonate fragment, it shown depositional process. Inter particles and intraparticle pore with filled by microsparite or cement (not big amount) in sample Sumuide C stronger compact than sample Sumuide A and Sumuide B, but lithic fragment and pores size less than sample Sumuide A because of cementation process.

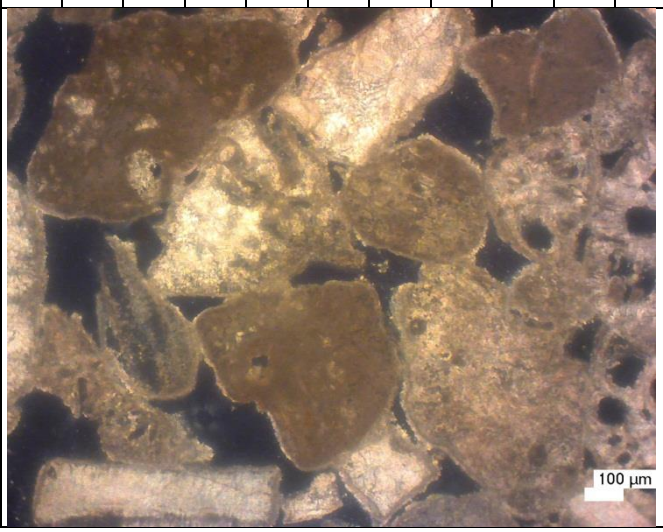
Code D.12: Anthropogenic Beachrock (Synthetic)	**Name**: Anthropogenic Beachrock
Location : -	

PPL

	1	2	3	4	5	6	7	8	9	10	11
A											
B											
C											
D											
E											
F											
G											
H											
I											
J											

100 µm

XPL

	1	2	3	4	5	6	7	8	9	10	11
A											
B											
C											
D											
E											
F											
G											
H											
I											
J											

Note :

- Thickness of thinsection >0.03 mm (± 0.04mm), make a difficult to observed the matrixs.

Texture and Description

Grain size clay to sand (0,04 -3mm). Bad sorted with shape of grain particle angular-sub rounded, but within altered remains fossil fragment. Open fabric grain supported, dominated by foraminifera, coral and lithic. There is found matrix micro quartz (part of lithic aggregate) inside re-microcrystalline fossils and also micrite (mud carbonate).

Main Compositions

- **Foraminifera [15%]:** as fragment Ø 2-5 mm (F1-H3 with uncleaned shaped, surrounding with cement.
- **Coral Fragment [10%] %]** as a fragment with variation sized between 0,5-4 mm.
- **Shell Fragment [15%]:** as a part of fragment.
- **Micrite [10%]:** dark color organic micrite as clay grain size that occur from depositional, Grain size <0,04mm whereas grain particles fragment as smoothed aggregate.
- **Pore [30%]:** as pores inside the rock because of interparticle grain contacted and intraparticle fossil, really rare with cement material (sparite).
- **Lithic (quartz) [5%]:** as a lithic fragment and matrix with size 0,3-0,5 mm whereas birefringence ordo 1, anhedral.

Microfacies :

-

Diagenesis characteristics:

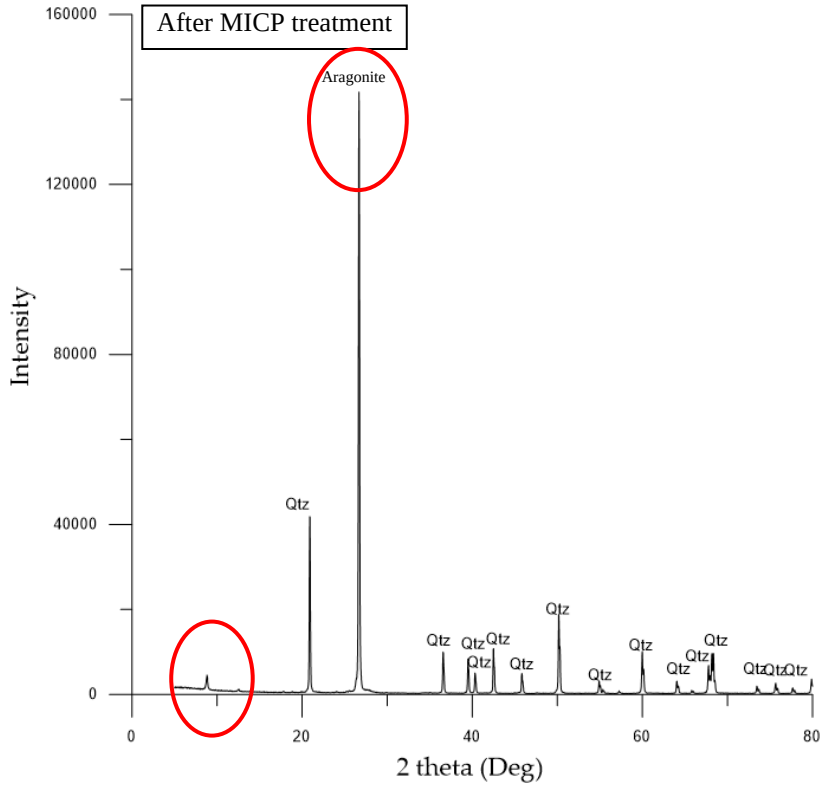
Dominant with cementation process

Pore system:
Interparticle and intra particle (Choquette and pray 1970)
Interpretation:
Interparticle type and intra particle high permeability not much as strong enough based on grain particle contact. For making anthropogenic beachrock, is made from coral sand so in this thin section contain with fragment of foraminifera and also coral, cement process as aragonite not only filled inside carbonate particle pores but also non carbonate particles. The cementation process using microbial activities precipitated surrounding the fragment particles.

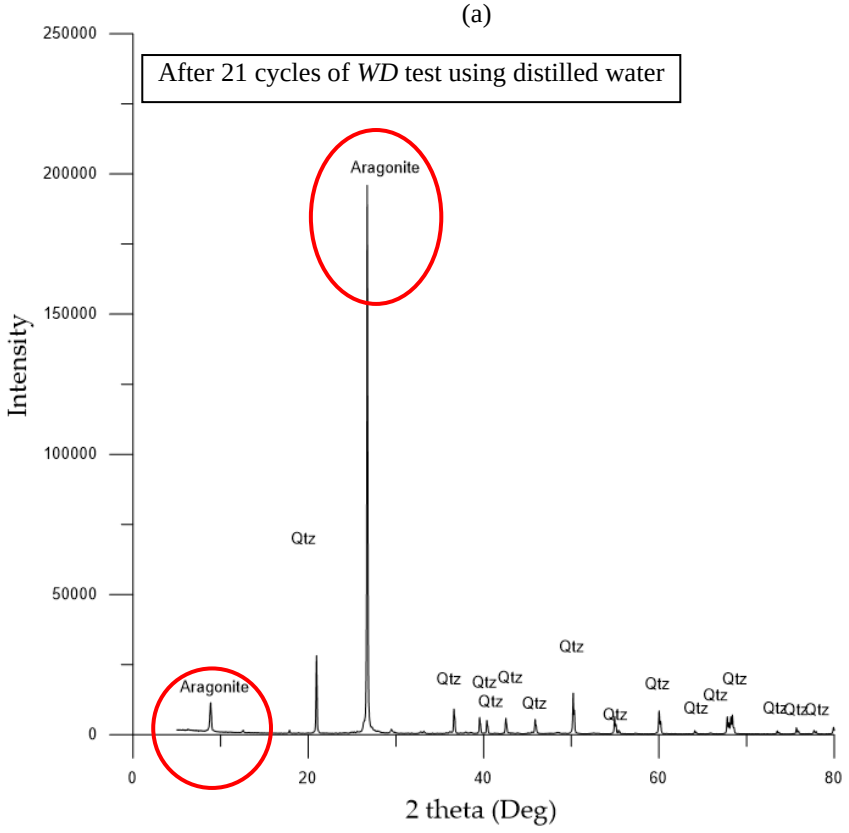
uyutuytAPPENDIXES E

XRD results before and after durability *wetting-drying* test

E.1 Mikawa sand

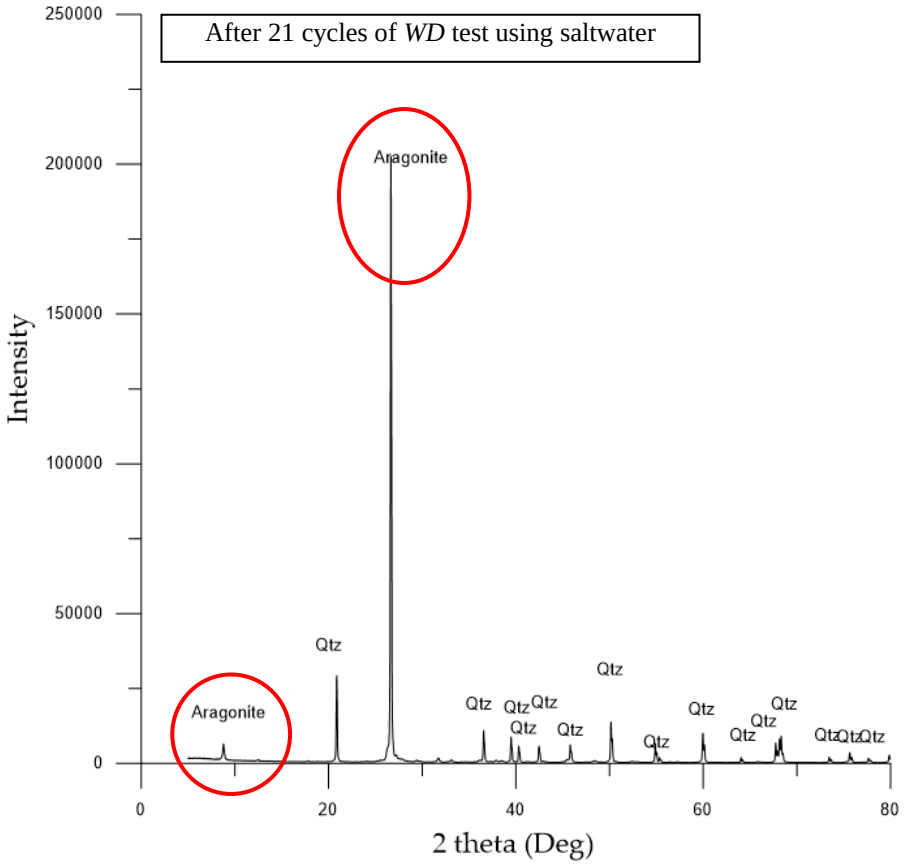


(a)



(b)

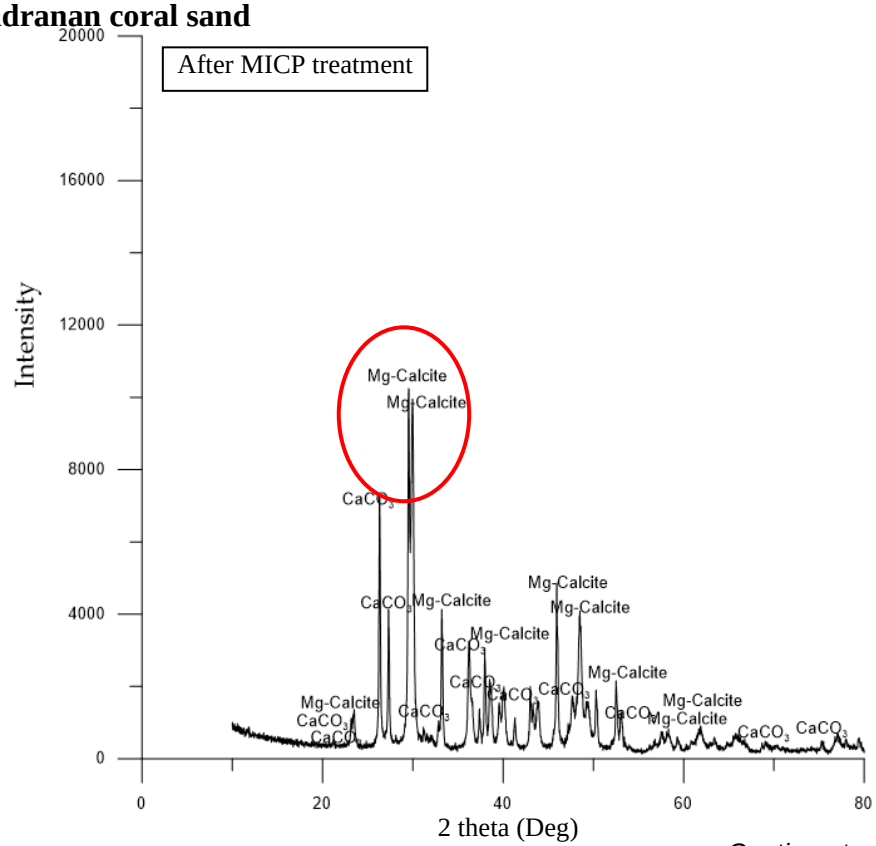
Continue to next page



(c)

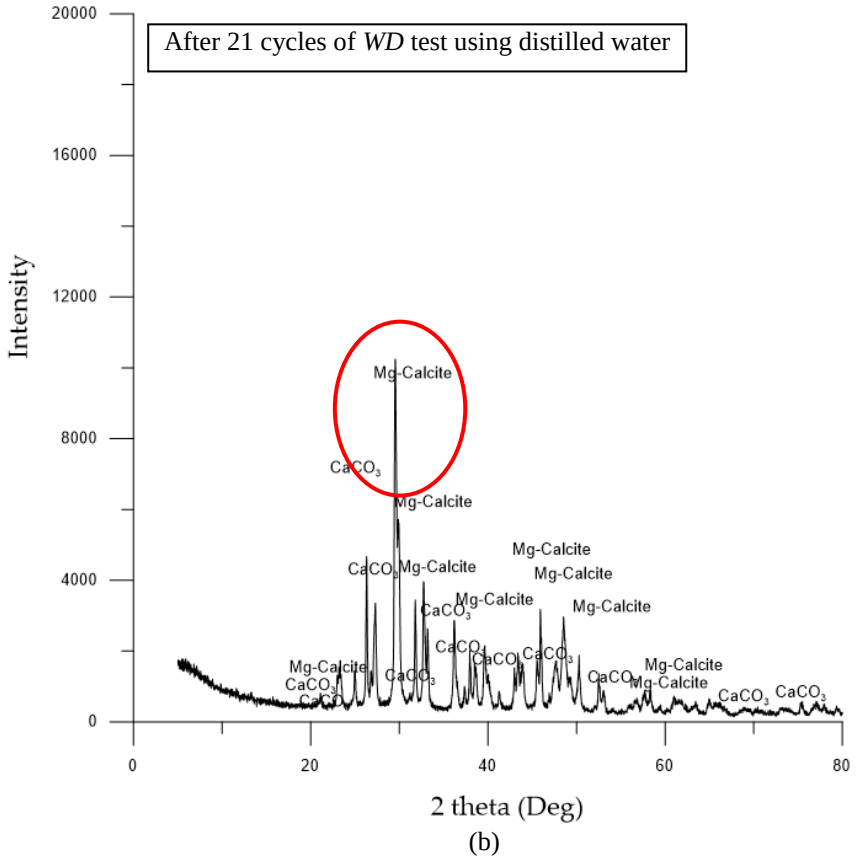
Figure E.1. Graphic XRD analysis pattern of Mikawa sand (a) before MICP treatment, (b) after MICP treatment, (c) MICP treated after 21 WD cycle under distilled water, and (d) MICP treated after 21 WD cycle under saltwater.

E.2 Krakal-Sadranan coral sand

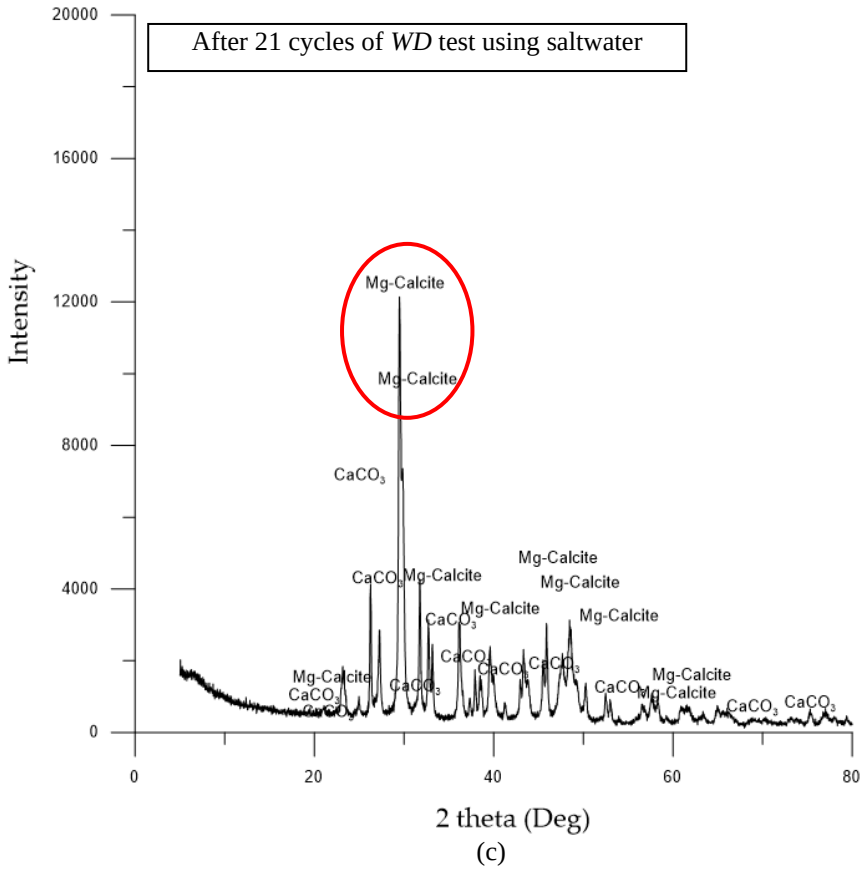


(a)

Continue to next page



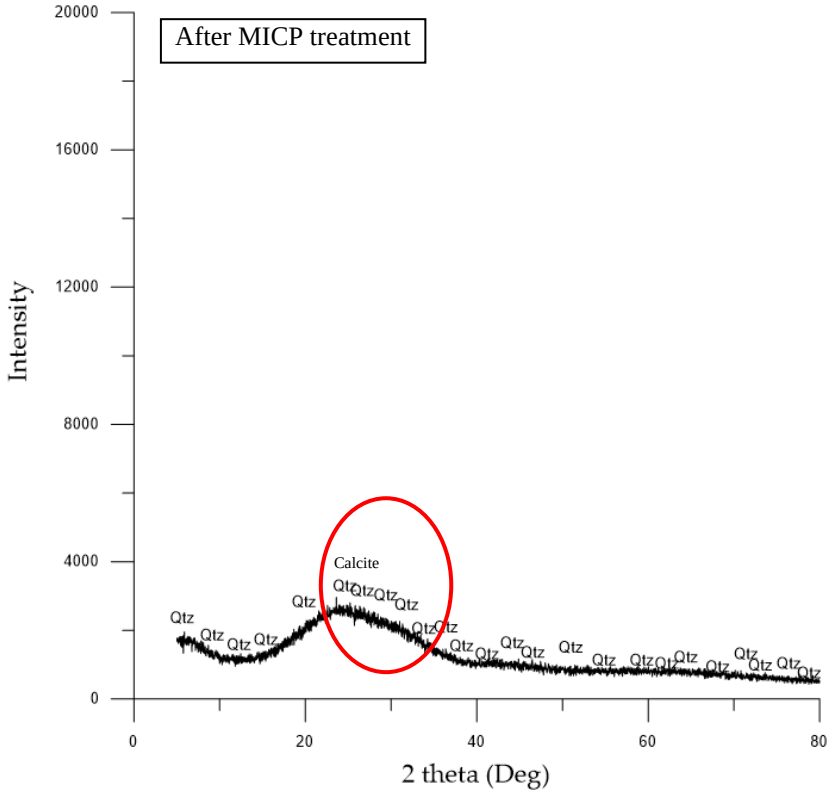
(b)



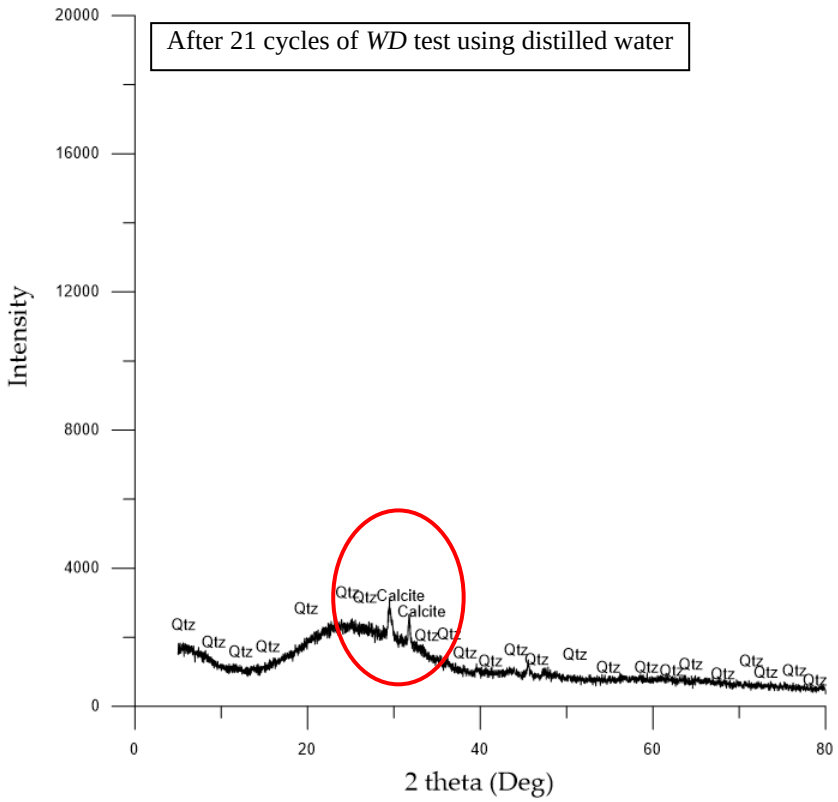
(c)

Figure E.2. Graphic XRD analysis pattern of Krakal-Sadranan coral sand (a) before MICP treatment, (b) after MICP treatment, (c) MICP treated after 21 WD cycle under distilled water, and (d) MICP treated after 21 WD cycle under saltwater.

E.3 Glass beads

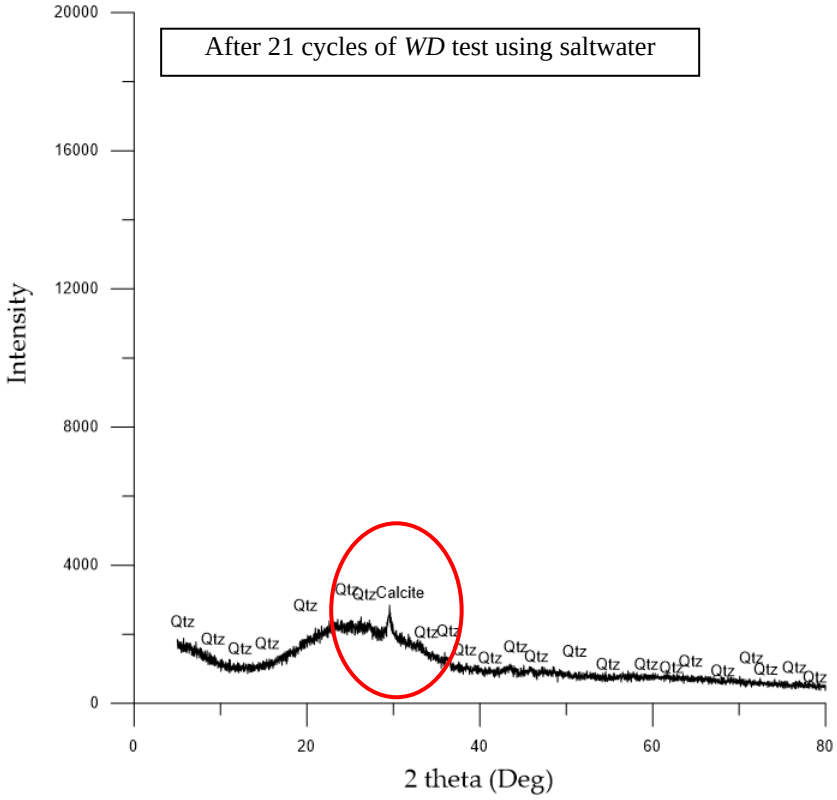


(a)



(b)

Continue to next page



(c)

Figure E.3. Graphic XRD analysis pattern of glass beads (a) before MICP treatment, (b) after MICP treatment, (c) MICP treated after 21 WD cycle under distilled water, and (d) MICP treated after 21 WD cycle under saltwater.

APPENDIXES F
XRD results of the MICP beach sand treatment using cheap chemical reagents

F.1 Coral Krakal-Sadranan sand

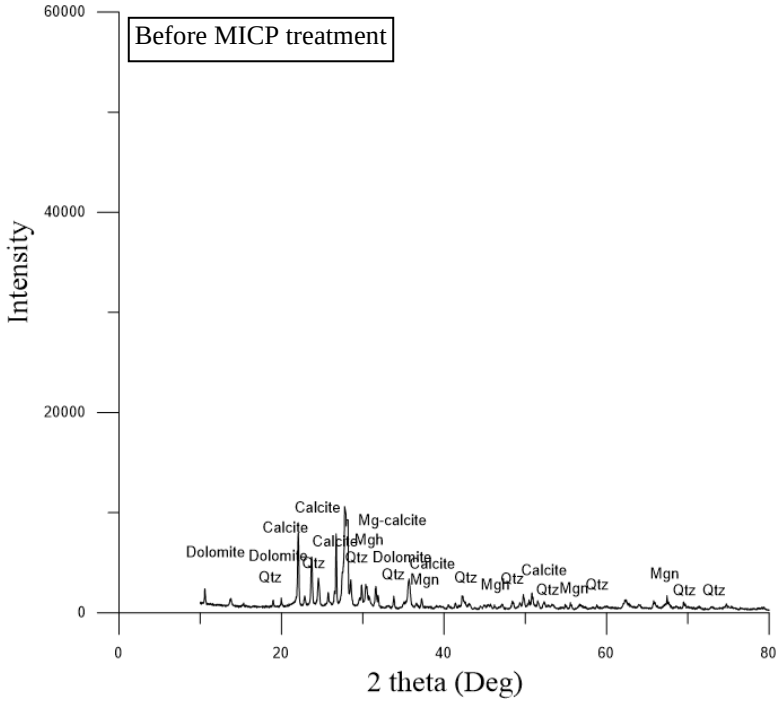


Figure F.1. Graphic XRD analysis of coral sands Krakal-Sadranan.

F.2 Coral Krakal-Sadranan sand treated with standard chemical

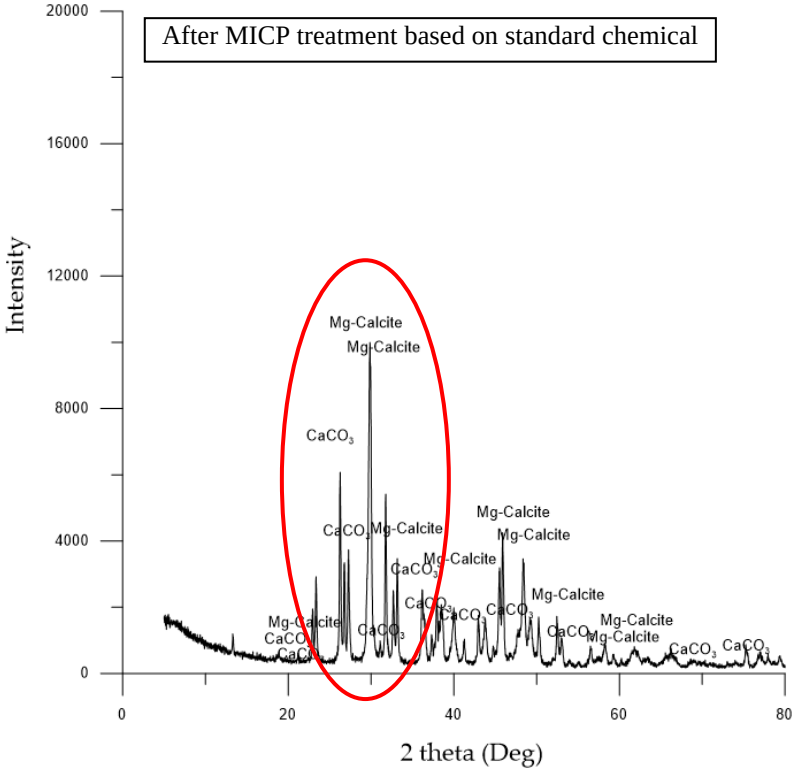


Figure F.2. Graphic XRD analysis pattern of MICP treatment based on standard chemical

F.3 Krakal-Sadranan coral sand treated with snow-melting reagent

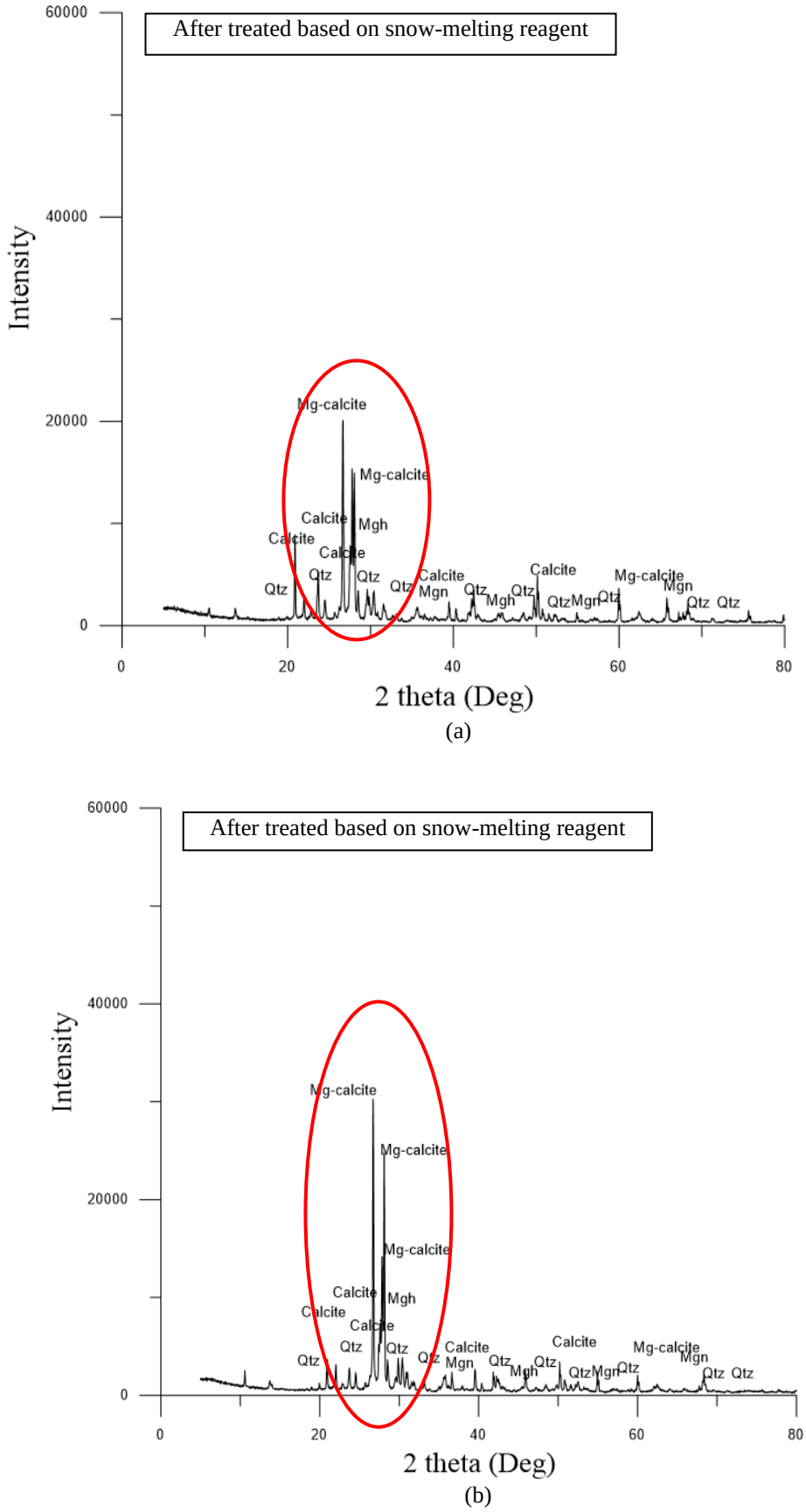
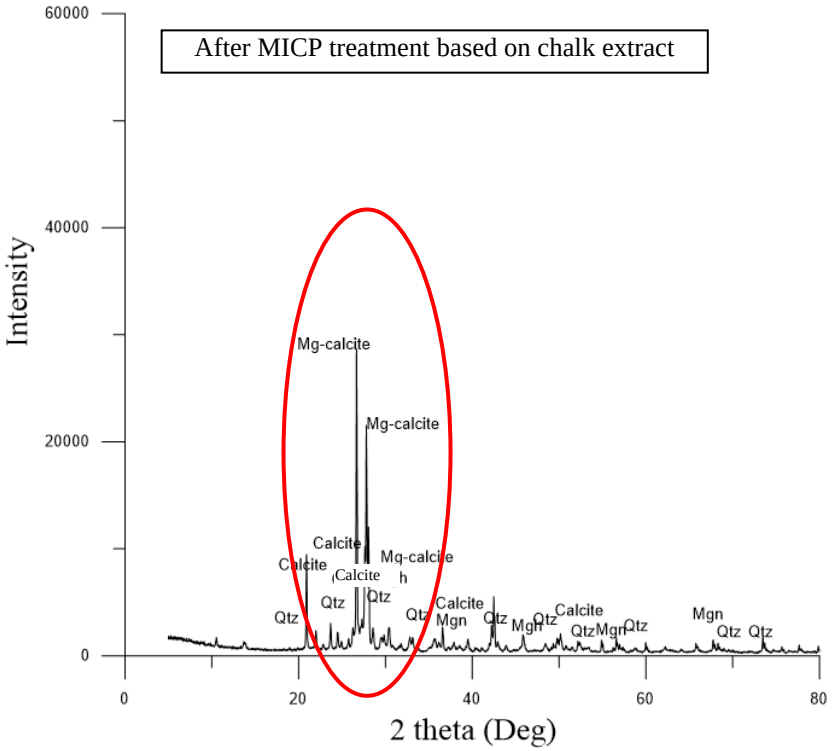
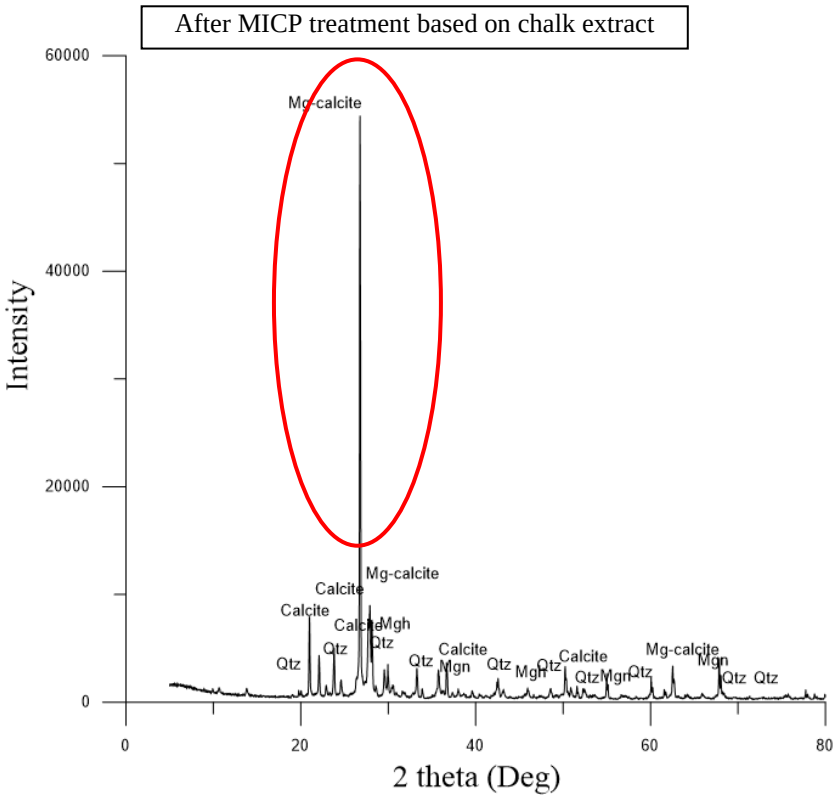


Figure F.3. Graphic XRD analysis pattern of MICP treatment based on snow-melting reagent (a) sample A and (b) sample B.

F.4 Krakal-Sadranan coral sand treated with chalk extract



(a)



(b)

Figure F.4. Graphic XRD analysis pattern of MICP treatment based on chalk extract (a) sample A and (b) sample B.